

LA-UR-03-1987

*Approved for public release;
distribution is unlimited*

Title: **MCNP — A General Monte Carlo
N-Particle Transport Code, Version 5**

Volume I: Overview and Theory

Authors: **X-5 Monte Carlo Team**

April 24, 2003 (Revised 10/3/05)



Los Alamos National Laboratory, an affirmative action/equal opportunity employer, is operated by the University of California for the U.S. Department of Energy under contract W-7405-ENG-36. By acceptance of this article, the publisher recognizes that the U.S. Government retains a nonexclusive, royalty-free license to publish or reproduce the published form of this contribution, or to allow others to do so, for U.S. Government purposes. Los Alamos National Laboratory requests that the publisher identify this article as work performed under the auspices of the U.S. Department of Energy. Los Alamos National Laboratory strongly supports academic freedom and a researcher's right to publish; as an institution, however, the Laboratory does not endorse the viewpoint of a publication or guarantee its technical correctness.

Form 836 (8/00)

MCNP, MCNP5, and “MCNP Version 5” are trademarks of the Regents of the University of California, Los Alamos National Laboratory.

COPYRIGHT NOTICE & DISCLAIMER

This material was prepared by the University of California (University) under Contract W-7405-ENG-36 with the U.S. Department of Energy (DOE). All rights in the material are reserved by DOE on behalf of the Government and the University pursuant to the contract.

This report was prepared as an account of work sponsored by an agency of the United States Government. Neither the United States Government nor any agency thereof, nor any of their employees, makes any warranty, express or implied, or assumes any legal liability or responsibility for the accuracy, completeness, or usefulness of any information, apparatus, product, or process disclosed, or represents that its use would not infringe privately owned rights. Reference herein to any specific commercial product, process, or service by trade name, trademark, manufacturer, or otherwise, does not necessarily constitute or imply its endorsement, recommendation, or favoring by the United States Government or any agency thereof. The views and opinions of authors expressed herein do not necessarily state or reflect those of the United States government or any agency thereof.

FOREWORD

This manual is a practical guide for the use of the general-purpose Monte Carlo code MCNP. The previous version of the manual (LA-13709-M, March 2000) has been corrected and updated to include the new features found in MCNP Version 5 (MCNP5). The manual has also been split into 3 volumes:

Volume I:	MCNP Overview and Theory	Chapters 1, 2 and Appendices G, H
Volume II:	MCNP User's Guide	Chapters 1, 3, 4, 5 and Appendices A, B, I, J, K
Volume III:	MCNP Developer's Guide	Appendices C, D, E, F

Volume I (LA-UR-03-1987) provides an overview of the capabilities of MCNP5 and a detailed discussion of the theoretical basis for the code. The first chapter provides introductory information about MCNP5. The second chapter describes the mathematics, data, physics, and Monte Carlo simulation techniques which form the basis for MCNP5. This discussion is not meant to be exhaustive — details of some techniques and of the Monte Carlo method itself are covered by references to the literature.

Volume II (LA-CP-03-0245) provides detailed specifications for MCNP5 input and options, numerous example problems, and a discussion of the output generated by MCNP5. The first chapter is a primer on basic MCNP5 use. The third chapter shows the user how to prepare input for the code. The fourth chapter contains several examples, and the fifth chapter explains the output. The appendices provide information on the available data libraries for MCNP, the format for several input/output files, and plotting the geometry, tallies, and cross-sections.

Volume III (LA-CP-03-0284) provides details on how to install MCNP on various computer systems, how to modify the code, the meaning of some of the code variables, and data layouts for certain arrays.

The Monte Carlo method for solving transport problems emerged from work done at Los Alamos during World War II. The method is generally attributed to Fermi, von Neumann, Ulam, Metropolis, and Richtmyer. MCNP, first released in 1977, is the successor to their work and has been under continuous development for the past 25 years. Neither the code nor the manual is static. The code is changed as needs arise, and the manual is changed to reflect the latest version of the code. This particular manual refers to Version 5.

MCNP5 and this manual are the product of the combined effort of many people in the Diagnostics Applications Group (X-5) in the Applied Physics Division (X Division) at the Los Alamos National Laboratory:

X-5 Monte Carlo Team

Thomas E. Booth	H. Grady Hughes	Anthony Zukaitis
Forrest B. Brown	Russell D. Mosteller	Marsha Boggs, (CCN-12)
Jeffrey S. Bull	Richard E. Prael	Roger Martz (CCN-7)
R. Arthur Forster	Avneet Sood	
John T. Goorley	Jeremy E. Sweezy	

X-5 Data Team

Joann M. Campbell	Robert C. Little	Morgan C. White
Stephanie C. Frankle		

Technical Editors

Sheila M. Girard

The code and manual can be obtained from the Radiation Safety Information Computational Center (RSICC), P. O. Box 2008, Oak Ridge, TN, 37831-6362.

Jeremy E. Sweezy
MCNP Team Leader
<jsweezy@lanl.gov>

**MCNP – A General Monte Carlo N-Particle Transport Code
Version 5**

**X-5 Monte Carlo Team
Diagnostics Applications Group
Los Alamos National Laboratory**

ABSTRACT

MCNP is a general-purpose Monte Carlo N-Particle code that can be used for neutron, photon, electron, or coupled neutron/photon/electron transport, including the capability to calculate eigenvalues for critical systems. The code treats an arbitrary three-dimensional configuration of materials in geometric cells bounded by first- and second-degree surfaces and fourth-degree elliptical tori.

Pointwise cross-section data are used. For neutrons, all reactions given in a particular cross-section evaluation (such as ENDF/B-VI) are accounted for. Thermal neutrons are described by both the free gas and $S(\alpha,\beta)$ models. For photons, the code accounts for incoherent and coherent scattering, the possibility of fluorescent emission after photoelectric absorption, and absorption in electron-positron pair production. Electron/positron transport processes account for angular deflection through multiple Coulomb scattering, collisional energy loss with optional straggling, and the production of secondary particles including K x-rays, knock-on and Auger electrons, bremsstrahlung, and annihilation gamma rays from positron annihilation at rest. Electron transport does not include the effects of external or self-induced electromagnetic fields. Photonuclear physics is available for a limited number of isotopes.

Important standard features that make MCNP very versatile and easy to use include a powerful general source, criticality source, and surface source; both geometry and output tally plotters; a rich collection of variance reduction techniques; a flexible tally structure; and an extensive collection of cross-section data.

Volume I: Overview and Theory

CHAPTER 1 - MCNP OVERVIEW	1
MCNP AND THE MONTE CARLO METHOD	1
Monte Carlo Method vs. Deterministic Method	2
The Monte Carlo Method	2
INTRODUCTION TO MCNP FEATURES	4
Nuclear Data and Reactions	4
Source Specification	5
Tallies and Output	5
Estimation of Monte Carlo Errors	6
Variance Reduction	8
MCNP GEOMETRY	12
Cells	13
Surface Type Specification	17
Surface Parameter Specification	17
REFERENCES	19
 CHAPTER 2 - GEOMETRY, DATA, PHYSICS, AND MATHEMATICS	 1
INTRODUCTION	1
History	1
MCNP Structure	4
History Flow	5
GEOMETRY	7
Complement Operator	8
Repeated Structure Geometry	9
Surfaces	9
CROSS SECTIONS	14
Neutron Interaction Data: Continuous-Energy and Discrete-Reaction	16
Photon Interaction Data	20
Electron Interaction Data	23
Neutron Dosimetry Cross Sections	23
Neutron Thermal $S(\alpha,\beta)$ Tables	24
Multigroup Tables	24
PHYSICS	25
Weight	25
Particle Tracks	27
Neutron Interactions	27
Photon Interactions	57
Electron Interactions	67
TALLIES	80
Surface Current Tally	84
Flux Tallies	85
Track Length Cell Energy Deposition Tallies	87
Pulse Height Tallies	89

Flux at a Detector	91
Additional Tally Features	104
ESTIMATION OF THE MONTE CARLO PRECISION	108
Monte Carlo Means, Variances, and Standard Deviations	109
Precision and Accuracy	110
The Central Limit Theorem and Monte Carlo Confidence Intervals	112
Estimated Relative Errors in MCNP	113
MCNP Figure of Merit	116
Separation of Relative Error into Two Components	118
Variance of the Variance	120
Empirical History Score Probability Density Function $f(x)$	122
Forming Statistically Valid Confidence Intervals	127
A Statistically Pathological Output Example	131
VARIANCE REDUCTION	134
General Considerations	134
Variance Reduction Techniques	139
CRITICALITY CALCULATIONS	163
Criticality Program Flow	164
Estimation of k_{eff} Confidence Intervals and Prompt Neutron Lifetimes	167
Recommendations for Making a Good Criticality Calculation	183
VOLUMES AND AREAS	185
Rotationally Symmetric Volumes and Areas	186
Polyhedron Volumes and Areas	186
Stochastic Volume and Area Calculation	187
PLOTTER	188
RANDOM NUMBERS	191
PERTURBATIONS	192
Derivation of the Operator	192
Limitations	199
Accuracy	199
REFERENCES	201
APPENDIX G - MCNP DATA LIBRARIES	1
ENDF/B REACTION TYPES	1
$S(\alpha,\beta)$ DATA FOR USE WITH THE MTn CARD	5
NEUTRON CROSS-SECTION LIBRARIES	9
MULTIGROUP DATA	40
PHOTOATOMIC DATA	43
PHOTONUCLEAR DATA	58
DOSIMETRY DATA	60
REFERENCES	74
APPENDIX H - FISSION SPECTRA CONSTANTS	
AND FLUX-TO-DOSE FACTORS	1
CONSTANTS FOR FISSION SPECTRA	1
Constants for the Maxwell Fission Spectrum (Neutron-induced)	1
Constants for the Watt Fission Spectrum	3

FLUX-TO-DOSE CONVERSION FACTORS	3
Biological Dose Equivalent Rate Factors	4
Silicon Displacement Kerma Factors	5
REFERENCES	7

Volume II: User's Guide

CHAPTER 1 - PRIMER	1
MCNP INPUT FOR SAMPLE PROBLEM	1
INP File	3
Cell Cards	4
Surface Cards	5
Data Cards	6
HOW TO RUN MCNP	11
Execution Line	12
Interrupts	15
Running MCNP	15
TIPS FOR CORRECT AND EFFICIENT PROBLEMS	16
Problem Setup	16
Preproduction	16
Production	17
Criticality	17
REFERENCES	18
 CHAPTER 3 - DESCRIPTION OF MCNP INPUT	 1
INP FILE	1
Message Block	1
Initiate-Run	2
Continue-Run	2
Card Format	4
Particle Designators	7
Default Values	7
Input Error Messages	7
Geometry Errors	8
CELL CARDS	9
Shorthand Cell Specification	11
SURFACE CARDS	11
Surfaces Defined by Equations	11
Axisymmetric Surfaces Defined by Points	15
General Plane Defined by Three Points	17
Surfaces Defined by Macrobodyes	18
DATA CARDS	23

Problem Type (MODE) Card	24
Geometry Cards	24
Variance Reduction	33
Source Specification	52
Tally Specification	79
Material Specification	117
Energy and Thermal Treatment Specification	127
Problem Cutoff Cards	135
User Data Arrays	138
Peripheral Cards	139
SUMMARY OF MCNP INPUT FILE	157
Input Cards	157
Storage Limitations	160
REFERENCES	161
CHAPTER 4 - EXAMPLES	1
GEOMETRY SPECIFICATION	1
COORDINATE TRANSFORMATIONS	16
TR1 and M = 1 Case	18
TR2 and M = -1 Case	19
REPEATED STRUCTURE AND LATTICE EXAMPLES	20
TALLY EXAMPLES	39
FMn Examples (Simple Form)	39
FMn Examples (General Form)	41
FSn Examples	42
FTn Examples	44
Repeated Structure/Lattice Tally Example	45
TALLYX Subroutine Examples	49
SOURCE EXAMPLES	53
SOURCE SUBROUTINE	60
SRCDX SUBROUTINE	62
CHAPTER 5 - OUTPUT	1
DEMO PROBLEM AND OUTPUT	1
TEST1 PROBLEM AND OUTPUT	8
CONC PROBLEM AND OUTPUT	49
KCODE	63
EVENT LOG AND GEOMETRY ERRORS	110
Event Log	110
Debug Print for a Lost Particle	113
REFERENCES	114
APPENDIX A - SUMMARY OF MCNP COMMANDS	1
GENERAL INFO, FILE NAMES, EXECUTION LINE, UNITS	1
Form of Input (INP) File: Required to Initiate and Run a Problem	1
Form of CONTINUE Input File: Requires a RUNTPE file	2
MCNP File Names and Contents	2

MCNP Execution Line Options and Useful Combinations	3
MCNP Execution Lines for Various Types of Problems	4
MCNP Physical Units and Tally Units	4
MCNP Interrupts (press <cr> after each entry)	5
Example of an MCNP Fixed Source INP File	5
Example of a k_{eff} Eigenvalue INP File	6
INPUT (INP) FILE COMMANDS	7
Input Command Formats	7
Input Commands	8
Input Commands by Function	11
Concise Input Command Descriptions	14
GEOMETRY PLOTTING COMMANDS	44
Geometry Plotting Command Formats	44
Geometry Plotting Commands	45
Geometry Plotting Commands By Function	46
Concise Geometry Plotting Command Descriptions	47
TALLY AND CROSS-SECTION PLOTTING COMMANDS	50
Tally and Cross-Section Plotting Command Formats	50
Tally and Cross-Section Plotting Commands	50
Tally and Cross-Section Plotting Commands By Function	52
Concise Tally and Cross-Section Plotting Command Descriptions	54
APPENDIX B - MCNP GEOMETRY AND TALLY PLOTTING	1
SYSTEM GRAPHICS INFORMATION	1
X Windows	1
THE GEOMETRY PLOTTER	2
Geometry PLOT Input and Execute Line Options	2
Geometry Plot Commands Grouped by Function	4
Geometry Debugging and Plot Orientation	9
Interactive Geometry Plotting	10
THE MCPLOT TALLY AND CROSS-SECTION PLOTTER	14
Input for MCPLOT and Execution Line Options	15
Plot Conventions and Command Syntax	17
Plot Commands Grouped by Function	17
MCTAL Files	24
Example of Use of COPLOT	27
Normalization of Energy-Dependent Tally Plots	27
REFERENCES	41
APPENDIX I - PTRAC TABLES	1
APPENDIX J - MESH-BASED WWINP, WWOUT,	
AND WWONE FILE FORMAT	1
APPENDIX K - XSDIR DATA DIRECTORY FILE	1

Volume III: Developer's Guide

APPENDIX C - INSTALLING AND RUNNING MCNP ON VARIOUS SYSTEMS	1
A NEW BUILD SYSTEM FOR MCNP FORTRAN 90 ON UNIX	1
NEW UNIX BUILD SYSTEM DESCRIPTION	2
THE UNIX INSTALL UTILITY	4
UNIX CONFIGURATION WITH INSTALL UTILITY	5
UNIX CONFIGURATION WITHOUT INSTALL UTILITY	9
UNIX MODES OF OPERATION	12
Source Directory	12
Source/config Directory	12
Source/src Directory	15
Source/datasrc Directory	15
Source/dotcomm/src Directory	16
Testing/Regression Directory	16
INSTALLING AND BUILDING MCNP5 ON WINDOWS PCs	21
Installing MCNP5 on Windows PCs	22
Building MCNP on Windows PCs	26
PARALLEL CONFIGURATION INFORMATION	30
TESTING PERFORMED TO DATE	32
MODIFYING MCNP WITH PATCHES	34
MCNP VERIFICATION	38
CONVERTING CROSS-SECTION FILES WITH MAKXSF	39
REFERENCES	42
APPENDIX D - MODIFYING MCNP	1
PREPROCESSORS	1
PROGRAMMING LANGUAGE	1
SYMBOLIC NAMES	2
SYSTEM DEPENDENCE	2
COMMON BLOCKS	3
DYNAMICALLY ALLOCATED STORAGE	4
THE RUNTPE FILE	4
C FUNCTIONS	5
SUBROUTINE USAGE IN MCNP5	6
MCNP Structure	6
History Flow	7
REFERENCES	9
APPENDIX E - GLOBAL CONSTANTS, VARIABLES, AND ARRAYS	1
DICTIONARY OF SYMBOLIC NAMES	1
SOME IMPORTANT COMPLICATED ARRAYS	27
Source Arrays	27
Transport Arrays	28
Tally Arrays	30

Accounting Arrays	35
KCODE Arrays	40
Universe Map/Lattice Activity Arrays for Table 128	42
Weight Window Mesh Parameters	42
Perturbation Parameters	43
Macrobody and Identical Surface Arrays	44
DERIVED STRUCTURES	45
APPENDIX F - DATA TABLE FORMATS	1
DATA TYPES AND CLASSES	1
XSDIR— DATA DIRECTORY FILE	2
DATA TABLES	4
Locating Data on a Type 1 Table	4
Locating Data on a Type 2 Table	10
Locating Data Tables in MCNP	11
Individual Data Blocks	11
DATA BLOCKS FOR CONTINUOUS/DISCRETE NEUTRON TRANSPORT TABLES	11
DATA BLOCKS FOR DOSIMETRY TABLES	34
DATA BLOCKS FOR THERMAL $S(\alpha,\beta)$ TABLES	35
DATA BLOCKS FOR PHOTOATOMIC TRANSPORT TABLES	38
FORMAT FOR MULTIGROUP TRANSPORT TABLES	41
FORMAT FOR ELECTRON TRANSPORT TABLES	53
FORMAT FOR PHOTONUCLEAR TRANSPORT TABLES	53
Data Blocks for Photonuclear Transport Tables	54
REFERENCES	69
MCNP MANUAL INDEX	1

CHAPTER 1 - MCNP OVERVIEW

WHAT IS COVERED IN CHAPTER 1

Brief explanation of the Monte Carlo method
Summary of MCNP features
Introduction to geometry

Chapter 1 provides an overview of the MCNP Monte Carlo code with brief summaries of the material covered in-depth in later chapters. It begins with a short discussion of the Monte Carlo method. Five features of MCNP are introduced: (1) nuclear data and reactions, (2) source specifications, (3) tallies and output, (4) estimation of errors, and (5) variance reduction. The third section explains MCNP geometry setup, including the concept of cells and surfaces.

I. MCNP AND THE MONTE CARLO METHOD

MCNP is a general-purpose, continuous-energy, generalized-geometry, time-dependent, coupled neutron/photon/electron Monte Carlo transport code. It can be used in several transport modes: neutron only, photon only, electron only, combined neutron/photon transport where the photons are produced by neutron interactions, neutron/photon/electron, photon/electron, or electron/photon. The neutron energy regime is from 10^{-11} MeV to 20 MeV for all isotopes and up to 150 MeV for some isotopes, the photon energy regime is from 1 keV to 100 GeV, and the electron energy regime is from 1 KeV to 1 GeV. The capability to calculate k_{eff} eigenvalues for fissile systems is also a standard feature.

The user creates an input file that is subsequently read by MCNP. This file contains information about the problem in areas such as:

the geometry specification,
the description of materials and selection of cross-section evaluations,
the location and characteristics of the neutron, photon, or electron source,
the type of answers or tallies desired, and
any variance reduction techniques used to improve efficiency.

Each area will be discussed in the primer by use of a sample problem. Remember five “rules” when running a Monte Carlo calculation. They will be more meaningful as you read this manual and gain experience with MCNP, but no matter how sophisticated a user you may become, never forget the following five points:

1. Define and sample the geometry and source well.
2. You cannot recover lost information.
3. Question the stability and reliability of results.
4. Be conservative and cautious with variance reduction biasing.
5. The number of histories run is not indicative of the quality of the answer.

The following sections compare Monte Carlo and deterministic methods and provide a simple description of the Monte Carlo method.

A. *Monte Carlo Method vs. Deterministic Method*

Monte Carlo methods are very different from deterministic transport methods. Deterministic methods, the most common of which is the discrete ordinates method, solve the transport equation for the average particle behavior. By contrast, Monte Carlo obtains answers by simulating individual particles and recording some aspects (tallies) of their average behavior. The average behavior of particles in the physical system is then inferred (using the central limit theorem) from the average behavior of the simulated particles. Not only are Monte Carlo and deterministic methods very different ways of solving a problem, even what constitutes a solution is different. Deterministic methods typically give fairly complete information (for example, flux) throughout the phase space of the problem. Monte Carlo supplies information only about specific tallies requested by the user.

When Monte Carlo and discrete ordinates methods are compared, it is often said that Monte Carlo solves the integral transport equation, whereas discrete ordinates solves the integro-differential transport equation. Two things are misleading about this statement. First, the integral and integro-differential transport equations are two different forms of the same equation; if one is solved, the other is solved. Second, Monte Carlo “solves” a transport problem by simulating particle histories. A transport equation need not be written to solve a problem by Monte Carlo. Nonetheless, one can derive an equation that describes the probability density of particles in phase space; this equation turns out to be the same as the integral transport equation.

Without deriving the integral transport equation, it is instructive to investigate why the discrete ordinates method is associated with the integro-differential equation and Monte Carlo with the integral equation. The discrete ordinates method visualizes the phase space to be divided into many small boxes, and the particles move from one box to another. In the limit, as the boxes get progressively smaller, particles moving from box to box take a differential amount of time to move a differential distance in space. In the limit, this approaches the integro-differential transport equation, which has derivatives in space and time. By contrast, Monte Carlo transports particles between events (for example, collisions) that are separated in space and time. Neither differential space nor time are inherent parameters of Monte Carlo transport. The integral equation does not have terms involving time or space derivatives.

Monte Carlo is well suited to solving complicated three-dimensional, time-dependent problems. Because the Monte Carlo method does not use phase space boxes, there are no averaging approximations required in space, energy, and time. This is especially important in allowing detailed representation of all aspects of physical data.

B. *The Monte Carlo Method*

Monte Carlo can be used to duplicate theoretically a statistical process (such as the interaction of nuclear particles with materials) and is particularly useful for complex problems that cannot be modeled by computer codes that use deterministic methods. The individual probabilistic events that comprise a process are simulated sequentially. The probability distributions governing these

events are statistically sampled to describe the total phenomenon. In general, the simulation is performed on a digital computer because the number of trials necessary to adequately describe the phenomenon is usually quite large. The statistical sampling process is based on the selection of random numbers—analogue to throwing dice in a gambling casino—hence the name “Monte Carlo.” In particle transport, the Monte Carlo technique is pre-eminently realistic (a numerical experiment). It consists of actually following each of many particles from a source throughout its life to its death in some terminal category (absorption, escape, etc.). Probability distributions are randomly sampled using transport data to determine the outcome at each step of its life.

Event Log

1. Neutron scatter, photon production
2. Fission, photon production
3. Neutron capture
4. Neutron leakage
5. Photon scatter
6. Photon leakage
7. Photon capture

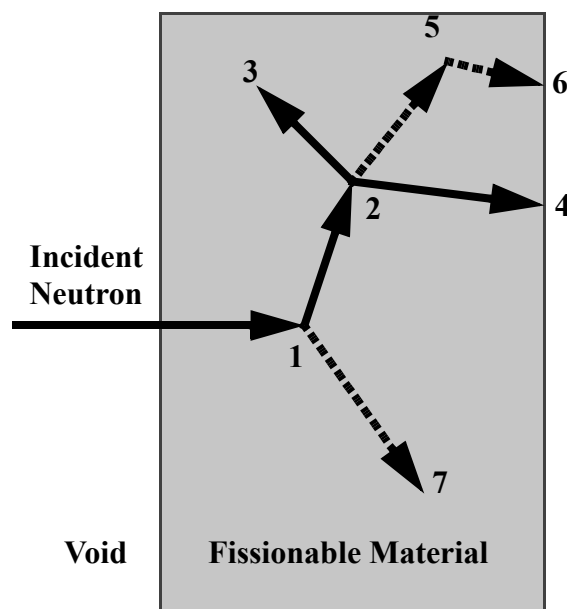


Figure 1-1.

Figure 1-1 represents the random history of a neutron incident on a slab of material that can undergo fission. Numbers between 0 and 1 are selected randomly to determine what (if any) and where interaction takes place, based on the rules (physics) and probabilities (transport data) governing the processes and materials involved. In this particular example, a neutron collision occurs at event 1. The neutron is scattered in the direction shown, which is selected randomly from the physical scattering distribution. A photon is also produced and is temporarily stored, or banked, for later analysis. At event 2, fission occurs, resulting in the termination of the incoming neutron and the birth of two outgoing neutrons and one photon. One neutron and the photon are banked for later analysis. The first fission neutron is captured at event 3 and terminated. The banked neutron is now retrieved and, by random sampling, leaks out of the slab at event 4. The fission-produced photon has a collision at event 5 and leaks out at event 6. The remaining photon generated at event 1 is now followed with a capture at event 7. Note that MCNP retrieves banked particles such that the last particle stored in the bank is the first particle taken out.

This neutron history is now complete. As more and more such histories are followed, the neutron and photon distributions become better known. The quantities of interest (whatever the user requests) are tallied, along with estimates of the statistical precision (uncertainty) of the results.

II. INTRODUCTION TO MCNP FEATURES

Various features, concepts, and capabilities of MCNP are summarized in this section. More detail concerning each topic is available in later chapters or appendices.

A. Nuclear Data and Reactions

MCNP uses continuous-energy nuclear and atomic data libraries. The primary sources of nuclear data are evaluations from the Evaluated Nuclear Data File (ENDF)¹ system, Advanced Computational Technology Initiative (ACTI),² the Evaluated Nuclear Data Library (ENDL)³, Evaluated Photon Data Library (EPDL),⁴ the Activation Library (ACTL)⁵ compilations from Livermore, and evaluations from the Nuclear Physics (T-16) Group^{6,7,8} at Los Alamos. Evaluated data are processed into a format appropriate for MCNP by codes such as NJOY.^{9,10} The processed nuclear data libraries retain as much detail from the original evaluations as is feasible to faithfully reproduce the evaluator's intent.

Nuclear data tables exist for neutron interactions, neutron-induced photons, photon interactions, neutron dosimetry or activation, and thermal particle scattering $S(\alpha,\beta)$. Most of the photon and electron data are atomic rather than nuclear in nature; photonuclear data are also included. Each data table available to MCNP is listed on a directory file, XSDIR. Users may select specific data tables through unique identifiers for each table, called ZAIDs. These identifiers generally contain the atomic number Z, mass number A, and library specifier ID.

Over 836 neutron interaction tables are available for approximately 100 different isotopes and elements. Multiple tables for a single isotope are provided primarily because data have been derived from different evaluations, but also because of different temperature regimes and different processing tolerances. More neutron interaction tables are constantly being added as new and revised evaluations become available. Neutron-induced photon production data are given as part of the neutron interaction tables when such data are included in the evaluations.

Photon interaction tables exist for all elements from $Z = 1$ through $Z = 100$. The data in the photon interaction tables allow MCNP to account for coherent and incoherent scattering, photoelectric absorption with the possibility of fluorescent emission, and pair production. Scattering angular distributions are modified by atomic form factors and incoherent scattering functions.

Cross sections for nearly 2000 dosimetry or activation reactions involving over 400 target nuclei in ground and excited states are part of the MCNP data package. These cross sections can be used as energy-dependent response functions in MCNP to determine reaction rates but cannot be used as transport cross sections.

Thermal data tables are appropriate for use with the $S(\alpha,\beta)$ scattering treatment in MCNP. The data include chemical (molecular) binding and crystalline effects that become important as the neutron's energy becomes sufficiently low. Data at various temperatures are available for light and heavy water, beryllium metal, beryllium oxide, benzene, graphite, polyethylene, and zirconium and hydrogen in zirconium hydride.

B. Source Specification

MCNP's generalized user-input source capability allows the user to specify a wide variety of source conditions without having to make a code modification. Independent probability distributions may be specified for the source variables of energy, time, position, and direction, and for other parameters such as starting cell(s) or surface(s). Information about the geometrical extent of the source can also be given. In addition, source variables may depend on other source variables (for example, energy as a function of angle) thus extending the built-in source capabilities of the code. The user can bias all input distributions.

In addition to input probability distributions for source variables, certain built-in functions are available. These include various analytic functions for fission and fusion energy spectra such as Watt, Maxwellian, and Gaussian spectra; Gaussian for time; and isotropic, cosine, and monodirectional for direction. Biasing may also be accomplished by special built-in functions.

A surface source allows particles crossing a surface in one problem to be used as the source for a subsequent problem. The decoupling of a calculation into several parts allows detailed design or analysis of certain geometrical regions without having to rerun the entire problem from the beginning each time. The surface source has a fission volume source option that starts particles from fission sites where they were written in a previous run.

MCNP provides the user three methods to define an initial criticality source to estimate k_{eff} , the ratio of neutrons produced in successive generations in fissile systems.

C. Tallies and Output

The user can instruct MCNP to make various tallies related to particle current, particle flux, and energy deposition. MCNP tallies are normalized to be per starting particle except for a few special cases with criticality sources. Currents can be tallied as a function of direction across any set of surfaces, surface segments, or sum of surfaces in the problem. Charge can be tallied for electrons and positrons. Fluxes across any set of surfaces, surface segments, sum of surfaces, and in cells, cell segments, or sum of cells are also available. Similarly, the fluxes at designated detectors (points or rings) are standard tallies, as well as radiography detector tallies. Fluxes can also be tallied on a mesh superimposed on the problem geometry. Heating and fission tallies give the energy deposition in specified cells. A pulse height tally provides the energy distribution of pulses created in a detector by radiation. In addition, particles may be flagged when they cross specified surfaces or enter designated cells, and the contributions of these flagged particles to the tallies are listed separately. Tallies such as the number of fissions, the number of absorptions, the total helium production, or any product of the flux times the approximately 100 standard ENDF reactions plus several nonstandard ones may be calculated with any of the MCNP tallies. In fact, any quantity of the form

$$C = \int \phi(E)f(E)dE$$

can be tallied, where $\phi(E)$ is the energy-dependent fluence, and $f(E)$ is any product or summation of the quantities in the cross-section libraries or a response function provided by the user. The

tallies may also be reduced by line-of-sight attenuation. Tallies may be made for segments of cells and surfaces without having to build the desired segments into the actual problem geometry. All tallies are functions of time and energy as specified by the user and are normalized to be per starting particle. Mesh tallies are functions of energy and are also normalized to be per starting particle.

In addition to the tally information, the output file contains tables of standard summary information to give the user a better idea of how the problem ran. This information can give insight into the physics of the problem and the adequacy of the Monte Carlo simulation. If errors occur during the running of a problem, detailed diagnostic prints for debugging are given. Printed with each tally is also its statistical relative error corresponding to one standard deviation. Following the tally is a detailed analysis to aid in determining confidence in the results. Ten pass/no-pass checks are made for the user-selectable tally fluctuation chart (TFC) bin of each tally. The quality of the confidence interval still cannot be guaranteed because portions of the problem phase space possibly still have not been sampled. Tally fluctuation charts, described in the following section, are also automatically printed to show how a tally mean, error, variance of the variance, and slope of the largest history scores fluctuate as a function of the number of histories run.

All tally results, except for mesh tallies, can be displayed graphically, either while the code is running or in a separate postprocessing mode.

D. Estimation of Monte Carlo Errors

MCNP tallies are normalized to be per starting particle and are printed in the output accompanied by a second number R , which is the estimated relative error defined to be one estimated standard deviation of the mean $S_{\bar{x}}$ divided by the estimated mean \bar{x} . In MCNP, the quantities required for this error estimate—the tally and its second moment—are computed after each complete Monte Carlo history, which accounts for the fact that the various contributions to a tally from the same history are correlated. For a well-behaved tally, R will be proportional to $1/\sqrt{N}$ where N is the number of histories. Thus, to halve R , we must increase the total number of histories fourfold. For a poorly behaved tally, R may increase as the number of histories increases.

The estimated relative error can be used to form confidence intervals about the estimated mean, allowing one to make a statement about what the true result is. The Central Limit Theorem states that as N approaches infinity there is a 68% chance that the true result will be in the range $\bar{x}(1 \pm R)$ and a 95% chance in the range $\bar{x}(1 \pm 2R)$. *It is extremely important to note that these confidence statements refer only to the precision of the Monte Carlo calculation itself and not to the accuracy of the result compared to the true physical value.* A statement regarding accuracy requires a detailed analysis of the uncertainties in the physical data, modeling, sampling techniques, and approximations, etc., used in a calculation.

The guidelines for interpreting the quality of the confidence interval for various values of R are listed in Table 1.1.

Table 1.1:
Guidelines for Interpreting the Relative Error R^*

<u>Range of R</u>	<u>Quality of the Tally</u>
0.5 to 1.0	Not meaningful
0.2 to 0.5	Factor of a few
0.1 to 0.2	Questionable
< 0.10	Generally reliable
< 0.05	Generally reliable for point detectors

* $R = S_{\bar{x}}/\bar{x}$ and represents the estimated relative error at the 1σ level. These interpretations of R assume that all portions of the problem phase space are being sampled well by the Monte Carlo process.

For all tallies except next-event estimators, hereafter referred to as point detector tallies, the quantity R should be less than 0.10 to produce generally reliable confidence intervals. Point detector results tend to have larger third and fourth moments of the individual tally distributions, so a smaller value of R , < 0.05, is required to produce generally reliable confidence intervals. The estimated uncertainty in the Monte Carlo result must be presented with the tally so that all are aware of the estimated precision of the results.

Keep in mind the footnote to Table 1.1. For example, if an important but highly unlikely particle path in phase space has not been sampled in a problem, the Monte Carlo results will not have the correct expected values and the confidence interval statements may not be correct. The user can guard against this situation by setting up the problem so as not to exclude any regions of phase space and by trying to sample all regions of the problem adequately.

Despite one's best effort, an important path may not be sampled often enough, causing confidence interval statements to be incorrect. To try to inform the user about this behavior, MCNP calculates a figure of merit (FOM) for one tally bin of each tally as a function of the number of histories and prints the results in the tally fluctuation charts at the end of the output. The FOM is defined as

$$FOM \equiv 1/(R^2 T)$$

where T is the computer time in minutes. The more efficient a Monte Carlo calculation is, the larger the FOM will be because less computer time is required to reach a given value of R .

The FOM should be approximately constant as N increases because R^2 is proportional to $1/N$ and T is proportional to N . *Always examine the tally fluctuation charts to be sure that the tally appears well behaved, as evidenced by a fairly constant FOM .* A sharp decrease in the FOM indicates that a seldom-sampled particle path has significantly affected the tally result and relative error estimate. In this case, the confidence intervals may not be correct for the fraction of the time that statistical theory would indicate. Examine the problem to determine what path is causing the large scores and try to redefine the problem to sample that path much more frequently.

After each tally, an analysis is done and additional useful information is printed about the TFC tally bin result. The nonzero scoring efficiency, the zero and nonzero score components of the relative error, the number and magnitude of negative history scores, if any, and the effect on the result if

the largest observed history score in the TFC were to occur again on the very next history are given. A table just before the TFCs summarizes the results of these checks for all tallies in the problem. Ten statistical checks are made and summarized in Table 160 after each tally, with a pass yes/no criterion. The empirical history score probability density function (PDF) for the TFC bin of each tally is calculated and displayed in printed plots.

The TFCs at the end of the problem include the variance of the variance (an estimate of the error of the relative error), and the slope (the estimated exponent of the PDF large score behavior) as a function of the number of particles started.

All this information provides the user with statistical information to aid in forming valid confidence intervals for Monte Carlo results. There is no GUARANTEE, however. The possibility always exists that some as yet unsampled portion of the problem may change the confidence interval if more histories were calculated. Chapter 2 contains more information about estimation of Monte Carlo precision.

E. Variance Reduction

As noted in the previous section, R (the estimated relative error) is proportional to $1/\sqrt{N}$, where N is the number of histories. For a given MCNP run, the computer time T consumed is proportional to N . Thus $R = C/\sqrt{T}$, where C is a positive constant. There are two ways to reduce R : (1) increase T and/or (2) decrease C . Computer budgets often limit the utility of the first approach. For example, if it has taken 2 hours to obtain $R = 0.10$, then 200 hours will be required to obtain $R = 0.01$. For this reason MCNP has special variance reduction techniques for decreasing C . (Variance is the square of the standard deviation.) The constant C depends on the tally choice and/or the sampling choices.

1. Tally Choice

As an example of the tally choice, note that the fluence in a cell can be estimated either by a collision estimate or a track length estimate. The collision estimate is obtained by tallying $1/\Sigma_t$ (Σ_t =macroscopic total cross section) at each collision in the cell and the track length estimate is obtained by tallying the distance the particle moves while inside the cell. Note that as Σ_t gets very small, very few particles collide but give enormous tallies when they do, producing a high variance situation (see page 2–118). In contrast, the track length estimate gets a tally from every particle that enters the cell. For this reason MCNP has track length tallies as standard tallies, whereas the collision tally is not standard in MCNP, except for estimating k_{eff} .

2. Nonanalog Monte Carlo

Explaining how sampling affects C requires understanding of the nonanalog Monte Carlo model.

The simplest Monte Carlo model for particle transport problems is the analog model that uses the natural probabilities that various events occur (for example, collision, fission, capture, etc.). Particles are followed from event to event by a computer, and the next event is always sampled (using the random number generator) from a number of possible next events according to the

natural event probabilities. This is called the analog Monte Carlo model because it is directly analogous to the naturally occurring transport.

The analog Monte Carlo model works well when a significant fraction of the particles contribute to the tally estimate and can be compared to detecting a significant fraction of the particles in the physical situation. There are many cases for which the fraction of particles detected is very small, less than 10^{-6} . For these problems analog Monte Carlo fails because few, if any, of the particles tally, and the statistical uncertainty in the answer is unacceptable.

Although the analog Monte Carlo model is the simplest conceptual probability model, there are other probability models for particle transport that estimate the same average value as the analog Monte Carlo model, while often making the variance (uncertainty) of the estimate much smaller than the variance for the analog estimate. This means that problems that would be impossible to solve in days of computer time with analog methods can be solved in minutes of computer time with nonanalog methods.

A nonanalog Monte Carlo model attempts to follow “interesting” particles more often than “uninteresting” ones. An “interesting” particle is one that contributes a large amount to the quantity (or quantities) that needs to be estimated. There are many nonanalog techniques, and all are meant to increase the odds that a particle scores (contributes). To ensure that the average score is the same in the nonanalog model as in the analog model, the score is modified to remove the effect of biasing (changing) the natural odds. Thus, if a particle is artificially made q times as likely to execute a given random walk, then the particle’s score is weighted by (multiplied by) $1/q$. The average score is thus preserved because the average score is the sum, over all random walks, of the probability of a random walk multiplied by the score resulting from that random walk.

A nonanalog Monte Carlo technique will have the same expected tallies as an analog technique if the expected weight executing any given random walk is preserved. For example, a particle can be split into two identical pieces and the tallies of each piece are weighted by $1/2$ of what the tallies would have been without the split. Such nonanalog, or variance reduction, techniques can often decrease the relative error by sampling naturally rare events with an unnaturally high frequency and weighting the tallies appropriately.

3. Variance Reduction Tools in MCNP

There are four classes of variance reduction techniques¹¹ that range from the trivial to the esoteric.

Truncation Methods are the simplest of variance reduction methods. They speed up calculations by truncating parts of phase space that do not contribute significantly to the solution. The simplest example is geometry truncation in which unimportant parts of the geometry are simply not modeled. Specific truncation methods available in MCNP are the energy cutoff and time cutoff.

Population Control Methods use particle splitting and Russian roulette to control the number of samples taken in various regions of phase space. In important regions many samples of low weight are tracked, while in unimportant regions few samples of high weight are tracked. A weight adjustment is made to ensure that the problem solution remains unbiased. Specific population

control methods available in MCNP are geometry splitting and Russian roulette, energy splitting/roulette, time splitting/roulette, weight cutoff, and weight windows.

Modified Sampling Methods alter the statistical sampling of a problem to increase the number of tallies per particle. For any Monte Carlo event it is possible to sample from any arbitrary distribution rather than the physical probability as long as the particle weights are then adjusted to compensate. Thus, with modified sampling methods, sampling is done from distributions that send particles in desired directions or into other desired regions of phase space such as time or energy, or change the location or type of collisions. Modified sampling methods in MCNP include the exponential transform, implicit capture, forced collisions, source biasing, and neutron-induced photon production biasing.

Partially-Deterministic Methods are the most complicated class of variance reduction methods. They circumvent the normal random walk process by using deterministic-like techniques, such as next event estimators, or by controlling the random number sequence. In MCNP these methods include point detectors, DXTRAN, and correlated sampling.

Variance reduction techniques, used correctly, can greatly help the user produce a more efficient calculation. Used poorly, they can result in a wrong answer with good statistics and few clues that anything is amiss. Some variance reduction methods have general application and are not easily misused. Others are more specialized and attempts to use them carry high risk. The use of weight windows tends to be more powerful than the use of importances but typically requires more input data and more insight into the problem. The exponential transform for thick shields is not recommended for the inexperienced user; rather, use many cells with increasing importances (or decreasing weight windows) through the shield. Forced collisions are used to increase the frequency of random walk collisions within optically thin cells but should be used only by an experienced user. The point detector estimator should be used with caution, as should DXTRAN.

For many problems, variance reduction is not just a way to speed up the problem but is absolutely necessary to get any answer at all. Deep penetration problems and pipe detector problems, for example, will run too slowly by factors of trillions without adequate variance reduction. Consequently, users have to become skilled in using the variance reduction techniques in MCNP. Most of the following techniques cannot be used with the pulse height tally.

The following summarizes briefly the main MCNP variance reduction techniques. Detailed discussion is in Chapter 2, page 2–134.

1. **Energy cutoff:** Particles whose energy is out of the range of interest are terminated so that computation time is not spent following them.
2. **Time cutoff:** Like the energy cutoff but based on time.
3. **Geometry splitting with Russian roulette:** Particles transported from a region of higher importance to a region of lower importance (where they will probably contribute little to the desired problem result) undergo Russian roulette; that is, some of those particles will be killed a certain fraction of the time, but survivors will be counted more by increasing their weight the remaining fraction of the time. In this way, unimportant particles are followed less often, yet the problem solution remains undistorted. On the other hand, if a particle is transported to a region of higher importance (where it will likely contribute

to the desired problem result), it may be split into two or more particles (or tracks), each with less weight and therefore counting less. In this way, important particles are followed more often, yet the solution is undistorted because, on average, total weight is conserved.

4. **Energy splitting/Russian roulette:** Particles can be split or rouletted upon entering various user-supplied energy ranges. Thus important energy ranges can be sampled more frequently by splitting the weight among several particles and less important energy ranges can be sampled less frequently by rouletting particles.
5. **Time splitting/Russian roulette:** Like energy splitting/roulette, but based on time.
6. **Weight cutoff/Russian roulette:** If a particle weight becomes so low that the particle becomes insignificant, it undergoes Russian roulette. Most particles are killed, and some particles survive with increased weight. The solution is unbiased because total weight is conserved, but computer time is not wasted on insignificant particles.
7. **Weight window:** As a function of energy, geometrical location, or both, low-weighted particles are eliminated by Russian roulette and high-weighted particles are split. This technique helps keep the weight dispersion within reasonable bounds throughout the problem. An importance generator is available that estimates the optimal limits for a weight window.
8. **Exponential transformation:** To transport particles long distances, the distance between collisions in a preferred direction is artificially increased and the weight is correspondingly artificially decreased. Because large weight fluctuations often result, it is highly recommended that the weight window be used with the exponential transform.
9. **Implicit absorption:** When a particle collides, there is a probability that it is absorbed by the nucleus. In analog absorption, the particle is killed with that probability. In implicit absorption, also known as implicit capture or survival biasing, the particle is never killed by absorption; instead, its weight is reduced by the absorption probability at each collision. Important particles are permitted to survive by not being lost to absorption. On the other hand, if particles are no longer considered useful after undergoing a few collisions, analog absorption efficiently gets rid of them.
10. **Forced collisions:** A particle can be forced to undergo a collision each time it enters a designated cell that is almost transparent to it. The particle and its weight are appropriately split into two parts, collided and uncollided. Forced collisions are often used to generate contributions to point detectors, ring detectors, or DXTRAN spheres.
11. **Source variable biasing:** Source particles with phase space variables of more importance are emitted with a higher frequency but with a compensating lower weight than are less important source particles. This technique can be used with pulse height tallies.
12. **Point and ring detectors:** When the user wishes to tally a flux-related quantity at a point in space, the probability of transporting a particle precisely to that point is vanishingly small. Therefore, pseudoparticles are directed to the point instead. Every time a particle history is born in the source or undergoes a collision, the user may require that a pseudoparticle be tallied at a specified point in space. In this way, many pseudoparticles of low weight reach the detector, which is the point of interest, even though no particle histories could ever reach the detector. For problems with rotational symmetry, the point may be represented by a ring to enhance the efficiency of the calculation.

13. ***DXTRAN***: DXTRAN, which stands for deterministic transport, improves sampling in the vicinity of detectors or other tallies. It involves deterministically transporting particles on collision to some arbitrary, user-defined sphere in the neighborhood of a tally and then calculating contributions to the tally from these particles. Contributions to the detectors or to the DXTRAN spheres can be controlled as a function of a geometric cell or as a function of the relative magnitude of the contribution to the detector or DXTRAN sphere.

The DXTRAN method is a way of obtaining large numbers of particles on user-specified “DXTRAN spheres.” DXTRAN makes it possible to obtain many particles in a small region of interest that would otherwise be difficult to sample. Upon sampling a collision or source density function, DXTRAN estimates the correct weight fraction that should scatter toward, and arrive without collision at, the surface of the sphere. The DXTRAN method then puts this correct weight on the sphere. The source or collision event is sampled in the usual manner, except that the particle is killed if it tries to enter the sphere because all particles entering the sphere have already been accounted for deterministically.

14. ***Correlated sampling***: The sequence of random numbers in the Monte Carlo process is chosen so that statistical fluctuations in the problem solution will not mask small variations in that solution resulting from slight changes in the problem specification. The i^{th} history will always start at the same point in the random number sequence no matter what the previous $i-1$ particles did in their random walks.

III. MCNP GEOMETRY

We will present here only basic introductory information about geometry setup, surface specification, and cell and surface card input. Areas of further interest would be the complement operator, use of parentheses, and repeated structure and lattice definitions, found in Chapter 2. Chapter 4 contains geometry examples and is recommended as a next step. Chapter 3 has detailed information about the format and entries on cell and surface cards and discusses macrobodies.

The geometry of MCNP treats an arbitrary 3-dimensional configuration of user-defined materials in geometric cells bounded by first- and second-degree surfaces and fourth-degree elliptical tori. The cells are defined by the intersections, unions, and complements of the regions bounded by the surfaces. Surfaces are defined by supplying coefficients to the analytic surface equations or, for certain types of surfaces, known points on the surfaces. MCNP also provides a “macrobody” capability, where basic shapes such as spheres, boxes, cylinders, etc., may be combined using boolean operators. This capability is essentially the same as the combinatorial geometry provided by other codes such as MORSE, KENO, and VIM.

MCNP has a more general geometry than is available in most combinatorial geometry codes. In addition to the capability of combining several predefined geometrical bodies, as in a combinatorial geometry scheme, MCNP gives the user the added flexibility of defining geometrical regions from all the first and second degree surfaces of analytical geometry and elliptical tori and then of combining them with boolean operators. The code does extensive internal

checking to find input errors. In addition, the geometry-plotting capability in MCNP helps the user check for geometry errors.

MCNP treats geometric cells in a Cartesian coordinate system. The surface equations recognized by MCNP are listed in Table 3.1 on page 3–13. The particular Cartesian coordinate system used is arbitrary and user defined, but the right-handed system shown in Figure 1-2 is usually chosen.

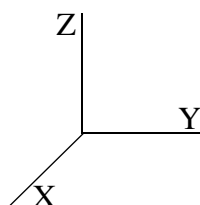


Figure 1-2.

Using the bounding surfaces specified on cell cards, MCNP tracks particles through the geometry, calculates the intersection of a track's trajectory with each bounding surface, and finds the minimum positive distance to an intersection. If the distance to the next collision is greater than this minimum distance and there are no DXTRAN spheres along the track, the particle leaves the current cell. At the appropriate surface intersection, MCNP finds the correct cell that the particle will enter by checking the sense of the intersection point for each surface listed for the cell. When a complete match is found, MCNP has found the correct cell on the other side and the transport continues.

A. Cells

When cells are defined, an important concept is that of the *sense* of all points in a cell with respect to a bounding surface. Suppose that $s = f(x,y,z) = 0$ is the equation of a surface in the problem. For any set of points (x,y,z) , if $s = 0$ the points are on the surface. However, for points not on the surface, if s is negative, the points are said to have a negative sense with respect to that surface and, conversely, a positive sense if s is positive. For example, a point at $x = 3$ has a positive sense with respect to the plane $x - 2 = 0$. That is, the equation $x - D = 3 - 2 = s = 1$ is positive for $x = 3$ (where $D = \text{constant}$).

Cells are defined on cell cards. Each cell is described by a cell number, material number, and material density followed by a list of operators and signed surfaces that bound the cell. If the sense is positive, the sign can be omitted. The material number and material density can be replaced by a single zero to indicate a void cell. The cell number must begin in columns 1–5. The remaining entries follow, separated by blanks. A more complete description of the cell card format can be found in Volume II. Each surface divides all space into two regions, one with positive sense with respect to the surface and the other with negative sense. The geometry description defines the cell to be the intersection, union, and/or complement of the listed regions.

The subdivision of the physical space into cells is not necessarily governed only by the different material regions, but may be affected by problems of sampling and variance reduction techniques

(such as splitting and Russian roulette), the need to specify an unambiguous geometry, and the tally requirements. The tally segmentation feature may eliminate most of the tally requirements.

Be cautious about making any one cell very complicated. With the union operator and disjointed regions, a very large geometry can be set up with just one cell. The problem is that for each track flight between collisions in a cell, the intersection of the track with each bounding surface of the cell is calculated, a calculation that can be costly if a cell has many surfaces. As an example, consider Figure 1-3a. It is just a lot of parallel cylinders and is easy to set up. However, the cell containing all the little cylinders is bounded by twelve surfaces (counting a top and bottom). A much more efficient geometry is seen in Figure 1-3b, where the large cell has been broken up into a number of smaller cells.

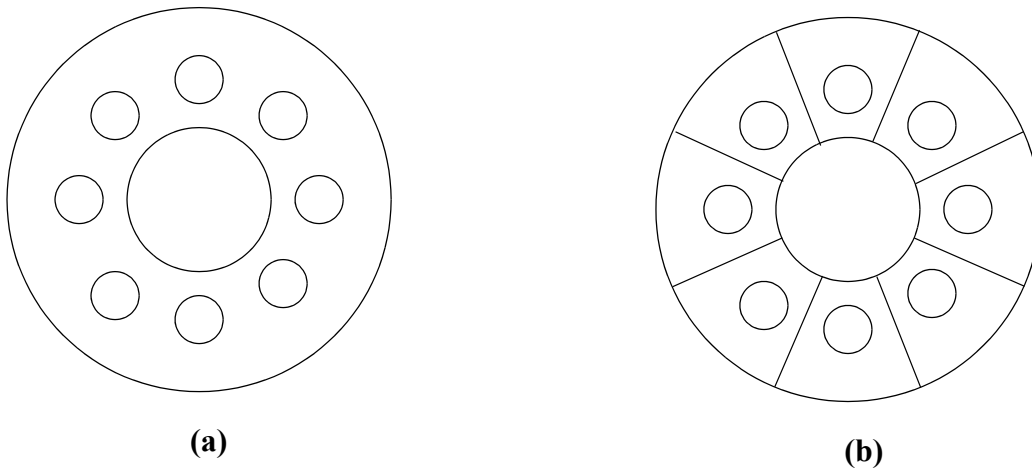


Figure 1-3.

1. Cells Defined by Intersections of Regions of Space

The intersection operator in MCNP is implicit; it is simply the blank space between two surface numbers on the cell card.

If a cell is specified using only intersections, all points in the cell must have the same sense with respect to a given bounding surface. This means that, for each bounding surface of a cell, all points in the cell must remain on only one side of any particular surface. Thus, there can be no concave corners in a cell specified only by intersections. Figure 1-4, a cell formed by the intersection of five surfaces (ignore surface 6 for the time being), illustrates the problem of concave corners by allowing a particle (or point) to be on two sides of a surface in one cell. Surfaces 3 and 4 form a concave corner in the cell such that points p_1 and p_2 are on the same side of surface 4 (that is, have the same sense with respect to 4) but point p_3 is on the other side of surface 4 (opposite sense). Points p_2 and p_3 have the same sense with respect to surface 3, but p_1 has the opposite sense. One way to remedy this dilemma (and there are others) is to add surface 6 between the 3/4 corner and surface 1 to divide the original cell into two cells.

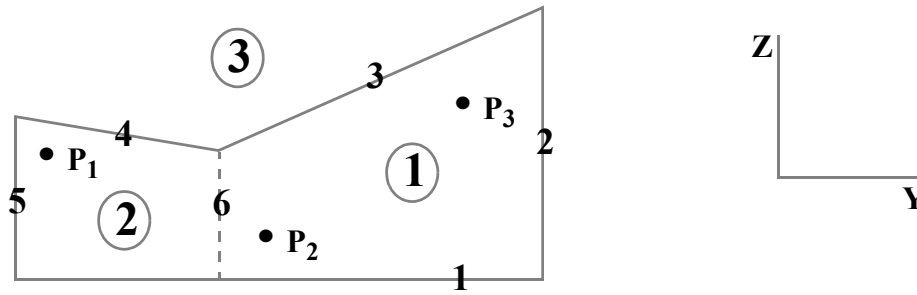


Figure 1-4.

With surface 6 added to Figure 1-4, the cell to the right of surface 6 is number 1 (cells indicated by circled numbers); to the left number 2; and the outside cell number 3. The cell cards (in two dimensions, all cells void) are

```
1  0  1  -2  -3  6
2  0  1  -6  -4  5
```

Cell 1 is a void and is formed by the intersection of the region above (positive sense) surface 1 with the region to the left (negative sense) of surface 2, intersected with the region below (negative sense) surface 3, and finally intersected with the region to the right (positive sense) of surface 6. Cell 2 is described similarly.

Cell 3 cannot be specified with the intersection operator. The following section about the union operator is needed to describe cell 3.

2. Cells Defined by Unions of Regions of Space

The union operator, signified by a colon on the cell cards, allows concave corners in cells and also cells that are completely disjoint. The intersection and union operators are binary Boolean operators, so their use follows Boolean algebra methodology; unions and intersections can be used in combination in any cell description.

Spaces on either side of the union operator are irrelevant, but remember that a space without the colon signifies an intersection. In the hierarchy of operations, intersections are performed first and then unions. There is no left to right ordering. Parentheses can be used to clarify operations and in some cases are required to force a certain order of operations. Innermost parentheses are cleared first. Spaces are optional on either side of a parenthesis. A parenthesis is equivalent to a space and signifies an intersection.

For example, let A and B be two regions of space. The region containing points that belong to both A and B is called the intersection of A and B. The region containing points that belong to A alone or to B alone or to both A and B is called the union of A and B. The shaded area in Figure 1-5a represents the union of A and B (or A : B), and the shaded area in Figure 1-5b represents the intersection of A and B (or A B). The only way regions of space can be added is with the union operator. An intersection of two spaces always results in a region no larger than either of the two

spaces. Conversely, the union of two spaces always results in a region no smaller than either of the two spaces.

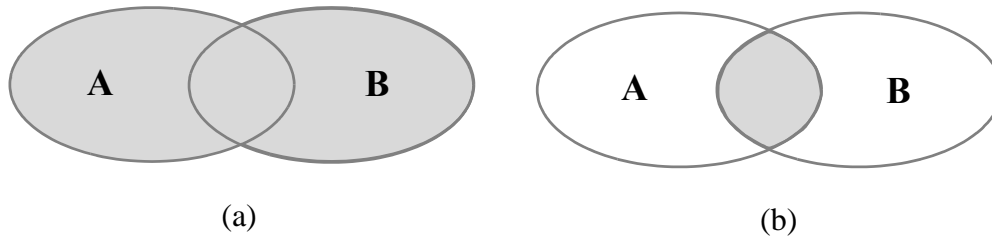


Figure 1-5.

A simple example will further illustrate the concept of Figure 1-5 and the union operator to solidify the concept of adding and intersecting regions of space to define a cell. See also the second example in Chapter 4. In Figure 1-6 we have two infinite planes that meet to form two cells. Cell 1 is easy to define; it is everything in the universe to the right of surface 1 (that is, a positive sense) that is also in common with (or intersected with) everything in the universe below surface 2 (that is, a negative sense). Therefore, the surface relation of cell 1 is $1 -2$.

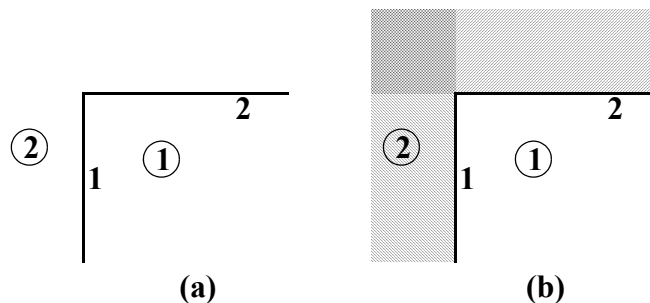


Figure 1-6.

Cell 2 is everything in the universe to the left (negative sense) of surface 1 plus everything in the universe above (positive sense) surface 2, or $-1 : 2$, illustrated in Figure 1-6b by all the shaded regions of space. If cell 2 were specified as $-1 : 2$, that would represent the region of space common to -1 and 2 , which is only the cross-hatched region in the figure and is obviously an improper specification for cell 2.

Returning to Figure 1-4 on page 1-15, if cell 1 is inside the solid black line and cell 2 is the entire region outside the solid line, then the MCNP cell cards in two dimensions are (assuming both cells are voids)

```
1  0  1  -2  (-3 : -4)  5
2  0  -5 : -1 : 2 : 3  4
```

Cell 1 is defined as the region above surface 1 intersected with the region to the left of surface 2, intersected with the union of regions below surfaces 3 and 4, and finally intersected with the region

to the right of surface 5. Cell 2 contains four concave corners (all except between surfaces 3 and 4), and its specification is just the converse (or complement) of cell 1. Cell 2 is the space defined by the region to the left of surface 5 plus the region below 1 plus the region to the right of 2 plus the space defined by the intersections of the regions above surfaces 3 and 4.

A simple consistency check can be noted with the two cell cards above. All intersections for cell 1 become unions for cell 2 and vice versa. The senses are also reversed.

Note that in this example, all corners less than 180 degrees in a cell are handled by intersections, and all corners greater than 180 degrees are handled by unions.

To illustrate some of the concepts about parentheses, assume an intersection is thought of mathematically as multiplication and a union is thought of mathematically as addition. Parentheses are removed first, with multiplication being performed before addition. The cell cards for the example cards above from Figure 1-4 may be written in the form

$$\begin{array}{ll} 1 & a \cdot b \cdot (c + d) \cdot e \\ 2 & e + a + b + c \cdot d \end{array}$$

Note that parentheses are required for the first cell but not for the second, although the second could have been written as $e + a + b + (c \cdot d)$, $(e + a + b) + (c \cdot d)$, $(e) + (a) + (b) + (c \cdot d)$, etc.

Several more examples using the union operator are given in Chapter 4. Study them to get a better understanding of this powerful operator that can greatly simplify geometry setups.

B. Surface Type Specification

The first- and second-degree surfaces plus the fourth-degree elliptical and degenerate tori of analytical geometry are all available in MCNP. The surfaces are designated by mnemonics such as C/Z for a cylinder parallel to the z -axis. A cylinder at an arbitrary orientation is designated by the general quadratic (GQ) mnemonic. A paraboloid parallel to a coordinate axis is designated by the special quadratic (SQ) mnemonic. The 29 mnemonics representing various types of surfaces are listed in Table 3.1 on page 3–13.

C. Surface Parameter Specification

There are two ways to specify surface parameters in MCNP: (1) by supplying the appropriate coefficients needed to satisfy the surface equation, and (2) by specifying known geometrical points on a surface that is rotationally symmetric about a coordinate axis.

1. Coefficients for the Surface Equations

The first way to define a surface is to use one of the surface-type mnemonics from Table 3.1 on page 3–13 and to calculate the appropriate coefficients needed to satisfy the surface equation.

For example, a sphere of radius 3.62 cm with the center located at the point (4,1,-3) is specified by

S 4 1 -3 3.62

An ellipsoid whose axes are not parallel to the coordinate axes is defined by the GQ mnemonic plus up to 10 coefficients of the general quadratic equation. Calculating the coefficients can be (and frequently is) nontrivial, but the task is greatly simplified by defining an auxiliary coordinate system whose axes coincide with the axes of the ellipsoid. The ellipsoid is easily defined in terms of the auxiliary coordinate system, and the relationship between the auxiliary coordinate system and the main coordinate system is specified on a TRn card, described on page 3–30.

The use of the SQ and GQ surfaces is determined by the orientation of the axes. One should always use the simplest possible surface in describing geometries; for example, using a GQ surface instead of an S to specify a sphere will require more computational effort for MCNP.

2. Points that Define a Surface

The second way to define a surface is to supply known points on the surface. This method is convenient if you are setting up a geometry from something like a blueprint where you know the coordinates of intersections of surfaces or points on the surfaces. When three or more surfaces intersect at a point, this second method also produces a more nearly perfect point of intersection if the common point is used in the surface specification. It is frequently difficult to get complicated surfaces to meet at one point if the surfaces are specified by the equation coefficients. Failure to achieve such a meeting can result in the unwanted loss of particles.

There are, however, restrictions that must be observed when specifying surfaces by points that do not exist when specifying surfaces by coefficients. Surfaces described by points must be either skew planes or surfaces rotationally symmetric about the x , y , or z axes. They must be unique, real, and continuous. For example, points specified on both sheets of a hyperboloid are not allowed because the surface is not continuous. However, it is valid to specify points that are all on one sheet of the hyperboloid. (See the X, Y, Z, and P input card descriptions on page 3–15 for additional explanation.)

IV. REFERENCES

1. P. F. Rose, Compiler and Editor, "ENDF-201, ENDF/B-VI Summary Documentation," BNL-NCS-17541, Brookhaven National Laboratory (October 1991).
2. S. C. Frankle, R. C. Reedy, and P. G. Young, "ACTI An MCNP Data Library for Prompt Gamma-ray Spectroscopy," 12th Biennial Radiation Protection and Shielding Topical Meeting, Santa Fe, NM, April 15-19, 2002.
3. R. J. Howerton, D. E. Cullen, R. C. Haight, M. H. MacGregor, S. T. Perkins, and E. F. Plechaty, "The LLL Evaluated Nuclear Data Library (ENDL): Evaluation Techniques, Reaction Index, and Descriptions of Individual Reactions," Lawrence Livermore National Laboratory report UCRL-50400, Vol. 15, Part A (September 1975).
4. D. E. Cullen, M. H. Chen, J. H. Hubbell, S. T. Perkins, E. F. Plechaty, J. A. Rathkopf, and J. H. Scofield, "Tables and Graphs of Photon Interaction Cross Sections from 10 eV to 100 GeV Derived from the LLNL Evaluated Photon Data Library (EPDL)," Lawrence Livermore National Laboratory report UCRL-50400, Volume 6, Rev. 4, Part A: Z = 1 to 50 and Part B: Z = 51 to 100 (1989).
5. M. A. Gardner and R. J. Howerton, "ACTL: Evaluated Neutron Activation Cross-Section Library-Evaluation Techniques and Reaction Index," Lawrence Livermore National Laboratory report UCRL-50400, Vol. 18 (October 1978).
6. E. D. Arthur and P. G. Young, "Evaluated Neutron-Induced Cross Sections for $^{54,56}\text{Fe}$ to 40 MeV," Los Alamos Scientific Laboratory report LA-8626-MS (ENDF-304) (December 1980).
7. D. G. Foster, Jr. and E. D. Arthur, "Average Neutronic Properties of "Prompt" Fission Products," Los Alamos National Laboratory report LA-9168-MS (February 1982).
8. E. D. Arthur, P. G. Young, A. B. Smith, and C. A. Philis, "New Tungsten Isotope Evaluations for Neutron Energies Between 0.1 and 20 MeV," *Trans. Am. Nucl. Soc.* **39**, 793 (1981).
9. R. E. MacFarlane and D. W. Muir, "The NJOY Nuclear Data Processing System Version 91," Los Alamos National Laboratory report LA-12740-M, (October 1994).
10. R. E. MacFarlane, D. W. Muir, and R. M. Boicourt, "The NJOY Nuclear Data Processing System, Volume I: User's Manual," Los Alamos National Laboratory report LA-9303-M, Vol. I (ENDF-324) (May 1982).
R. E. MacFarlane, D. W. Muir, and R. M. Boicourt, "The NJOY Nuclear Data Processing System, Volume II: The NJOY, RECONR, BROADR, HEATR, and THERMR Modules," Los Alamos National Laboratory report LA-9303-M, Vol. II (ENDF-324) (May 1982).
11. R. A. Forster, R. C. Little, J. F. Briesmeister, and J. S. Hendricks, "MCNP Capabilities For Nuclear Well Logging Calculations," *IEEE Transactions on Nuclear Science*, **37** (3), 1378 (June 1990)
12. A. Geist et al, "PVM 3 User's Guide and Reference Manual," ORNL/TM-12187, Oak Ridge National Laboratory (1993).
13. G. McKinney, "A Practical Guide to Using MCNP with PVM," *Trans. Am. Nucl. Soc.* **71**, 397 (1994).
14. G. McKinney, "MCNP4B Multiprocessing Enhancements Using PVM," Los Alamos National Laboratory memorandum X-6:GWM-95-212 (1995).

CHAPTER 2 - GEOMETRY, DATA, PHYSICS, AND MATHEMATICS

I. INTRODUCTION

Chapter 2 discusses the mathematics and physics of MCNP, including geometry, cross-section libraries, sources, variance reduction schemes, Monte Carlo simulation of neutron and photon transport, and tallies. This discussion is not meant to be exhaustive; many details of the particular techniques and of the Monte Carlo method itself will be found elsewhere. Carter and Cashwell's book *Particle-Transport Simulation with the Monte Carlo Method*,¹ a good general reference on radiation transport by Monte Carlo, is based upon what is in MCNP. A more recent reference is Lux and Koblinger's book, *Monte Carlo Particle Transport Methods: Neutron and Photon Calculations*.² Methods of sampling from standard probability densities are discussed in the Monte Carlo samplers by Everett and Cashwell.³

MCNP was originally developed by the Monte Carlo Group, currently the Diagnostic Applications Group, (Group X-5) in the Applied Physics Division (X Division) at the Los Alamos National Laboratory. Group X-5 improves MCNP (releasing a new version every two to three years), maintains it at Los Alamos and at other laboratories where we have collaborators or sponsors, and provides limited free consulting and support for MCNP users. MCNP is distributed to other users through the Radiation Safety Information Computational Center (RSICC) at Oak Ridge, Tennessee, and the OECD/NEA data bank in Paris, France. There are about 250 MCNP users at Los Alamos and 3000 users at 200 installations worldwide.

MCNP is comprised of about 425 subroutines written in Fortran 90 and C. MCNP has been made as system independent as possible to enhance its portability, and has been written to comply with the ANSI Fortran 90 standard. With one source code, MCNP is supported on many platforms. MCNP takes advantage of parallel computer architectures using three parallel models. MCNP supports threading using the OpenMP model. Distributed processing is supported through the use of both the Message Passing Interface (MPI) model and the Parallel Virtual Machine (PVM) software from Oak Ridge. MCNP also combines threading with both MPI and PVM.

A. History

The Monte Carlo method is generally attributed to scientists working on the development of nuclear weapons in Los Alamos during the 1940s. However, its roots go back much farther.

Perhaps the earliest documented use of random sampling to solve a mathematical problem was that of Comte de Buffon in 1772.⁴ A century later people performed experiments in which they threw a needle in a haphazard manner onto a board ruled with parallel straight lines and inferred the value of π from observations of the number of intersections between needle and lines.^{5,6} Laplace suggested in 1786 that π could be evaluated by random sampling.⁷ Lord Kelvin appears to have used random sampling to aid in evaluating some time integrals of the kinetic energy that appear in the kinetic theory of gasses⁸ and acknowledged his secretary for performing calculations for more than 5000 collisions.⁹

According to Emilio Segrè, Enrico Fermi's student and collaborator, Fermi invented a form of the Monte Carlo method when he was studying the moderation of neutrons in Rome.^{9,10} Though Fermi did not publish anything, he amazed his colleagues with his predictions of experimental results. After indulging himself, he would reveal that his “guesses” were really derived from the statistical sampling techniques that he performed in his head when he couldn't fall asleep.

During World War II at Los Alamos, Fermi joined many other eminent scientists to develop the first atomic bomb. It was here that Stan Ulam became impressed with electromechanical computers used for implosion studies. Ulam realized that statistical sampling techniques were considered impractical because they were long and tedious, but with the development of computers they could become practical. Ulam discussed his ideas with others like John von Neumann and Nicholas Metropolis. Statistical sampling techniques reminded everyone of games of chance, where randomness would statistically become resolved in predictable probabilities. It was Nicholas Metropolis who noted that Stan had an uncle who would borrow money from relatives because he “just had to go to Monte Carlo” and thus named the mathematical method “Monte Carlo.”¹⁰

Meanwhile, a team of wartime scientists headed by John Mauchly was working to develop the first electronic computer at the University of Pennsylvania in Philadelphia. Mauchly realized that if Geiger counters in physics laboratories could count, then they could also do arithmetic and solve mathematical problems. When he saw a seemingly limitless array of women cranking out firing tables with desk calculators at the Ballistic Research Laboratory at Aberdeen, he proposed¹⁰ that an electronic computer be built to deal with these calculations. The result was ENIAC (Electronic Numerical Integrator and Computer), the world's first computer, built for Aberdeen at the University of Pennsylvania. It had 18,000 double triode vacuum tubes in a system with 500,000 solder joints.¹⁰

John von Neumann was a consultant to both Aberdeen and Los Alamos. When he heard about ENIAC, he convinced the authorities at Aberdeen that he could provide a more exhaustive test of the computer than mere firing-table computations. In 1945 John von Neumann, Stan Frankel, and Nicholas Metropolis visited the Moore School of Electrical Engineering at the University of Pennsylvania to explore using ENIAC for thermonuclear weapon calculations with Edward Teller at Los Alamos.¹⁰ After the successful testing and dropping of the first atomic bombs a few months later, work began in earnest to calculate a thermonuclear weapon. On March 11, 1947, John von Neumann sent a letter to Robert Richtmyer, leader of the Theoretical Division at Los Alamos, proposing use of the statistical method to solve neutron diffusion and multiplication problems in fission devices.¹⁰ His letter was the first formulation of a Monte Carlo computation for an electronic computing machine. In 1947, while in Los Alamos, Fermi invented a mechanical device called FERMIAC¹¹ to trace neutron movements through fissionable materials by the Monte Carlo Method.

By 1948 Stan Ulam was able to report to the Atomic Energy Commission that not only was the Monte Carlo method being successfully used on problems pertaining to thermonuclear as well as fission devices, but also it was being applied to cosmic ray showers and the study of partial differential equations.¹⁰ In the late 1940s and early 1950s, there was a surge of papers describing the Monte Carlo method and how it could solve problems in radiation or particle transport and other areas.^{12,13,14} Many of the methods described in these papers are still used in Monte Carlo today, including the method of generating random numbers¹⁵ used in MCNP. Much of the interest

was based on continued development of computers such as the Los Alamos MANIAC (Mechanical Analyzer, Numerical Integrator, and Computer) in March, 1952.

The Atomic Energy Act of 1946 created the Atomic Energy Commission to succeed the Manhattan Project. In 1953 the United States embarked upon the “Atoms for Peace” program with the intent of developing nuclear energy for peaceful applications such as nuclear power generation. Meanwhile, computers were advancing rapidly. These factors led to greater interest in the Monte Carlo method. In 1954 the first comprehensive review of the Monte Carlo method was published by Herman Kahn¹⁶ and the first book was published by Cashwell and Everett¹⁷ in 1959.

At Los Alamos, Monte Carlo computer codes developed along with computers. The first Monte Carlo code was the simple 19-step computing sheet in John von Neumann's letter to Richtmyer. But as computers became more sophisticated, so did the codes. At first the codes were written in machine language and each code would solve a specific problem. In the early 1960s, better computers and the standardization of programming languages such as Fortran made possible more general codes. The first Los Alamos general-purpose particle transport Monte Carlo code was MCS,¹⁸ written in 1963. Scientists who were not necessarily experts in computers and Monte Carlo mathematical techniques now could take advantage of the Monte Carlo method for radiation transport. They could run the MCS code to solve modest problems without having to do either the programming or the mathematical analysis themselves. MCS was followed by MCN¹⁹ in 1965. MCN could solve the problem of neutrons interacting with matter in a three-dimensional geometry and used physics data stored in separate, highly-developed libraries.

In 1973 MCN was merged with MCG,²⁰ a Monte Carlo gamma code that treated higher energy photons, to form MCNG, a coupled neutron-gamma code. In 1977 MCNG was merged with MCP,²⁰ a Monte Carlo Photon code with detailed physics treatment down to 1 keV, to accurately model neutron-photon interactions. The code has been known as MCNP ever since. Though at first MCNP stood for Monte Carlo Neutron Photon, now it stands for Monte Carlo N-Particle. Other major advances in the 70s included the present generalized tally structure, automatic calculation of volumes, and a Monte Carlo eigenvalue algorithm to determine k_{eff} for nuclear criticality (KCODE).

In 1983 MCNP3 was released, entirely rewritten in ANSI standard Fortran 77. MCNP3 was the first MCNP version internationally distributed through the Radiation Shielding and Information Center at Oak Ridge, Tennessee. Other 1980s versions of MCNP were MCNP3A (1986) and MCNP3B (1988), that included tally plotting graphics (MCPLLOT), the present generalized source, surface sources, repeated structures/lattice geometries, and multigroup/adjoint transport.

MCNP4 was released in 1990 and was the first UNIX version of the code. It accommodated N-particle transport and multitasking on parallel computer architectures. MCNP4 added electron transport (patterned after the Integrated TIGER Series (ITS) electron physics),²¹ the pulse height tally (F8), a thick-target bremsstrahlung approximation for photon transport, enabled detectors and DXTRAN with the $S(\alpha,\beta)$ thermal treatment, provided greater random number control, and allowed plotting of tally results while the code was running.

MCNP4A, released in 1993, featured enhanced statistical analysis, distributed processor multitasking for running in parallel on a cluster of scientific workstations, new photon libraries,

ENDF-6 capabilities, color X-Windows graphics, dynamic memory allocation, expanded criticality output, periodic boundaries, plotting of particle tracks via SABRINA, improved tallies in repeated structures, and many smaller improvements.

MCNP4B, released in 1997, featured differential operator perturbations, enhanced photon physics equivalent to ITS3.0, PVM load balance and fault tolerance, cross-section plotting, postscript file plotting, 64-bit workstation upgrades, PC X-windows, inclusion of LAHET HMCNP, lattice universe mapping, enhanced neutron lifetimes, coincident-surface lattice capability, and many smaller features and improvements.

MCNP4C, released in 2000, featured an unresolved resonance treatment, macrobodies, superimposed importance mesh, perturbation enhancements, electron physics enhancements, plotter upgrades, cumulative tallies, parallel enhancements and other small features and improvements.

MCNP5, released in 2003, is rewritten in ANSI standard Fortran 90. It includes the addition of photonuclear collision physics, superimposed mesh tallies, time splitting, and plotter upgrades. MCNP5 also includes parallel computing enhancements with the addition of support for OpenMP and MPI.

Large production codes such as MCNP have revolutionized science — not only in the way it is done, but also by becoming the repositories for physics knowledge. MCNP represents over 500 person-years of sustained effort. The knowledge and expertise contained in MCNP is formidable.

Current MCNP development is characterized by a strong emphasis on quality control, documentation, and research. New features continue to be added to the code to reflect new advances in computer architecture, improvements in Monte Carlo methodology, and better physics models. MCNP has a proud history and a promising future.

B. MCNP Structure

MCNP is written in ANSI-Standard Fortran 90.²² Global data is shared via Fortran modules. See Appendix E for a list of data modules and their purposes. The general internal structure of MCNP is as follows:

Initiation (IMCN):

- Read input file (INP) to get dimensions;
- Set up variable dimensions or dynamically allocated storage;
- Re-read input file (INP) to load input;
- Process source;
- Process tallies;
- Process materials specifications including masses without loading the data files;
- Calculate cell volumes and surface areas.

Interactive Geometry Plot (PLOT).

Cross-section Processing (XACT):

- Load libraries;

- Eliminate excess neutron data outside problem energy range;
- Doppler broaden elastic and total cross sections to the proper temperature if the problem temperature is higher than the library temperature;
- Process multigroup libraries;
- Process electron libraries including calculation of range tables, straggling tables, scattering angle distributions, and bremsstrahlung.

MCRUN sets up multitasking and multiprocessing, runs histories, and returns to print, write RUNTPE dumps, or process another criticality cycle.

Under MCRUN, MCNP runs neutron, photon, or electron histories:

- Start a source particle;
- Find the distance to the next boundary, cross the surface and enter the next cell;
- Find the total neutron cross section and process neutron collisions producing photons as appropriate;
- Find the total photon cross section and process photon collisions producing electrons as appropriate;
- Use the optional thick-target bremsstrahlung approximation if no electron transport;
- Follow electron tracks;
- Process optional multigroup collisions;
- Process detector tallies or DXTRAN;
- Process surface, cell, and pulse height tallies.

Periodically write output file, restart dumps, update to next criticality cycle, rendezvous for multitasking and updating detector and DXTRAN Russian roulette criteria, etc.:

- Go to the next criticality cycle;
- Print output file summary tables;
- Print tallies;
- Generate weight windows.

Plot tallies, cross sections, and other data (MCPLLOT).

GKS graphics simulation routines.

PVM and MPI distributed processor multiprocessing routines.

Random number generator and control.

Mathematics, character manipulation, and other slave routines.

C. History Flow

The basic flow of a particle history for a coupled neutron/photon/electron problem is handled as follows:

For a given history, the random number sequence is set up and the number of the history, NPS, is incremented. The flag IPT is set for the type of particle being run: 1 for a neutron, 2 for a photon, and 3 for an electron. Some arrays and variables are initialized to zero. The branch of the history, NODE, is set to 1.

Next, the appropriate source routine is called. Source options are the standard fixed sources, the surface source, the criticality source, or a user-provided source. All of the parameters describing the particle are set in these source routines, including position, direction of flight, energy, weight,

time, and starting cell (and possibly surface), by sampling the various distributions described on the source input control cards. Several checks are made at this time to verify that the particle is in the correct cell or on the correct surface, and directed toward the correct cell.

Next, the initial parameters of the first fifty particle histories are printed. Then some of the summary information is incremented (see Appendix E for an explanation of these arrays). Energy, time, and weight are checked against cutoffs. A number of error checks are made. Detector contributions are scored, and then DXTRAN is called (if used in the problem) to create particles on the spheres. The particles are saved in the bank for later tracking. Bookkeeping is started for the pulse height cell tally energy balance. The weight window game is played, with any additional particles from splitting put into the bank and any losses to Russian roulette terminated.

Then the actual particle transport is started. For an electron source, electrons are run separately. For a neutron or photon source, the intersection of the particle trajectory with each bounding surface of the cell is calculated. The minimum positive distance DLS to the cell boundary indicates the next surface JSU the particle is heading toward. The distance to the nearest DXTRAN sphere is calculated, as is the distance to time cutoff, and energy boundary for multigroup charged particles. The cross sections for cell ICL are calculated using a binary table lookup in data tables for neutrons or photons. (New to MCNP5, the total photon cross section may include the photonuclear portion of the cross section, if photonuclear physics is in use. See page 3–129 for a discussion of turning photonuclear physics on.) The total cross section is modified by the exponential transformation if necessary. The distance to the next collision is determined (if a forced collision is required, the uncollided part is banked). The track length of the particle in the cell is found as the minimum of the distance to collision, the distance to the surface JSU, one mean free path (in the case of a mesh-based weight window), the distance to a DXTRAN sphere, the distance to time cutoff, or the distance to energy boundary. Track length cell tallies are then incremented. Some summary information is incremented. The particle's parameters (time, position, and energy) are then updated. If the particle's distance to a DXTRAN sphere (of the same type as the current particle) is equal to the minimum track length, the particle is terminated because particles reaching the DXTRAN sphere are already accounted for by the DXTRAN particles from each collision. If the particle exceeds the time cutoff, the track is terminated. If the particle was detected leaving a DXTRAN sphere, the DXTRAN flag is set to zero and the weight cutoff game is played. The particle is either terminated to weight cutoff or survives with an increased weight. Weight adjustments then are made for the exponential transformation.

If the minimum track length is equal to the distance-to-surface crossing, the particle is transported to surface JSU, any surface tallies are processed, and the particle is processed for entering the next cell. Reflecting surfaces, periodic boundaries, geometry splitting, Russian roulette from importance sampling, and loss to escape are treated. For splitting, one bank entry of NPA particle tracks is made for an (NPA+1)-for-1 split. The bank entries or retrievals are made on a last-in, first-out basis. The history is continued by going back to the previous paragraph and repeating the steps.

If the distance to collision is less than the distance to surface, or if a multigroup charged particle reaches the distance to energy boundary, the particle undergoes a collision. For neutrons, the collision analysis determines which nuclide is involved in the collision, samples the target velocity of the collision nuclide for the free gas thermal treatment, generates and banks any photons (ACEGAM), handles analog capture or capture by weight reduction, plays the weight cutoff game,

handles $S(\alpha, \beta)$ thermal collisions and elastic or inelastic scattering. For criticality problems, fission sites are stored for subsequent generations. Any additional tracks generated in the collision are put in the bank. The energies and directions of particles exiting the collision are determined. Multigroup and multigroup/adjoint collisions are treated separately. The collision process and thermal treatments are described in more detail later in this chapter (see page 2–28).

The collision analysis for photons is similar to that for neutrons, but includes either the simple or the detailed physics treatments. (See page 3–129 for a discussion of turning photonuclear physics on.) The simple physics treatment is valid only for photon interactions with free electrons, i.e. it does not account for electron binding effects when sampling emission distributions; the detailed treatment is the default and includes form factors and Compton profiles for electron binding effects, coherent (Thomson) scatter, and fluorescence from photoelectric capture (see page 2–57). New as of MCNP5, there may also be photonuclear physics (if photonuclear physics is in use). Additionally, photonuclear biasing is available (similar to forced collisions) to split the photon (updating the weight by the interaction probabilities) and force one part to undergo a photoatomic collision and the second part to undergo a photonuclear collision. The collision analysis samples for the collision nuclide, treats photonuclear collisions, treats photoelectric absorption, or capture (with fluorescence in the detailed physics treatment), incoherent (Compton) scatter (with Compton profiles and incoherent scattering factors in the detailed physics treatment to account for electron binding), coherent (Thomson) scatter for the detailed physics treatment only (again with form factors), and pair production. Secondary particles from photonuclear collisions (either photons or neutrons) are sampled using the same routines as for inelastic neutron collisions (see Elastic and Inelastic Scattering on page 2–35). Electrons are generated for incoherent scatter, pair production, and photoelectric absorption. These electrons may be assumed to deposit all their energy instantly if IDES=1 on the PHYS:P card, or they may produce electrons with the thick-target bremsstrahlung approximation (default for MODE P problems, IDES=0 on the PHYS:P card), or they may undergo full electron transport (default for MODE P E problems, IDES=0 on the PHYS:P card.) Multigroup or multigroup/adjoint photons are treated separately.

After the surface crossing or collision is processed, transport continues by calculating the distance to cell boundary, and so on. Or if the particle involved in the collision was killed by capture or variance reduction, the bank is checked for any remaining progeny, and if none exists, the history is terminated. Appropriate summary information is incremented, the tallies of this particular history are added to the total tally data, the history is terminated, and a return is made.

For each history, checks are made to see if output is required or if the job should be terminated because enough histories have been run or too little time remains to continue. For continuation, HISTORY is called again. Otherwise a return is made to MCRUN, and the summary information and tally data are printed.

II. GEOMETRY

The basic MCNP geometry concepts, discussed in Chapter 1, include the sense of a cell, the intersection and union operators, and surface specification. Covered in this section are the complement operator; the repeated structure capability; an explanation of two surfaces, the cone and the torus; and a description of ambiguity, reflecting, white, and periodic boundary surfaces.

A. Complement Operator

The complement operator provides no new capability over the intersection and union operators. It is just a shorthand cell-specifying method that implicitly uses the intersection and union operators.

The complement operator is the # symbol. The complement operator can be thought of as standing for *not in*. There are two basic uses of the operator:

- #*n* means that the description of the current cell is the complement of the description of cell *n*.
- #(...) means complement the portion of the cell description in the parentheses (usually just a list of surfaces describing another cell).

In the first of the two above forms, MCNP performs five operations: (1) the symbol # is removed, (2) parentheses are placed around *n*, (3) any intersections in *n* become unions, (4) any unions in *n* are replaced by back-to-back parentheses, “)(“, which is an intersection, and (5) the senses of the surfaces defining *n* are reversed.

A simple example is a cube. We define a two-cell geometry with six surfaces, where cell 1 is the cube and cell 2 is the outside world:

```
1  0 -1 2 -3 4 -5 6
2  0 1:-2: 3:-4: 5:-6
```

Note that cell 2 is everything in the universe that is *not in* cell 1, or

```
2  0 #1
```

The form #(n) is not allowed; it is functionally available as the equivalent of $-n$.

CAUTION: Using the complement operator can destroy some of the necessary conditions for some cell volume and surface area calculations by MCNP. See page 4–15 for an example.

The complement operator can be easily abused if it is used indiscriminately. A simple example can best illustrate the problems. Figure 2-1 consists of two concentric spheres inside a box. Cell 4 can be described using the complement operator as

```
4  0  #3 #2 #1
```

Although cells 1 and 2 do not touch cell 4, to omit them would be incorrect. If they were omitted, the description of cell 4 would be everything in the universe that is not in cell 3. Since cells 1 and 2 are not part of cell 3, they would be included in cell 4. Even though surfaces 1 and 2 do not physically bound cell 4, using the complement operator as in this example causes MCNP to think that all surfaces involved with the complement do bound the cell. Even though this specification is correct and required by MCNP, the disadvantage is that when a particle enters cell 4 or has a collision in cell 4, MCNP must calculate the intersection of the particle's trajectory with all real

bounding surfaces of cell 4 plus any extraneous ones brought in by the complement operator. This intersection calculation is very expensive and can add significantly to the required computer time.

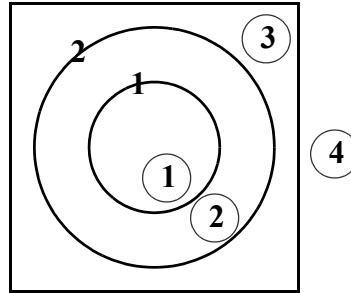


Figure 2-1

A better description of cell 4 would be to complement the description of cell 3 (omitting surface 2) by reversing the senses and interchanging union and intersection operators as illustrated in the cell cards that describe the simple cube in the preceding paragraphs.

B. Repeated Structure Geometry

The repeated structure geometry feature is explained in detail starting on page 3–25. The capabilities are only introduced here. Examples are shown in Chapter 4. The cards associated with the repeated structure feature are U (universe), FILL, TRCL, URAN, and LAT (lattice) and cell cards with LIKE m BUT.

The repeated structure feature makes it possible to describe only once the cells and surfaces of any structure that appears more than once in a geometry. This unit then can be replicated at other locations by using the “LIKE m BUT” construct on a cell card. The user specifies that a cell is filled with something called a universe. The U card identifies the universe, if any, to which a cell belongs. The FILL card specifies with which universe a cell is to be filled. A universe is either a lattice or an arbitrary collection of cells. The two types of lattice shapes, hexagonal prisms and hexahedra, need not be rectangular nor regular, but they must fill space exactly. Several concepts and cards combine in order to use this capability.

C. Surfaces

1. Explanation of Cone and Torus

Two surfaces, the cone and torus, require more explanation. The quadratic equation for a cone describes a cone of two sheets (just like a hyperboloid of two sheets)—one sheet is a cone of positive slope, and the other has a negative slope. A cell whose description contains a two-sheeted cone may require an ambiguity surface to distinguish between the two sheets. MCNP provides the option to select either of the two sheets; this option frequently simplifies geometry setups and eliminates any ambiguity. The +1 or the –1 entry on the cone surface card causes the one sheet cone treatment to be used. If the sign of the entry is positive, the specified sheet is the one that extends

to infinity in the positive direction of the coordinate axis to which the cone axis is parallel. The converse is true for a negative entry. This feature is available only for cones whose axes are parallel to the coordinate axes of the problem.

The treatment of fourth degree surfaces in Monte Carlo calculations has always been difficult because of the resulting fourth order polynomial (“quartic”) equations. These equations must be solved to find the intersection of a particle’s line of flight with a toroidal surface. In MCNP these equations must also be solved to find the intersection of surfaces in order to compute the volumes and surface areas of geometric regions of a given problem. In either case, the quartic equation,

$$x^4 + Bx^3 + Cx^2 + Dx + E = 0$$

is difficult to solve on a computer because of roundoff errors. For many years the MCNP toroidal treatment required 30 decimal digits (CDC double-precision) accuracy to solve quartic equations. Even then there were roundoff errors that had to be corrected by Newton-Raphson iterations. Schemes using a single-precision quartic formula solver followed by a Newton-Raphson iteration were inadequate because if the initial guess of roots supplied to the Newton-Raphson iteration is too inaccurate, the iteration will often diverge when the roots are close together.

The single-precision quartic algorithm in MCNP basically follows the quartic solution of Cashwell and Everett.²³ When roots of the quartic equation are well separated, a modified Newton-Raphson iteration quickly achieves convergence. But the key to this method is that if the roots are double roots or very close together, they are simply thrown out because a double root corresponds to a particle’s trajectory being tangent to a toroidal surface, and it is a very good approximation to assume that the particle then has no contact with the toroidal surface. In extraordinarily rare cases where this is not a good assumption, the particle would become “lost.” Additional refinements to the quartic solver include a carefully selected finite size of zero, the use of a cubic rather than a quartic equation solver whenever a particle is transported from the surface of a torus, and a gross quartic coefficient check to ascertain the existence of any real positive roots. As a result, the single-precision quartic solver is substantially faster than double-precision schemes, portable, and also somewhat more accurate.

In MCNP, elliptical tori symmetric about any axis parallel to a coordinate axis may be specified. The volume and surface area of various tallying segments of a torus usually will be calculated automatically.

2. Ambiguity Surfaces

The description of the geometry of a cell must eliminate any ambiguities as to which region of space is included in the cell. That is, a particle entering a cell should be able to determine uniquely which cell it is in from the senses of the bounding surfaces. This is not possible in a geometry such as shown in Figure 2-2 unless an *ambiguity surface* is specified. Suppose the figure is rotationally symmetric about the y-axis.

A particle entering cell 2 from the inner spherical region might think it was entering cell 1 because a test of the senses of its coordinates would satisfy the description of cell 1 as well as that of cell 2. In such cases, an ambiguity surface is introduced such as plane *a*. An ambiguity surface need not

be a bounding surface of a cell, but it may be and frequently is. It can also be the bounding surface of some cell other than the one in question. However, the surface must be listed among those in the problem and must not be a reflecting surface (see page 2–12). The description of cells 1 and 2 in Figure 2-2 is augmented by listing for each its sense

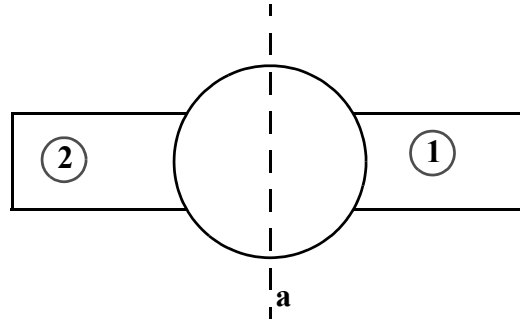


Figure 2-2

relative to surface *a* as well as that of each of its other bounding surfaces. A particle in cell 1 cannot have the same sense relative to surface *a* as does a particle in cell 2. More than one ambiguity surface may be required to define a particular cell.

A second example may help to clarify the significance of ambiguity surfaces. We would like to describe the geometry of Figure 2-3a. Without the use of an ambiguity surface, the result will be Figure 2-3b. Surfaces 1 and 3 are spheres about the origin, and surface 2 is a cylinder around the *y*-axis. Cell 1 is both the center and outside world of the geometry connected by the region interior to surface 2.

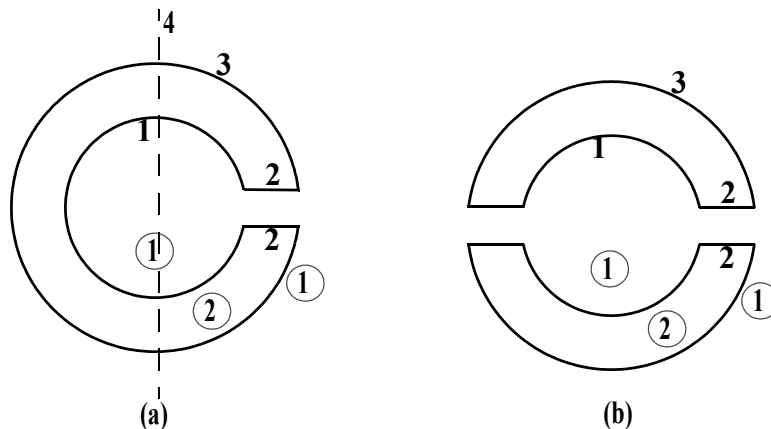


Figure 2-3

At first glance it may appear that cell 1 can easily be specified by $-1 : -2 : 3$ whereas cell 2 is simply #1. This results in Figure 2-3b, in which cell 1 is everything in the universe interior to surface 1 plus everything in the universe interior to surface 2 (remember the cylinder goes to plus and minus infinity) plus everything in the universe exterior to surface 3.

An ambiguity surface (plane 4 at $y = 0$) will solve the problem. Everything in the universe to the right of the ambiguity surface *intersected* with everything in the universe interior to the cylinder is a cylindrical region that goes to plus infinity but terminates at $y=0$. Therefore, $-1 : (4-2) : 3$ defines cell 1 as desired in Figure 2-3a. The parentheses in this last expression are not required because intersections are done before unions. Another expression for cell 2 rather than #1 is $1-3 \#(4-2)$.

For the user, ambiguity surfaces are specified the same way as any other surface—simply list the signed surface number as an entry on the cell card. For MCNP, if a particular ambiguity surface appears on cell cards with only one sense, it is treated as a true ambiguity surface. Otherwise, it still functions as an ambiguity surface but the TRACK subroutine will try to find intersections with it, thereby using a little more computer time.

3. Reflecting Surfaces

A surface can be designated a reflecting surface by preceding its number on the surface card with an asterisk. Any particle hitting a reflecting surface is specularly (mirror) reflected. Reflecting planes are valuable because they can simplify a geometry setup (and also tracking) in a problem. They can, however, make it difficult (or even impossible) to get the correct answer. The user is cautioned to check the source weight and tallies to ensure that the desired result is achieved. Any tally in a problem with reflecting planes should have the same expected result as the tally in the same problem without reflecting planes. Detectors or DXTRAN used with reflecting surfaces give WRONG answers (see page 2–101).

The following example illustrates the above points and should make MCNP users very cautious in the use of reflecting surfaces. Reflecting surfaces should never be used in any situation without a lot of thought.

Consider a cube of carbon 10 cm on a side sitting on top of a 5-MeV neutron source distributed uniformly in volume. The source cell is a 1-cm-thick void completely covering the bottom of the carbon cube and no more. The average neutron flux across any one of the sides (but not top or bottom) is calculated to be $0.150 (\pm 0.5\%)$ per cm^2 per starting neutron from an MCNP F2 tally, and the flux at a point at the center of the same side is $1.55\text{e-}03 \text{ n/cm}^2 (\pm 1\%)$ from an MCNP F5 tally.

The cube can be modeled by half a cube and a reflecting surface. All dimensions remain the same except the distance from the tally surface to the opposite surface (which becomes the reflecting surface) is 5 cm. The source cell is cut in half also. Without any source normalization, the flux across the surface is now $0.302 (\pm 0.5\%)$, which is twice the flux in the nonreflecting geometry. The detector flux is $2.58\text{E-}03 (\pm 1\%)$, which is *less* than twice the point detector flux in the nonreflecting problem.

The problem is that for the surface tally to be correct, the starting weight of the source particles has to be normalized; it should be half the weight of the nonreflected source particles. The detector results will always be wrong (and lower) for the reason discussed on page 2–101.

In this particular example, the normalization factor for the starting weight of source particles should be 0.5 because the source volume is half of the original volume. Without the normalization,

the full weight of source particles is started in only half the volume. These normalization factors are problem dependent and should be derived very carefully.

Another way to view this problem is that the tally surface has doubled because of the reflecting surface; two scores are being made across the tally surface when one is made across each of two opposite surfaces in the nonreflecting problem. The detector has doubled too, except that the contributions to it from beyond the reflecting surface are not being made, see page 2-101.

4. White Boundaries

A surface can be designated a white boundary surface by preceding its number on the surface card with a plus. A particle hitting a white boundary is reflected with a cosine distribution, $p(\mu) = \mu$, relative to the surface normal; that is, $\mu = \sqrt{\xi}$, where ξ is a random number. White boundary surfaces are useful for comparing MCNP results with other codes that have white boundary conditions. They also can be used to approximate a boundary with an infinite scatterer. They make absolutely no sense in problems with next-event estimators such as detectors or DXTRAN (see page 2-101) and should always be used with caution.

5. Periodic Boundaries

Periodic boundary conditions can be applied to pairs of planes to simulate an infinite lattice. Although the same effect can be achieved with an infinite lattice, the periodic boundary is easier to use, simplifies comparison with other codes having periodic boundaries, and can save considerable computation time. There is approximately a 55% run-time penalty associated with repeated structures and lattices that can be avoided with periodic boundaries. However, collisions and other aspects of the Monte Carlo random walk usually dominate running time, so the savings realized by using periodic boundaries are usually much smaller. A simple periodic boundary problem is illustrated in Figure 2-4.

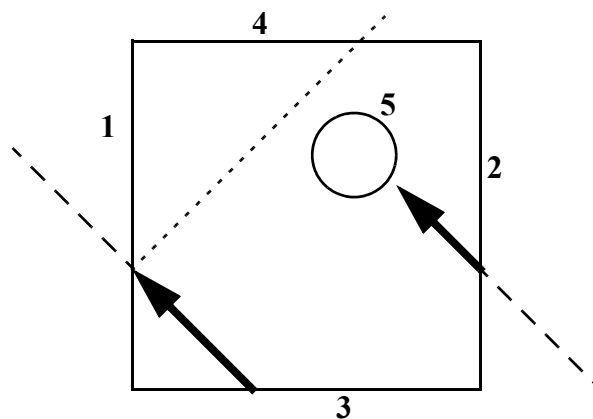


Figure 2-4

It consists of a square reactor lattice infinite in the z direction and 10 cm on a side in the x and y directions with an off-center 1-cm radius cylindrical fuel pin. The MCNP surface cards are:

1	-2	px	-5			
2	-1	px	5			
3	-4	py	-5			
4	-3	py	5			
5		c/z	-2	4	1	

The negative entries before the surface mnemonics specify periodic boundaries. Card one says that surface 1 is periodic with surface 2 and is a px plane. Card two says that surface 2 is periodic with surface 1 and is a px plane. Card three says that surface 3 is periodic with surface 4 and is a py plane. Card four says that surface 4 is periodic with surface 3 and is a py plane. Card five says that surface 5 is an infinite cylinder parallel to the z-axis. A particle leaving the lattice out the left side (surface 1) reenters on the right side (surface 2). If the surfaces were reflecting, the reentering particle would miss the cylinder, shown by the dotted line. In a fully specified lattice and in the periodic geometry, the reentering particle will hit the cylinder as it should.

Much more complicated examples are possible, particularly hexagonal prism lattices. In all cases, MCNP checks that the periodic surface pair matches properly and performs all the necessary surface rotations and translations to put the particle in the proper place on the corresponding periodic plane.

The following limitations apply:

- Periodic boundaries cannot be used with next event estimators such as detectors or DXTRAN (see page 2–101);
- All periodic surfaces must be planes;
- Periodic planes cannot also have a surface transformation;
- The periodic cells may be infinite or bounded by planes on the top or bottom that must be reflecting or white boundaries but not periodic;
- Periodic planes can only bound other periodic planes or top and bottom planes;
- A single zero-importance cell must be on one side of each periodic plane;
- All periodic planes must have a common rotational vector normal to the geometry top and bottom.

III. CROSS SECTIONS

The MCNP code package is incomplete without the associated nuclear data tables. The kinds of tables available and their general features are outlined in this section. The manner in which information contained on nuclear data tables is used in MCNP is described in Section IV beginning on page 2–25.

There are two broad objectives in preparing nuclear data tables for MCNP. First, the data available to MCNP should reproduce the original evaluated data as much as is practical. Second, new data should be brought into the MCNP package in a timely fashion, thereby giving users access to the most recent evaluations.

Nine classes of data tables exist for MCNP. They are: (1) continuous-energy neutron interaction data; (2) discrete reaction neutron interaction data; (3) continuous-energy photoatomic interaction

data; (4) continuous-energy photonuclear interaction data; (5) neutron dosimetry cross sections; (6) neutron $S(\alpha,\beta)$ thermal data; (7) multigroup neutron, coupled neutron/photon, and charged particles masquerading as neutrons; (8) multigroup photon; and (9) electron interaction data.

It is understood that photoatomic and electron data are atomic in nature, i.e. one elemental table is acceptable for any isotope of the element. For example, any isotope of tungsten may use a table with a ZA of 74000. Likewise, it is understood that neutron and photonuclear tables are nuclear (or isotopic) in nature, i.e. each isotope requires its own table. For tables describing these reactions, it is necessary to have a table for every isotope in a material. (Note that some older neutron evaluations are “elemental” in that they combine the reactions on several isotopes into a single table.) For example, natural tungsten would need tables with ZA equal 74180, 74182, 74183, 74184 and 74186. This can create difficulties when specifying material definitions. This has been true in the past, e.g. no neutron table exists for 74180 (0.13 atom percent) and it is typically ignored. This is even more true now that tables must be selected for both neutron and photonuclear interactions. The MPN card has been introduced to alleviate this problem.

In MODE N problems, one continuous-energy or discrete-reaction neutron interaction table is required for each isotope in the problem (some older “elemental” tables are available for neutron interactions). In MODE P problems, one photoatomic interaction table is required for each element and one photonuclear table is required for each isotope (if photonuclear physics is in use). In MODE E problems, one electron interaction table is required for each element. Dosimetry and thermal data are optional. Cross sections from dosimetry tables can be used as response functions with the FM card to determine reaction rates. Thermal $S(\alpha,\beta)$ tables should be used if the neutrons are transported at sufficiently low energies that molecular binding effects are important.

MCNP can read from data tables in two formats. Data tables are transmitted between computer installations as ASCII text files using an 80-column card-image Binary Coded Decimal (BCD) format (Type-1 format). If desired, an auxiliary processing code, MAKXSF, converts these files into unformatted binary files (Type-2 format), allowing faster access of the data during execution of MCNP and reduced disk-space for storing the files. The data contained on a table are independent of how they are stored.

The format for each class of ACE table is given in full detail in Appendix F. This appendix may be useful for users making extensive modifications to MCNP involving cross sections or for users debugging MCNP at a fairly high level.

The available data tables are listed in Appendix G. Each data table is identified by a ZAID. The general form of a ZAID is ZZZAAA.nnX, where ZZZ is the atomic number, AAA is the atomic mass number, nn is the unique evaluation identifier, and X indicates the class of data. For elemental evaluations AAA=000. Data tables are selected by the user with the Mn, MPNn and MTn cards.

In the remainder of this section we describe several characteristics of each class of data such as evaluated sources, processing tools, and differences between data on the original evaluation and on the MCNP data tables. The means of accessing each class of data through MCNP input will be detailed, and some hints will be provided on how to select the appropriate data tables.

A. *Neutron Interaction Data: Continuous-Energy and Discrete-Reaction*

In neutron problems, one neutron interaction table is required for each isotope (or element if using the older “elemental” tables) in the problem. The form of the ZAIDs is ZZZAAA.nnC for a continuous-energy table and ZZZAAA.nnD for a discrete reaction table. The neutron interaction tables available to MCNP are listed in Table G.2 of Appendix G. (It should be noted that although all nuclear data tables in Appendix G are available to users at Los Alamos, users at other installations will generally have only a subset of the tables available. Also note that your institution may make their own tables available to you.)

For most materials, there are many cross-section sets available (represented by different values of nn in the ZAIDs) because of multiple sources of evaluated data and different parameters used in processing the data. An evaluated nuclear data set is produced by analyzing experimentally measured cross sections and combining those data with the predictions of nuclear model calculations in an attempt to extract the most accurate interaction description. Preparing evaluated cross-section sets has become a discipline in itself and has developed since the early 1960s. In the US, researchers at many of the national laboratories as well as several industrial firms are involved in such work. The American evaluators joined forces in the mid-1960s to create the national ENDF system.²⁴

There has been some confusion due to the use of the term ENDF to refer to both a library and a format. The US effort to create a national evaluated nuclear data library led to formation of the Cross Section Evaluation Working Group (CSEWG) in the 1960s. This body standardized the ENDF format, which is used to store evaluated nuclear data files, and created the US ENDF/B library that contains the set of data evaluations currently recommended by CSEWG. Each update of the ENDF/B library receives a unique identifier (discussed below). While ENDF began as a US effort, over time other data centers have adopted the ENDF storage format for their own use (this international standardization has encouraged and facilitated many collaborations). Today the ENDF-6 format (note that the Arabic number 6 indicates the ENDF format version) has become the international standard for storing evaluated nuclear data and is used by data centers in Europe, Japan, China, Russia, Korea and elsewhere. The user should be aware that there are many evaluated nuclear data libraries of which ENDF/B is only one.

It is worth discussing the ENDF/B library for a moment. The US-based CSEWG meets once a year to discuss and approve changes to the ENDF/B library. In order to track the updates to the ENDF/B library, the following notation has been adopted. The “/B” in ENDF/B is used to indicate the US data library as recommended by CSEWG. (There was at one time an ENDF/A that was a repository for other, possibly useful, data. However, this is no longer used.) The major version of the library is indicated by a Roman numeral, e.g. ENDF/B-V or ENDF/B-VI. Changes in the major version are generally tied to changes in the standard cross sections. (Many cross-section measurements are made relative to the standard cross sections, e.g. elastic scattering off hydrogen or the U235(n,f) cross section. When one of the standard cross sections is changed, the evaluated data that were based on that standard must be updated.) Within a major release, revisions are generally indicated as ENDF/B-VI.2 or ENDF/B-VI.6 where the “.2” and “.6” indicate release 2 and release 6, respectively. A release indicates that some evaluations have been revised, added or deleted. Users should note that neither a major release nor an interim release guarantee that a particular evaluation has been updated. In fact, only a few evaluations change in each release and

often the change is limited to a certain energy region. This numbering scheme simply indicates that something within the data library has changed. It is up to the user to read the accompanying documentation to determine exactly what, if anything, changed. Each ACE table provided with the MCNP package is listed in Appendix G where its lineage (e.g. ENDF/B-V.0 or ENDF/B-VI.2) is given. The ENDF/B evaluations are available through the National Nuclear Data Center at Brookhaven National Laboratory (<http://www.nndc.bnl.gov/>).

In addition to the ENDF/B library, many other data centers provide libraries of evaluated data. These include the Japanese Atomic Energy Research Institute's (JAERI) JENDL library, the European JEFF library maintained by the Nuclear Energy Agency (NEA), the Chinese Nuclear Data Center's (CNDC) CENDL library, and the Russian BOFOD library. Other libraries also exist. These centers may provide processed versions of their library in MCNP ACE format. Contact the appropriate center for more information.

In recent years the primary evaluated source of neutron interaction data provided as part of the MCNP code package has been the ENDF/B library (i.e. ENDF/B-V and ENDF/B-VI). However, these have been supplemented with evaluated neutron interaction data tables from other sources, in particular data from Lawrence Livermore National Laboratory's Evaluated Nuclear Data Library (ENDL)²⁵ library and supplemental evaluations performed in the Nuclear Physics Group in the Theoretical Division at Los Alamos.^{26,27,28} The package also includes older evaluations from previous versions of ENDF/B, ENDL, the Los Alamos Master Data File,²⁹ and the Atomic Weapons Research Establishment in Great Britain.

MCNP does not access evaluated data directly from the ENDF format; these data must first be processed into ACE format. (ACE is an acronym for A Compact ENDF. A better description of ACE is that it is the processed data for use in MCNP, as these files are often not compact.) The very complex processing codes used for this purpose include NJOY³⁰ for evaluated data in ENDF-5 and ENDF-6 format and MCPOINT³¹ for evaluated data in the ENDL format.

Data on the MCNP neutron interaction tables include cross sections and emission distributions for secondary particles. Cross sections for all reactions given in the evaluated data are specified. For a particular table, the cross sections for each reaction are given on one energy grid that is sufficiently dense that linear-linear interpolation between points reproduces the evaluated cross sections within a specified tolerance. Over the years this tolerance has been tightened as computer memory has increased. In general, the tables currently available have cross sections that are reproduced to a tolerance of 1% or less, although many recent tables have been created with tolerances of 0.1%. Depending primarily on the number of resolved resonances for each isotope, the resulting energy grid may contain up to ~100,000 points (see Appendix G for information about specific tables).

Angular distributions for neutron (and photonuclear) collisions are given in each table for all reactions emitting neutrons or photons (note that older neutron tables may not include photon distributions). The distributions are typically given in the center-of-mass system for elastic scattering and discrete-level inelastic scattering. Other distributions may be given in either the center-of-mass or laboratory system as specified by the ENDF-6 scattering law from which they are derived. Angular distributions are given on a reaction-dependent grid of incident energies.

The sampled angle of scattering uniquely determines the secondary energy for elastic scattering and discrete-level inelastic scattering. For other inelastic reactions, energy distributions of the scattered particles are provided in each table. As with angular distributions, the energy distributions are given on a reaction-dependent grid of incident energies. The energy and angle of particles scattered by inelastic collisions is sampled in a stochastic manner such that the overall emission distribution and energy are preserved for many collisions but not necessarily for any single collision.

When neutron evaluations contain data about secondary photon production, that information appears in the MCNP neutron interaction tables. Many processed data sets contain photon production cross sections, photon angular distributions, and photon energy distributions for each neutron reaction that produces secondary photons. However, the user should be aware that not all evaluations include this information and the information is sometimes approximate, e.g. individual gamma lines may be lumped into average photon emission bins.

Other miscellaneous information on the neutron (and photonuclear) interaction tables includes the atomic weight ratio of the target nucleus, the Q-values of each reaction, and nubar ($\bar{\nu}$) data (the average number of neutrons per fission) for fissionable isotopes. In many cases both prompt and total $\bar{\nu}$ are given. Prompt $\bar{\nu}$ is the default for all but KCODE criticality problems, and total $\bar{\nu}$ is the default for KCODE criticality problems. The TOTNU input card can be used to change the default.

Approximations must be made when processing an evaluated data set into ACE format. As mentioned above, cross sections are reproduced to within a certain tolerance, generally less than 1%. Until recently, evaluated angular distributions for non-isotropic secondary particles could only be approximated on ACE tables by 32 equally-probable cosine bins. This approximation is extremely fast to use but may not adequately represent a distribution originally given as a 20th-order Legendre polynomial. Starting with MCNP version 4C, tabular angular distributions may be used to represent the scattering angle with a tolerance generally between 0.1% to 1% or better. On the whole, the approximations within more recent ACE tables are small, and MCNP interaction data tables for neutron (and photonuclear) collisions are extremely faithful representations of the original evaluated data.

Discrete-reaction tables are identical to continuous-energy tables except that in the discrete reaction tables all cross sections have been averaged into 262 groups. The averaging is done with a flat weighting function. This is not a multigroup representation; the cross sections are simply given as histograms rather than as continuous curves. The remaining data (angular distributions, energy distributions, $\bar{\nu}$, etc.) are identical in discrete-reaction and continuous-energy neutron tables. Discrete-reaction tables have been provided in the past as a method of shrinking the required data storage to enhance the ability to run MCNP on small machines or in a time-sharing environment. Given the advances in computing speed and storage, they are no longer necessary and **should not** be used. Their original purpose was for preliminary scoping studies. They were **never** recommended as a substitute for the continuous-energy tables when performing final calculations.

The matter of how to select the appropriate neutron interaction tables for your calculation is now discussed. Multiple tables for the same isotope are differentiated by the “nn” evaluation identifier portion of the ZAID. The easiest choice for the user is not to enter the nn at all. If no identifier nn

is entered, MCNP will select the first match found in the directory file XSDIR. The XSDIR file provided as part of the MCNP package contains the evaluations in the recommended (by the nuclear data team at LANL) order. Thus, the user can select the currently recommended table by entering only the ZZZAAA portion (without the nn) of the ZAID on the Mn card. The default nnX can be changed for all isotopes of a material by using the NLIB keyword entry on the Mm card. Given the NLIB option, MCNP will choose only tables with the given nn identifier. However, if a specific table is desired, MCNP will always use the table requested by a fully specified ZAID, i.e. ZZZAAA.nnX.

Careful users will want to think about what neutron interaction tables to choose. There is, unfortunately, no strict formula for choosing the tables. The following guidelines and observations are the best that can be offered:

1. Users should, in general, use the most recent data available. The nuclear data evaluation community works hard to continually update these libraries with the most faithful representations of the cross sections and emission distributions.
2. Consider checking the sensitivity of the results to various sets of nuclear data. Try, for example, a calculation with ENDF/B-VI.6 cross sections, and then another with ENDL cross sections. If the results of a problem are extremely sensitive to the choice of nuclear data, it is advisable to find out why.
3. Consider differences in evaluators' philosophies. The Physical Data Group at Livermore is justly proud of its extensive cross-section efforts; their evaluations manifest a philosophy of reproducing the data with the fewest number of points. Livermore evaluations are available mainly in the “.40C” series. We at Los Alamos are particularly proud of the evaluation work being carried out in the Nuclear Physics Group T-16; generally, these evaluations are the most complex because they are the most thorough. Recent evaluations from Los Alamos are available in the “.66c” series.
4. Be aware of the neutron energy spectrum in your problem. For high-energy problems, the “thinned” and discrete reaction data are probably not bad approximations. Conversely, it is essential to use the most detailed continuous-energy set available for problems influenced strongly by transport through the resonance region.
5. Check the temperature at which various data tables have been processed. Do not use a set that is Doppler broadened to 3,000 K for a room temperature calculation.
6. For a coupled neutron/photon problem, be careful that the tables you choose have photon production data available. If possible, use the more-recent sets that have been processed into expanded photon production format.
7. Users should be aware of the differences between the “.50C” series of data tables and the “.51C” series. Both are derived from ENDF/B-V. The “.50C” series is the most faithful reproduction of the evaluated data. The “.51C” series, also called the “thinned” series, has been processed with a less rigid tolerance than the “.50C” series. As with discrete reaction data tables, although by no means to the same extent, users should be careful when using the “thinned” data for transport through the resonance region.
8. In general, use the best data available. It is understood that the latest evaluations tend to be more complex and therefore require more memory and longer execution times. If you are limited by available memory, try to use smaller data tables such as thinned or

discrete-reaction for the minor isotopes in the calculation. Discrete reaction data tables might be used for a parameter study, followed by a calculation with the full continuous-energy data tables for confirmation.

In conclusion, the additional time necessary to choose appropriate neutron interaction data tables rather than simply to accept the defaults often will be rewarded by increased understanding of your calculation.

B. Photon Interaction Data

Photon interaction cross sections are required for all photon problems. Photon interactions can now account for both photoatomic and photonuclear events. Because these events are different in nature, i.e. elemental versus isotopic, the data are stored on separate tables.

Photoatomic data are stored on ACE tables that use ZAIDs with the form ZZZ000.nnP. There are currently four photoatomic interaction data libraries: *nn* equal 01, 02, 03 and 04.

The “01p” ACE tables were introduced in 1982 and combine data from several sources. The incoherent, coherent, photoelectric and pair production cross sections, the coherent form factors, and incoherent scattering function for this data set come from two sources. For *Z* equal to 84, 85, 87, 88, 89, 91, and 93, these values are based on the compilation of Storm and Israel³² and include data for incident photon energies from 1 keV to 15 MeV. For all other elements from *Z* equal to 1 through 94, the data are based on ENDF/B-IV³³ and include data for incident photon energies from 1 keV to 100 MeV. Fluorescence data for *Z* equal to 1 through 94 are taken from work by Everett and Cashwell³⁴ as derived from multiple sources.

The “02p” ACE tables were introduced in 1993 and are an extension of the “01p” to higher incident energies.³⁵ Below 10 MeV the data are identical to the “01p” data (i.e. the cross sections, form factors, scattering function, and fluorescence data in this region are identical). From 10 MeV to the top of the table (either 15 or 100 MeV, depending on the table) the cross-section values are smoothly transitioned from the “01p” values to the values from the Livermore Evaluated Photon Data Library (EPDL89).³⁶ Above this transition region, the cross section values are derived from the EPDL89 data and are given for incident energies up to 100 GeV. The pair production threshold was also corrected for some tables.

The “03p” ACE tables were introduced in 2002 and are an extension of the “02p” tables to include additional data. The energy of a photon after an incoherent (Compton) collision is a function of the momentum of the bound electron involved in the collision. To calculate this effect (which is seen as a broadening of the Compton peak), it is necessary to know the probability with which a photon interacts with an electron from a particular shell and the momentum profile for the electrons of each shell. The probabilities and momentum profile data of Biggs et al.³⁷ are included in the “03p” tables. All other data in the “03p” are identical to the “02p” data. The ability to use the new data for broadening of the Compton scattering energy requires MCNP5 or later; however, these tables are compatible with older versions of the code (you simply will not access or use the new data).

The “04p” ACE tables were introduced in 2002 and contain the first completely new data set since 1982. These tables were processed from the ENDF/B-VI.8 library. (The ENDF/B-VI.8

photoatomic and atomic relaxation data are in turn based upon the EPDL97³⁸ library.) They include incoherent, coherent, photoelectric and pair production cross sections for incident energies from 1 keV to 100 GeV and Z equal to 1 to 100. They also include coherent form factors, incoherent scattering functions, and fluorescence data derived from the ENDF/B-VI.8 data. It should be noted that the form factor and scattering data have been evaluated and stored on the traditional fixed grid (see the photon table description in Appendix F). The fluorescence data use the traditional scheme defined by Everett and Cashwell³⁴ but updated and consistent with the new data. Also included are the bound electron momenta of Biggs et al.³⁷ (i.e. identical to those data in the “03p” tables). This is the recommended data set.

For each element the photoatomic interaction libraries contain an energy grid—explicitly including the photoelectric edges and the pair production threshold—the incoherent, coherent, photoelectric and pair production cross sections (all stored as the logarithm of the value to facilitate log-log interpolation). The total cross section is not stored; instead it is calculated from the partial cross sections as needed. The energy grid for each table is tailored specifically for that element. The average material heating due to photon scattering is calculated by the processing code and included as a tabulation on the main energy grid. The incoherent scattering function and coherent form factors are tabulated as a function of momentum transfer on a predefined, fixed-momenta grid. Average fluorescence data (according to the scheme of Everett and Cashwell³⁴) are also included. The most recent data (on the 03p and 04p libraries) also include momentum profile data for broadening of the photon energy from Compton scattering from bound electrons.

The determination of directions and energies of atomically scattered photons requires information different from the sets of angular and energy distributions found on neutron interaction tables. The angular distribution for fluorescence x-rays from the relaxation cascade after a photoelectric event is isotropic. The angular distributions for coherent and incoherent scattering come from sampling the well-known Thomson and Klein-Nishina formulas, respectively. By default, this sampling accounts for the form factor and scattering function data at incident energies below 100 MeV. Above, 100 MeV (or at the user’s request) the form factor and scattering function data are ignored (a reasonable approximation for high-energy photons). The energy of an incoherently scattered photon is calculated from the sampled scattering angle. If available, this energy is modified to account for the momentum of the bound electron.

Very few approximations are made in the various processing codes used to transfer photon data from ENDF into the format of MCNP photon interaction tables. Cross sections are reproduced exactly as given (except as the logarithm of the value). Form factors and scattering functions are reproduced as given; however, the momentum transfer grid on which they are tabulated may be different from that of the original evaluation (see the description of the photoatomic table in Appendix F for the momenta grid used by all photoatomic tables). Heating numbers are calculated values, not given in evaluated sets, but inferred from them. Fluorescence data are calculated using the scheme developed by Everett and Cashwell.³⁴

Photonuclear data are stored on ACE tables that use ZAIDs with the form ZZZAAA.nnU. New to MCNP5, photon interactions can include photonuclear events. However, the current data distribution includes tables for only 13 nuclides. Because of this, photonuclear physics must be explicitly turned on. If on, a table must be provided for each nuclide of every material or a fatal error will occur and the simulation will not run. This situation should improve sometime relatively

soon. More than 150 other photonuclear data evaluations exist; these were created as part of an IAEA collaboration.³⁹ These evaluations have been processed and are available for beta testing use through the nuclear data website at Los Alamos National Laboratory (see <http://t2.lanl.gov/> and click on photonuclear). These files need peer review and validation testing before becoming part of the official MCNP data package.

Photonuclear interaction data describe nuclear events with specific isotopes. The reaction descriptions use the same ENDF-6 format as used for neutron data. Their processing, storage as ACE tables, and sampling in a simulation are completely analogous to what is done for neutrons. See the previous discussion of the neutron data for more details. Note that the photonuclear data available so far are complete in the sense that they provide secondary particle distributions for all light-particles, i.e. photons, neutrons, protons, alphas, etc. At this time, MCNP makes use of the photon and neutron emission distributions.

The selection of photon interaction data has become more complicated. Let us first examine the simple cases. Photon or photon/electron problems where photonuclear events are to be ignored (i.e. photonuclear physics is explicitly off) should specify the material composition on the Mn card by mass or weight fraction of each element, i.e. using the form ZZZ000 to describe each element. Partial ZAID specification, i.e. only ZZZ000 with no library evaluation number *nn*, will choose the default table (the first table listed in the XSDIR). This will be overridden if the evaluation identifier *nn* is given by the PLIB option, e.g. PLIB=02p will select all photoatomic tables for that material from the 02p data set. Specifying a full ZAID, e.g. 13000.03p, will override any other selection and always result in selecting that specific table. The next most simple case is a coupled neutron-photon problem that will explicitly ignore photonuclear events. In this case, one should specify the material composition according to the rules discussed in the previous section on neutron data tables. Given an isotopic material component, e.g. 13027, the appropriate elemental photoatomic table will be selected, e.g. 13000. If no evaluation identifier is given, the default (first) table from the XSDIR will be used. If a particular evaluation set is desired, the PLIB option on the Mn card may be used to select all photoatomic tables from a given library. It is recommended in all cases that the photoatomic tables for any given problem all be from the same library (these data sets are created *in masse* and thus are self-consistent across a library).

The most complicated case for material definition is the selection of tables for coupled neutron-photon problems where photonuclear events are not ignored. In such a case, the composition must be chosen based on the availability of most appropriate isotopic neutron and photonuclear tables as needed for the specific problem at hand. The MPNn card may be used to accommodate mismatches in the availability of specific isotopes (see page 3–120). As always, a fully specified ZAID, e.g. 13027.24u, will ensure that a specific table is selected. The PNLIB option on the material card may be used to select all photonuclear tables from a specific evaluation set *nn*. Otherwise, the isotope ZZZAAA will select the first match in the XSDIR file. Note that if no photonuclear table is available for the isotope ZZZAAA, the problem will report the error and will not run. See the discussion in the description of the MPNn card for more information on page 3–120).

C. *Electron Interaction Data*

Electron interaction data tables are required both for problems in which electrons are actually transported, and for photon problems in which the thick-target bremsstrahlung model is used. Electron data tables are identified by ZAIDs of the form ZZZ000.nnE, and are selected by default when the problem mode requires them. There are two electron interaction data libraries: el (ZAID endings of .01e) and el03 (ZAID endings of .03e).

The electron libraries contain data on an element-by-element basis for atomic numbers from Z equal 1 to 94. The library data contain energies for tabulation, radiative stopping power parameters, bremsstrahlung production cross sections, bremsstrahlung energy distributions, K-edge energies, Auger electron production energies, parameters for the evaluation of the Goudsmit-Saunderson theory for angular deflections based on the Riley cross-section calculation, and Mott correction factors to the Rutherford cross sections also used in the Goudsmit-Saunderson theory. The el03 library also includes the atomic data of Carlson used in the density effect calculation. Internal to the code at run-time, data are calculated for electron stopping powers and ranges, K x-ray production probabilities, knock-on probabilities, bremsstrahlung angular distributions, and the Landau-Blunck-Leisegang theory of energy-loss fluctuations. The el03 library is derived from the ITS3.0 code system.⁴⁰ Discussions of the theoretical basis for these data and references to the relevant literature are presented in Section IV-E beginning on page 2–67 of this chapter.

The hierarchy rules for electron cross sections require that each material must use the same electron library. If a specific ZAID is selected on a material card, such as specifying ZZZ000.01E, that choice of library will be used as the default for all elements in that material. Alternatively, the default electron library for a given material can be chosen by specifying ELIB = nnE on the M card. Under no circumstances should data tables from different libraries be specified for use in the same material (e.g., "m6 12000.01e 1 20000.03e 1" should not be used). This will result in a fatal error as reported at run-time. Overriding this error with a FATAL option will result in **unreliable** results. In the absence of any specification, MCNP will use the first electron data table listed in the XSDIR cross-section directory file for the relevant element.

D. *Neutron Dosimetry Cross Sections*

Dosimetry cross-section tables cannot be used for transport through material. These incomplete cross-section sets provide energy-dependent neutron cross sections to MCNP for use as response functions with the FM tally feature, e.g. they may be used in the calculation of a reaction rate. ZAIDs for dosimetry tables are of the form ZZZAAA.nnY. Remember, dosimetry cross-section tables have no effect on the particle transport of a problem.

The available dosimetry cross sections are from three sources: ENDF/B–V Dosimetry Tape 531, ENDF/B–V Activation Tape 532, and ACTL⁴¹—an evaluated neutron activation cross-section library from the Lawrence Livermore National Laboratory. Various codes have been used to process evaluated dosimetry data into the format of MCNP dosimetry tables.

Data on dosimetry tables are simply energy-cross-section pairs for one or more reactions. The energy grids for all reactions are independent of each other. Interpolation between adjacent energy points can be specified as histogram, linear-linear, linear-log, log-linear, or log-log. With the

exception of the tolerance involved in any reconstruction of pointwise cross sections from resonance parameters, evaluated dosimetry cross sections can be reproduced on the MCNP data tables with no approximation.

ZAIDs for dosimetry tables must be entered on material cards that are referenced by FM cards; under **no** circumstances may a material card specifying dosimetry data tables be referenced by a cell card. The complete ZAID, ZZZAAA.nnY, must be given; there are no defaults for dosimetry tables.

E. Neutron Thermal $S(\alpha,\beta)$ Tables

Thermal $S(\alpha,\beta)$ tables are not required, but they are absolutely essential to get correct answers in problems involving neutron thermalization. Thermal tables have ZAIDs of the form XXXXXX.nnT, where XXXXXX is a mnemonic character string. The data on these tables encompass those required for a complete representation of thermal neutron scattering by molecules and crystalline solids. The source of $S(\alpha,\beta)$ data is a special set of ENDF tapes.⁴² The THERMR and ACER modules of the NJOY³⁰ system have been used to process the evaluated thermal data into a format appropriate for MCNP.

Data are for neutron energies generally less than 4 eV. Cross sections are tabulated on table-dependent energy grids; inelastic scattering cross sections are always given and elastic scattering cross sections are sometimes given. Correlated energy-angle distributions are provided for inelastically scattered neutrons. A set of equally probable final energies is tabulated for each of several initial energies. Further, a set of equally probable cosines or cosine bins is tabulated for each combination of initial and final energies. Elastic scattering data can be derived from either an incoherent or a coherent approximation. In the incoherent case, equally probable cosines or cosine bins are tabulated for each of several incident neutron energies. In the coherent case, scattering cosines are determined from a set of Bragg energies derived from the lattice parameters. During processing, approximations to the evaluated data are made when constructing equally probable energy and cosine distributions.

ZAIDs for the thermal tables are entered on an MTn card that is associated with an existing Mn card. The thermal table generally will provide data for one component of a material—for example, hydrogen in light water. Thermal ZAIDs may be entered on the MTn card(s) as XXXXXX, XXXXXX.nn, or XXXXXX.nnT.

F. Multigroup Tables

Multigroup cross-section libraries are the only libraries allowed in multigroup/adjoint problems. Neutron multigroup problems cannot be supplemented with $S(\alpha,\beta)$ thermal libraries; the thermal effects must be included in the multigroup neutron library. Photon problems cannot be supplemented with electron libraries; the electrons must be part of the multigroup photon library. The form of the ZAID is ZZZAAA.nnM for neutrons (or other particles masquerading as neutrons) or ZZZAAA.nnG for photons.

Although continuous-energy data are more accurate than multigroup data, the multigroup option is useful for a number of important applications: (1) comparison of deterministic (S_n) transport codes to Monte Carlo; (2) use of adjoint calculations in problems where the adjoint method is more efficient; (3) generation of adjoint importance functions; (4) cross-section sensitivity studies; (5) solution of problems for which continuous-cross sections are unavailable; and (6) charged particle transport using the Boltzmann-Fokker-Planck algorithm in which charged particles masquerade as neutrons.

Multigroup cross sections are very problem dependent. Some multigroup libraries are available from the Transport Methods Group at Los Alamos but must be used with caution. Users are encouraged to generate or get their own multigroup libraries and then use the supplementary code CRSRD⁴³ to convert them to MCNP format. Reference 43 describes the conversion procedure. This report also describes how to use both the multigroup and adjoint methods in MCNP and presents several benchmark calculations demonstrating the validity and effectiveness of the multigroup/adjoint method.

To generate cross-section tables for electron/photon transport problems that will use the multigroup Boltzmann-Fokker-Planck algorithm,⁴⁴ the CEPXS⁴⁷ code developed by Sandia National Laboratory and available from RSICC can be used. The CEPXS manuals describe the algorithms and physics database upon which the code is based; the physics package is essentially the same as ITS version 2.1. The keyword "MONTE-CARLO" is needed in the CEPXS input file to generate a cross-section library suitable for input into CRSRD; this undocumented feature of the CEPXS code should be approached with caution.

IV. PHYSICS

The physics of neutron, photon, and electron interactions is the very essence of MCNP. This section may be considered a software requirements document in that it describes the equations MCNP is intended to solve. All the sampling schemes essential to the random walk are presented or referenced. But first, particle weight and particle tracks, two concepts that are important for setting up the input and for understanding the output, are discussed in the following sections.

A. Weight

At the most fundamental level, weight is a tally multiplier. That is, the tally contribution for a weight w is the unit weight tally contribution multiplied by w . Weight is an adjustment for deviating from a direct physical simulation of the transport process. Note that if a Monte Carlo code always sampled from the same distributions as nature does, then the Monte Carlo code would have the same mean and variance as seen in nature. Quite often, the natural variance is unacceptably high and the Monte Carlo code modifies the sampling using some form of "variance reduction" (see Section VII on page 2-134). The variance reduction methods use weighting schemes to produce the same mean as the natural transport process, but with lower calculational variance than the natural variance of the transport process.

With the exception of the pulse height tally (F8), all tallies in MCNP are made by individual particles. In this case, weight is assigned to the individual particles as a "particle weight." The

manual discusses the "particle weight" cases first and afterward discusses the weight associated with the F8 tally.

1. Particle Weight

If MCNP were used only to simulate exactly physical transport, then each MCNP particle would represent one physical particle and would have unit weight. However, for computational efficiency, MCNP allows many techniques that do not exactly simulate physical transport. For instance, each MCNP particle might represent a number w of particles emitted from a source. This number w is the initial weight of the MCNP particle. The w physical particles all would have different random walks, but the one MCNP particle representing these w physical particles will only have one random walk. Clearly this is not an exact simulation; however, the true number of physical particles is preserved in MCNP in the sense of statistical averages and therefore in the limit of a large number of MCNP source particles (of course including particle production or loss if they occur). Each MCNP particle result is multiplied by the weight so that the full results of the w physical particles represented by each MCNP particle are exhibited in the final results (tallies). This procedure allows users to normalize their calculations to whatever source strength they desire. The default normalization is to weight one per MCNP particle. A second normalization to the number of Monte Carlo histories is made in the results so that the expected means will be independent of the number of source particles actually initiated in the MCNP calculation.

The utility of particle weight, however, goes far beyond simply normalizing the source. Every Monte Carlo biasing technique alters the probabilities of random walks executed by the particles. The purpose of such biasing techniques is to increase the number of particles that sample some part of the problem of special interest (1) without increasing (sometimes actually decreasing) the sampling of less interesting parts of the problem, and (2) without erroneously affecting the expected mean physical result (tally). This procedure, properly applied, increases precision in the desired result compared to an unbiased calculation taking the same computing time. For example, if an event is made $\sqrt{2}$ times as likely to occur (as it would occur without biasing), the tally ought to be multiplied by $1/\sqrt{2}$ so that the expected average tally is unaffected. This tally multiplication can be accomplished by multiplying the particle weight by $1/\sqrt{2}$ because the tally contribution by a particle is always multiplied by the particle weight in MCNP. Note that weights need not be integers.

In short, particle weight is a number carried along with each MCNP particle, representing that particle's relative contribution to the final tallies. Its magnitude is determined to ensure that whenever MCNP deviates from an exact simulation of the physics, the expected physical result nonetheless is preserved in the sense of statistical averages, and therefore in the limit of large MCNP particle numbers. Its utility is in the manipulation of the number of particles, sampling just a part of the problem to achieve the same results and precision, obviating a full unbiased calculation which has a longer computing time.

2. Pulse Height Tally (F8) Weight

Unlike other tallies in MCNP, the pulse height tally depends on a collection of particles instead of just individual particles. Because of this, a weight is assigned to each collection of tallying particles. It is this "collective weight" that multiplies the F8 tally, not the particle weight.

When variance reduction is used, a "collective weight" is assigned to every collection of particles. If variance reduction techniques have made a collection's random walk q times as likely as without variance reduction, then the collective weight is multiplied by $1/q$ so that the expected F8 tally of the collection is preserved. The interested reader should consult Refs. 45 and 46 for more details.

B. Particle Tracks

When a particle starts out from a source, a particle track is created. If that track is split 2 for 1 at a splitting surface or collision, a second track is created and there are now two tracks from the original source particle, each with half the single track weight. If one of the tracks has an $(n,2n)$ reaction, one more track is started for a total of three. A track refers to each component of a source particle during its history. Track length tallies use the length of a track in a given cell to determine a quantity of interest, such as fluence, flux, or energy deposition. Tracks crossing surfaces are used to calculate fluence, flux, or pulse-height energy deposition (surface estimators). Tracks undergoing collisions are used to calculate multiplication and criticality (collision estimators).

Within a given cell of fixed composition, the method of sampling a collision along the track is determined using the following theory. The probability of a first collision for a particle between l and $l + dl$ along its line of flight is given by

$$p(l)dl = e^{-\Sigma_t l} \Sigma_t dl \quad ,$$

where Σ_t is the macroscopic total cross section of the medium and is interpreted as the probability per unit length of a collision. Setting ξ the random number on $[0,1)$, to be

$$\xi = \int_0^l e^{-\Sigma_t s} \Sigma_t ds = 1 - e^{-\Sigma_t l} \quad ,$$

it follows that

$$l = -\frac{1}{\Sigma_t} \ln(1 - \xi) \quad .$$

But, because $1 - \xi$ is distributed in the same manner as ξ and hence may be replaced by ξ , we obtain the well-known expression for the distance to collision,

$$l = -\frac{1}{\Sigma_t} \ln(\xi) \quad .$$

C. Neutron Interactions

When a particle (representing any number of neutrons, depending upon the particle weight) collides with a nucleus, the following sequence occurs:

1. the collision nuclide is identified;

2. either the $S(\alpha, \beta)$ treatment is used or the velocity of the target nucleus is sampled for low-energy neutrons;
3. photons are optionally generated for later transport;
4. neutron capture (that is, neutron disappearance by any process) is modeled;
5. unless the $S(\alpha, \beta)$ treatment is used, either elastic scattering or an inelastic reaction (including fission) is selected, and the new energy and direction of the outgoing track(s) are determined;
6. if the energy of the neutron is low enough and an appropriate $S(\alpha, \beta)$ table is present, the collision is modeled by the $S(\alpha, \beta)$ treatment instead of by step 5.

1. Selection of Collision Nuclide

If there are n different nuclides forming the material in which the collision occurred, and if ξ is a random number on the unit interval $[0,1)$, then the k^{th} nuclide is chosen as the collision nuclide if

$$\sum_{i=1}^{k-1} \Sigma_{ti} < \xi \sum_{i=1}^n \Sigma_{ti} \leq \sum_{i=1}^k \Sigma_{ti}$$

where Σ_{ti} is the macroscopic total cross section of nuclide i . If the energy of the neutron is low enough (below about 4 eV) and the appropriate $S(\alpha, \beta)$ table is present, the total cross section is the sum of the capture cross section from the regular cross-section table and the elastic and inelastic scattering cross sections from the $S(\alpha, \beta)$ table. Otherwise, the total cross section is taken from the regular cross-section table and is adjusted for thermal effects as described below.

2. Free Gas Thermal Treatment

A collision between a neutron and an atom is affected by the thermal motion of the atom, and in most cases, the collision is also affected by the presence of other atoms nearby. The thermal motion cannot be ignored in many applications of MCNP without serious error. The effects of nearby atoms are also important in some applications. MCNP uses a thermal treatment based on the free gas approximation to account for the thermal motion. It also has an explicit $S(\alpha, \beta)$ capability that takes into account the effects of chemical binding and crystal structure for incident neutron energies below about 4 eV, but is available for only a limited number of substances and temperatures. The $S(\alpha, \beta)$ capability is described later on page 2-54.

The free gas thermal treatment in MCNP assumes that the medium is a free gas and also that, in the range of atomic weight and neutron energy where thermal effects are significant, the elastic scattering cross section at zero temperature is nearly independent of the energy of the neutron, and that the reaction cross sections are nearly independent of temperature. These assumptions allow MCNP to have a thermal treatment of neutron collisions that runs almost as fast as a completely nonthermal treatment and that is adequate for most practical problems.

With the above assumptions, the free gas thermal treatment consists of adjusting the elastic cross section and taking into account the velocity of the target nucleus when the kinematics of a collision are being calculated. The MCNP free gas thermal treatment effectively applies to elastic scattering only.

Cross-section libraries processed by NJOY already include Doppler broadening of elastic, capture, fission, and other low-threshold absorption cross-sections (<1 eV). Inelastic cross sections are never broadened by NJOY.

a. Adjusting the Elastic Cross Section: The first aspect of the free gas thermal treatment is to adjust the zero-temperature elastic cross section by raising it by the factor

$$F = (1 + 0.5/a^2) \operatorname{erf}(a) + \exp(-a^2)/(a\sqrt{\pi}) \quad ,$$

where $a = \sqrt{AE/kT}$, A = atomic weight, E = neutron energy, and T = temperature. For speed, F is approximated by $F = 1 + 0.5/a^2$ when $a \geq 2$ and by linear interpolation in a table of 51 values of aF when $a < 2$. Both approximations have relative errors less than 0.0001. The total cross section also is increased by the amount of the increase in the elastic cross section.

The adjustment to the elastic and total cross sections is done partly in the setup of a problem and partly during the actual transport calculation. No adjustment is made if the elastic cross section in the data library was already processed to the temperature that is needed in the problem. If all of the cells that contain a particular nuclide have the same temperature, which is constant in time, that is different from the temperature of the library, the elastic and total cross sections for that nuclide are adjusted to that temperature during the setup so that the transport will run a little faster. Otherwise, these cross sections are reduced, if necessary, to zero temperature during the setup and the thermal adjustment is made when the cross sections are used. For speed, the thermal adjustment is omitted if the neutron energy is greater than $500 kT/A$. At that energy the adjustment of the elastic cross section would be less than 0.1%.

b. Sampling the Velocity of the Target Nucleus: The second aspect of the free gas thermal treatment takes into account the velocity of the target nucleus when the kinematics of a collision are being calculated. The target velocity is sampled and subtracted from the velocity of the neutron to get the relative velocity. The collision is sampled in the target-at-rest frame and the outgoing velocities are transformed to the laboratory frame by adding the target velocity.

There are different schools of thought as to whether the relative energy between the neutron and target, E_r , or the laboratory frame incident neutron energy (target-at-rest), E_o , should be used for all the kinematics of the collision. E_o is used in MCNP to obtain the distance-to-collision, select the collision nuclide, determine energy cutoffs, generate photons, generate fission sites for the next generation of a KCODE criticality problem, for $S(\alpha, \beta)$ scattering, and for capture. E_r is used for everything else in the collision process, namely elastic and inelastic scattering, including fission and (n,xn) reactions. It is shown in Eqn. 2.1 that E_r is based upon v_{rel} that is based upon the elastic scattering cross section, and, therefore, E_r is truly valid only for elastic scatter. However, the only significant thermal reactions for stable isotopes are absorption, elastic scattering, and fission. ^{181}Ta has a 6 keV threshold inelastic reaction; all other stable isotopes have higher inelastic thresholds. Metastable nuclides like ^{242m}Am have inelastic reactions all the way down to zero, but these inelastic reaction cross sections are neither constant nor $1/v$ cross sections and these nuclides are generally too massive to be affected by the thermal treatment anyway. Furthermore, fission is very insensitive to incident neutron energy at low energies. The fission secondary energy and angle distributions are nearly flat or constant for incident energies below about 500 keV. Therefore, it makes no significant difference if E_r is used only for elastic scatter or for other inelastic collisions as well. At thermal energies, whether E_r or E_o is used only makes a difference for elastic scattering.

If the energy of the neutron is greater than $400\text{ }kT$ and the target is not ^1H , the velocity of the target is set to zero. Otherwise, the target velocity is sampled as follows. The free-gas kernel is a thermal interaction model that results in a good approximation to the thermal flux spectrum in a variety of applications and can be sampled without tables. The effective scattering cross section in the laboratory system for a neutron of kinetic energy E is

$$\sigma_s^{eff}(E) = \frac{1}{v_n} \iint \sigma_s(v_{rel}) v_{rel} p(V) dv \frac{d\mu_t}{2} \quad (2.1)$$

Here, v_{rel} is the relative velocity between a neutron moving with a scalar velocity v_n and a target nucleus moving with a scalar velocity V , and μ_t is the cosine of the angle between the neutron and the target direction-of-flight vectors. The equation for v_{rel} is

$$v_{rel} = (v_n^2 + V^2 - 2v_n V \mu_t)^{\frac{1}{2}}$$

The scattering cross section at the relative velocity is denoted by $\sigma_s(v_{rel})$, and $p(V)$ is the probability density function for the Maxwellian distribution of target velocities,

$$p(V) = \frac{4}{\pi^{1/2}} \beta^3 V^2 e^{-\beta^2 V^2}$$

with β defined as

$$\beta = \left(\frac{AM_n}{2kT} \right)^{\frac{1}{2}},$$

where A is the mass of a target nucleus in units of the neutron mass, M_n is the neutron mass in $\text{MeV}\cdot\text{sh}^2/\text{cm}^2$, and kT is the equilibrium temperature of the target nuclei in MeV .

The most probable scalar velocity V of the target nuclei is $1/\beta$, which corresponds to a kinetic energy of kT for the target nuclei. This is not the average kinetic energy of the nuclei, which is $3kT/2$. The quantity that MCNP expects on the TMPn input card is kT and not just T (see page 3–132). Note that kT is not a function of the particle mass and is therefore the kinetic energy at the most probable velocity for particles of any mass.

Equation (2.1) implies that the probability distribution for a target velocity V and cosine μ_t is

$$P(V, \mu_t) = \frac{\sigma_s(v_{rel}) v_{rel} P(V)}{2\sigma_s^{eff}(E) v_n}.$$

It is assumed that the variation of $\sigma_s(v)$ with target velocity can be ignored. The justification for this approximation is that (1) for light nuclei, $\sigma_s(v_{rel})$ is slowly varying with velocity, and (2) for heavy nuclei, where $\sigma_s(v_{rel})$ can vary rapidly, the moderating effect of scattering is small so that

the consequences of the approximation will be negligible. As a result of the approximation, the probability distribution actually used is

$$P(V, \mu_t) \propto \sqrt{v_n^2 V^2 - 2Vv_n\mu_t} V^2 e^{-\beta^2 V^2} .$$

Note that the above expression can be written as

$$P(V, \mu_t) \propto \frac{\sqrt{v_n^2 + V^2 - 2Vv_n\mu_t}}{v_n + V} (V^3 e^{-\beta^2 V^2} + v_n V^2 e^{-\beta^2 V^2}) .$$

As a consequence, the following algorithm is used to sample the target velocity.

1. With probability $\alpha = 1 / (1 + (\sqrt{\pi}\beta v_n/2))$, the target velocity V is sampled from the distribution $P_1(V) = 2\beta^4 V^3 e^{-\beta^2 V^2}$. The transformation $V = \sqrt{y}/\beta$ reduces this distribution to the sampling distribution for $P(y) = ye^{-y}$. MCNP actually codes $1 - \alpha$.
2. With probability $1 - \alpha$, the target velocity is sampled from the distribution $P_2(V) = (4\beta^3/\sqrt{\pi})V^2 e^{-\beta^2 V^2}$. Substituting $V = y/\beta$ reduces the distribution to the sampling distribution for y : $P(y) = (4/\sqrt{\pi})y^2 e^{-y^2}$.
3. The cosine of the angle between the neutron velocity and the target velocity is sampled uniformly on the interval $-1 \leq \mu_t \leq +1$.
4. The rejection function $R(V, \mu_t)$ is computed using

$$R(V, \mu_t) = \frac{\sqrt{v_n^2 + V^2 - 2Vv_n\mu_t}}{v_n + V} \leq 1 .$$

With probability $R(V, \mu_t)$, the sampling is accepted; otherwise, the sampling is rejected and the procedure is repeated. The minimum efficiency of this rejection algorithm averaged over μ_t is 68% and approaches 100% as either the incident neutron energy approaches zero or becomes much larger than kT .

3. Optional Generation of Photons

Photons are generated if the problem is a combined neutron/photon run and if the collision nuclide has a nonzero photon production cross section. The number of photons produced is a function of neutron weight, neutron source weight, photon weight limits (entries on the PWT card), photon production cross section, neutron total cross section, cell importance, and the importance of the neutron source cell. No more than 10 photons may be born from any neutron collision. In a KCODE calculation, secondary photon production from neutrons is turned off during the inactive cycles.

Because of the many low-weight photons typically created by neutron collisions, Russian roulette is played for particles with weight below the bounds specified on the PWT card, resulting in fewer particles, each having a larger weight. The created photon weight before Russian roulette is

$$W_p = \frac{W_n \sigma_\gamma}{\sigma_T} ,$$

where W_p = photon weight,

W_n = neutron weight,

σ_γ = photon production cross section,

σ_T = total neutron cross section.

Both σ_γ and σ_T are evaluated at the incoming neutron energy without the effects of the thermal free gas treatment because nonelastic cross sections are assumed independent of temperature.

The Russian roulette game is played according to neutron cell importances for the collision and source cell. For a photon produced in cell i where the minimum weight set on the PWT card is W_i^{min} , let I_i be the neutron importance in cell i and let I_s be the neutron importance in the source cell. If $W_p > W_i^{min} * I_s / I_i$, one or more photons will be produced. The number of photons created is N_p , where $N_p = (W_p * I_i) / (5 * W_i^{min} * I_s) + 1$. $N_p \leq 10$. Each photon is stored in the bank with weight W_p / N_p . If $W_p < W_i^{min} * I_s / I_i$, Russian roulette is played and the photon survives with probability $W_p * I_i / (W_i^{min} * I_s)$ and is given the weight, $W_i^{min} * I_s / I_i$.

If weight windows are not used and if the weight of the starting neutrons is not unity, setting all the W_i^{min} on the PWT card to negative values will make the photon minimum weight relative to the neutron source weight. This will make the number of photons being created roughly proportional to the biased collision rate of neutrons. It is recommended for most applications that negative numbers be used and be chosen to produce from one to four photons per source neutron. The default values for W_i^{min} on the PWT card are -1, which should be adequate for most problems using cell importances.

If energy-independent weight windows are used, the entries on the PWT card should be the same as on the WWN1:P card. If energy-dependent photon weight windows are used, the entries on the PWT card should be the minimum WWNn:P entry for each cell, where n refers to the photon weight window energy group. This will cause most photons to be born within the weight window bounds.

Any photons generated at neutron collision sites are temporarily stored in the bank. There are two methods for determining the exiting energies and directions, depending on the form in which the processed photon production data are stored in a library. The first method has the evaluated photon production data processed into an “expanded format.”⁴⁸ In this format, energy-dependent cross sections, energy distributions, and angular distributions are explicitly provided for every photon-producing neutron interaction. In the second method, used with data processed from older evaluations, the evaluated photon production data have been collapsed so that the only information

about secondary photons is in a matrix of 20 equally probable photon energies for each of 30 incident neutron energy groups. The sampling techniques used in each method are now described.

a. Expanded Photon Production Method: In the expanded photon production method, the reaction n responsible for producing the photon is sampled from

$$\sum_{i=1}^{n-1} \sigma_i < \xi \sum_{i=1}^N \sigma_i \leq \sum_{i=1}^n \sigma_i$$

where ξ is a random number on the interval (0,1), N is the number of photon production reactions, and σ_i is the photon production cross section for reaction i at the incident neutron energy. Note that there is no correlation between the sampling of the type of photon production reaction and the sampling of the type of neutron reaction described on page 2–35.

Just as every neutron reaction (for example, $(n,2n)$) has associated energy-dependent angular and energy distributions for the secondary neutrons, every photon production reaction (for example, $(n,p\gamma)$) has associated energy-dependent angular and energy distributions for the secondary photons. The photon distributions are sampled in much the same manner as their counterpart neutron distributions.

All non-isotropic secondary photon angular distributions are represented by either 32 equiprobable cosine bins or by a tabulated angular distribution. The distributions are given at a number of incident neutron energies. All photon-scattering cosines are sampled in the laboratory system. The sampling procedure is identical to that described for secondary neutrons on page 2–36.

Secondary photon energy distributions are also a function of incident neutron energy. There are two representations of secondary photon energy distributions allowed in ENDF-6 format: tabulated spectra and discrete (line) photons. Correspondingly, there are two laws used in MCNP for the determination of secondary photon energies. Law 4 provides for representation of a tabulated photon spectra possibly including discrete lines. Law 2 is used solely for discrete photons. These laws are described in more detail beginning on page 2–41.

The expanded photon production method has clear advantages over the original 30 x 20 matrix method described below. In coupled neutron/photon problems, users should attempt to specify data sets that contain photon production data in expanded format. Such data sets are identified by “yes” entries in the GPD column in Table G.2 in Appendix G. However, it should be noted that the evaluations from which these data are processed may not include all discrete lines of interest; evaluators may have binned sets of photons into average spectra that simply preserve the energy distribution.

b. 30 x 20 Photon Production Method: For lack of better terminology, we will refer to the photon production data contained in older libraries as “30 x 20 photon production” data. In contrast to expanded photon production data, there is no information about individual photon production reactions in the 30 x 20 data. This method is not used in modern tables and is only included to maintain backwards compatibility for very old data libraries.

The only secondary photon data are a 30 x 20 matrix of photon energies; that is, for each of 30 incident neutron energy groups there are 20 equally probable exiting photon energies. There is no information regarding secondary photon angular distributions; therefore, all photons are taken to be produced isotropically in the laboratory system.

There are several problems associated with 30 x 20 photon production data. The 30 x 20 matrix is an inadequate representation of the actual spectrum of photons produced. In particular, discrete photon lines are not well represented, and the high-energy tail of a photon continuum energy distribution is not well sampled. Also, the multigroup representation is not consistent with the continuous-energy nature of MCNP. Finally, not all photons should be produced isotropically. None of these problems exists for data processed into the expanded photon production format.

4. Absorption

Absorption is treated in one of two ways: analog or implicit. Either way, the incident incoming neutron energy does not include the relative velocity of the target nucleus from the free gas thermal treatment because nonelastic reaction cross sections are assumed to be nearly independent of temperature. That is, only the scattering cross section is affected by the free gas thermal treatment. The terms “absorption” and “capture” are used interchangeably for non-fissile nuclides, both meaning (n,0n). For fissile nuclides, “absorption” includes both capture and fission reactions.

a. Analog Absorption: In analog absorption, the particle is killed with probability σ_a/σ_T , where σ_a and σ_T are the absorption and total cross sections of the collision nuclide at the incoming neutron energy. The absorption cross section is specially defined for MCNP as the sum of all (n,x) cross sections, where x is anything except neutrons. Thus σ_a is the sum of $\sigma_{n,g}$, $\sigma_{n,a}$, $\sigma_{n,d}$, σ_f ... etc. For all particles killed by analog absorption, the entire particle energy and weight are deposited in the collision cell.

b. Implicit Absorption: For implicit absorption, also called survival biasing, the neutron weight W_n is reduced to W_n as follows:

$$W_n = \left(1 - \frac{\sigma_a}{\sigma_T}\right) * W_n$$

If the new weight W_n is below the problem weight cutoff (specified on the CUT card), Russian roulette is played, resulting overall in fewer particles with larger weight.

For implicit absorption, a fraction σ_a/σ_T of the incident particle weight and energy is deposited in the collision cell corresponding to that portion of the particle that was absorbed. Implicit absorption is the default method of neutron absorption in MCNP.

c. Implicit Absorption Along a Flight Path: Implicit absorption also can be done continuously along the flight path of a particle trajectory as is the common practice in astrophysics. In this case, the distance to scatter, rather than the distance to collision, is sampled. The distance to scatter is

$$l = -\frac{1}{\Sigma_s} \ln(1 - \xi) \quad .$$

The particle weight at the scattering point is reduced to account for the expected absorption along the flight path,

$$W' = W e^{-\Sigma_a l} \quad ,$$

where W' = reduced weight after expected absorption along flight path,
 W = weight at the start of the flight path,
 σ_a = absorption cross section,
 σ_s = scattering cross section,
 σ_t = $\sigma_s + \sigma_a$ = total cross section,
 l = distance to scatter, and
 ξ = random number.

Implicit absorption along a flight path is a special form of the exponential transformation coupled with implicit absorption at collisions. (See the description of the exponential transform on page 2–148.) The path length is stretched in the direction of the particle, $\mu = 1$, and the stretching parameter is $p = \Sigma_a/\Sigma_t$. Using these values the exponential transform and implicit absorption at collisions yield the identical equations as does implicit absorption along a flight path.

Implicit absorption along a flight path is invoked in MCNP as a special option of the exponential transform variance reduction method. It is most useful in highly absorbing media, that is, Σ_a/Σ_t approaches 1. When almost every collision results in absorption, it is very inefficient to sample distance to collision. However, implicit absorption along a flight path is discouraged. In highly absorbing media, there is usually a superior set of exponential transform parameters. In relatively nonabsorbing media, it is better to sample the distance to collision than the distance to scatter.

5. Elastic and Inelastic Scattering

If the conditions for the $S(\alpha, \beta)$ treatment are not met, the particle undergoes either an elastic or inelastic collision. The selection of an elastic collision is made with the probability

$$\frac{\sigma_{el}}{\sigma_{in} + \sigma_{el}} = \frac{\sigma_{el}}{\sigma_T - \sigma_a}$$

where

σ_{el} is the elastic scattering cross section.

σ_{in} is the inelastic cross section; includes any neutron-out process— (n, n') , (n, f) , (n, np) , etc.

σ_a is the absorption cross section; $\Sigma\sigma(n, x)$, where $x \neq n$, that is, all neutron disappearing reactions.

σ_T is the total cross section, $\sigma_T = \sigma_{el} + \sigma_{in} + \sigma_a$.

Both σ_{el} and σ_T are adjusted for the free gas thermal treatment at thermal energies.

The selection of an inelastic collision is made with the remaining probability

$$\frac{\sigma_{in}}{\sigma_T - \sigma_a} \quad .$$

If the collision is determined to be inelastic, the type of inelastic reaction, n , is sampled from

$$\sum_{i=1}^{n-1} \sigma_i < \xi \sum_{i=1}^N \sigma_i \leq \sum_{i=1}^n \sigma_i \quad ,$$

where ξ is a random number on the interval $[0,1)$, N is the number of inelastic reactions, and σ_i is the i^{th} inelastic reaction cross section at the incident neutron energy.

Directions and energies of all outgoing particles from neutron collisions are determined by sampling data from the appropriate cross-section table. Angular distributions are provided and sampled for scattered neutrons resulting from either elastic or discrete-level inelastic events; the scattered neutron energy is then calculated from two-body kinematics. For other reaction types, a variety of data representations is possible. These representations may be divided into two types: (a) the outgoing energy and outgoing angle are sampled independently of each other, or (b) the outgoing energy and outgoing angle are correlated. In the latter case, the outgoing energy may be specified as a function of the sampled outgoing angle, or the outgoing angle may be specified as a function of the sampled outgoing energy. Details of the possible data representations and sampling schemes are provided in the following sections.

a. Sampling of Angular and Energy Distributions: The cosine of the angle between incident and exiting particle directions, μ , is sampled from angular distribution tables in the collision nuclide's cross-section library. The cosines are either in the center-of-mass or target-at-rest system, depending on the type of reaction. Data are provided at a number of incident neutron energies. If E is the incident neutron energy, if E_n is the energy of table n , and if E_{n+1} is the energy of table $n + 1$, then a value of μ is sampled from table $n + 1$ with probability $(E - E_n)/(E_{n+1} - E_n)$ and from table n with probability $(E_{n+1} - E)/(E_{n+1} - E_n)$. There are two options in MCNP for representing and sampling a non-isotropic scattering cosine. The first method involves the use of 32 equally probable cosine bins. The second method is to sample a tabulated distribution as a function of μ .

When the method with 32 equiprobable cosine bins is employed, a random number ξ on the interval $[0,1)$ is used to select the i^{th} cosine bin such that $I = 32 \cdot \xi + 1$. The value of μ is then computed as

$$\mu = \mu_i + (32 \cdot \xi - i)(\mu_{i+1} - \mu_i) \quad .$$

The method of 32 equiprobable cosine bins accurately represents high-probability regions of the scattering probability; however, it can be a very crude approximation in low-probability regions. For example, it accurately represents the forward scattering in a highly forward-peaked distribution, but may represent all the back angle scattering using only one or a few bins.

A new, more rigorous angular distribution representation was implemented in MCNP 4C. This new representation features a tabulation of the probability density function (PDF) as a function of the cosine of the scattering angle. Interpolation of the PDF between cosine values may be either by histogram or linear-linear interpolation. The new tabulated angular distribution allows more accurate representations of original evaluated distributions (typically given as a set of Legendre polynomials) in both high-probability and low-probability regions.

Tabular angular distributions are equivalent to tabular energy distribution (as defined using ENDF law 4) except that the sampled value is the cosine of the scattering angle, and discrete lines are not allowed. For each incident neutron energy E_i there is a pointer to a table of cosines $\mu_{i,k}$, probability density functions $p_{i,k}$, and cumulative density functions $c_{i,k}$. The index i and the interpolation fraction r are found on the incident energy grid for the incident energy E_{in} such that

$$E_i < E_{in} < E_{i+1} \quad \text{and}$$

$$E_{in} = E_i + r(E_{i+1} - E_i) \quad .$$

A random number, ξ_1 , on the unit interval [0,1) is used to sample a cosine bin k from the cumulative density function

$$c_{l,k} < \xi_1 < c_{l,k+1} \quad ,$$

where $l = i$ if $\xi_2 > r$ and $l = i+1$ if $\xi_2 < r$, and ξ_2 is a random number on the unit interval. For histogram interpolation the sampled cosine is

$$\mu' = \mu_{l,k} + \frac{(\xi_1 - c_{l,k})}{p_{l,k}} \quad .$$

For linear-linear interpolation the sampled cosine is

$$\mu' = \mu_{l,k} + \frac{\sqrt{P_{l,k}^2 + 2 \left[\frac{p_{l,k+1} - p_{l,k}}{\mu_{l,k+1} - \mu_{l,k}} \right] (\xi_1 - c_{l,k}) - p_{l,k}}}{\left[\frac{p_{l,k+1} - p_{l,k}}{\mu_{l,k+1} - \mu_{l,k}} \right]}$$

If the emitted angular distribution for some incident neutron energy is isotropic, μ is chosen from $\mu = \xi'$, where ξ' is a random number on the interval $[-1,1)$. Strictly, in MCNP random numbers are always furnished on the interval [0,1). Thus, to compute ξ' on $[-1,1)$ we calculate $\xi' = 2\xi - 1$, where ξ is a random number on [0,1).

The ENDF-6 format also has various formalisms to describe correlated secondary energy-angle spectra. These are discussed later in this chapter.

For elastic scattering, inelastic level scattering, and some ENDF-6 inelastic reactions, the scattering cosine is chosen in the center-of-mass system. Conversion must then be made to μ_{lab} , the cosine in the target-at-rest system. For other inelastic reactions, the scattering cosine is sampled directly in the target-at-rest system.

The incident particle direction cosines (u_o, v_o, w_o) are rotated to new outgoing target-at-rest system cosines (u, v, w) through a polar angle whose cosine is μ_{lab} , and through an azimuthal angle sampled uniformly. For random numbers ξ_1 and ξ_2 on the interval $[-1,1)$ with rejection criterion $\xi_1^2 \xi_2^2 \leq 1$, the rotation scheme is (Ref. 2 page 54):

$$\begin{aligned} u &= u_o \mu_{lab} + \frac{\sqrt{1 - \mu_{lab}^2} (\xi_1 u_o w_o - \xi_2 v_o)}{\sqrt{(\xi_1^2 + \xi_2^2)(1 - w_o^2)}} \\ v &= v_o \mu_{lab} + \frac{\sqrt{1 - \mu_{lab}^2} (\xi_1 v_o w_o + \xi_2 u_o)}{\sqrt{(\xi_1^2 + \xi_2^2)(1 - w_o^2)}} \\ w &= w_o \mu_{lab} - \frac{\xi_1 \sqrt{(1 - \mu_{lab}^2)(1 - w_o^2)}}{\sqrt{(\xi_1^2 + \xi_2^2)}} \end{aligned}$$

If $1 - w_o^2 \sim 0$, then

$$\begin{aligned} u &= u_o \mu_{lab} + \frac{\sqrt{1 - \mu_{lab}^2} (\xi_1 u_o v_o + \xi_2 w_o)}{\sqrt{(\xi_1^2 + \xi_2^2)(1 - v_o^2)}} \\ v &= v_o \mu_{lab} - \frac{\xi_1 \sqrt{(1 - \mu_{lab}^2)(1 - v_o^2)}}{\sqrt{(\xi_1^2 + \xi_2^2)}} \\ w &= w_o \mu_{lab} + \frac{\sqrt{1 - \mu_{lab}^2} (\xi_1 w_o v_o - \xi_2 u_o)}{\sqrt{(\xi_1^2 + \xi_2^2)(1 - v_o^2)}} \end{aligned}$$

If the scattering distribution is isotropic in the target-at-rest system, it is possible to use an even simpler formulation that takes advantage of the exiting direction cosines, (u, v, w), being independent of the incident direction cosines, (u_o, v_o, w_o). In this case,

$$\begin{aligned} u &= 2\xi_1^2 + 2\xi_2^2 - 1 \quad , \\ v &= \xi_1 \sqrt{\frac{1 - u^2}{\xi_1^2 + \xi_2^2}} \quad , \end{aligned}$$

$$w = \xi_2 \sqrt{\frac{1 - u^2}{\xi_1^2 + \xi_2^2}} ,$$

where ξ_1 and ξ_2 are rejected if $\xi_1^2 + \xi_2^2 > 1$.

b. Energy from Elastic Scattering: Once the particle direction is sampled from the appropriate angular distribution tables, then the exiting energy, E_{out} , is dictated by two-body kinematics:

$$\begin{aligned} E_{out} &= \frac{1}{2} E_{in} [(1 - \alpha) \mu_{cm} + 1 + \alpha] \\ &= E_{in} \left[\frac{1 + A^2 + 2A \mu_{cm}}{(1 + A)^2} \right] , \end{aligned}$$

where E_{in} = incident neutron energy, μ_{cm} = center-of-mass cosine of the angle between incident and exiting particle directions,

$$\alpha = \left(\frac{A - 1}{A + 1} \right)^2$$

and A = mass of collision nuclide in units of the mass of a neutron (atomic weight ratio).

c. Inelastic Reactions: The treatment of inelastic scattering depends upon the particular inelastic reaction chosen. Inelastic reactions are defined as (n, y) reactions such as (n, n') , $(n, 2n)$, (n, f) , $(n, n'\alpha)$ in which y includes at least one neutron.

For many inelastic reactions, such as $(n, 2n)$, more than one neutron can be emitted for each incident neutron. The weight of each exiting particle is always the same as the weight of the incident particle minus any implicit capture. The energy of exiting particles is governed by various scattering laws that are sampled independently from the cross-section files for each exiting particle. Which law is used is prescribed by the particular cross-section evaluation used. In fact, more than one law can be specified, and the particular one used at a particular time is decided with a random number. In an $(n, 2n)$ reaction, for example, the first particle emitted may have an energy sampled from one or more laws, but the second particle emitted may have an energy sampled from one or more different laws, depending upon specifications in the nuclear data library. Because emerging energy and scattering angle is sampled independently for each particle, there is no correlation between the emerging particles. Hence energy is not conserved in an individual reaction because, for example, a 14-MeV particle could conceivably produce two 12-MeV particles in a single reaction. But the net effect of many particle histories is unbiased because on the average the correct amount of energy is emitted. Results are biased only when quantities that depend upon the correlation between the emerging particles are being estimated.

Users should note that MCNP follows a very particular convention. The exiting particle energy and direction are always given in the target-at-rest (laboratory) coordinate system. For the kinematical calculations in MCNP to be performed correctly, the angular distributions for elastic, discrete

inelastic level scattering, and some ENDF-6 inelastic reactions *must* be given in the center-of-mass system, and the angular distributions for all other reactions *must* be given in the target-at-rest system. MCNP does not stop if this convention is not adhered to, but the results will be erroneous. In the checking of the cross-section libraries prepared for MCNP at Los Alamos, however, careful attention has been paid to ensure that these conventions are followed.

The exiting particle energy and direction in the target-at-rest (laboratory) coordinate system are related to the center-of-mass energy and direction as follows:¹

$$E' = E'_{cm} + \left[\frac{E + 2\mu_{cm}(A + 1)\sqrt{EE'_{cm}}}{(A + 1)^2} \right] ; \text{ and}$$

$$\mu_{lab} = \mu_{cm}\sqrt{\frac{E'_{cm}}{E'}} + \frac{1}{A + 1}\sqrt{\frac{E}{E'}}$$

where

- E' = exiting particle energy (laboratory),
- E'_{cm} = exiting particle energy (center-of-mass),
- E = incident particle energy (laboratory),
- μ_{cm} = cosine of center-of-mass scattering angle,
- μ_{lab} = cosine of laboratory scattering angle, and
- A = atomic weight ratio (mass of nucleus divided by mass of incident particle).

For point detectors it is necessary to convert

$$p(\mu_{lab}) = p(\mu_{cm})\frac{d\mu_{cm}}{d\mu_{lab}} ,$$

where

$$\mu_{cm} = \mu_{lab}\sqrt{\frac{E'}{E'_{cm}}} - \frac{1}{A + 1}\sqrt{\frac{E}{E'_{cm}}} \text{ and}$$

$$\begin{aligned} \frac{d\mu_{cm}}{d\mu_{lab}} &= \frac{E'/E'_{cm}}{\sqrt{\frac{E'}{E'_{cm}}} - \frac{\mu_{lab}}{A + 1}\sqrt{\frac{E}{E'_{cm}}}} \\ &= \frac{\sqrt{\frac{E'}{E'_{cm}}}}{1 - \frac{\mu_{lab}}{A + 1}\sqrt{\frac{E}{E'}}} . \end{aligned}$$

d. Nonfission Inelastic Scattering and Emission Laws: Nonfission inelastic reactions are handled differently from fission inelastic reactions. For each nonfission reaction N_p particles are emitted, where N_p is an integer quantity specified for each reaction in the cross-section data library of the collision nuclide. The direction of each emitted particle is independently sampled from the appropriate angular distribution table, as was described earlier. The energy of each emitted particle is independently sampled from one of the following scattering or emission laws. Energy and angle are correlated only for ENDF-6 laws 44 and 67. For completeness and convenience, all the laws are listed together, regardless of whether the law is appropriate for nonfission inelastic scattering (for example, Law 3), fission spectra (for example, Law 11), both (for example, Law 9), or neutron-induced photon production (for example, Law 2). The conversion from center-of-mass to target-at-rest (laboratory) coordinate systems is given in the above equations.

Law 1 (ENDF law 1): Equiprobable energy bins.

The index i and the interpolation fraction r are found on the incident energy grid for the incident energy E_{in} such that

$$E_i < E_{in} < E_{i+1} \quad \text{and}$$

$$E_{in} = E_i + r(E_{i+1} - E_i) \quad .$$

A random number on the unit interval ξ_l is used to select an equiprobable energy bin k from the K equiprobable outgoing energies E_{ik}

$$k = \xi_l K + 1 \quad .$$

Then scaled interpolation is used with random numbers ξ_2 and ξ_3 on the unit interval. Let

$$E_1 = E_{i,1} + r(E_{i+1,1} - E_{i,1}) \quad \text{and}$$

$$E_K = E_{i,K} + r(E_{i+1,K} - E_{i,K}) \quad ; \text{ and}$$

$$l = i \quad \text{if } \xi_3 > r \quad \text{or}$$

$$l = i + 1 \quad \text{if } \xi_3 < r \quad \text{and}$$

$$E' = E_{l,k} + \xi_2(E_{l,k+1} - E_{l,k}) \quad ; \quad \text{then}$$

$$E_{out} = E_1 + \frac{(E' - E_{l,1})(E_K - E_1)}{E_{l,K} - E_{l,1}} \quad .$$

Law 2 Discrete photon energy.

The value provided in the library is E_g . The secondary photon energy E_{out} is either

$$E_{out} = E_g \quad \text{for non-primary photons or}$$

$$E_{out} = E_g + [A/(A+1)]E_{in} \quad \text{for primary photons,}$$

where A is the atomic weight to neutron weight ratio of the target and E_{in} is the incident neutron energy.

Law 3 (ENDF law 3): Inelastic scattering (n, n') from nuclear levels.
The value provided in the library is Q .

$$E_{out} = \left(\frac{A}{A+1} \right)^2 \left[E_{in} - \frac{Q(A+1)}{A} \right] .$$

Law 4 Tabular distribution (ENDF law 4).

For each incident neutron energy E_i there is a pointer to a table of secondary energies $E_{i,k}$, probability density functions $p_{i,k}$, and cumulative density functions $c_{i,k}$. The index i and the interpolation fraction r are found on the incident energy grid for the incident energy E_{in} such that

$$E_i < E_{in} < E_{i+1} \quad \text{and}$$

$$E_{in} = E_i + r(E_{i+1} - E_i) .$$

The tabular distribution at each E_i may be composed of discrete lines, a continuous spectra, or a mixture of discrete lines superimposed on a continuous background. If discrete lines are present, there must be the same number of lines (given one per bin) in each table. The sampling of the emission energy for the discrete lines (if present) is handled separately from the sampling for the continuous spectrum (if present). A random number, ξ_1 , on the unit interval $[0,1)$ is used to sample a second energy bin k from the cumulative density function.

If discrete lines are present, the algorithm first checks to see if the sampled bin is within the discrete line portion of the table as determined by

$$c_{i,k} + r(c_{i+1,k} - c_{i,k}) < \xi_1 < c_{i,k+1} + r(c_{i+1,k+1} - c_{i,k+1})$$

If this condition is met, then the sampled energy E' for the discrete line is interpolated between incident energy grids as

$$E' = E_{i,k} + r(E_{i+1,k} - E_{i,k}) .$$

If a discrete line has been sampled, the energy sampling is finished. If a discrete line has not been sampled, the secondary energy is sampled from the remaining continuous background.

For continuous distributions, the secondary energy bin k is sampled from

$$c_{l,k} < \xi_1 < c_{l,k+1} ,$$

where $l = i$ if $\xi_2 > r$ and $l = i + 1$ if $\xi_2 < r$, and ξ_2 is a random number on the unit interval. For histogram interpolation the sampled energy is

$$E' = E_{l,k} + \frac{(\xi_1 - c_{l,k})}{P_{l,k}} .$$

For linear-linear interpolation the sampled energy is

$$E' = E_{l,k} + \left\{ \frac{\sqrt{P_{l,k}^2 + 2 \left[\frac{P_{l,k+1} - P_{l,k}}{E_{l,k+1} - E_{l,k}} \right] (\xi_1 - c_{l,k}) - P_{l,k}}}{\left[\frac{P_{l,k+1} - P_{l,k}}{E_{l,k+1} - E_{l,k}} \right]} \right\}$$

The secondary energy is then interpolated between the incident energy bins i and $i + 1$ to properly preserve thresholds. Let

$$E_1 = E_{i,1} + r(E_{i+1,1} - E_{i,1}) \quad \text{and}$$

$$E_K = E_{i,K} + r(E_{i+1,K} - E_{i,K}) ; \quad \text{then}$$

$$E_{out} = E_1 + \frac{(E' - E_{l,1})(E_K - E_1)}{(E_{l,K} - E_{l,1})} .$$

The final step is to adjust the energy from the center-of-mass system to the laboratory system, if the energies were given in the center-of-mass system.

Law 4 is an independent distribution, i.e. the emission energy and angle are not correlated. The outgoing angle is selected from the angular distribution as described on page 2–36. Data tables built using this methodology are designed to sample the distribution correctly in a statistical sense and will not necessarily sample the exact distribution for any specific collision.

Law 5 (ENDF law 5): General evaporation spectrum.

The function $g(x)$ is tabulated versus χ and the energy is tabulated versus incident energy E_{in} . The law is then

$$f(E_{in} \rightarrow E_{out}) = g\left(\frac{E_{out}}{T(E_{in})}\right) .$$

This density function is sampled by

$$E_{out} = \chi(\xi) T(E_{in}),$$

where $T(E_{in})$ is a tabulated function of the incident energy and $c(\xi)$ is a table of equiprobable χ values.

Law 7 (ENDF law 7): Simple Maxwell Fission Spectrum.

$$f(E_{in} \rightarrow E_{out}) = C * \sqrt{E_{out}} e^{-E_{out}/T(E_{in})}$$

The nuclear temperature $T(E_{in})$ is a tabulated function of the incident energy. The normalization constant C is given by

$$C^{-1} = T^{3/2} \left[\left(\frac{\sqrt{\pi}}{2} \right) \operatorname{erf} \left(\sqrt{\frac{(E_{in} - U)}{T}} \right) - \sqrt{\frac{(E_{in} - U)}{T}} e^{-(E_{in} - U)/T} \right]$$

U is a constant provided in the library and limits E_{out} to $0 \leq E_{out} \leq E_{in} - U$. In MCNP this density function is sampled by the rejection scheme

$$E_{out} = -T(E_{in}) \left[\frac{\xi_1^2 \ln \xi_3}{\xi_1^2 + \xi_2^2} + \ln \xi_4 \right],$$

where ξ_1, ξ_2, ξ_3 , and ξ_4 are random numbers on the unit interval. ξ_1 and ξ_1 are rejected if $\xi_1^2 + \xi_2^2 > 1$.

Law 9 (ENDF law 9): Evaporation spectrum.

$$f(E_{in} \rightarrow E_{out}) = C E_{out} e^{-E_{out}/T(E_{in})},$$

where the nuclear temperature $T(E_{in})$ is a tabulated function of the incident energy. The energy U is provided in the library and is assigned so that E_{out} is limited by $0 \leq E_{out} \leq E_{in} - U$. The normalization constant C is given by

$$C^{-1} = T^2 [1 - e^{-(E_{in} - U)/T} (1 + (E_{in} - U)/T)]$$

In MCNP this density function is sampled by

$$E_{out} = -T(E_{in}) \ln(\xi_1 \xi_2),$$

where ξ_1 and ξ_2 are random numbers on the unit interval, and ξ_1 and ξ_2 are rejected if $E_{out} > E_{in} - U$.

Law 11 (ENDF law 11): Energy Dependent Watt Spectrum.

$$f(E_{in} \rightarrow E_{out}) = C e^{-E_{out}/a(E_{in})} \sinh \sqrt{b(E_{in}) E_{out}}.$$

The constants a and b are tabulated functions of incident energy and U is a constant from the library. The normalization constant C is given by

$$c^{-1} = \frac{1}{2} \sqrt{\frac{\pi a^3 b}{4}} \exp\left(\frac{ab}{4}\right) \left[\operatorname{erf}\left(\sqrt{\frac{(E_{in} - U)}{a}} - \sqrt{\frac{ab}{4}}\right) + \operatorname{erf}\left(\sqrt{\frac{(E_{in} - U)}{a}} + \sqrt{\frac{ab}{4}}\right) \right] \\ - a \exp\left[-\frac{(E_{in} - U)}{a}\right] \sinh \sqrt{b(E_{in} - U)},$$

where the constant U limits the range of outgoing energy so that $0 \leq E_{out} \leq E_{in} - U$. This density function is sampled as follows. Let

$$g = \sqrt{\left(1 + \frac{ab}{8}\right)^2 - 1} + \left(1 + \frac{ab}{8}\right). \quad \text{Then } E_{out} = -ag \ln \xi_1.$$

E_{out} is rejected if

$$[(1 - g)(1 - \ln \xi_1) - \ln \xi_2]^2 > bE_{out} \quad ,$$

where ξ_1 and ξ_2 are random numbers on the unit interval.

Law 22 (UK law 2): Tabular linear functions of incident energy out.

Tables of P_{ij} , C_{ij} , and T_{ij} are given at a number of incident energies E_i . If $E_i \leq E_{in} < E_{i+1}$ then the i^{th} P_{ij} , C_{ij} , and T_{ij} tables are used.

$$E_{out} = C_{ik}(E_{in} - T_{ik}) \quad ,$$

where k is chosen according to

$$\sum_{j=1}^k P_{ij} < \xi \leq \sum_{j=1}^{k+1} P_{ij} \quad ,$$

where ξ is a random number on the unit interval $[0,1)$.

Law 24 (UK law 6): Equiprobable energy multipliers. The law is

$$E_{out} = E_{in} T(E_{in}) \quad .$$

The library provides a table of K equiprobable energy multipliers $T_{i,k}$ for a grid of incident neutron energies E_i . For incident energy E_{in} such that

$$E_i < E_{in} < E_{i+1} \quad ,$$

the random numbers ξ_1 and ξ_2 on the unit interval are used to find T :

$$k = \xi_1 K + 1$$

$$T = T_{i,k} + \xi_2 (T_{i,k+1} - T_{i,k}) \quad \text{and then}$$

$$E_{out} = E_{in} T \quad .$$

Law 44 Tabular Distribution (ENDF Law=1 Lang=2, Kalbach-87 correlated energy-angle scattering). Law 44 is an extension of Law 4. For each incident energy E_i there is a pointer to a table of secondary energies $E_{i,k}$, probability density functions $p_{i,k}$, cumulative density functions $c_{i,k}$, precompound fractions $R_{i,k}$, and angular distribution slope values $A_{i,k}$. The secondary emission energy is found exactly as stated in the Law 4 description on page 2–42. Unlike Law 4, Law 44 includes a correlated angular distribution associated

with each incident energy E_i as given by the Kalbach parameters $R_{i,k}$, and $A_{i,k}$. Thus, the sampled emission angle is dependent on the sampled emission energy.

The sampled values for R and A are interpolated on both the incident and outgoing energy grids. For discrete spectra,

$$A = A_{i,k} + r(A_{i+1,k} - A_{i,k}) \quad \text{and}$$

$$R = R_{i,k} + r(R_{i+1,k} - R_{i,k}) .$$

For continuous spectra with histogram interpolation,

$$A = A_{i,k} \quad \text{and}$$

$$R = R_{i,k}$$

For continuous spectra with linear-linear interpolation,

$$A = A_{l,k} + (A_{l,k+1} - A_{l,k})(E' - E_{l,k}) / (E_{l,k+1} - E_{l,k}) \quad \text{and}$$

$$R = R_{l,k} + (R_{l,k+1} - R_{l,k})(E' - E_{l,k}) / (E_{l,k+1} - E_{l,k}) .$$

The outgoing neutron center-of-mass scattering angle μ is sampled from the Kalbach density function

$$p(\mu, E_{in}, E_{out}) = \frac{1}{2} \frac{A}{\sinh(A)} [\cosh(A\mu) + R \sinh(A\mu)]$$

using the random numbers ξ_3 and ξ_4 on the unit interval as follows. If $\xi_3 > R$, then let

$$T = (2\xi_4 - 1) \sinh(A) \quad \text{and}$$

$$\mu = \ln(T + \sqrt{T^2 + 1}) / A ,$$

or if $\xi_3 < R$, then

$$\mu = \ln \left[\xi_4 e^A + (1 - \xi_4) e^{-A} \right] / A .$$

As with Law 4, the emission energy and angle are transformed from the center-of-mass to the laboratory system as necessary.

Law 61 Tabular Distribution (ENDF Law=1 Lang=0, 12 or 14; correlated energy-angle scattering). Law 61 is an extension of Law 4. For each incident energy E_i there is a pointer to a table of secondary energies $E_{i,k}$, probability density functions $p_{i,k}$, cumulative density functions $c_{i,k}$, and pointers to tabulated angular distributions $L_{i,k}$. The secondary emission

energy is found exactly as stated in the Law 4 description on page 2–42. Unlike Law 4, Law 61 includes a correlated angular distribution associated with each incident energy E_i as given by the tabular angular distribution located using the pointers $L_{i,k}$. Thus, the sampled emission angle is dependent on the sampled emission energy.

If the secondary distribution is given using histogram interpolation, the angular distribution located at $L_{i,k}$ is used to sample the emission angle. If the secondary distribution is specified as linear interpolation between energy points, $L_{i,k}$ is chosen by selecting the bin closest to the randomly sampled cumulative distribution function (CDF) point. If the value of $L_{i,k}$ is zero, the angle is sampled from an isotropic distribution as described on page 2–37. If the value of $L_{i,k}$ is positive, it points to a tabular angular distribution which is then sampled as described on page 2–37.

As with Law 4, the emission energy and angle are transformed from the center-of-mass to the laboratory system as necessary.

Law 66 N-body phase space distribution (ENDF law 6).

The phase space distribution for particle i in the center-of-mass coordinate system is:

$$P_i(\mu, E_{in}, T) = C_n \sqrt{T} (E_i^{max} - T)^{3n/2 - 4} ,$$

where all energies and angles are also in the center-of-mass system and E_i^{max} is the maximum possible energy for particle i , μ and T . T is used for calculating E_{out} . The C_n normalization constants for $n = 3, 4, 5$ are:

$$C_3 = \frac{4}{\pi (E_i^{max})^2} ,$$

$$C_4 = \frac{105}{32 (E_i^{max})^{7/2}} , \quad \text{and}$$

$$C_5 = \frac{256}{14\pi (E_i^{max})^5} .$$

E_i^{max} is a fraction of the energy available, E_a ,

$$E_i^{max} = \frac{M - m_i}{M} E_a ,$$

where M is the total mass of the n particles being treated, m_i is the mass of particle i , and

$$E_a = \frac{m_T}{m_p + m_T} E_{in} + Q ,$$

where m_T is the target mass and m_p is the projectile mass. For neutrons,

$$\frac{m_T}{m_p + m_T} = \frac{A}{A + 1}$$

and for a total mass ratio $A_p = M/m_i$,

$$\frac{M - m_i}{M} = \frac{A_p - 1}{A_p} .$$

Thus,

$$E_i^{max} = \frac{A_p - 1}{A_p} \left(\frac{A}{A + 1} E_{in} + Q \right) .$$

The total mass A_p and the number of particles in the reaction n are provided in the data library. The outgoing energy is sampled as follows.

Let ξ_i , $i = 1, 9$ be random numbers on the unit interval. Then from rejection technique R28 from the Monte Carlo Sampler,³ accept ξ_1 and ξ_2 if

$$\xi_1^2 + \xi_2^2 \leq 1$$

and accept ξ_3 and ξ_4 if

$$\xi_3^2 + \xi_4^2 \leq 1 .$$

Then let

$$p = \xi_5 \text{ if } n = 3 ,$$

$$p = \xi_5 \xi_6 \text{ if } n = 4 , \quad \text{and}$$

$$p = \xi_5 \xi_6 \xi_7 \xi_8 \text{ if } n = 5 ,$$

and let

$$x = \frac{-\xi_1 \ln(\xi_1^2 + \xi_2^2)}{(\xi_1^2 + \xi_2^2)} - \ln \xi_9 ,$$

$$y = \frac{-\xi_3 \ln(\xi_3^2 + \xi_4^2)}{(\xi_3^2 + \xi_4^2)} - \ln p , \quad \text{and}$$

$$T = \frac{x}{x + y} ;$$

then

$$E_{out} = T E_i^{max} .$$

The cosine of the scattering angle is always sampled isotropically in the center-of-mass system using another random number ξ_2 on the unit interval:

$$\mu = 2\xi_2 - 1 \quad .$$

Law 67 Correlated energy-angle scattering (ENDF law 7).

For each incident neutron energy, first the exiting particle direction μ is sampled as described on page 2–36. In other Law data, first the exiting particle energy is sampled and then the angle is sampled. The index i and the interpolation fraction r are found on the incident energy grid for the incident energy E_{in} , such that

$$E_i < E_{in} < E_{i+1} \quad \text{and}$$

$$E_{in} = E_i + r(E_{i+1} - E_i) \quad .$$

For each incident energy E_i there is a table of exiting particle direction cosines $\mu_{i,j}$ and locators $L_{i,j}$. This table is searched to find which ones bracket μ , namely,

$$\mu_{i,j} < \mu < \mu_{i,j+1} \quad .$$

Then the secondary energy tables at $L_{i,j}$ and $L_{i,j+1}$ are sampled for the outgoing particle energy. The secondary energy tables consist of a secondary energy grid $E_{i,j,k}$, probability density functions $p_{i,j,k}$, and cumulative density functions $c_{i,j,k}$. A random number ξ_1 on the unit interval is used to pick between incident energy indices: if $\xi_1 < r$ then $l = i + 1$; otherwise, $l = i$. Two more random numbers ξ_2 and ξ_3 on the unit interval are used to determine interpolation energies. If $\xi_2 < (\mu - \mu_{l,j})/(\mu_{l,j+1} - \mu_{l,j})$, then

$$E_{i,k} = E_{i,j+1,k} \quad \text{and} \quad m = j + 1, \quad \text{if} \quad l = i \quad .$$

Otherwise,

$$E_{i,k} = E_{i,j,k} \quad \text{and} \quad m = j, \quad \text{if} \quad l = i \quad .$$

If $\xi_3 < (\mu - \mu_{i+1,j})/(\mu_{i+1,j+1} - \mu_{i+1,j})$, then

$$E_{i+1,k} = E_{i+1,j+1,k} \quad \text{and} \quad m = j + 1, \quad \text{if} \quad l = i + 1 \quad .$$

Otherwise,

$$E_{i+1,k} = E_{i+1,j,k} \quad \text{and} \quad m = j, \quad \text{if} \quad l = i + 1 \quad .$$

A random number ξ_4 on the unit interval is used to sample a secondary energy bin k from the cumulative density function

$$c_{l,m,k} < \xi_4 < c_{l,m,k+1} \quad .$$

For histogram interpolation the sampled energy is

$$E' = E_{l,m,k} + \frac{(\xi_4 - c_{l,m,k})}{P_{l,m,k}}.$$

For linear-linear interpolation the sampled energy is

$$E' = E_{l,m,k} + \left\{ \frac{\sqrt{P_{l,m,k}^2 + 2 \left[\frac{P_{l,m,k+1} - P_{l,m,k}}{E_{l,m,k+1} - E_{l,m,k}} \right] (\xi_4 - c_{l,m,k}) - P_{l,m,k}}}{\left[\frac{P_{l,m,k+1} - P_{l,m,k}}{E_{l,m,k+1} - E_{l,m,k}} \right]} \right\}.$$

The final outgoing energy E_{out} uses scaled interpolation. Let

$$E_1 = E_{i,1} + r(E_{i+1,1} - E_{i,1})$$

$$\text{and } E_K = E_{i,K} + r(E_{i+1,K} - E_{i,K}).$$

$$\text{Then } E_{out} = E_1 + \frac{(E' - E_{l,1})(E_K - E_1)}{(E_{l,K} - E_{l,1})}.$$

e. Emission from Fission: For any fission reaction a number of neutrons, n , is emitted according to the value of $\bar{\nu}(E_{in})$. Depending on the type of problem (fixed source or KCODE) and on user input (TOTNU card), MCNP may use either prompt $\bar{\nu}_p(E_{in})$ or total $\bar{\nu}_t(E_{in})$. For either case, the average number of neutrons per fission, $\bar{\nu}(E_{in})$, may be a tabulated function of energy or a polynomial function of energy.

If the fifth entry on the PHYS:N card is zero (default), then n is sampled between I (the largest integer less than $\bar{\nu}(E_{in})$) and $I + 1$ by

$$n = I + 1 \quad \text{if } \xi \leq \bar{\nu}(E_{in}) - I$$

$$n = I \quad \text{if } \xi > \bar{\nu}(E_{in}) - I, \text{ where } \xi \text{ is a random number.}$$

If more microscopically correct fission neutron multiplicities are desired for fixed source problems, the fifth entry on the PHYS:N card can be used to select which set of Gaussian widths are used to sample the actual number of neutrons from fission that typically range from 0 to 7 or 8.⁴⁹ For a given fission event, there is a probability P_n that n neutrons are emitted. This distribution is generally called the neutron multiplicity distribution. Fission neutron multiplicity distributions are known to be well reproduced by simple Gaussian distributions,⁵⁰

$$P_0 = \frac{1}{\sqrt{2\pi\sigma^2}} \int_{-\infty}^{1/2} \exp\left(\frac{-(x - \bar{\nu} + b)^2}{2\sigma^2}\right) dx, \quad (2.2)$$

and

$$P_{n \neq 0} = \frac{1}{\sqrt{2\pi\sigma^2}} \int_{n-1/2}^{n+1/2} \exp\left(\frac{-(x - \bar{v} + b)^2}{2\sigma^2}\right) dx,$$

where \bar{v} is the mean multiplicity, b is a small adjustment to make the mean equal to \bar{v} , and σ is the Gaussian width. For the range of realistic widths, the adjustment b can be accurately expressed as a single smooth function of $(\bar{v} + 0.5)/\sigma$.⁵¹ To determine the value of σ from experimental data, many authors have minimized the chi-squared

$$x^2(\sigma) = \sum_n \left[\frac{P_n^{\text{exp}} - P_n(\sigma)}{\Delta P_n^{\text{exp}}} \right]^2, \quad (2.3)$$

where ΔP_n^{exp} is the uncertainty in the experimentally measured multiplicity distribution P_n^{exp} . The factorial moments of the neutron multiplicity distribution ($\bar{v}_i = \Sigma P_n n! / (n - i)!$) emitted by a multiplying sample can be expressed as a function of the factorial moments for spontaneous and induced fission.⁵² Therefore, for many applications it is not necessary to know the details of the neutron multiplicity distribution, but it is more important to know the corresponding first three factorial moments. A reevaluation of the existing spontaneous fission and neutron induced fission data has been performed⁵¹ where the widths of Gaussians are adjusted to fit the measured second and third factorial moments. This reevaluation was done by minimizing the chi-squared

$$x^2(\sigma) = \sum_{i=2}^3 \left[\frac{v_i(P_n^{\text{exp}}) - v_i(P_n(\sigma))}{\Delta v_i^{\text{exp}}} \right]^2. \quad (2.4)$$

These results are summarized in Table 2.1. Despite the change in emphasis from the detailed shape to the moments of the distributions, the inferred widths are little changed from those obtained by others. However, by minimizing the chi-squared in Eq. (2.4) the inferred widths are guaranteed to be in reasonable agreement with the measured second and third factorial moments. The widths obtained using Eq. (2.4) give Gaussian distributions that reproduce the experimental second and third factorial moments to better than 0.6%. The adjustment parameter b ensures that the first moment (\bar{v}) is accurately reproduced. If the chi-squared in Eq. (2.3) is used, then the second and third factorial moments can differ from the experimental values by as much as 10%.

Table 2.1
Recommended Gaussian
Widths⁵¹ from Eq. (2.4)

Reaction	σ
²³³ U(n,f)	1.070
²³⁵ U(n,f)	1.088
²³⁸ U(n,f)	1.116

Table 2.1 (Continued)
Recommended Gaussian
Widths⁵¹ from Eq. (2.4)

Reaction	σ
²³⁹ Pu(n,f)	1.140
²⁴¹ Pu(n,f)	1.150
²³⁸ Pu SF ¹	1.135
²⁴⁰ Pu SF	1.151
²⁴² Pu SF	1.161
²⁴² Cm SF	1.091
²⁴⁴ Cm SF	1.103
²⁴⁶ Cm SF	1.098
²⁴⁸ Cm SF	1.108
²⁵⁰ Cf SF	1.220
²⁵² Cf SF	1.245
²⁵⁴ Cf SF	1.215
²⁵⁴ Fm SF	1.246

¹SF: Spontaneous fission.

Assuming that the widths of the multiplicity distributions are independent of the initial excitation energy of the fissioning system,⁵¹ the relationship between different factorial moments is easily calculated as a function of $\bar{\nu}$. The corresponding calculated relationships between the first three factorial moments are in good agreement with experimental neutron induced fission data up to an incoming neutron energy of 10 MeV.⁵¹ This implies that an energy independent width can be used with confidence up to an incoming neutron energy of at least 10 MeV. The Gaussian widths in Table 2.1 are used for fission multiplicity sampling in MCNP when the fifth entry on the PHYS:N card is 1. Induced fission multiplicities for isotopes not listed in Table 2.1 use a Gaussian width that is linearly dependent on the mass number of the fissioning system.⁵¹

The direction of each emitted neutron is sampled independently from the appropriate angular distribution table by the procedure described on page 2–36.

The energy of each fission neutron is determined from the appropriate emission law. These laws are discussed in the preceding section. MCNP then models the transport of the first neutron out after storing all other neutrons in the bank.

f. Prompt and Delayed Neutron Emission: If (1) MCNP is using $\bar{\nu}_t$, (2) the data for the collision isotope includes delayed-neutron spectra, and (3) the use of detailed delayed-neutron data has not been preempted (on the PHYS:N card), then each fission neutron is first determined by MCNP to be either a prompt fission neutron or a delayed fission neutron. Assuming analog

sampling, the type of emitted neutron is determined from the ratio of delayed $\bar{\nu}(E_{in})$ to total $\bar{\nu}(E_{in})$ as

if $\xi \leq \bar{\nu}_d(E_{in}) / \bar{\nu}_{tot}(E_{in})$, produce a delayed neutron, or

if $\xi > \bar{\nu}_d(E_{in}) / \bar{\nu}_{tot}(E_{in})$, produce a prompt neutron,

where $\bar{\nu}_d$ is the expected number of delayed neutrons.

If the neutron is determined to be a prompt fission neutron, it is emitted instantaneously, and the emission laws (angle and energy) specified for prompt fission are sampled.

If the neutron is determined to be a delayed fission neutron, then MCNP first samples for the decay group by using the specified abundances. Then, the time delay is sampled from the exponential density with decay constant specified for the sampled decay group.

Finally, the emission laws (angle and energy) specified for that decay group are then sampled. Since the functionality in MCNP to produce delayed neutrons using appropriate emission data is new, we include next a somewhat more expanded description.

A small but important fraction (~1%) of the neutrons emitted in fission events are delayed neutrons emitted as a result of fission-product decay at times later than prompt fission neutrons. MCNP users have always been able to specify whether or not to include delayed fission neutrons by using either $\bar{\nu}_t$ (prompt plus delayed) or $\bar{\nu}_p$ (prompt only). However, in versions of MCNP up through and including 4B, all fission neutrons (whether prompt or delayed) were produced instantaneously and with an energy sampled from the spectra specified for prompt fission neutrons.

For many applications this approach is adequate. However, it is another example of a data approximation that is unnecessary. Therefore, Versions 4C and later of MCNP allow delayed fission neutrons to be sampled (either analog or biased) from time and energy spectra as specified in nuclear data evaluations. The libraries with detailed delayed fission neutron data are listed in Table G-2 with a “yes” in the “DN” column.

The explicit sampling of a delayed-neutron spectrum implemented in MCNP 4C has two effects. One is that the delayed neutron spectra have the correct energy distribution; they tend to be softer than the prompt spectra. The second is that experiments measuring neutron decay after a pulsed source can now be modeled with MCNP because the delay in neutron emission following fission is properly accounted for. In this treatment, a natural sampling of prompt and delayed neutrons is implemented as the default and an additional delayed neutron biasing control is available to the user via the PHYS:N card. The biasing allows the number of delayed neutrons produced to be increased artificially because of the low probability of a delayed neutron occurrence. The delayed neutron treatment is intended to be used with the TOTNU option in MCNP, giving the user the flexibility to use the time-dependent treatment of delayed neutrons whenever the delayed data are available.

The impact of sampling delayed-neutron energy spectra on reactivity calculations has been studied.⁵³ As expected, most of the reactivity impacts are very small, although changes of 0.1-0.2%

in k_{eff} were observed for certain cases. Overall, inclusion of delayed-neutron spectra can be expected to produce small positive reactivity changes for systems with significant fast neutron leakage and small negative changes for some systems in which a significant fraction of the fissions occurs in isotopes with an effective fission threshold (e.g., ^{238}U and ^{240}Pu).

6. The $S(\alpha,\beta)$ Treatment

The $S(\alpha,\beta)$ thermal scattering treatment is a complete representation of thermal neutron scattering by molecules and crystalline solids. Two processes are allowed: (1) inelastic scattering with cross section σ_{in} and a coupled energy-angle representation derived from an ENDF $S(\alpha,\beta)$ scattering law, and (2) elastic scattering with no change in the outgoing neutron energy for solids with cross section σ_{el} and an angular treatment derived from lattice parameters. The elastic scattering treatment is chosen with probability $\sigma_{el}/(\sigma_{el} + \sigma_{in})$. This thermal scattering treatment also allows the representation of scattering by multiatomic molecules (for example, BeO).

For the inelastic treatment, the distribution of secondary energies is represented by a set of equally probable final energies (typically 16 or 32) for each member of a grid of initial energies from an upper limit of typically 4 eV down to 10^{-5} eV, along with a set of angular data for each initial and final energy. The selection of a final energy E' given an initial energy E can be characterized by sampling from the distribution

$$p(E' | E_i < \xi < E_{i+1}) = \frac{1}{N} \sum_{j=1}^N \delta[E' - \rho E_{i,j} - (1 - \rho)E_{i+1,j}] ,$$

where E_i and E_{i+1} are adjacent elements on the initial energy grid,

$$\rho = \frac{E_{i+1} - E}{E_{i+1} - E_i} ,$$

N is the number of equally probable final energies, and E_{ij} is the j^{th} discrete final energy for incident energy E_i .

There are two allowed schemes for the selection of a scattering cosine following selection of a final energy and final energy index j . In each case, the $(i,j)^{th}$ set of angular data is associated with the energy transition $E = E_i \rightarrow E' = E_{i,j}$.

(1) The data consist of sets of equally probable discrete cosines $\mu_{i,j,k}$ for $k = 1, \dots, v$ with v typically 4 or 8. An index k is selected with probability $1/v$, and μ is obtained by the relation

$$\mu = \rho \mu_{i,j,k} + (1 - \rho) \mu_{i+1,j,k} .$$

(2) The data consist of bin boundaries of equally probable cosine bins. In this case, random linear interpolation is used to select one set or the other, with ρ being the probability of selecting the set corresponding to incident energy E_i . The subsequent procedure consists of sampling for one of the equally probable bins and then choosing μ uniformly in the bin.

For elastic scattering, the above two angular representations are allowed for data derived by an incoherent approximation. In this case, one set of angular data appears for each incident energy and is used with the interpolation procedures on incident energy described above.

For elastic scattering, when the data have been derived in the coherent approximation, a completely different representation occurs. In this case, the data actually stored are the set of parameters D_k , where

$$\sigma_{eI} = D_k/E \quad \text{for} \quad E_{bk} \leq E < E_{bk+1}$$

$$\sigma_{eI} = (0)/E \quad \text{for} \quad E < E_{B1}$$

and E_{Bk} are Bragg energies derived from the lattice parameters. For incident energy E such that $E_{Bk} \leq E \leq E_{Bk+1}$,

$$P_i = D_i/D_k \quad \text{for} \quad i = 1, \dots, k$$

represents a discrete cumulative probability distribution that is sampled to obtain index i , representing scattering from the i^{th} Bragg edge. The scattering cosine is then obtained from the relationship

$$\mu = 1 - 2E_{Bi}/E \quad .$$

Using next event estimators such as point detectors with $S(\alpha, \beta)$, scattering cannot be done exactly because of the discrete scattering angles. MCNP uses an approximate scheme^{54,55} that in the next event estimation calculation replaces discrete lines with histograms of width

$$\delta\mu < .1 \quad .$$

See also page 2-104.

7. Probability Tables for the Unresolved Resonance Range

Within the unresolved resonance range (e.g., in ENDF/B-VI, 2.25 - 25 keV for ²³⁵U, 10 - 149.03 keV for ²³⁸U, and 2.5 - 30 keV for ²³⁹Pu), continuous-energy neutron cross sections appear to be smooth functions of energy. This behavior occurs not because of the absence of resonances, but rather because the resonances are so close together that they are unresolved. Furthermore, the smoothly-varying cross sections do not account for resonance self-shielding effects, which may be significant for systems whose spectra peak in or near the unresolved resonance range.

Fortunately, the resonance self-shielding effects can be represented accurately in terms of probabilities based on a stratified sampling technique. This technique produces tables of probabilities for the cross sections in the unresolved resonance range. Sampling the cross section in a random walk from these probability tables is a valid physics approximation so long as the average energy loss in a single collision is much greater than the average width of a resonance; that is, if the narrow resonance approximation⁵⁶ is valid. Then the detail in the resonance structure following a collision is statistically independent of the magnitude of the cross sections prior to the collision.

The utilization of probability tables is not a new idea in Monte Carlo applications. A code⁵⁷ to calculate such tables for Monte Carlo fast reactor applications was utilized in the early 1970s. Temperature-difference Monte Carlo calculations⁵⁸ and a summary of the VIM Monte Carlo code⁵⁹ that uses probability tables are pertinent early examples. Versions of MCNP up through and including 4B did not take full advantage of the unresolved resonance data provided by evaluators. Instead, smoothly varying average cross sections were used in the unresolved range. As a result, any neutron self-shielding effects in this energy range were unaccounted for. Better utilizations of unresolved data have been known and demonstrated for some time, and the probability table treatment has been incorporated⁶⁰ into MCNP Version 4C and its successors. The column “UR” in Table G.2 of Appendix G lists whether unresolved resonance probability table data is available for each nuclide library.

Sampling cross sections from probability tables is straightforward. At each of a number of incident energies there is a table of cumulative probabilities (typically 20) and the value of the near-total, elastic, fission, and radiative capture cross sections and heat deposition numbers corresponding to those probabilities. These data supplement the usual continuous data; if probability tables are turned off (PHYS:N card), then the usual smooth cross section is used. But if the probability tables are turned on (default), if they exist for the nuclide of a collision, and if the energy of the collision is in the unresolved resonance energy range of the probability tables, then the cross sections are sampled from the tables. The near-total is the total of the elastic, fission, and radiative capture cross sections; it is not the total cross section, which may include other absorption or inelastic scatter in addition to the near-total. The radiative capture cross section is not the same as the usual MCNP capture cross section, which is more properly called “destruction” or absorption and includes not only radiative capture but all other reactions not emitting a neutron. Sometimes the probability tables are provided as factors (multipliers of the average or underlying smooth cross section) which adds computational complexity but now includes any structure in the underlying smooth cross section.

It is essential to maintain correlations in the random walk when using probability tables to properly model resonance self-shielding. Suppose we sample the 17th level (probability) from the table for a given collision. This position in the probability table must be maintained for the neutron trajectory until the next collision, regardless of particle splitting for variance reduction or surface crossings into various other materials whose nuclides may or may not have probability table data. Correlation must also be retained in the unresolved energy range when two or more cross-section sets for an isotope that utilize probability tables are at different temperatures.

The impact of the probability-table approach has been studied⁷¹ and found to have negligible impact for most fast and thermal systems. Small but significant changes in reactivity may be observed for plutonium and ²³³U systems, depending upon the detailed shape of the spectrum. However, the probability-table method can produce substantial increases in reactivity for systems that include large amounts of ²³⁸U and have high fluxes within the unresolved resonance region. Calculations for such systems will produce significantly *nonconservative* results unless the probability-table method is employed.

D. Photon Interactions

Sampling of a collision nuclide, analog capture, implicit capture, and many other aspects of photon interactions such as variance reduction, are the same as for neutrons. The collision physics are completely different.

MCNP has two photon interaction models: simple and detailed.

The simple physics treatment ignores coherent (Thomson) scattering and fluorescent photons from photoelectric absorption. It is intended for high-energy photon problems or problems where electrons are free and is also important for next event estimators such as point detectors, where scattering can be nearly straight ahead with coherent scatter. The simple physics treatment uses implicit capture unless overridden with the CUT:P card, in which case it uses analog capture.

The detailed physics treatment includes coherent (Thomson) scattering and accounts for fluorescent photons after photoelectric absorption. Form factors and Compton profiles are used to account for electron binding effects. Analog capture is always used. The detailed physics treatment is used below energy EMCPF on the PHYS:P card, and because the default value of EMCPF is 100 MeV, that means it is almost always used by default. It is the best treatment for most applications, particularly for high Z nuclides or deep penetration problems.

The generation of electrons from photons is handled three ways. These three ways are the same for both the simple and detailed photon physics treatments. (1) If electron transport is turned on (Mode P E), then all photon collisions except coherent scatter can create electrons that are banked for later transport. (2) If electron transport is turned off (no E on the Mode card), then a thick-target bremsstrahlung model (TTB) is used. This model generates electrons, but assumes that they are locally slowed to rest. Any bremsstrahlung photons produced by the nontransported electrons are then banked for later transport. Thus electron-induced photons are not neglected, but the expensive electron transport step is omitted. (The TTB production model contains many approximations compared to models used in actual electron transport. In particular, the bremsstrahlung photons inherit the direction of the parent electron.) (3) If IDES = 1 on the PHYS:P card, then all electron production is turned off, no electron-induced photons are created, and all electron energy is assumed to be locally deposited.

The TTB approximation is the default for MODE P problems. In MODE P E problems, it plays a role when the energy cutoff for electrons is greater than that for photons. In this case, the TTB model is used in the terminal processing of the electrons to account for the few low-energy bremsstrahlung photons that would be produced at the end of the electrons' range.

1. Simple Physics Treatment

The simple physics treatment is intended primarily for higher energy photons. It is inadequate for high Z nuclides or deep penetration problems. The physical processes treated are photoelectric effect, pair production, Compton scattering from free electrons, and (optionally) photonuclear interactions (described on page 2–64). The photoelectric effect is regarded as an absorption (without fluorescence). The kinematics of Compton scattering is assumed to be with free electrons (without the use of form factors or Compton profiles). The total scattering cross section, however,

includes the incoherent scattering factor regardless of the use of simple or detailed physics. Thus, strict comparisons with codes using only the Klein-Nishina differential cross section are not valid. Highly forward coherent Thomson scattering is ignored. Thus the total cross section σ_t is regarded as the sum of three components:

$$\sigma_t = \sigma_{pe} + \sigma_{pp} + \sigma_s \quad .$$

a. Photoelectric effect: This is treated as a pure absorption by implicit capture with a corresponding reduction in the photon weight WGT , and hence does not result in the loss of a particle history except for Russian roulette played on the weight cutoff. The noncaptured weight $WGT(1 - \sigma_{pe}/\sigma_t)$ is then forced to undergo either pair production or Compton scattering. The captured weight either is assumed to be locally deposited or becomes a photoelectron for electron transport or for the TTB approximation.

b. Pair production: In a collision resulting in pair production [probability $\sigma_{pp}/(\sigma_t - \sigma_{pe})$], either an electron-positron pair is created for further transport (or the TTB treatment) and the photon disappears, or it is assumed that the kinetic energy $WGT(E - 1.022)$ MeV of the electron-positron pair produced is deposited as thermal energy at the time and point of collision, with isotropic production of one photon of energy 0.511 MeV headed in one direction and another photon of energy 0.511 MeV headed in the opposite direction. The rare single 1.022-MeV annihilation photon is ignored. The relatively unimportant triplet production process is also ignored. The simple physics treatment for pair production is the same as the detailed physics treatment that is described in detail below.

c. Compton scattering: The alternative to pair production is Compton scattering on a free electron, with probability $\sigma_s/(\sigma_t - \sigma_{pe})$. In the event of such a collision, the objective is to determine the energy E' of the scattered photon, and $\mu = \cos\theta$ for the angle θ of deflection from the line of flight. This yields at once the energy $WGT(E - E')$ deposited at the point of collision and the new direction of the scattered photon. The energy deposited at the point of collision can then be used to make a Compton recoil electron for further transport or for the TTB approximation.

The differential cross section for the process is given by the Klein-Nishina formula¹

$$K(\alpha, \mu)d\mu = \pi r_o^2 \left(\frac{\alpha'}{\alpha} \right)^2 \left[\frac{\alpha'}{\alpha} + \frac{\alpha}{\alpha'} + \mu^2 - 1 \right] d\mu \quad , \quad (2.5)$$

where r_o is the classical electron radius 2.817938×10^{-13} cm, α and α' are the incident and final photon energies in units of 0.511 MeV [$\alpha = E/(mc^2)$, where m is the mass of the electron and c is the speed of light], and $\alpha' = \alpha/[1 + \alpha(1 - \mu)]$.

The Compton scattering process is sampled exactly by Kahn's method⁷² below 1.5 MeV and by Koblinger's method⁷³ above 1.5 MeV as analyzed and recommended by Blomquist and Gelbard.⁷⁴

For next event estimators such as detectors and DXTRAN, the probability density for scattering toward the detector point must be calculated:

$$p(\mu) = \frac{1}{\sigma_1^K(Z, \alpha)} K(\alpha, \mu) ,$$

where $\sigma_1^K(Z, \alpha)$ is the total Klein-Nishina cross section obtained by integrating $K(\alpha, \mu)$ over all angles for energy α . This is a difficult integration, so the empirical formula of Hastings² is used:

$$\sigma_1^K(Z, \alpha) = \pi r_o^2 \frac{c_1 \eta^2 + c_2 \eta + c_3}{\eta^3 + d_1 \eta^2 + d_2 \eta + d_3} ,$$

where $\eta = 1 + .222037a$, $c1 = 1.651035$, $c2 = 9.340220$, $c3 = -8.325004$, $d1 = 12.501332$, $d2 = -14.200407$, and $d3 = 1.699075$. Thus,

$$p(\mu) = \frac{\eta^3 + d_1 \eta^2 + d_2 \eta + d_3}{c_1 \eta^2 + c_2 \eta + c_3} \left(\frac{\alpha'}{\alpha} \right)^2 \left(\frac{\alpha}{\alpha'} + \frac{\alpha'}{\alpha} + \mu^2 - 1 \right) .$$

Above 100 MeV, where the Hastings fit is no longer valid, the approximation

$$\sigma_1^K(Z, \alpha) = \sigma_1(Z, \alpha)/Z$$

is made so that

$$p(\mu) = \frac{Z \pi r_o^2}{\sigma_1(Z, \alpha)} \left(\frac{\alpha'}{\alpha} \right)^2 \left(\frac{\alpha}{\alpha'} + \frac{\alpha'}{\alpha} + \mu^2 - 1 \right) .$$

2. Detailed Physics Treatment

The detailed physics treatment includes coherent (Thomson) scattering and accounts for fluorescent photons after photoelectric absorption. Again, photonuclear interactions may (optionally) be included (see page 2–64). Form factors are used with coherent and incoherent scattering to account for electron binding effects. Photo-neutron reactions can also be included for select isotopes. Analog capture is always used, as described below under photoelectric effect. The detailed physics treatment is used below energy EMCPF on the PHYS:P card, and because the default value of EMCPF is 100 MeV, that means it is almost always used by default. It is the best treatment for most applications, particularly for high Z nuclides or deep penetration problems.

The detailed physics treatment for next event estimators such as point detectors is inadvisable, as explained on page 2–64, unless the NOCOH=1 option is used on the PHYS:P card to turn off coherent scattering.

a. Incoherent (Compton) Scattering: To model Compton scattering it is necessary to determine the angle θ of scattering from the incident line of flight (and thus the new direction), the new energy E' of the photon, and the recoil kinetic energy of the electron, $E - E'$. The recoil kinetic energy can be deposited locally, can be transported in Mode P E problems, or (default) can be treated with the TTB approximation.

Incoherent scattering is assumed to have the differential cross section

$\sigma_I(Z, \alpha, \mu)d\mu = I(Z, \nu)K(\alpha, \mu)d\mu$, where $I(Z, \nu)$ is an appropriate scattering factor modifying the Klein-Nishina cross section in Eq. (2.2).

Qualitatively, the effect of $I(Z, \nu)$ is to decrease the Klein-Nishina cross section (per electron) more extremely in the forward direction, for low E and for high Z independently. For any Z , $I(Z, \nu)$ increases from $I(Z, 0) = 0$ to $I(Z, \infty) = Z$. The parameter ν is the inverse length $\nu = \sin(\theta/2)/\lambda = \kappa\alpha\sqrt{1-\mu}$ where $\kappa = 10^{-8}m_o c/(h\sqrt{2}) = 29.1445\text{cm}^{-1}$. The maximum value of ν is $\nu_{max} = \kappa\alpha\sqrt{2} = 41.2166\alpha$ at $\mu = -1$. The essential features of $I(Z, \nu)$ are indicated in Figure 2-5.

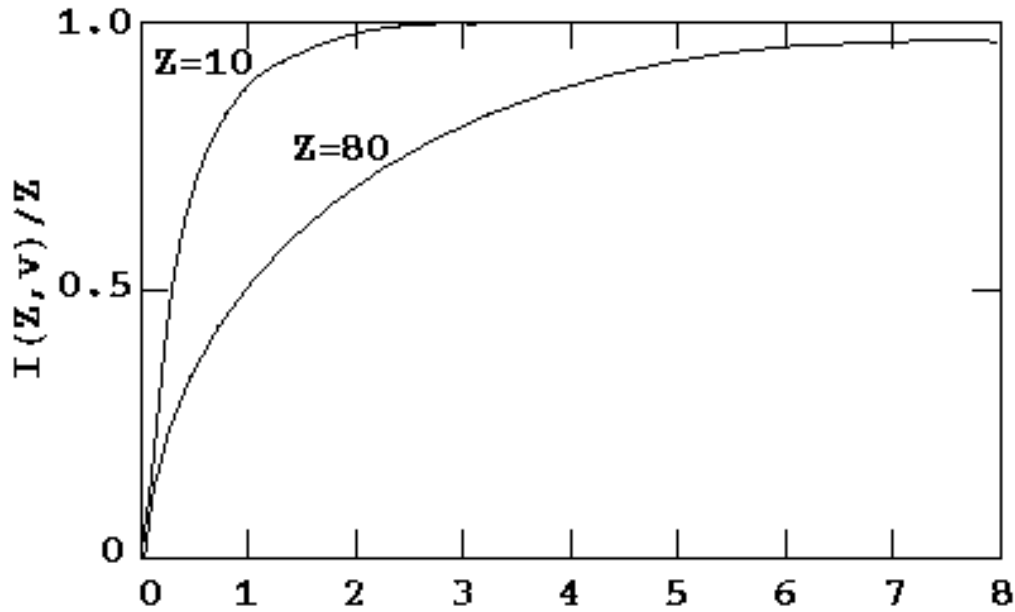


Figure 2-5

For hydrogen, an exact expression for the form factor is used:⁷⁵

$$I(1, \nu) = 1 - \frac{1}{\left(1 + \frac{1}{2}f^2\nu^2\right)^4},$$

where f is the inverse fine structure constant, $f = 137.0393$, and $f/\sqrt{2} = 96.9014$.

The Klein-Nishina formula is sampled exactly by Kahn's method⁷² below 1.5 MeV and by Koblinger's method⁷³ above 1.5 MeV as analyzed and recommended by Blomquist and Gelbard.⁷⁴ The outgoing energy E' and angle μ are rejected according to the form factors.

For next event estimators such as detectors and DXTRAN, the probability density for scattering toward the detector point must be calculated:

$$p(\mu) = \frac{1}{\sigma_1(Z, \alpha)} I(Z, \nu) K(\alpha, \mu) = \frac{\pi r_o^2}{\sigma_1(Z, \alpha)} I(Z, \nu) \left(\frac{\alpha'}{\alpha} \right)^2 \left(\frac{\alpha}{\alpha'} + \frac{\alpha'}{\alpha} + \mu^2 - 1 \right) .$$

where $\pi r_o^2 = 2494351$ and $\sigma_1(Z, \alpha)$ and $I(Z, \nu)$ are looked up in the data library.

The new energy, E' , of the photon accounts for the effects of a bound electron. The electron binding effect on the scattered photon's energy distribution appears as a broadening of the energy spectrum due to the precollision momentum of the electron. This effect on the energy distribution of the incoherently scattered photon is called Doppler broadening.

The Hartree-Fock Compton profiles, $J(p_z)$, are used to account for the effects of a bound electron on the energy distribution of the scattered photon. These Compton profiles are a collection of orbital and total atom data tabulated as a function of the projected precollision momentum of the electron. Values of the Compton profiles for the elements are published in tabular form by Biggs, et al.³⁷ as a function of p_z .

The scattered energy of a Doppler broadened photon can be calculated by selecting an orbital shell, sampling the projected momentum from the Compton profile, and calculating the scattered photon energy, E' , from:

$$p_z = -137 \frac{E - E' - EE'(1 - \cos(\theta))/mc^2}{\sqrt{E^2 + E'^2 - 2EE' \cos(\theta)}}$$

The Compton profiles are related to the incoherent scattering function, $I(Z, \nu)$ by:

$$I(Z, \nu) = \sum_k \int_{-\infty}^{p_z^{max}} J_k(p_z, Z) dp_z$$

where k refers to the particular electron subshell, $J_k(p_z, Z)$ is the Compton profile of the k^{th} shell for a given element, and p_z^{max} is the maximum momentum transferred and is calculated using $E' = E - E_{binding}$.

b. Coherent (Thomson) Scattering: Thomson scattering involves no energy loss, and thus is the only photon process that cannot produce electrons for further transport and that cannot use the TTB approximation. Only the scattering angle θ is computed, and then the transport of the photon continues.

The differential cross section is $\sigma_2(Z, \alpha, \mu) d\mu = C^2(Z, \nu) T(\mu) d\mu$, where $C(Z, \nu)$ is a form factor modifying the energy-independent Thomson cross section $T(\mu) = \pi r_o^2 (1 + \mu^2) d\mu$.

The general effect of $C^2(Z, \nu)/Z^2$ is to decrease the Thomson cross section more extremely for backward scattering, for high E , and low Z . This effect is opposite in these respects to the effect of

$I(Z, \nu)/Z$ on $K(\alpha, \mu)$ in incoherent (Compton) scattering. For a given Z , $C(Z, \nu)$ decreases from $C(Z, 0) = Z$ to $C(Z, \infty) = 0$. For example, $C(Z, \nu)$ is a rapidly decreasing function of μ as μ varies from +1 to -1, and therefore the coherent cross section is peaked in the forward direction. At high energies of the incoming photon, coherent scattering is strongly forward and can be ignored. The parameter ν is the inverse length $\nu = \sin(\theta/2)/\lambda = \kappa\alpha\sqrt{1-\mu}$, where $\kappa = 10^{-8} m_o c / (h\sqrt{2}) = 29.1445 \text{ cm}^{-1}$. The maximum value of ν is $\nu_{\max} = \kappa\alpha\sqrt{2} = 41.2166\alpha$ at $\mu = -1$. The square of the maximum value is $\nu_{\max}^2 = 1698.8038\alpha^2$. The qualitative features of $C(Z, \nu)$ are shown in Figure 2-6.

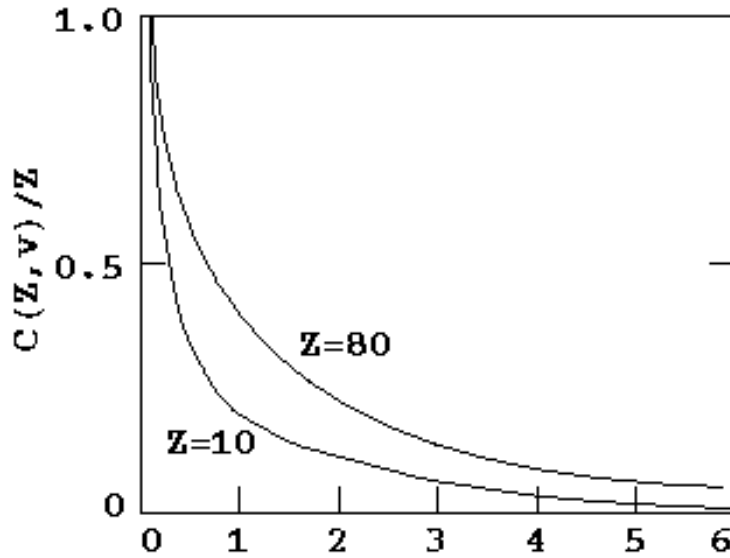


Figure 2-6

For next event estimators, one must evaluate the probability density function

$p(\mu) = \pi r_0^2 (1 + \mu^2) C^2(Z, \nu) / \sigma_2(Z, \alpha)$ for given μ . Here $\sigma_2(Z, \alpha)$ is the integrated coherent cross section. The value of $C^2(Z, \nu)$ at $\nu = \kappa\alpha\sqrt{1-\mu}$ must be interpolated in the original $C^2(Z, \nu_i)$ tables separately stored on the cross-section library for this purpose.

Note that at high energies, coherent scattering is virtually straight ahead with no energy loss; thus, it appears from a transport viewpoint that no scattering took place. For a point detector to sample this scattering, the point must lie on the original track ($\mu \cong 1$), which is seldom the case. Thus, photon point detector variances generally will be much greater with detailed photon physics than with simple physics unless coherent scattering is turned off with $\text{NOCOH} = 1$ on the PHYS:P card, as explained on page 2-64.

c. Photoelectric effect: The photoelectric effect consists of the absorption of the incident photon of energy E , with the consequent emission of several fluorescent photons and the ejection (or excitation) of an orbital electron of binding energy $e < E$, giving the electron a kinetic energy of $E - e$. Zero, one, or two fluorescent photons are emitted. These three cases are now described.

(1) Zero photons greater than 1 keV are emitted. In this event, the cascade of electrons that fills up the orbital vacancy left by the photoelectric ejection produces electrons and low-energy photons (Auger effect). These particles can be followed in Mode P E problems, or be treated with the TTB approximation, or be assumed to deposit energy locally. Because no photons are emitted by fluorescence (some may be produced by electron transport or the TTB model), the photon track is terminated. This photoelectric “capture” of the photon is scored like analog capture in the summary table of the output file. Implicit capture is not possible.

(2) One fluorescent photon of energy greater than 1 keV is emitted. The photon energy E' is the difference in incident photon energy E , less the ejected electron kinetic energy $E - e$, less a residual excitation energy e' that is ultimately dissipated by further Auger processes. This dissipation leads to additional electrons or photons of still lower energy. The ejected electron and any Auger electrons can be transported or treated with the TTB approximation. In general,

$$E' = E - (E - e) - e' = e - e'.$$

These primary transactions are taken to have the full fluorescent yield from all possible upper levels e' , but are apportioned among the x-ray lines $K\alpha_1$, ($L_3 \rightarrow K$); $K\alpha_2$, ($L_2 \rightarrow K$); $K\beta'_1$, (mean $M \rightarrow K$); and $K\beta'_2$, (mean $N \rightarrow K$).

(3) Two fluorescence photons can occur if the residual excitation e' of process (2) exceeds 1 keV. An electron of binding energy e'' can fill the orbit of binding energy e' , emitting a second fluorescent photon of energy $E'' = e' - e''$. As before, the residual excitation e'' is dissipated by further Auger events and electron production that can be modeled with electron transport in Mode P E calculations, approximated with the TTB model, or assumed to deposit all energy locally. These secondary transitions come from all upper shells and go to L shells. Thus the primary transitions must be $K\alpha_1$ or $K\alpha_2$ to leave an L shell vacancy.

Each fluorescent photon born as discussed above is assumed to be emitted isotropically and can be transported, provided that $E', E'' > 1 \text{ keV}$. The binding energies e , e' , and e'' are very nearly the x-ray absorption edges because the x-ray absorption cross section takes an abrupt jump as it becomes energetically possible to eject (or excite) the electron of energy first $E \cong e''$, then e' , then e , etc. The jump can be as much as a factor of 20 (for example, K-carbon).

A photoelectric event is terminal for elements $Z < 12$ because the possible fluorescence energy is below 1 keV. The event is only a single fluorescence of energy above 1 keV for $31 > Z \geq 12$, but double fluorescence (each above 1 keV) is possible for $Z \geq 31$. For $Z \geq 31$, primary lines $K\alpha_1$, $K\alpha_2$, and $K\beta'_1$ are possible and, in addition, for $Z \geq 37$, the $K\beta'_2$ line is possible.

In all photoelectric cases where the photon track is terminated because either no fluorescent photons are emitted or the ones emitted are below the energy cutoff, the termination is considered to be caused by analog capture in the output file summary table (and not energy cutoff).

d. Pair Production: This process is considered only in the field of a nucleus. The threshold is $2mc^2[1 + (m/M)] \cong 1.022 \text{ MeV}$, where M is the nuclear mass and m is the mass of the electron. There are three cases:

(1) In the case of electron transport (Mode P E), the electron and positron are created and banked and the photon track terminates.

(2) For Mode P problems with the TTB approximation, both an electron and positron are produced but not transported. Both particles can make TTB approximation photons. The positron is then considered to be annihilated locally and a photon pair is created as in case (3).

(3) For Mode P problems when positrons are not created by the TTB approximation, the incident photon of energy E vanishes. The kinetic energy of the created positron/electron pair, assumed to be $E - 2mc^2$, is deposited locally at the collision point. The positron is considered to be annihilated with an electron at the point of collision, resulting in a pair of photons, each with the incoming photon weight, and each with an energy of $mc^2 = 0.511$ MeV. The first photon is emitted isotropically, and the second is emitted in the opposite direction. The very rare single-annihilation photon of 1.022 MeV is ignored.

e. Caution for detectors and coherent scattering: The use of the detailed photon physics treatment is not recommended for photon next event estimators (such as point detectors and ring detectors) nor for DXTRAN, unless coherent scatter is turned off with the NOCOH = 1 option on the PHYS:P card. Alternatively, the simple physics treatment (EMCPF < .001 on the PHYS:P card) can be used. Turning off coherent scattering can improve the figure of merit (see page 2–116) by more than a factor of 10 for tallies with small relative errors because coherent scattering is highly peaked in the forward direction. Consequently, coherent scattering becomes undersampled because the photon must be traveling directly at the detector point and undergo a coherent scattering event. When the photon is traveling nearly in the direction of the point detector or the chosen point on a ring detector or DXTRAN sphere, the PSC term, $p(\mu)$, of the point detector (see page 2–91) becomes very large, causing a huge score for the event and severely affecting the tally. Remember that $p(\mu)$ is not a probability (that can be no larger than unity); it is a probability density function (the derivative of the probability) and can approach infinity for highly forward-peaked scattering. Thus the undersampled coherent scattering event is characterized by many low scores to the detector when the photon trajectory is away from the detector ($p(\mu) = \text{small}$) and a very few, very large scores ($p(\mu) = \text{huge}$) when the trajectory is nearly aimed at the detector. Such undersampled events cause a sudden increase in both the tally and the variance, a sudden drop in the figure of merit, and a failure to pass the statistical checks for the tally as described on page 2–129.

3. Photonuclear Physics Treatment

New in MCNP5, photonuclear physics may be included when handling a photon collision. A photonuclear interaction begins with the absorption of a photon by a nucleus. There are several mechanisms by which this can occur. The nuclear data files currently available focus on the energy range up to 150 MeV incident photon energy. The value of 150 MeV was chosen as this energy is just below the threshold for the production of pions and the subsequent need for much more complicated nuclear modeling. Below 150 MeV, the primary mechanisms for photoabsorption are the excitation of either the giant dipole resonance or a quasi-deuteron nucleon pair.

The giant dipole resonance (GDR) absorption mechanism can be conceptualized as the electromagnetic wave, the photon, interacting with the dipole moment of the nucleus as a whole.

This results in a collective excitation of the nucleus. It is the most likely process (that is, the largest cross section) by which photons interact with the nucleus. (Expected peak cross sections of 6-10 millibarns are seen for the light isotopes and 600-800 millibarns are not uncommon for the heavy elements. Thus, photonuclear collisions may account for a theoretical maximum of 5-6% of the photon collisions.) The GDR occurs with highest probability when the wavelength of the photon is comparable to the size of the nucleus. This typically occurs for photon energies in the range of 5-20 MeV and has a resonance width of a few MeV. For deformed nuclei, a double peak is seen due to the variation of the nuclear radius. Outside of this resonance region, the cross section for a GDR reaction becomes negligible. A more complete description of this process can be found in the text by Bohr and Mottelson.⁶¹

The quasi-deuteron (QD) absorption mechanism can be conceptualized as the electromagnetic wave interacting with the dipole moment of a correlated neutron-proton pair. In this case, the neutron-proton pair can be thought of as a QD having a dipole moment with which the photon can interact. This mechanism is not as intense as the GDR but it provides a significant background cross section for all incident photon energies above the relevant particle separation threshold. The seminal work describing this process was published by Levinger.^{62,63} Recent efforts to model this process include the work of Chadwick et al.⁶⁴

Once the photon has been absorbed by the nucleus, one or more secondary particle emissions can occur. For the energy range in question (that is, below 150 MeV) these reactions may produce a combination of gamma-rays, neutrons, protons, deuterons, tritons, helium-3 particles, alphas, and fission fragments. The threshold for the production of a given secondary particle is governed by the separation energy of that particle, typically a few MeV to as much as a few 10s of MeV. Most of these particles are emitted via pre-equilibrium and equilibrium mechanisms though it is possible, but rare, to have a direct emission.

Pre-equilibrium emission can be conceptualized as a particle within the nucleus that receives a large amount of energy from the absorption mechanism and escapes the binding force of the nucleus after at least one but very few interactions with other nuclei. (This is in contrast to a direct emission where the emission particle escapes the nucleus without any interactions.) Typically this occurs from QD absorption of the photon where the incident energy is initially split between the neutron-proton pair. Particles emitted by this process tend to be characterized by higher emission energies and forward-peaked angular distributions.

Equilibrium emission can be conceptualized as particle evaporation. This process typically occurs after the available energy has been generally distributed among the nucleons. In the classical sense, particles boil out of the nucleus as they penetrate the nuclear potential barrier. The barrier may contain contributions from coulomb potential (for charged particles) and effects of angular momentum conservation. It should be noted that for heavy elements, evaporation neutrons are emitted preferentially as they are not subject to the coulomb barrier. Particles emitted by this process tend to be characterized by isotropic angular emission and evaporation energy spectra. Several references are available on the general emission process after photoabsorption.^{65,66,67}

For all of the emission reactions discussed thus far, the nucleus will most probably be left in an excited state. It will subsequently relax to the ground state by the emission of one or more gamma-rays. The gamma-ray energies follow the well known patterns for relaxation. The only reactions

that do not produce gamma-rays are direct reactions where the photon is absorbed and all available energy is transferred to a single emission particle leaving the nucleus in the ground state.

Reactions at higher energies (above the pion production threshold) require more complete descriptions of the underlying nuclear physics. The delta resonance and other absorption mechanisms become significant and the amount of energy involved in the reaction presents the opportunity for the production of more fundamental particles. While beyond the scope of this current work, descriptions of the relevant physics may be found in the paper by Fasso et al.⁶⁸

New photonuclear data tables are used to extend the traditional photon collision routines. Because of the sparsity of photonuclear data, the user is allowed to toggle photonuclear physics on or off (with the fourth entry on the PHYS:p card) and the code defaults to off. Once turned on, the total photon cross section, photoatomic plus photonuclear (i.e. the photonuclear cross section is absent from this calculation when photonuclear physics is off), is used to determine the distance to the next photon collision. For simple physics, this implies the sum of the photoelectric, pair production, incoherent and photonuclear cross sections. Detailed physics includes the additional coherent cross section in this sum.

The toggle for turning on and off photonuclear physics is also used to select biased or unbiased photonuclear collisions. For the unbiased option, the type of collision is sampled as either photonuclear or photoatomic based on the ratio of the partial cross sections. The biased option is similar to forced collisions. At the collision site, the particle is split into two parts, one forced to undergo photoatomic interaction and the other photonuclear. The weight of each particle is adjusted by the ratio of their actual collision probability. The photoatomic sampling routines (as described in sections 1 and 2 above) are used to sample the emission characteristics for secondary electrons and photons from a photoatomic collision. The emission characteristics for secondary particles from photonuclear collisions are handled independently.

Once it has been determined that a photon will undergo a photonuclear collision, the emission particles are sampled as follows. First, the appropriate collision isotope is selected based on the ratio of the total photonuclear cross section from each relevant table. Note that photoatomic collisions are sampled from a set of elemental tables whereas photonuclear collisions are sampled from a set of isotopic tables. Next, the code computes the ratio of the production cross section to the total cross section for each secondary particle undergoing transport. Based on this ratio, an integer number of emission particles are sampled. If weight games (i.e. weight cut-offs or weight windows) are being used, these secondary particles are subjected to splitting or roulette to ensure that the sampled particles will be of an appropriate weight. The emission parameters for each secondary particle are then sampled independently from the reaction laws provided in the data. Last, tallies and summary information are appropriately updated, applicable variance reduction games are performed, and the emitted particle is banked for further transport.

Note that photonuclear physics was implemented in the traditional Monte Carlo style as a purely statistical based process. This means that photons undergoing a photonuclear interaction produce an average number of emission particles. For multiple particle emission, the particles may not be sampled from the same reaction; for example, if two neutrons are sampled, one may be from the (g,2n) distributions and the second from the (g,np) distributions. (Note that the photonuclear data use the same energy/angle distributions that have been used for neutrons and the same internal

coding for sampling. See “Nonfission Inelastic Scattering and Emission Laws” on page 2–41) This generalized particle production method is statistically correct for large sampling populations and lends itself to uncomplicated biasing schemes. It is (obviously) not microscopically correct. (It is not possible to perform microscopically correct sampling given the current set of data tables.)

Because of the low probability of a photon undergoing a photonuclear interaction, the use of biased photonuclear collisions may be necessary. However, caution should be exercised when using this option as it can lead to large variations in particle weights. It is important to check the summary tables to determine if appropriate weight cutoff or weight windows have been set. That is, check to see if weight cutoffs or weight windows are causing more particle creation and destruction than expected. It is almost always necessary to adjust the default neutron weight cutoff (when using only weight cutoffs with photonuclear biasing) as it will roulette a large fraction of the attempts to create secondary photoneutrons.

More information about the photonuclear physics included in MCNP can be found in White.^{69,70}

E. Electron Interactions

The transport of electrons and other charged particles is fundamentally different from that of neutrons and photons. The interaction of neutral particles is characterized by relatively infrequent isolated collisions, with simple free flight between collisions. By contrast, the transport of electrons is dominated by the long-range Coulomb force, resulting in large numbers of small interactions. As an example, a neutron in aluminum slowing down from 0.5 MeV to 0.0625 MeV will have about 30 collisions, while a photon in the same circumstances will experience fewer than ten. An electron accomplishing the same energy loss will undergo about 10^5 individual interactions. This great increase in computational complexity makes a single-collision Monte Carlo approach to electron transport unfeasible for most situations of practical interest.

Considerable theoretical work has been done to develop a variety of analytic and semi-analytic multiple-scattering theories for the transport of charged particles. These theories attempt to use the fundamental cross sections and the statistical nature of the transport process to predict probability distributions for significant quantities, such as energy loss and angular deflection. The most important of these theories for the algorithms in MCNP are the Goudsmit-Saunderson⁷⁶ theory for angular deflections, the Landau⁷⁷ theory of energy-loss fluctuations, and the Blunck-Leisegang⁷⁸ enhancements of the Landau theory. These theories rely on a variety of approximations that restrict their applicability, so that they cannot solve the entire transport problem. In particular, it is assumed that the energy loss is small compared to the kinetic energy of the electron.

In order to follow an electron through a significant energy loss, it is necessary to break the electron's path into many steps. These steps are chosen to be long enough to encompass many collisions (so that multiple-scattering theories are valid) but short enough that the mean energy loss in any one step is small (so that the approximations necessary for the multiple-scattering theories are satisfied). The energy loss and angular deflection of the electron during each of the steps can then be sampled from probability distributions based on the appropriate multiple-scattering theories. This accumulation of the effects of many individual collisions into single steps that are sampled probabilistically constitutes the “condensed history” Monte Carlo method.

The most influential reference for the condensed history method is the 1963 paper by Martin J. Berger.⁷⁹ Based on the techniques described in that work, Berger and Stephen M. Seltzer developed the ETRAN series of electron/photon transport codes.⁸⁰ These codes have been maintained and enhanced for many years at the National Bureau of Standards (now the National Institute of Standards and Technology). The ETRAN codes are also the basis for the Integrated TIGER Series,⁸¹ a system of general-purpose, application-oriented electron/photon transport codes developed and maintained by John A. Halbleib and his collaborators at Sandia National Laboratories in Albuquerque, New Mexico. The electron physics in MCNP is essentially that of the Integrated TIGER Series, Version 3.0. The ITS radiative and collisional stopping power and bremsstrahlung production models were integrated into MCNP 4C.

1. Electron Steps and Substeps

The condensed random walk for electrons can be considered in terms of a sequence of sets of values

$$(0, E_0, t_0, \mathbf{u}_0, \mathbf{r}_0), (s_1, E_1, t_1, \mathbf{u}_1, \mathbf{r}_1), (s_2, E_2, t_2, \mathbf{u}_2, \mathbf{r}_2), \dots$$

where s_n , E_n , t_n , \mathbf{u}_n , and \mathbf{r}_n are the total path length, energy, time, direction, and position of the electron at the end of n steps. On the average, the energy and path length are related by

$$E_{n-1} - E_n = - \int_{s_{n-1}}^{s_n} \frac{dE}{ds} ds, \quad (2.6)$$

where $-dE/ds$ is the total stopping power in energy per unit length. This quantity depends on energy and on the material in which the electron is moving. ETRAN-based codes customarily choose the sequence of path lengths $\{s_n\}$ such that

$$\frac{E_n}{E_{n-1}} = k, \quad (2.7)$$

for a constant k . The most commonly used value is $k = 2^{-1/8}$, which results in an average energy loss per step of 8.3%.

Electron steps with (energy-dependent) path lengths $s = s_n - s_{n-1}$ determined by Eqs. 2.3-2.4 are called *major steps* or *energy steps*. The condensed random walk for electrons is structured in terms of these energy steps. For example, all precalculated and tabulated data for electrons are stored on an energy grid whose consecutive energy values obey the ratio in Eq. 2.4. In addition, the Landau and Blunck-Leisegang theories for energy straggling are applied once per energy step. (But see page 2–74 below for a more detailed option.) For a single step, the angular scattering could also be calculated with satisfactory accuracy, since the Goudsmit-Saunderson theory is valid for arbitrary angular deflections. However, the representation of the electron's trajectory as the result of many small steps will be more accurate if the angular deflections are also required to be small. Therefore, the ETRAN codes and MCNP further break the electron steps into smaller substeps. A major step of path length s is divided into m substeps, each of path length s/m . Angular deflections and the production of secondary particles are sampled at the level of these substeps. The integer m depends

only on material (average atomic number Z). Appropriate values for m have been determined empirically, and range from $m = 2$ for $Z < 6$ to $m = 15$ for $Z > 91$.

In some circumstances, it may be desirable to increase the value of m for a given material. In particular, a very small material region may not accommodate enough substeps for an accurate simulation of the electron's trajectory. In such cases, the user can increase the value of m with the ESTEP option on the material card. The user can gain some insight into the selection of m by consulting Print Table 85 in the MCNP output. Among other information, this table presents a quantity called DRANGE as a function of energy. DRANGE is the size of an energy step in g/cm^2 . Therefore, DRANGE/m is the size of a substep in the same units, and if ρ is the material density in g/cm^3 , then $\text{DRANGE}/(m\rho)$ is the length of a substep in cm. This quantity can be compared with the smallest dimension of a material region. A reasonable rule of thumb is that an electron should make at least ten substeps in any material of importance to the transport problem.

2. Condensed Random Walk

In the initiation phase of a transport calculation involving electrons, all relevant data are either precalculated or read from the electron data file and processed. These data include the electron energy grid, stopping powers, electron ranges, energy step ranges, substep lengths, and probability distributions for angular deflections and the production of secondary particles. Although the energy grid and electron steps are selected according to Eqs. 2.3-2.4, energy straggling, the analog production of bremsstrahlung, and the intervention of geometric boundaries and the problem time cutoff will cause the electron's energy to depart from a simple sequence s_n satisfying Eq. 2.4. Therefore, the necessary parameters for sampling the random walk will be interpolated from the points on the energy grid.

At the beginning of each major step, the collisional energy loss rate is sampled (unless the logic described on page 2-74 is being used). In the absence of energy straggling, this will be a simple average value based on the nonradiative stopping power described in the next section. In general, however, fluctuations in the energy loss rate will occur. The number of substeps m per energy step will have been preset, either from the empirically-determined default values, or by the user, based on geometric considerations. At most m substeps will be taken in the current major step with the current value for the energy loss rate. The number of substeps may be reduced if the electron's energy falls below the boundary of the current major step, or if the electron reaches a geometric boundary. In these circumstances, or upon the completion of m substeps, a new major step is begun, and the energy loss rate is resampled.

With the possible exception of the energy loss and straggling calculations, the detailed simulation of the electron history takes place in the sampling of the substeps. The Goudsmit-Saunderson⁷⁶ theory is used to sample from the distribution of angular deflections, so that the direction of the electron can change at the end of each substep. Based on the current energy loss rate and the substep length, the projected energy for the electron at the end of the substep is calculated. Finally, appropriate probability distributions are sampled for the production of secondary particles. These include electron-induced fluorescent X-rays, "knock-on" electrons (from electron-impact ionization), and bremsstrahlung photons.

Note that the length of the substep ultimately derives from the total stopping power used in Eq. 2.3, but the projected energy loss for the substep is based on the nonradiative stopping power. The reason for this difference is that the sampling of bremsstrahlung photons is treated as an essentially analog process. When a bremsstrahlung photon is generated during a substep, the photon energy is subtracted from the projected electron energy at the end of the substep. Thus the radiative energy loss is explicitly taken into account, in contrast to the collisional (nonradiative) energy loss, which is treated probabilistically and is not correlated with the energetics of the substep. Two biasing techniques are available to modify the sampling of bremsstrahlung photons for subsequent transport. However, these biasing methods do not alter the linkage between the analog bremsstrahlung energy and the energetics of the substep.

MCNP uses identical physics for the transport of electrons and positrons, but distinguishes between them for tallying purposes, and for terminal processing. Electron and positron tracks are subject to the usual collection of terminal conditions, including escape (entering a region of zero importance), loss to time cutoff, loss to a variety of variance-reduction processes, and loss to energy cutoff. The case of energy cutoff requires special processing for positrons, which will annihilate at rest to produce two photons, each with energy $m c^2 = 0.511008$ MeV.

3. Stopping Power

a. Collisional Stopping Power

Berger⁷⁹ gives the restricted electron collisional stopping power, i.e., the energy loss per unit path length to collisions resulting in fractional energy transfers ε less than an arbitrary maximum value ε_m , in the form

$$-\left(\frac{dE}{ds}\right)_{\varepsilon_m} = NZC \left\{ \ln \frac{E^2(\tau+2)}{2I^2} + f^-(\tau, \varepsilon_m) - \delta \right\}, \quad (2.8)$$

where

$$\begin{aligned} f^-(\tau, \varepsilon_m) = & -1 - \beta^2 + \left(\frac{\tau}{\tau+1}\right)^2 \frac{\varepsilon_m^2}{2} + \frac{2\tau+1}{(\tau+1)^2} \ln(1 - \varepsilon_m) \\ & + \ln[4\varepsilon_m(1 - \varepsilon_m)] + \frac{1}{1 - \varepsilon_m}. \end{aligned} \quad (2.9)$$

Here ε and ε_m represent energy transfers as fractions of the electron kinetic energy E ; I is the mean ionization potential in the same units as E ; β is v/c ; τ is the electron kinetic energy in units of the electron rest mass; δ is the density effect correction (related to the polarization of the medium); Z is the average atomic number of the medium; N is the atom density of the medium in cm^{-3} ; and the coefficient C is given by

$$C = \frac{2\pi e^4}{mv^2}, \quad (2.10)$$

where m , e , and v are the rest mass, charge, and speed of the electron, respectively. The density effect correction δ is calculated using the prescriptions of Sternheimer, Berger and Seltzer⁸² when using data from the el03 library and using the method of Sternheimer and Peierls⁸³ when using data from the el library.

The ETRAN codes and MCNP do not make use of restricted stopping powers, but rather treat all collisional events in an uncorrelated, probabilistic way. Thus, only the total energy loss to collisions is needed, and Eqs. 2.5–2.6 can be evaluated for the special value $\varepsilon_m = 1/2$. The reason for the $1/2$ is the indistinguishability of the two outgoing electrons. The electron with the larger energy is, by definition, the primary. Therefore, only the range $\varepsilon < 1/2$ is of interest. With $\varepsilon_m = 1/2$, Eq. 2.6 becomes

$$f^-(\tau, \varepsilon_m) = -\beta^2 + (1 - \ln 2) + \left(\frac{1}{8} + \ln 2\right) \left(\frac{\tau}{\tau + 1}\right)^2. \quad (2.11)$$

On the right side of Eq. 2.5, we can express both E and I in units of the electron rest mass. Then E can be replaced by τ on the right side of the equation. We also introduce supplementary constants

$$\begin{aligned} C2 &= \ln(2I^2), \\ C3 &= 1 - \ln 2, \\ C4 &= \frac{1}{8} + \ln 2, \end{aligned} \quad (2.12)$$

so that Eq. 2.5 becomes

$$-\left(\frac{dE}{ds}\right) = NZ \frac{2\pi e^4}{mv^2} \left\{ \ln[\tau^2(\tau + 2)] - C2 + C3 - \beta^2 + C4 \left(\frac{\tau}{\tau + 1}\right)^2 - \delta \right\} \quad (2.13)$$

This is the collisional energy loss rate in MeV/cm in a particular medium. In MCNP, we are actually interested in the energy loss rate in units of MeV barns (so that different cells containing the same material need not have the same density). Therefore, we divide Eq. 2.10 by N and multiply by the conversion factor 10^{24} barns/cm². We also use the definition of the fine structure constant

$$\alpha = \frac{2\pi e^2}{hc},$$

where h is Planck's constant, to eliminate the electronic charge e from Eq. 2.10. The result is as follows:

$$-\left(\frac{dE}{ds}\right) = \frac{10^{24} \alpha^2 h^2 c^2}{2\pi m c^2} Z \left\{ \ln[\tau^2(\tau + 2)] - C2 + C3 - \beta^2 + C4 \left(\frac{\tau}{\tau + 1}\right)^2 - \delta \right\} \frac{1}{\beta^2} \quad (2.14)$$

This is the form actually used in MCNP to preset the collisional stopping powers at the energy boundaries of the major energy steps.

The mean ionization potential and density effect correction depend upon the state of the material, either gas or solid. In the fit of Sternheimer and Peierls⁸³ the physical state of the material also modifies the density effect calculation. In the Sternheimer, Berger and Seltzer⁸² treatment, the calculation of the density effect uses the conduction state of the material to determine the contribution of the outermost conduction electron to the ionization potential. The occupation numbers and atomic binding energies used in the calculation are from Carlson.⁸⁴

b. Radiative Stopping Power

The radiative stopping power is

$$-\left. \frac{dE}{ds} \right|_{rad} = 10^{24} Z(Z + \bar{\eta})(\alpha r_e^2)(T + mc^2)\Phi_{rad}^{(n)}$$

where $\Phi_{rad}^{(n)}$ is the scaled electron-nucleus radiative energy-loss cross section based upon evaluations by Berger and Seltzer for data from either the el or the el03 library (details of the numerical values of the data on the el03 library can be found in Refs. 85, 86, and 87; $\bar{\eta}$ is a parameter to account for the effect of electron-electron bremsstrahlung (it is unity when using data from the el library and, when using data from the el03 library, it is based upon the work of S. Seltzer and M. Berger^{85,86,87} and can be different from unity); α is the fine structure constant; mc^2 is the mass energy of an electron; and r_e is the classical electron radius. The dimensions of the radiative stopping power are the same as the collisional stopping power.

4. Energy Straggling

Because an energy step represents the cumulative effect of many individual random collisions, fluctuations in the energy loss rate will occur. Thus the energy loss will not be a simple average Δ ; rather there will be a probability distribution $f(s, \Delta) d\Delta$ from which the energy loss Δ for the step of length s can be sampled. Landau⁷⁷ studied this situation under the simplifying assumptions that the mean energy loss for a step is small compared with the electron's energy, that the energy parameter ξ defined below is large compared with the mean excitation energy of the medium, that the energy loss can be adequately computed from the Rutherford⁸⁸ cross section, and that the formal upper limit of energy loss can be extended to infinity. With these simplifications, Landau found that the energy loss distribution can be expressed as

$$f(s, \Delta) d\Delta = \phi(\lambda) d\lambda$$

in terms of $\phi(\lambda)$, a universal function of a single scaled variable

$$\lambda = \frac{\Delta}{\xi} - \ln \left[\frac{2\xi m v^2}{(1 - \beta^2) I^2} \right] + \delta + \beta^2 - 1 + \gamma \cdot$$

Here m and v are the mass and speed of the electron, δ is the density effect correction, β is v/c , I is the mean excitation energy of the medium, and γ is Euler's constant ($\gamma = 0.5772157\dots$). The parameter ξ is defined by

$$\xi = \frac{2\pi e^4 N Z}{m v^2} s ,$$

where e is the charge of the electron and $N Z$ is the number density of atomic electrons, and the universal function is

$$\phi(\lambda) = \frac{1}{2\pi i} \int_{x-i\infty}^{x+i\infty} e^{\mu \ln \mu + \lambda \mu} d\mu ,$$

where x is a positive real number specifying the line of integration.

For purposes of sampling, $\phi(\lambda)$ is negligible for $\lambda < -4$, so that this range is ignored. Börsch-Supan⁸⁹ originally tabulated $\phi(\lambda)$ in the range $-4 \leq \lambda \leq 100$, and derived for the range $\lambda > 100$ the asymptotic form

$$\phi(\lambda) \approx \frac{1}{w^2 + \pi^2} ,$$

in terms of the auxiliary variable w , where

$$\lambda = w + \ln w + \gamma - \frac{3}{2} .$$

Recent extensions⁹⁰ of Börsch-Supan's tabulation have provided a representation of the function in the range $-4 \leq \lambda \leq 100$ in the form of five thousand equally probable bins in λ . In MCNP, the boundaries of these bins are saved in the array **eqbm(mlam)**, where **mlam** = 5001. Sampling from this tabular distribution accounts for approximately 98.96% of the cumulative probability for $\phi(\lambda)$. For the remaining large- λ tail of the distribution, MCNP uses the approximate form $\phi(\lambda) \approx w^{-2}$, which is easier to sample than $(w^2 + \pi^2)^{-1}$, but is still quite accurate for $\lambda > 100$.

Blunck and Leisegang⁷⁸ have extended Landau's result to include the second moment of the expansion of the cross section. Their result can be expressed as a convolution of Landau's distribution with a Gaussian distribution:

$$f^*(s, \Delta) = \frac{1}{\sqrt{2\pi}\sigma} \int_{-\infty}^{+\infty} f(s, \Delta') \exp\left[-\frac{(\Delta - \Delta')^2}{2\sigma^2}\right] d\Delta' .$$

Blunck and Westphal⁹¹ provided a simple form for the variance of the Gaussian:

$$\sigma_{BW}^2 = 10eV \cdot Z^{4/3} \bar{\Delta} .$$

Subsequently, Chechin and Ermilova⁹² investigated the Landau/Blunck-Leisegang theory, and derived an estimate for the relative error

$$\varepsilon_{CE} \approx \left[\frac{10\xi}{I} \left(1 + \frac{\xi}{10I} \right)^3 \right]^{-\frac{1}{2}}$$

caused by the neglect of higher-order moments. Based on this work, Seltzer⁹³ describes and recommends a correction to the Blunck-Westphal variance:

$$\sigma = \frac{\sigma_{BW}}{1 + 3\varepsilon_{CE}} .$$

This value for the variance of the Gaussian is used in MCNP.

Examination of the asymptotic form for $\phi(\lambda)$ shows that unrestricted sampling of λ will not result in a finite mean energy loss. Therefore, a material- and energy-dependent cutoff λ_c is imposed on the sampling of λ . In the initiation phase of an MCNP calculation, the code makes use of two preset arrays, **flam**(**mlanc**) and **avlm**(**mlanc**), with **mlanc** = 1591. The array **flam** contains candidate values for λ_c in the range $-4 \leq \lambda_c \leq 50000$; the array **avlm** contains the corresponding expected mean values for the sampling of λ . For each material and electron energy, the code uses the known mean collisional energy loss Δ , interpolating in this tabular function to select a suitable value for λ_c , which is then stored in the dynamically-allocated array **flc**. During the transport phase of the calculation, the value of **flc** applicable to the current material and electron energy is used as an upper limit, and any sampled value of λ greater than the limit is rejected. In this way, the correct mean energy loss is preserved.

5. Logic for Sampling Energy Straggling

The Landau theory described in the previous section provides an energy-loss distribution determined by the energy E of the electron, the path-length s to be traversed, and the properties of the material. Let us symbolize a sampling of this distribution as an application of a straggling operator $L(E, s, \Delta)$ that provides a sampled value of the energy loss Δ . In versions of MCNP earlier than MCNP5, release 1.40, all parameters needed for sampling straggling were precomputed and associated with the standard energy boundaries E_n and the corresponding ranges s_n . In effect the code was restricted to calculations based on discrete arguments of the operator $L(E_n, s_n, \bar{\Delta}_n)$. As a result, the proper assignment of an electron transport step to an energy group n required a rather subtle logic. Eventually, two algorithms for apportioning straggled energy loss to electron substeps were made available. With release 1.40, a third algorithm is provided, as discussed below.

a. MCNP Energy Indexing Algorithm

The first energy indexing algorithm (also called the "bin-centered" treatment) developed for MCNP is arguably the less successful of the two existing algorithms, but for historical reasons

remains the default option. It was an attempt to keep the electron substeps aligned as closely as possible with the energy groups that were used for their straggling samples. A simplified description of the MCNP algorithm is as follows. An electron of energy E is assigned to the group n such that $E_n > E \geq E_{n+1}$. A straggled energy loss Δ is sampled from $L(E_n, s_n, \bar{\Delta}_n)$. The electron attempts to traverse m substeps, each of which is assigned the energy loss Δ/m . If m substeps are completed, the process starts over with the assignment of a new energy group. However, if the electron crosses a cell boundary, or if the electron energy falls below the current group, the loop over m is abandoned, even if fewer than m substeps have been completed, and the energy group is reassigned.

Since the straggling parameters are pre-computed at the midpoints of the energy groups, this algorithm does succeed in assigning to each substep a straggled energy loss based on parameters that are as close as possible to the beginning energy of the substep. However, there are two problems with the current MCNP approach. First, there is a high probability that the electron will not actually complete the expected range s_n for which the energy loss was sampled, in which case the energy loss relies on a linear interpolation in a theory that is clearly nonlinear. Second, the final substep of each sequence using the sampled energy loss from $L(E_n, s_n, \bar{\Delta}_n)$ will frequently fall partially in the next-lower energy group $n + 1$, but no substep using the sample from $L(E_n, s_n, \bar{\Delta}_n)$ will ever be partially in the higher group $n - 1$. This results in a small, but potentially significant systematic error. (See for example the investigations of Schaart et al.⁹⁴ and references therein.)

b. ITS Energy Indexing Algorithm

Developed for the ITS codes earlier than the MCNP algorithm, this method (also called the "nearest-group-boundary" treatment) was added to the MCNP code in order to explore some of the energy-dependent artifacts of the condensed history approach, and in order to offer more consistency with the TIGER Series codes. This algorithm differs from the default treatment in two ways. First, the electron is initially assigned to a group n such that

$$(E_{n-1} + E_n)/2 > E \geq (E_n + E_{n+1})/2.$$

In other words, the electron is assigned to the group whose upper limit is closest to the electron's energy. Second, although the electron will be reassigned when it enters a new geometric cell, it will not be reassigned merely for falling out of the current energy group. These differences serve to reduce the number of times that unwanted imposition of linear interpolation on partial steps occurs, and to allow more equal numbers of excursions above and below the energy group from which the Landau sampling was made. As Ref. 94 shows, these advantages make the ITS algorithm a more accurate representation of the energy loss process, as indicated in comparisons with reference calculations and experiments. Nevertheless, although the reliance on linear interpolation and the systematic errors are reduced, neither is completely eliminated. It is straightforward to create example calculations that show unphysical artifacts in the ITS algorithm as well as in the MCNP logic.

The "nearest-group-boundary" treatment is selected by setting the 18th entry of the DBCN card to 1. For example, the card "DBCN 17J 1" selects this straggling logic without affecting any of the other DBCN options.

c. New Energy- and Step-Specific Method

It is easy to express what we would like to see in the straggling logic. For an electron with energy E about to traverse a step of length s , we would like to sample the straggling from the operator $L(E, s, \bar{\Delta})$ without regard to the prearranged energy boundaries E_n . In the MCNP5 RSICC release 1.40, we have now brought this situation about. A new Fortran 90 module has been installed to deal with straggling data. Those parameters that are separate from the individual straggling events are still precomputed, but each electron transport step can now sample its energy loss separately from adjacent steps, and specifically for its current energy and planned step length. Using this approach, we largely eliminate the linear interpolations and energy misalignments of the earlier algorithms and obviate the need for a choice of energy group. At the time of the MCNP5 1.40 release, the new straggling logic is included in the code, but is still being tested. Preliminary results⁹⁵ indicate that a more accurate and stable estimate of the straggling is obtained, and a variety of unphysical artifacts are eliminated.

The new logic is selected by setting the 18th entry of the DBCN card to 2, for example with the card "DBCN 17J 2".

6. Angular Deflections

The ETRAN codes and MCNP rely on the Goudsmit-Saunderson⁷⁶ theory for the probability distribution of angular deflections. The angular deflection of the electron is sampled once per substep according to the distribution

$$F(s, \mu) = \sum_{l=0}^{\infty} \left(l + \frac{1}{2} \right) \exp(-sG_l) P_l(\mu) \quad ,$$

where s is the length of the substep, $\mu = \cos\theta$ is the angular deflection from the direction at the beginning of the substep, $P_l(\mu)$ is the l^{th} Legendre polynomial, and G_l is

$$G_l = 2\pi N \int_{-1}^{+1} \frac{d\sigma}{d\Omega} [1 - P_l(\mu)] d\mu \quad ,$$

in terms of the microscopic cross section $d\sigma/d\Omega$, and the atom density N of the medium.

For electrons with energies below 0.256 MeV, the microscopic cross section is taken from numerical tabulations developed from the work of Riley.⁹⁶ For higher-energy electrons, the microscopic cross section is approximated as a combination of the Mott⁹⁷ and Rutherford⁸⁸ cross sections, with a screening correction. Seltzer⁸⁰ presents this "factored cross section" in the form

$$\frac{d\sigma}{d\Omega} = \frac{Z^2 e^2}{p^2 v^2 (1 - \mu + 2\eta)^2} \left[\frac{(d\sigma/d\Omega)_{Mott}}{(d\sigma/d\Omega)_{Rutherford}} \right],$$

where e , p , and v are the charge, momentum, and speed of the electron, respectively. The screening correction η was originally given by Molière⁹⁸ as

$$\eta = \frac{1}{4} \left(\frac{\alpha mc}{0.885p} \right)^2 Z^{2/3} [1.13 + 3.76(\alpha Z/\beta)^2],$$

where α is the fine structure constant, m is the rest mass of the electron, and $\beta = v/c$. MCNP now follows the recommendation of Seltzer,⁸⁰ and the implementation in the Integrated TIGER Series, by using the slightly modified form

$$\eta = \frac{1}{4} \left(\frac{\alpha mc}{0.885p} \right)^2 Z^{2/3} \left[1.13 + 3.76(\alpha Z/\beta)^2 \sqrt{\frac{\tau}{\tau + 1}} \right],$$

where τ is the electron energy in units of electron rest mass. The multiplicative factor in the final term is an empirical correction which improves the agreement at low energies between the factored cross section and the more accurate partial-wave cross sections of Riley.

7. Bremsstrahlung

When using data from the el library, for the sampling of bremsstrahlung photons, MCNP relies primarily on the Bethe-Heitler⁹⁹ Born-approximation results that have been used until rather recently⁸⁵ in ETRAN. A comprehensive review of bremsstrahlung formulas and approximations relevant to the present level of the theory in MCNP can be found in the paper of Koch and Motz.¹⁰⁰ Particular prescriptions appropriate to Monte Carlo calculations have been developed by Berger and Seltzer.¹⁰¹ For the ETRAN-based codes, this body of data has been converted to tables including bremsstrahlung production probabilities, photon energy distributions, and photon angular distributions.

For data tables on the el03 library, the production cross section for bremsstrahlung photons and energy spectra are from the evaluation by Seltzer and Berger.^{85,86,87} We summarize the salient features of the evaluation below; more details can be found in the evaluators' documentation. The evaluation uses detailed calculations of the electron-nucleus bremsstrahlung cross section for electrons with energies below 2 MeV and above 50 MeV. The evaluation below 2 MeV uses the results of Pratt, Tseng, and collaborators, based on numerical phase-shift calculations.^{102,103,104} For 50 MeV and above, the analytical theory of Davies, Bethe, Maximom, and Olsen¹⁰⁵ is used and is supplemented by the Elwert Coulomb¹⁰⁶ correction factor and the theory of the high-frequency limit or tip region given by Jabbur and Pratt.¹⁰⁷ Screening effects are accounted for by the use of Hartree-Fock atomic form factors.¹⁰⁸ The values between these firmly grounded theoretical limits are found by a cubic-spline interpolation as described in Refs. 85 and 86. Seltzer reports good agreement between interpolated values and those calculated by Tseng and Pratt¹⁰⁹ for 5 and 10 MeV electrons in aluminum and uranium. Electron-electron bremsstrahlung is also included in the cross-section evaluation based on the theory of Haug¹¹⁰ with screening corrections derived from Hartree-Fock incoherent scattering factors.¹⁰⁸ The energy spectra for the bremsstrahlung photons are provided in the evaluation. No major changes were made to the tabular

angular distributions, which are internally calculated when using the el library, except to make finer energy bins over which the distribution is calculated.

MCNP addresses the sampling of bremsstrahlung photons at each electron substep. The tables of production probabilities are used to determine whether a bremsstrahlung photon will be created. For data from the el03 library, the bremsstrahlung production is sampled according to a Poisson distribution along the step so that none, one or more photons could be produced; the el library allows for either none or one bremsstrahlung photon in a substep. If a photon is produced, the new photon energy is sampled from the energy distribution tables. By default, the angular deflection of the photon from the direction of the electron is also sampled from the tabular data. The direction of the electron is unaffected by the generation of the photon because the angular deflection of the electron is controlled by the multiple scattering theory. However, the energy of the electron at the end of the substep is reduced by the energy of the sampled photon because the treatment of electron energy loss, with or without straggling, is based only on nonradiative processes.

There is an alternative to the use of tabular data for the angular distribution of bremsstrahlung photons. If the fourth entry on the PHYS:E card is 1, then the simple, material-independent probability distribution

$$p(\mu)d\mu = \frac{1 - \beta^2}{2(1 - \beta\mu)^2}d\mu \quad , \quad (2.15)$$

where $\mu = \cos\theta$ and $\beta = v/c$, will be used to sample for the angle of the photon relative to the direction of the electron according to the formula

$$\mu = \frac{2\xi - 1 - \beta}{2\xi\beta - 1 - \beta} \quad ,$$

where ξ is a random number. This sampling method is of interest only in the context of detectors and DXTRAN spheres. A set of source contribution probabilities $p(\mu)$ consistent with the tabular data is not available. Therefore, detector and DXTRAN source contributions are made using Eq. 2.12. Specifying that the generation of bremsstrahlung photons rely on Eq. 2.12 allows the user to force the actual transport to be consistent with the source contributions to detectors and DXTRAN.

8. K-shell Electron Impact Ionization and Auger Transitions

Data tables on the el03 library use the same K-shell impact ionization calculation (based upon ITS1.0) as data tables on the el library, except for how the emission of relaxation photons is treated; the el03 evaluation model has been modified to be consistent with the photo-ionization relaxation model. In the el evaluation, a K-shell impact ionization event generated a photon with the average K-shell energy. The el03 evaluation generates photons with energies given by Everett and Cashwell.³⁴ Both el03 and el treatments only take into account the highest Z component of a material. Thus inclusion of trace high Z impurities could mask K-shell impact ionization from other dominant components.

Auger transitions are handled the same for data tables from the el03 and el libraries. If an atom has undergone an ionizing transition and can undergo a relaxation, if it does not emit a photon it will

emit an Auger electron. The difference between el and el03 is the energy with which an Auger electron is emitted, given by $E_A = E_{\bar{K}}$ or $E_A = E_{\bar{K}} - 2E_{\bar{L}}$ for el or el03, respectively. The el value is that of the highest energy Auger electron while the el03 value is the energy of the most probable Auger electron. It should be noted that both models are somewhat crude.

9. Knock-On Electrons

The Møller cross section¹¹¹ for scattering of an electron by an electron is

$$\frac{d\sigma}{d\varepsilon} = \frac{C}{E} \left\{ \frac{1}{\varepsilon^2} + \frac{1}{(1-\varepsilon)^2} + \left(\frac{\tau}{\tau+1} \right)^2 - \frac{2\tau+1}{(\tau+1)^2} \frac{1}{\varepsilon(1-\varepsilon)} \right\} , \quad (2.16)$$

where ε , τ , E , and C have the same meanings as in Eqs. 2.5-2.7. When calculating stopping powers, one is interested in all possible energy transfers. However, for the sampling of transportable secondary particles, one wants the probability of energy transfers greater than some ε_c representing an energy cutoff, below which secondary particles will not be followed. This probability can be written

$$\sigma(\varepsilon_c) = \int_{\varepsilon_c}^{1/2} \frac{d\sigma}{d\varepsilon} d\varepsilon .$$

The reason for the upper limit of 1/2 is the same as in the discussion of Eq. 2.8. Explicit integration of Eq. 2.13 leads to

$$\sigma(\varepsilon_c) = \frac{C}{E} \left\{ \frac{1}{\varepsilon_c} - \frac{1}{1-\varepsilon_c} + \left(\frac{\tau}{\tau+1} \right)^2 \left(\frac{1}{2} - \varepsilon_c \right) - \frac{2\tau+1}{(\tau+1)^2} \ln \frac{1-\varepsilon_c}{\varepsilon_c} \right\} .$$

Then the normalized probability distribution for the generation of secondary electrons with $\varepsilon > \varepsilon_c$ is given by

$$g(\varepsilon, \varepsilon_c) d\varepsilon = \frac{1}{\sigma(\varepsilon_c)} \frac{d\sigma}{d\varepsilon} d\varepsilon . \quad (2.17)$$

At each electron substep, MCNP uses $\sigma(\varepsilon_c)$ to determine randomly whether knock-on electrons will be generated. If so, the distribution of Eq. 2.14 is used to sample the energy of each secondary electron. Once an energy has been sampled, the angle between the primary direction and the direction of the newly generated secondary particle is determined by momentum conservation. This angular deflection is used for the subsequent transport of the secondary electron. However, neither the energy nor the direction of the primary electron is altered by the sampling of the secondary particle. On the average, both the energy loss and the angular deflection of the primary electron have been taken into account by the multiple scattering theories.

10. Multigroup Boltzmann–Fokker–Planck Electron Transport

The electron physics described above can be implemented into a multigroup form using a hybrid multigroup/continuous-energy method for solving the Boltzmann–Fokker–Planck equation as

described by Morel.⁴⁴ The multigroup formalism for performing charged particle transport was pioneered by Morel and Lorence⁴⁷ for use in deterministic transport codes. With a first order treatment for the continuous slowing down approximation (CSDA) operator, this formalism is equally applicable to a standard Monte Carlo multigroup transport code as discussed by Sloan.¹¹² Unfortunately, a first order treatment is not adequate for many applications. Morel, et al. have addressed this difficulty by developing a hybrid multigroup/continuous energy algorithm for charged particles that retains the standard multigroup treatment for large-angle scattering, but treats exactly the CSDA operator. As with standard multigroup algorithms, adjoint calculations are performed readily with the hybrid scheme.

The process for performing an MCNP/MGBFP calculation for electron/photon transport problems involves executing three codes. First the CEPXS⁴⁷ code is used to generate coupled electron–photon multigroup cross sections. Next the CRSRD code casts these cross sections into a form suitable for use in MCNP by adjusting the discrete ordinate moments into a Radau quadrature form that can be used by a Monte Carlo code. CRSRD also generates a set of multigroup response functions for dose or charge deposition that can be used for response estimates for a forward calculation or for sources in an adjoint calculation. Finally, MCNP is executed using these adjusted multigroup cross sections. Some applications of this capability for electron/photon transport have been presented in Ref. 113.

V. TALLIES

MCNP automatically creates standard summary information that gives the user a better insight into the physics of the problem and the adequacy of the Monte Carlo simulation including: a complete accounting of the creation and loss of all tracks and their energy; the number of tracks entering and reentering a cell plus the track population in the cell; the number of collisions in a cell; the average weight, mean free path, and energy of tracks in a cell; the activity of each nuclide in a cell (that is, how particles interacted with each nuclide, not the radioactivity); and a complete weight balance for each cell.

MCNP also provides seven standard tally types. These include seven standard neutron tallies, six standard photon tallies, and four standard electron tallies. These basic tallies can be modified by the user in many ways. All tallies are normalized to be per starting particle except in KCODE criticality problems, which are normalized to be per fission neutron generation. The MCNP tally plotter provides graphical displays of the results (see Appendix B).

<u>Tally Mnemonic</u>				<u>Description</u>	
F1:N	or	F1:P	or	F1:E	Surface current
F2:N	or	F2:P	or	F2:E	Surface flux
F4:N	or	F4:P	or	F4:E	Track length estimate of cell flux
F5a:N	or	F5a:P			Flux at a point or ring detector
F6:N	or	F6:P	or	F6:N,P	Track length estimate of energy deposition
F7:N					Track length estimate of fission energy deposition
F8:N	or	F8:P	or	F8:E	Pulse height tally
			or	F8:P,E	

The above seven tally categories represent the basic MCNP tally types. To have many tallies of a given type, add multiples of 10 to the tally number. For example, F1, F11, F21,...,F981, F991 are all type F1 tallies. Particle type is specified by appending a colon and the particle designator. For example, F11:N and F96:N are neutron tallies and F2:P and F25:P are photon tallies. F6 tallies can be for both neutrons and photons – for example, F16:N,P. All F8 tallies (except F8:N) are for both photons and electrons; that is, F8:P, F8:E, and F8:P,E are all identical. *It should be noted that although F8:N is also allowed, it is not advised, because MCNP neutron transport does not currently sample joint collision exit densities in an analog (for example, energy conserving) way.*

The units of each tally are derived from the units of the source. If the source has units of particles per unit time, current tallies are particles per unit time and flux tallies are particles per unit time per unit area. When the source has units of particles, current tallies have units of particles and flux tallies actually represent fluences with units of particles per unit area. A steady-state flux solution can be obtained by having a source with units of particles per unit time and integrating the tally over all time (that is, omitting the Tn card). The average flux in a time bin can be obtained from the fluence tally for a time-dependent source by dividing the tally by the time bin width in shakes. These tallies can all be made per unit energy by dividing each energy bin by the energy bin width.

Extensive statistical analysis of tally convergence is applied to the tally fluctuation bin of each tally (see page 3–107). Ten statistical checks are made, including the variance of the variance and the Pareto slope of the history score probability density function. These checks are described in detail in Section VI beginning on page 2–108 .

The tally quantities actually scored in MCNP before the final normalization per starting particle are presented in Table 2.2. The table also gives the physical quantity that corresponds to each tally, and it defines much of the notation used in the remainder of this section.

Table 2.2
Tally Quantities Scored

<u>Tally</u>	<u>Score</u>	<u>Physical Quantity</u>	<u>Units</u>
F1	W	$J = \int dE \int dt \int dA \int d\Omega \hat{\Omega} \cdot \hat{n} \psi(\vec{r}, \hat{\Omega}, E, t)$	particles
F2	$\frac{W}{ \mu A}$	$\bar{\phi}_S = \frac{1}{A} \int dE \int dt \int dA \int d\Omega \psi(\vec{r}, \hat{\Omega}, E, t)$	particles/cm ²
F4	$W \frac{T_l}{V}$	$\bar{\phi}_V = \frac{1}{V} \int dE \int dt \int dV \int d\Omega \psi(\vec{r}, \hat{\Omega}, E, t)$	particles/cm ²
F5	$\frac{W \cdot p(\hat{\Omega}_P) e^{-\lambda}}{R^2}$	$\phi_P = \int dE \int dt \int d\Omega \psi(\vec{r}_P, \hat{\Omega}, E, t)$	particles/cm ²
F6	$WT_l \sigma_t(E) H(E) \frac{\rho_a}{m}$	$H_t = \frac{\rho_a}{m} \int dE \int dt \int dV \int d\Omega \sigma_t(E) H(E) \psi(\vec{r}, \hat{\Omega}, E, t)$	MeV/g
F7	$WT_l \sigma_f(E) Q \frac{\rho_a}{m}$	$H_f = \frac{\rho_a}{m} Q \int dE \int dt \int dV \int d\Omega \sigma_f(E) \psi(\vec{r}, \hat{\Omega}, E, t)$	MeV/g
F8	W_C put in bin E_D	pulses	pulses

W	=	particle weight
W_C	=	collective weight from a history for pulse height tally; see subsection D, page 2–89.
$\vec{r}, \hat{\Omega}, E, t$	=	particle position vector (cm), direction vector, energy (MeV), and time (sh; 1sh = 10^{-8} s)
μ	=	$\hat{\Omega} \cdot \hat{n}$, cosine of angle between surface normal \hat{n} and particle trajectory $\hat{\Omega}$
A, V	=	surface area (cm^2) and volume (cm^3) (calculated by the code or input by the user)
T_l	=	track length (cm) = event transit time \times particle velocity
$p(\hat{\Omega}_P)$	=	probability density function for scattering (or starting) in the direction $\hat{\Omega}_P$ towards the point detector (Azimuthal symmetry is assumed)
λ	=	total number of mean free paths from particle location to detector
R	=	distance to detector from a source or collision event
$\sigma_t(E)$	=	microscopic total cross section (barns)
$\sigma_f(E)$	=	microscopic fission cross section (barns)
$H(E)$	=	heating number (MeV/collision)
E_D	=	total energy deposited by a history in a detector; see subsection D, page 2–89
ρ_a	=	atom density (atoms/barn-cm)
ρ_g	=	mass density (g/cm^3) (not used in Table 2.1 but used later in this chapter)
m	=	cell mass (g)
Q	=	fission heating Q-value (MeV)
ψ	=	angular flux familiar from nuclear reactor theory; ^{114,115} $\psi(\vec{r}, \hat{\Omega}, E, t) = vn(\vec{r}, \hat{\Omega}, E, t)$, where n is the particle density (particles/ $\text{cm}^3/\text{MeV}/\text{steradian}$) and v is velocity in cm/sh. Thus, the units of ψ are particles/ $\text{cm}^2/\text{sh}/\text{MeV}/\text{steradian}$.
J	=	total (not net) current crossing a surface
$\bar{\phi}_S$	=	average flux on a surface
$\bar{\phi}_V$	=	average flux in a cell (volume)
ϕ_P	=	flux at a point
\vec{r}_P	=	point at which ϕ_P is estimated (location of point detector)
H_t	=	total energy deposition in a cell (MeV/g)
H_f	=	total fission energy deposition in a cell (MeV/g).

Adding an asterisk (*Fn) changes the units into an energy tally and multiplies each tally as indicated in Table 2.3. For an F8 pulse height tally, the asterisk changes the tally from deposition of pulses to an energy deposition tally and a plus changes the tally to a charge deposition tally.

Table 2.3
Tallies Modified with an Asterisk or Plus

<u>Tally</u>	<u>Score</u>	<u>Units</u>
*F1	WE	MeV
*F2	$\frac{WE}{ \mu A}$	MeV/cm ²
*F4	$\frac{WT_l E}{V}$	MeV/cm ²
*F5	$\frac{W \cdot p(\hat{\Omega}_D) e^{-\lambda} E}{R^2}$	MeV/cm ²
*F6	$1.60219 \times 10^{-22} \frac{\text{jerks}}{\text{MeV}} WT_l \sigma_t(E) H(E) \frac{\rho_a}{m}$	jerks/g
*F7	$1.60219 \times 10^{-22} \frac{\text{jerks}}{\text{MeV}} WT_l \sigma_f(E) Q \frac{\rho_a}{m}$	jerks/g
*F8	$E_D \times W_C$ put in bin E_D	MeV
+ F8	$\pm W_C$ put in bin E_D	charge

In addition to the standard tallies, MCNP has one special tally type, the superimposed mesh tally. This feature allows the user to tally particles on a mesh independent of the problem geometry. Currently only track-length (type 4) mesh tallies have been implemented. Other track-length quantities such as heating and energy deposition can be calculated with the use of a tally multiplier (FM) card. Mesh tallies are invoked by using the FMESH card. As in the F card, a unique number is assigned to each mesh tally. Since only track-length mesh tallies are available, the mesh tally number must end with a 4, and it must not be identical to any number that is used to identify an F4 tally. The track length is computed over the mesh tally cells, and is normalized to be per starting particle, except in KCODE criticality calculations.

Not all features of the standard tallies have been implemented in the mesh tallies. For example, no tally fluctuation statistics are given for mesh tallies; the only error information provided is the relative error for each mesh cell. Features that can be used with the mesh tallies are multiplying the result by the particle energy (*FMESH format), dose functions, and tally multipliers. Time binning is not a feature of the mesh tallies.

The definitions of the current and flux in the sections that follow come from nuclear reactor theory^{114,115} but are related to similar quantities in radiative transfer theory. The MCNP angular

flux multiplied by the particle energy is the same as the intensity in radiative transfer theory. The MCNP total flux at energy E multiplied by the particle energy E equals the integrated energy density times the speed of light in radiative transfer theory. The MCNP current multiplied by the particle energy is analogous to the radiative flux crossing an area in radiative transfer theory. The MCNP particle fluence multiplied by the particle energy is the same as the fluence in radiative transfer theory.

Nuclear reactor theory has given the terms *flux* and *current* quite different meanings^{114,115} than they have in other branches of physics; terminology from other fields should not be confused with that used in this manual.

Rigorous mathematical derivations of the basic tallies are given in Ref. 116. Somewhat heuristic derivations follow. Note that the surface current is a *total* but the cell and surface fluxes are *averages*.

A. Surface Current Tally

The F1 tally is a simple count of the number of particles, represented by the Monte Carlo weight, crossing a surface in specified bins. The number of particles at time t , in a volume element $d\vec{r}$, with directions within $d\Omega$, and energies within dE is $n(\vec{r}, \Omega, E, t)d\vec{r}d\Omega dE$. Let the volume element $d\vec{r}$ contain the surface element dA (with surface normal \hat{n}) and along Ω for a distance vdt , as depicted in Figure 2-7. Then the differential volume element is $d\vec{r} = vdt|\hat{\Omega} \cdot \hat{n}|dA$. All the particles within this volume element (with directions within $d\Omega$ and energies within dE) will cross surface dA in time dt . Thus, the number of particles crossing surface dA in time dt is $|\hat{\Omega} \cdot \hat{n}|vn(\vec{r}, \Omega, E, t)d\Omega dE dt dA$. The number of particles crossing surface A in energy bin i , time bin j , and angle bin k is thus

$$\int_{E_i} dE \int_{t_j} dt \int_{\Omega_k} d\Omega \int dA |\hat{\Omega} \cdot \hat{n}| vn(\vec{r}, \hat{\Omega}, E, t)$$

The range of integration over energy, time, and angle (cosine) is controlled by E, T, and C cards. If the range of integration is over all angles (no C card), then the F1 tally is a count of the number of particles with any trajectory crossing the surface (in each energy and time bin) and thus has no direction associated with it.

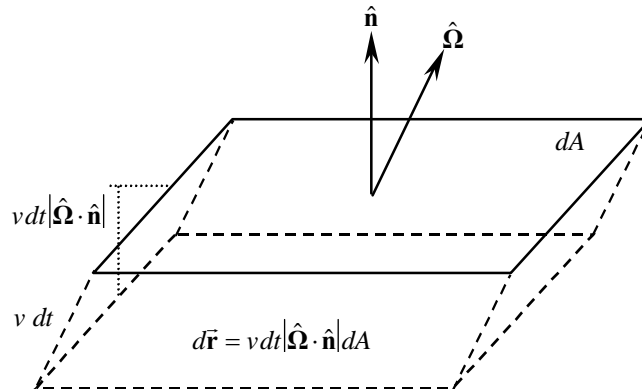


Figure 2-7. Diagram for description of the surface current tally.

Note that the MCNP current J of Table 2.2 is the total current, not the net current. (It is the total number of particles crossing a surface.) Frequently, the net current, rather than the total current, is desired. Defining the partial currents crossing in the positive and negative directions (“right” and “left” or “up” and “down”) as¹¹⁵

$$J_{\pm} = \int dE \int dt \int dA \int_{\substack{\hat{\Omega} \cdot \hat{n} > 0 \\ \hat{\Omega} \cdot \hat{n} < 0}} d\hat{\Omega} |\hat{\Omega} \cdot \hat{n}| \psi(\vec{r}, \hat{\Omega}, E, t),$$

the net current across the surface is $J_{net} = J_+ - J_-$. (The total current of Table 2.2 is $J = J_+ + J_-$.) The partial currents J_{\pm} across a surface can be calculated in MCNP using an F1 tally with two cosine bins, one each for $-1 \leq \mu < 0$ and $0 < \mu \leq 1$.

The units of the F1 tally are those of the source. If the source has units of particles per unit time, the tally has units of particles per unit time. When the source has units of particles, the tally has units of particles. The SD card can be used to input a constant that divides the tally. In other words, if x is input on the SD card, the tally will be divided by x .

B. Flux Tallies

Defining the scalar flux $\phi(\vec{r}, E, t) = \int d\hat{\Omega} \psi(\vec{r}, \hat{\Omega}, E, t)$ [$\phi(\vec{r}, E, t) d\vec{r} dE$ is the total scalar flux in volume element $d\vec{r}$ about \vec{r} and energy element dE about E] and, introducing energy and time bins, the integrals of Table 2.2 for the F2, F4, and F5 tallies can be recast as

$$F2 = \frac{1}{A} \int_{E_i} dE \int_{t_j} dt \int dA \phi(\vec{r}, E, t),$$

$$F4 = \frac{1}{V} \int_{E_i} dE \int_{t_j} dt \int dV \phi(\vec{r}, E, t) \text{ and}$$

$$F5 = \int_{E_i} dE \int_{t_j} dt \phi(\vec{r}_P, E, t).$$

The range of integration over energy and time can be tailored by E and T cards. If no E card is present, the integration limits are the same as the limits for the corresponding cross sections used. The F4 cell flux and F2 surface flux tallies are discussed in this section. The F5 detector flux tally is discussed on page 2–89.

1. Track Length Estimate of Cell Flux (F4)

The average particle flux in a cell (from Table 2.2) can be written

$$\begin{aligned}\bar{\phi}_V &= \frac{1}{V} \int dE \int dt \int dV \int d\Omega \psi(\vec{r}, \hat{\Omega}, E, t) \\ &= \frac{1}{V} \int dE \int dV \int d\Omega \int dt v n(\vec{r}, \hat{\Omega}, E, t) \\ &= \frac{1}{V} \int dE \int dV \int dt v N(\vec{r}, E, t),\end{aligned}$$

where $N(\vec{r}, E, t) = \int d\Omega n(\vec{r}, \hat{\Omega}, E, t)$ is the density of particles, regardless of their trajectories, at a point. Defining ds to be the differential unit of track length and noting that $ds = vdt$ yields

$$\bar{\phi}_V = \frac{1}{V} \int dE \int dV \int ds N(\vec{r}, E, t).$$

The quantity $N(\vec{r}, E, t)ds$ may be thought of as a track length density; thus, the average flux can be estimated by summing track lengths. MCNP estimates $\bar{\phi}_V$ by summing WT_l/V for all particle tracks in the cell. Time- and energy-dependent subdivisions of $\bar{\phi}_V$ are made by binning the track lengths in appropriate time and energy bins. The track length estimator is generally quite reliable because there are frequently many tracks in a cell (compared to the number of collisions), leading to many contributions to this tally.

The SD card can be used to input a new volume that divides the tally. In other words, if V' is input on the SD card, the tally will be divided by V' instead of V . There are cases where MCNP cannot calculate the volume of a taller region. In these cases, the user must input an entry on an SD card corresponding to the taller cell.

2. Surface Flux (F2)

The average particle scalar flux on a surface ($\bar{\phi}_S$ of Table 2.2) is estimated using a surface crossing estimator that may be thought of as the limiting case of the cell flux or track length estimator when the cell becomes infinitely thin, as illustrated in Figure 2-8.

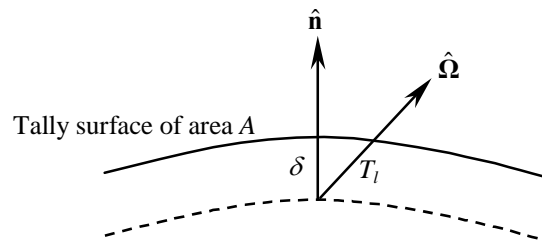


Figure 2-8. Diagram for description of the surface flux tally.

As the cell thickness δ approaches zero, the cell volume approaches $A\delta$ and the track length through the cell approaches $\delta/|\hat{\Omega} \cdot \hat{n}|$. Thus,

$$\begin{aligned}
 \bar{\phi}_S &= \lim_{\delta \rightarrow 0} \bar{\phi}_V \\
 &= \lim_{\delta \rightarrow 0} \frac{WT_l}{V} \\
 &= \lim_{\delta \rightarrow 0} \frac{W}{A\delta} \frac{\delta}{|\hat{\Omega} \cdot \hat{n}|} \\
 &= \frac{W}{A|\mu|} .
 \end{aligned}$$

A more formal derivation of the surface flux estimator may be found in Ref. 116.

For particles grazing the surface, $1/|\mu|$ is very large and MCNP approximates the surface flux estimator in order to satisfy the requirement of one central limit theorem. An unmodified surface flux estimator has an infinite variance, and thus confidence intervals could not be formed via the central limit theorem, because the central limit theorem requires a finite variance. For this reason, MCNP sets $|\mu| = 0.05$ when $|\mu| < 0.10$; because of this approximation, the F2 tally is not an exact estimate of the surface flux.

The SD card can be used to input a new area that divides the tally. In other words, if A' is input on the SD card, the tally will be divided by A' instead of A .

The F2 tally is essential for stochastic calculation of surface areas when the normal analytic procedure fails (see page 2-187).

C. *Track Length Cell Energy Deposition Tallies*

The F6 and F7 cell heating and energy deposition tallies are track length flux tallies modified to tally a reaction rate convolved with an energy-dependent heating function $[(H \text{ or } Q)\sigma\rho_a\phi]$ from Table 2.2] instead of a flux. The derivation of such modified track length estimators along the lines of the derivation of the track length flux estimator in subsection B.1 on page 2-85 is straightforward. The heating tallies are merely flux tallies (F4) multiplied by an energy-dependent multiplier (FM card); the equivalence is shown in this section.

The units of the heating tally are MeV/g. An asterisk (*F6 and *F7) changes the units to jerks/g ($1 \text{ MeV} = 1.6021910^{-22} \text{ jerks}$) (the asterisk causes the tally to be multiplied by a constant rather than by energy as in the other tallies). The SD card can be used to input a new mass that divides the tally. In other words, if m' is input on the SD card, the tally will be divided by m' instead of m .

As with the F4 tally, there are cases where MCNP cannot calculate the area of a tally surface. In such cases, the user must input an entry on an SD card corresponding to the surface tally.

Energy deposition for photons and electrons can be computed with the *F8 tally. See page 2-89. However, this is not a track length estimator.

The F7 tally includes the gamma-ray heating because the fission photons are deposited locally. The F6:N tally deposits the photons elsewhere, so it does not include gamma-ray heating. Thus, for fissionable materials, the F7:N result will be greater than the F6:N result even though F7:N includes only fission and F6 includes all reactions. The true heating is found by summing the neutron and photon F6 tallies in a coupled neutron/photon calculation. In a neutron-only problem, F6 will give the right heating of light materials only if, in the physical experiment, *all* photons escape the geometry. F7 will give about the right heating of fissionable materials only if, in the physical experiment, no photons come from elsewhere, all fission photons are immediately captured, and nonfission reactions can be ignored. By definition, the F7 tally cannot be used for photons. Examples of the mnemonic used to combine neutron and photon F6 tallies are F6:N,P and F516:P,N.

MCNP computes heating as specified in Table 2.2, with a heating function [$H(E)$ or Q] modifying a track length reaction rate tally. In other words, the average energy deposited for all reactions at the incident particle energy is used in the tally, regardless of the actual reaction that might be sampled at the next collision. The heating functions are tabulated in the nuclear data by incident energy (except for fission Q-values). Great care should be taken to understand exactly what the heating functions include and how they were computed. The functions $H(E)$ and Q from Table 2.2 are generally defined and computed for tabulation in the data tables as follows:

1. F6 Neutrons

The heating number is $H(E) = E - \sum_i p_i(E)[\bar{E}_{i,out}(E) - Q_i + \bar{E}_{i,\gamma}(E)]$, where

$$\begin{aligned} p_i(E) &= \frac{\sigma_i(E)}{\sigma_T(E)} = \text{probability of reaction } i \text{ at neutron incident energy } E \\ \bar{E}_{i,out}(E) &= \text{average exiting neutron energy for reaction } i \text{ at neutron incident energy } E \\ Q_i &= \text{Q-value of reaction } i \\ \bar{E}_{i,\gamma}(E) &= \text{average exiting gamma energy for reaction } i \text{ at neutron incident energy } E \end{aligned}$$

2. F6 Photons

The heating number is $H(E) = E - \sum_{i=1}^3 p_i(E)[\bar{E}_{i,out}(E)]$, where

$$\begin{aligned} i = 1 &\rightarrow \text{incoherent (Compton) scattering with form factors} \\ i = 2 &\rightarrow \text{pair production; } \bar{E}_{i,out}(E) = 2m_0c^2 = 1.022016 \text{ MeV } (m_0c^2 \text{ is the rest-mass energy of an electron)} \\ i = 3 &\rightarrow \text{photoelectric absorption; } \bar{E}_{i,out}(E) = 0 \\ p_i(E) &= \text{probability of reaction } i \text{ at gamma incident energy } E \\ \bar{E}_{i,out}(E) &= \text{average exiting gamma energy for reaction } i \text{ at neutron incident energy } E. \end{aligned}$$

The pulse height tally is analogous to a physical detector. The F8 energy bins correspond to the total energy deposited in a detector in the specified channels by each physical particle (history). All the other MCNP tallies record the energy of a scoring track in the energy bin.

In an experimental configuration, suppose a source emits 100 photons at 10 MeV, and ten of these get to the detector cell. Further, suppose that the first photon (and any of its progeny created in the cell) deposits 1 keV in the detector before escaping, the second deposits 2 keV, and so on up to the tenth photon which deposits 10 keV. Then the pulse height measurement at the detector would be one pulse in the 1 keV energy bin, 1 pulse in the 2 keV energy bin, and so on up to 1 pulse in the 10 keV bin.

In the analogous MCNP pulse height tally, the source cell is credited with the energy times the weight of the source particle. When a particle crosses a surface, the energy times the weight of the particle is subtracted from the account of the cell that it is leaving and is added to the account of the cell that it is entering. The energy is the kinetic energy of the particle plus $2m_0c^2 = 1.022016$ if the particle is a positron. At the end of the history, the account in each tally cell is divided by the source weight. The resulting energy determines which energy bin the score is put in. The value of the score is the source weight for an F8 tally and the source weight times the energy in the account for a *F8 tally. The value of the score is zero if no track entered the cell during the history.

The pulse height tally depends on sampling the joint density of all particles exiting a collision event. MCNP does not currently sample this joint density for neutron collisions. MCNP neutron physics is nonanalog (in the joint density sampling), particularly in the way that multiple neutrons exiting a collision are totally uncorrelated and do not even conserve energy except in an average sense over many neutron histories. Thus, neutron F8 tallies must be done with extreme caution when more than one neutron can exit a collision.

Another aspect of the pulse height tally that is different from other MCNP tallies is that F8:P, F8:E and F8:P,E are all equivalent. All the energy from both photons and electrons, if present, will be deposited in the cell, no matter which tally is specified.

When the pulse height tally is used with energy bins, care must be taken because of negative scores from nonanalog processes and zero scores caused by particles passing through the pulse height cell without depositing energy. In some codes, like the Integrated TIGER Series, these events cause large contributions to the lowest energy bin pulse height score. In other codes no contribution is made. MCNP compromises by counting these events in a zero bin and an epsilon bin so that these scores can be segregated out. It is recommended that your energy binning for an F8 tally be something like

E8 0 1.e-5 1. 2. 3. 4. 5. ...

Knock-on electrons in MCNP are nonanalog in that the energy loss is included in the multiple scattering energy loss rate rather than subtracted out at each knock-on event. Thus knock-ons can cause negative energy pulse height scores. These scores will be caught in the 0 energy bin. If they are a large fraction of the total F8 tally, then the tally is invalid because of nonanalog events. Another situation is differentiating zero contributions from particles not entering the cell and particles entering the cell but not depositing any energy. These are differentiated in MCNP by

causing an arbitrary $1.e-12$ energy loss for particles just passing through the cell. These will appear in the 0-epsilon bin.

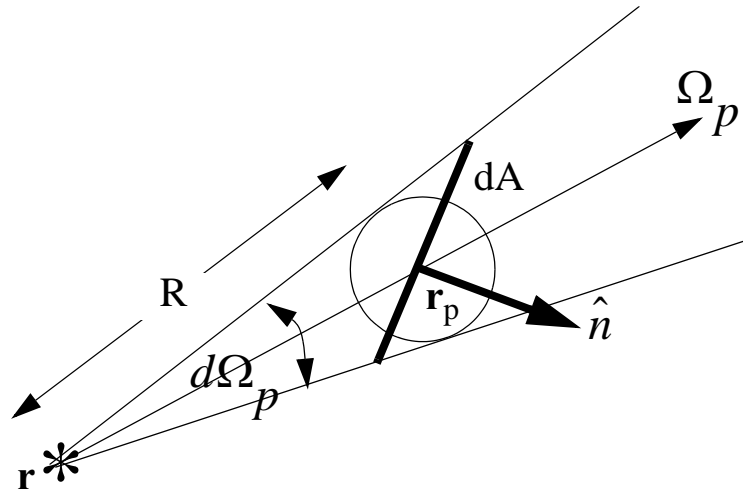
E. Flux at a Detector

The neutral particle flux can be estimated at a point (or ring) using the point (or ring) detector next-event estimator. Neutral particle flux images using an array of point detectors—one detector for each pixel—can also be estimated. Detectors can yield anomalous statistics and must be used with caution. Detectors also have special variance reduction features, such as a highly advantageous DD card Russian roulette game. Whenever a user-supplied source is specified, a user-supplied source angle probability density function must also be provided.

1. Point Detector

A point detector is a deterministic estimate (from the current event point) of the flux at a point in space. Contributions to the point detector tally are made at source and collision events throughout the random walk. The point detector tally (F5) may be considered a limiting case of a surface flux tally (F2), as will be shown below.

Consider the point detector to be a sphere whose radius is shrinking to zero. Figure 2-9 shows the details.



\mathbf{r} = source or collision point

\mathbf{r}_p = detector point

Figure 2-9

Let Ω_p be in the direction to the center of the sphere, i.e., in the direction $\mathbf{r}_p - \mathbf{r}$. Let $d\Omega_p$ be the solid angle subtended by the sphere from \mathbf{r} , and let dA be defined by the intersection of an arbitrary plane (passing through the detector point) and the collapsing cone.

In order to contribute to a flux tally upon crossing dA , the particle has to do two things. First, the particle must scatter toward dA (i.e. into solid angle $d\Omega_p$); this occurs with probability

$$p(\Omega_p)d\Omega_p \quad .$$

Second, the particle must have a collisionless free-flight for the distance $R = |\mathbf{r}_p - \mathbf{r}|$ (along Ω_p) to the sphere; this occurs with probability

$$e^{-\int_0^R -\Sigma_t(s)ds} \quad ,$$

where $\Sigma_t(s)$ is the total macroscopic cross section at a distance s (along Ω_p) from the source or collision point. The probability that these two events both occur is

$$p(\Omega_p)d\Omega_p e^{-\int_0^R -\Sigma_t(s)ds} \quad .$$

Define η to be the cosine of the angle between the particle direction and the unit normal ($\hat{\mathbf{n}}$) to area dA :

$$\eta = \Omega_p \cdot \hat{\mathbf{n}} \quad .$$

If a particle of weight w reaches dA , it will contribute $w/(|\eta|dA)$ to the flux (compare F2 tally on page 2–86).

As the sphere shrinks to a point, the solid angle subtended by dA is $d\Omega_p = |\eta|dA/R^2$. (The sides of the cone in the figure become parallel and the cone resembles a cylinder near the shrinking sphere.) Thus the tally becomes

$$F5 = p(\Omega_p)d\Omega_p e^{-\int_0^R -\Sigma_t(s)ds} \frac{w}{|\eta|dA} = wp(\Omega_p) \frac{|\eta|dA}{R^2} \frac{1}{|\eta|dA} e^{-\int_0^R -\Sigma_t(s)ds}$$

or

$$F5 = w \frac{p(\Omega_p)}{R^2} e^{-\int_0^R -\Sigma_t(s)ds} \quad .$$

In all the scattering distributions and in the standard sources, MCNP assumes azimuthal symmetry. This provides some simplification. The angle Ω_p can be expressed in polar coordinates with the incoming particle direction being the polar axis. The azimuthal angle is ϕ and the cosine of the polar angle is μ . The probability density of scattering into $d\Omega_p$ can then be written in terms of a probability density in μ, ϕ . That is,

$$p(\Omega_p) d\Omega_p = p(\mu, \phi) d\mu d\phi \quad .$$

Defining the PDF for scattering at μ as

$$p(\mu) = \int_0^{2\pi} p(\mu, \phi) d\phi$$

and, recalling that $p(\mu, \phi)$ is independent of ϕ , yields

$$p(\mu, \phi) = \frac{p(\mu)}{2\pi} .$$

Substituting this into the last expression for the F5 tally yields

$$F5 = w \frac{p(\mu)}{2\pi R^2} e^{-\int_0^R \Sigma_t(s) ds} .$$

A point detector tally is known as a “next-event estimator” because it is a tally of the flux at a point as if the "next event" were a particle trajectory directly to the detector point without further collision.

A contribution to the point detector is made at every source or collision event. The $e^{-\lambda}$ term accounts for attenuation between the present event and the detector point. The $1/2\pi R^2$ term accounts for the solid angle effect. The $p(\mu)$ term accounts for the probability of scattering toward the detector instead of the direction selected in the random walk. For an isotropic source or scatter, $p(\mu) = 0.5$ and the solid angle terms reduce to the expected $1/4\pi R^2$. (Note that $p(\mu)$ can be larger than unity because it is the value of a density function and not a probability.) Each contribution to the detector can be thought of as the transport of a pseudoparticle to the detector.

The R^2 term in the denominator of the point detector causes a singularity that makes the theoretical variance of this estimator infinite. That is, if a source or collision event occurs near the detector point, R approaches zero and the flux approaches infinity. The technique is still valid and unbiased, but convergence is slower and often impractical. If the detector is not in a source or scattering medium, a source or collision close to the detector is impossible. For problems where there are many scattering events near the detector, a cell or surface estimator should be used instead of a point detector tally. If there are so few scattering events near the detector that cell and surface tallies are impossible, a point detector can still be used with a specified average flux region close to the detector. This region is defined by a fictitious sphere of radius R_o surrounding the point detector. R_o can be specified either in centimeters or in mean free paths. If R_o is specified in centimeters and if $R < R_o$, the point detector estimation inside R_o is assumed to be the average flux uniformly distributed in volume.

$$\begin{aligned} \Phi(R < R_o) &= \frac{\int \Phi dV}{\int dV} \\ &= Wp(\mu) \frac{\int_0^{R_o} e^{(-\Sigma_t r)} 4\pi r^2 dr}{\frac{4}{3}\pi R_o^3} \\ &= \frac{Wp(\mu)(1 - e^{-\Sigma_t R_o})}{\frac{2}{3}\pi R_o^3 \Sigma_t} . \end{aligned}$$

If $\Sigma_t = 0$, the detector is not in a scattering medium, no collision can occur, and

$$\Phi(R < R_o, \Sigma_t = 0) = \frac{Wp(\mu)R_o}{\frac{2}{3}\pi R_o^3} .$$

If the fictitious sphere radius is specified in mean free paths λ_0 , then $\lambda_0 = \Sigma_t R_o$ and

$$\Phi(\lambda < \lambda_0) = \frac{Wp(\mu)(1 - e^{-\lambda_0})\Sigma_t^2}{\frac{2}{3}\pi\lambda_0^3} .$$

The choice of R_o may require some experimentation. For a detector in a void region or a region with very few collisions (such as air), R_o can be set to zero. For a typical problem, setting R_o to a mean free path or some fraction thereof is usually adequate. If R_o is in centimeters, it should correspond to the mean free path for some average energy in the sphere. Be certain when defining R_o that the sphere it defines does not encompass more than one material unless you understand the consequences. This is especially true when defining R_o in terms of mean free path because R_o becomes a function of energy and can vary widely. In particular, if R_o is defined in terms of mean free paths and if a detector is on a surface that bounds a void on one side and a material on the other, the contribution to the detector from the direction of the void will be zero even though the importance of the void is nonzero. The reason is simply that the volume of the artificial sphere is infinite in a void. Contributions to the detector from the other direction (that is, across the material) will be accounted for.

Detectors differing only in R_o are coincident detectors (see page 2–103), and there is little cost incurred by experimenting with several detectors that differ only by R_o in a single problem.

2. Ring Detector

A ring detector¹¹⁷ tally is a point detector tally in which the point detector location is not fixed but rather sampled from some location on a ring. Most of the previous section on point detectors applies to ring detectors as well. In MCNP three ring detector tallies, FX, FY, and FZ, correspond to rings located rotationally symmetric about the x , y , and z coordinate axes. A ring detector usually enhances the efficiency of point detectors for problems that are rotationally symmetric about a coordinate axis. Ring detectors also can be used for problems where the user is interested in the average flux at a point on a ring about a coordinate axis.

Although the ring detector is based on the point detector that has a $1/R^2$ singularity and an unbounded variance, the ring detector has a finite variance and only a $1/R_{min}$ singularity, where R_{min} is the minimum distance between the contributing point and the detector ring.¹¹⁸

In a cylindrically symmetric system, the flux is constant on a ring about the axis of symmetry. Hence, one can sample uniformly for positions on the ring to determine the flux at any point on the ring. The ring detector efficiency is improved by biasing the selection of point detector locations to favor those near the contributing collision or source point. This bias results in the same total

number of detector contributions, but the large contributions are sampled more frequently, reducing the relative error.

For isotropic scattering in the lab system, experience has shown that a good biasing function is proportional to $e^{-P}R^{-2}$, where P is the number of mean free paths and R is the distance from the collision point to the detector point. For most practical applications, using a biasing function involving P presents prohibitive computational complexity except for homogeneous medium problems. For air transport problems, a biasing function resembling e^{-P} has been used with good results. A biasing function was desired that would be applicable to problems involving dissimilar scattering media and would be effective in reducing variance. The function R^{-2} meets these requirements.

In Figure 2-10, consider a collision point, (x_o, y_o, z_o) at a distance R from a point detector location (x, y, z) . The point (x, y, z) is to be selected from points on a ring of radius r that is symmetric about the y-axis in this case.

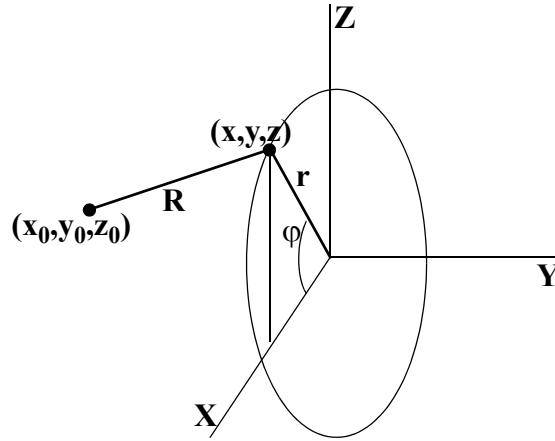


Figure 2-10

To sample a position (x, y, z) on the ring with a $1/R^2$ bias, we pick ϕ from the density function $p(\phi) = C/(2\pi R^2)$, where C is a normalization constant. To pick ϕ from $p(\phi)$, let ξ be a random number on the unit interval. Then

$$\begin{aligned}\xi &= \frac{C}{2\pi} \int_{-\pi}^{\phi} \frac{d\phi'}{R^2} \\ &= \frac{C}{2\pi} \int_{-\pi}^{\phi} \frac{d\phi'}{(x_o - r \cos \phi')^2 + (y_o - y)^2 + (z_o - r \sin \phi')^2} \\ &= \frac{C}{2\pi} \int_{-\pi}^{\phi} \frac{d\phi'}{a + b \cos \phi' + c \sin \phi'}\end{aligned}$$

$$= \frac{1}{\pi} \tan^{-1} \left\{ \frac{1}{C} \left[(a-b) \tan \frac{\varphi}{2} + c \right] \right\} + \frac{1}{2} ,$$

where

$$\begin{aligned} a &= r^2 + x_o^2 + (y - y_o)^2 + z_o^2 \\ b &= -2rx_o \\ c &= -2rz_o \\ C &= (a^2 - b^2 - c^2)^{1/2}. \end{aligned}$$

The above expression is valid if $a^2 > b^2 + c^2$, which is true except for collisions exactly on the ring.

Solving for $\tan \frac{\varphi}{2}$,

$$\tan \frac{\varphi}{2} = \frac{1}{a-b} \left\{ C \tan \left[\pi \left(\xi - \frac{1}{2} \right) \right] - c \right\} .$$

Letting $t = \tan \varphi/2$,

$$\begin{aligned} \text{then } x &= r \cos \varphi = r(1 - t^2)/(1 + t^2) \\ y &= y \text{ (fixed)} \\ z &= r \sin \varphi = 2rt/(1 + t^2). \end{aligned}$$

For ring detectors, the $1/R^2$ biasing has been supplemented when it is weak to include a biasing based on angle to select the point on the ring. This angle is in the plane of the ring and is relative to the shortest line from the collision point to the detector ring. The angle that would most likely be selected would pick the same point on the ring as a straight line through the axis of the problem, the collision point, and the ring. The angle least likely to be picked would choose the point on the opposite side of the ring. This approach will thus make scores with smaller attenuations more often. This supplemental biasing is achieved by requiring that $a \leq 3/2(b^2 + c^2)^{1/2}$ in the above equation.

If the radius of the ring is very large compared to the dimensions of the scattering media (such that the detector sees essentially a point source in a vacuum), the ring detector is still more efficient than a point detector. The reason for this unexpected behavior is that the individual scores to the ring detector for a specific history have a mean closer to the true mean than to the regular point detector contributions. That is, the point detector contributions from one history will tend to cluster about the wrong mean because the history will not have collisions uniformly in volume throughout the problem, whereas the ring detector will sample many paths through the problem geometry to get to different points on the ring.

3. Flux Image Detectors

Flux image detector tallies are an array of point detectors close enough to one another to generate an image based on the point detector fluxes. Each detector point represents one pixel of the flux image. The source need not be embedded in the object. The particle creating the image does not have to be the source particle type. Three types of neutral particle flux image tallies can be made:^{119,120}

- Flux Image Radiograph (FIR), a flux image radiograph on a planar image surface;
- Flux Image on a Cylinder (FIC), a flux image on a cylindrical image surface; and
- Flux Image by Pinhole (FIP), a flux image by pinhole on a planar image surface.

When these flux image tallies are used with FSn and Cn cards to construct a virtual image grid, millions of point detectors can be created—one detector for each pixel—to produce a flux image. The FSn card is used to define the image pixels along the s -axis. The Cn card defines the pixels along the t -axis. The relationship of the s -axis, t -axis, and reference direction for the planar image grid is defined by the right-hand rule. Since the orientation of the s -axis and the t -axis is dependent on the reference direction in the geometry coordinate system, the MCNP tally output should be examined to see the direction cosines of these two planar image grid axes. The image grid SHOULD NOT be in a scattering material because the point detector average flux neighborhood is not used for flux image tallies.

a. Radiograph Image Tallies FIR and FIC

Both the FIR and FIC tallies act like film for an x-ray type image (that is, a transmitted image for neutrons or photons). The diagram in Figure 2-11 shows how the FIR planar rectangular grid image is defined for a source particle passing through an object and scattering in an object. An FIC cylindrical surface grid generates an image on a cylinder as shown in Figure 2-12 for the particles generated inside the object.

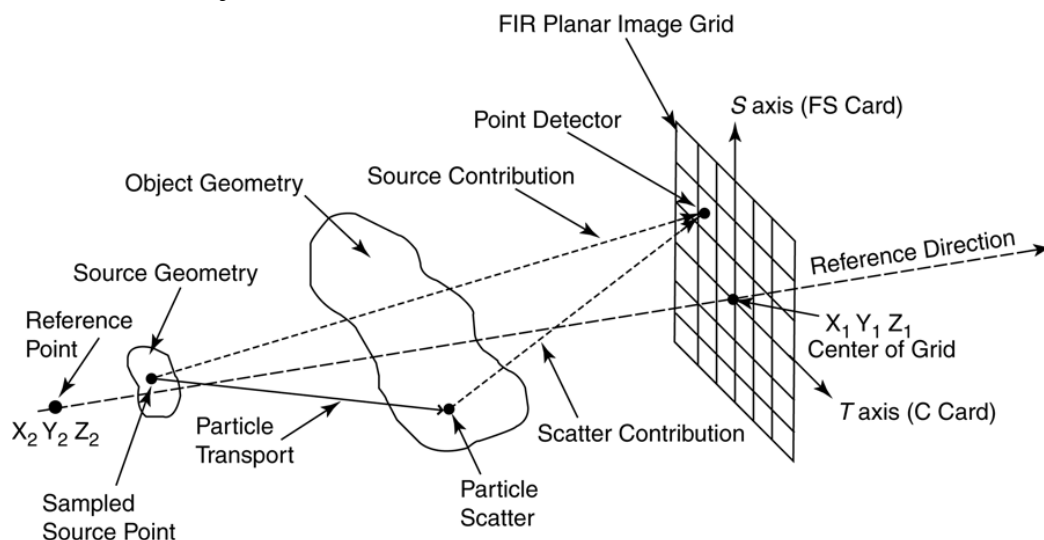


Figure 2-11
Diagram of an FIR (Flux Image Radiograph) tally for a source external to the object.

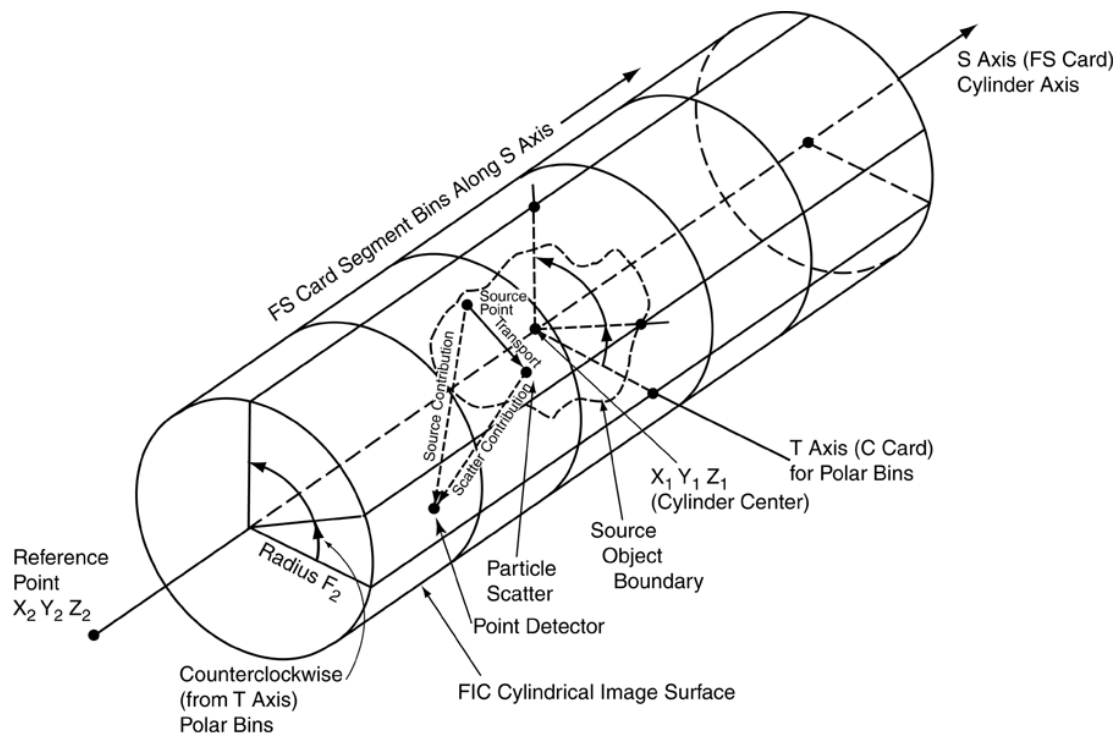


Figure 2-12

Diagram of an FIC (Flux Image on a Cylinder) tally for a source internal to the object.

In both cases, a ray-trace point-detector flux contribution is made to every image grid bin (pixel) from each source and scatter event. Allowing each event to contribute to all pixels reduces statistical fluctuations across the grid that would occur if the grid location for the contribution were selected randomly. For each source and scatter event, the direction cosines to a pixel detector point are determined. The option exists to select a random position in the pixel. The same relative random offset is used for all pixels for a source or scatter event. The random detector location in a pixel changes from event to event. The option also exists to select the point detector location at the center of each pixel when the center flux is desired.

A standard point detector attenuated ray-trace flux contribution to the image pixel is then made. A new direction cosine is determined for each pixel followed by the new ray-trace flux calculation. These tallies automatically create a source-only contribution and a total for each pixel. Standard point detector tally modifications can be made to the image tally, for example, by using the FM, PD, and FT cards.

b. Pinhole Image Tally FIP

The Flux Image by Pinhole (FIP) tally uses a pinhole (as in a pinhole camera) to create a neutron or photon image onto a planar rectangular grid that acts much like photographic film. Figure 2-13 is a diagram of the FIP image tally. Each source and scatter event contributes to one point detector on the image grid pixel intersected by the particle trajectory through the pinhole.

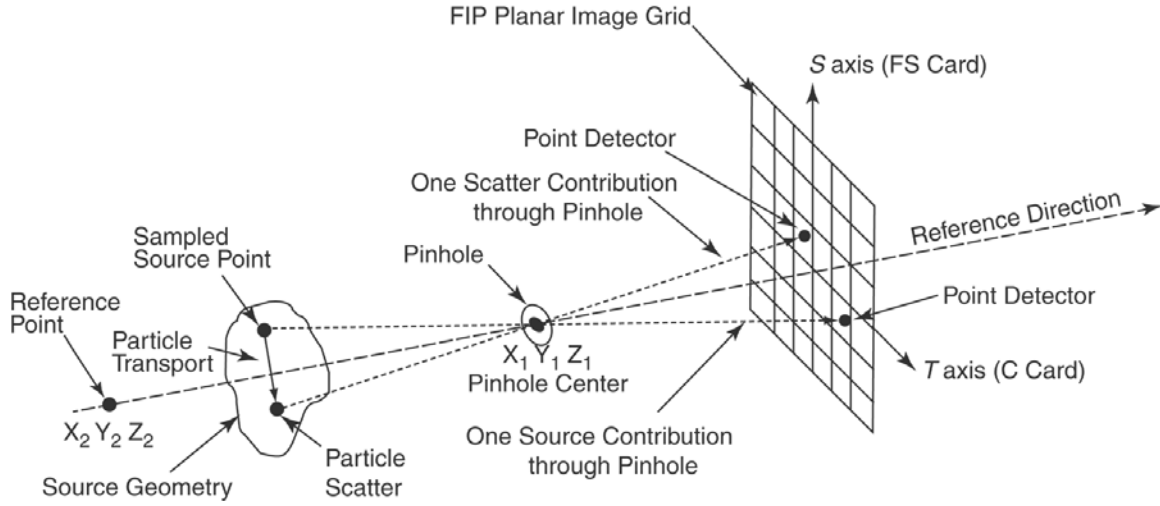


Figure 2-13

Diagram of an FIP (Flux Image by Pinhole) tally for a source internal to the object.

The particle event point and the virtual pinhole point (sampled uniformly in area if a radius is specified) are used to define the direction cosines of the contribution to be made from the source or scatter location through the pinhole to one image grid element (pixel). Once this direction is established, a ray-trace point detector flux contribution is made to the intersected pixel including attenuation by any material along that path. No source or scattering events on the image grid side of the pinhole will contribute to the image.

The pinhole and associated grid will image both direct source contributions and the direct plus any scattered contributions. Standard tally modifications can be made to the image tally, for example, by using the FM, PD, and FT cards.

The magnitude of the flux contribution through the pinhole to a pixel is calculated as follows. The flux at a pinhole point P is $\phi_P(\vec{\Omega})$, where $\vec{\Omega}$ is the direction that intersects the pinhole at point P . Define μ to be the cosine of the angle between the detector trajectory and the reference direction, which is perpendicular to the plane of the pinhole. The particle weight per unit pinhole area (or the particle current per unit pinhole area) is $\phi_P(\vec{\Omega})\mu$. The weight in a small area dA in the pinhole is $\phi_P(\vec{\Omega})\mu dA$. The total particle weight W integrated over the pinhole area A_P is:

$$W = \int_{A_P} \phi_P(\vec{\Omega})\mu dA \quad .$$

The FIP tally selects one particle trajectory to carry this weight. This trajectory should be sampled in dA from

$$p(\vec{\Omega})d(\vec{\Omega}) = \frac{\phi_P(\vec{\Omega})\mu dA}{\int_{A_P} \phi_P(\vec{\Omega})\mu dA} \quad .$$

Instead, the pinhole point P sampling is biased to be uniform in the pinhole area A_P ; that is,

$$b(\vec{\Omega})d(\vec{\Omega}) = \frac{dA}{A_P} .$$

To account for this biased sampling, the weight W of the sample must be multiplied by

$$w_m(\vec{\Omega}) = \frac{p(\vec{\Omega})}{b(\vec{\Omega})} = \frac{A_P \phi_P(\vec{\Omega}) \mu}{\int \phi_P(\vec{\Omega}) \mu dA} .$$

Thus, an unbiased estimate of the sampled weight going through dA at the pinhole is

$$W_P(\vec{\Omega}) = W w_m(\vec{\Omega}) \text{ or}$$

$$W_P(\vec{\Omega}) = \int \phi_P(\vec{\Omega}) \mu dA \frac{A_P \phi_P(\vec{\Omega}) \mu}{\int \phi_P(\vec{\Omega}) \mu dA} = A_P \phi_P(\vec{\Omega}) \mu .$$

Now that an unbiased estimate of the weight through dA is obtained, an unbiased estimate of the weight arriving on the image plane can also be obtained. If $\lambda(\vec{\Omega})$ is the optical path along $\vec{\Omega}$ from the sampled pinhole point to the image plane, then the weight $W_{\text{pixel}}(\vec{\Omega})$ arriving at the pixel in the image plane is

$$W_{\text{pixel}}(\vec{\Omega}) = W_P(\vec{\Omega}) e^{-\lambda(\vec{\Omega})} = A_P \phi_P(\vec{\Omega}) \mu e^{-\lambda(\vec{\Omega})} .$$

The surface flux at the image plane is estimated by the $W_{\text{pixel}}(\vec{\Omega})$ divided by μ (note that the pinhole plane and image plane are parallel) divided by pixel area A_{pixel} . Therefore, the surface flux at the intersected pixel is

$$\phi_{\text{pixel}}(\vec{\Omega}) = \frac{\phi_P(\vec{\Omega}) e^{-\lambda(\vec{\Omega})} A_P}{A_{\text{pixel}}} .$$

Thus, the flux at the pixel is just the $e^{-\lambda(\vec{\Omega})}$ attenuated flux at the pinhole scaled by the ratio of A_P (where the weight W passes through) to the A_{pixel} (the pixel where the flux $\phi_{\text{pixel}}(\vec{\Omega})$ is scored). If a perfect pinhole with no pinhole area is used, then A_P is defined to be unity.

4. General Considerations of Point Detector Estimators

a. Pseudoparticles and detector reliability: Point and ring detectors are Monte Carlo methods wherein the simulation of particle transport from one place to another is deterministically short-circuited. Transport from the source or collision point to the detector is replaced by a deterministic estimate of the potential contribution to the detector. This transport between the source or collision point and the detector can be thought of as being via “pseudoparticles.” Pseudoparticles undergo no further collisions. These particles do not reduce the weight or otherwise affect the random walk of the particles that produced them. They are merely estimates of a potential contribution. The only resemblance to Monte Carlo particles is that the quantity they

estimate requires an attenuation term that must be summed over the trajectory from the source or collision to the detector. Thus most of the machinery for transporting particles can also be used for the pseudoparticles. No records (for example, tracks entering) are kept about pseudoparticle passage.

Because detectors rely on pseudoparticles rather than particle simulation by random walk, they should be considered only as a very useful last resort. Detectors are unbiased estimators, but their use can be tricky, misleading, and occasionally unreliable. Consider the problem illustrated in Figure 2-14.

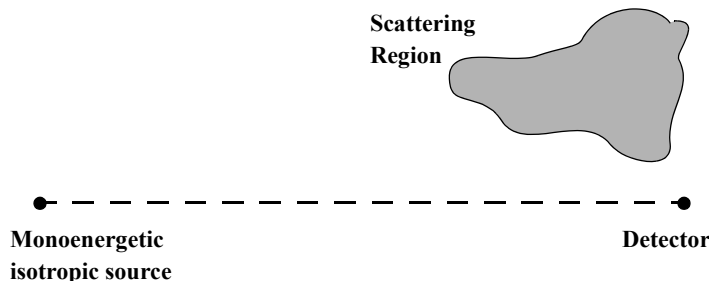


Figure 2-14

The monoenergetic isotropic point source always will make the same contribution to the point detector, so the variance of that contribution will be zero. If no particles have yet collided in the scattering region, the detector tally will be converged to the source contribution, which is wrong and misleading. But as soon as a particle collides in the scattering region, the detector tally and its variance will jump. Then the detector tally and variance will steadily decrease until the next particle collides in the scattering region, at which time there will be another jump.

These jumps in the detector score and variance are characteristic of undersampling important regions. Next event estimators are prone to undersampling as already described on page 2–64 for the $p(\mu)$ term of photon coherent scattering. The jump discussed here is from the sudden change in the R and possibly λ terms. Jumps in the tally caused by undersampling can be eliminated only by better sampling of the undersampled scattering region that caused them.

Biasing Monte Carlo particles toward the tally region would cause the scattering region to be sampled better, thus eliminating the jump problem. It is recommended that detectors be used with caution and with a complete understanding of the nature of next event estimators. When detectors are used, the tally fluctuation charts printed in the output file should be examined closely to see the degree of the fluctuations. Also the detector diagnostic print tables should be examined to see if any one pseudoparticle trajectory made an unusually large contribution to the tally. Detector results should be viewed suspiciously if the relative error is greater than 5%. Close attention should be paid to the tally statistical analysis and the ten statistical checks described on page 2–129.

b. Detectors and reflecting, white, or periodic surfaces: Detectors used with reflecting, white, or periodic surfaces give wrong answers because pseudoparticles travel only in straight lines. Consider Figure 2-15, with a point detector and eight source cells. The imaginary cells and point detector are also shown on the other side of the mirror. The solid line shows the source contribution from the indicated cell. MCNP does not allow for the dashed-line contribution on the

other side of the reflecting surface. The result is that contributions to the detector will always be from the solid path instead of from a mixture of solid and dashed contributions. This same situation occurs at every collision. Therefore, the detector tally will be lower (with the same starting weight) than the correct answer and should not be used with reflecting, white, or periodic surfaces. The effect is even worse for problems with multiple reflecting, white, or periodic surfaces.

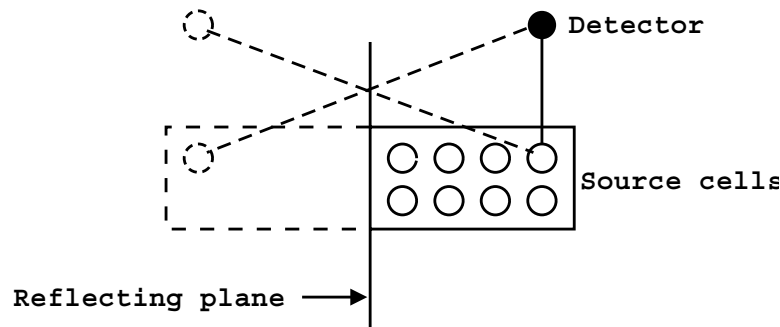


Figure 2-15

c. Variance reduction schemes for detectors: Pseudoparticles of point detectors are not subject to the variance reduction schemes applied to particles of the random walk. They do not split according to importances, weight windows, etc., although they are terminated by entering zero importance cells. However, two Russian roulette games are available specifically for detector pseudoparticles.

The PD card can be used to specify the pseudoparticle generation probability for each cell. The entry for each cell i is p_i where $0 \leq p_i \leq 1$. Pseudoparticles are created with probability p_i and weight $1/p_i$. If $p_i = 1$, which is the default, every source or collision event produces a pseudoparticle. If $p_i = 0$, no pseudoparticle is produced. Setting $p_i = 0$ in a cell that can actually contribute to a detector erroneously biases the detector tally by eliminating such contributions. Thus $p_i = 0$ should be used only if the true probability of scoring is zero or if the score from cell i is unwanted for some legitimate reason such as problem diagnostics. Fractional entries of p_i should be used with caution because the PD card applies equally to all pseudoparticles. The DD card can be used to Russian roulette just the unimportant pseudoparticles. However, the DD card roulette game often requires particles to travel some distance along their trajectory before being killed. When cells are many mean-free paths from the detector, the PD card may be preferable.

The DD card controls both the detector diagnostic printing and a Russian roulette game played on pseudoparticles in transit to detectors. The Russian roulette game is governed by the input parameter k that controls a comparison weight w_c internal to MCNP, such that

$$\begin{aligned} w_c &= -k \text{ if } k < 0; \\ w_c &= 0 \text{ if } k = 0; \\ w_c &= 0 \text{ if } k > 0 \text{ and } N \leq 200; \\ w_c &= (k/N) \sum_i^I \phi_i \text{ if } k > 0 \text{ and } N > 200, \\ &\text{where } N = \text{number of histories run so far,} \end{aligned}$$

I = number of pseudoparticles started so far,
 $\phi_i = Wp(\mu)e^{-\lambda/(2\pi R^2)}$,
 I = contribution of the i^{th} pseudoparticle to the detector tally.

When each pseudoparticle is generated, W , $p(\mu)$, and R are already known before the expensive tracking process is undertaken to determine λ . If $Wp(\mu)/(2\pi R^2) < w_c$, the pseudoparticle contribution to the detector ϕ_i will be less than the comparison weight. Playing Russian roulette on all pseudoparticles with $\phi_i < w_c$ avoids the expensive tracking of unimportant pseudoparticles. Most are never started. Some are started but are rouletted as soon as λ has increased to the point where $Wp(\mu)e^{-\lambda/(2\pi R^2)} < w_c$. Rouletting pseudoparticles whose expected detector contribution is small also has the added benefit that those pseudoparticles surviving Russian roulette now have larger weights, so the disparity in particle weights reaching the detector is reduced. Typically, using the DD card will increase the efficiency of detector problems by a factor of ten. This Russian roulette is so powerful that it is one of two MCNP variance reduction options that is turned on by default. The default value of k is 0.1. The other default variance reduction option is implicit capture.

The DD card Russian roulette game is almost foolproof. Performance is relatively insensitive to the input value of k . For most applications the default value of $k = 0.1$ is adequate. Usually, choose k so that there are 1–5 transmissions (pseudoparticle contributions) per source history. If k is too large, too few pseudoparticles are sampled; thus $k \geq 1$ is a fatal error.

Because a random number is used for the Russian roulette game invoked by $k > 0$, the addition of a detector tally affects the random walk tracking processes. Detectors are the only tallies that affect results. If any other tally type is added to a problem, the original problem tallies remain unchanged. Because detectors use the default DD card Russian roulette game, and that game affects the random number sequence, the whole problem will track differently and the original tallies will agree only to within statistics. Because of this tracking difference, it is recommended that $k < 0$ be used once a good guess at w_c can be made. This is especially important if a problem needs to be debugged by starting at some history past the first one. Also, $k < 0$ makes the first 200 histories run faster.

There are two cases when it is beneficial to turn off the DD card Russian roulette game by setting $k = 0$. First, when looking at the tail of a spectrum or some other low probability event, the DD card roulette game will preferentially eliminate small scores and thus eliminate the very phenomenon of interest. For example, if energy bias is used to preferentially produce high energy particles, these biased particles will have a lower weight and thus preferentially will be rouletted by the DD card game. Second, in very deep penetration problems, pseudoparticles will sometimes go a long way before being rouletted. In this rare case it is wasteful to roulette a pseudoparticle after a great deal of time has been spent following it and perhaps a fractional PD card should be used or, if possible, a cell or surface tally.

d. Coincident detectors: Because tracking pseudoparticles is very expensive, MCNP uses a single pseudoparticle for multiple detectors, known as coincident detectors, that must be identical in:

geometric location,
particle type (that is, neutron or photon),
upper time bin limit,

DD card Russian Roulette control parameter, k , and
PD card entries, if any.

Energy bins, time bins, tally multipliers, response functions, fictitious sphere radii, user-supplied modifications (TALLYX), etc., can all be different. Coincident detectors require little additional computational effort because most detector time is spent in tracking a pseudoparticle. Multiple detectors using the same pseudoparticle are almost “free.”

e. Direct vs. total contribution: Unless specifically turned off by the user, MCNP automatically prints out both the direct and total detector contribution. Recall that pseudoparticles are generated at source and collision events. The direct contribution is that portion of the tally from pseudoparticles born at source events. The total contribution is the total tally from both source and collision events. For Mode N P problems with photon detectors, the direct contribution is from pseudophotons born in neutron collisions. The direct contributions for detailed photon physics will be smaller than the simple physics direct results because coherent scattering is included in the detailed physics total cross section and omitted in the simple physics treatment.

f. Angular distribution functions for point detectors: All detector estimates require knowledge of the $p(\mu)$ term, the value of the probability density function at an angle θ , where $\mu = \cos \theta$. This quantity is available to MCNP for the standard source and for all kinds of collisions. For user-supplied source subroutines, MCNP assumes an isotropic distribution

$$p(\mu)d\mu = \frac{d\Omega}{4\pi} = \int_0^{2\pi} \frac{d\mu d\phi}{4\pi} = \frac{1}{2}d\mu \quad .$$

Therefore, the variable PSC = $p(\mu) = 1/2$. If the source distribution is not isotropic in a user-supplied source subroutine, the user must also supply a subroutine SRCDX if there are any detectors or DXTRAN spheres in the problem. In subroutine SRCDX, the variable PSC must be set for each detector and DXTRAN sphere. An example of how this is done and also a description of several other source angular distribution functions is in Chapter 4.

g. Detectors and the $S(\alpha,\beta)$ thermal treatment: The $S(\alpha,\beta)$ thermal treatment poses special challenges to next event estimators because the probability density function for angle has discrete lines to model Bragg scattering and other molecular effects. Therefore, MCNP has an approximate model⁵⁴ that, for the PSC calculation (not the transport calculation), replaces the discrete lines with finite histograms of width $\mu < .1$.

This approximation has been demonstrated to accurately model the discrete line $S(\alpha,\beta)$ data. In cases where continuous data is approximated with discrete lines, the approximate scheme cancels the errors and models the scattering better than the random walk.⁵⁵ Thus the $S(\alpha,\beta)$ thermal treatment can be used with confidence with next event estimators like detectors and DXTRAN.

F. Additional Tally Features

The standard MCNP tally types can be controlled, modified, and beautified by other tally cards. These cards are described in detail in Chapter 3; an overview is given here.

1. Bin Limit Control

The integration limits of the various tally types can be controlled by E, T, C, and FS cards. The E card establishes energy bin ranges; the T card establishes time bin ranges; the C card establishes cosine bin ranges; and the FS card segments the surface or cell of a tally into subsurface or subcell bins.

2. Flagging

Cell and surface flagging cards, CF and SF, determine where the different portions of a tally originate.

Example: F4 1
 CF4 2 3 4

The flux tally for cell 1 is output twice: first, the total flux in cell 1; and second, the flagged tally, or that portion of the flux caused by particles having passed through cells 2, 3, or 4.

3. Multipliers and Modification

MCNP tallies can be modified in many different ways. The EM, TM, and CM cards multiply the quantities in each energy, time, or cosine bin by a different constant. This capability is useful for modeling response functions or changing units. For example, a surface current tally can have its units changed to per steradian by entering the inverse steradian bin sizes on the CM card.

The DE and DF cards allow modeling of an energy-dependent dose function that is a continuous function of energy from a table whose data points need not coincide with the tally energy bin structure (E card). An example of such a dose function is the flux-to-radiation dose conversion factor given in Appendix H.

The FM card multiplies the F1, F2, F4, and F5 tallies by any continuous-energy quantity available in the data libraries. For example, average heating numbers $H_{avg}(E)$ and total cross section $\sigma_T(E)$ are stored on the MCNP data libraries. An F4 tally multiplied by $\sigma_T H_{avg}(E) \rho_a / \rho_g$ converts it to an F6 tally, or an F5 detector tally multiplied by the same quantity calculates heating at a point (see page 2–91). The FM card can modify any flux or current tally of the form $\int \phi(E) dE$ into $\int R(E) \phi(E) dE$, where $R(E)$ is any combination of sums and products of energy-dependent quantities known to MCNP.

The FM card can also model attenuation. Here the tally is converted to $\int \phi(E) e^{-\sigma_t(E) \rho_a x} dE$, where x is the thickness of the attenuator, ρ_a is its atom density, and σ_t is its total cross section. Double parentheses allow the calculation of $\int \phi(E) e^{-\sigma_t(E) \rho_a x} R(E) dE$. More complex expressions of $\sigma_t(E) \rho_a x$ are allowed so that many attenuators may be stacked. This is useful for calculating attenuation in line-of-sight pipes and through thin foils and detector coatings, particularly when done in conjunction with point and ring detector tallies. Beware, however, that attenuation assumes

that the attenuated portion of the tally is lost from the system by capture or escape and cannot be scattered back in.

Two special FM card options are available. The first option sets $R(E) = 1/\phi(E)$ to score tracks or collisions. The second option sets $R(E) = 1/velocity$ to score population or prompt removal lifetime.

4. Special Treatments

A number of special tally treatments are available using the FT tally card. A brief description of each one follows.

a. Change current tally reference vector: F1 current tallies measure bin angles relative to the surface normal. They can be binned relative to any arbitrary vector defined with the FRV option.

b. Gaussian energy broadening: The GEB option can be used to better simulate a physical radiation detector in which energy peaks exhibit Gaussian energy broadening. The tallied energy is broadened by sampling from the Gaussian:

$$f(E) = Ce^{-\left(\frac{E-E_o}{A}\right)^2},$$

where E = the broadened energy;
 E_o = the unbroadened energy of the tally;
 C = a normalization constant; and
 A = the Gaussian width.

The Gaussian width is related to the full width half maximum (FWHM) by

$$A = \frac{FWHM}{2\sqrt{\ln 2}} = .60056120439322 * FWHM$$

The desired FWHM is specified by the user-provided constants, a, b, and c, where

$$FWHM = a + b\sqrt{E + cE^2}.$$

The FWHM is defined as $FWHM = 2(E_{FWHM} - E_o)$,

where E_{FWHM} is such that $f(E_{FWHM}) = \frac{1}{2} f(E_o)$

and $f(E_o)$ is the maximum value of $f(E)$.

c. Time convolution: Because the geometry and material compositions are independent of time, except in the case of time-dependent temperatures, the expected tally $T(t, t + \tau)$ at time $t + \tau$ from a source particle emitted at time t is identical to the expected tally $T(0, \tau)$ from a source particle

emitted at time 0. Thus, if a calculation is performed with all source particles started at $t = 0$, one has an estimate of $T(0, \tau)$ and the tallies T_{Q_i} from a number of time-distributed sources. $Q_i(t)$ can be calculated at time η as

$$T_{Q_i}(\eta) = \int_a^b Q_i(t)T(t, \eta)dt = \int_a^b Q_i(t)T(0, \eta - t)dt \quad ,$$

by sampling t from $Q_i(t)$ and recording each particle's tally (shifted by t), or after the calculation by integrating $Q_i(t)$ multiplied by the histogram estimate of $T(0, \eta - t)$. The latter method is used in MCNP to simulate a source as a square pulse starting at time a and ending at time b , where a and b are supplied by the TMC option.

d. Binning by the number of collisions: Tallies can be binned by the number of collisions that caused them with the INC option and an FU card. A current tally, for example, can be subdivided into the portions of the total current coming from particles that have undergone zero, one, two, three, ... collisions before crossing the surface. In a point detector tally, the user can determine what portion of the score came from particles having their 1st, 2nd, 3rd, ... collision. Collision binning is particularly useful with the exponential transform because the transform reduces variance by reducing the number of collisions. If particles undergoing many collisions are the major contributor to a tally, then the exponential transform is ill-advised. When the exponential transform is used, the portion of the tally coming from particles having undergone many collisions should be small.

e. Binning by detector cell: The ICD option with an FU card is used to determine what portion of a detector tally comes from what cells. This information is similar to the detector diagnostics print, but the FT card can be combined with energy and other binning cards. The contribution to the normalized rather than unnormalized tally is printed.

f. Binning by source distribution: The SCX and SCD options are used to bin a tally score according to what source distribution caused it.

g. Binning by multigroup particle type: The PTT option with an FU card is used to bin multigroup tallies by particle type. The MCNP multigroup treatment is available for neutron, coupled neutron/photon, and photon problems. However, charged particles or any other combinations of particles can be run with the various particles masquerading as neutrons and are printed out in the OUTP file as if they were neutrons. With the PTT option, the tallies can be segregated into particle types by entering atomic weights in units of MeV on the FU card. The FU atomic weights must be specified to within 0.1% of the true atomic weight in MeV units; thus FU .511 specifies an electron, but .510 is not recognized.

h. Binning by particle charge: The ELC option allows binning F1 current tallies by particle charge. There are three ELC options:

1. Cause negative electrons to make negative scores and positrons to make positive scores. Note that by tallying positive and negative numbers the relative error is unbounded and this tally may be difficult to converge.

2. Segregate electrons and positrons into separate bins plus a total bin. There will be three bins (positron, electron, and total) all with positive scores. The total bin will be the same as the single tally bin without the ELC option.
3. Segregate electrons and positrons into separate bins plus a total bin, with the electron bin scores being all negative to reflect their charge. The bins will be for positrons (positive scores), electrons (negative scores), and total. The total bin will be the same as the single bin with the first ELC option above (usually with negative scores because there are more electrons than positrons).

5. User Modification

If the above capabilities do not provide exactly what is desired, tallies can be modified by a user-supplied TALLYX subroutine (FU card). As with a user-supplied SOURCE subroutine, which lets the users provide their own specialized source, the TALLYX subroutine lets the user modify any tally, with all the programming changes conveniently located in a single subroutine.

6. Tally Output Format

Not only can users change the contents of MCNP tallies, the output format can be modified as well. Any desired descriptive comment can be added to the tally title by the tally comment (FC) card. The printing order can be changed (FQ card) so that instead of, for instance, getting the default output blocks in terms of time vs. energy, they could be printed in blocks of segment vs. cosine. The tally bin that is monitored for the tally fluctuation chart printed at the problem end and used in the statistical analysis of the tally can be selected (TF card). Detector tally diagnostic prints are controlled with the DD card. Finally, the PRINT card controls what optional tables are displayed in the output file.

VI. ESTIMATION OF THE MONTE CARLO PRECISION

Monte Carlo results represent an average of the contributions from many histories sampled during the course of the problem. An important quantity equal in stature to the Monte Carlo answer (or tally) itself is the statistical error or uncertainty associated with the result. The importance of this error and its behavior versus the number of histories cannot be overemphasized because the user not only gains insight into the quality of the result, but also can determine if a tally appears statistically well behaved. If a tally is not well behaved, the estimated error associated with the result generally will not reflect the true confidence interval of the result and, thus, the answer could be completely erroneous. MCNP contains several quantities that aid the user in assessing the quality of the confidence interval.¹²¹

The purpose of this section is to educate MCNP users about the proper interpretation of the MCNP estimated mean, relative error, variance of the variance, and history score probability density function. Carefully check tally results and the associated tables in the tally fluctuation charts to ensure a well-behaved and properly converged tally.

A. Monte Carlo Means, Variances, and Standard Deviations

Monte Carlo results are obtained by sampling possible random walks and assigning a score x_i (for example, x_i = energy deposited by the i^{th} random walk) to each random walk. Random walks typically will produce a range of scores depending on the tally selected and the variance reduction chosen.

Suppose $f(x)$ is the history score probability density function for selecting a random walk that scores x to the tally being estimated. The true answer (or mean) is the expected value of x , $E(x)$, where

$$E(x) = \int xf(x)dx = \text{true mean.}$$

The function $f(x)$ is seldom explicitly known; thus, $f(x)$ is implicitly sampled by the Monte Carlo random walk process. The true mean then is estimated by the sample mean \bar{x} where

$$\bar{x} = \frac{1}{N} \sum_{i=1}^N x_i, \quad (2.18)$$

where x_i is the value of x selected from $f(x)$ for the i^{th} history and N is the number of histories calculated in the problem. The Monte Carlo mean \bar{x} is the average value of the scores x_i for all the histories calculated in the problem. The relationship between $E(x)$ and \bar{x} is given by the Strong Law of Large Numbers¹ that states that if $E(x)$ is finite, \bar{x} tends to the limit $E(x)$ as N approaches infinity.

The variance of the population of x values is a measure of the spread in these values and is given by¹

$$\sigma^2 = \int (x - E(x))^2 f(x) dx = E(x^2) - (E(x))^2.$$

The square root of the variance is σ , which is called the standard deviation of the population of scores. As with $E(x)$, σ is seldom known but can be estimated by Monte Carlo as S , given by (for large N)

$$S^2 = \frac{\sum_{i=1}^N (x_i - \bar{x})^2}{N - 1} \approx \overline{x^2} - \bar{x}^2 \quad (2.19a)$$

and

$$\overline{x^2} = \frac{1}{N} \sum_{i=1}^N x_i^2. \quad (2.19b)$$

The quantity S is the estimated standard deviation of the population of x based on the values of x_i that were actually sampled.

The estimated variance of \bar{x} is given by

$$S_{\bar{x}}^2 = \frac{S^2}{N} . \quad (2.20)$$

These formulas do not depend on any restriction on the distribution of x or \bar{x} (such as normality) beyond requiring that $E(x)$ and σ^2 exist and are finite. The estimated standard deviation of the mean \bar{x} is given by $S_{\bar{x}}$.

It is important to note that $S_{\bar{x}}$ is proportional to $1/\sqrt{N}$, which is the inherent drawback to the Monte Carlo method. To halve $S_{\bar{x}}$, four times the original number of histories must be calculated, a calculation that can be computationally expensive. The quantity $S_{\bar{x}}$ can also be reduced for a specified N by making S smaller, reducing the inherent spread of the tally results. This can be accomplished by using variance reduction techniques such as those discussed in Section VII of this chapter beginning on page 2–134.

B. Precision and Accuracy

There is an extremely important difference between precision and accuracy of a Monte Carlo calculation. As illustrated in Figure 2-16, precision is the uncertainty in \bar{x} caused by the statistical

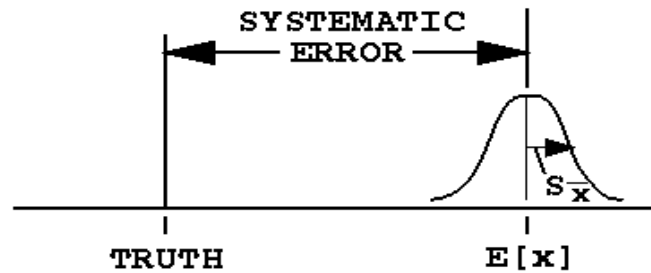


Figure 2-16

fluctuations of the x_i 's for the portion of physical phase space sampled by the Monte Carlo process. Important portions of physical phase space might not be sampled because of problem cutoffs in time or energy, inappropriate use of variance reduction techniques, or an insufficient sampling of important low-probability events. Accuracy is a measure of how close the expected value of \bar{x} , $E(x)$, is to the true physical quantity being estimated. The difference between this true value and $E(x)$ is called the systematic error, which is seldom known. Error or uncertainty estimates for the results of Monte Carlo calculations refer only to the precision of the result and not to the accuracy. It is quite possible to calculate a highly precise result that is far from the physical truth because nature has not been modeled faithfully.

1. Factors Affecting Problem Accuracy

Three factors affect the accuracy of a Monte Carlo result: (1) the code, (2) problem modeling, and (3) the user. Code factors encompass: the physics features included in a calculation as well as the mathematical models used; uncertainties in the data, such as the transport and reaction cross sections, Avogadro's number, atomic weights, etc.; the quality of the representation of the differential cross sections in energy and angle; and coding errors (bugs). All of the applicable physics must be included in a calculation to produce accurate results. Even though the evaluations are not perfect, more faithful representation of the evaluator's data should produce more accurate results. The descending order of preference for Monte Carlo data for calculations is continuous energy, thinned continuous energy, discrete reaction, and multigroup. Coding errors can always be a problem because no large code is bug-free. MCNP, however, is a very mature, heavily used production code. With steadily increasing use over the years, the likelihood of a serious coding error continues to diminish.

The second area, problem-modeling factors, can quite often contribute to a decrease in the accuracy of a calculation. Many calculations produce seemingly poor results because the model of the energy and angular distribution of the radiation source is not adequate. Two other problem-modeling factors affecting accuracy are the geometrical description and the physical characteristics of the materials in the problem.

The third general area affecting calculational accuracy involves user errors in the problem input or in user-supplied subroutines and patches to MCNP. The user can also abuse variance reduction techniques such that portions of the physical phase space are not allowed to contribute to the results. Checking the input and output carefully can help alleviate these difficulties. A last item that is often overlooked is a user's thorough understanding of the relationship of the Monte Carlo tallies to any measured quantities being calculated. Factors such as detector efficiencies, data reduction and interpretation, etc., must be completely understood and included in the calculation, or the comparison is not meaningful.

2. Factors Affecting Problem Precision

The precision of a Monte Carlo result is affected by four user-controlled choices: (1) forward vs. adjoint calculation, (2) tally type, (3) variance reduction techniques, and (4) number of histories run.

The choice of a forward vs. adjoint calculation depends mostly on the relative sizes of the source and detector regions. Starting particles from a small region is easy to do, whereas transporting particles to a small region is generally hard to do. Because forward calculations transport particles from source to detector regions, forward calculations are preferable when the detector (or tally) region is large and the source region is small. Conversely, because adjoint calculations transport particles backward from the detector region to the source region, adjoint calculations are preferable when the source (or tally) region is large and the detector region is small. MCNP can be run in multigroup adjoint mode. There is no continuous-energy adjoint capability.

As alluded to above, the smaller the tally region, the harder it becomes to get good tally estimates. An efficient tally will average over as large a region of phase space as practical. In this connection,

tally dimensionality is extremely important. A one-dimensional tally is typically 10 to 100 times easier to estimate than a two-dimensional tally, which is 10 to 100 times easier than a three-dimensional tally. This fact is illustrated in Figure 2-22 later in this section.

Variance reduction techniques can be used to improve the precision of a given tally by increasing the nonzero tallying efficiency and by decreasing the spread of the nonzero history scores. These two components are depicted in a hypothetical $f(x)$ shown in Figure 2-17. See page 2-122 for

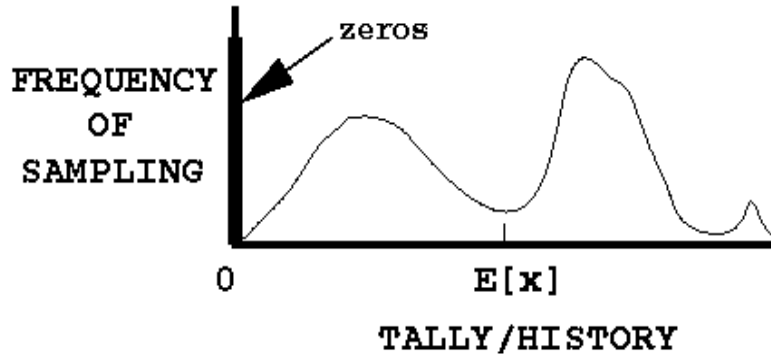


Figure 2-17

more discussion about the empirical $f(x)$ for each tally fluctuation chart bin. A calculation will be more precise when the history-scoring efficiency is high and the variance of the nonzero scores is low. The user should strive for these conditions in difficult Monte Carlo calculations. Examples of these two components of precision are given on page 2-118.

More histories can be run to improve precision (see subsection C below). Because the precision is proportional to $1/\sqrt{N}$, running more particles is often costly in computer time and therefore is viewed as the method of last resort for difficult problems.

C. The Central Limit Theorem and Monte Carlo Confidence Intervals

To define confidence intervals for the precision of a Monte Carlo result, the Central Limit Theorem¹ of probability theory is used, stating that

$$\lim_{N \rightarrow \infty} Pr \left[E(x) + \alpha \frac{\sigma}{\sqrt{N}} < \bar{x} < E(x) + \beta \frac{\sigma}{\sqrt{N}} \right] = \frac{1}{\sqrt{2\pi}} \int_{\alpha}^{\beta} e^{-t^2/2} dt \quad ,$$

where α and β can be any arbitrary values and $Pr[Z]$ means the probability of Z . In terms of the estimated standard deviation of \bar{x} , $S_{\bar{x}}$, this may be rewritten in the following approximation for large N :

$$Pr \left(\left[\alpha S_{\bar{x}} < \frac{\bar{x} - E(x)}{\sigma/\sqrt{N}} < \beta S_{\bar{x}} \right] \right) \approx \frac{1}{\sqrt{2\pi}} \int_{\alpha}^{\beta} e^{-t^2/2} dt \quad .$$

This crucial theorem states that for large values of N (that is, as N tends to infinity) and identically distributed independent random variables x_i with finite means and variances, the distribution of the \bar{x} 's approaches a normal distribution. Therefore, for any distribution of tallies (an example is

shown in Figure 2-17), the distribution of resulting \bar{x} 's will be approximately normally distributed, as shown in Figure 2-16, with a mean of $E(x)$. If S is approximately equal to σ , which is valid for a statistically significant sampling of a tally (that is, N has tended to infinity), then

$$\bar{x} - S_{\bar{x}} < E(x) < \bar{x} + S_{\bar{x}}, \sim 68\% \text{ of the time and} \quad (2.21a)$$

$$\bar{x} - 2S_{\bar{x}} < E(x) < \bar{x} + 2S_{\bar{x}}, \sim 95\% \text{ of the time} \quad (2.21b)$$

from standard tables for the normal distribution function. Eq. (2.18a) is a 68% confidence interval and Eq. (2.18b) is a 95% confidence interval.

The key point about the validity of these confidence intervals is that the physical phase space must be adequately sampled by the Monte Carlo process. If an important path in the geometry or a window in the cross sections, for example, has not been well sampled, both \bar{x} and $S_{\bar{x}}$ will be unknowingly incorrect and the results will be wrong, usually tending to be too small. The user must take great care to be certain that adequate sampling of the source, transport, and any tally response functions have indeed taken place. Additional statistical quantities to aid in the assessment of proper confidence intervals are described in later portions of this section beginning on page 2-127.

D. *Estimated Relative Errors in MCNP*

All standard MCNP tallies are normalized to be per starting particle history (except for some criticality calculations) and are printed in the output with a second number, which is the estimated relative error defined as

$$R \equiv S_{\bar{x}} / \bar{x} \quad (2.22a)$$

The relative error is a convenient number because it represents statistical precision as a fractional result with respect to the estimated mean.

Combining Eqs. (2.15), (2.16), and (2.17), R can be written (for large N) as

$$R = \left[\frac{1}{N} \left(\frac{\overline{x^2}}{\bar{x}^2} - 1 \right) \right]^{1/2} = \left[\frac{\sum_{i=1}^N x_i^2}{(\sum_{i=1}^N x_i)^2} - \frac{1}{N} \right]^{1/2}. \quad (2.22b)$$

Several important observations about the relative error can be made from Eq. (2.19b). First, if all the x_i 's are nonzero and equal, R is zero. Thus, low-variance solutions should strive to reduce the spread in the x_i 's. If the x_i 's are all zero, R is defined to be zero. If only one nonzero score is made, R approaches unity as N becomes large. Therefore, for x_i 's of the same sign, $S_{\bar{x}}$ can never be greater than \bar{x} because R never exceeds unity. For positive and negative x_i 's, R can exceed unity. The range of R values for x_i 's of the same sign is therefore between zero and unity.

To determine what values of R lead to results that can be stated with confidence using Eqs. (2.6), consider Eq. (2.19b) for a difficult problem in which nonzero scores occur very infrequently. In this case,

$$\frac{1}{N} \ll \frac{\sum_{i=1}^N x_i^2}{(\sum_{i=1}^N x_i)^2} . \quad (2.23a)$$

For clarity, assume that there are n out of N ($n \ll N$) nonzero scores that are identical and equal to x . With these two assumptions, R for “difficult problems” becomes

$$R_{D.P.} \sim \left[\frac{nx^2}{n^2 x^2} \right]^{1/2} = \frac{1}{\sqrt{n}}, n \ll N . \quad (2.23b)$$

This result is expected because the limiting form of a binomial distribution with infrequent nonzero scores and large N is the Poisson distribution, which is the form in Eq. (2.20b) used in detector “counting statistics.”

Table 2.4
Estimated Relative Error R vs. Number of Identical Tallies n for Large N

n	1	4	16	25	100	400
R	1.0	0.5	0.25	0.20	0.10	0.05

Through use of Eq. (2.20), a table of R values versus the number of tallies or “counts” can be generated as shown in Table 2.4. A relative error of 0.5 is the equivalent of four counts, which is hardly adequate for a statistically significant answer. Sixteen counts is an improvement, reducing R to 0.25, but still is not a large number of tallies. The same is true for n equals 25. When n is 100, R is 0.10, so the results should be much improved. With 400 tallies, an R of 0.05 should be quite good indeed.

Based on this qualitative analysis and the experience of Monte Carlo practitioners, Table 2.5 presents the recommended interpretation of the estimated 1σ confidence interval $\bar{x}(1 \pm R)$ for various values of R associated with an MCNP tally. These guidelines were determined empirically, based on years of experience using MCNP on a wide variety of problems. Just before the tally fluctuation charts, a “Status of Statistical Checks” table prints how many tally bins of each tally have values of R exceeding these recommended guidelines.

Table 2.5
Guidelines for Interpreting the Relative Error R^a

<u>Range of R</u>	<u>Quality of the Tally</u>
0.5 to 1	Garbage
0.2 to 0.5	Factor of a few
0.1 to 0.2	Questionable
< 0.10	Generally reliable except for point detector
< 0.05	Generally reliable for point detector

^a $R = S_x/\bar{x}$ and represents the estimated statistical relative error at the 1σ level. These interpretations of R assume that all portions of the problem phase space have been well sampled by the Monte Carlo process. Please use statistical checks for detailed information.

Point detector tallies generally require a smaller value of R for valid confidence interval statements because some contributions, such as those near the detector point, are usually extremely important and may be difficult to sample well. Experience has shown that for R less than 0.05, point detector results are generally reliable. For an R of 0.10, point detector tallies may only be known within a factor of a few and sometimes not that well (see the pathological example on page 2–131.)

MCNP calculates the relative error for each tally bin in the problem using Eq. (2.19b). Each x_i is defined as the total contribution from the i^{th} starting particle and all resulting progeny. This definition is important in many variance reduction methods, multiplying physical processes such as fission or (n, xn) neutron reactions that create additional neutrons, and coupled neutron/photon/electron problems. The i^{th} source particle and its offspring may thus contribute many times to a tally and all of these contributions are correlated because they are from the same source particle.

Figure 2-18 represents the MCNP process of calculating the first and second moments of each tally bin and relevant totals using three tally storage blocks of equal length for each tally bin. The hypothetical grid of tally bins in the bottom half of Figure 2-18 has 24 tally bins including the time and energy totals. During the course of the i^{th} history, sums are performed in the first MCNP tally storage block. Some of the tally bins receive no contributions and others receive one or more contributions. At the conclusion of the i^{th} history, the sums are added to the second MCNP tally storage block. The sums in the first MCNP tally storage block are squared and added to the third tally storage block. The first tally storage block is then filled with zeros and history $i + 1$ begins. After the last history N , the estimated tally means are computed using the second MCNP tally storage block and Eq. (2.15). The estimated relative errors are calculated using the second and third MCNP tally storage blocks and Eq. (2.19b). This method of estimating the statistical uncertainty of the result produces the best estimate because the batch size is one, which minimizes the variance of the variance.^{122,123}

Note that there is no guarantee that the estimated relative error will decrease inversely proportional to the \sqrt{N} as required by the Central Limit Theorem because of the statistical nature of the tallies. Early in the problem, R will generally have large statistical fluctuations. Later, infrequent large

contributions may cause fluctuations in $S_{\bar{x}}$ and to a lesser extent in \bar{x} and therefore in R . MCNP calculates a *FOM* for one bin of each numbered tally to aid the user in determining the statistical behavior as a function of N and the efficiency of the tally.

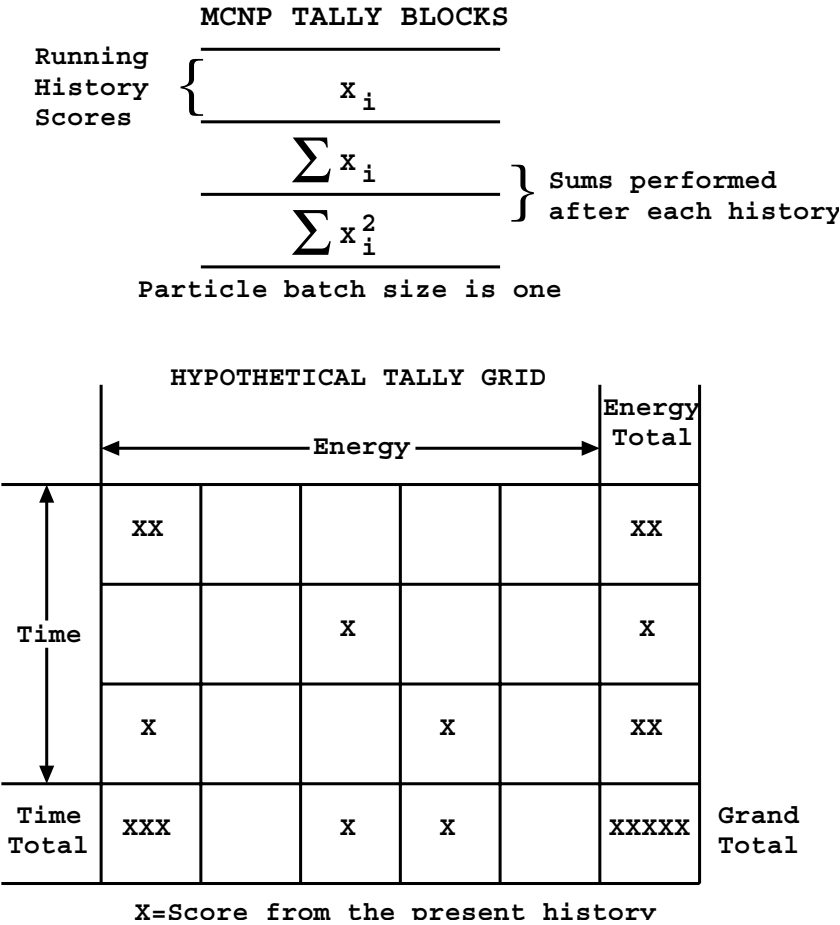


Figure 2-18

E. MCNP Figure of Merit

The estimated relative error squared, R^2 , should be proportional to $1/N$, as shown by Eq. (2.19b). The computer time T used in an MCNP problem should be directly proportional to N ; therefore, R^2T should be approximately a constant within any one Monte Carlo run. It is convenient to define a figure of merit (*FOM*) of a tally to be

$$FOM \equiv \frac{1}{R^2 T} \quad . \tag{2.24a}$$

MCNP prints the *FOM* for one bin of each numbered tally as a function of N , where the unit of computer time T is minutes. The table is printed in particle increments of 1000 up to 20,000 histories. Between 20,000 and 40,000 histories, the increment is doubled to 2000. This trend

continues, producing a table of up to 20 entries. The default increment can be changed by the 5th entry on the PRDMP card.

The *FOM* is a very important statistic about a tally bin and should be studied by the user. It is a tally reliability indicator in the sense that if the tally is well behaved, the *FOM* should be approximately a constant with the possible exception of statistical fluctuations very early in the problem. An order-of-magnitude estimate of the expected fractional statistical fluctuations in the *FOM* is $2R$. This result assumes that both the relative statistical uncertainty in the relative error is of the order of the relative error itself and the relative error is small compared to unity. The user should always examine the tally fluctuation charts at the end of the problem to check that the *FOMs* are approximately constant as a function of the number of histories for each tally.

The numerical value of the *FOM* can be better appreciated by considering the relation

$$R = 1/\sqrt{FOM * T} \quad (2.24b)$$

Table 2.6 shows the expected value of R that would be produced in a one-minute problem ($T = 1$) as a function of the value of the *FOM*. It is clearly advantageous to have a large *FOM* for a problem because the computer time required to reach a desired level of precision is proportionally reduced. Examination of Eq. (2.21b) shows that doubling the *FOM* for a problem will reduce the computer time required to achieve the same R by a factor of two.

Table 2.6
***R* Values as a Function of the *FOM* for $T = 1$ Minute**

<i>FOM</i>	1	10	100	1000	10000
<i>R</i>	1.0	0.32	0.10	0.032	0.010

Another interpretation for the *FOM* involves defining the problem's particle computation rate t as

$$t = N/T \quad (2.24c)$$

where t is the number of particles per minute for a problem on a specific computer and N is the number of particles run in the problem. Substituting Eq. (2.21c) into Eq. (2.21a) and using Eqs. (2.16a), (2.17), and (2.19a), the *FOM* becomes

$$FOM = t \cdot (\bar{x}/S)^2 \quad (2.24d)$$

where S is the estimated standard deviation of the sampled population (not the mean). The squared quantity is a ratio of the desired result divided by a measure of the spread in the sampled values. This ratio is called the tally signal-to-noise ratio:

$$\text{signal-to-noise ratio} = \bar{x}/S \quad (2.24e)$$

The quantity \bar{x}/S approaches the expected value of the signal-to-noise ratio for a problem tally bin as N becomes large. Using Eq. (2.21e), the *FOM* becomes

$$FOM = t(\text{signal-to-noise ratio})^2 \quad (2.24f)$$

The *FOM* is directly proportional to the particles per minute t (as would be expected) and the tally bin signal-to-noise ratio squared. The tally bin signal-to-noise ratio is dependent on the shape of the underlying history score probability density function $f(x)$ for the tally bin (see page 2–122). To increase the *FOM*, t and/or the signal-to-noise ratio can be increased. Since \bar{x} should be the same for the problems with different variance reduction, increasing the *FOM* is equivalent to increasing t/S^2 (decreasing S with variance reduction techniques often decreases t). It is usually worthwhile to optimize the tally efficiency by intelligently running various variance reduction methods and using the largest *FOM* consistent with good phase-space sampling (good sampling can often be inferred by examining the cell particle activity in Print Table 126). MCNP prints both the empirical $f(x)$ and signal-to-noise ratio for the tally fluctuation chart bin of each tally in Print Table 161.

In summary, the *FOM* has three uses. One important use is as a tally reliability indicator. If the *FOM* is not approximately a constant (except for statistical fluctuations early in the problem), the confidence intervals may not overlap the expected score value, $E(x)$, the expected fraction of the time (see page 2–109). A second use for the *FOM* is to optimize the efficiency of the Monte Carlo calculation by making several short test runs with different variance reduction parameters and then selecting the problem with the largest *FOM*. Remember that the statistical behavior of the *FOM* (that is, R) for a small number of histories may cloud the selection of techniques competing at the same level of efficiency. A third use for the *FOM* is to estimate the computer time required to reach a desired value of R by using $T \sim 1/(R^2 FOM)$.

F. Separation of Relative Error into Two Components

Three factors that affect the efficiency of a Monte Carlo problem are (1) history-scoring efficiency, (2) dispersions in nonzero history scores, and (3) computer time per history. All three factors are included in the *FOM*. The first two factors control the value of R ; the third is T .

The relative error can be separated into two components: the nonzero history-scoring efficiency component R_{eff}^2 and the intrinsic spread of the nonzero x_i scores R_{int}^2 . Defining q to be the fraction of histories producing nonzero x_i 's, Eq. 2.19b can be rewritten as

$$R = \frac{\sum_{i=1}^N x_i^2}{(\sum_{i=1}^N x_i)^2} - \frac{1}{N} = \frac{\sum_{x_i \neq 0} x_i^2}{(\sum_{x_i \neq 0} x_i)^2} - \frac{1}{N} = \frac{\sum_{x_i \neq 0} x_i^2}{(\sum_{x_i \neq 0} x_i)^2} - \frac{1}{qN} + \frac{1-q}{qN} \quad (2.25a)$$

Note by Eq. 2.19b that the first two terms are the relative error of the qN nonzero scores. Thus defining,

$$R_{int}^2 = \frac{\sum_{x_i \neq 0} x_i^2}{(\sum_{x_i \neq 0} x_i)^2} - \frac{1}{qN} \quad \text{and} \quad (2.25b)$$

$$R_{eff}^2 = (1 - q)/(qN) \quad \text{yields} \quad (2.25c)$$

$$R^2 = R_{eff}^2 + R_{int}^2 \quad . \quad (2.25d)$$

For identical nonzero x_i 's, R_{int}^2 is zero and for a 100% scoring efficiency, R_{eff}^2 is zero. It is usually possible to increase q for most problems using one or more of the MCNP variance reduction techniques. These techniques alter the random walk sampling to favor those particles that produce a nonzero tally. The particle weights are then adjusted appropriately so that the expected tally is preserved. This topic is described in Section VII (Variance Reduction) beginning on page 2-134. The sum of the two terms of Eq. (2.22d) produces the same result as Eq. (2.19b). Both R_{int}^2 and R_{eff}^2 are printed for the tally fluctuation chart bin of each tally so that the dominant component of R can be identified as an aid to making the calculation more efficient.

These equations can be used to better understand the effects of scoring inefficiency; that is, those histories that do not contribute to a tally. Table 2.7 shows the expected values of R_{eff} as a function of q and the number of histories N . This table is appropriate for identical nonzero scores and represents the theoretical minimum relative error possible for a specified q and N . It is no surprise that small values of q require a compensatingly large number of particles to produce precise results.

Table 2.7
Expected Values of R_{eff} as a Function of q and N

$\frac{q}{N}$	<u>0.001</u>	<u>0.01</u>	<u>0.1</u>	<u>0.5</u>
10^3	0.999	0.315	0.095	0.032
10^4	0.316	0.099	0.030	0.010
10^5	0.100	0.031	0.009	0.003
10^6	0.032	0.010	0.003	0.001

A practical example of scoring inefficiency is the case of infrequent high-energy particles in a down-scattering-only problem. If only a small fraction of all source particles has an energy in the highest energy tally bin, the dominant component of the relative error will probably be the scoring efficiency because only the high-energy source particles have a nonzero probability of contributing to the highest energy bin. For problems of this kind, it is often useful to run a separate problem starting only high-energy particles from the source and to raise the energy cutoff. The much-improved scoring efficiency will result in a much larger *FOM* for the high-energy tally bins.

To further illustrate the components of the relative error, consider the five examples of selected discrete probability density functions shown in Figure 2-19. Cases I and II have no dispersion in the nonzero scores, cases III and IV have 100% scoring efficiency, and case V contains both

elements contributing to R . The most efficient problem is case III. Note that the scoring inefficiency contributes 75% to R in case V, the second worst case of the five.

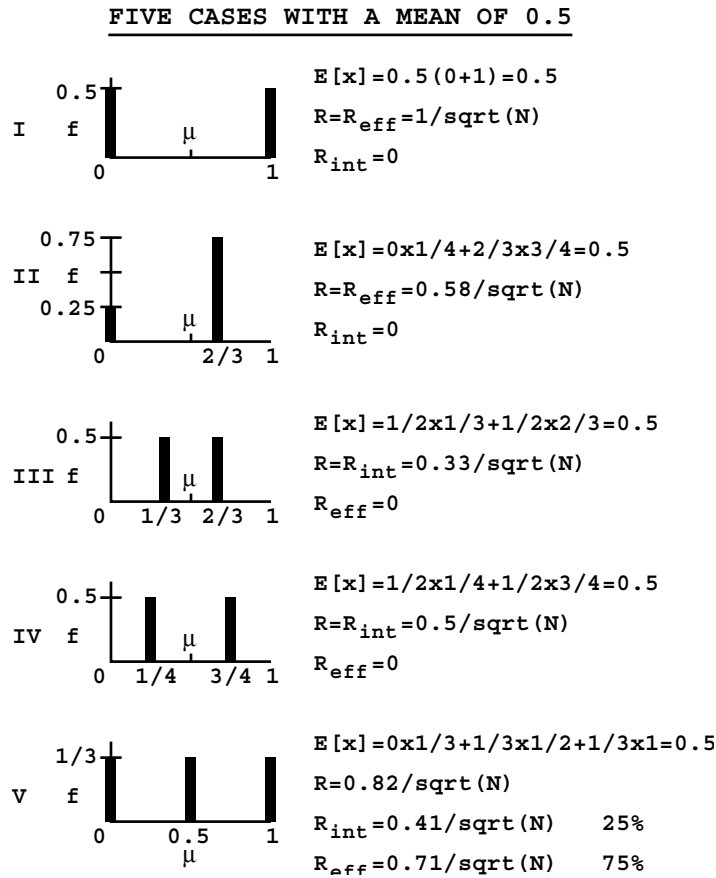


Figure 2-19

G Variance of the Variance

Previous sections have discussed the relative error R and figure of merit FOM as measures of the quality of the mean. A quantity called the relative variance of the variance (VOV) is another useful tool that can assist the user in establishing more reliable confidence intervals. The VOV is the estimated relative variance of the estimated R . The VOV involves the estimated third and fourth moments of the empirical history score PDF $f(x)$ and is much more sensitive to large history score fluctuations than is R . The magnitude and NPS behavior of the VOV are indicators of tally fluctuation chart (TFC) bin convergence. Early work was done by Estes and Cashwell¹²² and Pederson¹²⁴ later reinvestigated this statistic to determine its usefulness.

The VOV is a quantity that is analogous to the square of the R of the mean, except it is for R instead of the mean. The estimated relative VOV of the mean is defined as

$$VOV = S^2(S_{\bar{x}}^2)/S_{\bar{x}}^4$$

where S_x^2 is the estimated variance of x and $S^2(S_x^2)$ is the estimated variance in S_x^2 . The VOV is a measure of the relative statistical uncertainty in the estimated R and is important because S must be a good approximation of σ to use the Central Limit Theorem to form confidence intervals.

The VOV for a tally bin¹²⁴ is

$$VOV = \Sigma(x_i - \bar{x})^4 / (\Sigma(x_i - \bar{x})^2)^2 - 1/N . \quad (2.26)$$

This is the fourth central moment minus the second central moment squared, normed by the product of N and the second central moment squared.

When Eq. (2.23) is expanded in terms of sums of powers of x_i , it becomes

$$VOV = \frac{\Sigma x_i^4 - 4\Sigma x_i \Sigma x_i^3 / N + 6\Sigma x_i^2 (\Sigma x_i)^2 / N^2 - 3(\Sigma x_i)^4 / N^3}{(\Sigma x_i^2 - (\Sigma x_i)^2 / N)^2} - \frac{1}{N}$$

or

$$VOV = \frac{\Sigma x_i^4 - 4\Sigma x_i \Sigma x_i^3 / N + 8\Sigma x_i^2 (\Sigma x_i)^2 / N^2 - 4(\Sigma x_i)^4 / N^3 - (\Sigma x_i^2)^2 / N}{(\Sigma x_i^2 - (\Sigma x_i)^2 / N)^2} \quad (2.27)$$

Now consider the truncated Cauchy formula for the following analysis. The truncated Cauchy is similar in shape to some difficult Monte Carlo tallies. After numerous statistical experiments on sampling a truncated positive Cauchy distribution

$$\text{Cauchy } f(x) = 2/\pi(1 + x^2), 0 \leq x \leq x_{max} , \quad (2.28)$$

it is concluded that the VOV should be below 0.1 to improve the probability of forming a reliable confidence interval. The quantity 0.1 is a convenient value and is why the VOV is used for the statistical check and not the square root of the VOV (R of the R). Multiplying numerator and denominator of Eq. (2.24) by $1/N$ converts the terms into \bar{x}^n , averages, and shows that the VOV is expected to decrease as $1/N$.

It is interesting to examine the VOV for the n identical history scores x ($n \ll N$) that were used to analyze R in Table 2.4, page 2–114. The VOV behaves as $1/n$ in this limit. Therefore, ten identical history scores would be enough to satisfy the VOV criterion, a factor of at least ten less than the R criterion. There are two reasons for this phenomenon: 1) it is more important to know R well than the VOV in forming confidence intervals; and 2) the history scores will ordinarily not be identical and thus the fourth moment terms in the VOV will increase rapidly over the second moment terms in R.

The behavior of the VOV as a function of N for the TFC bin is printed in the OUTP file. Because the VOV involves third and fourth moments, the VOV is a much more sensitive indicator to large

history scores than the R, which is based on first and second moments. The desired VOV behavior is to decrease inversely with N . This criterion is deemed to be a necessary, but not sufficient, condition for a statistically well-behaved tally result. A tally with a VOV that matches this criteria is NOT guaranteed to produce a high quality confidence interval because undersampling of high scores will also underestimate the higher score moments.

To calculate the VOV of every tally bin, put a nonzero 15th entry on the DBCN card. This option creates two additional history score moment tables each of length MXF in the TAL array to sum x_i^3 and x_i^4 (see Figure 2-18). This option is not the default because the amount of tally storage will increase by 2/5, which could be prohibitive for a problem with many tally bins. The magnitude of the VOV in each tally bin is reported in the “Status of Statistical Checks” table. History-dependent checks of the VOV of all tally bins can be done by printing the tallies to the output file at some frequency using the PRDMP card.

H. Empirical History Score Probability Density Function $f(x)$

1. Introduction

This section discusses another statistic that is useful in assessing the quality of confidence intervals from Monte Carlo calculations. Consider a generic Monte Carlo problem with difficult to sample, but extremely important, large history scores. This type of problem produces three possible scenarios.¹²¹

The first, and obviously desired, case is a correctly converged result that produces a statistically correct confidence interval. The second case is the sampling of an infrequent, but very large, history score that causes the mean and R to increase and the FOM to decrease significantly. This case is easily detectable by observing the behavior of the FOM and the R in the TFCs.

The third and most troublesome case yields an answer that appears statistically converged based on the accepted guidelines described previously, but in fact may be substantially smaller than the correct result because the large history tallies were not well sampled. This situation of too few large history tallies is difficult to detect. The following sections discuss the use of the empirical history score PDF $f(x)$ to gain insight into the TFC bin result. A pathological example to illustrate the third case follows.

2. The History Score Probability Density Function $f(x)$

A history score posted to a tally bin can be thought of as having been sampled from an underlying and generally unknown history score PDF $f(x)$, where the random variable x is the score from one complete particle history to a tally bin. The history score can be either positive or negative. The quantity $f(x)dx$ is the probability of selecting a history score between x and $x + dx$ for the tally bin. Each tally bin will have its own $f(x)$.

The most general form for expressing $f(x)$ mathematically is

$$f(x) = f_c(x) + \sum_{i=1}^n p_i \delta(x - x_i) \quad ,$$

where $f_c(x)$ is the continuous nonzero part and $\sum_{i=1}^n p_i \delta(x - x_i)$ represents the n different discrete components occurring at x_i with probability p_i . An $f(x)$ could be composed of either or both parts of the distribution. A history score of zero is included in $f(x)$ as the discrete component $\delta(x - 0)$.

By the definition of a PDF,

$$\int_{-\infty}^{\infty} f(x) dx \equiv 1 \quad .$$

As discussed on page 2-109, $f(x)$ is used to estimate the mean, variance, and higher moment quantities such as the VOV.

3. The Central Limit Theorem and $f(x)$

As discussed on page 2-112, the Central Limit Theorem (CLT) states that the estimated mean will appear to be sampled from a normal distribution with a known standard deviation $\sigma/(\sqrt{N})$ when N approaches infinity. In practice, σ is NOT known and must be approximated by the estimated standard deviation S . The major difficulty in applying the CLT correctly to a Monte Carlo result to form a confidence interval is knowing when N has approached infinity.

The CLT requires the first two moments of $f(x)$ to exist. Nearly all MCNP tally estimators (except point detectors with zero neighborhoods in a scattering material and some exponential transform problems) satisfy this requirement. Therefore, the history score PDF $f(x)$ also exists. One can also examine the behavior of $f(x)$ for large history scores to assess if $f(x)$ appears to have been “completely” sampled. If “complete” sampling has occurred, the largest values of the sampled x ’s should have reached the upper bound (if such a bound exists) or should decrease faster than $1/x^3$ so that $E(x^2) = \int_{-\infty}^{\infty} x^2 f(x) dx$ exists (σ is assumed to be finite in the CLT). Otherwise, N is assumed not to have approached infinity in the sense of the CLT. This is the basis for the use of the empirical $f(x)$ to assess Monte Carlo tally convergence.

The argument should be made that since S must be a good estimate of σ , the expected value of the fourth history score moment $E(x^4) = \int_{-\infty}^{\infty} x^4 f(x) dx$ should exist. It will be assumed that only the second moment needs to exist so that the $f(x)$ convergence criterion will be relaxed somewhat. Nevertheless, this point should be kept in mind.

4. Analytic Study of $f(x)$ for Two-State Monte Carlo Problems

Booth^{125,126} examined the distribution of history scores analytically for both an analog two-state splitting problem and two exponential transform problems. This work provided the theoretical

foundation for statistical studies¹²⁷ on relevant analytic functions to increase understanding of confidence interval coverage rates for Monte Carlo calculations.

It was found that the two-state splitting problem $f(x)$ decreases geometrically as the score increases by a constant increment. This is equivalent to a negative exponential behavior for a continuous $f(x)$. The $f(x)$ for the exponential transform problem decreases geometrically with geometrically increasing x . Therefore, the splitting problem produces a linearly decreasing $f(x)$ for the history score on a lin-log plot of the score probability versus score. The exponential transform problem generates a linearly decreasing score behavior (with high score negative exponential roll off) on a log-log plot of the score probability versus score plot. In general, the exponential transform problem is the more difficult to sample because of the larger impact of the low-probability high scores.

The analytic shapes were compared with a comparable problem calculated with a modified version of MCNP. These shapes of the analytic and empirical $f(x)$ s were in excellent agreement.¹²⁷

5. Proposed Uses for the Empirical $f(x)$ in Each TFC Bin

Few papers discuss the underlying or empirical $f(x)$ for Monte Carlo transport problems.^{128,121} MCNP provides a visual inspection and analysis of the empirical $f(x)$ for the TFC bin of each tally. This analysis helps to determine if there are any unsampled regions (holes) or spikes in the empirical history score PDF $f(x)$ at the largest history scores.

The most important use for the empirical $f(x)$ is to help determine if N has approached infinity in the sense of the CLT so that valid confidence intervals can be formed. It is assumed that the underlying $f(x)$ satisfies the CLT requirements; therefore, so should the empirical $f(x)$. Unless there is a largest possible history score, the empirical $f(x)$ must eventually decrease more steeply than

x^{-3} for the second moment $\left(\int_{-\infty}^{\infty} x^2 f(x) dx\right)$ to exist. It is postulated¹²⁹ that if such decreasing

behavior in the empirical $f(x)$ with no upper bound has not been observed, then N is not large enough to satisfy the CLT because $f(x)$ has not been completely sampled. Therefore, a larger N is required before a confidence interval can be formed. It is important to note that this convergence criterion is NOT affected by any correlations that may exist between the estimated mean and the estimated R . In principle, this lack of correlation should make the $f(x)$ diagnostic robust in assessing “complete” sampling.

Both the analytic and empirical history score distributions suggest that large score fill-in and one or more extrapolation schemes for the high score tail of the $f(x)$ could provide an estimate of scores not yet sampled to help assess the impact of the unsampled tail on the mean. The magnitude of the unsampled tail will surely affect the quality of the tally confidence interval.

6. Creation of $f(x)$ for TFC Bins

The creation of the empirical $f(x)$ in MCNP automatically covers nearly all TFC bin tallies that a user might reasonably be expected to make, including the effect of large and small tally multipliers. A logarithmically spaced grid is used for accumulating the empirical $f(x)$ because the tail behavior is assumed to be of the form $1/x^n$, $n > 3$ (unless an upper bound for the history scores exists). This

grid produces an equal width histogram straight line for $f(x)$ on a log-log plot that decreases n decades in $f(x)$ per decade increase in x .

Ten bins per x decade are used and cover the unnormalized tally range from 10^{-30} to 10^{30} . The term “unnormalized” indicates that normalizations that are not performed until the end of the problem, such as cell volume or surface area, are not included in $f(x)$. The user can multiply this range at the start of the problem by the 16th entry on the DBCN card when the range is not sufficient. Both history score number and history score for the TFC bin are tallied in the x grid.

With this x grid in place, the average empirical $f(\bar{x}_i)$ between x_i and x_{i+1} is defined to be

$$f(\bar{x}_i) = (\text{number of history scores in } i^{\text{th}} \text{ score bin}) / N(x^{i+1} - x^i),$$

where $x^{i+1} = 1.2589 x^i$. The quantity 1.2589 is $10^{0.1}$ and comes from 10 equally spaced log bins per decade. The calculated $f(\bar{x}_i)$ s are available on printed plots or by using the “z” plot option (MCPLLOT) with the TFC command mnemonics. Any history scores that are outside the x grid are counted as either above or below to provide this information to the user.

Negative history scores can occur for some electron charge deposition tallies. The MCNP default is that any negative history score will be lumped into one bin below the lowest history score in the built-in grid (the default is 1×10^{-30}). If DBCN(16) is negative, $f(-x)$ will be created from the negative scores and the absolute DBCN(16) value will be used as the score grid multiplier. Positive history scores then will be lumped into the lowest bin because of the sign change.

Figure 2-20 and Figure 2-21 show two simple examples of empirical $f(x)$ s from MCNP for 10 million histories each. Figure 2-20 is from an energy leakage tally directly from a source that is uniform in energy from 0 to 10 MeV. The analytic $f(x)$ is a constant 0.1 between 0 and 10 MeV. The empirical $f(x)$ shows the sampling, which is 0.1 with statistical noise at the lower x bins where fewer samples are made in the smaller bins.

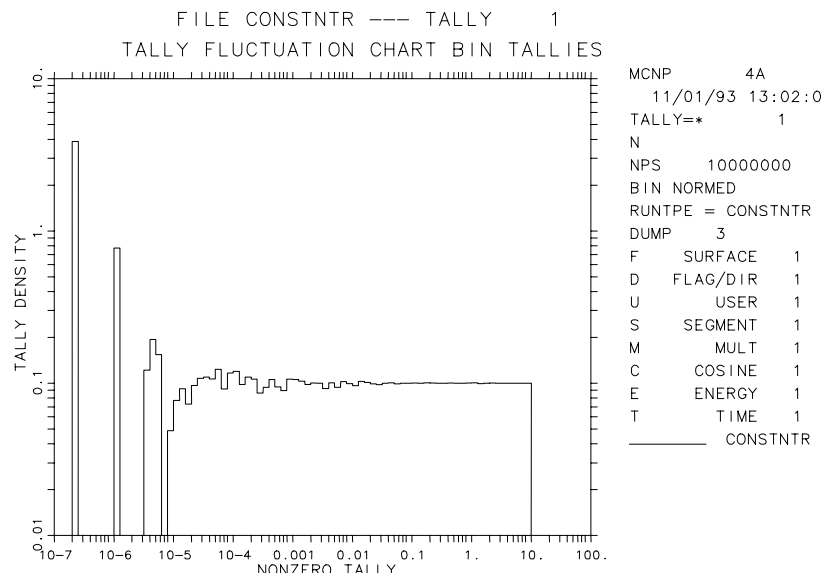


Figure 2-20

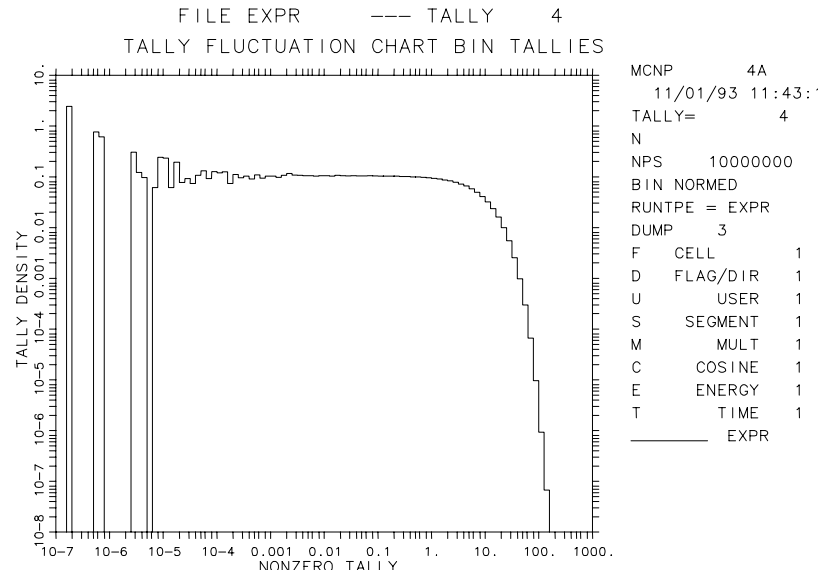


Figure 2-21

Figure 2-21 shows the sampled distance to first collision in a material that has a macroscopic cross section of about 0.1 cm^{-1} . This analytic function is a negative exponential given by $f(x) = \Sigma \exp^{-\Sigma x}$ (see page 2-27) with a mean of 10. The empirical $f(x)$ transitions from a constant 0.1 at values of x less than unity to the expected negative exponential behavior.

7. Pareto Fit to the Largest History Scores for the TFC Bin

The slope n in $1/x^n$ of the largest history tallies x must be estimated to determine if and when the largest history scores decrease faster than $1/x^3$. The 201 largest history scores for each TFC bin are continuously updated and saved during the calculation. A generalized Pareto function¹³⁰

$$\text{Pareto } f(x) = a^{-1}(1 + kx/a)^{-(1/k)-1}$$

is used to fit the largest x 's. This function fits a number of extreme value distributions including $1/x^n$, exponential ($k = 0$), and constant ($k = -1$). The large history score tail fitting technique uses the robust "simplex" algorithm,¹³¹ which finds the values of a and k that best fit the largest history scores by maximum likelihood estimation.

The number of history score tail points used for the Pareto fit is a maximum of 201 points because this provides about 10% precision¹³⁰ in the slope estimator at $n = 3$. The precision increases for smaller values of n and vice versa. The number of points actually used in the fit is the lesser of 5% of the nonzero history scores or 201. The minimum number of points used for a Pareto fit is 25 with at least two different values, which requires 500 nonzero history scores with the 5% criterion. If less than 500 history scores are made in the TFC bin, no Pareto fit is made.

From the Pareto fit, the slope of $f(x_{\text{large}})$ is defined to be

$$SLOPE \equiv (1/k) + 1 \quad .$$

A SLOPE value of zero is defined to indicate that not enough $f(x_{large})$ tail information exists for a SLOPE estimate. The SLOPE is not allowed to exceed a value of 10 (a “perfect score”), which would indicate an essentially negative exponential decrease. If the 100 largest history scores all have values with a spread of less than 1%, an upper limit is assumed to have been reached and the SLOPE is set to 10. The SLOPE should be greater than 3 to satisfy the second moment existence requirement of the CLT. Then, $f(x)$ will appear to be “completely” sampled and hence N will appear to have approached infinity.

A printed plot of $f(x)$ is automatically generated in the OUTP file if the SLOPE is less than 3 (or if any of the other statistical checks described in the next section do not pass). If $0 < \text{SLOPE} < 10$, several “S’s” appear on the printed plot to indicate the Pareto fit, allowing the quality of the fit to the largest history scores to be assessed visually. If the largest scores are not Pareto in shape, the SLOPE value may not reflect the best estimate of the largest history score decrease. A new SLOPE can be estimated graphically. A blank or 162 on the PRINT card also will cause printed plots of the first two cumulative moments of the empirical $f(x)$ to be made. Graphical plots of various $f(x)$ quantities can be made using the “z” plot option (MC PLOT) with the TFC plot command. These plots should be examined for unusual behavior in the empirical $f(x)$, including holes or spikes in the tail. MCNP tries to assess both conditions and prints a message if either condition is found.

I. Forming Statistically Valid Confidence Intervals

The ultimate goal of a Monte Carlo calculation is to produce a valid confidence interval for each tally bin. Section VI has described different statistical quantities and the recommended criteria to form a valid confidence interval. Detailed descriptions of the information available in the output for all tally bins and the TFC bins are now discussed.

1. Information Available for Forming Statistically Valid Confidence

The R is calculated for every user-specified tally bin in the problem. The VOV and the shifted confidence interval center, discussed below, can be obtained for all bins with a nonzero entry for the 15th entry on the DBCN card at problem initiation.

a. R Magnitude Comparisons With MCNP Guidelines: The quality of MCNP Monte Carlo tallies historically has been associated with two statistical checks that have been the responsibility of the user: 1) for all tally bins, the estimated relative error magnitude rules-of-thumb that are shown in Figure 2-5 (that is, $R < 0.1$ for nonpoint detector tallies and $R < 0.05$ for point detector tallies); and 2) a statistically constant FOM in the user-selectable (TFn card) TFC bin so that the estimated R is decreasing by $1/\sqrt{N}$ as required by the CLT.

In an attempt to make the user more aware of the seriousness of checking these criteria, MCNP provides checks of the R magnitude for all tally bins. A summary of the checks is printed in the “Status of Statistical Checks” table. Messages are provided to the user giving the results of these checks.

b. Asymmetric Confidence Intervals: A correlation exists between the estimated mean and the estimated uncertainty in the mean.¹²⁴ If the estimated mean is below the expected value, the estimated uncertainty in the mean $S_{\bar{x}}$ will most likely be below its expected value. This correlation

is also true for higher moment quantities such as the VOV. The worst situation for forming valid confidence intervals is when the estimated mean is much smaller than the expected value, resulting in smaller than predicted coverage rates. To correct for this correlation and improve coverage rates, one can estimate a statistic shift in the midpoint of the confidence interval to a higher value. The estimated mean is unchanged.

The shifted confidence interval midpoint is the estimated mean plus a term proportional to the third central moment. The term arises from an Edgeworth expansion¹²⁴ to attempt to correct the confidence interval for non-normality effects in the estimate of the mean. The adjustment term is given by

$$SHIFT = \Sigma(x_i - \bar{x})^3 / (2S^2N) \quad .$$

Substituting for the estimated mean and expanding produces

$$SHIFT = (\Sigma x_i^3 - 3\Sigma x_i^2 \Sigma x_i / N + 2(\Sigma x_i)^3 / N^2) / 2(N\Sigma x_i^2 - (\Sigma x_i)^2) \quad .$$

The *SHIFT* should decrease as $1/N$. This term is added to the estimated mean to produce the midpoint of the now asymmetric confidence interval about the mean. This value of the confidence interval midpoint can be used to form the confidence interval about the estimated mean to improve coverage rates of the true, but unknown, mean $E(x)$. The estimated mean plus the *SHIFT* is printed automatically for the TFC bin for all tallies. A nonzero entry for the 15th DBCN card entry produces the shifted value for all tally bins.

This correction approaches zero as N approaches infinity, which is the condition required for the CLT to be valid. Kalos¹³² uses a slightly modified form of this correction to determine if the requirements of the CLT are “substantially satisfied.” His relation is

$$\left| \Sigma(x_i - \bar{x})^3 \right| \ll S^3 \sqrt{N} \quad ,$$

which is equivalent to

$$SHIFT \ll S_{\bar{x}} / 2 \quad .$$

The user is responsible for applying this check.

c. Forming Valid Confidence Intervals for Non-TFC Bins: The amount of statistical information available for non-TFC bins is limited to the mean and R. The VOV and the center of the asymmetric confidence can be obtained for all tally bins with a nonzero 15th entry on the DBCN card in the initial problem. The magnitude criteria for R (and the VOV, if available) should be met before forming a confidence interval. If the shifted confidence interval center is available, it should be used to form asymmetric confidence intervals about the estimated mean.

History dependent information about R (and the VOV, if available) for non-TFC bins can be obtained by printing out the tallies periodically during a calculation using the PRDMP card. The

N -dependent behavior of R can then be assessed. The complete statistical information available can be obtained by creating a new tally and selecting the desired tally bin with the TFN card.

2. Information Available for Forming Statistically Valid Confidence Intervals for TFC Bins

Additional information about the statistical behavior of each TFC bin result is available. A TFC bin table is produced by MCNP after each tally to provide the user with detailed information about the apparent quality of the TFC bin result. The contents of the table are discussed in the following subsections, along with recommendations for forming valid confidence intervals using this information.

a. TFC Bin Tally Information: The first part of the TFC bin table contains information about the TFC bin result including the mean, R , scoring efficiency, the zero and nonzero history score components of R (see page 2-118), and the shifted confidence interval center. The two components of R can be used to improve the problem efficiency by either improving the history scoring efficiency or reducing the range of nonzero history scores.

b. The Largest TFC Bin History Score Occurs on the Next History: There are occasions when the user needs to make a conservative estimate of a tally result. Conservative is defined so that the results will not be less than the expected result. One reasonable way to make such an estimate is to assume that the largest observed history score would occur again on the very next history, $N + 1$.

MCNP calculates new estimated values for the mean, R , VOV, FOM, and shifted confidence interval center for the TFC bin result for this assumption. The results of this proposed occurrence are summarized in the TFC bin information table. The user can assess the impact of this hypothetical happening and act accordingly.

c. Description of the 10 Statistical Checks for the TFC Bin: MCNP prints the results of ten statistical checks of the tally in the TFC bin at each print. In a "Status of Statistical Checks" table, the results of these ten checks are summarized at the end of the output for all TFC bin tallies. The quantities involved in these checks are the estimated mean, R , VOV, FOM, and the large history score behavior of $f(x)$. Passing all of the checks should provide additional assurance that any confidence intervals formed for a TFC bin result will cover the expected result the correct fraction of the time. At a minimum, the results of these checks provide the user with more information about the statistical behavior of the result in the TFC bin of each tally.

The following 10 statistical checks are made on the TFCs printed at the end of the output for desirable statistical properties of Monte Carlo solutions:

MEAN

- (1) a nonmonotonic behavior (no up or down trend) in the estimated mean as a function of the number histories N for the last half of the problem;

R

- (2) an acceptable magnitude of the estimated R of the estimated mean (< 0.05 for a point detector tally or < 0.10 for a non-point detector tally);
- (3) a monotonically decreasing R as a function of the number histories N for the last half of the problem;
- (4) a $1/\sqrt{N}$ decrease in the R as a function of N for the last half of the problem;

VOV

- (5) the magnitude of the estimated VOV should be less than 0.10 for all types of tallies;
- (6) a monotonically decreasing VOV as a function of N for the last half of the problem;
- (7) a $1/N$ decrease in the VOV as a function of N for the last half of the problem;

FOM

- (8) a statistically constant value of the FOM as a function of N for the last half of the problem;
- (9) a nonmonotonic behavior in the FOM as a function of N for the last half of the problem; and

$f(x)$

- (10) the SLOPE (see page 2–126) of the 25 to 201 largest positive (negative with a negative DBCN(16) entry) history scores x should be greater than 3.0 so that the second moment $\int_{-\infty}^{\infty} x^2 f(x) dx$ will exist if the SLOPE is extrapolated to infinity.

The seven N -dependent checks for the TFC bin are for the last half of the problem. The last half of the problem should be well behaved in the sense of the CLT to form the most valid confidence intervals. “Monotonically decreasing” in checks 3 and 5 allows for some increases in both R and the VOV. Such increases in adjacent TFC entries are acceptable and usually do not, by themselves, cause poor confidence intervals. A TFC bin R that does not pass check 3, by definition in MCNP, does not pass check 4. Similarly, a TFC bin VOV that does not pass check 6, by definition, does not pass check 7.

A table is printed after each tally for the TFC bin result that summarizes the results and the pass or no-pass status of the checks. Both asymmetric and symmetric confidence intervals are printed for the one, two, and three σ levels when all of the statistical checks are passed. These intervals can be expected to be correct with improved probability over historical rules of thumb. This is NOT A GUARANTEE, however; there is always a possibility that some as-yet-unsampled portion of the problem would change the confidence interval if more histories were calculated. A WARNING is printed if one or more of these ten statistical checks is not passed, and one page of printed plot information about $f(x)$ is produced for the user to examine.

An additional information-only check is made on the largest five $f(x)$ score grid bins to determine if there are bins that have no samples or if there is a spike in an $f(x)$ that does not appear to have an upper limit. The result of the check is included in the TFC summary table for the user to consider. This check is not a pass or no-pass test because a hole in the tail may be appropriate for a discrete

$f(x)$ or an exceptional sample occurred with so little impact that none of the ten checks was affected. The empirical $f(x)$ should be examined to assess the likelihood of “complete” sampling.

d. Forming Valid TFC Bin Confidence Intervals: For TFC bin results, the highest probability of creating a valid confidence interval occurs when all of the statistical checks are passed. Not passing several of the checks is an indication that the confidence interval is less likely to be correct. A monotonic trend in the mean for the last half of the problem is a strong indicator that the confidence interval is likely to produce incorrect coverage rates. The magnitudes of R and the VOV should be less than the recommended values to increase the likelihood of a valid confidence interval. Small jumps in the R, VOV, and/or the FOM as a function of N are not threatening to the quality of a result. The slope of $f(x)$ is an especially strong indicator that N has not approached infinity in the sense of the CLT. If the slope appears too shallow (< 3), check the printed plot of $f(x)$ to see that the estimated Pareto fit is adequate. The use of the shifted confidence interval is recommended, although it will be a small effect for a well-converged problem.

The last half of the problem is determined from the TFC. The more information available about the last half of the problem, the better the N -dependent checks will be. Therefore, a problem that has run 40,000 histories will have 20 TFC N entries, which is more N entries than a 50,000 history problem with 13 entries. It is possible that a problem that passes all tests at 40,000 may not pass all the tests at 40,001. As is always the case, the user is responsible for deciding when a confidence interval is valid. These statistical diagnostics are designed to aid in making this decision.

J. *A Statistically Pathological Output Example*

A statistically pathological test problem is discussed in this section. The problem calculates the surface neutron leakage flux above 12 MeV from an isotropic 14 MeV neutron point source of unit strength at the center of a 30-cm-thick concrete shell with an outer radius of 390 cm. Point and ring detectors were deliberately used to estimate the surface neutron leakage flux with highly inefficient, long-tailed $f(x)$ s. The input is shown on page 5–49.

The variance reduction methods used were implicit capture with weight cutoff, low-score point detector Russian roulette, and a 0.5 mean free path (4 cm) neighborhood around the detectors to produce large, but finite, higher moments. Other tallies or variance reduction methods could be used to make this calculation much more efficient, but that is not the object of this example. A surface flux estimator would have been over a factor of 150 to 30,000 times more efficient than ring and point detectors, respectively.

Figure 2-22 shows MCNP plots of the estimated mean, R, VOV and slope of the history score PDF as a function of N values of 20,000 (left column) and 5 million (right column). The ring detector results are shown as the solid line and the point detector result is the dashed line.

Column 1 shows the results as a function of N for 20,000 histories. The point detector result at 14,000 histories (not shown) was $1.41 \times 10^{-8} \text{ n/cm}^2/\text{s}$ ($R=0.041$). The FOM varied somewhat randomly between about 800 and 1160 for the last half of the problem. With no other information, this result could be accepted by even a careful Monte Carlo practitioner. However, the VOV never gets close to the required 0.1 value and the slope of the unbounded $f(x)$ is less than 1.4. This slope could not continue indefinitely because even the mean of $f(x)$ would not exist. Therefore, a

confidence interval should not be formed for this tally. At 20,000 histories, R increases substantially and the FOM crashes, indicating serious problems with the result.

The ring detector result is having problems of its own. The ring detector result for 14,000 histories was $4.60 \times 10^{-8} \text{ n/cm}^2/\text{s}$ (R=0.17, VOV = 0.35, slope=2.1, FOM=67). None of the plotted quantities satisfies the required convergence criteria. The correct detector result, obtained from a 5 million history ring detector tally, is $5.72 \times 10^{-8} \text{ n/cm}^2/\text{s}$ (R=0.0169, VOV=0.023, slope=4.6, FOM=19). The apparently converged 14,000 history point detector result is a factor of four below the correct result!

If you were to run 200,000 histories, you would see the point detector result increasing to $3.68 \times 10^{-8} \text{ n/cm}^2/\text{s}$ (R=0.20, VOV=0.30, slope=1.6, FOM=1.8). The magnitudes of R and the VOV are much too large for the point detector result to be accepted. The slope of $f(x)$ is slowly increasing, but has only reached a value of 1.6. This slope is still far too shallow compared to the required value of 3.0.

The ring detector result of $5.06 \times 10^{-8} \text{ n/cm}^2/\text{s}$ (R=0.0579, VOV=0.122, slope=2.8, FOM=22) at 192,000 histories is interesting. All of these values are close to being acceptable, but just miss the requirements. The ring detector result is more than two estimated standard deviations below the correct result.

Column 2 shows the results as a function of N for 5 million histories. The ring detector result of $5.72 \times 10^{-8} \text{ n/cm}^2/\text{s}$ (R=0.0169, VOV=0.023, slope=4.6, FOM=19) now appears very well behaved in all categories. This tally passed all 10 statistical checks. There appears to be no reason to question the validity of this tally. The point detector result is $4.72 \times 10^{-8} \text{ n/cm}^2/\text{s}$ (R=0.11, VOV=0.28, slope=2.1, FOM=0.45). The result is clearly improving, but does not meet the acceptable criteria for convergence. This tally did not pass 3 out 10 statistical checks.

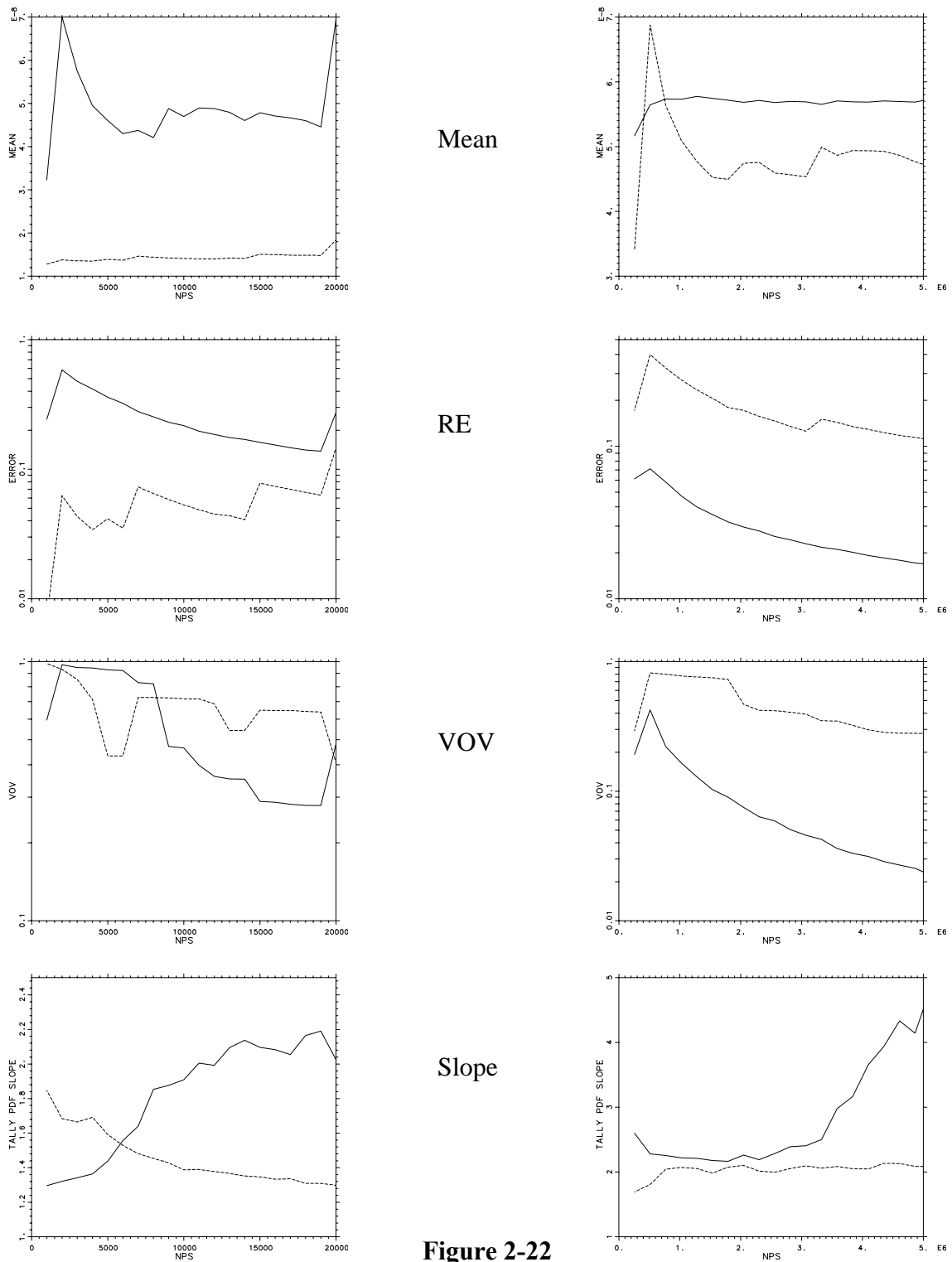


Figure 2-22

When you compare the empirical point detector $f(x)$ s for 14,000 and 200 million histories you see that the 14,000 history $f(x)$ clearly has unsampled regions in the tail, indicating incomplete $f(x)$ sampling.¹²⁹ For the point detector, seven decades of x have been sampled by 200 million histories

compared to only three decades for 14,000 histories. The largest x 's occur from the extremely difficult to sample histories that have multiple small energy loss collisions close to the detector. The 200 million history point detector result is $5.41 \times 10^{-8} n/cm^2/s$ ($R=0.035$, $VOV=0.60$, $slope=2.4$, $FOM=0.060$). The point detector $f(x)$ slope is increasing, but still is not yet completely sampled. This tally did not pass 6 of 10 checks with 200 million histories. The result is about 1.5 estimated standard deviations below the correct answer. It is important to note that calculating a large number of histories DOES NOT guarantee a precise result. The more compact empirical ring $f(x)$ for 20 million histories appears to be completely sampled because of the large slope. The results for 1 billion histories are shown in Ref. 121.

For difficult to sample problems such as this example, it is possible that an even larger history score could occur that would cause the VOV and possibly the slope to have unacceptable values. The mean and RE will be much less affected than the VOV. The additional running time required to reach acceptable values for the VOV and the slope could be prohibitive. The large history score should NEVER be discarded from the tally result. It is important that the cause for the large history score be completely understood. If the score was created by a poorly sampled region of phase space, the problem should be modified to provide improved phase space sampling. It is also possible that the large score was created by an extremely unlikely set of circumstances that occurred "early" in the calculation. In this situation, if the RE is within the guidelines, the empirical $f(x)$ appears to be otherwise completely sampled, and the largest history score appears to be a once in a lifetime occurrence, a good confidence interval can still be formed. If a conservative (large) answer is required, the printed result that assumes the largest history score occurs on the very next history can be used.

Comparing several empirical $f(x)$ s for the above problem with 200 million histories that have been normalized so that the mean of each $f(x)$ is unity, you see that the point detector at 390 cm clearly is quite Cauchy-like (see Eq. (2.25) for many decades.¹²⁸ The point detector at 4000 cm is a much easier tally (by a factor of 10,000) as exhibited by the much more compact empirical $f(x)$. The large-score tail decreases in a manner similar to the negative exponential $f(x)$. The surface flux estimator is the most compact $f(x)$ of all. The blip on the high-score tail is caused by the average cosine approximation of 0.05 between cosines of 0 and 0.1 (see page 2-87). This tally is 30,000 times more efficient than the point detector tally.

VII. VARIANCE REDUCTION

A. General Considerations

1. Variance Reduction and Accuracy

Variance-reducing techniques in Monte Carlo calculations reduce the computer time required to obtain results of sufficient precision. Note that precision is only one requirement for a good Monte Carlo calculation. Even a zero variance calculation cannot accurately predict natural behavior if other sources of error are not minimized. Factors affecting accuracy were discussed in Section VI beginning on page 2-108.

2. Two Choices That Affect Efficiency

The efficiency of a Monte Carlo calculation is affected by two choices, tally type and random walk sampling. The tally choice (for example, point detector flux tally vs. surface crossing flux tally) amounts to trying to obtain the best results from the random walks sampled. The chosen random walk sampling amounts to preferentially sampling “important” random walks at the expense of “unimportant” random walks. (A random walk is important if it has a large affect on a tally.) These two choices usually affect the time per history and the history variance as described in the next section on page 2–136. MCNP estimates tallies of the form

$$\langle T \rangle = \int d\vec{r} \int d\vec{v} \int dt N(\vec{r}, \vec{v}, t) T(\vec{r}, \vec{v}, t)$$

by sampling particle histories that statistically produce the correct particle density $N(\vec{r}, \vec{v}, t)$. The tally function $T(\vec{r}, \vec{v}, t)$ is zero except where a tally is required. For example, for a surface crossing tally (*FI*), T will be one on the surface and zero elsewhere. MCNP variance reduction techniques allow the user to try to produce better statistical estimates of N where T is large, usually at the expense of poorer estimates where T is zero or small.

There are many ways to statistically produce $N(\vec{r}, \vec{v}, t)$. Analog Monte Carlo simply samples the events according to their natural physical probabilities. In this way, an analog Monte Carlo calculation estimates the number of physical particles executing any given random walk. Nonanalog techniques do not directly simulate nature. Instead, nonanalog techniques are free to do anything if N , hence $\langle T \rangle$, is preserved. This preservation is accomplished by adjusting the weight of the particles. The weight can be thought of as the number of physical particles represented by the MCNP particle (see page 2–25). Every time a decision is made, the nonanalog techniques require that the expected weight associated with each outcome be the same as in the analog game. In this way, the expected number of physical particles executing any given random walk is the same as in the analog game.

For example, if an outcome “A” is made q times as likely as in the analog game, when a particle chooses outcome “A,” its weight must be multiplied by q^{-1} to preserve the expected weight for outcome “A.” Let p be the analog probability for outcome “A”; then pq is the nonanalog probability for outcome “A.” If w_0 is the current weight of the particle, then the expected weight for outcome “A” in the analog game is $w_0 * p$ and the expected weight for outcome “A” in the nonanalog game is $(w_0/q) * pq$.

MCNP uses three basic types of nonanalog games: (1) splitting, (2) Russian roulette, and (3) sampling from nonanalog probability density functions. The previous paragraph discusses type 3. Splitting refers to dividing the particle's weight among two or more daughter particles and following the daughter particles independently. Usually the weight is simply divided evenly among k identical daughter particles whose characteristics are identical to the parent except for a factor $1/k$ in weight (for example, splitting in the weight window). In this case the expected weight is clearly conserved because the analog technique has one particle of weight w_0 at (\vec{r}, \vec{v}, t) , whereas the splitting results in k particles of weight w_0/k at (\vec{r}, \vec{v}, t) . In both cases the outcome is weight w_0 at (\vec{r}, \vec{v}, t) .

Other splitting techniques split the parent particle into k , typically two, differing daughter particles. The weight of the j^{th} daughter represents the expected number of physical particles that would select outcome j from a set of k mutually exclusive outcomes. For example, the MCNP forced collision technique considers two outcomes: (1) the particle reaches a cell boundary before collision, or (2) the particle collides before reaching a cell boundary. The forced collision technique divides the parent particle representing w_0 physical particles into two daughter particles, representing w_1 physical particles that are uncollided and w_2 physical particles that collide. The uncollided particle of weight w_1 is then put on the cell boundary. The collision site of the collided particle of weight w_2 is selected from a conditional distance-to-collision probability density, the condition being that the particle must collide in the cell. This technique preserves the expected weight colliding at any point in the cell as well as the expected weight not colliding. A little simple mathematics is required to demonstrate this technique.

Russian roulette takes a particle at (\vec{r}, \vec{v}, t) of weight w_0 and turns it into a particle of weight $w_1 > w_0$ with probability w_0/w_1 and kills it (that is, weight=0) with probability $(1 - (w_0/w_1))$. The expected weight at (\vec{r}, \vec{v}, t) is $w_1 * (w_0/w_1) + (1 - (w_0/w_1)) * 0 = w_0$, the same as in the analog game.

Some techniques use a combination of these basic games and DXTRAN uses all three.

3. Efficiency, Time per History, and History Variance

Recall from page 2-116 that the measure of efficiency for MCNP calculations is the *FOM*: $FOM \equiv 1/(R^2 T)$, where

$$\begin{aligned} R^2 &= \text{sample relative standard deviation of the mean and} \\ T &= \text{computer time for the calculation (in minutes).} \end{aligned}$$

Recall from Eqns. 2.17 and 2.19a that $R = (S/\sqrt{N})/\bar{x}$, where

$$\begin{aligned} S^2 &= \text{sample history variance,} \\ N &= \text{number of particles, and} \\ \bar{x} &= \text{sample mean.} \end{aligned}$$

Generally we are interested in obtaining the smallest R in a given time T . The equation above indicates that to decrease R it is desirable to: 1) decrease S and 2) increase N ; that is, decrease the time per particle history. Unfortunately, these two goals usually conflict. Decreasing S normally requires more time because better information is required. Increasing N normally increases S because there is less time per history to obtain information. However, the situation is not hopeless. It is often possible either to decrease S substantially without decreasing N too much or to increase N substantially without increasing S too much, so that R decreases.

Many variance reduction techniques in MCNP attempt to decrease R by either producing or destroying particles. Some techniques do both. In general, techniques that produce tracks work by decreasing S (we hope much faster than N decreases) and techniques that destroy tracks work by increasing N (we hope much faster than S increases).

4. Strategy

Successful use of MCNP variance reduction techniques is often difficult, tending to be more art than science. The introduction of the weight window generator has improved things, but the user is still fundamentally responsible for the choice and proper use of variance reducing techniques. Each variance reduction technique has its own advantages, problems, and peculiarities. However, there are some general principles to keep in mind while developing a variance reduction strategy.

Not surprisingly, the general principles all have to do with understanding both the physical problem and the variance reduction techniques available to solve the problem. If an analog calculation will not suffice to calculate the tally, there must be something special about the particles that tally. The user should understand the special nature of those particles that tally. Perhaps, for example, only particles that scatter in particular directions can tally. After the user understands why the tallying particles are special, MCNP techniques can be selected (or developed by the user) that will increase the number of special particles followed.

After the MCNP techniques are selected the user typically has to supply appropriate parameters to the variance reduction techniques. This is probably more difficult than is the selection of techniques. The first guess at appropriate parameters typically comes either from experience with similar problems or from experience with an analog calculation of the current problem. It is usually better to err on the conservative side; that is, too little biasing rather than too much biasing. After the user has supplied parameters for the variance reduction techniques, a short Monte Carlo run is done so that the effectiveness of the techniques and parameters can be monitored with the MCNP output.

The MCNP output contains much information to help the user understand the sampling. This information should be examined to ensure that

- (1) the variance reduction techniques are improving the sampling of the particles that tally;
- (2) the variance reduction techniques are working cooperatively; that is, one is not destructively interfering with another;
- (3) the *FOM* table is not erratic, which would indicate poor sampling; and
- (4) there is nothing that looks obviously ridiculous.

Unfortunately, analyzing the output information requires considerable thought and experience. Reference 133 shows in detail strategies and analysis for a particular problem.

After ascertaining that the techniques are improving the calculation, the user makes a few more short runs to refine the parameters until the sampling no longer improves. The weight window generator can also be turned on to supply information about the importance function in different regions of the phase space. This rather complex subject is described on page 2-146.

5. Erratic Error Estimates

Erratic error estimates are sometimes observed in MCNP calculations. In fact, the primary reason for the Tally Fluctuation Chart (TFC) table in the MCNP output is to allow the user to monitor the

FOM and the relative error as a function of the number of histories. With few exceptions, such as an analog point detector embedded in a scattering medium with $R_0 = 0$ (a practice highly discouraged), MCNP tallies are finite variance tallies. For finite variance tallies the relative error should decrease roughly as $1/\sqrt{N}$ so the *FOM* should be roughly constant and the ten statistical checks of the tallies (see page 2–129) should all be passed. If the statistical checks are not passed, the error estimates should be considered erratic and unreliable, no matter how small the relative error estimate is.

Erratic error estimates occur typically because a high-weight particle tallies from an important region of phase space that has not been well sampled. A high-weight particle in a given region of phase space is a particle whose weight is some nontrivial fraction of all the weight that has tallied from that region because of all previous histories. A good example is a particle that collides very close to a point or ring detector. If not much particle weight has previously collided that close to the detector, the relative error estimate will exhibit a jump for that history. Another example is coherent photon scattering towards a point detector (see page 2–64).

To avoid high-weight particles in important regions, the user should try to ensure that these regions are well sampled by many particles and try to minimize the weight fluctuation among these particles. Thus the user should try to use biasing techniques that preferentially push particles into important regions without introducing large weight fluctuations in these regions. The weight window can often be very useful in minimizing weight fluctuations caused by other variance reduction techniques.

If, despite a user's efforts, an erratic error estimate occurs, the user should obtain event logs for those particles causing the estimate to be erratic. The event logs should be studied to learn what is special about these particles. When the special nature of these particles is understood, the user can adjust the variance reduction techniques to sample these particles more often. Thus their weight will be smaller and they will not be as likely to cause erratic estimates. *Under absolutely no circumstances should these particles be discarded or ignored!* The fact that these particles contribute very heavily to the tally indicates that they are important to the calculation and the user should try to sample more of them.

6. Biasing Against Random Walks of Presumed Low Importance

It was mentioned earlier that one should be cautious and conservative when applying variance reduction techniques. Many more people get into trouble by overbiasing than by underbiasing. Note that preferentially sampling some random walks means that some walks will be sampled (for a given computer time) less frequently than they would have been in an analog calculation. Sometimes these random walks are so heavily biased against that very few, or even none, are ever sampled in an actual calculation because not enough particles are run.

Suppose that (on average) for every million histories only one track enters cell 23. Further suppose that a typical run is 100,000 histories. On any given run it is unlikely that a track enters cell 23. Now suppose that tracks entering cell 23 turn out to be much more important than a user thought. Maybe 10% of the answer should come from tracks entering cell 23. The user could run 100,000 particles and get 90% of the true tally with an estimated error of 1%, with absolutely no indication that anything is amiss. However, suppose the biasing had been set such that (on average) for every

10,000 particles, one track entered cell 23, about 10 tracks total. The tally probably will be severely affected by at least one high weight particle and will hover closer to the true tally with a larger and perhaps erratic error estimate. The essential point is this: following ten tracks into cell 23 does not cost much computer time and it helps ensure that the estimated error cannot be low when the tally is seriously in error. Always make sure that all regions of the problem are sampled enough to be certain that they are unimportant.

B. Variance Reduction Techniques

There are four classes of variance reduction techniques¹³⁴ that range from the trivial to the esoteric.

Truncation Methods are the simplest of variance reduction methods. They speed up calculations by truncating parts of phase space that do not contribute significantly to the solution. The simplest example is geometry truncation in which unimportant parts of the geometry are simply not modeled. Specific truncation methods available in MCNP are energy cutoff and time cutoff.

Population Control Methods use particle splitting and Russian roulette to control the number of samples taken in various regions of phase space. In important regions many samples of low weight are tracked, while in unimportant regions few samples of high weight are tracked. A weight adjustment is made to ensure that the problem solution remains unbiased. Specific population control methods available in MCNP are geometry splitting and Russian roulette, energy splitting/roulette, time splitting/roulette, weight cutoff, and weight windows.

Modified Sampling Methods alter the statistical sampling of a problem to increase the number of tallies per particle. For any Monte Carlo event it is possible to sample from any arbitrary distribution rather than the physical probability as long as the particle weights are then adjusted to compensate. Thus with modified sampling methods, sampling is done from distributions that send particles in desired directions or into other desired regions of phase space such as time or energy, or change the location or type of collisions. Modified sampling methods in MCNP include the exponential transform, implicit capture, forced collisions, source biasing, and neutron-induced photon production biasing.

Partially-Deterministic Methods are the most complicated class of variance reduction methods. They circumvent the normal random walk process by using deterministic-like techniques, such as next event estimators, or by controlling the random number sequence. In MCNP these methods include point detectors, DXTRAN, and correlated sampling.

The available MCNP variance reduction techniques are described below.

1. Energy Cutoff

The energy cutoff in MCNP is either a single user-supplied, problem-wide energy level or a cell-dependent energy level. Particles are terminated when their energy falls below the energy cutoff. The energy cutoff terminates tracks and thus decreases the time per history. The energy cutoff should be used only when it is known that low-energy particles are either of zero or almost zero importance. An energy cutoff is like a Russian roulette game with zero survival probability. A number of pitfalls exist.

1. Remember that low-energy particles can often produce high-energy particles (for example, fission or low-energy neutrons inducing high-energy photons). Thus, even if a detector is not sensitive to low-energy particles, the low-energy particles may be important to the tally.
2. The CUT card energy cutoff is the same throughout the entire problem. Often low-energy particles have zero importance in some regions and high importance in others, and so a cell-dependent energy cutoff is also available with the ELPT card.
3. The answer will be biased (low) if the energy cutoff is killing particles that might otherwise have contributed. Furthermore, as $N \rightarrow \infty$ the apparent error will go to zero and therefore mislead the unwary. Serious consideration should be given to two techniques discussed later, energy roulette and space-energy weight window, that are always unbiased.

The energy cutoff has one advantage not directly related to variance reduction. A lower energy cutoff requires more cross sections so that computer memory requirements go up and interactive computing with a timesharing system is degraded.

2. Time Cutoff

The time cutoff in MCNP is a single user-supplied, problem-wide time value. Particles are terminated when their time exceeds the time cutoff. The time cutoff terminates tracks and thus decreases the computer time per history. A time cutoff is like a Russian roulette game with zero survival probability. The time cutoff should only be used in time-dependent problems where the last time bin will be earlier than the cutoff.

Although the energy and time cutoffs are similar, more caution must be exercised with the energy cutoff because low energy particles can produce high energy particles, whereas a late time particle cannot produce an early time particle.

3. Geometry Splitting with Russian Roulette

Geometry splitting/Russian roulette is one of the oldest and most widely used variance-reducing techniques in Monte Carlo codes. When used judiciously, it can save substantial computer time. As particles migrate in an important direction, they are increased in number to provide better sampling, but if they head in an unimportant direction, they are killed in an unbiased manner to avoid wasting time on them. Oversplitting, however, can substantially waste computer time. Splitting generally decreases the history variance but increases the time per history, whereas Russian roulette generally increases the history variance but decreases the time per history.

Each cell in the problem geometry setup is assigned an importance I by the user on the IMP input card. The number I should be proportional to the estimated value that particles in the cell have for the quantity being scored. When a particle of weight W passes from a cell of importance I to one of higher importance I' , the particle is split into a number of identical particles of lower weight according to the following recipe. If I'/I is an integer n ($n \geq 2$), the particle is split into n identical particles, each weighing W/n . Weight is preserved in the integer splitting process. If I'/I is not an integer but still greater than 1, splitting is done probabilistically so that the expected number of splits is equal to the importance ratio. Denoting $n = [I'/I]$ to be the largest integer in I'/I ,

$p = I'/I - n$ is defined. Then with probability p , $n + 1$ particles are used, and with probability $1 - p$, n particles are used. For example, if I'/I is 2.75, 75% of the time split 3 for 1 and 25% of the time split 2 for 1. The weight assigned to each particle is $W \cdot I/I'$, which is the expected weight, to minimize dispersion of weights.

On the other hand, if a particle of weight W passes from a cell of importance I to one of lower importance I' , so that $I'/I < 1$, Russian roulette is played and the particle is killed with probability $1 - (I'/I)$, or followed further with probability I'/I and weight $W \cdot I/I'$.

Geometry splitting with Russian roulette is very reliable. It can be shown that the weights of all particle tracks are the same in a cell no matter which geometrical path the tracks have taken to get to the cell, assuming that no other biasing techniques, e.g. implicit capture, are used. The variance of any tally is reduced when the possible contributors all have the same weight.

The assigned cell importances can have any value—they are not limited to integers. However, adjacent cells with greatly different importances place a greater burden on reliable sampling. Once a sample track population has deteriorated and lost some of its information, large splitting ratios (like 20 to 1) can build the population back up, but nothing can regain the lost information. It is generally better to keep the ratio of adjacent importances small (for example, a factor of a few) and have cells with optical thicknesses in the penetration direction less than about two mean free paths. MCNP prints a warning message if adjacent importances or weight windows have a ratio greater than 4. PRINT TABLE 120 in the OUTP file lists the affected cells and ratios.

Generally, in a deep penetration shielding problem the sample size (number of particles) diminishes to almost nothing in an analog simulation, but splitting helps keep the size built up. A good rule is to keep the population of tracks traveling in the desired direction more or less constant—that is, approximately equal to the number of particles started from the source. A good initial approach is to split the particles 2 for 1 wherever the track population drops by a factor of 2. Near-optimum splitting usually can be achieved with only a few iterations and additional iterations show strongly diminishing returns. Note that in a combined neutron/photon problem, importances will probably have to be set individually for neutrons and for photons.

MCNP never splits into a void, although Russian roulette can be played entering a void. Splitting into a void accomplishes nothing except extra tracking because all the split particles must be tracked across the void and they all make it to the next surface. The split should be done according to the importance ratio of the last nonvoid cell departed and the first nonvoid cell entered. Note four more items:

1. Geometry splitting/Russian roulette works well only in problems that do not have extreme angular dependence. In the extreme case, splitting/Russian roulette can be useless if no particles ever enter an important cell where the particles can be split.
2. Geometry splitting/Russian roulette will preserve weight variations. The technique is “dumb” in that it never looks at the particle weight before deciding appropriate action. An example is geometry splitting/Russian roulette used with source biasing.
3. Geometry splitting/Russian roulette are turned on or off together.

4. Particles are killed immediately upon entering a zero importance cell, acting as a geometry cutoff.

4. Energy Splitting/Roulette and Time Splitting/Roulette

a. Energy Splitting/Roulette

Energy splitting and roulette typically are used together, but the user can specify only one if desired. Energy splitting/roulette is independent of spatial cell. If the problem has a space-energy dependence, the space-energy dependent weight window is normally a better choice.

1. Splitting: In some cases, particles are more important in some energy ranges than in others. For example, it may be difficult to calculate the number of ^{235}U fissions because the thermal neutrons are also being captured and not enough thermal neutrons are available for a reliable sample. In this case, once a neutron falls below a certain energy level it can be split into several neutrons with an appropriate weight adjustment. A second example involves the effect of fluorescent emission after photoelectric absorption. With energy splitting, the low-energy photon track population can be built up rather than rapidly depleted, as would occur naturally with the high photoelectric absorption cross section. Particles can be split as they move up or down in energy at up to five different energy levels.
2. Russian roulette: In many cases the number of tracks increases with decreasing energy, especially neutrons near the thermal energy range. These tracks can have many collisions requiring appreciable computer time. They may be important to the problem and cannot be completely eliminated with an energy cutoff, but their number can be reduced by playing a Russian roulette game to reduce their number and computer time.

If a track's energy drops through a prescribed energy level, the roulette game is played, based on the input value of the survival probability. If the game is won, the track's history is continued, but its weight is increased by the reciprocal of the survival probability to conserve weight.

b. Time Splitting/Roulette

Time splitting/roulette is similar to the energy splitting and roulette game just discussed, except a particle's time can only increase, in contrast with a particle's energy that may increase or decrease. Time splitting/roulette is independent of spatial cell. If the problem has a space-time dependence, the space-time dependent weight window is normally a better choice.

1. Splitting: In some cases, particles are more important later in time. For example, if a detector responds primarily to late time particles, then it may be useful to split the particles as time increases.
2. Russian roulette: In some cases there may be too many late time particles for optimal calculational efficiency, and the late time particles can be rouletted.

5. Weight Cutoff

In weight cutoff, Russian roulette is played if a particle's weight drops below a user-specified weight cutoff. The particle is either killed or its weight is increased to a user-specified level. The weight cutoff was originally envisioned for use with geometry splitting/Russian roulette and implicit capture, see page 2–150. Because of this intent,

1. The weight cutoffs in cell j depend not only on $WC1$ and $WC2$ on the CUT card, but also on the cell importances.
2. Implicit capture is always turned on (except in detailed photon physics) whenever a nonzero $WC1$ is specified.

Referring to item 1 above, the weight cutoff is applied when the particle's weight falls below $R_j * WC2$, where R_j is the ratio of the source cell importance (IMP card) to cell j 's importance. With probability $W/(WC1 * R_j)$ the particle survives with new weight $WC1 * R_j$; otherwise the particle is killed. When $WC1$ and $WC2$ on the CUT card are negative, the weight cutoff is scaled to the minimum source weight of a particle so that source particles are not immediately killed by falling below the cutoff.

As mentioned earlier, the weight cutoff game was originally envisioned for use with geometry splitting and implicit capture. To illustrate the need for a weight cutoff when using implicit capture, consider what can happen without a weight cutoff. Suppose a particle is in the interior of a very large medium and there are neither time nor energy cutoffs. The particle will go from collision to collision, losing a fraction of its weight at each collision. Without a weight cutoff, a particle's weight would eventually be too small to be representable in the computer, at which time an error would occur. If there are other loss mechanisms (for example, escape, time cutoff, or energy cutoff), the particle's weight will not decrease indefinitely, but the particle may take an unduly long time to terminate.

Weight cutoff's dependence on the importance ratio can be easily understood if one remembers that the weight cutoff game was originally designed to solve the low-weight problem sometimes produced by implicit capture. In a high-importance region, the weights are low by design, so it makes no sense to play the same weight cutoff game in high- and low-importance regions.

Comments: Many techniques in MCNP cause weight change. The weight cutoff was really designed with geometry splitting and implicit capture in mind. Care should be taken in the use of other techniques.

Weight cutoff games are unlike time and energy cutoffs. In time and energy cutoffs, the random walk is always terminated when the threshold is crossed. Potential bias may result if the particle's importance was not zero. A weight cutoff (weight roulette would be a better name) does not bias the game because the weight is increased for those particles that survive.

Setting the weight cutoff is not typically an easy task and requires thought and experimentation. Essentially the user must guess what weight is worth following and start experimenting with weight cutoffs in that vicinity.

6. Weight Window

The weight window Figure 2-23 is a phase space splitting and Russian roulette technique. The phase space may be space-energy, space-time, or space.

For each phase space cell, the user supplies a lower weight bound. The upper weight bound is a user-specified multiple of the lower weight bound. These weight bounds define a window of acceptable weights. If a particle is below the lower weight bound, Russian roulette is played and the particle's weight is either increased to a value within the window or the particle is terminated. If a particle is above the upper weight bound, it is split so that all the split particles are within the window. No action is taken for particles within the window.

Figure 2-24 is a more detailed picture of the weight window. Three important weights define the weight window in a phase space cell.

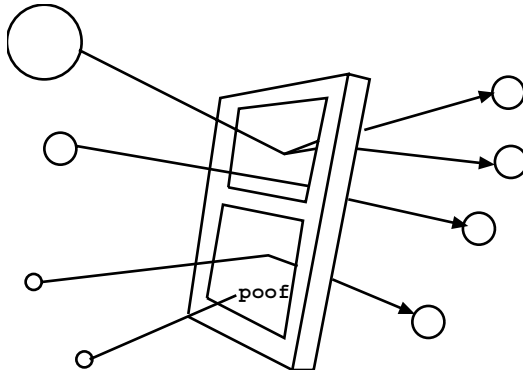


Figure 2-23

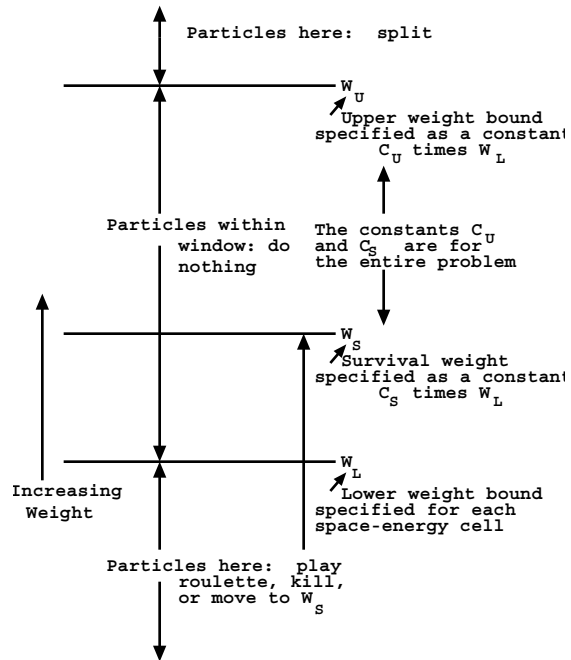


Figure 2-24

1. W_L , the lower weight bound,
2. W_S , the survival weight for particles playing roulette, and
3. W_U , the upper weight bound.

The user specifies W_L for each phase space cell on WWN cards. W_S and W_U are calculated using two problem-wide constants, C_S and C_U (entries on the WWP card), as $W_S = C_S W_L$ and $W_U = C_U W_L$. Thus all cells have an upper weight bound C_U times the lower weight bound and a survival weight C_S times the lower weight bound.

Although the weight window can be effective when used alone, it was designed for use with other biasing techniques that introduce a large variation in particle weight. In particular, a particle may have several “unpreferred” samplings, each of which will cause the particle weight to be multiplied by a weight factor substantially larger than one. Any of these weight multiplications by itself is usually not serious, but the cumulative weight multiplications can seriously degrade calculational efficiency. Worse, the error estimates may be misleading until enough extremely high-weight particles have been sampled. Monte Carlo novices are prone to be misled because they do not have enough experience reading and interpreting the summary information on the sampling supplied by MCNP. Hence, a novice may put more faith in an answer than is justified.

Although it is impossible to eliminate all pathologies in Monte Carlo calculations, a properly specified weight window goes far toward eliminating the pathology referred to in the preceding paragraph. As soon as the weight gets above the weight window, the particle is split and subsequent weight multiplications will thus be multiplying only a fraction of the particle’s weight (before splitting). Thus, it is hard for the tally to be severely perturbed by a particle of extremely large weight. In addition, low-weight particles are rouletted, so time is not wasted following particles of trivial weight.

One cannot ensure that every history contributes the same score (a zero variance solution), but by using a window inversely proportional to the importance, one can ensure that the mean score from any track in the problem is roughly constant. (A weight window generator exists to estimate these importance reciprocals; see page 2–146.) In other words, the window is chosen so that the track weight times the mean score (for unit track weight) is approximately constant. Under these conditions, the variance is due mostly to the variation in the number of contributing tracks rather than the variation in track score.

Thus far, two things remain unspecified about the weight window: the constant of inverse proportionality and the width of the window. It has been observed empirically that an upper weight bound five times the lower weight bound works well, but the results are reasonably insensitive to this choice anyway. The constant of inverse proportionality is chosen so that the lower weight bound in some reference cell is chosen appropriately. In most instances the constant should be chosen so that the source particles start within the window.

1. Weight Window Compared to Geometry Splitting: Although both techniques use splitting and Russian roulette, there are some important differences.
 - a. The weight window is space-energy dependent or space-time dependent. Geometry splitting is only space dependent.
 - b. The weight window discriminates on particle weight before deciding appropriate action. Geometry splitting is done regardless of particle weight.
 - c. The weight window works with absolute weight bounds. Geometry splitting is done on the ratio of the importance across a surface.
 - d. The weight window can be applied at surfaces, collision sites, or both. Geometry splitting is applied only at surfaces.

- e. The weight window can control weight fluctuations introduced by other biasing techniques by requiring all particles in a cell to have weight $W_L < W < W_U$. The geometry splitting will preserve any weight fluctuations because it is weight independent.
 - f. In the rare case where no other weight modification schemes are present, importances will cause all particles in a given cell to have the same weight. Weight windows will merely bound the weight.
 - g. The weight windows can be turned off for a given cell or energy regime by specifying a zero lower bound. This is useful in long or large regions where no single importance function applies. Care should be used because when the weight window is turned off at collisions, the weight cutoff game is turned on, sometimes causing too many particles to be killed.
 - h. For repeated structures, the geometry splitting uses the product of the importances at the different levels. No product is used for the weight windows.
2. The Weight Window Generator: The generator is a method that automatically generates weight window importance functions.¹³⁵ The task of choosing importances by guessing, intuition, experience, or trial and error is simplified and insight into the Monte Carlo calculation is provided.

Although the window generator has proved very useful, two caveats are appropriate. The generator is by no means a panacea for all importance sampling problems and certainly is not a substitute for thinking on the user's part. In fact, in most instances, the user will have to decide when the generator's results look reasonable and when they do not. After these disclaimers, one might wonder what use to make of a generator that produces both good and bad results. To use the generator effectively, it is necessary to remember that the generated parameters are only statistical estimates and that these estimates can be subject to considerable error. Nonetheless, practical experience indicates that a user can learn to use the generator effectively to solve some very difficult transport problems.

Examples of the weight window generator are given in Refs. 133 and 135 and should be examined before using the generator. Note that this importance estimation scheme works regardless of what other variance reduction techniques are used in a calculation.

3. Theory: The importance of a particle at a point P in phase space equals the expected score a unit weight particle will generate. Imagine dividing the phase space into a number of phase space "cells" or regions. The importance of a cell then can be defined as the expected score generated by a unit weight particle after entering the cell. Thus, with a little bookkeeping, the cell's importance can be estimated as

$$\text{Importance (expected score)} = \frac{\text{total score because of particles (and their progeny) entering the cell}}{\text{total weight entering the cell}}$$

After the importances have been generated, MCNP assigns weight windows inversely proportional to the importances. Then MCNP supplies the weight windows in an output file suitable for use as an input file in a subsequent calculation. The spatial portion of the phase space is divided using either standard MCNP cells or a superimposed mesh grid, which can be either rectangular or cylindrical. The energy portion of the phase space is divided using the WWGE card. The time portion of the phase space can be divided also. The constant of proportionality is specified on the WWG card.

4. Limitations of the Weight-Window Generator: The principal problem encountered when using the generator is bad estimates of the importance function because of the statistical nature of the generator. In particular, unless a phase space region is sampled adequately, there will be either no generator importance estimate or an unreliable one. The generator often needs a very crude importance guess just to get any tally; that is, the generator needs an initial importance function to estimate a (we hope) better one for subsequent calculations.

Fortunately, in most problems the user can guess some crude importance function sufficient to get enough tallies for the generator to estimate a new set of weight windows. Because the weight windows are statistical, several iterations usually are required before the optimum importance function is found for a given tally. The first set of generated weight windows should be used in a subsequent calculation, which generates a better set of windows, etc.

In addition to iterating on the generated weight windows, the user must exercise some degree of judgment. Specifically, in a typical generator calculation, some generated windows will look suspicious and will have to be reset. In MCNP, this task is simplified by an algorithm that automatically scrutinizes cell-based importance functions, either input by the user or generated by a generator. By flagging the generated windows that are more than a factor of 4 different from those in adjacent spatial regions, often it is easy to determine which generated weight windows are likely to be statistical flukes that should be revised before the next generator iteration. For example, suppose the lower weight bounds in adjacent cells were 0.5, 0.3, 0.9, 0.05, 0.03, 0.02, etc.; here the user would probably want to change the 0.9 to something like 0.1 to fit the pattern, reducing the 18:1 ratio between cells 3 and 4.

The weight window generator also will fail when phase space is not sufficiently subdivided and no single set of weight window bounds is representative of the whole region. It is necessary to turn off the weight windows (by setting a lower bound of zero) or to further subdivide the geometry or energy phase space. Use of a superimposed importance mesh grid for weight window generation is a good way to subdivide the spatial portion of the phase space without complicating the MCNP cell geometry.

On the other hand, the weight window generator will also fail if the phase space is too finely subdivided and subdivisions are not adequately sampled. Adequate sampling of the important regions of phase space is always key to accurate Monte Carlo calculations, and the weight window generator is a tool to help the user determine the important phase space regions. When using the mesh-based weight window generator, resist the temptation to create mesh cells that are too small.

7. Exponential Transform

The exponential transform samples the distance to collision from a nonanalog probability density function. Although many impressive results are claimed for the exponential transform, it should be remembered that these results are usually obtained for one-dimensional geometries and quite often for energy-independent problems. A review article by Clark¹³⁶ gives theoretical background and sample results for the exponential transform. Sarkar and Prasad¹³⁷ have done a purely analytical analysis for the optimum transform parameter for an infinite slab and one energy group. The exponential transform allows particle walks to move in a preferred direction by artificially reducing the macroscopic cross section in the preferred direction and increasing the cross section in the opposite direction according to

$$\Sigma_t^* = \Sigma_t(1 - p\mu) \quad ,$$

where

- Σ_t^* = fictitious transformed cross section,
- Σ_t = true total cross section,
- Σ_a = absorption cross section,
- Σ_s = scattering cross section,
- p = the exponential transform parameter used to vary the degree of biasing $|p| < 1$ can be a constant or $p = \Sigma_a/\Sigma_t$, in which case $\Sigma_t^* = \Sigma_s$, and
- μ = cosine of the angle between the preferred direction and the particle's direction. $|\mu| \leq 1$. The preferred direction can be specified on a VECT card.

At a collision a particle's weight is multiplied by a factor w_c (derived below) so that the expected weight colliding at any point is preserved. The particle's weight is adjusted such that the weight multiplied by the probability that the next collision is in ds about s remains constant.

The probability of colliding in ds about s is

$$\Sigma e^{-\Sigma s} ds \quad ,$$

where Σ is either Σ_t or Σ_t^* , so that preserving the expected collided weight requires

$$\Sigma_t e^{-\Sigma_t s} ds = w_c \Sigma_t^* e^{-\Sigma_t^* s} ds \quad ,$$

or

$$w_c = \frac{\Sigma_t e^{-\Sigma_t s}}{\Sigma_t^* e^{-\Sigma_t^* s}} = \frac{e^{-\rho \Sigma_t \mu s}}{1 - p\mu} \quad .$$

If the particle reaches a cell surface, time cutoff, DXTRAN sphere, or tally segment instead of colliding, the particle's weight is adjusted so that the weight, multiplied by the probability that the particle travels a distance s to the surface, remains constant. The probability of traveling a distance s without collision is

$$e^{-\Sigma s} ,$$

so that preserving the expected uncollided weight requires

$$e^{-\Sigma_t s} = w_s e^{-\Sigma_t^* s} , \text{ or}$$

$$w_s = \frac{e^{-\Sigma_t s}}{e^{-\Sigma_t^* s}} = e^{-\rho \Sigma_t \mu s} .$$

For one-dimensional deep penetration through highly absorbing media, the variance typically will decrease as p goes from zero to some p' , and then increase as p goes from p' to one. For $p < p'$, the solution is “underbiased” and for $p > p'$, the solution is “overbiased.”

Choosing p' is usually a matter of experience, although some insight may be gleaned by understanding what happens in severely underbiased and severely overbiased calculations. For illustration, apply the variance analysis of page 2–118 to a deep penetration problem when the exponential transform is the only nonanalog technique used. In a severely underbiased calculation ($p \rightarrow 0$), very few particles will score, but those that do will all contribute unity. Thus the variance in an underbiased system is caused by a low scoring efficiency rather than a large dispersion in the weights of the penetrating particles. In a severely overbiased system ($p \rightarrow 1$) particles will score, but there will be a large dispersion in the weights of the penetrating particles with a resulting increase in variance.

Comments: MCNP gives a warning message if the exponential transform is used without a weight window. There are numerous examples where an exponential transform without a weight window gives unreliable means and error estimates. However, with a good weight window both the means and errors are well behaved. The exponential transform works best on highly absorbing media and very poorly on highly scattering media. For neutron penetration of concrete or earth, experience indicates that a transform parameter $p = 0.7$ is about optimal. For photon penetration of high-Z material, even higher values such as $p = 0.9$ are justified.

The following explains what happens with an exponential transform without a weight window. For simplicity consider a slab of thickness T with constant Σ_t . Let the tally be a simple count (F1 tally) of the weight penetrating the slab and let the exponential transform be the only nonanalog technique used. Suppose for a given penetrating history that there are k flights, m that collide and n that do not collide. The penetrating weight is thus:

$$w_p = \prod_{i=1}^m \frac{e^{-\rho \Sigma_t \mu_i s_i}}{(1 - p \mu_i)} \prod_{j=m+1}^k e^{-\rho \Sigma_t \mu_j s_j} .$$

However, the particle's penetration of the slab means that

$$\sum_{l=1}^k \mu_l s_l = T \quad \text{and hence}$$

$$w_p = e^{-\rho \Sigma_t T} \prod_{i=1}^m (1 - p \mu_i)^{-1}.$$

The only variation in w_p is because of the $(1 - p\mu)^{-1}$ factors that arise only from collisions. For a perfectly absorbing medium, every particle that penetrates scores exactly $e^{-\rho \Sigma_t T}$. If a particle has only a few collisions, the weight variation will be small compared to a particle that has many collisions. The weight window splits the particle whenever the weight gets too large, depriving the particle of getting a whole series of weight multiplications upon collision that are substantially greater than one.

By setting $p = \Sigma_a / \Sigma_t$ and $\mu = 1$ so that $\Sigma^* = \Sigma_s$, we sample distance to scatter rather than distance to collision. It is preferable to sample distance to scatter in highly absorbing media — in fact, this is the standard procedure for astrophysics problems. Sampling distance to scatter is also equivalent to implicit capture along a flight path (see page 2–34). However, in such highly absorbing media there is usually a more optimal choice of transform parameter, p , and it is usually preferable to take advantage of the directional component by not fixing $\mu = 1$.

8. Implicit Capture

“Implicit capture,” “survival biasing,” and “absorption by weight reduction” are synonymous. Implicit capture is a variance reduction technique applied in MCNP after the collision nuclide has been selected. Let

$$\begin{aligned} \sigma_{ti} &= \text{total microscopic cross section for nuclide } i \text{ and} \\ \sigma_{ai} &= \text{microscopic absorption cross section for nuclide } i. \end{aligned}$$

When implicit capture is used rather than sampling for absorption with probability $\sigma_{ai} / \sigma_{ti}$, the particle always survives the collision and is followed with new weight: $W * (1 - \sigma_{ai} / \sigma_{ti})$. Implicit capture is a splitting process where the particle is split into absorbed weight (which need not be followed further) and surviving weight.

Implicit capture can also be done along a flight path rather than at collisions when a special form of the exponential transform is used. See page 2–34 for details.

Two advantages of implicit capture are

1. a particle that has finally, against considerable odds, reached the tally region and is not absorbed just before a tally is made, and

2. the history variance, in general, decreases when the surviving weight (that is, 0 or W) is not sampled, but an expected surviving weight is used instead (see weight cutoff, page 2–143).

Two disadvantages are

1. a fluctuation in particle weight is introduced, and
2. the time per history is increased (see weight cutoff, page 2–143).

9. Forced Collisions

The forced collision method is a variance reduction scheme that increases sampling of collisions in specified cells. Because detector contributions and DXTRAN particles arise only from collisions and at the source, it is often useful in certain cells to increase the number of collisions that can produce large detector contributions or large weight DXTRAN particles. Sometimes we want to sample collisions in a relatively thin cell (a fraction of a mean free path) to improve the estimate of quantities like a reaction rate or energy deposition or to cause collisions that are important to some other part of the problem.

The forced collision method splits particles into collided and uncollided parts. The collided part is forced to collide within the current cell. The uncollided part exits the current cell without collision and is stored in the bank until later when its track is continued at the cell boundary. Its weight is

$$W = W_0 e^{-\Sigma_t d} ,$$

where

- W_0 = current particle weight before forced collision,
- d = distance to cell surface in the particle's direction, and
- Σ_t = macroscopic total cross section of the cell material.

That is, the uncollided part is the current particle weight multiplied by the probability of exiting the cell without collision.

The collided part has weight $W = W_0(1 - e^{-\Sigma_t d})$, which is the current particle weight multiplied by the probability of colliding in the cell. The uncollided part is always produced. The collided part may be produced only a fraction f of the time, in which case the collided weight is $W_0(1 - e^{-\Sigma_t d})/f$. This is useful when several forced collision cells are adjacent or when too much time is spent producing and following forced collision particles.

The collision distance is sampled as follows. If $P(x)$ is the unconditional probability of colliding within a distance x , $P(x)/P(d)$ is the conditional probability of colliding within a distance x given that a collision is known to occur within a distance d . Thus the position x of the collision must be sampled on the interval $0 < x < d$ within the cell according to $\xi = P(x)/P(d)$, where $P(x) = 1 - e^{-x\Sigma_t}$ and ξ is a random number. Solving for x , one obtains

$$x = -\frac{1}{\Sigma_t} \ln[1 - \xi(1 - e^{-d\Sigma_t})] .$$

Because a forced collision usually yields a collided particle having a relatively small weight, care must be taken with the weight-cutoff game (page 2–143), the weight-window game (page 2–144), and subsequent collisions of the particle within the cell. The weight window game is not played on the surface of a forced collision cell that the particle is entering. For collisions inside the cell the user has two options.

Option 1: (negative entry for the cell on the forced collision card) After the forced collision, subsequent collisions of the particle are sampled normally. The weight cutoff game is turned off and detector contributions and DXTRAN particles are made before the weight window game is played. If weight windows are used, they should be set to the weight of the collided particle weight or set to zero if detector contributions or DXTRAN particles are desired.

Option 2: (positive entry for the cell on the forced collision card) After the forced collision, detector contributions or DXTRAN particles are made and either the weight cutoff or weight window game is played. Surviving collided particles undergo subsequent forced collisions. If weight windows are used, they should bracket the weight of particles entering the cell.

10. Source Variable Biasing

Provision is made for biasing the MCNP sources in any or all of the source variables specified. MCNP's source biasing, although not completely general, allows the production of more source particles, with suitably reduced weights, in the more important regimes of each variable. For example, one may start more “tracks” at high energies and in strategic directions in a shielding problem while correcting the distribution by altering the weights assigned to these tracks. Sizable variance reductions may result from such biasing of the source. Source biasing samples from a nonanalog probability density function.

If negative weight cutoff values are used on the CUT card, the weight cutoff is made relative to the lowest value of source particle weight generated by the biasing schemes.

1. **Biasing by Specifying Explicit Sampling Frequencies:** The SB input card determines source biasing for a particular variable by specifying the frequency at which source particles will be produced in the variable regime. If this fictitious frequency does not correspond to the fraction of actual source particles in a variable bin, the corrected weight of the source particles in a particular bin is determined by the ratio of the actual frequency (defined on the SP card) divided by the fictitious frequency (defined on the SB card) except for the lin-lin interpolation where it is defined to be the ratio of the actual to fictitious frequency evaluated at the exact value of the interpolated variable. The total weight of particles started in a given SI bin interval is thus conserved.
2. **Biasing by Standard Prescription:** Source biasing can use certain built-in prescriptions similar in principle to built-in analytic source distributions. These biasing options are detailed in the sections below for the appropriate source variables. The SB card input is analogous to that of an SP card for an analytic source distribution; that is, the first entry is a negative prescription number for the type of biasing required, followed by one or more optional user-specified parameters, which are discussed in the following sections.

a. Direction Biasing: The source direction can be biased (about a reference axis) by sampling from a continuous exponential function or by using cones of fixed size and starting a fixed fraction of particles within each cone. The user can bias particles in any arbitrary direction or combination of directions. The sampling of the azimuthal angle about the reference axis is not biased.

In general, continuous biasing is preferable to fixed cone biasing because cone biasing can cause problems from the discontinuities of source track weight at the cone boundaries. However, if the cone parameters (cone size and fraction of particles starting in the cone) are optimized through a parameter study and the paths that tracks take to contribute to tallies are understood, fixed cone biasing sometimes can outperform continuous biasing. Unfortunately, it is usually time consuming (both human and computer) and difficult to arrive at the necessary optimization.

Source directional biasing can be sampled from an exponential probability density function $p(\mu) = Ce^{K\mu}$, where C is a norming constant equal to $K/(e^K - e^{-K})$ and $\mu = \cos\theta$, where θ is an angle relative to the biasing direction. K is typically about 1; $K = 3.5$ defines the ratio of weight of tracks starting in the biasing direction to tracks starting in the opposite direction to be 1/1097. This ratio is equal to e^{-2K} .

Table 2.8 may help to give the user a feel for the biasing parameter K .

Table 2.8
Exponential Biasing Parameter

<u>K</u>	<u>Cumulative Probability</u>	<u>Theta</u>	<u>Weight</u>	<u>K</u>	<u>Cumulative Probability</u>	<u>Theta</u>	<u>Weight</u>
.01	0	0	0.990	2.0	0	0	.245
	.25	60	0.995		.25	31	.325
	.50	90	1.000		.50	48	.482
	.75	120	1.005		.75	70	.931
	1.00	180	1.010		1.00	180	13.40
1.0	0	0	.432	3.5	0	0	.143
	.25	42	.552		.25	23	.190
	.50	64	.762		.50	37	.285
	.75	93	1.230		.75	53	.569
	1.00	180	3.195		1.00	180	156.5

From this table for $K = 1$, we see that half the tracks start in a cone of 64° opening about the axis, and the weight of tracks at 64° is 0.762 times the unbiased weight of source particles. $K = 0.01$ is almost equivalent to no biasing, and $K = 3.5$ is very strong.

Cone directional biasing can be invoked by specifying cone cosines on the SI card, the true distribution on the SP card, and the desired biasing probabilities on the SB card. Both histogram

and linear interpolation can be used. For example, consider the following case in which the true distribution is isotropic:

$$SIn - 1 \ v \ 1$$

$$SPn \ 0 \ \frac{1 + v}{2} \ \frac{1 - v}{2}$$

$$SBn \ 0 \ p_1 \ p_2$$

The direction cosine relative to the reference direction, say v , is sampled uniformly within the cone $v < \nu < 1$ with probability p_2 and within $-1 < \nu < v$ with the complementary probability p_1 . The weights assigned are $W(1 - v)/(2p_2)$ and $W(1 + v)/(2p_1)$, respectively. Note that for a very small cone defined by v and a high probability $p_2 \gg p_1$ for being within the cone, the few source particles generated outside the cone will have a very high weight that can severely perturb a tally.

b. Covering Cylinder Extent Biasing: This biasing prescription for the SDEF EXT variable allows the automatic spatial biasing of source particles in a cylindrical-source-covering-volume along the axis of the cylinder. Such biasing can aid in the escape of source particles from optically thick source regions and thus represents a variance reduction technique.

c. Covering Cylinder or Sphere Radial Biasing: This biasing prescription for the SDEF RAD variable allows for the radial spatial biasing of source particles in either a spherical or cylindrical source covering volume. Like the previous example of extent biasing, this biasing can be used to aid in the escape of source particles from optically thick source regions.

3. Biasing Standard Analytic Source Functions:¹³⁸ The preceding examples discuss the biasing of source variables by either input of specific sampling frequencies corresponding to SP card entries or by standard analytic biasing functions. A third biasing category can be used in conjunction with standard analytic source probability functions (for example, a Watt fission spectrum).

A negative entry on an SP card, that is,

$$SPn \ -i \ a \ b$$

causes MCNP to sample source distribution n from probability function i with input variables a, b, \dots . Sampling schemes are typically unbiasedable. For example, for

$$SPn \ -5 \ a$$

the evaporation spectrum $f(E) = C E \exp(-E/a)$ is sampled according to the sampling prescription $E = -a \log(\xi_1 * \xi_2)$, where ξ_{i1} and ξ_{i2} are random numbers. Biasing this sampling scheme is usually very difficult or impossible. Fortunately, there is an approximate method available in MCNP for biasing any arbitrary probability function.¹³⁸ The code approximates the function as a table, then uses the usual SB card biasing scheme to bias this approximate table function. The user inputs a coarse bin structure to govern the bias and the code adds up to 300 additional equiprobable bins to assure accuracy. For example, suppose we wish to sample the function

$$f(E) = C E \exp(-E/a)$$

and suppose that we want half the source to be in the range $.005 < E < .1$ and the other half to be in the range $.1 < E < 20$. Then the input is

```
SPn -5 a
SIn .005 .1 20
SBn C 0 .5 1 .
```

MCNP breaks up the function into 150 equiprobable bins below $E = .1$ and 150 more equiprobable bins above $E = .1$. Half the time E is chosen from the upper set of bins and half the time it is chosen from the lower set. Particles starting from the upper bins have a different weight from that of particles starting from the lower bins in order to adjust for the bias, and a detailed summary is provided when the PRINT option is used.

Note that in the above example the probability distribution function is truncated below $E = .005$ and above $E = 20$. MCNP prints out how much of the distribution is lost in this manner and reduces the weight accordingly.

It is possible for the user to choose a foolish biasing scheme. For example,

```
SPn -5 a
SIn .005 297I .1 20
SBn 0 1 298R
```

causes each of the 299 bins to be chosen with equal probability. This would be all right except that since there are never more than 300 equiprobable bins, this allocates only 1 equiprobable bin per user-supplied bin. The single equiprobable bin for $.1 < E < 20$ is inadequate to describe the distribution function over this range. Thus the table no longer approximates the function and the source will be sampled erroneously. MCNP issues an error message whenever too much of the source distribution is allocated to a single equiprobable bin, alerting users to a poor choice of binning which might inadequately represent the function. The coarse bins used for biasing should be chosen so that the probability function is roughly equally distributed among them.

11. Point Detector Tally

The point detector is a tally and does not bias random walk sampling. Recall from Section VI, however, that the tally choice affects the efficiency of a Monte Carlo calculation. Thus, a little will be said here in addition to the discussion in the tally section.

Although flux is a point quantity, flux at a point cannot be estimated by either a track-length tally (F4) or a surface flux tally (F2) because the probability of a track entering the volume or crossing the surface of a point is zero. For very small volumes, a point detector tally can provide a good estimate of the flux where it would be almost impossible to get either a track-length or surface-crossing estimate because of the low probability of crossing into the small volume.

It is interesting that a DXTRAN sphere of vanishingly small size with a surface-crossing tally across the diameter normal to the particle's trajectory is equivalent to a point detector. Thus, many of the comments on DXTRAN are appropriate and the DXC cards essentially are identical to the PD cards.

For a complete discussion of point detectors, see page 2–91.

12. DXTRAN

DXTRAN typically is used when a small region is being inadequately sampled because particles have a very small probability of scattering toward that region. To ameliorate this situation, the user can specify in the input file a DXTRAN sphere that encloses the small region. Upon collision (or exiting the source) outside the sphere, DXTRAN creates a special “DXTRAN particle” and deterministically scatters it toward the DXTRAN sphere and deterministically transports it, without collision, to the surface of the DXTRAN sphere. The collision itself is otherwise treated normally, producing a non-DXTRAN particle that is sampled in the normal way, with no reduction in weight. However, the non-DXTRAN particle is killed if it tries to enter the DXTRAN sphere. DXTRAN uses a combination of splitting, Russian roulette, and sampling from a nonanalog probability density function.

The subtlety about DXTRAN is how the extra weight created for the DXTRAN particles is balanced by the weight killed as non-DXTRAN particles cross the DXTRAN sphere. The non-DXTRAN particle is followed without any weight correction, so if the DXTRAN technique is to be unbiased, the extra weight put on the DXTRAN sphere by DXTRAN particles must somehow (on average) balance the weight of non-DXTRAN particles killed on the sphere.

1. DXTRAN Viewpoint 1: One can view DXTRAN as a splitting process (much like the forced collision technique) wherein each particle is split upon departing a collision (or source point) into two distinct pieces:
 - a. the weight that does not enter the DXTRAN sphere on the next flight, either because the particle is not pointed toward the DXTRAN sphere or because the particle collides before reaching the DXTRAN sphere, and
 - b. the weight that enters the DXTRAN sphere on the next flight.

Let w_0 be the weight of the particle before exiting the collision, let p_1 be the analog probability that the particle does not enter the DXTRAN sphere on its next flight, and let p_2 be the analog probability that the particle does enter the DXTRAN sphere on its next flight. The particle must undergo one of these mutually exclusive events, thus $p_1 + p_2 = 1$. The expected weight not entering the DXTRAN sphere is $w_1 = w_0 p_1$, and the expected weight entering the DXTRAN sphere is $w_2 = w_0 p_2$. Think of DXTRAN as deterministically splitting the original particle with weight w_0 into two particles, a non-DXTRAN (particle 1) particle of weight w_1 and a DXTRAN (particle 2) particle of weight w_2 . Unfortunately, things are not quite that simple.

Recall that the non-DXTRAN particle is followed with unreduced weight w_0 rather than weight $w_1 = w_0 p_1$. The reason for this apparent discrepancy is that the non-DXTRAN particle (particle 1) plays a Russian roulette game. Particle 1’s weight is increased from w_1 to w_0 by playing a Russian roulette game with survival probability $p_1 = w_1 / w_0$. The reason for playing this Russian roulette game is simply that p_1 is not known, so assigning weight $w_1 = p_1 w_0$ to particle 1 is impossible. However, it is possible to play the Russian roulette game without explicitly knowing p_1 . It is not magic, just slightly subtle.

The Russian roulette game is played by sampling particle 1 normally and keeping it only if it does not enter (on its next flight) the DXTRAN sphere; that is, particle 1 survives (by definition of p_1) with probability p_1 . Similarly, the Russian roulette game is lost if particle 1 enters (on its next flight) the DXTRAN sphere; that is, particle 1 loses the roulette with probability p_2 . To restate this idea, with probability p_1 , particle 1 has weight w_0 and does not enter the DXTRAN sphere and with probability p_2 , the particle enters the DXTRAN sphere and is killed. Thus, the expected weight not entering the DXTRAN sphere is $w_0 p_1 + 0 * p_2 = w_1$, as desired.

So far, this discussion has concentrated on the non-DXTRAN particle and ignored exactly what happens to the DXTRAN particle. The sampling of the DXTRAN particle will be discussed after a second viewpoint on the non-DXTRAN particle.

2. DXTRAN Viewpoint 2: This second way of viewing DXTRAN does not see DXTRAN as a splitting process but as an accounting process in which weight is both created and destroyed on the surface of the DXTRAN sphere. In this view, DXTRAN estimates the weight that should go to the DXTRAN sphere upon collision and creates this weight on the sphere as DXTRAN particles. If the non-DXTRAN particle does not enter the sphere, its next flight will proceed exactly as it would have without DXTRAN, producing the same tally contributions and so forth. However, if the non-DXTRAN particle's next flight attempts to enter the sphere, the particle must be killed or there would be (on average) twice as much weight crossing the DXTRAN sphere as there should be because the weight crossing the sphere has already been accounted for by the DXTRAN particle.
3. The DXTRAN Particle: Although the DXTRAN particle does not confuse people nearly as much as the non-DXTRAN particle, the DXTRAN particle is nonetheless subtle.

The most natural approach for scattering particles toward the DXTRAN sphere would be to sample the scattering angle Ω proportional to the analog density. This approach is not used because it is too much work to sample proportional to the analog density and because it is sometimes useful to bias the sampling.

To sample Ω in an unbiased fashion when it is known that Ω points to the DXTRAN sphere, one samples the conditional density

$$P_{con}(\Omega) = P(\Omega) / \int_{S(\Omega)} P(\Omega) d\Omega \quad (\text{the set } S(\Omega) \text{ points toward the sphere})$$

and multiplies the weight by $\int_{S(\Omega)} P(\Omega) d(\Omega)$, the probability of scattering into the cone (see Figure 2-25). However, it is too much work to calculate the above integral for each collision. Instead, an arbitrary density function $P_{arb}(\Omega)$ is sampled and the weight is multiplied by

$$\frac{P_{con}(\Omega)}{P_{arb}(\Omega)} = \frac{P(\Omega)}{P_{arb}(\Omega) \int_{S(\Omega)} P(\Omega) d(\Omega)} \quad .$$

The total weight multiplication is the product of the fraction of the weight scattering into the cone, $\int_{S(\Omega)} P(\Omega) d\Omega$, and the weight correction for sampling $P_{arb}(\Omega)$ instead of $P_{con}(\Omega)$. Thus, the weight correction on scattering is

$$\frac{P(\Omega)}{P_{arb}(\Omega)}.$$

If μ is the cosine of the angle between the scattering direction and the particle's incoming direction, then $P(\Omega) = P(\mu)/(2\pi)$ because the scattering is symmetric in the azimuthal angle. If η is the cosine of the angle with respect to the cone axis (see Figure 2-25) and if the azimuthal angle about the cone axis is uniformly sampled, then $P_{arb}(\Omega) = P_{arb}(\eta)/(2\pi)$. Thus

$$\frac{P(\mu)}{P_{arb}(\eta)} = \text{weight multiplier for DXTRAN particle.}$$

This result can be obtained more directly, but the other derivation does not explain why $P_{con}(\Omega)$ is not sampled.

Because $P_{arb}(\eta)$ is arbitrary, MCNP can choose a scheme that samples η from a two-step density that favors particles within the larger η interval. In fact, the inner DXTRAN sphere has to do only with this arbitrary density and is not essential to the DXTRAN concept. The DXTRAN particles are always created on the outside DXTRAN sphere, with the inner DXTRAN sphere defining only the boundary between the two steps in the density function.

After $\eta = \cos \theta$ has been chosen, the azimuthal angle ϕ is sampled uniformly on $[0, 2\pi]$; this completes the scattering. Recall, however, that the DXTRAN particle arrives at the DXTRAN sphere without collision. Thus the DXTRAN particle also has its weight multiplied by the negative exponential of the optical path between the collision site and the sphere. Thus the DXTRAN weight multiplication is:

$$\frac{P(\mu)}{P_{arb}(\eta)} \exp(-\lambda)$$

where λ is the number of mean free paths from the exit site to the chosen point on the DXTRAN sphere.

4. Inside the DXTRAN Sphere: So far, only collisions outside the DXTRAN sphere have been discussed. At collisions inside the DXTRAN sphere, the DXTRAN game is not played because first, the particle is already in the desired region, and second, it is impossible to define the angular cone of Figure 2-25. If there are several DXTRAN spheres and the collision occurs in sphere i , DXTRAN will be played for all spheres except sphere i .
5. Terminology—Real particle and Pseudoparticle: Sometimes the DXTRAN particle is called a pseudoparticle and the non-DXTRAN particle is called the original or real particle. The terms “real particle” and “pseudoparticle” are potentially misleading. Both

particles are equally real: both execute random walks, both carry nonzero weight, and both contribute to tallies. The only sense in which the DXTRAN particle should be considered “pseudo” or “not real” is during creation. A DXTRAN particle is created on the DXTRAN sphere, but creation involves determining what weight the DXTRAN particle should have upon creation. Part of this weight determination requires calculating the optical path between the collision site and the DXTRAN sphere. This is done in the same way as point detectors (see point detector pseudoparticles on page 2–100.) MCNP determines the optical path by tracking a pseudoparticle from the collision site to the DXTRAN sphere. This pseudoparticle is deterministically tracked to the DXTRAN sphere simply to determine the optical path. No distance to collision is sampled, no tallies are made, and no records of the pseudoparticle's passage are kept (for example, tracks entering). In contrast, once the DXTRAN particle is created at the sphere's surface, the particle is no longer a pseudoparticle. The particle has real weight, executes random walks, and contributes to tallies.

6. DXTRAN Details: To explain how the scheme works, consider the neighborhood of interest to be a spherical region surrounding a designated point in space. In fact, consider two spheres of arbitrary radii about the point $P_0 = (x_0, y_0, z_0)$. Further, assume that the particle having direction (u, v, w) collides at the point $P_1 = (x, y, z)$, as shown in Figure 2-25.

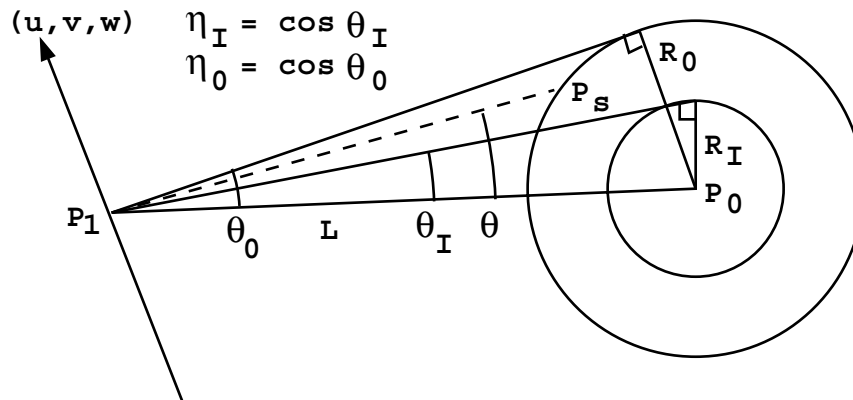


Figure 2-25

The quantities θ_I , θ_O , η_I , η_O , R_I , and R_0 are defined in the figure. Thus L , the distance between the collision point and center of the spheres, is

$$L = \sqrt{(x - x_0)^2 + (y - y_0)^2 + (z - z_0)^2} .$$

On collision, a DXTRAN particle is placed at a point on the outer sphere of radius R_0 as described below. Provision is made for biasing the contributions of these DXTRAN particles on the outer sphere within the cone defined by the inner sphere. The weight of the DXTRAN particle is adjusted to account for the probability of scattering in the direction of the point on the outer sphere and traversing the distance with no further collision.

The steps in sampling the DXTRAN particles are outlined:

$$\eta_I = \cos \theta_I = (L^2 - R_I^2)^{1/2} / L$$

$$\eta_O = \cos \theta_O = (L^2 - R_O^2)^{1/2} / L$$

Sample $\eta = \eta_I + \xi(1 - \eta_I)$ uniformly in $(\eta_I, 1)$ with probability

$$Q(1 - \eta_I) / [Q(1 - \eta_I) + \eta_I - \eta_O]$$

and with probability

$$(\eta_I - \eta_O) / [Q(1 - \eta_I) + \eta_I - \eta_O]$$

sample $\eta = \eta_O + \xi(\eta_I - \eta_O)$ uniformly in (η_O, η_I) . The quantity Q (equal to 5 in MCNP) is a factor that measures the importance assigned to scattering in the inner cone relative to the outer cone. Therefore, Q is also the ratio of weights for particles put in the two different cones.

With $\eta = \cos \theta$ chosen, a new direction (u', v', w') is computed by considering the rotation through the polar angle θ (and a uniform azimuthal angle ϕ) from the reference direction

$$\left(\frac{x_0 - x}{L}, \frac{y_0 - y}{L}, \frac{z_0 - z}{L} \right) .$$

The particle is advanced in the direction (u', v', w') to the surface of the sphere of radius R_0 . The new DXTRAN particle with appropriate direction and coordinates is banked. The weight of the DXTRAN particle is determined by multiplying the weight of the particle at collision by

$$v \cdot \frac{P(\mu) \{ Q(1 - \eta_I) + \eta_I - \eta_O \} e^{-\int_{P_I}^{P_S} \sigma_t(s) ds}}{Q}, \quad \eta_I \leq \eta \leq 1 \quad \text{and}$$

$$v \cdot P(\mu) \{ Q(1 - \eta_I) + \eta_I - \eta_O \} e^{-\int_{P_I}^{P_S} \sigma_t(s) ds}, \quad \eta_O \leq \eta \leq \eta_I$$

where

$$\begin{aligned} \mu &= uu' + vv' + ww', \\ P(\mu) &= \text{scattering probability density function for scattering through the angle } \cos^{-1} \mu \text{ in the lab system for the event sampled at } (x, y, z), \\ v &= \text{number of particles emitted from the event, and} \end{aligned}$$

$e^{-\int_{P_I}^{P_S} \Sigma_t(s) ds}$ = the attenuation along the line between $P_I(x,y,z)$ and P_S , the point on the sphere where the particle is placed.

In arriving at the weight factor, note that the density function for sampling η is given by

$$Q/[Q(1 - \eta_I) + \eta_I - \eta_O], \eta_I < \eta \leq 1$$

$$1/([Q(1 - \eta_I) + \eta_I - \eta_O]), \eta_O \leq \eta \leq \eta_I \quad .$$

Thus the weight of the DXTRAN particle is the weight of the incoming particle at P_I modified by the ratio of the probability density function for actually scattering from P_I and arriving at P_S without collision to the density function actually sampled in choosing P_S . Therefore, particles in the outer cone have weights $Q = 5$ times higher than the weights of similar particles in the inner cone.

The attenuation is calculated at the energy obtained by scattering through the angle μ . The energy is uniquely determined from μ in elastic scattering (and also in level scattering), whereas for other nonelastic events, the energy is sampled from the corresponding probability density function for energy, and may not depend on μ .

7. Auxiliary Games for DXTRAN: The major disadvantage to DXTRAN is the extra time consumed following DXTRAN particles with low weights. Three special games can control this problem:
 1. DXTRAN weight cutoffs,
 2. DXC games, and
 3. DD game.

Particles inside a DXTRAN sphere are not subject to the normal MCNP weight cutoff or weight window game. Instead DXTRAN spheres have their own weight cutoffs, allowing the user to roulette DXTRAN particles that, for one reason or another, do not have enough weight to be worth following.

Sometimes low-weighted DXTRAN particles occur because of collisions many free paths from the DXTRAN sphere. The exponential attenuation causes these particles to have extremely small weights. The DXTRAN weight cutoff will roulette these particles only after much effort has been spent producing them. The DXC cards are cell dependent and allow DXTRAN contributions to be taken only some fraction of the time. They work just like the PD cards for detectors (see page 2–102). The user specifies a probability p_i that a DXTRAN particle will be produced at a given collision or source sampling in cell i . The DXTRAN result remains unbiased because when a DXTRAN particle is produced its weight is multiplied by p_i^{-1} . (The non-DXTRAN particle is treated exactly as before, unaffected unless it enters the DXTRAN sphere, whereupon it is killed.) To see the utility, suppose that the DXTRAN weight cutoff was immediately killing 99% of the DXTRAN particles from cell i . Only 1% of the DXTRAN particles survive anyway, so it might be appropriate to produce only 1% ($p_i = .01$) and have these not be killed

immediately by the DXTRAN weight cutoff. Or the p_i 's can often be set such that all DXTRAN particles from all cells are created on the DXTRAN sphere with roughly the same weight. Choosing the p_i 's is often difficult and the method works well typically when the material exponential attenuation is the major source of the weight fluctuation.

Often the weight fluctuation arises because the probability $P(\mu)$ of scattering toward the DXTRAN sphere varies greatly, depending on what nuclide is hit and what the collision orientation is with respect to the DXTRAN sphere. For example, consider a highly forward-peaked scattering probability density. If the DXTRAN sphere were close to the particle's precollision direction, $P(\mu)$ will be large; if the DXTRAN sphere were at 105° to the precollision direction, $P(\mu)$ will be small. The DD game can be used to reduce the weight fluctuation on the DXTRAN sphere caused by these geometry effects, as well as the material exponential attenuation effects.

The DD game selectively roulettes the DXTRAN pseudoparticles during creation, depending on the DXTRAN particles' weight compared to some reference weight. This is the same game that is played on detector contributions, and is described on page 2–102. The reference weight can be either a fraction of the average of previous DXTRAN particle weights or a user input reference weight. Recall that a DXTRAN particle's weight is computed by multiplying the exit weight of the non-DXTRAN particle by a weight factor having to do with the scattering probability and the negative exponential of the optical path between the collision site and DXTRAN sphere. The optical path is computed by tracking a pseudoparticle from collision to the DXTRAN sphere. The weight of the pseudoparticle is monotonically decreasing, so the DD game compares the pseudoparticle's weight at the collision site and, upon exiting each cell, against the reference weight. A roulette game is played when the pseudoparticle's weight falls below the reference weight. The DD card stops tracking a pseudoparticle as soon as the weight becomes inconsequential, saving time by eliminating subsequent tracking.

8. Final Comments:

- a. DXTRAN should be used carefully in optically thick problems. Do not rely on DXTRAN to do penetration.
- b. If the source is user supplied, some provision must be made for obtaining the source contribution to particles on the DXTRAN sphere.
- c. Extreme care must be taken when more than one DXTRAN sphere is in a problem. Cross-talk between spheres can result in extremely low weights and an excessive growth in the number of particle tracks.
- d. Never put a zero on the DXC card. A zero will bias the calculation by not creating DXTRAN particles but still killing the non-DXTRAN particle if it enters the DXTRAN sphere.
- e. Usually there should be a rough balance in the summary table of weight created and lost by DXTRAN.
- f. DXTRAN cannot be used with reflecting surfaces for the same reasons that point detectors cannot be used with reflecting surfaces. See page 2–101 for further explanation.

- g. Both DXTRAN and point detectors track pseudoparticles to a point. Therefore, most of the discussion about detectors applies to DXTRAN. Refer to the section on detectors, page 2–91, for more information.

13. Correlated Sampling

Correlated sampling estimates the change in a quantity resulting from a small alteration of any type in a problem. This technique enables the evaluation of small quantities that would otherwise be masked by the statistical errors of uncorrelated calculations. MCNP correlates a pair of runs by providing each new history in the original and altered problems with the same starting pseudorandom number. The same sequence of subsequent numbers is used and each history tracks identically until the alteration causes the tracking to diverge. The sequencing of random numbers is done by incrementing the random number generator at the beginning of each history by a stride S of random numbers from the beginning of the previous history. The default value of S is 152,917. The stride should be a quantity greater than would be needed by most histories (see page 2–191).

MCNP does not provide an estimate of the error in the difference. Reference 133 shows how the error in the difference between two correlated runs can be estimated. A postprocessor code would have to be written to do this.

Correlated sampling should not be confused with more elaborate Monte Carlo perturbation schemes that calculate differences and their variances directly. MCNP also has a sophisticated perturbation capability.

VIII. CRITICALITY CALCULATIONS

Nuclear criticality, the ability to sustain a chain reaction by fission neutrons, is characterized by k_{eff} , the eigenvalue to the neutron transport equation. In reactor theory, k_{eff} is thought of as the ratio between the number of neutrons in successive generations, with the fission process regarded as the birth event that separates generations of neutrons.¹³⁹ For critical systems, $k_{eff} = 1$ and the chain reaction will just sustain itself. For subcritical systems, $k_{eff} < 1$ and the chain reaction will not sustain itself. For supercritical systems, $k_{eff} > 1$ and the number of fissions in the chain reaction will increase with time. In addition to the geometry description and material cards, all that is required to run a criticality problem is a KCODE card, described below, and an initial spatial distribution of fission points using either the KSRC card, the SDEF card, or an SRCTP file.

Calculating k_{eff} consists of estimating the mean number of fission neutrons produced in one generation per fission neutron started. A generation is the life of a neutron from birth in fission to death by escape, parasitic capture, or absorption leading to fission. In MCNP, the computational equivalent of a fission generation is a k_{eff} cycle; that is, a cycle is a computed estimate of an actual fission generation. Processes such as $(n,2n)$ and $(n,3n)$ are considered internal to a cycle and do not act as termination. Because fission neutrons are terminated in each cycle to provide the fission source for the next cycle, a single history can be viewed as continuing from cycle to cycle. The effect of the delayed neutrons is included by using the total $\bar{\nu}$ when the data are available. In a Mode N,P problem, secondary photon production from neutrons is turned off during inactive

cycles. MCNP uses three different estimators for k_{eff} . We recommend using, for the final k_{eff} result, the statistical combination of all three.¹⁴⁰

It is extremely important to emphasize that the result from a criticality calculation is a confidence interval for k_{eff} that is formed using the final estimated k_{eff} and the estimated standard deviation. A properly formed confidence interval from a valid calculation should include the true answer the fraction of time used to define the confidence interval. There will always be some probability that the true answer lies outside of a confidence interval.

Reference 141 is an introduction to using MCNP for criticality calculations, focusing on the unique aspects of setting up and running a criticality problem and interpreting the results. A quickstart chapter gets the new MCNP user on the computer running a simple criticality problem as quickly as possible.

A. *Criticality Program Flow*

Because the calculation of k_{eff} entails running successive fission cycles, criticality calculations have a different program flow than MCNP fixed source problems. They require a special criticality source that is incompatible with the surface source and user-supplied sources. Unlike fixed source problems, where the source being sampled throughout the problem never changes, the criticality source changes from cycle to cycle.

1. Criticality Problem Definition

To set up a criticality calculation, the user initially supplies an INP file that includes the KCODE card with the following information:

1. the nominal number of source histories, N , per k_{eff} cycle;
2. an initial guess of k_{eff} ;
3. the number of source cycles, I_c , to skip before k_{eff} accumulation; and
4. the total number of cycles, I_t , in the problem.

Other KCODE entries are discussed in Chapter 3, page 3–76. The initial spatial distribution of fission neutrons can be entered by using (1) the KSRC card with sets of x,y,z point locations, (2) the SDEF card to define points uniformly in volume, or (3) a file (SRCTP) from a previous MCNP criticality calculation. If the SDEF card is used, the default WGT value should not be changed. Any KSRC points in geometric cells that are void or have zero importance are rejected. The remaining KSRC points are duplicated or rejected enough times so the total number of points M in the source spatial distribution is approximately the nominal source size N . The energy of each source particle for the first k_{eff} cycle is selected from a generic Watt thermal fission distribution if it is not available from the SRCTP file.

2. Particle Transport for Each k_{eff} Cycle

In each k_{eff} cycle, M (varying with cycle) source particles are started isotropically. For the first cycle, these M points come from one of three user–selected source possibilities. For subsequent

cycles, these points are the ones written at collision sites from neutron transport in the previous cycle. The total source weight of each cycle is a constant N . That is, the weight of each source particle is N/M , so all normalizations occur as if N rather than M particles started in each cycle.

Source particles are transported through the geometry by the standard random walk process, except that fission is treated as capture, either analog or implicit, as defined on the PHYS:N or CUT:N card. At each collision point the following four steps are performed for the cycle:

1. the three prompt neutron lifetime estimates are accumulated;
2. if fission is possible, the three k_{eff} estimates are accumulated; and
3. if fission is possible, $n \geq 0$ fission sites (including the sampled outgoing energy of the fission neutron) at each collision are stored for use as source points in the next cycle,

where

n	=	$[W\bar{v}(\sigma_f/\sigma_t)(1/k_{eff}) + \text{random number}]$;
W	=	particle weight (before implicit capture weight reduction or analog capture);
\bar{v}	=	average number of neutrons produced by fission at the incident energy of this collision, with either prompt \bar{v} or total \bar{v} (default) used;
σ_f	=	microscopic material fission cross section;
σ_t	=	microscopic material total cross section; and
k_{eff}	=	estimated collision k_{eff} from previous cycle.

For the first cycle, use the second KCODE card entry.

$M = \sum n$ = number of fission source points to be used in the next cycle. The number of fission sites n stored at each collision is rounded up or down to an integer (including zero) with a probability proportional to its closeness to that integer. If the initial guess of k_{eff} is too low or too high, the number of fission sites written as source points for the next cycle will be, respectively, too high or too low relative to the desired nominal number N . A bad initial guess of k_{eff} causes only this consequence.

A very poor initial guess for the spatial distribution of fissions can cause the first cycle estimate of k_{eff} to be extremely low. This situation can occur when only a fraction of the fission source points enter a cell with a fissionable material. As a result, one of two error messages can be printed: (1) no new source points were generated, or (2) the new source has overrun the old source. The second message occurs when the MCNP storage for the fission source points is exceeded because the small k_{eff} that results from a poor initial source causes n to become very large.

The fission energy of the next-cycle neutron is sampled separately for each source point and stored for the next cycle. It is sampled from the same distributions as fissions would be sampled in the random walk based on the incident neutron energy and fissionable isotope. The geometric coordinates and cell of the fission site are also stored.

4. The collision nuclide and reaction are sampled (after steps 1, 2, and 3) but the fission reaction is not allowed to occur because fission is treated as capture. The fission neutrons

that would have been created are accrued by three different methods to estimate k_{eff} for this cycle. The three estimators are a collision estimator, an absorption estimator and a track length estimator as discussed in subsection B on page 2-167.

3. k_{eff} Cycle Termination

At the end of each k_{eff} cycle, a new set of M source particles has been written from fissions in that cycle. The number M varies from cycle to cycle but the total starting weight in each cycle is a constant N . These M particles are written to the SRCTP file at certain cycle intervals. The SRCTP file can be used as the initial source in a subsequent criticality calculation with a similar, though not identical, geometry. Also, k_{eff} quantities are accumulated, as is described below.

4. Convergence

The first I_c cycles in a criticality calculation are inactive cycles, where the spatial source changes from the initial definition to the correct distribution for the problem. No k_{eff} accumulation, summary table, activity table, or tally information is accrued for inactive cycles. Photon production, perturbations, and DXTRAN are turned off during inactive cycles. I_c is the third entry on the KCODE card for the number of k_{eff} cycles to be skipped before k_{eff} and tally accumulation. After the first I_c cycles, the fission source spatial distribution is assumed to have achieved equilibrium, active cycles begin, and k_{eff} and tallies are accumulated. Cycles are run until either a time limit is reached or the total cycles on the KCODE card have been completed.

Criticality calculations with MCNP are based on an iterative procedure called "power iteration."^{142,143} After assuming an initial guess for the fission source spatial distribution (i.e., first generation), histories are followed to produce a source for the next fission neutron generation and to estimate a new value for k_{eff} . The new fission source distribution is then used to follow histories for the second generation, producing yet another fission source distribution and estimate of k_{eff} . These generations (also called cycles or batches) are repeated until the source spatial distribution has converged. Once the fission source distribution has converged to its stationary state, tallies for reaction rates and k_{eff} may be accumulated by running additional cycles until the statistical uncertainties have become sufficiently small.

Analysis of the power iteration procedure for solving k_{eff} eigenvalue calculations¹⁴² shows that the convergence of the fission source distribution, \vec{S} , and the estimated eigenvalue, k_{eff} , can be modeled as

$$\vec{S}^{(n+1)} \approx \vec{S}_0 + a \left(\frac{k_1}{k_0} \right)^{n+1} \vec{S}_1 + \dots$$

$$k_{eff}^{(n+1)} \approx k_0 \left[1 - b \left(\frac{k_1}{k_0} \right)^n \left(1 - \frac{k_1}{k_0} \right) + \dots \right],$$

where \vec{S}_0 and k_0 are the fundamental eigenfunction and eigenvalue of the exact transport solution, \vec{S}_1 and k_1 are the eigenfunction and eigenvalue of the first higher mode, a and b are constants, and n is the number of cycles performed in the power iteration procedure. Note that k_0 is the expected value of k_{eff} , and that $k_0 > k_1 > 0$, so that (k_1/k_0) is less than 1. The quantity (k_1/k_0) is called the

dominance ratio (DR), and is the key physical parameter that determines the convergence rate of the power iteration procedure. The DR is a function of problem geometry and materials. As the number of cycles n becomes large, the error terms due to higher modes die off as DR^n , and the source distribution and k_{eff} approach their stationary, equilibrium values. For typical light-water reactor systems, the DR is often in the range 0.8-0.99, and 50-100 inactive cycles may be required for errors in the initial guess to die away sufficiently that the source and k_{eff} converge. For some critical systems (e.g., heavy-water reactors, fuel storage vaults), however, the DR may be very close to 1 (e.g., .99 or higher), and hundreds or thousands of inactive cycles may be required to attain source convergence.

It should also be noted that the source distribution \vec{S} and the eigenvalue k_{eff} do not converge in the same manner. The expression for $k_{eff}^{(n+1)}$ has the additional factor $(1-k_1/k_0)$ on the higher-mode error. For problems where the DR is very close to 1, the source distribution may take hundreds or thousands of cycles to converge (due to errors dying out as DR^n), while k_{eff} may converge rapidly (since its higher-mode error is damped by the additional factor $1-DR$, which may be very small). That is, k_{eff} will converge more rapidly than the source distribution. Thus, it is very important to examine the behavior of both k_{eff} and the source distribution when assessing problem convergence. **Both k_{eff} and the fission source distribution must converge before starting active cycles for tallies.** It is up to the user to specify the number of inactive cycles I_c to run in order to attain convergence. Most users will make a trial calculation (using a small number of histories per cycle, such as 1000) to examine the convergence behavior of k_{eff} and the source distribution, to determine a proper value for I_c , and then make a final calculation using a larger number of histories per cycle (e.g., 5000 or more) and sufficient active cycles to attain small uncertainties. To assist users in assessing convergence of criticality calculations, MCNP provides several statistical checks on k_{eff} , as discussed in the next sections. In addition, MCNP calculates a quantity called the entropy of the source distribution, H_{src} ,^{144,145} to assist users in assessing the convergence of the source distribution.

B. Estimation of k_{eff} Confidence Intervals and Prompt Neutron Lifetimes

The criticality eigenvalue k_{eff} and various prompt neutron lifetimes, along with their standard deviations, are automatically estimated in every criticality calculation in addition to any user-requested tallies. k_{eff} and the lifetimes are estimated for every active cycle, as well as averaged over all active cycles. k_{eff} and the lifetimes are estimated in three different ways. These estimates are combined¹⁴⁰ using observed statistical correlations to provide the optimum final estimate of k_{eff} and its standard deviation.

It is known¹⁴⁶ that the power iteration method with a fixed source size produces a very small negative bias Δk_{eff} in k_{eff} that is proportional to $1/N$. This bias is negligible¹⁴⁶ for all practical problems where N is greater than about 200 neutrons per cycle and as long as too many active cycles are not used. It has been shown¹⁴⁶ that this bias is less, probably much less, than one-half of one standard deviation for 400 active cycles when the ratio of the true k_{eff} standard deviation to k_{eff} is 0.0025 at the problem end.

In MCNP the definition of k_{eff} is:

$$k_{eff} = \frac{\text{fission neutrons in generation } i+1}{\text{fission neutrons in generation } i}$$

$$= \frac{\rho_a \int_V \int_0^\infty \int_E \int_\Omega v \sigma_f \Phi dV dt dE d\Omega}{\int_V \int_0^\infty \int_E \int_\Omega \nabla \cdot J dV dt dE d\Omega + \rho_a \int_V \int_0^\infty \int_E \int_\Omega (\sigma_c + \sigma_f + \sigma_m) \Phi dV dt dE d\Omega},$$

where the phase-space variables are t , E , and Ω for time, energy, direction, and implicitly r for position with incremental volume dV around r . The denominator is the loss rate, which is the sum of leakage, capture (n,0n), fission, and multiplicity (n,xn) terms. By particle balance, the loss rate is also the source rate, which is unity in a criticality calculation. If the number of fission neutrons produced in one generation is equal to the number in the previous generation, then the system is critical. If it is greater, the system is supercritical. If it is less, then the system is subcritical. The multiplicity term is:

$$\begin{aligned} & \rho_a \int_V \int_0^\infty \int_E \int_\Omega \sigma_m \Phi (dV dt) dE d\Omega \\ &= \rho_a \int_V \int_0^\infty \int_E \int_\Omega \sigma_{n,2n} \Phi dV dt dE d\Omega - 2\rho_a \int_V \int_0^\infty \int_E \int_\Omega \sigma_{n,2n} \Phi dV dt dE d\Omega \\ &+ \rho_a \int_V \int_0^\infty \int_E \int_\Omega \sigma_{n,3n} \Phi dV dt dE d\Omega - 3\rho_a \int_V \int_0^\infty \int_E \int_\Omega \sigma_{n,3n} \Phi dV dt dE d\Omega + \dots \end{aligned}$$

The above definition of k_{eff} comes directly from the time-integrated Boltzmann transport equation (without external sources):

$$\begin{aligned} & \int_V \int_0^\infty \int_E \int_\Omega \nabla \cdot J dV dt dE d\Omega + \rho_a \int_V \int_0^\infty \int_E \int_\Omega \sigma_T \Phi dV dt dE d\Omega \\ &= \frac{1}{k_{eff}} \rho_a \int_V \int_0^\infty \int_E \int_\Omega v \sigma_f \Phi dV dt dE d\Omega + \rho_a \int_V \int_0^\infty \int_E \int_\Omega \int_{E'} \sigma_s \Phi' dE' dV dt dE d\Omega \end{aligned}$$

which may be rewritten to look more like the definition of k_{eff} as:

$$\begin{aligned} & \int_V \int_0^\infty \int_E \int_\Omega \nabla \cdot J dV dt dE d\Omega \\ &+ \rho_a \int_V \int_0^\infty \int_E \int_\Omega (\sigma_c + \sigma_f + \sigma_{n,2n} + \sigma_{n,3n} + \dots) \Phi dV dt dE d\Omega \\ &= \frac{1}{k_{eff}} \rho_a \int_V \int_0^\infty \int_E \int_\Omega v \sigma_f \Phi dV dt dE d\Omega \\ &+ \rho_a \int_V \int_0^\infty \int_E \int_\Omega (2\sigma_{n,2n} + 3\sigma_{n,3n} + \dots) \Phi dV dt dE d\Omega \end{aligned}$$

The loss rate is on the left and the production rate is on the right.

The neutron prompt removal lifetime is the average time from the emission of a prompt neutron in fission to the removal of the neutron by some physical process such as escape, capture, or fission. Also, even with the TOTNU card to produce delayed neutrons as well as prompt neutrons (KCODE default), the neutrons are all born at time zero, so the removal lifetimes calculated in MCNP are prompt removal lifetimes, even if there are delayed neutrons.

The definition of the prompt removal lifetime¹⁴⁷ is

$$\tau_r = \frac{\int_V \int_0^\infty \int_E \int_\Omega \eta dV dt dE d\Omega}{\int_V \int_0^\infty \int_E \int_\Omega \nabla \cdot J dV dt dE d\Omega + \rho_a \int_V \int_0^\infty \int_E \int_\Omega (\sigma_c + \sigma_f + \sigma_m) \Phi dV dt dE d\Omega} ,$$

where η is the population per unit volume per unit energy per unit solid angle. In a multiplying system in which the population is increasing or decreasing on an asymptotic period, the population changes in accordance with

$$\eta = \eta_0 e^{(k_{eff}-1)t/\tau_r^+} ,$$

where τ_r^+ is the adjoint-weighted removal lifetime. MCNP calculates the nonadjoint-weighted prompt removal lifetime τ_r that can be significantly different in a multiplying system. In a nonmultiplying system, $k_{eff} = 0$ and $\tau_r \rightarrow \tau_r^+$, the population decays as

$$\eta = \eta_0 e^{-t/\tau_r} ,$$

where the nonadjoint-weighted removal lifetime τ_r is also the relaxation time.

Noting that the flux is defined as

$$\Phi = \eta v ,$$

where v is the speed, the MCNP nonadjoint-weighted prompt removal lifetime τ_r is defined as

$$\tau_r = \frac{\int_V \int_0^\infty \int_E \int_\Omega \frac{\Phi}{v} dV dt dE d\Omega}{\int_V \int_0^\infty \int_E \int_\Omega \nabla \cdot J dV dt dE d\Omega + \rho_a \int_V \int_0^\infty \int_E \int_\Omega (\sigma_c + \sigma_f + \sigma_m) \Phi dV dt dE d\Omega} .$$

The prompt removal lifetime is a fundamental quantity in the nuclear engineering point kinetics equation. It is also useful in nuclear well-logging calculations and other pulsed source problems because it gives the population time-decay constant.

1. Collision Estimators

The collision estimate for k_{eff} for any active cycle is:

$$k_{eff}^C = \frac{1}{N} \sum_i W_i \left[\frac{\sum_k f_k \bar{v}_k \sigma_{f_k}}{\sum_k f_k \sigma_{T_k}} \right] ,$$

where i is summed over all collisions in a cycle where fission is possible;
 k is summed over all nuclides of the material involved in the i^{th} collision;
 σ_{T_k} = total microscopic cross section;
 σ_{f_k} = microscopic fission cross section;
 \bar{v}_k = average number of prompt or total neutrons produced per fission by the collision nuclide at the incident energy;
 f_k = atomic fraction for nuclide k ;
 N = nominal source size for cycle; and
 W_i = weight of particle entering collision.

Because W_i represents the number of neutrons entering the i^{th} collision,

$$W_i \left[\frac{\sum_k f_k \bar{v}_k \sigma_{f_k}}{\sum_k f_k \sigma_{T_k}} \right]$$

is the expected number of neutrons to be produced from all fission processes in the collision. Thus k_{eff}^C is the mean number of fission neutrons produced per cycle. The collision estimator tends to be best, sometimes only marginally so, in very large systems.

The collision estimate of the prompt removal lifetime for any active cycle is the average time required for a fission source neutron to be removed from the system by either escape, capture (n,0n), or fission.

$$\tau_r^C = \frac{\sum W_e T_e + \sum (W_c + W_f) T_x}{\sum W_e + \sum (W_c + W_f)} ,$$

where T_e and T_x are the times from the birth of the neutron until escape or collision. W_e is the weight lost at each escape. $W_c + W_f$ is the weight lost to (n,0n) and fission at each collision,

$$W_c + W_f = W_i \frac{\sum_k f_k (\sigma_{c_k} + \sigma_{f_k})}{\sum_k f_k \sigma_{T_k}} ,$$

where σ_{c_k} is the microscopic capture (n,0n) cross section, and W_i is the weight entering the collision.

2. Absorption Estimators

The absorption estimator for k_{eff} for any active cycle is made when a neutron interacts with a fissionable nuclide. The estimator differs for analog and implicit absorption. For analog absorption,

$$k_{eff}^A = \frac{1}{N} \sum_i W_i \bar{v}_k \frac{\sigma_{f_k}}{\sigma_{c_k} + \sigma_{f_k}} ,$$

where i is summed over each analog absorption event in the k^{th} nuclide. Note that in analog absorption, the weight is the same both before and after the collision. Because analog absorption includes fission in criticality calculations, the frequency of analog absorption at each collision with nuclide k is $(\sigma_{c_k} + \sigma_{f_k})/\sigma_{T_k}$. The analog absorption k_{eff} estimate is very similar to the collision estimator of k_{eff} except that only the k^{th} absorbing nuclide, as sampled in the collision, is used rather than averaging over all nuclides.

For implicit absorption, the following is accumulated:

$$k_{eff}^A = \frac{1}{N} \sum_i W_i' \bar{v}_k \frac{\sigma_{f_k}}{\sigma_{c_k} + \sigma_{f_k}} ,$$

where i is summed over all collisions in which fission is possible and $W_i' = W_i(\sigma_{c_k} + \sigma_{f_k})/\sigma_{T_k}$ is the weight absorbed in the implicit absorption. The difference between the implicit absorption estimator k_{eff}^A and the collision estimator k_{eff}^C is that only the nuclide involved in the collision is used for the absorption k_{eff} estimate rather than an average of all nuclides in the material for the collision k_{eff} estimator.

The absorption estimator with analog absorption is likely to produce the smallest statistical uncertainty of the three estimators for systems where the ratio $\bar{v}_k \sigma_{f_k}/(\sigma_{c_k} + \sigma_{f_k})$ is nearly constant. Such would be the case for a thermal system with a dominant fissile nuclide such that the $1/\text{velocity}$ cross-section variation would tend to cancel.

The absorption estimate differs from the collision estimate in that the collision estimate is based upon the expected value at each collision, whereas the absorption estimate is based upon the events actually sampled at a collision. Thus all collisions will contribute to the collision estimate of k_{eff}^C and τ_r^C by the probability of fission (or capture for τ_r^C) in the material. Contributions to the absorption estimator will only occur if an actual fission (or capture for τ_r^A) event occurs for the sampled nuclide in the case of analog absorption. For implicit absorption, the contribution to the absorption estimate will only be made for the nuclide sampled.

The absorption estimate of the prompt removal lifetime for any active cycle is again the average time required for a fission source neutron to be removed from the system by either escape, capture (n,0n), or fission.

For implicit absorption,

$$\tau_r^A = \frac{\sum W_e T_e + \sum (W_c + W_f) T_x}{\sum W_e + \sum W_c + \sum W_f} ,$$

where

$$W_c + W_f = \frac{W_i(\sigma_{ck} + \sigma_{fk})}{\sigma_{T_k}} .$$

For analog absorption,

$$\tau_r^A = \frac{\sum W_e T_e + \sum W_c T_c + \sum W_f T_f}{\sum W_e + \sum W_c + \sum W_f} ,$$

where T_e , T_c , T_f , and T_x are the times from the birth of the neutron until escape, capture (n,0n), fission, or collision. W_e is the weight lost at each escape. W_c and W_f are the weights lost to capture (n,0n) and fission at each capture (n,0n) or fission event with the nuclide sampled for the collision.

3. Track Length Estimators

The track length estimator of k_{eff} is accumulated every time the neutron traverses a distance d in a fissionable material cell:

$$k_{eff}^{TL} = \frac{1}{N} \sum_i W_i \rho d \sum_k f_k \bar{v}_k \sigma_{f_k} ,$$

where i is summed over all neutron trajectories,
 ρ is the atomic density in the cell, and
 d is the trajectory track length from the last event.

Because $\rho d \sum_k f_k \bar{v}_k \sigma_{f_k}$ is the expected number of fission neutrons produced along trajectory d , k_{eff}^{TL} is a third estimate of the mean number of fission neutrons produced in a cycle per nominal fission source neutron.

The track length estimator tends to display the lowest variance for optically thin fuel cells (for example, plates) and fast systems where large cross-section variations because of resonances may cause high variances in the other two estimators.

The track length estimator for the prompt removal lifetime for each cycle is accumulated every time the neutron traverses a distance d in any material in any cell:

$$\tau_r^{TL} = \frac{\sum_i W_i d/v}{W_s} ,$$

where W_s is the source weight summed over all histories in the cycle and v is the velocity. Note that d/v is the time span of the track. Note further that:

$$\sum_i W_i d/v = \int_V \int_0^\infty \int_E \int_\Omega \frac{\Phi}{v} dV dt dE d\Omega ,$$

and in criticality problems:

$$\begin{aligned} W_s &= \frac{1}{k_{eff}} \rho_a \int_V \int_0^\infty \int_E \int_\Omega v \sigma_f \Phi dV dt dE d\Omega \\ &= \int_V \int_0^\infty \int_E \int_\Omega \nabla \cdot J dV dt dE d\Omega + \rho_a \int_V \int_0^\infty \int_E \int_\Omega (\sigma_c + \sigma_f + \sigma_m) \Phi dV dt dE d\Omega \end{aligned}$$

These relationships show how τ_r^{TL} is related to the definition of τ_r on page 2–169.

4. Other Lifetime Estimators

In addition to the collision, absorption, and track length estimators of the prompt removal lifetime τ_r , MCNP provides the escape, capture (n,0n), and fission prompt lifespans and lifetimes for all KCODE problems having a sufficient number of settle cycles. Further, the “average time of” printed in the problem summary table is related to the lifespans, and track-length estimates of many lifetimes can be computed using the $1/v$ tally multiplier option on the FM card for track-length tallies.

In KCODE problems, MCNP calculates the lifespan of escape l_e , capture (n,0n) l_c , fission l_f , and removal l_r :

$$l_e = \frac{\sum W_e T_e}{\sum W_e} ,$$

$$l_c = \frac{\sum W_c T_c}{\sum W_c} ,$$

$$l_f = \frac{\sum W_f T_f}{\sum W_f} , \quad \text{and}$$

$$l_r = \frac{\sum W_e T_e + \sum W_c T_c + \sum W_f T_f}{\sum W_e + \sum W_c + \sum W_f} .$$

These sums are taken over all the active histories in the calculation. (If $KC8 = 0$ on the KCODE card, then the sums are over both active and inactive cycle histories, but $KC8 = 1$, the default, is assumed for the remainder of this discussion.) The capture (n,0n) and fission contributions are accumulated at each collision with a nuclide, so these are absorption estimates. Thus,

$$l_r \approx \tau_r^A .$$

The difference is that τ_r^A is the average of the τ_r^A for each cycle and l_r is the average over all histories. $l_r = \tau_r^A$ if there is precisely one active cycle, but then neither τ_r^A nor l_r is printed out because there are too few cycles. The cycle average τ_r^A does not precisely equal the history average l_r because they are ratios.

l_e and l_c are the “average time to” escape and capture (n,0n) that is printed in the problem summary table for all neutron and photon problems.

$\frac{1}{N}\Sigma W_e$, $\frac{1}{N}\Sigma W_c$, and $\frac{1}{N}\Sigma W_f$ are the weight lost to escape, capture (n,0n), and fission in the problem summary table.

The “fractions” F_x printed out below the lifespan in the KCODE summary table are, for $x = e, c, f$, or r ,

$$F_x = \frac{W_x}{\Sigma W_e + \Sigma W_c + \Sigma W_f} .$$

The prompt lifetimes¹⁴⁷ for the various reactions τ_x are then

$$\tau_x = \frac{\tau_r}{F_x} = \frac{\int_V \int_0^\infty \frac{\Phi}{v} dV dt}{\rho_a \int_V \int_0^\infty \sigma_x \Phi dV dt} .$$

Both τ_r^A and the covariance-weighted combined estimator $\tau_r^{(C/A/T)}$ are used. Note again that the slight differences between similar quantities are because l_x and F_x are averaged over all active histories whereas τ_r^A and $\tau_r^{(C/A/T)}$ are averaged within each active cycle, and then the final values are the averages of the cycle values, i.e., history–averages vs. batch–averages.

The prompt removal lifetime can also be calculated using the F4 track-length tally with the $1/v$ multiplier option on the FM card and using the volume divided by the average source weight W_s as the multiplicative constant. The standard track length tally is then converted from

$$F4 = \int \Phi dt \quad \text{to}$$

$$F4 = \frac{V}{W_s} \int \frac{\Phi}{v} dt .$$

Remember to multiply by volume, either by setting the FM card constant to the volume or overriding the F4 volume divide by using segment divisors of unity on the SD card. W_s should be unity for KCODE calculations. The only difference between τ_r^{TL} and the modified F4 tally will be

any variations from unity in W_s and the error estimation, which will be batch-averaged for τ_r^{TL} and history-averaged for the F4 tally.

Lifetimes for all other processes also can be estimated by using the FM multiplier to calculate reaction rates as well (the numerator and denominator are separate tallies that must be divided by the user — see the examples in Chapters 4 and 5):

$$\tau_x^{TL} = \frac{(1/v \text{ multiplier})}{\text{reaction rate multiplier}} = \frac{\int_V \int_0^\infty \frac{\Phi}{v} dV dt}{\rho_a \int_V \int_0^\infty \sigma_x \Phi dV dt} .$$

Note that the lifetimes are inversely additive:

$$\frac{1}{\tau_r} = \frac{1}{\tau_e} + \frac{1}{\tau_c} + \frac{1}{\tau_f} .$$

5. Combined k_{eff} and τ_r Estimators

MCNP provides a number of combined k_{eff} and τ_r estimators that are combinations of the three individual k_{eff} and τ_r estimators using two at a time or all three. The combined k_{eff} and τ_r values are computed by using a maximum likelihood estimate, as outlined by Halperin¹⁴⁸ and discussed further by Urbatsch.¹⁴⁰ This technique, which is a generalization of the inverse variance weighting for uncorrelated estimators, produces the maximum likelihood estimate for the combined average k_{eff} and τ_r , which, for multivariate normality, is the almost–minimum variance estimate. It is “almost” because the covariance matrix is not known exactly and must be estimated. The three-combined k_{eff} and τ_r estimators are the best final estimates from an MCNP calculation.¹⁴⁰

This method of combining estimators can exhibit one feature that is disconcerting: sometimes (usually with highly positively correlated estimators) the combined estimate will lie outside the interval defined by the two or three individual average estimates. Statisticians at Los Alamos have shown¹⁴⁰ that this is the best estimate to use for a final k_{eff} and τ_r value. Reference 140 shows the results of one study of 500 samples from three highly positively correlated normal distributions, all with a mean of zero. In 319 samples, all three estimators fell on the same side of the expected value. This type of behavior occurs with high positive correlation because if one estimator is above or below the expected value, the others have a good probability of being on the same side of the expected value. The advantage of the three-combined estimator is that the Halperin algorithm correctly predicts that the true value will lie outside of the range.

6. Error Estimation and Estimator Combination

After the first I_c inactive cycles, during which the fission source spatial distribution is allowed to come into spatial equilibrium, MCNP begins to accumulate the estimates of k_{eff} and τ_r with those estimates from previous active (after the inactive) cycles. The relative error R of each quantity is estimated in the usual way as

$$R = \frac{1}{\bar{x}} \sqrt{\frac{x^2 - \bar{x}^2}{M-1}}$$

where M = the number of active cycles,

$$\bar{x} = \frac{1}{M} \sum_m x_m, \text{ and } \overline{x^2} = \frac{1}{M} \sum_m x_m^2, \quad ,$$

where x_m = a quantity, such as k_{eff}^C , from cycle m . This assumes that the cycle-to-cycle estimates of each k_{eff} are uncorrelated. This assumption generally is good for k_{eff} , but not for the eigenfunction (fluxes) of optically large systems.¹⁴⁹

MCNP also combines the three estimators in all possible ways and determines the covariance and correlations. The simple average of two estimators is defined as $x^{ij} = (1/2)(x^i + x^j)$, where, for example, x^i may be the collision estimator k_{eff}^C and x^j may be the absorption estimator k_{eff}^A .

The “combined average” of two estimators is weighted by the covariances as

$$x^{ij} = x^i - \frac{(x^i - x^j)(C_{ii} - C_{ij})}{(C_{ii} + C_{jj} - 2C_{ij})} = \frac{(C_{jj} - C_{ij})x^i + (C_{ii} - C_{ij})x^j}{(C_{ii} + C_{jj} - 2C_{ij})},$$

where the covariance C_{ij} is

$$C_{ij} = \frac{1}{m} \sum_m x_m^i x_m^j - \left(\frac{1}{M} \sum_m x_m^i \right) \left(\frac{1}{M} \sum_m x_m^j \right).$$

Note that $C_{ii} = \overline{x^2} - \bar{x}^2$ for estimator i .

The “correlation” between two estimators is a function of their covariances and is given by

$$\text{correlation} = \frac{C_{ij}}{\sqrt{|C_{ii}C_{jj}|}}.$$

The correlation will be between unity (perfect positive correlation) and minus one (perfect anti or negative correlation). If the correlation is one, no new information has been gained by the second estimator. If the correlation is zero, the two estimators appear statistically independent and the combined estimated standard deviation should be significantly less than either. If the correlation is negative one, even more information is available because the second estimator will tend to be low, relative to the expected value, when the first estimator is high and vice versa. Even larger improvements in the combined standard deviation should occur.

The combined average estimator (k_{eff} or τ_r) and the estimated standard deviation of all three estimators are based on the method of Halperin¹⁴⁸ and is much more complicated than the two-combination case. The improvements to the standard deviation of the three-combined estimator

will depend on the magnitude and sign of the correlations as discussed above. The details and analysis of this method are given in Ref. 140.

For many problems, all three estimators are positively correlated. The correlation will depend on what variance reduction (for example, implicit or analog capture) is used. Occasionally, the absorption estimator may be only weakly correlated with either the collision or track length estimator. It is possible for the absorption estimator to be significantly anticorrelated with the other two estimators for some fast reactor compositions and large thermal systems. Except in the most heterogeneous systems, the collision and track length estimators are likely to be strongly positively correlated.

There may be a negative bias¹⁴⁶ in the estimated standard deviation of k_{eff} for systems where the locations of fission sites in one generation are correlated with the locations of fission sites in successive generations. The statistical methods used in MCNP for estimating standard deviations in k_{eff} calculations do not account for the effects of intergenerational correlation, leading to underprediction of standard deviations. These systems are typically large with small neutron leakage. The magnitude of this effect can be estimated by batching the cycle k_{eff} values in batch sizes much greater than one cycle,¹⁴⁶ which MCNP provides automatically. For problems where there is a reason to suspect the results, a more accurate calculation of this effect can be done by making several independent calculations of the same problem (using different random number sequences) and observing the variance of the population of independent k_{eff} values. The larger the number of independent calculations that can be made, the better the distribution of k_{eff} values can be assessed.

7. Creating and Interpreting k_{eff} Confidence Intervals

The result of a Monte Carlo criticality calculation (or any other type of Monte Carlo calculation) is a confidence interval. For criticality, this means that the result is not just k_{eff} , but k_{eff} plus and minus some number of estimated standard deviations to form a confidence interval (based on the Central Limit Theorem) in which the true answer is expected to lie a certain fraction of the time. The number of standard deviations used (for example, from a Student's t Table) determines the fraction of the time that the confidence interval will include the true answer, for a selected confidence level. For example, a valid 99% confidence interval should include the true result 99% of the time. There is always some probability (in this example, 1%) that the true result will lie outside of the confidence interval. To reduce this probability to an acceptable level, either the confidence interval must be increased according to the desired Student's t percentile, or more histories need to be run to get a smaller estimated standard deviation.

MCNP uses three different estimators for k_{eff} . The advantages of each estimator vary with the problem: no one estimator will be the best for all problems. All estimators and their estimated standard deviations are valid under the assumption that they are unbiased and consistent, therefore representative of the true parameters of the population. This statement has been validated empirically¹⁴⁰ for all MCNP estimators for small dominance ratios. The batched k_{eff} results table should be used to estimate if the calculated batch-size-of-one k_{eff} standard deviation appears to be adequate.

The confidence interval based on the three-statistically-combined k_{eff} estimator is the recommended result to use for all final k_{eff} confidence interval quotations because all of the available information has been used in the final result. This estimator often has a lower estimated standard deviation than any of the three individual estimators and therefore provides the smallest valid confidence interval as well. The final estimated k_{eff} value, estimated standard deviation, and the estimated 68%, 95%, and 99% confidence intervals (using the correct number of degrees of freedom) are presented in the box on the k_{eff} results summary page of the output. If other confidence intervals are wanted, they can be formed from the estimated standard deviation of k_{eff} . At least 30 active cycles need to be run for the final k_{eff} results box to appear. Thirty cycles are required so that there are enough degrees of freedom to form confidence intervals using the well-known estimated standard deviation multipliers. (When constructing a confidence interval using any single k_{eff} estimator, its standard deviation, and a Student's t Table, there are $I_t - I_c - 1$ degrees of freedom. For the two- and three-combined k_{eff} estimators, there are $I_t - I_c - 2$ and $I_t - I_c - 3$ degrees of freedom, respectively.)

All of the k_{eff} estimators and combinations by two or three are provided in MCNP so that the user can make an alternate choice of confidence interval if desired. Based on statistical studies, using the individual k_{eff} estimator with the smallest estimated standard deviation is not recommended. Its use can lead to confidence intervals that do not include the true result the correct fraction of the time.¹⁴⁰ The studies have shown that the standard deviation of the three-combined k_{eff} estimator provides the correct coverage rates, assuming that the estimated standard deviations in the individual k_{eff} estimators are accurate. This accuracy can be verified by checking the batched k_{eff} results table. When significant anti-correlations occur among the estimators, the resultant much smaller estimated standard deviation of the three-combined average has been verified¹⁴⁰ by analyzing a number of independent criticality calculations.

8. Analysis to Assess the Validity of a Criticality Calculation

The two most important requirements for producing a valid criticality calculation for a specified geometry are sampling all of the fissionable material well and ensuring that the fundamental spatial mode was achieved before and maintained during the active k_{eff} cycles. MCNP has checks to assess the fulfillment of both of these conditions.

MCNP verifies that at least one fission source point was generated in each cell containing fissionable material. A WARNING message is printed on the k_{eff} results summary page that includes a list of cells that did not have any particles entering, and/or no collisions, and/or no fission source points. For repeated structure geometries, a source point in any one cell that is repeated will satisfy this test. For example, assume a problem with a cylinder and a cube that are both filled with the same universe, namely a sphere of uranium and the space outside the sphere. If a source point is placed in the sphere inside the cylinder but not in the sphere inside the cube, the test will be satisfied.

One basic assumption that is made for a good criticality calculation is that the normal spatial mode for the fission source has been achieved after I_c cycles were skipped. MCNP attempts to assess this condition in several ways. The estimated combined k_{eff} and its estimated standard deviation for the first and second active cycle halves of the problem are compared. A WARNING message is issued if either the difference of the two values of combined col/abs/track-length k_{eff} does not appear to

be zero or the ratio of the larger-to-the-smaller estimated standard deviations of the two col/abs/track-length k_{eff} is larger than expected. Failure of either or both checks implies that the two active halves of the problem do not appear to be the same and the output from the calculation should be inspected carefully.

MCNP checks to determine which number of cycles skipped produces the minimum estimated standard deviation for the combined k_{eff} estimator. If this number is larger than I_c , it may indicate that not enough inactive cycles were skipped. The table of combined k_{eff} -by-number-of-cycles skipped should be examined to determine if enough inactive cycles were skipped.

It is assumed that N is large enough so that the collection of active cycle k_{eff} estimates for each estimator will be normally distributed if the fundamental spatial mode has been achieved in I_c cycles and maintained for the rest of the calculation. To test this assumption, MCNP performs normality checks^{150,151} on each of the three k_{eff} estimator cycle data at the 95% and 99% confidence levels. A WARNING message is issued if an individual k_{eff} data set does not appear to be normally distributed at the 99% confidence level. This condition will happen to good data about 1% of the time. Unless there is a high positive correlation among the three estimators, it is expected to be rare that all three k_{eff} estimators will not appear normally distributed at the 99% confidence level when the normal spatial mode has been achieved and maintained. When the condition that all three sets of k_{eff} estimators do not appear to be normal at the 99% confidence level occurs, the box with the final k_{eff} will not be printed. The final confidence interval results are available elsewhere in the output. Examine the calculation carefully to see if the normal mode was achieved before the active cycles began. The normality checks are also made for the batched- k_{eff} and k_{eff} -by- cycles-skipped tables so that normality behavior can be studied by batch size and I_c .

These normality checks test the assumption that the individual cycle k_{eff} values behave in the assumed way. Even if the underlying individual cycle k_{eff} values are not normally distributed, the three average k_{eff} values and the combined k_{eff} estimator will be normally distributed if the conditions required by the Central Limit Theorem are met for the average. If required, this assumption can be tested by making several independent calculations to verify empirically that the population of the average k_{eff} values appears to be normally distributed with the same population variance as estimated by MCNP.

MCNP tests for a monotonic trend of the three-combined k_{eff} estimator over the last ten active cycles. This type of behavior is not expected in a well converged solution for k_{eff} and could indicate a problem with achieving or maintaining the normal spatial mode. A WARNING message is printed if such a monotonic trend is observed.

To assist users in assessing the convergence of the fission source spatial distribution, MCNP computes a quantity called the Shannon entropy of the fission source distribution, H_{src} .^{144,145} The Shannon entropy is a well-known concept from information theory and provides a single number for each cycle to help characterize convergence of the fission source distribution. It has been found that the Shannon entropy converges to a single steady-state value as the source distribution approaches stationarity. Line plots of Shannon entropy vs. cycle are easier to interpret and assess than are 2-D or 3-D plots of the source distribution vs. cycle.

To compute H_{src} , it is necessary to superimpose a 3-D grid on a problem encompassing all of the fissionable regions, and then to tally the number of fission sites in a cycle that fall into each of the grid boxes. These tallies may then be used to form a discretized estimate of the source distribution, $\{P_J, J=1, N_s\}$, where N_s is the number of grid boxes in the superimposed mesh, and $P_J = (\text{number of source sites in } J^{\text{th}} \text{ grid box}) / (\text{total number of source sites})$. Then, the Shannon entropy of the discretized source distribution for that cycle is given by

$$H_{src} = - \sum_{J=1}^{N_s} P_J \cdot \ln_2(P_J) .$$

H_{src} varies between 0 for a point distribution to $\ln_2(N_s)$ for a uniform distribution. Also note that as P_J approaches 0, $P_J \ln_2(P_J)$ approaches 0. MCNP prints H_{src} for each cycle of a KCODE calculation. Plots of H_{src} vs. cycle can also be obtained during or after a calculation, using the z option and requesting plots for "kcode 6." The user may specify a particular grid to use in determining H_{src} by means of the HSRC input card. If the HSRC card is provided, users should specify a small number of grid boxes (e.g., 5-10 in each of the XYZ directions), chosen according to the symmetry of the problem and layout of the fuel regions. If the HSRC card is not provided, MCNP will automatically determine a grid that encloses all of the fission sites for the cycle. The number of grid boxes will be determined by dividing the number of histories per cycle by 20, and then finding the nearest integer for each direction that will produce this number of equal-sized grid boxes, although not fewer than 4x4x4 will be used.

Upon completion of the problem, MCNP will compute the average value of H_{src} for the last half of the active cycles, as well as its (population) standard deviation. MCNP will then report the first cycle found (active or inactive) where H_{src} falls within one standard deviation of its average for the last half of the cycles, along with a recommendation that at least that many cycles should be inactive. Plots of H_{src} vs. cycle should be examined to further verify that the number of inactive cycles is adequate for fission source convergence.

When running criticality calculations with MCNP, it is essential that users examine the convergence of both k_{eff} and the fission source distribution (using Shannon entropy). If either k_{eff} or the fission source distribution is not converged prior to starting the active cycles, then results from the calculations will not be correct.

9. Normalization of Standard Tallies in a Criticality Calculation

Track length fluxes, surface currents, surface fluxes, heating and detectors—all the standard MCNP tallies—can be made during a criticality calculation. The tallies are for one fission neutron generation. Biases may exist in these criticality results, but appear to be smaller than statistical uncertainties.¹⁴⁶ These tallied quantities are accumulated only after the I_c inactive cycles are finished. The tally normalization is per active source weight w , where $w = N * (I_t - I_c)$, and N is the nominal source size (from the KCODE card); I_t is the total number of cycles in the problem; and I_c is the number of inactive cycles (from KCODE card). The number w is appropriately adjusted if the last cycle is only partially completed. If the tally normalization flag (on the KCODE card) is turned on, the tally normalization is the actual number of starting particles during the active cycles rather than the nominal weight above. Bear in mind, however, that the source particle weights are

all set to $W = N/M$ so that the source normalization is based upon the nominal source size N for each cycle.

An MCNP tally in a criticality calculation is for one fission neutron being born in the system at the start of a cycle. The tally results must be scaled either by the total number of neutrons in a burst or by the neutron birth rate to produce, respectively, either the total result or the result per unit time of the source. The scaling factor is entered on the Fm card.

The statistical errors that are calculated for the tallies assume that all the neutron histories are independent. They are not independent because of the cycle-to-cycle correlations that become more significant for large or loosely-coupled systems. For some very large systems, the estimated standard deviation for a tally that involves only a portion of the problem has been observed to be underestimated by a factor of five or more (see Ref. 149 pages 42–44). This value also is a function of the size of the tally region. In the Ref. 149 slab reactor example, the entire problem (that is, k_{eff}) standard deviation was not underestimated at all. An MCNP study¹⁵² of the FFTF fast reactor indicates that 90% coverage rates for flux tallies are good, but that 2 out of 300 tallies were beyond four estimated standard deviations. Independent runs can be made to study the real eigenfunction distribution (that is, tallies) and the estimated standard deviations for difficult criticality calculations. This method is the only way to determine accurately these confidence intervals for large or loosely-coupled problems where intergeneration correlation is significant.

10. Neutron Tallies and the MCNP Net Multiplication Factor

The MCNP net multiplication factor M printed out on the problem summary page differs from the k_{eff} from the criticality code. We will examine a simple model to illustrate the approximate relationship between these quantities and compare the tallies between standard and criticality calculations.

Assume we run a standard MCNP calculation using a fixed neutron source distribution identical in space and energy to the source distribution obtained from the solution of an eigenvalue problem with $k_{eff} < 1$. Each generation will have the same space and energy distribution as the source. The contribution to an estimate of any quantity from one generation is reduced by a factor of k_{eff} from the contribution in the preceding generation. The estimate E_k of a tally quantity obtained in a criticality eigenvalue calculation is the contribution for one generation produced by a unit source of fission neutrons. An estimate for a standard MCNP fixed source calculation, E_s , is the sum of contributions for all generations starting from a unit source.

$$E_s = E_k + k_{eff}E_k + k_{eff}^2E_k + k_{eff}^3E_k + \dots = E_k / (1 - k_{eff}) \quad . \quad (2.29)$$

Note that $1/(1 - k_{eff})$ is the true system multiplication, often called the subcritical multiplication factor. The above result depends on our assumptions about the unit fission source used in the standard MCNP run. Usually, E_s will vary considerably from the above result, depending on the difference between the fixed source and the eigenmode source generated in the eigenvalue problem. E_s will be a fairly good estimate if the fixed source is a distributed source roughly approximating the eigenmode source. Tallies from a criticality calculation are appropriate only for a critical system and the tally results can be scaled to a desired fission neutron source (power) level or total neutron pulse strength.

In a fixed source MCNP problem, the net multiplication M is defined to be unity plus the gain G_f in neutrons from fission plus the gain G_x from nonfission multiplicative reactions. Using neutron weight balance (creation equals loss),

$$M = 1 + G_f + G_x = W_e + W_c \quad , \quad (2.30)$$

where W_e is the weight of neutrons escaped per source neutron and W_c is the weight of neutrons captured per source neutron. In a criticality calculation, fission is treated as an absorptive process; the corresponding relationship for the net multiplication is then

$$M^o = 1 + G_x^o = W_e^o + W_c^o + W_f^o \quad , \quad (2.31)$$

where the superscript o designates results from the criticality calculation and W_f^o is the weight of neutrons causing fission per source neutron. Because k_{eff} is the number of fission neutrons produced in a generation per source neutron, we can also write

$$k_{eff} = \bar{\nu} W_f^o \quad , \quad (2.32)$$

where $\bar{\nu}$ is the average number of neutrons emitted per fission for the entire problem. Making the same assumptions as above for the fixed source used in the standard MCNP calculation and using equations (2.26), (2.27), and (2.28), we obtain

$$M = W_e + W_c = \frac{W_e^o + W_c^o}{1 - k_{eff}} = \frac{M^o - W_f^o}{1 - k_{eff}}$$

or, by using (2.28) and (2.29),

$$M = \frac{M^o - \frac{k_{eff}}{\bar{\nu}}}{1 - k_{eff}} = \frac{1 - \frac{k_{eff}}{\bar{\nu}} + G_x^o}{1 - k_{eff}} \quad .$$

Often, the nonfission multiplicative reactions $G_x^o \ll 1$. This implies that k_{eff} can be **approximated** by k_{eff}^{FS} (from an appropriate **Fixed Source** calculation)

$$k_{eff} \approx k_{eff}^{FS} = \frac{M - 1}{M - \frac{1}{\bar{\nu}}} \quad , \quad (2.33)$$

when the two fission neutron source distributions are nearly the same. The average value of $\bar{\nu}$ in a problem can be calculated by dividing the fission neutrons gained by the fission neutrons lost as given in the totals of the neutron weight balance for physical events. Note, however, that the above estimate is subject to the same limitations as described in Eq. 2.26.

C. *Recommendations for Making a Good Criticality Calculation*

1. Problem Set-Up

As with any calculation, the geometry must be adequately and correctly specified to represent the true physical situation. Plot the geometry and check cells, materials, and masses for correctness. Specify the appropriate nuclear data, including $S(\alpha, \beta)$ thermal data, at the correct material temperatures. Do as good a job as possible to put initial fission source points in every cell with fissionable material. Try running short problems with both analog and implicit capture (see the PHYS:N card) to improve the figure of merit for the combined k_{eff} and any tallies being made. Follow the tips for good calculations listed at the end of Chapter 1.

2. Number of Neutrons per Cycle and Number of Cycles

Criticality calculations can suffer from two potential problems. The first is the failure to sufficiently converge the spatial distribution of the fission source from its initial guess to a distribution fluctuating around the fundamental eigenmode solution. It is recommended that the user make an initial run with a relatively small number of source particles per generation (perhaps 500 or 1000) and generously allow a large enough number of cycles so that the eigenvalue appears to be fluctuating about a constant value. The user should examine the results and continue the calculation if any trends in the eigenvalue are noticeable. The SRCTP file from the last k_{eff} cycle of the initial run can then be used as the source for the final production run to be made with a larger number of histories per cycle.

This convergence procedure can be extended for very slowly convergent problems—typically large, thermal, low-leakage systems, where a convergence run might be made with 500 or 1000 histories per cycle. Then a second convergence run would be made with 1000 histories per cycle, using the SRCTP file from the first run as an initial fission source guess. If the results from the second run appear satisfactory, then a final run might be made using 5000 or 10000 particles per cycle with the SRCTP file from the second run as an initial fission source guess. In the final run, only a few cycles should need to be skipped. The bottom line is this: skip enough cycles so that the normal spatial mode is achieved.

The second potential problem arises from the fact that the criticality algorithm produces a very small negative bias in the estimated eigenvalue. The bias depends upon $1/N$, where N is the number of source particles per generation. Thus, it is desirable to make N as large as possible. Any value of $N > 500$ should be sufficient to reduce the bias to a small level. The eigenvalue bias Δk_{eff} has been shown¹⁴⁶ to be

$$-\Delta k_{eff} = \frac{(I_t - I_c)}{2k_{eff}} (\sigma_{k_{eff}}^2 - \sigma_{approx}^2) \quad , \quad (2.34)$$

where $\sigma_{k_{eff}}$ is the true standard deviation for the final k_{eff} ,
 σ_{approx} is the approximate standard deviation computed assuming
the individual k_{eff} values are statistically independent, and
 $\sigma_{k_{eff}}^2 > \sigma_{approx}^2$.

The standard deviations are computed at the end of the problem. Because the σ^2 s decrease as $1/(I_t - I_c)$, Δk_{eff} is independent of the number of active cycles. Recall that Δk_{eff} is proportional to $1/N$, the number of neutrons per k_{eff} cycle.

Eqn. (2.31) can be written¹⁴⁶ as the following inequality:

$$\frac{|\Delta k_{eff}|}{\sigma k_{eff}} < \frac{(I_t - I_c) \sigma_{k_{eff}}}{2 k_{eff}} \quad (2.35)$$

This inequality is useful for determining an upper limit to the number of active cycles that should be used for a calculation without having Δk_{eff} dominate $\sigma_{k_{eff}}$. If $\sigma_{k_{eff}}/k_{eff}$ is 0.0010, which is a reasonable value for criticality calculations, and $I_t - I_c$ is 1000, then $|\Delta k_{eff}|/\sigma_{k_{eff}} < 0.5$ and Δk_{eff} will not dominate the k_{eff} confidence interval. If $\sigma_{k_{eff}}$ is reasonably well approximated by MCNP's estimated standard deviation, this ratio will be much less than 0.5.

The total running time for the active cycles is proportional to $N(I_t - I_c)$, and the standard deviation in the estimated eigenvalue is proportional to $1/\sqrt{N(I_t - I_c)}$. From the results of the convergence run, the total number of histories needed to achieve the desired standard deviation can be estimated.

It is recommended that 200 to 1000 active cycles be used. This large number of cycles will provide large batch sizes of k_{eff} cycles (for example, 40 batches of 10 cycles each for 400 active cycles) to compare estimated standard deviations with those obtained for a batch size of one k_{eff} cycle. For example, for 400 active cycles, 40 batches of 10 k_{eff} values are created and analyzed for a new average k_{eff} and a new estimated standard deviation. The behavior of the average k_{eff} by a larger number of cycles can also be observed to ensure a good normal spatial mode. Fewer than 30 active cycles is not recommended because trends in the average k_{eff} may not have enough cycles to develop.

3. Analysis of Criticality Problem Results

The goal of the calculation is to produce a k_{eff} confidence interval that includes the true result the desired fraction of the time. Check all WARNING messages. Understand their significance to the calculation. Study the results of the checks that MCNP makes that were described starting on page 2-178.

The criticality problem output contains a lot of useful information. Study it to make sure that: 1) the problem terminated properly; 2) enough cycles were skipped to ensure that the normal spatial mode for fission sources was achieved; 3) all cells with fissionable material were sampled; 4) the average combined k_{eff} appears to be varying randomly about the average value for the active cycles; 5) the average combined k_{eff} -by-cycles-skipped does not exhibit a trend during the latter stages of the calculation; 6) the confidence intervals for the batched (with at least 30 batch values) combined k_{eff} do not differ significantly from the final result; 7) the impact of having the largest of each of the three k_{eff} estimators occurring on the next cycle is not too great on the final confidence interval; and 8) the combined k_{eff} figure of merit should be stable. The combined k_{eff} figure of merit should be reasonably stable, but not as stable as a tally figure of merit because the number of histories for

each cycle is not exactly the same, and the combined k_{eff} relative error may experience some changes because of changes in the estimated covariance matrix for the three individual estimators.

Plots (using the z option) can be made of the three individual and average k_{eff} estimators by cycle, as well as the three-estimator-combined k_{eff} . Use these plots to better understand the results.

If there is concern about a calculation, the k_{eff} -by-cycles-skipped table presents the results that would be obtained in the final result box for differing numbers of cycles skipped. This information can provide insight into fission source spatial convergence, normality of the k_{eff} data sets, and changes in the 95% and 99% confidence intervals. If concern persists, a problem could be run that tallies the track length estimator k_{eff} using an F4:n tally and an FM card using the -6 and -7 reaction multipliers (see Chapter 4 for an example). In the most drastic cases, several independent calculations can be made and the variance of the k_{eff} values (and any other tallies) could be computed from the individual values.

If a conservative (too large) k_{eff} confidence interval is desired, the results from the largest k_{eff} occurring on the next cycle table can be used. This situation could occur with a maximum probability of $1/(I_t - I_c)$ for highly positively correlated k_{eff} values to $1/(I_t - I_c)^3$ for no correlation.

Finally, keep in mind the discussion starting on page 2-180. For large systems with a dominance ratio close to one, the estimated standard deviations for tallies could be much smaller than the true standard deviation. The cycle-to-cycle correlations in the fission sources are not taken into account, especially for any tallies that are not made over the entire problem. The only way to obtain the correct statistical errors in this situation is to run a series of independent problems using different random number sequences and analyze the sampled tally results to estimate the statistical uncertainties.

IX. VOLUMES AND AREAS

The particle flux in Monte Carlo transport problems often is estimated as the track length per unit volume or the number of particles crossing a surface per unit area. Therefore, knowing the volumes and surface areas¹⁵⁴ of the geometric regions in a Monte Carlo problem is essential. Knowing volumes is useful in calculating the masses and densities of cells and thus in calculating volumetric or mass heating. Furthermore, calculation of the mass of a geometry is frequently a good check on the accuracy of the geometry setup when the mass is known by other means.

Calculating volumes and surface areas in modern Monte Carlo transport codes is nontrivial. MCNP allows the construction of cells from unions and/or intersections of regions defined by an arbitrary combination of second-degree surfaces, toroidal fourth-degree surfaces, or both. These surfaces can have different orientations or be segmented for tallying purposes. The cells they form can even consist of several disjoint subcells. Cells can be constructed from quadrilateral or hexagonal lattices or can be embedded in repeated structures universes. Although such generality greatly increases the flexibility of MCNP, computing cell volumes and surface areas understandably requires increasingly elaborate computational methods.

MCNP automatically calculates volumes and areas of polyhedral cells and of cells or surfaces generated by surfaces of revolution about any axis, even a skew axis. If a tally is segmented, the segment volumes or areas are computed. For nonrotationally symmetric or nonpolyhedral cells, a stochastic volume and surface area method that uses ray tracing is available. See page 2–186.

A. *Rotationally Symmetric Volumes and Areas*

The procedure for computing volumes and surface areas of rotationally symmetric bodies follows:

1. Determine the common axis of symmetry of the cell.¹⁵⁴ If there is none and if the cell is not a polyhedron, MCNP cannot compute the volume (except stochastically) and the area of each bounding surface cannot be computed on the side of the asymmetric cell.
2. Convert the bounding surfaces to q-form:

$$ar^2 + br + cs^2 + ds + e = 0 \quad ,$$

where s is the axis of rotational symmetry in the r - s coordinate system. All MCNP surfaces except tori are quadratic surfaces and therefore can be put into q-form.

3. Determine all intersections of the bounding surfaces with each other in the r - s coordinate system. This procedure generally requires the solution of a quartic equation.²³ For spheres, ellipses, and tori, extra intersection points are added so that these surfaces are not infinite. The list of intersections are put in order of increasing s -coordinate. If no intersection is found, the surface is infinite; its volume and area on one side cannot be computed.
4. Integrate over each bounding surface segment between intersections:

$$V = \pi \int r^2 ds \quad \text{for volumes;}$$

$$A = 2\pi \int r \sqrt{1 + \left(\frac{dr}{ds}\right)^2} ds \quad \text{for surface areas.}$$

A bounding surface segment lies between two intersections that bound the cell of interest.

A numerical integration is required for the area of a toroidal surface; all other integrals are directly solved by integration formulas. The sense of a bounding surface to a cell determines the sign of V . The area of each surface is determined cell-by-cell twice, once for each side of the surface. An area will be calculated unless bounded on both sides by asymmetric or infinite cells.

B. *Polyhedron Volumes and Areas*

A polyhedron is a body bounded only by planes that can have an arbitrary orientation. The procedure for calculating the volumes and surface areas of polyhedra is as follows:

1. For each facet side (planar surface), determine the intersections (r_i, s_i) of the other bounding planes in the r - s coordinate system. The r - s coordinate system is redefined for each facet to be an arbitrary coordinate system in the plane of the facet.
2. Determine the area of the facet:

$$a = \frac{1}{2} \sum (s_{i+1} - s_i)(r_{i+1} + r_i) \quad ,$$

and the coordinates of its centroid, r_c, s_c :

$$r_c = 1/(6a) \sum (s_{i+1} - s_i)(r_{i+1}^2 + r_{i+1}r_i + r_i^2) \quad .$$

$$s_c = 1/(6a) \sum (r_{i+1} - r_i)(s_{i+1}^2 + s_{i+1}s_i + s_i^2) \quad .$$

The sums are over all bounding edges of the facet where i and $i + 1$ are the ends of the bounding edge such that, in going from i to $i + 1$, the facet is on the right side. As with rotationally symmetric cells, the area of a surface is determined cell-by-cell twice, once for each side. The area of a surface on one side is the sum over all facets on that side.

3. The volume of a polyhedron is computed by using an arbitrary reference plane. Prisms are projected from each facet normal to the reference plane, and the volume of each prism is $V = da \cos \theta$ where
 d = distance from reference plane to facet centroid;
 a = facet area; and
 θ = angle between the external normal of the facet and the positive normal of the reference plane.

The sum of the prism volumes is the polyhedron cell volume.

C. Stochastic Volume and Area Calculation

MCNP cannot calculate the volumes and areas of asymmetric, nonpolyhedral, or infinite cells. Also, in very rare cases, the volume and area calculation can fail because of roundoff errors. For these cases a stochastic estimation is possible by ray tracing. The procedure is as follows:

1. Void out all materials in the problem (VOID card).
2. Set all nonzero importances to one and all positive weight windows to zero.
3. Use a planar source with a source weight equal to the surface area to flood the geometry with particles. This will cause the particle flux throughout the geometry to statistically approach unity. Perhaps the best way to do a stochastic volume estimation is to use an inward-directed, biased cosine source on a spherical surface with weight equal to πr^2 .¹⁵³
4. Use the cell flux tally (F4) to tabulate volumes and the surface flux tally (F2) to tabulate areas. The cell flux tally is inversely proportional to cell volume. Thus in cells whose volumes are known, the unit flux will result in a tally of unity and, in cells whose volume is uncalculated, the unit flux will result in a tally of volumes. Similarly, the surface flux

tally is inversely proportional to area so that the unit flux will result in a tally of unity wherever the area is known and a tally of area wherever it is unknown.

X. PLOTTER

The MCNP plotter draws cross-sectional views of the problem geometry according to commands entered by the user. See Appendix B for the command vocabulary and examples of use. The pictures can be drawn on the screen of a terminal or to a postscript file as directed by the user. The pictures are drawn in a square viewport on the graphics device. The mapping between the viewport and the portion of the problem space to be plotted, called the window, is user-defined. A plane in problem space, the plot plane, is defined by specifying an origin \vec{r}_0 and two perpendicular basis vectors \vec{a} and \vec{b} . The size of the window in the plot plane is defined by specifying two extents. The picture appears in the viewport with the origin at the center, the first basis vector pointing to the right and the second basis vector pointing up. The width of the picture is twice the first extent and the height is twice the second extent. If the extents are unequal, the picture is distorted. The central task of the plotter is to plot curves representing the intersections of the surfaces of the geometry with the plot plane within the window.

All plotted curves are conics, defined here to include straight lines. The intersection of a plane with any MCNP surface that is not a torus is always a conic. A torus is plotted only if the plot plane contains the torus axis or is perpendicular to it, in which case the intersection curves are conics. The first step in plotting the curves is to find equations for them, starting from the equations for the surfaces of the problem. Equations are needed in two forms for each curve: a quadratic equation and a pair of parametric equations. The quadratic equations are needed to solve for the intersections of the curves. The parametric equations are needed for defining the points on the portions of the curves that are actually plotted.

The equation of a conic is

$$As^2 + 2Hst + Bt^2 + 2Gs + 2Ft + C = 0 \quad ,$$

where s and t are coordinates in the plot plane. They are related to problem coordinates (x,y,z) by

$$\vec{r} = \vec{r}_0 + s\vec{a} + t\vec{b}$$

or in matrix form

$$\begin{bmatrix} 1 \\ x \\ y \\ z \end{bmatrix} = \begin{bmatrix} 1 & 0 & 0 \\ x_0 & a_x & b_x \\ y_0 & a_y & b_y \\ z_0 & a_z & b_z \end{bmatrix} \begin{bmatrix} 1 \\ s \\ t \end{bmatrix} \text{ or } \begin{bmatrix} 1 \\ x \\ y \\ z \end{bmatrix} = PL \begin{bmatrix} 1 \\ s \\ t \end{bmatrix} \quad .$$

In matrix form the conic equation is

$$[1 \ s \ t] \begin{bmatrix} C & G & F \\ G & A & H \\ F & H & B \end{bmatrix} \begin{bmatrix} 1 \\ s \\ t \end{bmatrix} = 0 \text{ or } [1 \ s \ t] QM \begin{bmatrix} 1 \\ s \\ t \end{bmatrix} .$$

Thus, finding the equation of a curve to be plotted is a matter of finding the QM matrix, given the PL matrix and the coefficients of the surface.

Any surface in MCNP, except for tori, can be readily written as

$$Ax^2 + By^2 + Cz^2 + Dxy + Eyz + Fzx + Gx + Hy + Jz + K = 0 \quad ,$$

or in matrix form as

$$[1 \ x \ y \ z] \begin{bmatrix} K & G/2 & H/2 & J/2 \\ G/2 & A & D/2 & F/2 \\ H/2 & D/2 & B & E/2 \\ J/2 & F/2 & E/2 & C \end{bmatrix} \begin{bmatrix} 1 \\ x \\ y \\ z \end{bmatrix} = 0 \quad ,$$

or

$$[1 \ x \ y \ z] AM \begin{bmatrix} 1 \\ x \\ y \\ z \end{bmatrix} = 0 \quad .$$

The transpose of the transformation between (s,t) and (x,y,z) is

$$[1 \ x \ y \ z] = [1 \ s \ t] PL^T \quad ,$$

where PL^T is the transpose of the PL matrix. Substitution in the surface equation gives

$$[1 \ s \ t] PL^T AM PL \begin{bmatrix} 1 \\ s \\ t \end{bmatrix} = 0 \quad .$$

Therefore, $QM = PL^T AM PL$.

A convenient set of parametric equations for conics is

$$\begin{array}{ll} \text{straight line} & s = C_1 + C_2 p \\ & t = C_4 + C_5 p \\ \text{parabola} & s = C_1 + C_2 p + C_3 p^2 \\ & t = C_4 + C_5 p + C_6 p^2 \\ \text{ellipse} & s = C_1 + C_2 \sin p + C_3 \cos p \end{array}$$

$$\begin{array}{lcl} & t & = C_4 + C_5 \sin p + C_6 \cos p \\ \text{hyperbola} & s & = C_1 + C_2 \sinh p + C_3 \cosh p \\ & t & = C_4 + C_5 \sinh p + C_6 \cosh p. \end{array}$$

The type of a conic is determined by examination of the conic invariants,¹⁵⁵ which are simple functions of the elements of QM . Some of the surfaces produce two curves, such as the two branches of a hyperbola or two straight lines. A separate set of parametric coefficients, C_1 through C_6 , is needed for each curve in such cases. The parametric coefficients are found by transforming QM into yet another coordinate system where most of its elements are zero. The parametric coefficients are then simple functions¹⁵⁵ of the remaining elements. Finally, the coefficients are transformed from that coordinate system back to the (s,t) system.

For a plottable torus, the curves are either a pair of identical ellipses or a pair of concentric circles. The parametric coefficients are readily calculated from the surface coefficients and the elements of QM are simple functions of the parametric coefficients.

The next step is to reject all curves that lie entirely outside the window by finding the intersections of each curve with the straight line segments that bound the window, taking into account the possibility that an ellipse may lie entirely inside the window.

The remaining curves are plotted one at a time. The intersections of the current curve, with all of the other remaining curves and with the boundaries of the window, are found by solving the simultaneous equations

$$[1 \ s \ t] QM_i \begin{bmatrix} 1 \\ s \\ t \end{bmatrix} = 0 \quad ,$$

where $i = 1$ is the current curve and $i = 2$ is one of the other curves. This process generally requires finding the roots of a quartic. False roots and roots outside the window are rejected and the value of the parameter p for each remaining intersection is found. The intersections then are arranged in order of increasing values of p .

Each segment of the curve—the portion of the curve between two adjacent intersections—is examined to see whether and how it should be plotted. A point near the center of the segment is transformed back to the (x,y,z) coordinate system. All cells immediately adjacent to the surface at that point are found. If there is exactly one cell on each side of the surface and those cells are the same, the segment is not plotted. If there is exactly one cell on each side and those cells are different, the segment is plotted as a solid line. If anything else is found, the segment is plotted as a dotted line, which indicates either that there is an error in the problem geometry or that some other surface of the problem also intersects the plot plane along the segment.

If a curve to be plotted is not a straight line, it is plotted as a sequence of short straight lines between selected points on the curve. The points are selected according to the criterion that the middle of the line drawn between points must not lie farther from the nearest point on the true curve than the nominal resolution of the picture. The nominal resolution is fixed at 1/3000 of a side of the

viewport. This is a bit coarse for the best plotting devices and is quite a bit too fine for the worst ones, but it produces adequate pictures at reasonable cost.

XI. RANDOM NUMBERS

Like any other Monte Carlo program, MCNP uses a sequence of random numbers to sample from probability distributions. MCNP has always used the linear congruential scheme of Lehmer,¹⁵ though the mechanics of implementation have been modified for portability to different computer platforms. A random sequence of integers I_n is generated by

$$I_{n+1} = G I_n + C \mod 2^M, \quad n = 0, 1, \dots$$

where G is the random number multiplier, I_0 is the initial random seed, C is an additive constant, and M -bit integers and M -bit floating point mantissas are assumed. The random number is then

$$R_n = 2^{-M} I_n.$$

The MCNP5 random number generator¹⁶⁹ implements the above algorithm in portable Fortran 90 using either 48-bit integers (the default) or 63-bit integers.

The starting random number for history k is

$$I_0^{(k)} = G^{kS} I_0 + C (G^{kS} - 1) / (G - 1) \mod 2^M,$$

where S is the random number stride, that is, the number of random numbers allocated to each single history. This initial random number expression is evaluated very efficiently using a fast skip-ahead algorithm.¹⁶⁸ Successive random numbers for history k are then

$$I_n^{(k)} = G I_{n-1}^{(k)} + C \mod 2^M.$$

The default values of G , M , I_0 , S , and C , which can be changed with the RAND card, are

$$\begin{aligned} G &= 5^{19} = 19,073,486,328,125 \\ M &= 48 \\ C &= 0 \\ S &= 152,917 \\ I_0 &= 1 \end{aligned}$$

The values of G , M , and C may be changed by selecting another set of parameters using the RAND card. The 3 other sets of parameters use 63-bit integers and a nonzero additive constant C .

The period P of the MCNP algorithm using the default parameters is $P = 2^{46} \approx 7.04 \times 10^{13}$, and $P = 2^{63} \approx 9.2 \times 10^{18}$ for the extended random number parameters.

MCNP prints a WARNING and counts the number of histories for which the stride S is exceeded. MCNP also prints a WARNING if the period P is exceeded. Exceeding the stride or the period does

not result in wrong answers but may result in an underestimate of the variance. However, because the random numbers are used for very different purposes, MCNP seems quite insensitive to overrunning either the stride or the period.¹⁵⁶

Sometimes users wish to know how much of the variation between problems is purely statistical and the variance is insufficient to provide this information. In correlated sampling (see page 2–163) and criticality problems, the variances can be underestimated because of correlation between histories. In this case, rerun the problems with a different random number sequence, either by starting with a new random number or by changing the random number stride or multiplier on the RAND card. MCNP checks for and does not allow invalid choices, such as an even numbered initial random number that, after a few random numbers, would result in all subsequent random numbers being zero.

XII. PERTURBATIONS

The evaluation of response or tally sensitivities to cross-section data involves finding the ratio of the change in a tally to the infinitesimal change in the data, as given by the Taylor series expansion. In deterministic methods, this ratio is approximated by performing two calculations, one with the original data and one with the perturbed data. This approach is useful even when the magnitude of the perturbation becomes very small. In Monte Carlo methods, however, this approach fails as the magnitude of the perturbation becomes small because of the uncertainty associated with the response. For this reason, the differential operator technique was developed.

The differential operator perturbation technique as applied in the Monte Carlo method was introduced by Olhoeft¹⁵⁷ in the early 1960s. Nearly a decade after its introduction, this technique was applied to geometric perturbations by Takahashi.¹⁵⁸ A decade later, the method was generalized for perturbations in cross-section data by Hall^{159,160} and later Rief.¹⁶¹ A rudimentary implementation into MCNP followed shortly thereafter.¹⁶² With an enhancement of the user interface and the addition of second order effects, this implementation has evolved into a standard MCNP feature.

A. Derivation of the Operator

In the differential operator approach, a change in the Monte Carlo response c , due to changes in a related data set (represented by the parameter v), is given by a Taylor series expansion

$$\Delta c = \frac{dc}{dv} \cdot \Delta v + \frac{1}{2!} \cdot \frac{d^2c}{dv^2} \cdot \Delta v^2 + \dots + \frac{1}{n!} \cdot \frac{d^nc}{dv^n} \cdot \Delta v^n + \dots ,$$

where the n^{th} -order coefficient is

$$u_n = \frac{1}{n!} \cdot \frac{d^nc}{dv^n} .$$

This can be written as

$$u_n = \frac{1}{n!} \sum_{b \in B} \sum_{h \in H} x_b^n(h) \left(\frac{\partial^n c}{\partial x_b^n(h)} \right) ,$$

for the data set

$$x_b(h) = K_b(h) \cdot e^v; b \in B, h \in H ,$$

where $K_b(h)$ is some constant, B represents a set of macroscopic cross sections, and H represents a set of energies or an energy interval.

For a track-based response estimator

$$c = \sum_j t_j q_j ,$$

where t_j is the response estimator and q_j is the probability of path segment j (path segment j is comprised of segment $j - 1$ plus the current track). This gives

$$u_n = \frac{1}{n!} \sum_j \left[\sum_{b \in B} \sum_{h \in H} x_b^n(h) \left(\frac{\partial^n}{\partial x_b^n(h)} (t_j q_j) \right) \right] ,$$

or

$$u_n = \frac{1}{n!} \sum_j \gamma_{nj} t_j q_j ,$$

where

$$\gamma_{nj} \equiv \sum_{b \in B} \sum_{h \in H} x_b^n(h) \left(\frac{\partial^n}{\partial x_b^n(h)} (t_j q_j) \right) \left(\frac{1}{t_j q_j} \right) .$$

With some manipulations presented in Refs. 163 and 164, the path segment estimator $\gamma_{nj} t_j$ can be converted to a particle history estimator of the form

$$u_n = \sum_i V_{ni} P_i ,$$

where p_i is the probability of the i^{th} history and V_{ni} is the n^{th} -order coefficient estimator for history i , given by

$$V_{ni} \equiv \frac{1}{n!} \sum_{j'} \gamma_{nj'} t_{j'} .$$

Note that this sum involves only those path segments j' in particle history i . The Monte Carlo expected value of u_n becomes

$$\begin{aligned}\langle u_n \rangle &= \frac{1}{N} \sum_i V_{ni} \\ &= \frac{1}{Nn!} \sum_i \left(\sum_{j'} \gamma_{nj'} t_{j'} \right) \quad ,\end{aligned}$$

for a sample of N particle histories.

The probability of path segment j is the product of the track probabilities,

$$q_j = \prod_{k=0}^m r_k \quad ,$$

where r_k is the probability of track k and segment j contains $m + 1$ tracks. If the k^{th} track starts with a neutron undergoing reaction type “a” at energy E' and is scattered from angle θ' to angle θ and E , continues for a length λ_k , and collides, then

$$r_k = \left(\frac{x_a(E')}{x_T(E')} \right) P_a(E' \rightarrow E; \theta' \rightarrow \theta) dE d\theta (e^{-x_T(E)\lambda_k}) x_T(E) d\lambda_k \quad ,$$

where $x_a(E')$ is the macroscopic reaction cross section at energy E' , $x_T(E')$ is the total cross section at energy E' , and $P_a(E' \rightarrow E; \theta' \rightarrow \theta) dE d\theta$ is the probability distribution function in phase space of the emerging neutron. If the track starts with a collision and ends in a boundary crossing

$$r_k = \left(\frac{x_a(E')}{x_T(E')} \right) P_a(E' \rightarrow E; \theta' \rightarrow \theta) dE d\theta (e^{-x_T(E)\lambda_k}) \quad .$$

If the track starts with a boundary crossing and ends with a collision,

$$r_k = (e^{-x_T(E)\lambda_k}) x_T(E) \quad .$$

And finally, if the track starts and ends with boundary crossings

$$r_k = e^{-x_T(E)\lambda_k} \quad .$$

1. First Order

For a first-order perturbation, the differential operator becomes

$$\begin{aligned}\gamma_{1j'} &\equiv \sum_{b \in B} \sum_{h \in H} x_b(h) \left(\frac{\partial}{\partial x_b(h)} (t_{j'} q_{j'}) \right) \left(\frac{1}{t_{j'} q_{j'}} \right) \\ &= \sum_{b \in B} \sum_{h \in H} \left(\frac{x_b(h)}{q_{j'}} \frac{\partial q_{j'}}{\partial x_b(h)} + \frac{x_b(h)}{t_{j'}} \frac{\partial t_{j'}}{\partial x_b(h)} \right)\end{aligned}$$

whereas,

$$\frac{1}{q_{j'}} \frac{\partial q_{j'}}{\partial x_b(h)} = \sum_{k=0}^m \frac{1}{r_k} \frac{\partial r_k}{\partial x_b(h)} \quad .$$

then

$$\gamma_{1j'} = \sum_{k=0}^m \beta_{j'k} + R_{1j'} \quad ,$$

where

$$\begin{aligned}\beta_{j'k} &\equiv \sum_{b \in B} \sum_{h \in H} \left(\frac{x_b(h)}{r_k} \right) \left(\frac{\partial r_k}{\partial x_b(h)} \right) \\ &= \sum_{b \in B} \sum_{h \in H} \left(\delta_{hE'} \delta_{ba} - \frac{\delta_{hE'} x_b(E')}{x_T(E')} - \delta_{hE} x_b(E) \lambda_k + \frac{\delta_{hE} x_b(E)}{x_T(E)} \right)\end{aligned}$$

for a track segment k that starts with a particle undergoing reaction type “a” at energy E' and is scattered to energy E and collides after a distance λ_k . Note that δ_{hE} and δ_{ba} are unity if $h=E$ and $b=a$; otherwise they vanish. For other types of tracks (for which the various expressions for r_k were given in the previous section), that is, collision to boundary, boundary to collision, and boundary to boundary, derivatives of r_k can be taken leading to one or more of these four terms for $\beta_{j'k}$.

The second term of $\gamma_{1j'}$ is

$$R_{1j'} = \sum_{b \in B} \sum_{h \in H} \frac{x_b(h)}{t_{j'}} \frac{\partial t_{j'}}{\partial x_b(h)} \quad ,$$

where the tally response is a linear function of some combination of reaction cross sections, or

$$t_{j'} = \lambda_k \sum_{c \in C} x_c(E) \quad ,$$

where c is an element of the tally cross sections, $c \in C$, and may be an element of the perturbed cross sections, $c \in B$. Then,

$$R_{1j'} = \sum_{b \in B} \sum_{h \in H} \frac{x_b(h)}{\left(\sum_{c \in C} x_c(h) \right)} \frac{\partial}{\partial x_b(h)} \left(\sum_{c \in C} x_c(h) \right)$$

$$= \frac{\sum_{c \in B} \sum_{E \in H} x_c(E)}{\sum_{c \in C} x_c(E)} .$$

$R_{1j'}$ is the fraction of the reaction rate tally involved in the perturbation. If none of the nuclides participating in the tally is involved in the perturbation, then $R_{1j'} = 0$, which is always the case for F1, F2, and F4 tallies without FM cards. For F4 tallies with an FM card, if the FM card multiplicative constant is positive (no flag to multiply by atom density) it is assumed that the FM tally cross sections are unaffected by the perturbation and $R_{1j'} = 0$. For KCODE k_{eff} track length estimates, F6 and F7 heating tallies, and F4 tallies with FM cards with negative multipliers (multiply by atom density to get macroscopic cross sections), if the tally cross section is affected by the perturbation, then $R_{1j'} > 0$. For k_{eff} and F6 and F7 tallies in perturbed cells where all nuclides are perturbed, generally $R_{1j'} = 1$.

Finally, the expected value of the first-order coefficient is

$$\langle u_1 \rangle = \frac{1}{N} \sum_i \left[\sum_{j'} \left(\sum_{k=0}^m \beta_{j'k} + R_{1j'} \right) t_{j'} \right] .$$

2. Second Order

For a second-order perturbation, the differential operator becomes

$$\gamma_{2j'} \equiv \sum_{b \in B} \sum_{h \in H} x_b^2(h) \left(\frac{\partial^2}{\partial x_b^2(h)} (t_{j'} q_{j'}) \right) \left(\frac{1}{t_{j'} q_{j'}} \right)$$

$$= \sum_{b \in B} \sum_{h \in H} \frac{x_b^2(h)}{t_{j'} q_{j'}} \left(t_{j'} \frac{\partial^2 q_{j'}}{\partial x_b^2(h)} + 2 \frac{\partial q_{j'}}{\partial x_b(h)} \frac{\partial t_{j'}}{\partial x_b(h)} + q_{j'} \frac{\partial^2 t_{j'}}{\partial x_b^2(h)} \right) .$$

Whereas $t_{j'}$ is a linear function of $x_b(h)$, then

$$\frac{\partial^2 t_{j'}}{\partial x_b^2(h)} = 0$$

and by taking first and second derivatives of the r_k terms of $q_{j'}$ as for the first-order perturbation,

$$\gamma_{2j'} = \sum_{k=0}^m (\alpha_{j'k} - \beta_{j'k}^2) - R_{1j'}^2 + \left(\sum_{k=0}^m \beta_{j'k} + R_{1j'} \right)^2 ,$$

where

$$\begin{aligned} \alpha_{j'k} = & \sum_{b \in B} \sum_{h \in H} \left(\frac{2\delta_{hE'} x_b^2(E')}{x_T^2(E')} - \frac{2\delta_{hE'} \delta_{ba} x_b(E')}{x_T(E')} + \delta_{hE'} x_b^2 \lambda_k^2 - \frac{2\delta_{hE'} x_b^2(E) \lambda_k}{x_T(E)} \right. \\ & \left. + 2 \left(\delta_{hE'} \delta_{ba} - \frac{x_b(E') \delta_{hE'}}{x_t(E')} \right) \left(\frac{x_b(E) \delta_{hE}}{x_t(E)} - \lambda_k \delta_{hE} x_b(E) \right) \right) . \end{aligned}$$

The expected value of the second-order coefficient is

$$\langle u_2 \rangle = \frac{1}{2N} \sum_i \left[\sum_{j'} \left(\sum_{k=0}^m (\alpha_{j'k} - \beta_{j'k}^2) - R_{ij'}^2 + \left(\sum_{k=0}^m \beta_{j'k} + R_{1j'} \right)^2 \right) t_{j'} \right] ,$$

where $\beta_{j'k}$ and $\alpha_{j'k}$ are given by one or more terms as described above for track k and $R_{1j'}$ is again the fraction of the perturbation with nuclides participating in the tally.

3. Implementation in MCNP

The total perturbation printed in the MCNP output file is

$$\langle \Delta c \rangle = \frac{1}{N} \sum_i \sum_{j'} \Delta c_{j'} \quad .$$

For each history i and path j' ,

$$\Delta c_{j'} = \frac{dc_{j'}}{dv} \cdot \Delta v + \frac{1}{2} \cdot \frac{d^2 c_{j'}}{dv^2} \cdot \Delta v^2 \quad .$$

Let the first-order perturbation with $R_{1j'} = 0$ be

$$P_{1j'} = \sum_{j'} \left(\sum_{k=0}^m \beta_{j'k} \right) t_{j'} \quad ,$$

and let the second-order perturbation with $R_{1j'} = 0$ be

$$P_{2j'} = \sum_{j'} \left(\sum_{k=0}^m (\alpha_{j'k} - \beta_{j'k}^2) \right) t_{j'} \quad .$$

Then the Taylor series expansion for $R_{1j'} = 0$ is

$$\Delta c_{j'} = \left(P_{1j'} \Delta v + \frac{1}{2} (P_{2j'} + P_{1j'}^2) \Delta v^2 \right) t_{j'} \quad .$$

If $R_{1j'} \neq 0$ then

$$\begin{aligned} \Delta c_{j'} &= \left[(P_{1j'} + R_{1j'}) \Delta v + \frac{1}{2} (P_{2j'} - R_{1j'}^2 + (P_{1j'} + R_{1j'})^2) \Delta v^2 \right] t_{j'} \\ &= \left[P_{1j'} \Delta v + \frac{1}{2} (P_{2j'} + P_{1j'}^2) \Delta v^2 + R_{1j'} \Delta v + P_{1j'} R_{1j'} \Delta v^2 \right] t_{j'} \quad . \end{aligned}$$

That is, the $R_{1j'} \neq 0$ case is just a correction to the $R_{1j'} = 0$ case.

In MCNP, $P_{1j'}$ and $P_{2j'}$ are accumulated along every track length through a perturbed cell. All perturbed tallies are multiplied by

$$P_{1j'} \Delta v + \frac{1}{2} (P_{2j'} + P_{1j'}^2) \Delta v^2 \quad ,$$

and then if $R_{1j'} \neq 0$ the tally is further corrected by

$$R_{1j'} \Delta v + P_{1j'} R_{1j'} \Delta v^2 \quad .$$

$R_{1j'}$ is the fraction of the reaction rate tally involved in the perturbation. $R_{1j'} = 0$ for F1, F2, F4 tallies without FM cards, and F4 tallies with FM cards with positive multiplicative constants.

B. Limitations

Although it is always a high priority to minimize the limitations of any MCNP feature, the perturbation technique has the limitations given below. Chapter 3, page 3–154, has examples you can refer to.

1. A fatal error is generated if a PERT card attempts to unvoid a region. The simple solution is to include the material in the unperturbed problem and void the region of interest with the PERT card. See Appendix B of Ref. 165.
2. A fatal error is generated if a PERT card attempts to alter a material composition in such a way as to introduce a new nuclide. The solution is to set up the unperturbed problem with a mixture of both materials and introduce PERT cards to remove each. See Appendix B of Ref. 165.
3. The track length estimate of k_{eff} in KCODE criticality calculations assumes the fundamental eigenfunction (fission distribution) is unchanged in the perturbed configuration.
4. DXTRAN, point detector tallies, and pulse height tallies are not currently compatible with the PERT card.
5. While there is no limit to the number of perturbations, they should be kept to a minimum, as each perturbation can degrade performance by 10–20%.
6. Use caution in selecting the multiplicative constant and reaction number on FM cards used with F4 tallies in perturbation problems.
7. The METHOD keyword can indicate if a perturbation is so large that higher than second-order terms are needed to prevent inaccurate tallies.
8. If a perturbation changes the relative concentrations of nuclides (MAT keyword) it is assumed that the perturbation contribution from each nuclide is independent (that is, second-order differential cross terms are neglected).

C. Accuracy

Analyzing the first- and second-order perturbation results presented in Ref. 166 leads to the following rules of thumb. The first-order perturbation estimator typically provides sufficient accuracy for response or tally changes that are less than 5%. The default first- plus second-order estimator offers acceptable accuracy for response changes that are less than 20–30%. This upper bound depends on the behavior of the response as a function of the perturbed parameter. The magnitude of the second-order estimator is a good measure of the range of applicability. If this magnitude exceeds 30% of the first-order estimator, it is likely that higher-order terms are needed for an accurate prediction. The METHOD keyword on the PERT card allows one to tally the second-order term separate from the first. See Chapter 3, page 3–153.

The MCNP perturbation capability assumes that changes in the relative concentrations or densities of the nuclides in a material are independent and neglects the cross-differential terms in the second-order perturbation term when changing two or more cross sections at once. In some cases there will be a large FALSE second-order perturbation term. See Chapter 3, page 3–154 for further discussion and examples. Reference 166 provides more discussion and a method for calculating the cross terms.

The MCNP perturbation capability has been shown to be inaccurate for some large but very localized perturbations in criticality problems. An alternative implementation that only requires postprocessing standard MCNP tallies has been shown to be much more accurate in some cases. See Ref. 167.

XIII. REFERENCES

1. L. L. Carter and E. D. Cashwell, *Particle Transport Simulation with the Monte Carlo Method*, ERDA Critical Review Series, TID-26607 (1975).
2. Ivan Lux and Laszlo Koblinger, *Monte Carlo Particle Transport Methods: Neutron and Photon Calculations*, CRC Press, Boca Raton (1991).
3. C. J. Everett and E. D. Cashwell, "A Third Monte Carlo Sampler," Los Alamos National Laboratory Report, LA-9721-MS, (March 1983).
4. G. Comte de Buffon, "Essai d'arithmetique morale," *Supplement a la Naturelle*, Vol. 4, 1777.
5. A Hall, "On an Experimental Determination of Pi," *Messeng. Math.*, 2, 113-114 (1873).
6. J. M. Hammersley and D. C. Handscomb, *Monte Carlo Methods*, John Wiley & Sons, New York (1964).
7. Marquis Pierre-Simon de Laplace, *Theorie Analytique des Probabilities*, Livre 2 pp. 356-366 contained in *Oeuvres Completes de Laplace, de L'Academie des Sciences*, Paris, Vol. 7, part 2, 1786.
8. Lord Kelvin, "Nineteenth Century Clouds Over the Dynamical Theory of Heat and Light," *Philosophical Magazine*, series 6, 2, 1 (1901).
9. W. W. Wood, "Early History of Computer Simulations in Statistical Mechanics and Molecular Dynamics," International School of Physics "Enrico Fermi," Varenna, Italy, 1985, Molecular-Dynamics Simulation of Statistical Mechanical Systems, XCVII Corso (Soc. Italiana di Fisica, Bologna) (1986).
10. Necia Grant Cooper, Ed., *From Cardinals to Chaos — Reflections on the Life and Legacy of Stanislaw Ulam*, Cambridge University Press, New York (1989).
11. "Fermi Invention Rediscovered at LASL," *The Atom*, Los Alamos Scientific Laboratory (October 1966).
12. N. Metropolis and S. Ulam, "The Monte Carlo Method," *J. Amer. Stat. Assoc.*, 44, 335 (1949).
13. Herman Kahn, "Modifications of the Monte Carlo Method," *Proceeding, Seminar on Scientific Computation*, Nov. 1949, IBM, New York, 20-27 (1950).
14. A. S. Householder, G. E. Forsythe, and H. H. Germond, Ed., *Monte Carlo Methods*, NBS Applied Mathematics Series, Vol. 12, 6, (1951).
15. D. H. Lehmer, "Mathematical Methods in Large-Scale Computing Units," *Ann. Comp. Lab.*, Harvard Univ. 26, 141-146 (1951).
16. Herman Kahn, "Applications of Monte Carlo," AECU-3259 Report, Rand Corporation, Santa Monica, CA, (1954).
17. E. D. Cashwell and C. J. Everett, *A Practical Manual on the Monte Carlo Method for Random Walk Problems*, Pergamon Press, Inc., New York (1959).
18. Robert R. Johnston, "A General Monte Carlo Neutronics Code," Los Alamos Scientific Laboratory Report, LAMS-2856 (March 1963).
19. E. D. Cashwell, J. R. Neergaard, W. M. Taylor, and G. D. Turner, "MCN: A Neutron Monte Carlo Code," Los Alamos Scientific Laboratory Report, LA-4751 (January 1972).
20. E. D. Cashwell, J. R. Neergaard, C. J. Everett, R. G. Schrandt, W. M. Taylor, and G. D. Turner, "Monte Carlo Photon Codes: MCG and MCP," Los Alamos National Laboratory Report, LA-5157-MS (March 1973).

21. J. A. Halblieb and T. A. Mehlhorn, "ITS: The Integrated TIGER Series of Coupled Electron/Photon Monte Carlo Transport Codes," Sandia National Laboratory Report, SAND 84-0573 (1984).
22. American National Standard for Programming Language - Fortran - Extended, American National Standards Institute, ANSI X3.198-1992, New York, NY, September 1992.
23. E. D. Cashwell and C. J. Everett, "Intersection of a Ray with a Surface of Third or Fourth Degree," Los Alamos Scientific Laboratory Report, LA-4299 (December 1969).
24. R. Kinsey, "Data Formats and Procedures for the Evaluated Nuclear Data File, ENDF," Brookhaven National Laboratory Report, BNL-NCS-50496 (ENDF 102) 2nd Edition (ENDF/B-V) (October 1979).
25. R. J. Howerton, D. E. Cullen, R. C. Haight, M. H. MacGregor, S. T. Perkins, and E. F. Plechaty, "The LLL Evaluated Nuclear Data Library (ENDL): Evaluation Techniques, Reaction Index, and Descriptions of Individual Reactions," Lawrence Livermore Scientific Laboratory Report UCRL-50400, Vol. 15, Part A (September 1975).
26. E. D. Arthur and P. G. Young, "Evaluated Neutron-Induced Cross Sections for $^{54,56}\text{Fe}$ to 40 MeV," Los Alamos National Laboratory report LA-8626-MS (ENDF-304) (December 1980).
27. D. G. Foster, Jr. and E. D. Arthur, "Average Neutronic Properties of "Prompt" Fission Products," Los Alamos National Laboratory report LA-9168-MS (February 1982).
28. E. D. Arthur, P. G. Young, A. B. Smith, and C. A. Philis, "New Tungsten Isotope Evaluations for Neutron Energies Between 0.1 and 20 MeV," *Trans. Am. Nucl. Soc.* **39**, 793 (1981).
29. M. W. Asprey, R. B. Lazarus, and R. E. Seamon, "EVXS: A Code to Generate Multigroup Cross Sections from the Los Alamos Master Data File," Los Alamos Scientific Laboratory report LA-4855 (June 1974).
30. R. E. MacFarlane, D. W. Muir, and R. M. Boicourt, "The NJOY Nuclear Data Processing System, Volume I: User's Manual," Los Alamos National Laboratory report LA-9303-M, Vol. I (ENDF-324) (May 1982).
R. E. MacFarlane, D. W. Muir, and R. M. Boicourt, "The NJOY Nuclear Data Processing System, Volume II: The NJOY, RECONR, BROADR, HEATR, and THERMR Modules," Los Alamos National Laboratory report LA-9303-M, Vol. II (ENDF-324) (May 1982).
31. R. J. Howerton, R. E. Dye, P. C. Giles, J. R. Kimlinger, S. T. Perkins and E. F. Plechaty, "Omega Documentation," Lawrence Livermore National Laboratory report UCRL-50400, Vol. 25 (August 1983).
32. E. Storm and H. I. Israel, "Photon Cross Sections from 0.001 to 100 MeV for Elements 1 through 100," Los Alamos Scientific Laboratory report LA-3753 (November 1967).
33. J. H. Hubbell, W. J. Veigele, E. A. Briggs, R. T. Brown, D. T. Cromer and R. J. Howerton, "Atomic Form Factors, Incoherent Scattering Functions, and Photon Scattering Cross Sections," *J. Phys. Chem. Ref. Data* **4**, 471 (1975).
34. C. J. Everett and E. D. Cashwell, "MCP Code Fluorescence-Routine Revision," Los Alamos Scientific Laboratory report LA-5240-MS (May 1973).
35. H. Grady Hughes, "Information on the MCPLIB02 Photon Library," Los Alamos National Laboratory report LA-UR-08-539 (January 23, 1993).
36. D. E. Cullen, M. H. Chen, J. H. Hubbell, S. T. Perkins, E. F. Plechaty, J. A. Rathkopf, and J. H. Scofield, "Tables and Graphs of Photon-Interaction Cross Sections from 10 eV to 100 GeV Derived from the LLNL Evaluated Photon Data Library (EPDL)," Lawrence Livermore National Laboratory report UCRL-50400, Vol. 6 (October 31, 1989).

37. F. Biggs, L. B. Mendelsohn, and J. B. Mann, "Hartree-Fock Compton Profiles for the Elements," *Atomic Data and Nuclear Data Tables*, Vol. 16, No. 3, pp. 201-309 (1975).
38. D. E. Cullen, J. H. Hubbell, and L. D. Kissel, "EPDL97: The Evaluated Photon Data Library, '97 Version," UCRL-50400, Vol. 6, Rev. 5, Lawrence Livermore National Laboratory (1997).
39. P. Oblozinsky, ed., "Handbook on Photonuclear Data for Applications: Cross-Sections and Spectra," IAEA-TECDOC-1178, International Atomic Energy Agency: Vienna, Austria (2000).
40. J. A. Halbleib, R. P. Kensek, T. A. Mehlhorn, G. D. Valdez, S. M. Seltzer, and M. J. Berger, "ITS Version 3.0: Integrated TIGER Series of Coupled Electron/Photon Monte Carlo Transport Codes," SAND91-1634 (1992).
41. M. A. Gardner and R. J. Howerton, "ACTL: Evaluated Neutron Activation Cross-Section Library—Evaluation Techniques and Reaction Index," Lawrence Livermore National Laboratory report UCRL-50400, Vol. 18 (October 1978).
42. J. U. Koppel and D. H. Houston, "Reference Manual for ENDF Thermal Neutron Scattering Data," General Atomics report GA-8744, Revised (ENDF-269) (July 1978).
43. J. C. Wagner, E. L. Redmond II, S. P. Palmtag, and J. S. Hendricks, "MCNP: Multigroup/Adjoint Capabilities," Los Alamos National Laboratory report, LA-12704 (December 1993).
44. J. E. Morel, L. J. Lorence, Jr., R. P. Kensek, J. A. Halbleib, and D. P. Sloan, "A Hybrid Multigroup/Continuous-Energy Monte Carlo Method for Solving the Boltzmann-Fokker-Planck Equation," *Nucl. Sci. Eng.*, **124**, p. 369-389 (1996).
45. Thomas E. Booth, "Monte Carlo Variance Reduction Approaches for Non-Boltzmann Tallies," Los Alamos National Laboratory report LA-12433 (December 1992).
46. Thomas E. Booth, "Pulse Height Tally Variance Reduction in MCNP," Los Alamos National Laboratory report LA-13955 (2002).
47. L. J. Lorence, Jr., J. E. Morel, G. D. Valdez, "Physics Guide to CEPXS: A Multigroup Coupled Electron-Photon Cross-Section Generating Code, Version 1.0," SAND89-1685 (1989) and "User's Guide to CEPXS/ONED--ANT: A One-Dimensional Coupled Electron-Photon Discrete Ordinates Code Package, Version 1.0," SAND89-1661 (1989) and L. J. Lorence, Jr., W. E. Nelson, J. E. Morel, "Coupled Electron-Photon Transport Calculations Using the Method of Discrete-Ordinates," *IEEE/NSREC*, Vol. NS-32, No. 6, Dec. 1985.
48. R. C. Little and R. E. Seamon, "Neutron-Induced Photon Production in MCNP," *Sixth International Conference on Radiation Shielding*, Vol. I, p. 151 (May 1983).
49. H. Grady Hughes and Robert G. Schrandt, "Gaussian Sampling of Fission Neutron Multiplicity," Los Alamos National Laboratory memorandum X-6:HG-86-264 (1986).
50. J. Terrell, "Distribution of Fission Neutron Numbers," *Phys. Rev. C*, **1**, 783 (1957).
51. J. P. Lestone, "Energy and Isotope Dependence of Neutron Multiplicity Distributions," (submitted to *Nucl. Sci. Eng.*) Los Alamos National Laboratory report LA-UR-05-0288 (2005).
52. K. Böhnelt, "The Effect of Multiplication on the Quantitative Determination of Spontaneously Fissioning Isotopes by Neutron Correlation Analysis," *Nucl. Sci. Eng.*, **90**, 75 (1985).
53. R. D. Mosteller and C. J. Werner, "Reactivity Impact of Delayed Neutron Spectra on MCNP Calculations," in *Transactions of American Nuclear Society*, Vol. 82, pp. 235-236 (2000).
54. J. S. Hendricks and R. E. Prael, "Monte Carlo Next-Event Estimates from Thermal Collisions," *Nucl. Sci. Eng.*, **109** (3) pp. 150-157 (October 1991).

55. J. S. Hendricks, R. E. Prael, "MCNP $S(\alpha,\beta)$ Detector Scheme," Los Alamos National Laboratory report, LA-11952 (October 1990).
56. G. I. Bell and S. Glasstone, *Nuclear Reactor Theory* (Van Nostrand Reinhold Company, New York, 1970).
57. J. M. Otter, R. C. Lewis, and L. B. Levitt, "UBR, A Code to Calculate Unresolved Resonance Cross Section Probability Tables," AI-AEC-13024 (July 1972).
58. R. E. Prael, "Application of the Probability Table Method to Monte Carlo Temperature Difference Calculations," *Transactions of the American Nuclear Society*, Vol 17, p. 261 (November 1973).
59. R. N. Blomquist, R. M. Lell, and E. M. Gelbard, "VIM - A Continuous Energy Monte Carlo Code at ANL," *A Review of the Theory and Application of Monte Carlo Methods*, April 21-23, 1980, Oak Ridge, Tennessee, ORNL/RSIC-44.
60. L. L. Carter, R. C. Little, J. S. Hendricks, and R. E. MacFarlane, "New Probability Table Treatment in MCNP for Unresolved Resonances," *1998 ANS Radiation Protection and Shielding Division Topical Conference*, April 19-23, 1998, Nashville, TN, Vol. II, pp. 341- 347.
61. A. Bohr and B. R. Mottelson, *Nuclear Structure*, 2nd Ed. (World Scientific: Singapore, 1998).
62. J. S. Levinger, "Neutron Production by Complete Absorption of High-Energy Photons," *Nucleonics*, Vol. 6, No. 5, pp. 64-67 (1950).
63. J. S. Levinger, "The High Energy Nuclear Photoeffect," *Physical Review*, Vol. 84, No. 1, pp. 43-51 (1951).
64. M. B. Chadwick, P. Oblozinsky, P. E. Hodgson, and G. Reffo, "Pauli-Blocking in the Quasideuteron Model of Photoabsorption," *Physical Review C*, Vol. 44, No. 2, pp. 814-823 (1991).
65. J. R. Wu and C. C. Chang, "Pre-Equilibrium Particle Decay in the Photonuclear Reactions," *Physical Review C*, Vol. 16, No. 5, pp. 1812-1824 (1977).
66. M. Blann, B. L. Berman, and T. T. Komoto, "Precompound-Model Analysis of Photoneutron Reaction," *Physical Review C*, Vol. 28, No. 6, pp. 2286-2298 (1983).
67. M. B. Chadwick, P. G. Young, and S. Chibas, "Photonuclear Angular-Distribution Systematics in the Quasideuteron Regime," *Journal of Nuclear Science and Technology*, Vol. 32, No. 11, pp. 1154-1158 (1995).
68. A. Fasso, A. Ferrari, and P. R. Sala, "Total Giant Resonance Photonuclear Cross Sections for Light Nuclei: A Database for the FLUKA Monte Carlo Transport Code," *Third Specialists Meeting on Shielding Aspects of Accelerators, Targets, and Irradiation Facilities*, SATIF-3, Tohoku University, Sendai, Japan (Organization for Economic Cooperation and Development Nuclear Energy Agency: Paris, France, 1997)
69. M. C. White, "Development and Implementation of Photonuclear Cross-Section Data for Mutually Coupled Neutron-Photon Transport Calculations in the Monte Carlo N-Particle (MCNP) Radiation Transport Code," Ph.D. thesis, University of Florida (2000).
70. M. C. White, R. C. Little, and M. B. Chadwick, "Photonuclear Physics in MCNP(X)," *ANS Conference on Nuclear Applications of Accelerator Technology*, Long Beach, California, November 14-18, 1999.
71. R. D. Mosteller and R. C. Little, "Impact of MCNP Unresolved Resonance Probability Table Treatment on Uranium and Plutonium Benchmarks," *Sixth International Conference on Nuclear Criticality Safety (ICNC '99)*, September 20-24, 1999, Versailles, France, pp. 522-531.

72. H. Kahn, "Applications of Monte Carlo," AEC-3259 The Rand Corporation (April 1956).
73. L. Koblinger, "Direct Sampling from the Klein-Nishina Distribution for Photon Energies Above 1.4 MeV," *Nucl. Sci. Eng.*, **56**, 218 (1975).
74. R. N. Blomquist and E. M. Gelbard, "An Assessment of Existing Klein-Nishina Monte Carlo Sampling Methods," *Nucl. Sci. Eng.*, **83**, 380 (1983).
75. G. W. Grodstein, "X-Ray Attenuation Coefficients from 10 keV to 100 MeV," National Bureau of Standards, Circular No. 583 (1957).
76. S. Goudsmit and J. L. Saunderson, "Multiple Scattering of Electrons," *Phys. Rev.* **57** (1940) 24.
77. L. Landau, "On the Energy Loss of Fast Particles by Ionization," *J. Phys. USSR* **8** (1944) 201.
78. O. Blunck and S. Leisegang, "Zum Energieverlust schneller Elektronen in dünnen Schichten," *Z. Physik* **128** (1950) 500.
79. M. J. Berger, "Monte Carlo Calculation of the Penetration and Diffusion of Fast Charged Particles," in *Methods in Computational Physics, Vol. 1*, edited by B. Alder, S. Fernbach, and M. Rotenberg, (Academic Press, New York, 1963) 135.
80. Stephen M. Seltzer, "An Overview of ETRAN Monte Carlo Methods," in *Monte Carlo Transport of Electrons and Photons*, edited by Theodore M. Jenkins, Walter R. Nelson, and Alessandro Rindi, (Plenum Press, New York, 1988) 153.
81. J. Halbleib, "Structure and Operation of the ITS Code System," in *Monte Carlo Transport of Electrons and Photons*, edited by Theodore M. Jenkins, Walter R. Nelson, and Alessandro Rindi, (Plenum Press, New York, 1988) 249.
82. R. M. Sternheimer, M. J. Berger, and S. M. Seltzer, "Density Effect for the Ionization Loss of Charged Particles in Various Substances," *Phys. Rev.* **B26** (1982) 6067.
83. R. M. Sternheimer and R. F. Peierls, "General Expression for the Density Effect for the Ionization Loss of Charged Particles," *Phys. Rev.* **B3** (1971) 3681.
84. T. A. Carlson, *Photoelectron and Auger Spectroscopy*, Plenum Press, New York, N.Y. 1975.
85. Stephen M. Seltzer, "Cross Sections for Bremsstrahlung Production and Electron Impact Ionization," in *Monte Carlo Transport of Electrons and Photons*, edited by Theodore M. Jenkins, Walter R. Nelson, and Alessandro Rindi, (Plenum Press, New York, 1988) 81.
86. S. M. Seltzer and M. J. Berger, "Bremsstrahlung Spectra from Electron Interactions with Screened atomic Nuclei and Orbital Electrons", *Nucl. Instr. Meth.* **B12** (1985) 95.
87. S. M. Seltzer and M. J. Berger, "Bremsstrahlung Energy Spectra from Electrons with Kinetic Energy 1 keV - 10 GeV Incident on Screened Nuclei and Orbital Electrons of Neutral Atoms with Z=1 to 100", *Atom. Data and Nuc. Data Tables* **35**, (1986) 345.
88. E. Rutherford, "The Scattering of α and β Particles by Matter and the Structure of the Atom," *Philos. Mag.* **21** (1911) 669.
89. W. Börsch-Supan, "On the Evaluation of the Function $\phi(\lambda) = \frac{1}{2\pi i} \int_{\sigma-i\infty}^{\sigma+i\infty} e^{\mu \ln \mu + \lambda \mu} d\mu$ for Real Values of λ ," *J. Res. National Bureau of Standards* **65B** (1961) 245.
90. J. A. Halbleib, R. P. Kensek, T. A. Mehlhorn, G. D. Valdez, S. M. Seltzer, and M. J. Berger, "ITS Version 3.0: The Integrated TIGER Series of Coupled Electron/Photon Monte Carlo Transport Codes," Sandia National Laboratories report SAND91-1634 (March 1992).
91. O. Blunck and K. Westphal, "Zum Energieverlust energiereicher Elektronen in dünnen Schichten," *Z. Physik* **130** (1951) 641.
92. V. A. Chechin and V. C. Ermilova, "The Ionization-Loss Distribution at Very Small Absorber Thickness," *Nucl. Instr. Meth.* **136** (1976) 551.

93. Stephen M. Seltzer, "Electron-Photon Monte Carlo Calculations: The ETRAN Code," *Appl. Radiat. Isot.* Vol. 42, No. 10 (1991) pp. 917-941.
94. D. R. Schaart, J. T. M. Jansen, J. Zoetelief, and P. F. A. de Leege, "A Comparison of MCNP4C Electron Transport with ITS 3.0 and Experiment at Incident Energies Between 100 keV and 20 MeV: Influence of Voxel Size, Substeps, and Energy Indexing Algorithm," *Phys. Med. Biol.*, **47**, pp. 1459-1484 (2002).
95. H. Grady Hughes, "Improved Logic for Sampling Landau Straggling in MCNP5," American Nuclear Society 2005 Mathematics and Computation Topical Meeting, Los Alamos National Laboratory report LA-UR-05-4404 (2005).
96. M. E. Riley, C. J. MacCallum, and F. Biggs, "Theoretical Electron-Atom Elastic Scattering Cross Sections. Selected Elements, 1 keV to 256 keV," *Atom. Data and Nucl. Data Tables* **15** (1975) 443.
97. N. F. Mott, "The Scattering of Fast Electrons by Atomic Nuclei," *Proc. Roy. Soc. (London)* **A124** (1929) 425.
98. G. Moliere, "Theorie der Streuung schneller geladener Teilchen II: Mehrfach- und Vielfachstreuung," *Z. Naturforsch* **3a** (1948) 78.
99. H. A. Bethe and W. Heitler, "On Stopping of Fast Particles and on the Creation of Positive Electrons," *Proc. Roy. Soc. (London)* **A146** (1934) 83.
100. H. W. Koch and J. W. Motz, "Bremsstrahlung Cross-Section Formulas and Related Data," *Rev. Mod. Phys.* **31** (1959) 920.
101. Martin J. Berger and Stephen M. Seltzer, "Bremsstrahlung and Photoneutrons from Thick Tungsten and Tantalum Targets," *Phys. Rev.* **C2** (1970) 621.
102. R. H. Pratt, H. K. Tseng, C. M. Lee, L. Kissel, C. MacCallum, and M. Riley, "Bremsstrahlung Energy Spectra from Electrons of Kinetic Energy $1 \text{ keV} \leq T \leq 2000 \text{ keV}$ Incident on Neutral Atoms $2 < Z < 92$," *Atom. Data and Nuc. Data Tables* **20**, (1977) 175; errata in **26** (1981) 477.
103. H. K. Tseng and R. H. Pratt, "Exact Screened Calculations of Atomic-Field Bremsstrahlung," *Phys. Rev.* **A3** (1971) 100.
104. H. K. Tseng and R. H. Pratt, "Electron Bremsstrahlung from Neutral Atoms," *Phys. Rev. Lett.* **33** (1974) 516.
105. H. Davies, H. A. Bethe, and L. C. Maximom, "Theory of Bremsstrahlung and Pair Production. II. Integral Cross Section for Pair Production," *Phys. Rev.* **93** (1954) 788; and H. Olsen, "Outgoing and Ingoing Waves in Final States and Bremsstrahlung," *Phys. Rev.* **99** (1955) 1335.
106. G. Elwert, "Verschärte Berechnung von Intensität und Polarisation im Kontinuierlichen Röntgenspektrum," *Ann. Physik* **34** (1939) 178.
107. R. J. Jabbur and R. H. Pratt, "High-Frequency Region of the Spectrum of Electron and Positron Bremsstrahlung," *Phys. Rev.* **129** (1963) 184; and "High-Frequency Region of the Spectrum of Electron and Positron Bremsstrahlung II," *Phys. Rev.* **133** (1964) 1090.
108. J. H. Hubbell, W. J. Veigele, E. A. Briggs, R. T. Brown, D. T. Cromer, and R. J. Howerton, "Atomic Form Factors, Incoherent Scattering Functions, and Photon Scattering Cross Sections," *J. Phys. Chem. Ref. Data* **4** (1975) 471; and J. H. Hubbell and I. Overbo, "Relativistic Atomic Form Factors and Photon Coherent Scattering Cross sections," *J. Phys. Chem. Ref. Data* **8** (1979) 69.
109. H. K. Tseng and R. H. Pratt, "Electron Bremsstrahlung Energy Spectra Above 2 MeV," *Phys. Rev.* **A19** (1979) 1525.
110. E. Haug, "Bremsstrahlung and Pair Production in the field of free Electrons," *Z. Naturforsch.* **30a** (1975) 1099.

111. C. Møller, "Zur Theorie des Durchgang schneller Elektronen durch Materie," *Ann. Physik.* **14** (1932) 568.
112. D. P. Sloan, "A New Multigroup Monte Carlo Scattering Algorithm Suitable for Neutral and Charged-Particle Boltzmann and Fokker-Planck Calculations," Ph.D. dissertation, Sandia National Laboratories report SAND83-7094, (May 1983).
113. K. J. Adams and M. Hart, "Multigroup Boltzmann-Fokker-Planck Electron Transport Capability in MCNP," *Trans. Am. Nucl. Soc.*, **73**, 334 (1995).
114. G. I. Bell and S. Glasstone, *Nuclear Reactor Theory*, Krieger Publishing Company, Malabar, Florida, Chap. 1 (org. 1970, reprint 1985).
115. E. E. Lewis and W. F. Miller, Jr., *Computational Methods of Neutron Transport*, American Nuclear Society, Inc., La Grange Park, Illinois, Chap.1 (1993).
116. A. Dubi, "Monte Carlo Calculations for Nuclear Reactors," in *CRC Handbook of Nuclear Reactors Calculations*, Yigel Ronen, Ed., CRC Press, Inc., Boca Raton, Florida, Vol. II, Chap II (1986).
117. J. E. Stewart, "A General Point-on-a-Ring Detector," *Transactions of the American Nuclear Society*, **28**, 643 (1978).
118. R. A. Forster, "Ring Detector and Angle Biasing," Los Alamos Scientific Laboratory technical memorandum TD-6-8-79 (July 1979).
119. Edward C. Snow and John D. Court, "Radiography Image Detector Capability in MCNP4B," *Trans. Am. Nucl. Soc.* **79**, 99 (1998).
120. *MCNPX User's Manual*, Version 2.4.0, Los Alamos National Laboratory report LA-CP-02-408, September 2002.
121. S. P. Pederson, R. A. Forster, and T. E. Booth, "Confidence Interval Procedures for Monte Carlo Transport Simulations," *Nucl. Sci. Eng.* **127**, 54-77 (1997).
122. Guy Estes and Ed Cashwell, "MCNP1B Variance Error Estimator," TD-6-27-78(8/31/78).
123. A. Dubi, "On the Analysis of the Variance in Monte Carlo Calculations," *Nucl. Sci. Eng.*, **72**, 108 (1979). See also I. Lux, "On Efficient Estimation of Variances," *Nucl. Sci. Eng.*, **92**, 607 (1986).
124. Shane P. Pederson, "Mean Estimation in Highly Skewed Samples," Los Alamos National Laboratory Report LA-12114-MS (1991).
125. T. E. Booth, "Analytic Comparison of Monte Carlo Geometry Splitting and Exponential Transform," *Trans. Am. Nucl. Soc.*, **64**, 303 (1991).
126. T. E. Booth, "A Caution on Reliability Using "Optimal" Variance Reduction Parameters," *Trans. Am. Nucl. Soc.*, **66**, 278 (1991).
127. T. E. Booth, "Analytic Monte Carlo Score Distributions for Future Statistical Confidence Interval Studies," *Nucl. Sci. Eng.*, **112**, 159 (1992).
128. R. A. Forster, "A New Method of Assessing the Statistical Convergence of Monte Carlo Solutions," *Trans. Am. Nucl. Soc.*, **64**, 305 (1991).
129. R. A. Forster, S. P. Pederson, T. E. Booth, "Two Proposed Convergence Criteria for Monte Carlo Solutions," *Trans. Am. Nucl. Soc.*, **64**, 305 (1991).
130. J. R. M. Hosking and J. R. Wallis, "Parameter and Quantile Estimation for the Generalized Pareto Distribution," *Technometrics*, **29**, 339 (1987).
131. W. H. Press, B. P. Flannery, S. A. Teukolsky, and W. T. Vetterling, *Numerical Recipes: The Art of Scientific Computing (Fortran Version)*, Cambridge University Press (1990).
132. Malvin H. Kalos, Paula A Whitlock, *Monte Carlo Methods, Volume I: Basics*, John Wiley & Sons, New York, 1987.

133. T. E. Booth, "A Sample Problem for Variance Reduction in MCNP," Los Alamos National Laboratory report LA-10363-MS (June 1985).
134. R. A. Forster, R. C. Little, J. F. Briesmeister, and J. S. Hendricks, "MCNP Capabilities For Nuclear Well Logging Calculations," *IEEE Transactions on Nuclear Science*, **37** (3), 1378 (June 1990).
135. T. E. Booth and J. S. Hendricks, "Importance Estimation in Forward Monte Carlo Calculations," *Nucl. Tech./Fusion*, **5** (1984).
136. F. H. Clark, "The Exponential Transform as an Importance-Sampling Device, A Review," ORNL-RSIC-14 (January 1966).
137. P. K. Sarkar and M. A. Prasad, "Prediction of Statistical Error and Optimization of Biased Monte Carlo Transport Calculations," *Nucl. Sci. Eng.*, **70**, 243-261, (1979).
138. J. S. Hendricks, "Construction of Equiprobable Bins for Monte Carlo Calculation," *Trans. Am. Nucl. Soc.*, **35**, 247 (1980).
139. G. Bell and S. Glasstone, *Nuclear Reactor Theory*, Litton Educational Publishing, Inc., 1970.
140. T. J. Urbatsch, R. A. Forster, R. E. Prael, and R. J. Beckman, "Estimation and Interpretation of k_{eff} Confidence Intervals in MCNP," Los Alamos National Laboratory report LA-12658, (November 1995).
141. C. D. Harmon II, R. D. Busch, J. F. Briesmeister, and R. A. Forster, "Criticality Calculations with MCNP, A Primer," Nuclear Criticality Safety Group, University of New Mexico, Los Alamos National Laboratory, (December 1993).
142. F. B. Brown, "Fundamentals of Monte Carlo Particle Transport," Los Alamos National Laboratory report LA-UR-05-4983 (2005).
143. S. Nakamura, *Computational Methods in Engineering and Science*, R. E. Krieger Publishing Company, Malabar, FL (1986).
144. T. Ueki and F. B. Brown, "Stationarity Diagnostics Using Shannon Entropy in Monte Carlo Criticality Calculation I: F Test," *Trans. Am. Nuc.*, **87**, 156 (2002), and Los Alamos National Laboratory report LA-UR-02-3783 (2002).
145. T. Ueki and F. B. Brown, "Stationarity and Source Convergence Diagnostics in Monte Carlo Criticality Calculation," M&C 2003, ANS Topical Meeting, Gatlinburg, Tennessee (April 2003), and Los Alamos National Laboratory report LA-UR-02-6228 (2002).
146. E. M. Gelbard and R. Prael, "Computations of Standard Deviations in Eigenvalue Calculations," *Progress in Nuclear Energy*, **24**, p 237 (1990).
147. G. D. Spriggs, R. D. Busch, K. J. Adams, D. K. Parsons, L. Petrie, and J. S. Hendricks, "On the Definition of Neutron Lifetimes in Multiplying and Nonmultiplying Systems," Los Alamos National Laboratory Report, LA-13260-MS, (March 1997).
148. M. Halperin, "Almost Linearly-Optimum Combination of Unbiased Estimates," *Amer. Stat. Ass. J.*, **56**, 36-43 (1961).
149. R. C. Gast and N. R. Candelore, "The Recap-12 Monte Carlo Eigenfunction Strategy and Uncertainties," WAPD-TM-1127 (L) (1974).
150. S. S. Shapiro and M. B. Wilk, "An Analysis of Variance Test for Normality," *Biometrika*, **52**, p. 591 (1965).
151. R. B. D'Agostino, "An Omnibus Test of Normality for Moderate and Large Size Samples," *Biometrika*, **58**, p. 341 (1971).
152. L. L. Carter, T. L. Miles, and S. E. Binney, "Quantifying the Reliability of Uncertainty Predictions in Monte Carlo Fast Reactor Physics Calculations," *Nucl. Sci. Eng.*, **113**, p. 324 (1993).

153. K. M. Case, F. de Hoffmann, and G. Placzek, *Introduction to the Theory of Neutron Diffusion, Volume I*, Los Alamos Scientific Laboratory report (June 1953).
154. J. S. Hendricks, "Calculation of Cell Volumes and Surface Areas in MCNP," Los Alamos National Laboratory report LA-8113-MS (January 1980).
155. B. Spain, *Analytical Conics*, Pergamon, 1957.
156. J. S. Hendricks, "Effects of Changing the Random Number Stride in Monte Carlo Calculations," *Nucl. Sci. Eng.*, **109** (1) pp. 86-91 (September 1991).
157. J. E. Olhoeft, "The Doppler Effect for a Non-Uniform Temperature Distribution in Reactor Fuel Elements," WCAP-2048, Westinghouse Electric Corporation, Atomic Power Division, Pittsburgh (1962).
158. H. Takahashi, "Monte Carlo Method for Geometrical Perturbation and its Application to the Pulsed Fast Reactor," *Nucl. Sci. Eng.*, **41**, p. 259 (1970).
159. M. C. Hall, "Monte Carlo Perturbation Theory in Neutron Transport Calculations," Ph.D. Thesis, University of London (1980).
160. M. C. Hall, "Cross-Section Adjustment with Monte Carlo Sensitivities: Application to the Winfrith Iron Benchmark," *Nucl. Sci. Eng.* **81**, p. 423 (1982).
161. H. Rief, "Generalized Monte Carlo Perturbation Algorithms for Correlated Sampling and a Second-Order Taylor Series Approach," *Ann. Nucl. Energy* **11**, p. 455 (1984).
162. G. McKinney, "A Monte Carlo (MCNP) Sensitivity Code Development and Application," M. S. Thesis, University of Washington, (1984).
163. G. W. McKinney, "Theory Related to the Differential Operator Perturbation Technique," Los Alamos National Laboratory Memo, X-6:GWM-94-124 (1994).
164. A. K. Hess, L. L. Carter, J. S. Hendricks, and G. W. McKinney, "Verification of the MCNP Perturbation Correction Feature for Cross-Section Dependent Tallies," Los Alamos National Laboratory report LA-13520 (October 1998).
165. G. W. McKinney and J. L. Iverson, "Verification of the Monte Carlo Differential Operator Technique for MCNP," Los Alamos National Laboratory Report LA-13098, (February 1996).
166. J. A. Favorite and D. Kent Parsons, "Second-Order Cross Terms in Monte Carlo Differential Operator Perturbation Estimates," *Proceedings of International Conference, Mathematical Methods for Nuclear Applications*, Salt Lake City, Utah, September 9-13, 2001.
167. J. A. Favorite, "An Alternative Implementation of the Differential Operator (Taylor Series) Perturbation Method for Monte Carlo Criticality Problems," *Nucl. Sci. Eng.*, **142**, pp. 327-341 (2002).
168. F. B. Brown, "Random Number Generation with Arbitrary Strides," *Trans. Am. Nucl. Soc.* **71**, 202 (1994).
169. F. B. Brown and Y. Nagaya, "The MCNP5 Random Number Generator," *Trans. Am. Nucl. Soc.* **87**, 230-232 (2002).

APPENDIX G - MCNP DATA LIBRARIES

Appendix G is divided into eight sections. Section I lists some of the more frequently used ENDF/B reaction types that can be used with the FMn input card, Sections II through VII provide details about the data libraries available for use with MCNP, and Section VIII is a list of references. Information about any specific data library, as well as other useful information, can be found on the following Data Team web site: <http://www-xdiv.lanl.gov/PROJECTS/DATA/nuclear/nuclear.html>

	<u>Page</u>
I. ENDF/B Reaction Types	G-1
II. $S(\alpha, \beta)$ Data for Use with the MTm Card	G-5
III. Neutron Cross Section Libraries	G-9
IV. Multigroup Data	G-40
V. Photoatomic Data	G-43
VI. Photonuclear Data	G-58
VII. Dosimetry Data	G-60
VIII. References	G-74

I. ENDF/B REACTION TYPES

The following partial list includes some of the more useful reactions for use with the FMn input card and with the cross-section plotter (see pages 3-99 and B-14.) The complete ENDF/B list can be found in the ENDF/B manual.¹ The MT column lists the ENDF/B reaction number. The FM column lists special MCNP reaction numbers that can be used with the FM card and cross-section plotter.

The nomenclature between MCNP and ENDF/B is inconsistent in that MCNP often refers to the number of the reaction type as R whereas ENDF/B uses MT, but they are the same. The problem arises because MCNP has an MT input card used for the $S(\alpha, \beta)$ thermal treatment. However, the nomenclature between Monte Carlo transport and Deterministic transport techniques can be radically different. See Reference 2 on page G-74 for more information.

Generally only a subset of reactions is available for a particular nuclide. Some reaction data are eliminated by MCNP in cross-section processing if they are not required by the problem. Examples are photon production in a MODE N problem or certain reaction cross sections not requested on an FM card. FM numbers should be used when available rather than MT numbers. If an MT number is requested, the equivalent FM number will be displayed on the legend of cross-section plots.

Neutron Continuous-energy and Discrete Reactions:

<u>MT</u>	<u>FM</u>	<u>Microscopic Cross-Section Description</u>
1	-1	Total (see Note 1)
2	-3	Elastic (see Note 1)
16		(n,2n)
17		(n,3n)
18		Total fission (n,fx) if and only if MT=18 is used to specify fission in the original evaluation.
	-6	Total fission cross section. (equal to MT=18 if MT=18 exists; otherwise equal to the sum of MTs 19, 20, 21, and 38.)
19		(n,f)
20		(n,n'f)
21		(n,2nf)
22		(n,n'α)
28		(n,n'p)
32		(n,n'd)
33		(n,n't)
38		(n,3nf)
51		(n,n') to 1 st excited state
52		(n,n') to 2 nd excited state
.		.
90		(n,n') to 40 th excited state
91		(n,n') to continuum
101	-2	Absorption: sum of MT=102-117 (neutron disappearance; does not include fission)
102		(n,γ)
103		(n,p)
104		(n,d)
105		(n,t)
106		(n, ³ He)
107		(n,α)

In addition, the following special reactions are available for many nuclides:

202	-5	total photon production
203		total proton production (see Note 2)
204		total deuterium production (see Note 2)
205		total tritium production (see Note 2)
206		total ³ He production (see Note 2)
207		total alpha production (see Note 2)
301	-4	average heating numbers (MeV/collision)
	-7	nubar (prompt or total)
	-8	fission Q (in print table 98, but not plots)

S(α,β):

<u>MT</u>	<u>FM</u>	<u>Microscopic Cross-Section Description</u>
1		Total cross section
2		Elastic scattering cross-section
4		Inelastic scattering cross-section

Neutron and Photon Multigroup:

<u>MT</u>	<u>FM</u>	<u>Microscopic Cross-Section Description</u>
1	-1	Total cross section
18	-2	Fission cross section
	-3	Nubar data
	-4	Fission chi data
101	-5	Absorption cross section
	-6	Stopping powers
	-7	Momentum transfers
n		Edit reaction n
202		Photon production
301		Heating number
318		Fission Q
401		Heating number times total cross section

Photoatomic Data:

<u>MT</u>	<u>FM</u>	<u>Microscopic Cross-Section Description</u>
501	-5	Total
504	-1	Incoherent (Compton + Form Factor)
502	-2	Coherent (Thomson + Form Factor)
522	-3	Photoelectric with fluorescence
516	-4	Pair production
301	-6	Heating number

Electrons (see Note 3):

<u>MT</u>	<u>FM</u>	<u>Microscopic Cross-Section Description</u>
	1	de/dx electron collision stopping power
	2	de/dx electron radiative stopping power
	3	de/dx total electron stopping power
	4	electron range
	5	electron radiation yield
	6	relativistic β^2
	7	stopping power density correction
	8	ratio of rad/col stopping powers
	9	drange
	10	dyield

11	rng array values
12	qav array values
13	ear array values

Notes:

1. At the time they are loaded, the total and elastic cross sections from the data library are thermally adjusted by MCNP to the temperature of the problem, if that temperature is different from the temperature at which the cross-section set was processed (see page 2-29). If different cells have different temperatures, the cross sections first are adjusted to zero degrees and adjusted again to the appropriate cell temperatures during transport. The cross-section plot will *never* display the *transport* adjustment. Therefore, for plotting, reactions 1 and -1 are equivalent and reactions 2 and -3 are equivalent. But for the FM card, reactions -1 and -3 will use the zero degree data and reactions 1 and 2 will use the transport-adjusted data. For example, if a library evaluated at 300° is used in a problem with cells at 400° and 500°, the cross-section plotter and MT = -1 and MT = -3 options on the FM card will use 0° data. The MT = 1 and MT = 2 options on the FM card will use 400° and 500° data.
2. The user looking for total production of p, d, t, ³He and ⁴He should be warned that in some evaluations, such processes are represented using reactions with MT (or R) numbers other than the standard ones given in the above list. This is of particular importance with the so-called “pseudolevel” representation of certain reactions which take place in light isotopes. For example, the ENDF/B-V evaluation of carbon includes cross sections for the (n,n'³α) reaction in MT = 52 to 58. The user interested in particle production from light isotopes should check for the existence of pseudolevels and thus possible deviations from the above standard reaction list.
3. Two electron transport libraries, el and el03, are maintained. The electron transport algorithms and data in MCNP were adapted from the ITS code.³ The el library was developed and released in 1990 in conjunction with the addition of electron transport into MCNP4; the electron transport algorithms and data correspond (roughly) to that found in ITS version 1. The el03 library⁴ was developed and released in 2000 in conjunction with upgrades to the electron physics package; these upgrades correspond (roughly) to that of ITS version 3. The MT numbers for use in plotting the cross-section values for these tables should be taken from the Print Table 85 column headings and are not from ENDF.

II. S(α,β) DATA FOR USE WITH THE MTn CARD

Table G .1 lists all the S(α,β) data libraries that are maintained. The number(s) in parentheses following the description in words [Beryllium Metal (4009)] specify the nuclides for which the S(α,β) data are valid. For example, lwtr.01t provides scattering data only for ^1H ; ^{16}O would still be represented by the default free-gas treatment. The entries in each of the columns of Table G .1 are described as follows:

ZAID	The table identification to be specified on MTn cards. The portion of the ZAID before the decimal point provides a shorthand alphanumeric description of the material. The two digits after the decimal point differentiate among different tables for the same material. The final character in the ZAID is a "t" which indicates a thermal S(α,β) table.
Source	There are currently three evaluated sources of MCNP S(α,β) tables: (1) ENDF5—Indicates that the data were processed from evaluations distributed by the National Nuclear Data Center at Brookhaven National Laboratory as part of ENDF/B-V. Note that these evaluations were carried over from ENDF/B-III. ⁵ (2) LANL89—Initial work on cold moderator scattering data performed at Los Alamos National Laboratory. ^{6,7} (3) ENDF6.3—Indicates that the data were processed from evaluations distributed by the National Nuclear Data Center at Brookhaven National Laboratory as part of ENDF/B-VI, Release 3. ⁸
Library	Name of the library that contains the data table for this ZAID.
Date Processed	Date that the data table was processed by the NJOY code.
Temperature	The temperature of the data in degrees Kelvin.
Number of Angles	The number of equally-likely discrete secondary cosines provided at each combination of incident and secondary energy for inelastic scattering and for each incident energy for incoherent elastic scattering.
Number of Energies	The number of secondary energies provided for each incident energy for inelastic scattering.
Elastic Scattering Data	There are three options: (1) none—no elastic scattering data for this material. (2) coh—coherent elastic scattering data provided for this material (Bragg scattering). (3) inco—incoherent elastic scattering data provided for this material.

Table G .1
Thermal $S(\alpha,\beta)$ Cross-Section Libraries

<u>ZAID</u>	<u>Source</u>	<u>Library Name</u>	<u>Date of Processing</u>	<u>Temp (K)</u>	<u>Num of Angles</u>	<u>Num of Energies</u>	<u>Elastic Data</u>
Beryllium Metal (4009)							
be.01t	endf5	tmccs	10/24/85	300	8	20	coh
be.04t	endf5	tmccs	10/24/85	600	8	20	coh
be.05t	endf5	tmccs	10/24/85	800	8	20	coh
be.06t	endf5	tmccs	10/24/85	1200	8	20	coh
be.60t	endf6.3	sab2002	09/13/99	294	16	64	coh
be.61t	endf6.3	sab2002	09/13/99	400	16	64	coh
be.62t	endf6.3	sab2002	09/13/99	600	16	64	coh
be.63t	endf6.3	sab2002	09/14/99	800	16	64	coh
be.64t	endf6.3	sab2002	09/14/99	1000	16	64	coh
be.65t	endf6.3	sab2002	09/14/99	1200	16	64	coh
be.69t	endf6.3	sab2002	09/17/99	77	16	64	coh
Benzene (1001, 6000, 6012)							
benz.01t	endf5	tmccs	09/08/86	300	8	32	none
benz.02t	endf5	tmccs	09/08/86	400	8	32	none
benz.03t	endf5	tmccs	09/08/86	500	8	32	none
benz.04t	endf5	tmccs	09/08/86	600	8	32	none
benz.05t	endf5	tmccs	09/08/86	800	8	32	none
benz.60t	endf6.3	sab2002	09/14/99	294	16	64	none
benz.61t	endf6.3	sab2002	09/14/99	400	16	64	none
benz.62t	endf6.3	sab2002	09/14/99	600	16	64	none
benz.63t	endf6.3	sab2002	09/14/99	800	16	64	none
Beryllium Oxide (4009, 8016)							
beo.01t	endf5	tmccs	09/08/86	300	8	32	coh
beo.04t	endf5	tmccs	09/08/86	600	8	32	coh
beo.05t	endf5	tmccs	09/08/86	800	8	32	coh
beo.06t	endf5	tmccs	09/08/86	1200	8	32	coh
beo.60t	endf6.3	sab2002	09/14/99	294	16	64	coh
beo.61t	endf6.3	sab2002	09/14/99	400	16	64	coh
beo.62t	endf6.3	sab2002	09/14/99	600	16	64	coh
beo.63t	endf6.3	sab2002	09/14/99	800	16	64	coh
beo.64t	endf6.3	sab2002	09/14/99	1000	16	64	coh
beo.65t	endf6.3	sab2002	09/14/99	1200	16	64	coh
Ortho Deuterium (1002)							
dortho.01t	lanl89	therxs	05/30/89	20	8	8	none
dortho.60t	endf6.3	sab2002	09/16/99	19	16	64	none
Para Deuterium (1002)							
dpara.01t	lanl89	therxs	05/30/89	20	8	8	none
dpara.60t	endf6.3	sab2002	09/16/99	19	16	64	none

Table G.1 (Cont.)
Thermal S(α,β) Cross-Section Libraries

<u>ZAID</u>	<u>Source</u>	<u>Library Name</u>	<u>Date of Processing</u>	<u>Temp (K)</u>	<u>Num of Angles</u>	<u>Num of Energies</u>	<u>Elastic Data</u>
Graphite (6000, 6012)							
grph.01t	endf5	tmccs	09/08/86	300	8	32	coh
grph.04t	endf5	tmccs	09/08/86	600	8	32	coh
grph.05t	endf5	tmccs	09/08/86	800	8	32	coh
grph.06t	endf5	tmccs	09/08/86	1200	8	32	coh
grph.07t	endf5	tmccs	09/08/86	1600	8	32	coh
grph.08t	endf5	tmccs	09/08/86	2000	8	32	coh
grph.60t	endf6.3	sab2002	09/14/99	294	16	64	coh
grph.61t	endf6.3	sab2002	09/14/99	400	16	64	coh
grph.62t	endf6.3	sab2002	09/14/99	600	16	64	coh
grph.63t	endf6.3	sab2002	09/14/99	800	16	64	coh
grph.64t	endf6.3	sab2002	09/14/99	1000	16	64	coh
grph.65t	endf6.3	sab2002	09/14/99	1200	16	64	coh
Hydrogen in Zirconium Hydride (1001)							
h/zr.01t	endf5	tmccs	10/22/85	300	8	20	inco
h/zr.02t	endf5	tmccs	10/22/85	400	8	20	inco
h/zr.04t	endf5	tmccs	10/22/85	600	8	20	inco
h/zr.05t	endf5	tmccs	10/22/85	800	8	20	inco
h/zr.06t	endf5	tmccs	10/22/85	1200	8	20	inco
h/zr.60t	endf6.3	sab2002	09/14/99	294	16	64	inco
h/zr.61t	endf6.3	sab2002	09/14/99	400	16	64	inco
h/zr.62t	endf6.3	sab2002	09/14/99	600	16	64	inco
h/zr.63t	endf6.3	sab2002	09/14/99	800	16	64	inco
h/zr.64t	endf6.3	sab2002	09/14/99	1000	16	64	inco
h/zr.65t	endf6.3	sab2002	09/14/99	1200	16	64	inco
Ortho Hydrogen (1001)							
hortho.01t	lanl89	therxs	03/03/89	20	8	8	none
hortho.60t	endf6.3	sab2002	01/21/03	19	16	64	none
hortho.61t	endf6.3	sab2002	06/14/00	20	16	64	none
hortho.62t	endf6.3	sab2002	06/14/00	21	16	64	none
hortho.63t	endf6.3	sab2002	06/14/00	22	16	64	none
hortho.64t	endf6.3	sab2002	06/14/00	23	16	64	none
hortho.65t	endf6.3	sab2002	06/14/00	24	16	64	none
hortho.66t	endf6.3	sab2002	06/14/00	25	16	64	none

Table G .1 (Cont.)
Thermal $S(\alpha,\beta)$ Cross-Section Libraries

<u>ZAID</u>	<u>Source</u>	<u>Library Name</u>	<u>Date of Processing</u>	<u>Temp (K)</u>	<u>Num of Angles</u>	<u>Num of Energies</u>	<u>Elastic Data</u>
Para Hydrogen (1001)							
hpara.01t	lanl89	therxs	03/03/89	20	8	8	none
hpara.60t	endf6.3	sab2002	06/14/00	19	16	64	none
hpara.61t	endf6.3	sab2002	06/13/00	20	16	64	none
hpara.62t	endf6.3	sab2002	06/14/00	21	16	64	none
hpara.63t	endf6.3	sab2002	06/14/00	22	16	64	none
hpara.64t	endf6.3	sab2002	06/14/00	23	16	64	none
hpara.65t	endf6.3	sab2002	06/14/00	24	16	64	none
hpara.66t	endf6.3	sab2002	06/14/00	25	16	64	none
Deuterium in Heavy Water (1002)							
hwtr.01t	endf5	tmccs	10/22/85	300	8	20	none
hwtr.02t	endf5	tmccs	10/22/85	400	8	20	none
hwtr.03t	endf5	tmccs	10/22/85	500	8	20	none
hwtr.04t	endf5	tmccs	10/22/85	600	8	20	none
hwtr.05t	endf5	tmccs	10/22/85	800	8	20	none
hwtr.60t	endf6.3	sab2002	09/14/99	294	16	64	none
hwtr.61t	endf6.3	sab2002	01/20/03	400	16	64	none
hwtr.62t	endf6.3	sab2002	09/14/99	600	16	64	none
hwtr.63t	endf6.3	sab2002	09/14/99	800	16	64	none
hwtr.64t	endf6.3	sab2002	01/20/03	1000	16	64	none
Hydrogen in Liquid Methane (1001)							
lmeth.01t	lanl89	therxs	04/10/88	100	8	8	none
lmeth.60t	endf6.3	sab2002	09/17/99	100	16	64	none
Hydrogen in Light Water (1001)							
lwtr.01t	endf5	tmccs	10/22/85	300	8	20	none
lwtr.02t	endf5	tmccs	10/22/85	400	8	20	none
lwtr.03t	endf5	tmccs	10/22/85	500	8	20	none
lwtr.04t	endf5	tmccs	10/22/85	600	8	20	none
lwtr.05t	endf5	tmccs	10/22/85	800	8	20	none
lwtr.60t	endf6.3	sab2002	09/13/99	294	16	64	none
lwtr.61t	endf6.3	sab2002	09/13/99	400	16	64	none
lwtr.62t	endf6.3	sab2002	09/13/99	600	16	64	none
lwtr.63t	endf6.3	sab2002	09/13/99	800	16	64	none
lwtr.64t	endf6.3	sab2002	01/21/03	1000	16	64	none
Hydrogen in Polyethylene (1001)							
poly.01t	endf5	tmccs	10/22/85	300	8	20	inco
poly.60t	endf6.3	sab2002	09/14/99	294	16	64	inco
Hydrogen in Solid Methane (1001)							
smeth.01t	lanl89	therxs	04/10/88	22	8	8	inco
smeth.60t	endf6.3	sab2002	09/17/99	22	16	64	inco

Table G .1 (Cont.)
Thermal $S(\alpha,\beta)$ Cross-Section Libraries

<u>ZAID</u>	<u>Source</u>	<u>Library Name</u>	<u>Date of Processing</u>	<u>Temp (K)</u>	<u>Num of Angles</u>	<u>Num of Energies</u>	<u>Elastic Data</u>
Zirconium in Zirconium Hydride (40000, 40090, 40091, 40092, 40094, 40096)							
zr/h.01t	endf5	tmccs	09/08/86	300	8	32	inco
zr/h.02t	endf5	tmccs	09/08/86	400	8	32	inco
zr/h.04t	endf5	tmccs	09/08/86	600	8	32	inco
zr/h.05t	endf5	tmccs	09/08/86	800	8	32	inco
zr/h.06t	endf5	tmccs	09/08/86	1200	8	32	inco
zr/h.60t	endf6.3	sab2002	09/14/99	294	16	64	inco
zr/h.61t	endf6.3	sab2002	09/14/99	400	16	64	inco
zr/h.62t	endf6.3	sab2002	09/14/99	600	16	64	inco
zr/h.63t	endf6.3	sab2002	09/14/99	800	16	64	inco
zr/h.64t	endf6.3	sab2002	09/14/99	1000	16	64	inco
zr/h.65t	endf6.3	sab2002	09/14/99	1200	16	64	inco

III. NEUTRON CROSS-SECTION LIBRARIES

Table G .2 lists all the continuous-energy and discrete neutron data libraries that are maintained. **Not all libraries are publicly available.** The entries in each of the columns of Table G .2 are described as follows:

ZAID	<p>The nuclide identification number with the form ZZZAAA.nnX, where ZZZ is the atomic number</p> <p>AAA is the mass number (000 for elements)</p> <p>nn is the unique table identification number</p> <p>X = C for continuous-energy neutron tables</p> <p>X = D for discrete-reaction tables</p>
Atomic Weight Ratio	<p>The atomic weight ratio (AWR) is the ratio of the atomic mass of the nuclide to a neutron. This is the AWR that is contained in the original evaluation and that was used in the NJOY processing of the evaluation.</p>
Library	<p>Name of the library that contains the data file for that ZAID. The number in brackets following a file name refers to one of the special notes at the end of Table G .2.</p>
Source	<p>Indicates the originating evaluation for that data file.</p> <p>ENDF/B-V.# or ENDF/B-VI.# (such as B-V.0 and B-VI.1) are the Evaluated Nuclear Data Files, a US effort coordinated by the National Nuclear Data Center at Brookhaven National Laboratory. The evaluations are updated periodically by evaluators from all over the world, and the release number of the evaluation is given. This is not necessarily the same as the ENDF revision number for that evaluation.</p>

For example, Pu-243 is noted as ENDF/B-VI.2 as it was first released with Release 2 of ENDF/B-VI, but it is Revision 1 of that evaluation.

LLNL – evaluated nuclear data libraries compiled by the Nuclear Data Group at Lawrence Livermore National Laboratory. The number in the library name indicates the year the library was produced or received.

LANL – evaluations from the Nuclear Physics Group T-16 at Los Alamos National Laboratory.

:T or :X – the original evaluation has been modified by the Los Alamos National Laboratory Groups T-16 or X-5.

Evaluation Date	Denotes the year that the evaluation was completed or accepted. In cases where this information is not known, the date that the data library was produced is given. It is rare that a completely new evaluation is produced. Most often, only a section of an existing evaluation is updated, but a new evaluation date is assigned. This can be misleading for the users, and we encourage you to read the File 1 information for data tables important to your application to understand the history of a specific evaluation. This information is available from the Data Team's web site. The notation "<1985" means "before" 1985.
Temperature	<p>Indicates the temperature (°K) at which the data were processed. The temperature enters into the processing of the evaluation of a data file only through the Doppler broadening of cross sections. The user must be aware that without the proper use of the TMP card, MCNP will attempt to correct the data libraries to the default 300°K by modifying the elastic and total cross sections <i>only</i>.</p> <p>Doppler broadening refers to a change in cross section resulting from thermal motion (translation, rotation and vibration) of nuclei in a target material. Doppler broadening is done on all cross sections for incident neutrons (nonrelativistic energies) on a target at some temperature (Temp) in which the free-atom approximation is valid. In general an increase in the temperature of the material containing neutron-absorbing nuclei in a homogeneous system results in Doppler broadening of resonances and an increase in resonance absorption. Furthermore, a constant cross section at zero °K goes to 1/v behavior as the temperature increases. You should not only use the best evaluations but also use evaluations that are at temperatures approximating the temperatures in your application.</p>
Length	The total length of a particular cross-section file in words. It is understood that the actual storage requirement in an MCNP problem will often be less because certain data that are not needed for a problem may be expunged.
Number of Energies	The number of energy points (NE) on the grid used for the neutron cross section for that data file. In general, a finer energy grid (or greater

number of points) indicates a more accurate representation of the cross sections, particularly through the resonance region.

E_{max}	The maximum incident neutron energy for that data file. For all incident neutron energies greater than E_{max} , MCNP assumes the last cross-section value given.
GPD	“yes” means that photon-production data are included; “no” means that such data are not included.
\bar{v}	for fissionable material, \bar{v} indicates the type of fission nu data available. “pr” indicates that only prompt nu data are given; “tot” indicates that only total nu data are given; “both” indicates that prompt and total nu are given.
CP	“yes” indicates that secondary charged-particles data are present; “no” indicates that such data are not present.
DN	“yes” indicates that delayed neutron data are present; “no” indicates that such data are not present.
UR	“yes” indicates that unresolved resonance data are present; “no” indicates that such data are not present.

Numbers in brackets [] refer to notes on page G-39.

Table G.2 contains no indication of a “recommended” library for each isotope. Because of the wide variety of applications MCNP is used to simulate, no one data set is “best.” The default cross-section set for each isotope is determined by the XSDIR file being used (see page 2-18).

Finally, you can introduce a cross-section library of your own by using the XS input card.

APPENDIX G - MCNP DATA LIBRARIES
NEUTRON CROSS-SECTION LIBRARIES

Table G.2
Continuous-Energy and Discrete Neutron Data Libraries Maintained by X-5

<u>Z</u> <u>A</u> <u>I</u> <u>D</u>	<u>A</u> <u>W</u> <u>R</u>	<u>L</u> <u>i</u> <u>b</u> <u>r</u> <u>a</u> <u>r</u> <u>y</u> <u>N</u> <u>a</u> <u>m</u> <u>e</u>	<u>S</u> <u>o</u> <u>u</u> <u>r</u> <u>c</u> <u>e</u>	<u>E</u> <u>v</u> <u>a</u> <u>l</u> <u>D</u> <u>a</u> <u>t</u> <u>e</u>	<u>T</u> <u>e</u> <u>m</u> <u>p</u> <u>(</u> <u>°</u> <u>K</u> <u>)</u>	<u>L</u> <u>e</u> <u>n</u> <u>g</u> <u>t</u> <u>h</u> <u>w</u> <u>o</u> <u>r</u> <u>d</u> <u>s</u>	<u>N</u> <u>E</u>	<u>E</u> _{max} <u>(</u> <u>M</u> <u>e</u> <u>V</u> <u>)</u>	<u>G</u> <u>P</u> <u>D</u>	<u>U</u>	<u>C</u> <u>P</u>	<u>D</u> <u>N</u>	<u>U</u> <u>R</u>
Z = 1 ***** Hydrogen *****													
** H-1 **													
1001.24c	0.9991	la150n	B-VI.6	1998	293.6	10106	686	150.0	yes	no	yes	no	no
1001.42c	0.9992	endl92	LLNL	<1992	300.0	1968	121	30.0	yes	no	no	no	no
1001.50c	0.9992	rmccs	B-V.0	1977	293.6	2766	244	20.0	yes	no	no	no	no
1001.50d	0.9992	drmcscs	B-V.0	1977	293.6	3175	263	20.0	yes	no	no	no	no
1001.53c	0.9992	endl5mt[1]	B-V.0	1977	587.2	4001	394	20.0	yes	no	no	no	no
1001.60c	0.9992	endlf60	B-VI.1	1989	293.6	3484	357	100.0	yes	no	no	no	no
1001.62c	0.9992	actia	B-VI.8	1998	293.6	10128	688	150.0	yes	no	yes	no	no
1001.66c	0.9992	endlf66a	B-VI.6:X	1998	293.6	10128	688	150.0	yes	no	yes	no	no
** H-2 **													
1002.24c	1.9968	la150n	B-VI.6	1997	293.6	10270	538	150.0	yes	no	yes	no	no
1002.50c	1.9968	endlf5p	B-V.0	1967	293.6	3987	214	20.0	yes	no	no	no	no
1002.50d	1.9968	dre5	B-V.0	1967	293.6	4686	263	20.0	yes	no	no	no	no
1002.55c	1.9968	rmccs	LANL/T	1982	293.6	5981	285	20.0	yes	no	no	no	no
1002.55d	1.9968	drmcscs	LANL/T	1982	293.6	5343	263	20.0	yes	no	no	no	no
1002.60c	1.9968	endlf60	B-VI.0	1967[2]	293.6	2704	178	20.0	yes	no	no	no	no
1002.66c	1.9968	endlf66a	B-VI.6	1997	293.6	10270	538	150.0	yes	no	yes	no	no
** H-3 **													
1003.42c	2.9901	endl92	LLNL	<1992	300.0	2308	52	30.0	no	no	no	no	no
1003.50c	2.9901	rmccs	B-V.0	1965	293.6	2428	184	20.0	no	no	no	no	no
1003.50d	2.9901	drmcscs	B-V.0	1965	293.6	2807	263	20.0	no	no	no	no	no
1003.60c	2.9901	endlf60	B-VI.0	1965	293.6	3338	180	20.0	no	no	no	no	no
1003.66c	2.9901	endlf66a	B-VI.0	1965	293.6	5782	389	20.0	no	no	no	no	no
1003.69c	2.9896	t16_2003	LANL/T16	2001	293.6	11206	468	20.0	no	no	no	no	no
Z = 2 ***** Helium *****													
** He-3 **													
2003.42c	2.9901	endl92	LLNL	<1992	300.0	1477	151	30.0	yes	no	no	no	no
2003.50d	2.9901	drmcscs	B-V.0	1971	293.6	2612	263	20.0	no	no	no	no	no
2003.50c	2.9901	rmccs	B-V.0	1971	293.6	2320	229	20.0	no	no	no	no	no
2003.60c	2.9890	endlf60	B-VI.1	1990	293.6	2834	342	20.0	no	no	no	no	no
2003.66c	2.9890	endlf66a	B-VI.1	1990	293.6	9679	668	20.0	no	no	yes	no	no
** He-4 **													
2004.42c	3.9682	endl92	LLNL	<1992	300.0	1332	49	30.0	no	no	no	no	no
2004.50c	4.0015	rmccs	B-V.0	1973	293.6	3061	345	20.0	no	no	no	no	no
2004.50d	4.0015	drmcscs	B-V.0	1973	293.6	2651	263	20.0	no	no	no	no	no
2004.60c	4.0015	endlf60	B-VI.0	1973	293.6	2971	327	20.0	no	no	no	no	no
2004.62c	3.9682	actia	B-VI.8	1973	293.6	5524	588	20.0	no	no	no	no	no
2004.66c	3.9682	endlf66a	B-VI.0:X	1973	293.6	5524	588	20.0	no	no	no	no	no
Z = 3 ***** Lithium *****													
** Li-6 **													
3006.42c	5.9635	endl92	LLNL	<1992	300.0	7805	294	30.0	yes	no	no	no	no
3006.50c	5.9634	rmccs	B-V.0	1977	293.6	9932	373	20.0	yes	no	no	no	no
3006.50d	5.9634	drmcscs	B-V.0	1977	293.6	8716	263	20.0	yes	no	no	no	no
3006.60c	5.9634	endlf60	B-VI.1	1989	293.6	12385	498	20.0	yes	no	no	no	no
3006.66c	5.9634	endlf66a	B-VI.1	1989	293.6	28012	870	20.0	yes	no	no	no	no
** Li-7 **													
3007.42c	6.9557	endl92	LLNL	<1992	300.0	5834	141	30.0	yes	no	no	no	no
3007.50d	6.9557	dre5	B-V.0	1972	293.6	4935	263	20.0	yes	no	no	no	no
3007.50c	6.9557	endlf5p	B-V.0	1972	293.6	4864	343	20.0	yes	no	no	no	no
3007.55c	6.9557	rmccs	B-V.2	1979	293.6	13171	328	20.0	yes	no	no	no	no
3007.55d	6.9557	drmcscs	B-V.2	1979	293.6	12647	263	20.0	yes	no	no	no	no
3007.60c	6.9557	endlf60	B-VI.0	1988	293.6	14567	387	20.0	yes	no	no	no	no
3007.66c	6.9557	endlf66a	B-VI.0	1988	293.6	19559	677	20.0	yes	no	no	no	no

Table G.2 (Cont.)
Continuous-Energy and Discrete Neutron Data Libraries Maintained by X-5

<u>Z</u> <u>A</u> <u>I</u> <u>D</u>	<u>A</u> <u>W</u> <u>R</u>	<u>L</u> <u>i</u> <u>b</u> <u>r</u> <u>a</u> <u>r</u> <u>y</u> <u>N</u> <u>a</u> <u>m</u> <u>e</u>	<u>S</u> <u>o</u> <u>u</u> <u>r</u> <u>c</u> <u>e</u>	<u>E</u> <u>v</u> <u>a</u> <u>l</u> <u>D</u> <u>a</u> <u>t</u> <u>e</u>	<u>T</u> <u>e</u> <u>m</u> <u>p</u> <u>(</u> <u>°</u> <u>K</u> <u>)</u>	<u>L</u> <u>e</u> <u>n</u> <u>g</u> <u>t</u> <u>h</u> <u>w</u> <u>o</u> <u>r</u> <u>d</u> <u>s</u>	<u>N</u> <u>E</u>	<u>E</u> _{max} <u>(</u> <u>M</u> <u>e</u> <u>V</u> <u>)</u>	<u>G</u> <u>P</u> <u>D</u>	<u>U</u>	<u>C</u> <u>P</u>	<u>D</u> <u>N</u>	<u>U</u> <u>R</u>
Z = 4 ***** Beryllium *****													
** Be-7 **													
4007.42c	6.9567	endl92	LLNL	<1992	300.0	1544	127	30.0	yes	no	no	no	no
** Be-9 **													
4009.21c	8.9348	100xs[3]	LANL/T:X	1989	300.0	28964	316	100.0	yes	no	no	no	no
4009.24c	8.9347	la150n	LANL	1989	293.6	68468	619	100.0	yes	no	yes	no	no
4009.50c	8.9348	rmccs	B-V.0	1976	293.6	8886	329	20.0	yes	no	no	no	no
4009.50d	8.9348	drmcscs	B-V.0	1976	293.6	8756	263	20.0	yes	no	no	no	no
4009.60c	8.9348	endf60	B-VI.0	1986	293.6	64410	276	20.0	yes	no	no	no	no
4009.62c	8.9348	actia	B-VI.8	2000	293.6	115407	514	20.0	yes	no	yes	no	no
4009.66c	8.9348	endf66a	B-VI.0	1986	293.6	113907	538	20.0	yes	no	yes	no	no
Z = 5 ***** Boron *****													
** B-10 **													
5010.42c	9.9269	endl92	LLNL	<1992	300.0	4733	175	30.0	yes	no	no	no	no
5010.50d	9.9269	drmcscs	B-V.0	1977	293.6	12322	263	20.0	yes	no	no	no	no
5010.50c	9.9269	rmccs	B-V.0	1977	293.6	20200	514	20.0	yes	no	no	no	no
5010.53c	9.9269	endf5mt[1]	B-V.0	1977	587.2	23676	700	20.0	yes	no	no	no	no
5010.60c	9.9269	endf60	B-VI.1	1989	293.6	27957	673	20.0	yes	no	no	no	no
5010.66c	9.9269	endf66a	B-VI.1	1989	293.6	51569	1035	20.0	yes	no	no	no	no
** B-11 **													
5011.42c	10.9147	endl92	LLNL	<1992	300.0	4285	244	30.0	yes	no	no	no	no
5011.50d	10.9150	dre5	B-V.0	1974	293.6	2812	263	20.0	no	no	no	no	no
5011.50c	10.9150	endf5p	B-V.0	1974	293.6	4344	487	20.0	no	no	no	no	no
5011.55d	10.9150	drmcscs	B-V.0:T	1971[4]	293.6	7106	263	20.0	yes	no	no	no	no
5011.55c	10.9150	rmccsa	B-V.0:T	1971[4]	293.6	12254	860	20.0	yes	no	no	no	no
5011.56d	10.9147	newxsd	LANL/T	1986	293.6	17348	263	20.0	yes	no	no	no	no
5011.56c	10.9147	newxs	LANL/T	1986	293.6	56929	1762	20.0	yes	no	no	no	no
5011.60c	10.9147	endf60	B-VI.0	1989	293.6	108351	2969	20.0	yes	no	no	no	no
5011.66c	10.9147	endf66a	B-VI.0:X	1989	293.6	149785	3442	20.0	yes	no	yes	no	no
Z = 6 ***** Carbon *****													
** C-nat**													
6000.24c	11.8980	la150n	B-VI.6	1996	293.6	79070	1267	150.0	yes	no	yes	no	no
6000.50d	11.8969	drmcscs	B-V.0	1977	293.6	16844	263	20.0	yes	no	no	no	no
6000.50c	11.8969	rmccs	B-V.0	1977	293.6	23326	875	20.0	yes	no	no	no	no
6000.60c	11.8980	endf60	B-VI.1	1989	293.6	22422	978	32.0	yes	no	no	no	no
6000.66c	11.8980	endf66a	B-VI.6	1989	293.6	79070	1267	150.0	yes	no	yes	no	no
** C-12 **													
6012.21c	11.8969	100xs[3]	LANL/T:X	1989	300.0	28809	919	100.0	yes	no	no	no	no
6012.42c	11.8969	endl92	LLNL	<1992	300.0	6229	191	30.0	yes	no	no	no	no
6012.50d	11.8969	drmcscs[5]	B-V.0	1977	293.6	16844	263	20.0	yes	no	no	no	no
6012.50c	11.8969	rmccs[5]	B-V.0	1977	293.6	23326	875	20.0	yes	no	no	no	no
** C-13 **													
6013.42c	12.8916	endl92	LLNL	<1992	300.0	5993	429	30.0	yes	no	no	no	no
Z = 7 ***** Nitrogen *****													
** N-14 **													
7014.24c	13.8827	la150n	B-VI.6	1997	293.6	144740	1824	150.0	yes	no	yes	no	no
7014.42c	13.8828	endl92	LLNL	<1992	300.0	20528	770	30.0	yes	no	no	no	no
7014.50c	13.8830	rmccs	B-V.0	1973	293.6	45457	1196	20.0	yes	no	no	no	no
7014.50d	13.8830	drmcscs	B-V.0	1973	293.6	26793	263	20.0	yes	no	no	no	no
7014.60c	13.8828	endf60	LANL/T	1992	293.6	60397	1379	20.0	yes	no	no	no	no
7014.62c	13.8828	actia	B-VI.8	2000	293.6	145340	1824	150.0	yes	no	yes	no	no
7014.66c	13.8828	endf66a	B-VI.6	1997	293.6	144740	1824	150.0	yes	no	yes	no	no

Table G.2 (Cont.)
Continuous-Energy and Discrete Neutron Data Libraries Maintained by X-5

<u>Z</u> <u>A</u> <u>I</u> <u>D</u>	<u>A</u> <u>W</u> <u>R</u>	<u>Library</u> <u>Name</u>	<u>Source</u>	<u>Eval</u> <u>Date</u>	<u>Temp</u> <u>(°K)</u>	<u>Length</u> <u>words</u>	<u>NE</u>	<u>E_{max}</u> <u>(MeV)</u>	<u>GPD</u>	<u>U</u>	<u>CP</u>	<u>DN</u>	<u>UR</u>
** N-15 **													
7015.42c	14.8713	endl92	LLNL	<1992	300.0	22590	352	30.0	yes	no	no	no	no
7015.55c	14.8710	rmccsa	LANL/T	1983	293.6	20920	744	20.0	yes	no	no	no	no
7015.55d	14.8710	drmcsc	LANL/T	1983	293.6	15273	263	20.0	yes	no	no	no	no
7015.60c	14.8710	endf60	B-VI.0	1993	293.6	24410	653	20.0	yes	no	no	no	no
7015.66c	14.8710	endf66a	B-VI.0	1993	293.6	31755	880	20.0	yes	no	no	no	no
Z = 8 ***** Oxygen *****													
** O-16 **													
8016.21c	15.8575	100xs[3]	LANL/T:X	1989	300.0	45016	1427	100.0	yes	no	no	no	no
8016.24c	15.8531	la150n	B-VI.6	1996	293.6	164461	1935	150.0	yes	no	yes	no	no
8016.42c	15.8575	endl92	LLNL	<1992	300.0	9551	337	30.0	yes	no	no	no	no
8016.50c	15.8580	rmccs	B-V.0	1972	293.6	37942	1391	20.0	yes	no	no	no	no
8016.50d	15.8580	drmcsc	B-V.0	1972	293.6	20455	263	20.0	yes	no	no	no	no
8016.53c	15.8580	endf5mt[1]	B-V.0	1972	587.2	37989	1398	20.0	yes	no	no	no	no
8016.54c	15.8580	endf5mt[1]	B-V.0	1972	880.8	38017	1402	20.0	yes	no	no	no	no
8016.60c	15.8532	endf60	B-VI.0	1990	293.6	58253	1609	20.0	yes	no	no	no	no
8016.62c	15.8575	actia	B-VI.8	2000	293.6	407432	2759	150.0	yes	no	yes	no	no
8016.66c	15.8532	endf66a	B-VI.6	1996	293.6	164461	1935	150.0	yes	no	yes	no	no
** O-17 **													
8017.60c	16.8531	endf60	B-VI.0	1978	293.6	4200	335	20.0	no	no	no	no	no
8017.66c	16.8531	endf66a	B-VI.0	1978	293.6	8097	612	20.0	no	no	no	no	no
Z = 9 ***** Fluorine *****													
** F-19 **													
9019.42c	18.8352	endl92	LLNL	<1992	300.0	37814	1118	30.0	yes	no	no	no	no
9019.50c	18.8350	endf5p	B-V.0	1976	293.6	44130	1569	20.0	yes	no	no	no	no
9019.50d	18.8350	dre5	B-V.0	1976	293.6	23156	263	20.0	yes	no	no	no	no
9019.51d	18.8350	drmcsc	B-V.0	1976	293.6	23156	263	20.0	yes	no	no	no	no
9019.51c	18.8350	rmccs	B-V.0	1976	293.6	41442	1541	20.0	yes	no	no	no	no
9019.60c	18.8350	endf60	B-VI.0	1990	300.0	93826	1433	20.0	yes	no	no	no	no
9019.62c	18.8350	actia	B-VI.8	2000	293.6	127005	1888	20.0	yes	no	yes	no	no
9019.66c	18.8350	endf66a	B-VI.0:X	1990	293.6	122324	1870	20.0	yes	no	yes	no	no
Z = 10 ***** Neon *****													
** Ne-20 **													
10020.42c	19.8207	endl92	LLNL	<1992	300.0	14286	1011	30.0	yes	no	no	no	no
Z = 11 ***** Sodium *****													
** Na-23 **													
11023.42c	22.7923	endl92	LLNL	<1992	300.0	19309	1163	30.0	yes	no	no	no	no
11023.50c	22.7920	endf5p	B-V.0	1977	293.6	52252	2703	20.0	yes	no	no	no	no
11023.50d	22.7920	dre5	B-V.0	1977	293.6	41665	263	20.0	yes	no	no	no	no
11023.51d	22.7920	drmcsc	B-V.0	1977	293.6	41665	263	20.0	yes	no	no	no	no
11023.51c	22.7920	rmccs	B-V.0	1977	293.6	48863	2228	20.0	yes	no	no	no	no
11023.60c	22.7920	endf60	B-VI.1	1977	293.6	50294	2543	20.0	yes	no	no	no	no
11023.62c	22.7920	actia	B-VI.8	2000	293.6	69562	3239	20.0	yes	no	no	no	no
11023.66c	22.7920	endf66a	B-VI.1	1977	293.6	64249	3239	20.0	yes	no	no	no	no

Table G.2 (Cont.)
Continuous-Energy and Discrete Neutron Data Libraries Maintained by X-5

<u>Z</u> <u>A</u> <u>I</u> <u>D</u>	<u>A</u> <u>W</u> <u>R</u>	<u>L</u> <u>i</u> <u>b</u> <u>r</u> <u>a</u> <u>r</u> <u>y</u> <u>N</u> <u>a</u> <u>m</u> <u>e</u>	<u>S</u> <u>o</u> <u>u</u> <u>r</u> <u>c</u> <u>e</u>	<u>E</u> <u>v</u> <u>a</u> <u>l</u> <u>D</u> <u>a</u> <u>t</u> <u>e</u>	<u>T</u> <u>e</u> <u>m</u> <u>p</u> <u>(</u> <u>°</u> <u>K</u> <u>)</u>	<u>L</u> <u>e</u> <u>n</u> <u>g</u> <u>t</u> <u>h</u> <u>w</u> <u>o</u> <u>r</u> <u>d</u> <u>s</u>	<u>N</u> <u>E</u>	<u>E</u> _{max} <u>(</u> <u>M</u> <u>e</u> <u>V</u> <u>)</u>	<u>G</u> <u>P</u> <u>D</u>	<u>U</u>	<u>C</u> <u>P</u>	<u>D</u> <u>N</u>	<u>U</u> <u>R</u>
Z = 12 ***** Magnesium *****													
** Mg-nat**													
12000.42c	24.0962	endl92	LLNL	<1992	300.0	9288	468	30.0	yes	no	no	no	no
12000.50d	24.0963	dre5	B-V.0	1978	293.6	14070	263	20.0	yes	no	no	no	no
12000.50c	24.0963	endf5u	B-V.0	1978	293.6	56334	2430	20.0	yes	no	no	no	no
12000.51c	24.0963	rmccs	B-V.0	1978	293.6	48917	1928	20.0	yes	no	no	no	no
12000.51d	24.0963	drnccs	B-V.0	1978	293.6	14070	263	20.0	yes	no	no	no	no
12000.60c	24.0963	endf60	B-VI.0	1978	293.6	55776	2525	20.0	yes	no	no	no	no
12000.61c	24.0963	actib	B-VI.8	2000	77.0	69108	3213	20.0	yes	no	no	no	no
12000.62c	24.0963	actia	B-VI.8	2000	293.6	68746	3172	20.0	yes	no	no	no	no
12000.64c	24.0963	endf66d	B-VI.0	1978	77.0	67880	3213	20.0	yes	no	no	no	no
12000.66c	24.0963	endf66a	B-VI.0	1978	293.6	67511	3172	20.0	yes	no	no	no	no
Z = 13 ***** Aluminum *****													
** Al-27 **													
13027.21c	26.7498	100xs[3]	LANL/T:X	1989	300.0	35022	1473	100.0	yes	no	no	no	no
13027.24c	26.7497	la150n	B-VI.6	1997	293.6	214549	3148	150.0	yes	no	yes	no	no
13027.42c	26.7498	endl92	LLNL	<1992	300.0	32388	1645	30.0	yes	no	no	no	no
13027.50d	26.7500	drnccs	B-V.0	1973	293.6	41947	263	20.0	yes	no	no	no	no
13027.50c	26.7500	rmccs	B-V.0	1973	293.6	54162	2028	20.0	yes	no	no	no	no
13027.60c	26.7500	endf60	B-VI.0	1973	293.6	55427	2241	20.0	yes	no	no	no	no
13027.61c	26.7497	actib	B-VI.8	2000	77.0	220073	3038	150.0	yes	no	yes	no	no
13027.62c	26.7497	actia	B-VI.8	2000	293.6	220418	3081	150.0	yes	no	yes	no	no
13027.64c	26.7497	endf66d	B-VI.6	1997	77.0	213659	3037	150.0	yes	no	yes	no	no
13027.66c	26.7497	endf66a	B-VI.6	1997	293.6	214004	3036	150.0	yes	no	yes	no	no
13027.91c	26.7497	actib[6]	B-VI.8	2000	77.0	220104	3038	150.0	yes	no	yes	no	no
13027.92c	26.7497	actia[6]	B-VI.8	2000	293.6	220449	3081	150.0	yes	no	yes	no	no
Z = 14 ***** Silicon *****													
** Si-nat**													
14000.21c	27.8440	100xs[3]	LANL/T:X	1989	300.0	76399	2883	100.0	yes	no	no	no	no
14000.42c	27.8442	endl92	LLNL	<1992	300.0	16696	855	30.0	yes	no	no	no	no
14000.50c	27.8440	endf5p	B-V.0	1976	293.6	98609	2440	20.0	yes	no	no	no	no
14000.50d	27.8440	dre5	B-V.0	1976	293.6	69498	263	20.0	yes	no	no	no	no
14000.51c	27.8440	rmccs	B-V.0	1976	293.6	88129	1887	20.0	yes	no	no	no	no
14000.51d	27.8440	drnccs	B-V.0	1976	293.6	69498	263	20.0	yes	no	no	no	no
14000.60c	27.8440	endf60	B-VI.0	1976	293.6	104198	2824	20.0	yes	no	no	no	no
** Si-28 **													
14028.24c	27.7370	la150n	LANL	1997	293.6	264892	7417	150.0	yes	no	yes	no	no
14028.61c	27.7370	actib	B-VI.6	1997	77.0	264592	7472	150.0	yes	no	yes	no	no
14028.62c	27.7370	actia	B-VI.6	1997	293.6	263728	7364	150.0	yes	no	yes	no	no
14028.64c	27.7370	endf66d	B-VI.6	1997	77.0	264592	7472	150.0	yes	no	yes	no	no
14028.66c	27.7370	endf66a	B-VI.6	1997	293.6	263728	7364	150.0	yes	no	yes	no	no
** Si-29 **													
14029.24c	28.7280	la150n	B-VI.6	1997	293.6	252663	4878	150.0	yes	no	yes	no	no
14029.61c	28.7280	actib	B-VI.8	1999	77.0	252671	4879	150.0	yes	no	yes	no	no
14029.62c	28.7280	actia	B-VI.8	1999	293.6	252591	4869	150.0	yes	no	yes	no	no
14029.64c	28.7280	endf66d	B-VI.6	1997	77.0	252791	4894	150.0	yes	no	yes	no	no
14029.66c	28.7280	endf66a	B-VI.6	1997	293.6	252615	4872	150.0	yes	no	yes	no	no
** Si-30 **													
14030.24c	29.7160	la150n	B-VI.6	1997	293.6	195933	5791	150.0	yes	no	yes	no	no
14030.61c	29.7160	actib	B-VI.6	1997	77.0	196252	5831	150.0	yes	no	yes	no	no
14030.62c	29.7160	actia	B-VI.6	1997	293.6	195852	5781	150.0	yes	no	yes	no	no
14030.64c	29.7160	endf66d	B-VI.6	1997	77.0	196252	5831	150.0	yes	no	yes	no	no
14030.66c	29.7160	endf66a	B-VI.6	1997	293.6	195852	5781	150.0	yes	no	yes	no	no

Table G.2 (Cont.)
Continuous-Energy and Discrete Neutron Data Libraries Maintained by X-5

<u>Z</u> <u>A</u> <u>I</u> <u>D</u>	<u>A</u> <u>W</u> <u>R</u>	<u>L</u> <u>i</u> <u>b</u> <u>r</u> <u>a</u> <u>r</u> <u>y</u> <u>N</u> <u>a</u> <u>m</u> <u>e</u>	<u>S</u> <u>o</u> <u>u</u> <u>r</u> <u>c</u> <u>e</u>	<u>E</u> <u>v</u> <u>a</u> <u>l</u> <u>D</u> <u>a</u> <u>t</u> <u>e</u>	<u>T</u> <u>e</u> <u>m</u> <u>p</u> <u>(</u> <u>°</u> <u>K</u> <u>)</u>	<u>L</u> <u>e</u> <u>n</u> <u>g</u> <u>t</u> <u>h</u> <u>w</u> <u>o</u> <u>r</u> <u>d</u> <u>s</u>	<u>N</u> <u>E</u>	<u>E</u> _{max} <u>(</u> <u>M</u> <u>e</u> <u>V</u> <u>)</u>	<u>G</u> <u>P</u> <u>D</u>	<u>U</u>	<u>C</u> <u>P</u>	<u>D</u> <u>N</u>	<u>U</u> <u>R</u>
Z = 15 ***** Phosphorus *****													
** P-31 **													
15031.24c	30.7080	la150n	B-VI.6	1997	293.6	71942	990	150.0	yes	no	yes	no	no
15031.42c	30.7077	endl92	LLNL	<1992	300.0	6805	224	30.0	yes	no	no	no	no
15031.50c	30.7080	endf5u	B-V.0	1977	293.6	5733	326	20.0	yes	no	no	no	no
15031.50d	30.7080	dre5	B-V.0	1977	293.6	5761	263	20.0	yes	no	no	no	no
15031.51d	30.7080	drmcsc	B-V.0	1977	293.6	5761	263	20.0	yes	no	no	no	no
15031.51c	30.7080	rmccs	B-V.0	1977	293.6	5732	326	20.0	yes	no	no	no	no
15031.60c	30.7080	endf60	B-VI.0	1977	293.6	6715	297	20.0	yes	no	no	no	no
15031.66c	30.7080	endf66a	B-VI.6	1997	293.6	71942	990	150.0	yes	no	yes	no	no
Z = 16 ***** Sulfur *****													
** S-nat**													
16000.60c	31.7882	endf60	B-VI.0	1979	293.6	108683	8382	20.0	yes	no	no	no	no
16000.61c	31.7888	actib	B-VI.8	2000	77.0	162749	10459	20.0	yes	no	no	no	no
16000.62c	31.7888	actia	B-VI.8	2000	293.6	160505	10272	20.0	yes	no	no	no	no
16000.64c	31.7882	endf66d	B-VI.0	1979	77.0	162138	10460	20.0	yes	no	no	no	no
16000.66c	31.7882	endf66a	B-VI.0	1979	293.6	159894	10273	20.0	yes	no	no	no	no
** S-32 **													
16032.42c	31.6974	endl92	LLNL	<1992	300.0	6623	307	30.0	yes	no	no	no	no
16032.50c	31.6970	endf5u	B-V.0	1977	293.6	6789	363	20.0	yes	no	no	no	no
16032.50d	31.6970	dre5	B-V.0	1977	293.6	6302	263	20.0	yes	no	no	no	no
16032.51c	31.6970	rmccs	B-V.0	1977	293.6	6780	362	20.0	yes	no	no	no	no
16032.51d	31.6970	drmcsc	B-V.0	1977	293.6	6302	263	20.0	yes	no	no	no	no
16032.60c	31.6970	endf60	B-VI.0	1977	293.6	7025	377	20.0	yes	no	no	no	no
16032.61c	31.6970	actib	B-VI.8	2000	77.0	14930	885	20.0	yes	no	no	no	no
16032.62c	31.6970	actia	B-VI.8	2000	293.6	16050	993	20.0	yes	no	no	no	no
16032.64c	31.6970	endf66d	B-VI.0	1977	77.0	12714	885	20.0	yes	no	no	no	no
16032.66c	31.6970	endf66a	B-VI.0	1977	293.6	13834	993	20.0	yes	no	no	no	no
Z = 17 ***** Chlorine *****													
** Cl-nat**													
17000.42c	35.1484	endl92	LLNL	<1992	300.0	12012	807	30.0	yes	no	no	no	no
17000.50d	35.1480	dre5	B-V.0	1967	293.6	18209	263	20.0	yes	no	no	no	no
17000.50c	35.1480	endf5p	B-V.0	1967	293.6	23313	1499	20.0	yes	no	no	no	no
17000.51c	35.1480	rmccs	B-V.0	1967	293.6	21084	1375	20.0	yes	no	no	no	no
17000.51d	35.1480	drmcsc	B-V.0	1967	293.6	18209	263	20.0	yes	no	no	no	no
17000.60c	35.1480	endf60	B-VI.0	1967	293.6	24090	1816	20.0	yes	no	no	no	no
17000.64c	35.1480	endf66d	B-VI.0	1967	77.0	44517	2799	20.0	yes	no	no	no	no
17000.66c	35.1480	endf66a	B-VI.0	1967	293.6	45407	2888	20.0	yes	no	no	no	no
** Cl-35 **													
17035.61c	34.6684	actib	B-VI.8	2000	77.0	316441	7217	20.0	yes	no	yes	no	no
17035.62c	34.6684	actia	B-VI.8	2000	293.6	311841	6987	20.0	yes	no	yes	no	no
** Cl-37 **													
17037.61c	36.6483	actib	B-VI.8	2000	77.0	137963	3495	20.0	yes	no	yes	no	no
17037.62c	36.6483	actia	B-VI.8	2000	293.6	137404	3425	20.0	yes	no	yes	no	no
Z = 18 ***** Argon *****													
** Ar-nat**													
18000.35c	39.6048	rmccsa	LLNL	<1985	0.0	5585	259	20.0	yes	no	no	no	no
18000.35d	39.6048	drmcsc	LLNL	<1985	0.0	14703	263	20.0	yes	no	no	no	no
18000.42c	39.6048	endl92	LLNL	<1992	300.0	5580	152	30.0	yes	no	no	no	no
18000.59c	39.6048	misc5xs[7,8]	LANL/T	1982	293.6	3473	252	20.0	yes	no	no	no	no

Table G.2 (Cont.)
Continuous-Energy and Discrete Neutron Data Libraries Maintained by X-5

<u>Z</u> <u>A</u> <u>I</u> <u>D</u>	<u>A</u> <u>W</u> <u>R</u>	<u>L</u> <u>i</u> <u>b</u> <u>r</u> <u>a</u> <u>r</u> <u>y</u> <u>N</u> <u>a</u> <u>m</u> <u>e</u>	<u>S</u> <u>o</u> <u>u</u> <u>r</u> <u>c</u> <u>e</u>	<u>E</u> <u>v</u> <u>a</u> <u>l</u> <u>D</u> <u>a</u> <u>t</u> <u>e</u>	<u>T</u> <u>e</u> <u>m</u> <u>p</u> <u>(</u> <u>°</u> <u>K</u> <u>)</u>	<u>L</u> <u>e</u> <u>n</u> <u>g</u> <u>t</u> <u>h</u> <u>w</u> <u>o</u> <u>r</u> <u>d</u> <u>s</u>	<u>N</u> <u>E</u>	<u>E</u> _{max} <u>(</u> <u>M</u> <u>e</u> <u>V</u> <u>)</u>	<u>G</u> <u>P</u> <u>D</u>	<u>U</u>	<u>C</u> <u>P</u>	<u>D</u> <u>N</u>	<u>U</u> <u>R</u>
Z = 19 ***** Potassium *****													
** K-nat**													
19000.42c	38.7624	endl92	LLNL	<1992	300.0	11060	544	30.0	yes	no	no	no	no
19000.50c	38.7660	endf5u	B-V.0	1974	293.6	22051	1243	20.0	yes	no	no	no	no
19000.50d	38.7660	dre5	B-V.0	1974	293.6	23137	263	20.0	yes	no	no	no	no
19000.51d	38.7660	drmcscs	B-V.0	1974	293.6	23137	263	20.0	yes	no	no	no	no
19000.51c	38.7660	rmccs	B-V.0	1974	293.6	18798	1046	20.0	yes	no	no	no	no
19000.60c	38.7660	endf60	B-VI.0	1974	293.6	24482	1767	20.0	yes	no	no	no	no
19000.62c	38.7660	actia	B-VI.8	2000	293.6	52304	2734	20.0	yes	no	no	no	no
19000.66c	38.7660	endf66a	B-VI.0	1974	293.6	51384	2734	20.0	yes	no	no	no	no
Z = 20 ***** Calcium *****													
** Ca-nat**													
20000.24c	39.7360	la150n	B-VI.6	1997	293.6	187818	4470	150.0	yes	no	yes	no	no
20000.42c	39.7357	endl92	LLNL	<1992	300.0	13946	1002	30.0	yes	no	no	no	no
20000.50c	39.7360	endf5u	B-V.0	1976	293.6	62624	2394	20.0	yes	no	no	no	no
20000.50d	39.7360	dre5	B-V.0	1976	293.6	29033	263	20.0	yes	no	no	no	no
20000.51d	39.7360	drmcscs	B-V.0	1976	293.6	29033	263	20.0	yes	no	no	no	no
20000.51c	39.7360	rmccs	B-V.0	1976	293.6	53372	1796	20.0	yes	no	no	no	no
20000.60c	39.7360	endf60	B-VI.0	1980	293.6	76468	2704	20.0	yes	no	no	no	no
20000.61c	39.7360	actib	B-VI.8	2000	77.0	185636	4178	150.0	yes	no	yes	no	no
20000.62c	39.7360	actia	B-VI.8	2000	293.6	187296	4344	150.0	yes	no	yes	no	no
20000.64c	39.7360	endf66d	B-VI.6	1997	77.0	184909	4179	150.0	yes	no	yes	no	no
20000.66c	39.7360	endf66a	B-VI.6	1997	293.6	186569	4345	150.0	yes	no	yes	no	no
** Ca-40 **													
20040.21c	39.6193	100xs[3]	LANL/T:X	1989	300.0	53013	2718	100.0	yes	no	no	no	no
Z = 21 ***** Scandium *****													
** Sc-45 **													
21045.60c	44.5679	endf60	B-VI.2	1992	293.6	105627	10639	20.0	yes	no	no	no	no
21045.62c	44.5679	actia	B-VI.8:X	2000	293.6	267570	22382	20.0	yes	no	no	no	no
21045.66c	44.5679	endf66a	B-VI.2:X	1992	293.6	256816	22383	20.0	yes	no	no	no	no
Z = 22 ***** Titanium *****													
** Ti-nat**													
22000.42c	47.4885	endl92	LLNL	<1992	300.0	8979	608	30.0	yes	no	no	no	no
22000.50c	47.4676	endf5u	B-V.0	1977	293.6	54801	4434	20.0	yes	no	no	no	no
22000.50d	47.4676	dre5	B-V.0	1977	293.6	10453	263	20.0	yes	no	no	no	no
22000.51d	47.4676	drmcscs	B-V.0	1977	293.6	10453	263	20.0	yes	no	no	no	no
22000.51c	47.4676	rmccs	B-V.0	1977	293.6	31832	1934	20.0	yes	no	no	no	no
22000.60c	47.4676	endf60	B-VI.0	1977	293.6	76454	7761	20.0	yes	no	no	no	no
22000.61c	47.4676	actib	B-VI.8	2000	77.0	131345	11427	20.0	yes	no	no	no	no
22000.62c	47.4676	actia	B-VI.8	2000	293.6	125641	10859	20.0	yes	no	no	no	no
22000.64c	47.4676	endf66d	B-VI.0	1977	77.0	131040	11428	20.0	yes	no	no	no	no
22000.66c	47.4676	endf66a	B-VI.0	1977	293.6	125336	10860	20.0	yes	no	no	no	no
Z = 23 ***** Vanadium *****													
** V-nat**													
23000.50d	50.5040	dre5	B-V.0	1977	293.6	8868	263	20.0	yes	no	no	no	no
23000.50c	50.5040	endf5u	B-V.0	1977	293.6	38312	2265	20.0	yes	no	no	no	no
23000.51c	50.5040	rmccs	B-V.0	1977	293.6	34110	1899	20.0	yes	no	no	no	no
23000.51d	50.5040	drmcscs	B-V.0	1977	293.6	8868	263	20.0	yes	no	no	no	no
23000.60c	50.5040	endf60	B-VI.0	1988	293.6	167334	8957	20.0	yes	no	no	no	no
23000.62c	50.5040	actia	B-VI.8	2000	293.6	198692	10393	20.0	yes	no	no	no	no
23000.66c	50.5040	endf66a	B-VI.0	1988	293.6	192051	10393	20.0	yes	no	no	no	no

Table G.2 (Cont.)
Continuous-Energy and Discrete Neutron Data Libraries Maintained by X-5

<u>ZAID</u>	<u>AWR</u>	<u>Library</u> <u>Name</u>	<u>Source</u>	<u>Eval</u> <u>Date</u>	<u>Temp</u> <u>(°K)</u>	<u>Length</u> <u>words</u>	<u>NE</u>	<u>E_{max}</u> <u>(MeV)</u>	<u>GPD</u>	<u>U</u>	<u>CP</u>	<u>DN</u>	<u>UR</u>
** V-51 **													
23051.42c	50.5063	endl92	LLNL	<1992	300.0	94082	5988	30.0	yes	no	no	no	no
Z = 24 ***** Chromium *****													
** Cr-nat**													
24000.42c	51.5493	endl92	LLNL	<1992	300.0	12573	377	30.0	yes	no	no	no	no
24000.50d	51.5490	drmcscs	B-V.0	1977	293.6	30714	263	20.0	yes	no	no	no	no
24000.50c	51.5490	rmccs	B-V.0	1977	293.6	134454	11050	20.0	yes	no	no	no	no
** Cr-50 **													
24050.24c	49.5170	la150n	B-VI.6	1997	293.6	391112	28453	150.0	yes	no	yes	no	no
24050.60c	49.5170	endf60	B-VI.1	1989	293.6	119178	11918	20.0	yes	no	no	no	no
24050.61c	49.5170	actib	B-VI.8	2000	77.0	405367	29959	150.0	yes	no	yes	no	no
24050.62c	49.5170	actia	B-VI.8	2000	293.6	390799	28138	150.0	yes	no	yes	no	no
24050.64c	49.5170	endf66d	B-VI.6	1997	77.0	403120	29954	150.0	yes	no	yes	no	no
24050.66c	49.5170	endf66a	B-VI.6	1997	293.6	388600	28139	150.0	yes	no	yes	no	no
** Cr-52 **													
24052.24c	51.4940	la150n	B-VI.6	1997	293.6	346350	21232	150.0	yes	no	yes	no	no
24052.60c	51.4940	endf60	B-VI.1	1989	293.6	117680	10679	20.0	yes	no	no	no	no
24052.61c	51.4940	actib	B-VI.8	2000	77.0	344811	21143	150.0	yes	no	yes	no	no
24052.62c	51.4940	actia	B-VI.8	2000	293.6	342461	20849	150.0	yes	no	yes	no	no
24052.64c	51.4940	endf66d	B-VI.6	1997	77.0	344376	21132	150.0	yes	no	yes	no	no
24052.66c	51.4940	endf66a	B-VI.6	1997	293.6	342098	20847	150.0	yes	no	yes	no	no
** Cr-53 **													
24053.24c	52.4860	la150n	B-VI.6	1997	293.6	286602	13873	150.0	yes	no	yes	no	no
24053.60c	52.4860	endf60	B-VI.1	1989	293.6	114982	10073	20.0	yes	no	no	no	no
24053.61c	52.4860	actib	B-VI.8	2000	77.0	292322	14242	150.0	yes	no	yes	no	no
24053.62c	52.4860	actia	B-VI.8	2000	293.6	287642	13657	150.0	yes	no	yes	no	no
24053.64c	52.4860	endf66d	B-VI.6	1997	77.0	289469	14231	150.0	yes	no	yes	no	no
24053.66c	52.4860	endf66a	B-VI.6	1997	293.6	284837	13652	150.0	yes	no	yes	no	no
** Cr-54 **													
24054.24c	53.4760	la150n	B-VI.6	1997	293.6	259040	13750	150.0	yes	no	yes	no	no
24054.60c	53.4760	endf60	B-VI.1	1989	293.6	98510	9699	20.0	yes	no	no	no	no
24054.61c	53.4760	actib	B-VI.8	2000	77.0	262192	13814	150.0	yes	no	yes	no	no
24054.62c	53.4760	actia	B-VI.8	2000	293.6	260423	13593	150.0	yes	no	yes	no	no
24054.64c	53.4760	endf66d	B-VI.6	1997	77.0	259591	13819	150.0	yes	no	yes	no	no
24054.66c	53.4760	endf66a	B-VI.6	1997	293.6	257750	13589	150.0	yes	no	yes	no	no
Z = 25 ***** Manganese *****													
** Mn-55 **													
25055.42c	54.4661	endl92	LLNL	<1992	300.0	10262	460	30.0	yes	no	no	no	no
25055.50d	54.4661	dre5	B-V.0	1977	293.6	9681	263	20.0	yes	no	no	no	no
25055.50c	54.4661	endf5u	B-V.0	1977	293.6	105093	12525	20.0	yes	no	no	no	no
25055.51d	54.4661	drmcscs	B-V.0	1977	293.6	9681	263	20.0	yes	no	no	no	no
25055.51c	54.4661	rmccs	B-V.0	1977	293.6	25727	1578	20.0	yes	no	no	no	no
25055.60c	54.4661	endf60	B-VI.0	1988	293.6	184269	8207	20.0	yes	no	no	no	no
25055.61c	54.4661	actib	B-VI.8	2000	77.0	279378	11967	20.0	yes	no	yes	no	no
25055.62c	54.4661	actia	B-VI.8	2000	293.6	272554	11114	20.0	yes	no	yes	no	no
25055.64c	54.4661	endf66d	B-VI.5	1988	77.0	270711	11967	20.0	yes	no	yes	no	no
25055.66c	54.4661	endf66a	B-VI.5	1988	293.6	263887	11114	20.0	yes	no	yes	no	no
Z = 26 ***** Iron *****													
** Fe-nat**													
26000.21c	55.3650	100xs[3]	LANL/T:X	1989	300.0	149855	15598	100.0	yes	no	no	no	no
26000.42c	55.3672	endl92	LLNL	<1992	300.0	38653	3385	30.0	yes	no	no	no	no
26000.50c	55.3650	endf5p	B-V.0	1978	293.6	115447	10957	20.0	yes	no	no	no	no
26000.50d	55.3650	dre5	B-V.0	1978	293.6	33896	263	20.0	yes	no	no	no	no
26000.55d	55.3650	drmcscs	LANL/T	1986	293.6	72632	263	20.0	yes	no	no	no	no
26000.55c	55.3650	rmccs	LANL/T	1986	293.6	178392	6899	20.0	yes	no	no	no	no

Table G.2 (Cont.)
Continuous-Energy and Discrete Neutron Data Libraries Maintained by X-5

<u>Z</u> <u>A</u> <u>I</u> <u>D</u>	<u>A</u> <u>W</u> <u>R</u>	<u>L</u> <u>i</u> <u>b</u> <u>r</u> <u>a</u> <u>r</u> <u>y</u> <u>N</u> <u>a</u> <u>m</u> <u>e</u>	<u>S</u> <u>o</u> <u>u</u> <u>r</u> <u>c</u> <u>e</u>	<u>E</u> <u>v</u> <u>a</u> <u>l</u> <u>D</u> <u>a</u> <u>t</u> <u>e</u>	<u>T</u> <u>e</u> <u>m</u> <u>p</u> <u>(</u> <u>°</u> <u>K</u> <u>)</u>	<u>L</u> <u>e</u> <u>n</u> <u>g</u> <u>t</u> <u>h</u> <u>w</u> <u>o</u> <u>r</u> <u>d</u> <u>s</u>	<u>N</u> <u>E</u>	<u>E</u> _{max} <u>(</u> <u>M</u> <u>e</u> <u>V</u> <u>)</u>	<u>G</u> <u>P</u> <u>D</u>	<u>U</u>	<u>C</u> <u>P</u>	<u>D</u> <u>N</u>	<u>U</u> <u>R</u>
** Fe-54 **													
26054.24c	53.4760	la150n	B-VI.6	1996	293.6	311741	19323	150.0	yes	no	yes	no	no
26054.60c	53.4760	endf60	B-VI.1	1989	293.6	121631	10701	20.0	yes	no	no	no	no
26054.61c	53.4760	actib	B-VI.8	2000	77.0	318575	20129	150.0	yes	no	yes	no	no
26054.62c	53.4760	actia	B-VI.8	2000	293.6	311639	19262	150.0	yes	no	yes	no	no
26054.64c	53.4760	endf66d	B-VI.6	1996	77.0	317271	20129	150.0	yes	no	yes	no	no
26054.66c	53.4760	endf66a	B-VI.6	1996	293.6	310335	19262	150.0	yes	no	yes	no	no
** Fe-56 **													
26056.24c	55.4540	la150n	B-VI.6	1996	293.6	461888	25792	150.0	yes	no	yes	no	no
26056.60c	55.4540	endf60	B-VI.1	1989	293.6	174517	11618	20.0	yes	no	no	no	no
26056.61c	55.4540	actib	B-VI.8	2000	77.0	475976	26821	150.0	yes	no	yes	no	no
26056.62c	55.4540	actia	B-VI.8	2000	293.6	466257	25606	150.0	yes	no	yes	no	no
26056.64c	55.4540	endf66d	B-VI.6	1996	77.0	468162	26821	150.0	yes	no	yes	no	no
26056.66c	55.4540	endf66a	B-VI.6	1996	293.6	458443	25606	150.0	yes	no	yes	no	no
** Fe-57 **													
26057.24c	56.4460	la150n	B-VI.6	1996	293.6	315349	14285	150.0	yes	no	yes	no	no
26057.60c	56.4460	endf60	B-VI.1	1989	293.6	133995	7606	20.0	yes	no	no	no	no
26057.61c	56.4460	actib	B-VI.8	2000	77.0	319262	14390	150.0	yes	no	yes	no	no
26057.62c	56.4460	actia	B-VI.8	2000	293.6	318268	14266	150.0	yes	no	yes	no	no
26057.64c	56.4460	endf66d	B-VI.6	1996	77.0	316191	14390	150.0	yes	no	yes	no	no
26057.66c	56.4460	endf66a	B-VI.6	1996	293.6	315197	14266	150.0	yes	no	yes	no	no
** Fe-58 **													
26058.60c	57.4360	endf60	B-VI.1	1989	293.6	93450	6788	20.0	yes	no	no	no	no
26058.61c	57.4360	actib	B-VI.8	2000	77.0	169389	11556	20.0	yes	no	yes	no	no
26058.62c	57.4360	actia	B-VI.8	2000	293.6	165829	11111	20.0	yes	no	yes	no	no
26058.64c	57.4360	endf66d	B-VI.5	1989	77.0	165636	11556	20.0	yes	no	yes	no	no
26058.66c	57.4360	endf66a	B-VI.5	1989	293.6	162076	11111	20.0	yes	no	yes	no	no
Z = 27 ***** Cobalt *****													
** Co-59 **													
27059.42c	58.4269	endl92	LLNL	<1992	300.0	119231	13098	30.0	yes	no	no	no	no
27059.50d	58.4269	dre5	B-V.0	1977	293.6	11769	263	20.0	yes	no	no	no	no
27059.50c	58.4269	endf5u	B-V.0	1977	293.6	117075	14502	20.0	yes	no	no	no	no
27059.51d	58.4269	drmcsc	B-V.0	1977	293.6	11769	263	20.0	yes	no	no	no	no
27059.51c	58.4269	rmccs	B-V.0	1977	293.6	28355	1928	20.0	yes	no	no	no	no
27059.60c	58.4269	endf60	B-VI.2	1992	293.6	186618	11838	20.0	yes	no	no	no	no
27059.66c	58.4269	endf66a	B-VI.2	1992	293.6	266952	19759	20.0	yes	no	no	no	no
Z = 28 ***** Nickel *****													
** Ni-nat**													
28000.42c	58.1957	endl92	LLNL	<1992	300.0	44833	3116	30.0	yes	no	no	no	no
28000.50c	58.1826	rmccs	B-V.0	1977	293.6	139913	8927	20.0	yes	no	no	no	no
28000.50d	58.1826	drmcsc	B-V.0	1977	293.6	21998	263	20.0	yes	no	no	no	no
** Ni-58 **													
28058.24c	57.4380	la150n	B-VI.6	1997	293.6	613673	39258	150.0	yes	no	yes	no	no
28058.42c	57.4376	endl92	LLNL	<1992	300.0	38930	4914	30.0	yes	no	no	no	no
28058.60c	57.4380	endf60	B-VI.1	1989	293.6	172069	16445	20.0	yes	no	no	no	no
28058.61c	57.4380	actib	B-VI.8	2000	77.0	630981	40646	150.0	yes	no	yes	no	no
28058.62c	57.4380	actia	B-VI.8	2000	293.6	617974	39020	150.0	yes	no	yes	no	no
28058.64c	57.4380	endf66d	B-VI.6	1997	77.0	623330	40632	150.0	yes	no	yes	no	no
28058.66c	57.4380	endf66a	B-VI.6	1997	293.6	610483	39026	150.0	yes	no	yes	no	no
** Ni-60 **													
28060.24c	59.4160	la150n	B-VI.6	1997	293.6	408148	21448	150.0	yes	no	yes	no	no
28060.60c	59.4160	endf60	B-VI.1	1991	293.6	110885	10055	20.0	yes	no	no	no	no
28060.61c	59.4160	actib	B-VI.8	2000	77.0	424742	22574	150.0	yes	no	yes	no	no
28060.62c	59.4160	actia	B-VI.8	2000	293.6	407398	21131	150.0	yes	no	yes	no	no
28060.64c	59.4160	endf66d	B-VI.6	1997	77.0	420274	22569	150.0	yes	no	yes	no	no
28060.66c	59.4160	endf66a	B-VI.6	1997	293.6	403014	21133	150.0	yes	no	yes	no	no

Table G.2 (Cont.)
Continuous-Energy and Discrete Neutron Data Libraries Maintained by X-5

<u>ZAID</u>	<u>AWR</u>	<u>Library</u> <u>Name</u>	<u>Source</u>	<u>Eval</u> <u>Date</u>	<u>Temp</u> <u>(°K)</u>	<u>Length</u> <u>words</u>	<u>NE</u>	<u>E_{max}</u> <u>(MeV)</u>	<u>GPD</u>	<u>U</u>	<u>CP</u>	<u>DN</u>	<u>UR</u>
** Ni-61 **													
28061.24c	60.4080	la150n	B-VI.6	1997	293.6	244768	7384	150.0	yes	no	yes	no	no
28061.60c	60.4080	endf60	B-VI.1	1989	293.6	93801	5882	20.0	yes	no	no	no	no
28061.61c	60.4080	actib	B-VI.8	2000	77.0	247660	7438	150.0	yes	no	yes	no	no
28061.62c	60.4080	actia	B-VI.8	2000	293.6	247188	7379	150.0	yes	no	yes	no	no
28061.64c	60.4080	endf66d	B-VI.6	1997	77.0	245215	7440	150.0	yes	no	yes	no	no
28061.66c	60.4080	endf66a	B-VI.6	1997	293.6	244743	7381	150.0	yes	no	yes	no	no
** Ni-62 **													
28062.24c	61.3960	la150n	B-VI.6	1997	293.6	232065	9219	150.0	yes	no	yes	no	no
28062.60c	61.3960	endf60	B-VI.1	1989	293.6	82085	7230	20.0	yes	no	no	no	no
28062.61c	61.3960	actib	B-VI.8	2000	77.0	234983	9227	150.0	yes	no	yes	no	no
28062.62c	61.3960	actia	B-VI.8	2000	293.6	234511	9168	150.0	yes	no	yes	no	no
28062.64c	61.3960	endf66d	B-VI.6	1997	77.0	232193	9235	150.0	yes	no	yes	no	no
28062.66c	61.3960	endf66a	B-VI.6	1997	293.6	231705	9174	150.0	yes	no	yes	no	no
** Ni-64 **													
28064.24c	63.3790	la150n	B-VI.6	1997	293.6	197799	7958	150.0	yes	no	yes	no	no
28064.60c	63.3790	endf60	B-VI.1	1989	293.6	66656	6144	20.0	yes	no	no	no	no
28064.61c	63.3790	actib	B-VI.8	2000	77.0	199097	7992	150.0	yes	no	yes	no	no
28064.62c	63.3790	actia	B-VI.8	2000	293.6	198313	7894	150.0	yes	no	yes	no	no
28064.64c	63.3790	endf66d	B-VI.6	1997	77.0	198112	7997	150.0	yes	no	yes	no	no
28064.66c	63.3790	endf66a	B-VI.6	1997	293.6	197296	7895	150.0	yes	no	yes	no	no
Z = 29 ***** Copper *****													
** Cu-nat**													
29000.50d	63.5460	drmccs	B-V.0	1978	293.6	12777	263	20.0	yes	no	no	no	no
29000.50c	63.5460	rmccs	B-V.0	1978	293.6	51850	3435	20.0	yes	no	no	no	no
** Cu-63 **													
29063.24c	62.3890	la150n	B-VI.6	1998	293.6	329768	23123	150.0	yes	no	yes	no	no
29063.60c	62.3890	endf60	B-VI.2	1989	293.6	119097	11309	20.0	yes	no	no	no	no
29063.61c	62.3890	actib	B-VI.8	2000	77.0	348384	24556	150.0	yes	no	yes	no	no
29063.62c	62.3890	actia	B-VI.8	2000	293.6	335072	22892	150.0	yes	no	yes	no	no
29063.64c	62.3890	endf66d	B-VI.6	1997	77.0	339601	24549	150.0	yes	no	yes	no	no
29063.66c	62.3890	endf66a	B-VI.6	1997	293.6	326281	22884	150.0	yes	no	yes	no	no
** Cu-65 **													
29065.24c	64.3700	la150n	B-VI.6	1998	293.6	285628	17640	150.0	yes	no	yes	no	no
29065.60c	64.3700	endf60	B-VI.2	1989	293.6	118385	11801	20.0	yes	no	no	no	no
29065.61c	64.3700	actib	B-VI.8	2000	77.0	304772	18575	150.0	yes	no	yes	no	no
29065.62c	64.3700	actia	B-VI.8	2000	293.6	296916	17593	150.0	yes	no	yes	no	no
29065.64c	64.3700	endf66d	B-VI.6	1997	77.0	291518	18562	150.0	yes	no	yes	no	no
29065.66c	64.3700	endf66a	B-VI.6	1997	293.6	283630	17576	150.0	yes	no	yes	no	no
Z = 30 ***** Zinc *****													
** Zn-nat**													
30000.40c	64.8183	endl92	LLNL	<1992	300.0	271897	33027	30.0	yes	no	no	no	no
30000.42c	64.8183	endl92	LLNL:X	<1992	300.0	271897	33027	30.0	yes	no	no	no	no
Z = 31 ***** Gallium *****													
** Ga-nat**													
31000.42c	69.1211	endl92	LLNL	<1992	300.0	6311	219	30.0	yes	no	no	no	no
31000.50c	69.1211	rmccs	B-V.0	1980	293.6	7928	511	20.0	yes	no	no	no	no
31000.50d	69.1211	drmccs	B-V.0	1980	293.6	6211	263	20.0	yes	no	no	no	no
31000.60c	69.1211	endf60	B-VI.0	1980	293.6	9228	566	20.0	yes	no	no	no	no
31000.66c	69.1211	endf66a	B-VI.0	1980	293.6	14640	1130	20.0	yes	no	no	no	no
Z = 33 ***** Arsenic *****													
** As-74 **													
33074.42c	73.2889	endl92	LLNL	<1992	300.0	55752	6851	30.0	yes	no	no	no	no

Table G.2 (Cont.)
Continuous-Energy and Discrete Neutron Data Libraries Maintained by X-5

<u>Z</u> <u>A</u> <u>I</u> <u>D</u>	<u>A</u> <u>W</u> <u>R</u>	<u>L</u> <u>i</u> <u>b</u> <u>r</u> <u>a</u> <u>r</u> <u>y</u> <u>N</u> <u>a</u> <u>m</u> <u>e</u>	<u>S</u> <u>o</u> <u>u</u> <u>r</u> <u>c</u> <u>e</u>	<u>E</u> <u>v</u> <u>a</u> <u>l</u> <u>D</u> <u>a</u> <u>t</u> <u>e</u>	<u>T</u> <u>e</u> <u>m</u> <u>p</u> <u>(</u> <u>°</u> <u>K</u> <u>)</u>	<u>L</u> <u>e</u> <u>n</u> <u>g</u> <u>t</u> <u>h</u> <u>w</u> <u>o</u> <u>r</u> <u>d</u> <u>s</u>	<u>N</u> <u>E</u>	<u>E</u> _{max} <u>(</u> <u>M</u> <u>e</u> <u>V</u> <u>)</u>	<u>G</u> <u>P</u> <u>D</u>	<u>U</u>	<u>C</u> <u>P</u>	<u>D</u> <u>N</u>	<u>U</u> <u>R</u>
** As-75 **													
33075.35d	74.2780	drmccs	B-V.0	1974	0.0	8480	263	20.0	yes	no	no	no	no
33075.35c	74.2780	rmccsa	B-V.0	1974	0.0	50931	6421	20.0	yes	no	no	no	no
33075.42c	74.2780	endl92	LLNL	<1992	300.0	56915	6840	30.0	yes	no	no	no	no
Z = 35 ***** Bromine *****													
** Br-79 **													
35079.55c	78.2404	misc5xs[7,9]	LANL/T	1982	293.6	10431	1589	20.0	no	no	no	no	no
** Br-81 **													
35081.55c	80.2212	misc5xs[7,9]	LANL/T	1982	293.6	5342	831	20.0	no	no	no	no	no
Z = 36 ***** Krypton *****													
** Kr-78 **													
36078.50c	77.2510	rmccsa	B-V.0	1978	293.6	9057	939	20.0	no	no	no	no	no
36078.50d	77.2510	drmccs	B-V.0	1978	293.6	4358	263	20.0	no	no	no	no	no
36078.66c	77.2510	endf66a	B-VI.0	1978	293.6	27045	2221	20.0	no	no	no	no	no
** Kr-80 **													
36080.50d	79.2298	drmccs	B-V.0	1978	293.6	4276	263	20.0	no	no	no	no	no
36080.50c	79.2298	rmccsa	B-V.0	1978	293.6	10165	1108	20.0	no	no	no	no	no
36080.66c	79.2298	endf66a	B-VI.0	1978	293.6	26039	2361	20.0	no	no	no	no	no
** Kr-82 **													
36082.50d	81.2098	drmccs	B-V.0	1978	293.6	4266	263	20.0	no	no	no	no	no
36082.50c	81.2098	rmccsa	B-V.0	1978	293.6	7220	586	20.0	no	no	no	no	no
36082.59c	81.2098	misc5xs[7,8]	LANL/T	1982	293.6	7010	499	20.0	yes	no	no	no	no
36082.66c	81.2098	endf66a	B-VI.0	1978	293.6	19674	1296	20.0	no	no	no	no	no
** Kr-83 **													
36083.50c	82.2018	rmccsa	B-V.0	1978	293.6	8078	811	20.0	no	no	no	no	no
36083.50d	82.2018	drmccs	B-V.0	1978	293.6	4359	263	20.0	no	no	no	no	no
36083.59c	82.2018	misc5xs[7,8]	LANL/T	1982	293.6	8069	704	20.0	yes	no	no	no	no
36083.66c	82.2018	endf66a	B-VI.0	1978	293.6	21271	1760	20.0	no	no	no	no	no
** Kr-84 **													
36084.50c	83.1906	rmccsa	B-V.0	1978	293.6	9364	944	20.0	no	no	no	no	no
36084.50d	83.1906	drmccs	B-V.0	1978	293.6	4463	263	20.0	no	no	no	no	no
36084.59c	83.1906	misc5xs[7,8]	LANL/T	1982	293.6	10370	954	20.0	yes	no	no	no	no
36084.66c	83.1906	endf66a	B-VI.0	1978	293.6	24427	2098	20.0	no	no	no	no	no
** Kr-86 **													
36086.50c	85.1726	rmccsa	B-V.0	1975	293.6	10416	741	20.0	no	no	no	no	no
36086.50d	85.1726	drmccs	B-V.0	1975	293.6	4301	263	20.0	no	no	no	no	no
36086.59c	85.1726	misc5xs[7,8]	LANL/T	1982	293.6	8740	551	20.0	yes	no	no	no	no
36086.66c	85.1726	endf66a	B-VI.0	1978	293.6	22203	1425	20.0	no	no	no	no	no
Z = 37 ***** Rubidium *****													
** Rb-85 **													
37085.55c	84.1824	misc5xs[7,9]	LANL/T	1982	293.6	27304	4507	20.0	no	no	no	no	no
37085.66c	84.1824	endf66a	B-VI.0	1979	293.6	179843	15316	20.0	no	no	no	no	no
** Rb-87 **													
37087.55c	86.1626	misc5xs[7,9]	LANL/T	1982	293.6	8409	1373	20.0	no	no	no	no	no
37087.66c	86.1624	endf66b	B-VI.0	1979	293.6	42718	3637	20.0	no	no	no	no	no
Z = 39 ***** Yttrium *****													
** Y-88 **													
39088.42c	87.1543	endl92	LLNL	<1992	300.0	11682	181	30.0	yes	no	no	no	no
** Y-89 **													
39089.35c	88.1421	misc5xs[7]	LLNL	<1985	0.0	49885	6154	20.0	yes	no	no	no	no
39089.42c	88.1421	endl92	LLNL	<1992	300.0	69315	8771	30.0	yes	no	no	no	no
39089.50d	88.1421	dre5	B-V.0[10]	1985	293.6	2311	263	20.0	no	no	no	no	no
39089.50c	88.1421	endf5u	B-V.0[10]	1985	293.6	18631	3029	20.0	no	no	no	no	no

Table G.2 (Cont.)
Continuous-Energy and Discrete Neutron Data Libraries Maintained by X-5

<u>Z</u> <u>A</u> <u>I</u> <u>D</u>	<u>A</u> <u>W</u> <u>R</u>	<u>L</u> <u>i</u> <u>b</u> <u>r</u> <u>a</u> <u>r</u> <u>y</u> <u>N</u> <u>a</u> <u>m</u> <u>e</u>	<u>S</u> <u>o</u> <u>u</u> <u>r</u> <u>c</u> <u>e</u>	<u>E</u> <u>v</u> <u>a</u> <u>l</u> <u>D</u> <u>a</u> <u>t</u> <u>e</u>	<u>T</u> <u>e</u> <u>m</u> <u>p</u> <u>(</u> <u>°</u> <u>K</u> <u>)</u>	<u>L</u> <u>e</u> <u>n</u> <u>g</u> <u>t</u> <u>h</u> <u>w</u> <u>o</u> <u>r</u> <u>d</u> <u>s</u>	<u>N</u> <u>E</u>	<u>E</u> _{max} <u>(</u> <u>M</u> <u>e</u> <u>V</u> <u>)</u>	<u>G</u> <u>P</u> <u>D</u>	<u>U</u>	<u>C</u> <u>P</u>	<u>D</u> <u>N</u>	<u>U</u> <u>R</u>
39089.60c	88.1420	endf60	B-VI.0	1986	293.6	86556	9567	20.0	yes	no	no	no	no
39089.66c	88.1420	endf66b	B-VI.4	1986	293.6	144304	13207	20.0	yes	no	no	no	no

Z = 40 ***** Zirconium *****

** Zr-nat**

40000.42c	90.4364	endl92	LLNL	<1992	300.0	131855	17909	30.0	yes	no	no	no	no
40000.56d	90.4360	misc5xs[7,11]	B-V:X	1976	300.0	5400	263	20.0	no	no	no	no	no
40000.56c	90.4360	misc5xs[7,11]	B-V:X	1976	300.0	52064	7944	20.0	no	no	no	no	no
40000.57d	90.4360	misc5xs[7,11]	B-V:X	1976	300.0	5400	263	20.0	no	no	no	no	no
40000.57c	90.4360	misc5xs[7,11]	B-V:X	1976	300.0	16816	2116	20.0	no	no	no	no	no
40000.58c	90.4360	misc5xs[7,11]	B-V:X	1976	587.2	57528	8777	20.0	no	no	no	no	no
40000.60c	90.4360	endf60	B-VI.1	1976[11]	293.6	66035	10298	20.0	no	no	no	no	no
40000.66c	90.4360	endf66b	B-VI.1	1976	293.6	165542	22226	20.0	no	no	no	no	no

** Zr-90 **

40090.66c	89.1320	endf66b	B-VI.0:X	1976	293.6	51841	6243	20.0	no	no	no	no	no
-----------	---------	---------	----------	------	-------	-------	------	------	----	----	----	----	----

** Zr-91 **

40091.65c	90.1220	endf66e	B-VI.0:X	1976	3000.1	86834	10971	20.0	no	no	no	no	yes
40091.66c	90.1220	endf66b	B-VI.0:X	1976	293.6	106833	13828	20.0	no	no	no	no	yes

** Zr-92 **

40092.66c	91.1120	endf66b	B-VI.0:X	1976	293.6	82986	10664	20.0	no	no	no	no	no
-----------	---------	---------	----------	------	-------	-------	-------	------	----	----	----	----	----

** Zr-93 **

40093.50c	92.1083	kidman	B-V.0	1974	293.6	2579	236	20.0	no	no	no	no	no
-----------	---------	--------	-------	------	-------	------	-----	------	----	----	----	----	----

** Zr-94 **

40094.66c	93.0960	endf66b	B-VI.0:X	1976	293.6	86543	11144	20.0	no	no	no	no	no
-----------	---------	---------	----------	------	-------	-------	-------	------	----	----	----	----	----

** Zr-96 **

40096.66c	95.0810	endf66b	B-VI.0:X	1976	293.6	47405	5652	20.0	no	no	no	no	no
-----------	---------	---------	----------	------	-------	-------	------	------	----	----	----	----	----

Z = 41 ***** Niobium *****

** Nb-93 **

41093.24c	92.1051	la150n	LANL	1997	293.6	375888	23213	150.0	yes	no	yes	no	no
41093.42c	92.1083	endl92	LLNL	<1992	300.0	73324	9277	30.0	yes	no	no	no	no
41093.50c	92.1051	endf5p	B-V.0	1974	293.6	128960	17279	20.0	yes	no	no	no	no
41093.50d	92.1051	dre5	B-V.0	1974	293.6	10332	263	20.0	yes	no	no	no	no
41093.51c	92.1051	rmccs	B-V.0	1974	293.6	14675	963	20.0	yes	no	no	no	no
41093.51d	92.1051	drmcsc	B-V.0	1974	293.6	10332	263	20.0	yes	no	no	no	no
41093.60c	92.1051	endf60	B-VI.1	1990	293.6	110269	10678	20.0	yes	no	no	no	no
41093.66c	92.1051	endf66b	B-VI.6	1997	293.6	367638	23063	150.0	yes	no	yes	no	no

Z = 42 ***** Molybdenum *****

** Mo-nat**

42000.42c	95.1158	endl92	LLNL	<1992	300.0	9293	442	30.0	yes	no	no	no	no
42000.50d	95.1160	dre5	B-V.0	1979	293.6	7754	263	20.0	yes	no	no	no	no
42000.50c	95.1160	endf5u	B-V.0	1979	293.6	35634	4260	20.0	yes	no	no	no	no
42000.51c	95.1160	rmccs	B-V.0	1979	293.6	10139	618	20.0	yes	no	no	no	no
42000.51d	95.1160	drmcsc	B-V.0	1979	293.6	7754	263	20.0	yes	no	no	no	no
42000.60c	95.1160	endf60	B-VI.0	1979	293.6	45573	5466	20.0	yes	no	no	no	no
42000.66c	95.1160	endf66b	B-VI.0	1979	293.6	68710	7680	20.0	yes	no	no	no	no

** Mo-95 **

42095.50c	94.0906	kidman	B-V.0	1980	293.6	15411	2256	20.0	no	no	no	no	no
-----------	---------	--------	-------	------	-------	-------	------	------	----	----	----	----	----

Z = 43 ***** Technetium *****

** Tc-99 **

43099.50c	98.1500	kidman	B-V.0	1978	293.6	12152	1640	20.0	no	no	no	no	no
43099.60c	98.1500	endf60	B-VI.0	1978	293.6	54262	8565	20.0	no	no	no	no	no
43099.65c	98.1500	endf66e	B-VI.0	1978	3000.1	67583	8545	20.0	no	no	no	no	yes
43099.66c	98.1500	endf66b	B-VI.0	1978	293.6	90039	11753	20.0	no	no	no	no	yes

Table G.2 (Cont.)
Continuous-Energy and Discrete Neutron Data Libraries Maintained by X-5

<u>ZAID</u>	<u>AWR</u>	<u>Library</u> <u>Name</u>	<u>Source</u>	<u>Eval</u> <u>Date</u>	<u>Temp</u> <u>(°K)</u>	<u>Length</u> <u>words</u>	<u>NE</u>	<u>E_{max}</u> <u>(MeV)</u>	<u>GPD</u>	<u>U</u>	<u>CP</u>	<u>DN</u>	<u>UR</u>
Z = 44 ***** Ruthenium *****													
** Ru-101 **													
44101.50c	100.0390	kidman	B-V.0	1980	293.6	5299	543	20.0	no	no	no	no	no
** Ru-103 **													
44103.50c	102.0220	kidman	B-V.0	1974	293.6	3052	235	20.0	no	no	no	no	no
Z = 45 ***** Rhodium *****													
** Rh-103 **													
45103.50d	102.0210	drmccs	B-V.0	1978	293.6	4663	263	20.0	no	no	no	no	no
45103.50c	102.0210	rmccsa	B-V.0	1978	293.6	18870	2608	20.0	no	no	no	no	no
45103.65c	102.0210	endf66e	B-VI.0	1978	3000.1	83883	10715	20.0	no	no	no	no	yes
45103.66c	102.0210	endf66b	B-VI.0	1978	293.6	116685	15401	20.0	no	no	no	no	yes
** Rh-105 **													
45105.50c	104.0050	kidman	B-V.0	1974	293.6	1591	213	20.0	no	no	no	no	no
Z = 45 ***** Average fission product from Uranium-235 *****													
** U-235 fp **													
45117.90d	115.5446	drmccs	LANL/T	1982	293.6	9507	263	20.0	yes	no	no	no	no
45117.90c	115.5446	rmccs	LANL/T	1982	293.6	10314	399	20.0	yes	no	no	no	no
Z = 46 ***** Palladium *****													
** Pd-102 **													
46102.66c	101.0302	endf66b	B-VI.5	1996	293.6	148683	659	30.0	yes	no	yes	no	no
** Pd-104 **													
46104.66c	103.0114	endf66b	B-VI.5	1996	293.6	155873	1197	30.0	yes	no	yes	no	no
** Pd-105 **													
46105.50c	104.0040	kidman	B-V.0	1980	293.6	4647	505	20.0	no	no	no	no	no
46105.66c	104.0039	endf66b	B-VI.5	1996	293.6	634077	13480	30.0	yes	no	yes	no	no
** Pd-106 **													
46106.66c	104.9937	endf66b	B-VI.5	1996	293.6	150930	1154	30.0	yes	no	yes	no	no
** Pd-108 **													
46108.50c	106.9770	kidman	B-V.0	1980	293.6	4549	555	20.0	no	no	no	no	no
46108.66c	106.9769	endf66b	B-VI.5	1996	293.6	168900	1981	30.0	yes	no	yes	no	no
** Pd-110 **													
46110.66c	108.9610	endf66b	B-VI.5	1996	293.6	127359	862	30.0	yes	no	yes	no	no
Z = 46 ***** Average fission product from Plutonium-239 *****													
** Pu-239 fp **													
46119.90d	117.5255	drmccs	LANL/T	1982	293.6	9542	263	20.0	yes	no	no	no	no
46119.90c	117.5255	rmccs	LANL/T	1982	293.6	10444	407	20.0	yes	no	no	no	no
Z = 47 ***** Silver *****													
** Ag-nat**													
47000.55c	106.9420	rmccsa	LANL/T	1984	293.6	29092	2350	20.0	yes	no	no	no	no
47000.55d	106.9420	drmccs	LANL/T	1984	293.6	12409	263	20.0	yes	no	no	no	no
** Ag-107 **													
47107.42c	105.9867	endl92	LLNL	<1992	300.0	27108	2885	30.0	yes	no	no	no	no
47107.50c	105.9870	rmccsa	B-V.0	1978	293.6	12111	1669	20.0	no	no	no	no	no
47107.50d	105.9870	drmccs	B-V.0	1978	293.6	4083	263	20.0	no	no	no	no	no
47107.60c	105.9870	endf60	B-VI.0	1983	293.6	64008	10101	20.0	no	no	no	no	no
47107.66c	105.9870	endf66b	B-VI.0	1983	293.6	104321	13835	20.0	no	no	no	no	no

Table G.2 (Cont.)
Continuous-Energy and Discrete Neutron Data Libraries Maintained by X-5

<u>ZAID</u>	<u>AWR</u>	<u>Library</u> <u>Name</u>	<u>Source</u>	<u>Eval</u> <u>Date</u>	<u>Temp</u> <u>(°K)</u>	<u>Length</u> <u>words</u>	<u>NE</u>	<u>E_{max}</u> <u>(MeV)</u>	<u>GPD</u>	<u>U</u>	<u>CP</u>	<u>DN</u>	<u>UR</u>
** Ag-109 **													
47109.42c	107.9692	endl92	LLNL	<1992	300.0	33603	3796	30.0	yes	no	no	no	no
47109.50c	107.9690	rmccsa	B-V.0	1978	293.6	14585	2120	20.0	no	no	no	no	no
47109.50d	107.9690	drmcsc	B-V.0	1978	293.6	3823	263	20.0	no	no	no	no	no
47109.60c	107.9690	endf60	B-VI.0	1983	293.6	76181	11903	20.0	no	no	no	no	no
47109.66c	107.9690	endf66b	B-VI.0	1983	293.6	121474	16086	20.0	no	no	no	no	no
Z = 48 ***** Cadmium *****													
** Cd-nat**													
48000.42c	111.4443	endl92	LLNL	<1992	300.0	211537	29369	30.0	yes	no	no	no	no
48000.50d	111.4600	dre5	B-V.0	1974	293.6	3026	263	20.0	no	no	no	no	no
48000.50c	111.4600	endf5u	B-V.0	1974	293.6	19714	2981	20.0	no	no	no	no	no
48000.51c	111.4600	rmccsc	B-V.0	1974	293.6	6734	818	20.0	no	no	no	no	no
48000.51d	111.4600	drmcsc	B-V.0	1974	293.6	3026	263	20.0	no	no	no	no	no
** Cd-106 **													
48106.65c	105.0000	endf66e	B-VI.4	1996	3000.1	121059	10194	20.0	no	no	no	no	yes
48106.66c	105.0000	endf66b	B-VI.4	1996	293.6	151365	12949	20.0	no	no	no	no	yes
** Cd-108 **													
48108.65c	106.9770	endf66e	B-VI.4	1996	3000.1	112404	11496	20.0	no	no	no	no	yes
48108.66c	106.9770	endf66b	B-VI.4	1996	293.6	141658	14744	20.0	no	no	no	no	yes
** Cd-110 **													
48110.65c	108.9590	endf66e	B-VI.4:X	1996	3000.1	105350	10737	20.0	no	no	no	no	yes
48110.66c	108.9590	endf66b	B-VI.4:X	1996	293.6	133785	13902	20.0	no	no	no	no	yes
** Cd-111 **													
48111.66c	109.9520	endf66b	B-VI.3	1995	293.6	153808	16016	20.0	no	no	no	no	no
** Cd-112 **													
48112.65c	110.9420	endf66e	B-VI.4	1996	3000.1	101915	11153	20.0	no	no	no	no	yes
48112.66c	110.9420	endf66b	B-VI.4	1996	293.6	130334	14515	20.0	no	no	no	no	yes
** Cd-113 **													
48113.66c	111.9300	endf66b	B-VI.3	1995	293.6	97047	9799	20.0	no	no	no	no	no
** Cd-114 **													
48114.65c	112.9250	endf66e	B-VI.4	1996	3000.1	83882	10534	20.0	no	no	no	no	yes
48114.66c	112.9250	endf66b	B-VI.4	1996	293.6	102222	13154	20.0	no	no	no	no	yes
** Cd-116 **													
48116.65c	114.9090	endf66e	B-VI.4	1996	3000.1	55903	6607	20.0	no	no	no	no	yes
48116.66c	114.9090	endf66b	B-VI.4	1996	293.6	66642	8141	20.0	no	no	no	no	yes
Z = 49 ***** Indium *****													
** In-nat**													
49000.42c	113.8336	endl92	LLNL	<1992	300.0	65498	7870	30.0	yes	no	no	no	no
49000.60c	113.8340	endf60	B-VI.0	1990	293.6	93662	10116	20.0	yes	no	no	no	no
49000.66c	113.8340	endf66b	B-VI.0	1990	293.6	269821	30337	20.0	yes	no	no	no	no
Z = 49-50 ***** Fission Products *****													
** Avg fp **													
49120.42c	116.4906	endl92fp[12]	LLNL	<1992	300.0	12755	164	30.0	yes	no	no	no	no
49125.42c	116.4906	endl92fp[12]	LLNL	<1992	300.0	9142	119	30.0	yes	no	no	no	no
50120.35c	116.4906	rmccsc	LLNL	<1985	yes	8366	232	20.0	yes	no	no	no	no
50120.35d	116.4906	drmcsc	LLNL	<1985	yes	8963	263	20.0	yes	no	no	no	no
Z = 50 ***** Tin *****													
** Sn-nat**													
50000.40c	117.6704	endl92	LLNL	<1992	300.0	248212	34612	30.0	yes	no	no	no	no
50000.42c	117.6704	endl92	LLNL:X	<1992	300.0	248212	34612	30.0	yes	no	no	no	no

Table G.2 (Cont.)
Continuous-Energy and Discrete Neutron Data Libraries Maintained by X-5

<u>Z</u> <u>A</u> <u>I</u> <u>D</u>	<u>A</u> <u>W</u> <u>R</u>	<u>L</u> <u>i</u> <u>b</u> <u>r</u> <u>a</u> <u>r</u> <u>y</u> <u>N</u> <u>a</u> <u>m</u> <u>e</u>	<u>S</u> <u>o</u> <u>u</u> <u>r</u> <u>c</u> <u>e</u>	<u>E</u> <u>v</u> <u>a</u> <u>l</u> <u>D</u> <u>a</u> <u>t</u> <u>e</u>	<u>T</u> <u>e</u> <u>m</u> <u>p</u> <u>(</u> <u>°</u> <u>K</u> <u>)</u>	<u>L</u> <u>e</u> <u>n</u> <u>g</u> <u>t</u> <u>h</u> <u>w</u> <u>o</u> <u>r</u> <u>d</u> <u>s</u>	<u>N</u> <u>E</u>	<u>E</u> _{max} <u>(</u> <u>M</u> <u>e</u> <u>V</u> <u>)</u>	<u>G</u> <u>P</u> <u>D</u>	<u>U</u>	<u>C</u> <u>P</u>	<u>D</u> <u>N</u>	<u>U</u> <u>R</u>
Z = 51 ***** Antimony *****													
** Sb-nat**													
51000.42c	120.7041	endl92	LLNL	<1992	300.0	95953	10721	30.0	yes	no	no	no	no
Z = 53 ***** Iodine *****													
** I-127 **													
53127.42c	125.8143	endl92	LLNL	<1992	300.0	76321	10	30.0	yes	no	no	no	no
53127.55c	125.8140	misc5xs[7,9]	LANL/T	1982	293.6	59725	9423	20.0	no	no	no	no	no
53127.60c	125.8143	endf60[13]	LANL/T	1991	293.6	399760	7888	30.0	yes	no	no	no	no
53127.66c	125.8143	endf66b	B-VI.2	1991	293.6	373991	11519	30.0	yes	no	yes	no	no
** I-129 **													
53129.60c	127.7980	endf60	B-VI.0	1980	293.6	8792	1237	20.0	no	no	no	no	no
** I-135 **													
53135.50c	133.7510	kidman	B-V.0	1974	293.6	1232	194	20.0	no	no	no	no	no
Z = 54 ***** Xenon *****													
** Xe-nat**													
54000.42c	130.1721	endl92	LLNL	<1992	300.0	43411	5173	30.0	yes	no	no	no	no
** Xe-124 **													
54124.66c	122.8420	endf66b	B-VI.0	1978	293.6	21034	1979	20.0	no	no	no	no	no
** Xe-126 **													
54126.66c	124.8230	endf66b	B-VI.0	1978	293.6	21388	2133	20.0	no	no	no	no	no
** Xe-128 **													
54128.66c	126.8050	endf66b	B-VI.0	1978	293.6	32739	3817	20.0	no	no	no	no	no
** Xe-129 **													
54129.66c	127.7970	endf66b	B-VI.0	1978	293.6	118721	15971	20.0	no	no	no	no	no
** Xe-130 **													
54130.66c	128.7880	endf66b	B-VI.0	1978	293.6	34346	3984	20.0	no	no	no	no	no
** Xe-131 **													
54131.50c	129.7810	kidman	B-V.0	1978	293.6	22572	3376	20.0	no	no	no	no	no
54131.66c	129.7810	endf66b	B-VI.0	1978	293.6	79510	10434	20.0	no	no	no	no	no
** Xe-132 **													
54132.66c	130.7710	endf66b	B-VI.0	1978	293.6	17947	1709	20.0	no	no	no	no	no
** Xe-134 **													
54134.42c	132.7551	endl92	LLNL	<1992	300.0	8033	192	30.0	yes	no	no	no	no
54134.66c	132.7550	endf66b	B-VI.0	1978	293.6	15028	1349	20.0	no	no	no	no	no
** Xe-135 **													
54135.50c	133.7480	endf5mt[1]	B-V	1975	293.6	5529	704	20.0	no	no	no	no	no
54135.53c	133.7480	endf5mt[1]	B-V	1975	587.2	5541	706	20.0	no	no	no	no	no
54135.54c	133.7480	endf5mt[1]	B-V	1975	880.8	5577	712	20.0	no	no	no	no	no
** Xe-136 **													
54136.66c	134.7400	endf66b	B-VI.0	1978	293.6	10700	764	20.0	no	no	no	no	no
Z = 55 ***** Cesium *****													
** Cs-133 **													
55133.50c	131.7640	kidman	B-V.0	1978	293.6	26713	4142	20.0	no	no	no	no	no
55133.55c	131.7640	misc5xs[7,9]	LANL/T	1982	293.6	67893	11025	20.0	no	no	no	no	no
55133.60c	131.7640	endf60	B-VI.0	1978	293.6	54723	8788	20.0	no	no	no	no	no
55133.66c	131.7640	endf66b	B-VI.0	1978	293.6	141927	19648	20.0	no	no	no	no	no
** Cs-134 **													
55134.60c	132.7570	endf60	B-VI.0	1988	293.6	10227	1602	20.0	no	no	no	no	no
** Cs-135 **													
55135.50c	133.7470	kidman	B-V.0	1974	293.6	1903	199	20.0	no	no	no	no	no
55135.60c	133.7470	endf60	B-VI.0	1974	293.6	3120	388	20.0	no	no	no	no	no
** Cs-136 **													
55136.60c	134.7400	endf60	B-VI.0	1974	293.6	10574	1748	20.0	no	no	no	no	no
** Cs-137 **													
55137.60c	135.7310	endf60	B-VI.0	1974	293.6	2925	369	20.0	no	no	no	no	no

Table G.2 (Cont.)
Continuous-Energy and Discrete Neutron Data Libraries Maintained by X-5

<u>Z</u> <u>A</u> <u>I</u> <u>D</u>	<u>A</u> <u>W</u> <u>R</u>	<u>L</u> <u>i</u> <u>b</u> <u>r</u> <u>a</u> <u>r</u> <u>y</u> <u>N</u> <u>a</u> <u>m</u> <u>e</u>	<u>S</u> <u>o</u> <u>u</u> <u>r</u> <u>c</u> <u>e</u>	<u>E</u> <u>v</u> <u>a</u> <u>l</u> <u>D</u> <u>a</u> <u>t</u> <u>e</u>	<u>T</u> <u>e</u> <u>m</u> <u>p</u> <u>(</u> <u>°</u> <u>K</u> <u>)</u>	<u>L</u> <u>e</u> <u>n</u> <u>g</u> <u>t</u> <u>h</u> <u>w</u> <u>o</u> <u>r</u> <u>d</u> <u>s</u>	<u>N</u> <u>E</u>	<u>E</u> _{max} <u>(</u> <u>M</u> <u>e</u> <u>V</u> <u>)</u>	<u>G</u> <u>P</u> <u>D</u>	<u>U</u>	<u>C</u> <u>P</u>	<u>D</u> <u>N</u>	<u>U</u> <u>R</u>
Z = 56 ***** Barium *****													
** Ba-138 **													
56138.50c	136.7150	rmccs	B-V.0	1978	293.6	6018	292	20.0	yes	no	no	no	no
56138.50d	136.7150	drmcsc	B-V.0	1978	293.6	6320	263	20.0	yes	no	no	no	no
56138.60c	136.7150	endf60	B-VI.0	1978	293.6	7347	267	20.0	yes	no	no	no	no
56138.66c	136.7150	endf66b	B-VI.3	1994	293.6	79268	8920	20.0	yes	no	no	no	no
Z = 59 ***** Praseodymium *****													
** Pr-141 **													
59141.50c	139.6970	kidman	B-V.0	1980	293.6	15620	1354	20.0	no	no	no	no	no
Z = 60 ***** Neodymium *****													
** Nd-143 **													
60143.50c	141.6820	kidman	B-V.0	1980	293.6	17216	1701	20.0	no	no	no	no	no
** Nd-145 **													
60145.50c	143.6680	kidman	B-V.0	1980	293.6	38473	3985	20.0	no	no	no	no	no
** Nd-147 **													
60147.50c	145.6540	kidman	B-V.0	1979	293.6	1816	251	20.0	no	no	no	no	no
** Nd-148 **													
60148.50c	146.6460	kidman	B-V.0	1980	293.6	10867	1054	20.0	no	no	no	no	no
Z = 61 ***** Promethium *****													
** Pm-147 **													
61147.50c	145.6530	kidman	B-V.0	1980	293.6	9152	825	20.0	no	no	no	no	no
** Pm-148 **													
61148.50c	146.6470	kidman	B-V.0	1979	293.6	1643	257	20.0	no	no	no	no	no
** Pm-149 **													
61149.50c	147.6390	kidman	B-V.0	1979	293.6	2069	238	20.0	no	no	no	no	no
Z = 62 ***** Samarium *****													
** Sm-147 **													
62147.50c	145.6530	kidman	B-V.0	1980	293.6	33773	2885	20.0	no	no	no	no	no
62147.65c	145.6530	endf66e	B-VI.0	1980	3000.1	186194	15025	20.0	no	no	no	no	yes
62147.66c	145.6530	endf66b	B-VI.0	1980	293.6	315674	25815	20.0	no	no	no	no	yes
** Sm-149 **													
62149.49c	147.6380	uresa	B-VI.0	1978	300.0	57787	7392	20.0	no	no	no	no	yes
62149.50c	147.6380	endf5u	B-V.0	1978	293.6	15662	2008	20.0	no	no	no	no	no
62149.50d	147.6380	dre5	B-V.0	1978	293.6	4429	263	20.0	no	no	no	no	no
62149.65c	147.6380	endf66e	B-VI.0	1978	3000.1	47902	5399	20.0	no	no	no	no	yes
62149.66c	147.6380	endf66b	B-VI.0	1978	293.6	64240	7733	20.0	no	no	no	no	yes
** Sm-150 **													
62150.49c	148.6290	uresa	B-VI.2	1992	300.0	60992	8183	20.0	no	no	no	no	yes
62150.50c	148.6290	kidman	B-V.0	1974	293.6	9345	1329	20.0	no	no	no	no	no
** Sm-151 **													
62151.50c	149.6230	kidman	B-V.0	1980	293.6	7303	605	20.0	no	no	no	no	no
** Sm-152 **													
62152.49c	150.6150	uresa	B-VI.2	1992	300.0	203407	19737	20.0	no	no	no	no	yes
62152.50c	150.6150	kidman	B-V.0	1980	293.6	41252	4298	20.0	no	no	no	no	no

Table G.2 (Cont.)
Continuous-Energy and Discrete Neutron Data Libraries Maintained by X-5

<u>Z</u> <u>A</u> <u>I</u> <u>D</u>	<u>A</u> <u>W</u> <u>R</u>	<u>L</u> <u>i</u> <u>b</u> <u>r</u> <u>a</u> <u>r</u> <u>y</u> <u>N</u> <u>a</u> <u>m</u> <u>e</u>	<u>S</u> <u>o</u> <u>u</u> <u>r</u> <u>c</u> <u>e</u>	<u>E</u> <u>v</u> <u>a</u> <u>l</u> <u>D</u> <u>a</u> <u>t</u> <u>e</u>	<u>T</u> <u>e</u> <u>m</u> <u>p</u> <u>(</u> <u>°</u> <u>K</u> <u>)</u>	<u>L</u> <u>e</u> <u>n</u> <u>g</u> <u>t</u> <u>h</u> <u>w</u> <u>o</u> <u>r</u> <u>d</u> <u>s</u>	<u>N</u> <u>E</u>	<u>E</u> _{max} <u>(</u> <u>M</u> <u>e</u> <u>V</u> <u>)</u>	<u>G</u> <u>P</u> <u>D</u>	<u>U</u>	<u>C</u> <u>P</u>	<u>D</u> <u>N</u>	<u>U</u> <u>R</u>
Z = 63 ***** Europium *****													
** Eu-nat**													
63000.35c	150.6546	rmccsa	LLNL	<1985	yes	6926	364	20.0	yes	no	no	no	no
63000.35d	150.6546	drmcscs	LLNL	<1985	yes	6654	263	20.0	yes	no	no	no	no
63000.42c	150.6546	endl92	LLNL	<1992	300.0	37421	4498	30.0	yes	no	no	no	no
** Eu-151 **													
63151.49c	149.6230	uresa	B-VI.0	1986	300.0	147572	10471	20.0	yes	no	no	no	yes
63151.50c	149.6230	rmccs	B-V.0	1977	293.6	68057	5465	20.0	yes	no	no	no	no
63151.50d	149.6230	drmcscs	B-V.0	1977	293.6	10013	263	20.0	yes	no	no	no	no
63151.55d	149.6230	newxsd	LANL/T	1986	293.6	35199	263	20.0	yes	no	no	no	no
63151.55c	149.6230	newxs	LANL/T	1986	293.6	86575	4749	20.0	yes	no	no	no	no
63151.60c	149.6230	endlf60	B-VI.0	1986	293.6	96099	7394	20.0	yes	no	no	no	no
63151.65c	149.6230	endlf66e	B-VI.0	1986	3000.1	98867	5220	20.0	yes	no	no	no	yes
63151.66c	149.6230	endlf66b	B-VI.0	1986	293.6	155078	10841	20.0	yes	no	no	no	yes
** Eu-152 **													
63152.49c	150.6200	uresa	B-VI.0	1988	300.0	81509	6540	20.0	no	no	no	no	yes
63152.50d	150.6200	dre5	B-V.0	1973	293.6	5655	263	20.0	no	no	no	no	no
63152.50c	150.6200	endlf5u	B-V.0	1973	293.6	49313	4553	20.0	no	no	no	no	no
63152.65c	150.6200	endlf66e	B-VI.0	1988	3000.1	53516	3563	20.0	no	no	no	no	yes
63152.66c	150.6200	endlf66b	B-VI.0	1988	293.6	89485	6833	20.0	no	no	no	no	yes
** Eu-153 **													
63153.49c	151.6080	uresa	B-VI.0	1986	300.0	129446	8784	20.0	yes	no	no	no	yes
63153.50d	151.6070	drmcscs	B-V.0	1978	293.6	11244	263	20.0	yes	no	no	no	no
63153.50c	151.6070	rmccs	B-V.0	1978	293.6	55231	4636	20.0	yes	no	no	no	no
63153.55d	151.6080	newxsd	LANL/T	1986	293.6	36372	263	20.0	yes	no	no	no	no
63153.55c	151.6080	newxs	LANL/T	1986	293.6	72971	4174	20.0	yes	no	no	no	no
63153.60c	151.6080	endlf60	B-VI.0	1986	293.6	86490	6198	20.0	yes	no	no	no	no
63153.65c	151.6080	endlf66e	B-VI.0	1986	3000.1	93021	4791	20.0	yes	no	no	no	yes
63153.66c	151.6080	endlf66b	B-VI.0	1986	293.6	135491	9038	20.0	yes	no	no	no	yes
** Eu-154 **													
63154.49c	152.6000	uresa	B-VI.0	1989	300.0	72804	6627	20.0	no	no	no	no	yes
63154.50c	152.6000	endlf5u	B-V.0	1973	293.6	37008	4030	20.0	no	no	no	no	no
63154.50d	152.6000	dre5	B-V.0	1973	293.6	5458	263	20.0	no	no	no	no	no
63154.65c	152.6000	endlf66e	B-VI.0	1989	3000.1	54676	4078	20.0	no	no	no	no	yes
63154.66c	152.6000	endlf66b	B-VI.0	1989	293.6	80218	6916	20.0	no	no	no	no	yes
** Eu-155 **													
63155.50c	153.5920	kidman	B-V.0	1974	293.6	4532	273	20.0	no	no	no	no	no
63155.66c	153.5920	endlf66b	B-VI.1	1988	293.6	27638	2440	20.0	no	no	no	no	no
Z = 64 ***** Gadolinium *****													
** Gd-nat**													
64000.35c	155.8991	rmccsa	LLNL	<1985	yes	7878	454	20.0	yes	no	no	no	no
64000.35d	155.8991	drmcscs	LLNL	<1985	yes	6833	263	20.0	yes	no	no	no	no
** Gd-152 **													
64152.50c	150.6150	endlf5u	B-V.0	1977	293.6	26251	3285	20.0	no	no	no	no	no
64152.50d	150.6150	dre5	B-V.0	1977	293.6	5899	263	20.0	no	no	no	no	no
64152.55c	150.6150	misc5xs[7,14]	B-V.0:T	1986	293.6	32590	3285	20.0	yes	no	no	no	no
64152.60c	150.6150	endlf60	B-VI.0	1977	293.6	32760	4391	20.0	no	no	no	no	no
64152.65c	150.6150	endlf66e	B-VI.4	1994	3000.1	263235	20777	20.0	no	no	no	no	yes
64152.66c	150.6150	endlf66b	B-VI.4	1994	293.6	341562	29480	20.0	no	no	no	no	yes
** Gd-154 **													
64154.50d	152.5990	dre5	B-V.0	1977	293.6	5930	263	20.0	no	no	no	no	no
64154.50c	152.5990	endlf5u	B-V.0	1977	293.6	49572	7167	20.0	no	no	no	no	no
64154.55c	152.5990	misc5xs[7,14]	B-V.0:T	1986	293.6	59814	7167	20.0	yes	no	no	no	no
64154.60c	152.5990	endlf60	B-VI.0	1977	293.6	67662	10189	20.0	no	no	no	no	no
64154.65c	152.5990	endlf66e	B-VI.4	1994	3000.1	218806	21530	20.0	no	no	no	no	yes
64154.66c	152.5990	endlf66b	B-VI.4	1994	293.6	286357	31180	20.0	no	no	no	no	yes

Table G.2 (Cont.)
Continuous-Energy and Discrete Neutron Data Libraries Maintained by X-5

<u>Z</u> <u>A</u> <u>I</u> <u>D</u>	<u>A</u> <u>W</u> <u>R</u>	<u>L</u> <u>i</u> <u>b</u> <u>r</u> <u>a</u> <u>r</u> <u>y</u> <u>N</u> <u>a</u> <u>m</u> <u>e</u>	<u>S</u> <u>o</u> <u>u</u> <u>r</u> <u>c</u> <u>e</u>	<u>E</u> <u>v</u> <u>a</u> <u>l</u> <u>D</u> <u>a</u> <u>t</u> <u>e</u>	<u>T</u> <u>e</u> <u>m</u> <u>p</u> <u>(</u> <u>°</u> <u>K</u> <u>)</u>	<u>L</u> <u>e</u> <u>n</u> <u>g</u> <u>t</u> <u>h</u> <u>w</u> <u>o</u> <u>r</u> <u>d</u> <u>s</u>	<u>N</u> <u>E</u>	<u>E</u> _{max} <u>(</u> <u>M</u> <u>e</u> <u>V</u> <u>)</u>	<u>G</u> <u>P</u> <u>D</u>	<u>U</u>	<u>C</u> <u>P</u>	<u>D</u> <u>N</u>	<u>U</u> <u>R</u>
** Gd-155 **													
64155.50c	153.5920	endf5u	B-V.0	1977	293.6	44965	6314	20.0	no	no	no	no	no
64155.50d	153.5920	dre5	B-V.0	1977	293.6	6528	263	20.0	no	no	no	no	no
64155.55c	153.5920	misc5xs[7,14]	B-V.0:T	1986	293.6	54346	6314	20.0	yes	no	no	no	no
64155.60c	153.5920	endf60	B-VI.0	1977	293.6	61398	9052	20.0	no	no	no	no	no
64155.65c	153.5920	endf66e	B-VI.0	1977	3000.1	62954	6748	20.0	no	no	no	no	yes
64155.66c	153.5920	endf66b	B-VI.0	1977	293.6	106795	13011	20.0	no	no	no	no	yes
** Gd-156 **													
64156.50c	154.5830	endf5u	B-V.0	1977	293.6	37371	3964	20.0	no	no	no	no	no
64156.50d	154.5830	dre5	B-V.0	1977	293.6	6175	263	20.0	no	no	no	no	no
64156.55c	154.5830	misc5xs[7,14]	B-V.0:T	1986	293.6	44391	3964	20.0	yes	no	no	no	no
64156.60c	154.5830	endf60	B-VI.0	1977	293.6	42885	5281	20.0	no	no	no	no	no
64156.66c	154.5830	endf66b	B-VI.0	1977	293.6	79827	7354	20.0	no	no	no	no	no
** Gd-157 **													
64157.50d	155.5760	dre5	B-V.0	1977	293.6	6346	263	20.0	no	no	no	no	no
64157.50c	155.5760	endf5u	B-V.0	1977	293.6	38975	5370	20.0	no	no	no	no	no
64157.55c	155.5760	misc5xs[7,14]	B-V.0:T	1986	293.6	47271	5370	20.0	yes	no	no	no	no
64157.60c	155.5760	endf60	B-VI.0	1977	293.6	56957	8368	20.0	no	no	no	no	no
64157.65c	155.5760	endf66e	B-VI.0	1977	3000.1	71857	8101	20.0	no	no	no	no	yes
64157.66c	155.5760	endf66b	B-VI.0	1977	293.6	99199	12007	20.0	no	no	no	no	yes
** Gd-158 **													
64158.50d	156.5670	dre5	B-V.0	1977	293.6	5811	263	20.0	no	no	no	no	no
64158.50c	156.5670	endf5u	B-V.0	1977	293.6	95876	15000	20.0	no	no	no	no	no
64158.55c	156.5670	misc5xs[7,14]	B-V.0:T	1986	293.6	113916	15000	20.0	yes	no	no	no	no
64158.60c	156.5670	endf60	B-VI.0	1977	293.6	59210	8909	20.0	no	no	no	no	no
64158.66c	156.5670	endf66b	B-VI.0	1977	293.6	152895	19903	20.0	no	no	no	no	no
** Gd-160 **													
64160.50d	158.5530	dre5	B-V.0	1977	293.6	5030	263	20.0	no	no	no	no	no
64160.50c	158.5530	endf5u	B-V.0	1977	293.6	53988	8229	20.0	no	no	no	no	no
64160.55c	158.5530	misc5xs[7,14]	B-V.0:T	1986	293.6	65261	8229	20.0	yes	no	no	no	no
64160.60c	158.5530	endf60	B-VI.0	1977	293.6	54488	8304	20.0	no	no	no	no	no
64160.66c	158.5530	endf66b	B-VI.0	1977	293.6	90407	11183	20.0	no	no	no	no	no
Z = 67 ***** Holmium *****													
** Ho-165 **													
67165.35c	163.5135	rmccsa	LLNL	<1985	yes	54279	7075	20.0	yes	no	no	no	no
67165.35d	163.5135	drmcsc	LLNL	<1985	yes	7019	263	20.0	yes	no	no	no	no
67165.42c	163.5135	endl92	LLNL	<1992	300.0	103467	13884	30.0	yes	no	no	no	no
67165.55c	163.5130	newxs	LANL/T	1986	293.6	56605	2426	30.0	yes	no	no	no	no
67165.55d	163.5130	newxsd	LANL/T	1986	293.6	42266	263	20.0	yes	no	no	no	no
67165.60c	163.5130	endf60	B-VI.0	1988	293.6	75307	4688	30.0	yes	no	no	no	no
67165.66c	163.5130	endf66b	B-VI.5	1988	293.6	101124	6648	30.0	yes	no	no	no	no
Z = 69 ***** Thulium *****													
** Tm-169 **													
69169.55c	167.4830	misc5xs[7]	LANL/T	1986	300.0	47941	4738	20.0	no	no	no	no	no
Z = 71 ***** Lutetium *****													
** Lu-175 **													
71175.65c	173.4380	endf66e	B-VI.0	1967	3000.1	34931	3631	20.0	no	no	no	no	yes
71175.66c	173.4380	endf66b	B-VI.0	1967	293.6	42687	4739	20.0	no	no	no	no	yes
** Lu-176 **													
71176.65c	174.4300	endf66e	B-VI.0	1967	3000.1	37422	3903	20.0	no	no	no	no	yes
71176.66c	174.4300	endf66b	B-VI.0	1967	293.6	48096	5428	20.0	no	no	no	no	yes

Table G.2 (Cont.)
Continuous-Energy and Discrete Neutron Data Libraries Maintained by X-5

<u>Z</u> <u>A</u> <u>I</u> <u>D</u>	<u>A</u> <u>W</u> <u>R</u>	<u>L</u> <u>i</u> <u>b</u> <u>r</u> <u>a</u> <u>r</u> <u>y</u> <u>N</u> <u>a</u> <u>m</u> <u>e</u>	<u>S</u> <u>o</u> <u>u</u> <u>r</u> <u>c</u> <u>e</u>	<u>E</u> <u>v</u> <u>a</u> <u>l</u> <u>D</u> <u>a</u> <u>t</u> <u>e</u>	<u>T</u> <u>e</u> <u>m</u> <u>p</u> <u>(</u> <u>°</u> <u>K</u> <u>)</u>	<u>L</u> <u>e</u> <u>n</u> <u>g</u> <u>t</u> <u>h</u> <u>w</u> <u>o</u> <u>r</u> <u>d</u> <u>s</u>	<u>N</u> <u>E</u>	<u>E</u> _{max} <u>(</u> <u>M</u> <u>e</u> <u>V</u> <u>)</u>	<u>G</u> <u>P</u> <u>D</u>	<u>U</u>	<u>C</u> <u>P</u>	<u>D</u> <u>N</u>	<u>U</u> <u>R</u>
Z = 72 ***** Hafnium *****													
** Hf-nat**													
72000.42c	176.9567	endl92	LLNL	<1992	300.0	108989	14113	30.0	yes	no	no	no	no
72000.50d	176.9540	newxsd	B-V.0	1976	293.6	4751	263	20.0	no	no	no	no	no
72000.50c	176.9540	newxs	B-V.0	1976	293.6	52231	8270	20.0	no	no	no	no	no
72000.60c	176.9540	endf60	B-VI.0	1976	293.6	84369	13634	20.0	no	no	no	no	no
** Hf-174 **													
72174.65c	172.4460	endf66e	B-VI.2	1992	3000.1	35072	3834	20.0	no	no	no	no	yes
72174.66c	172.4460	endf66b	B-VI.2	1992	293.6	39545	4473	20.0	no	no	no	no	yes
** Hf-176 **													
72176.65c	174.4300	endf66e	B-VI.2	1992	3000.1	55807	6869	20.0	no	no	no	no	yes
72176.66c	174.4300	endf66b	B-VI.2	1992	293.6	66727	8429	20.0	no	no	no	no	yes
** Hf-177 **													
72177.65c	175.4230	endf66e	B-VI.2	1991	3000.1	115867	15278	20.0	no	no	no	no	yes
72177.66c	175.4230	endf66b	B-VI.2	1991	293.6	219075	30022	20.0	no	no	no	no	yes
** Hf-178 **													
72178.65c	176.4150	endf66e	B-VI.2	1991	3000.1	58452	7291	20.0	no	no	no	no	yes
72178.66c	176.4150	endf66b	B-VI.2	1991	293.6	67580	8595	20.0	no	no	no	no	yes
** Hf-179 **													
72179.65c	177.4090	endf66e	B-VI.2	1992	3000.1	79130	10151	20.0	no	no	no	no	yes
72179.66c	177.4090	endf66b	B-VI.2	1992	293.6	106850	14111	20.0	no	no	no	no	yes
** Hf-180 **													
72180.65c	178.4010	endf66e	B-VI.2	1991	3000.1	112444	15082	20.0	no	no	no	no	yes
72180.66c	178.4010	endf66b	B-VI.2	1991	293.6	145939	19867	20.0	no	no	no	no	yes
Z = 73 ***** Tantalum *****													
** Ta-181 **													
73181.42c	179.3936	endl92	LLNL	<1992	300.0	47852	4927	30.0	yes	no	no	no	no
73181.50d	179.4000	dre5	B-V.0	1972	293.6	16361	263	20.0	yes	no	no	no	no
73181.50c	179.4000	endf5u	B-V.0	1972	293.6	60740	6341	20.0	yes	no	no	no	no
73181.51c	179.4000	rmccs	B-V.0	1972	293.6	21527	753	20.0	yes	no	no	no	no
73181.51d	179.4000	drmcsc	B-V.0	1972	293.6	16361	263	20.0	yes	no	no	no	no
73181.60c	179.4000	endf60	B-VI.0	1972	293.6	91374	10352	20.0	yes	no	no	no	no
73181.64c	179.4000	endf66d	B-VI.0	1972	77.0	158545	17152	20.0	yes	no	no	no	no
73181.66c	179.4000	endf66b	B-VI.0	1972	293.6	140345	14877	20.0	yes	no	no	no	no
** Ta-182 **													
73182.49c	180.3870	uresa	B-VI.0	1971	300.0	20850	2463	20.0	no	no	no	no	yes
73182.60c	180.3870	endf60	B-VI.0	1971	293.6	12085	1698	20.0	no	no	no	no	no
73182.64c	180.3870	endf66d	B-VI.0	1971	77.0	29837	3020	20.0	no	no	no	no	yes
73182.65c	180.3870	endf66e	B-VI.0	1971	3000.1	25028	2333	20.0	no	no	no	no	yes
73182.66c	180.3870	endf66b	B-VI.0	1971	293.6	28577	2840	20.0	no	no	no	no	yes
Z = 74 ***** Tungsten *****													
** W-nat**													
74000.21c	182.2706	100xs[3]	LANL/T:X	1989	300.0	194513	21386	100.0	yes	no	no	no	no
74000.55c	182.2770	rmccs	B-V.2	1982	293.6	50639	1816	20.0	yes	no	no	no	no
74000.55d	182.2770	drmcsc	B-V.2	1982	293.6	34272	263	20.0	yes	no	no	no	no
** W-182 **													
74182.24c	180.3900	la150n	B-VI.6	1996	293.6	246875	16896	150.0	yes	no	yes	no	yes
74182.48c	180.3900	uresa[16]	B-VI.0	1980	300.0	150072	16495	20.0	no	no	no	no	yes
74182.50c	180.3900	endf5p	B-V.0	1973	293.6	94367	11128	20.0	yes	no	no	no	no
74182.50d	180.3900	dre5	B-V.0	1973	293.6	17729	263	20.0	yes	no	no	no	no
74182.55c	180.3900	rmccsa	B-V.2	1980	293.6	122290	13865	20.0	yes	no	no	no	no
74182.55d	180.3900	drmcsc	B-V.2	1980	293.6	26387	263	20.0	yes	no	no	no	no
74182.60c	180.3900	endf60	B-VI.0	1980	293.6	113177	12283	20.0	yes	no	no	no	no
74182.61c	180.3900	actib	B-VI.8	2000	77.0	269718.0	18237	150.0	yes	no	yes	no	yes
74182.62c	180.3900	actia	B-VI.8	2000	293.6	258342.0	16815	150.0	yes	no	yes	no	yes
74182.63c	180.3900	actib	B-VI.8	2000	3000.1	232047.0	13528	150.0	yes	no	yes	no	yes
74182.64c	180.3900	endf66d	B-VI.6	1996	77.0	257611	18238	150.0	yes	no	yes	no	yes
74182.65c	180.3900	endf66e	B-VI.6	1996	3000.1	219900	13524	150.0	yes	no	yes	no	yes
74182.66c	180.3900	endf66b	B-VI.6	1996	293.6	246251	16818	150.0	yes	no	yes	no	yes

Table G.2 (Cont.)
Continuous-Energy and Discrete Neutron Data Libraries Maintained by X-5

<u>ZAID</u>	<u>AWR</u>	<u>Library</u> <u>Name</u>	<u>Source</u>	<u>Eval</u> <u>Date</u>	<u>Temp</u> <u>(°K)</u>	<u>Length</u> <u>words</u>	<u>NE</u>	<u>E_{max}</u> <u>(MeV)</u>	<u>GPD</u>	<u>U</u>	<u>CP</u>	<u>DN</u>	<u>UR</u>
** W-183 **													
74183.24c	181.3800	la150n	B-VI.6	1996	293.6	217095	13034	150.0	yes	no	yes	no	yes
74183.48c	181.3800	uresa[16]	B-VI.0	1980	300.0	119637	12616	20.0	no	no	no	no	yes
74183.50c	181.3800	endf5p	B-V.0	1973	293.6	58799	5843	20.0	yes	no	no	no	no
74183.50d	181.3800	dre5	B-V.0	1973	293.6	19443	263	20.0	yes	no	no	no	no
74183.55d	181.3800	drmcscs	B-V.2	1980	293.6	26320	263	20.0	yes	no	no	no	no
74183.55c	181.3800	rmccsa	B-V.2	1980	293.6	79534	8083	20.0	yes	no	no	no	no
74183.60c	181.3800	endf60	B-VI.0	1980	293.6	89350	9131	20.0	yes	no	no	no	no
74183.61c	181.3800	actib	B-VI.8	2000	77.0	235761.0	14449	150.0	yes	no	yes	no	yes
74183.62c	181.3800	actia	B-VI.8	2000	293.6	224856.0	13086	150.0	yes	no	yes	no	yes
74183.63c	181.3800	actib	B-VI.8	2000	3000.1	198226.0	9757	150.0	yes	no	yes	no	yes
74183.64c	181.3800	endf66d	B-VI.6	1996	77.0	228392	14446	150.0	yes	no	yes	no	yes
74183.65c	181.3800	endf66e	B-VI.6	1996	3000.1	190833	9751	150.0	yes	no	yes	no	yes
74183.66c	181.3800	endf66b	B-VI.6	1996	293.6	217447	13078	150.0	yes	no	yes	no	yes
** W-184 **													
74184.24c	182.3700	la150n	B-VI.6	1996	293.6	192693	10180	150.0	yes	no	yes	no	yes
74184.48c	182.3700	uresa[16]	B-VI.0	1980	300.0	97118	9794	20.0	no	no	no	no	yes
74184.50c	182.3700	endf5p	B-V.0	1973	293.6	58870	6173	20.0	yes	no	no	no	no
74184.50d	182.3700	dre5	B-V.0	1973	293.6	17032	263	20.0	yes	no	no	no	no
74184.55d	182.3700	drmcscs	B-V.2	1980	293.6	26110	263	20.0	yes	no	no	no	no
74184.55c	182.3700	rmccsa	B-V.2	1980	293.6	80006	7835	20.0	yes	no	no	no	no
74184.60c	182.3700	endf60	B-VI.0	1980	293.6	78809	7368	20.0	yes	no	no	no	no
74184.61c	182.3700	actib	B-VI.8	2000	77.0	200883.0	10902	150.0	yes	no	yes	no	yes
74184.62c	182.3700	actia	B-VI.8	2000	293.6	194523.0	10107	150.0	yes	no	yes	no	yes
74184.63c	182.3700	actib	B-VI.8	2000	3000.1	181213.0	8443	150.0	yes	no	yes	no	yes
74184.64c	182.3700	endf66d	B-VI.6	1996	77.0	198499	10906	150.0	yes	no	yes	no	yes
74184.65c	182.3700	endf66e	B-VI.6	1996	3000.1	178773	8440	150.0	yes	no	yes	no	yes
74184.66c	182.3700	endf66b	B-VI.6	1996	293.6	192123	10109	150.0	yes	no	yes	no	yes
** W-186 **													
74186.24c	184.3600	la150n	B-VI.6	1996	293.6	187863	10848	150.0	yes	no	yes	no	yes
74186.48c	184.3600	uresa[16]	B-VI.0	1980	300.0	102199	10485	20.0	no	no	no	no	yes
74186.50d	184.3600	dre5	B-V.0	1973	293.6	17018	263	20.0	yes	no	no	no	no
74186.50c	184.3600	endf5p	B-V.0	1973	293.6	63701	6866	20.0	yes	no	no	no	no
74186.55d	184.3600	drmcscs	B-V.2	1980	293.6	26281	263	20.0	yes	no	no	no	no
74186.55c	184.3600	rmccsa	B-V.2	1980	293.6	83618	8342	20.0	yes	no	no	no	no
74186.60c	184.3600	endf60	B-VI.0	1980	293.6	82010	7793	20.0	yes	no	no	no	no
74186.61c	184.3600	actib	B-VI.8	2000	77.0	207824.0	11635	150.0	yes	no	yes	no	yes
74186.62c	184.3600	actia	B-VI.8	2000	293.6	202211.0	10833	150.0	yes	no	yes	no	yes
74186.63c	184.3600	actib	B-VI.8	2000	3000.1	190276.0	9128	150.0	yes	no	yes	no	yes
74186.64c	184.3600	endf66d	B-VI.6	1996	77.0	193372	11635	150.0	yes	no	yes	no	yes
74186.65c	184.3600	endf66e	B-VI.6	1996	3000.1	175817	9127	150.0	yes	no	yes	no	yes
74186.66c	184.3600	endf66c	B-VI.6	1996	293.6	187731	10829	150.0	yes	no	yes	no	yes

Z = 75 ***** Rhenium *****

** Re-185 **													
75185.32c	183.3612	misc5xs[7]	LLNL	<1985	yes	13650	1488	20.0	yes	no	no	no	no
75185.42c	183.3641	endl92	LLNL	<1992	300.0	23715	2214	30.0	yes	no	no	no	no
75185.50c	183.3640	rmccsa	B-V.0	1968	293.6	9190	1168	20.0	no	no	no	no	no
75185.50d	183.3640	drmcscs	B-V.0	1968	293.6	4252	263	20.0	no	no	no	no	no
75185.60c	183.3640	endf60	B-VI.0	1990	293.6	102775	16719	20.0	no	no	no	no	no
75185.65c	183.3640	endf66e	B-VI.0	1990	3000.1	179325	24470	20.0	no	no	no	no	yes
75185.66c	183.3640	endf66c	B-VI.0	1990	293.6	397396	55623	20.0	no	no	no	no	yes
** Re-187 **													
75187.32c	185.3539	misc5xs[7]	LLNL	<1985	yes	12318	1296	20.0	yes	no	no	no	no
75187.42c	185.3497	endl92	LLNL	<1992	300.0	20969	1821	30.0	yes	no	no	no	no
75187.50c	185.3500	rmccsa	B-V.0	1968	293.6	8262	959	20.0	no	no	no	no	no
75187.50d	185.3500	drmcscs	B-V.0	1968	293.6	4675	263	20.0	no	no	no	no	no
75187.60c	185.3500	endf60	B-VI.0	1990	293.6	96989	15624	20.0	no	no	no	no	no
75187.65c	185.3500	endf66e	B-VI.0	1990	3000.1	180705	24518	20.0	no	no	no	no	yes
75187.66c	185.3500	endf66c	B-VI.0	1990	293.6	358295	49888	20.0	no	no	no	no	yes

Table G.2 (Cont.)
Continuous-Energy and Discrete Neutron Data Libraries Maintained by X-5

<u>Z</u> <u>A</u> <u>I</u> <u>D</u>	<u>A</u> <u>W</u> <u>R</u>	<u>L</u> <u>i</u> <u>b</u> <u>r</u> <u>a</u> <u>r</u> <u>y</u> <u>N</u> <u>a</u> <u>m</u> <u>e</u>	<u>S</u> <u>o</u> <u>u</u> <u>r</u> <u>c</u> <u>e</u>	<u>E</u> <u>v</u> <u>a</u> <u>l</u> <u>D</u> <u>a</u> <u>t</u> <u>e</u>	<u>T</u> <u>e</u> <u>m</u> <u>p</u> <u>(</u> <u>°</u> <u>K</u> <u>)</u>	<u>L</u> <u>e</u> <u>n</u> <u>g</u> <u>t</u> <u>h</u> <u>w</u> <u>o</u> <u>r</u> <u>d</u> <u>s</u>	<u>N</u> <u>E</u>	<u>E</u> _{max} <u>(</u> <u>M</u> <u>e</u> <u>V</u> <u>)</u>	<u>G</u> <u>P</u> <u>D</u>	<u>U</u>	<u>C</u> <u>P</u>	<u>D</u> <u>N</u>	<u>U</u> <u>R</u>
Z = 77 ***** Iridium *****													
** Ir-nat**													
77000.55c	190.5630	misc5xs[7]	LANL/T	1986	300.0	43071	3704	20.0	no	no	no	no	no
** Ir-191 **													
77191.49c	189.3200	uresa	B-VI.4	1995	300.0	83955	8976	20.0	yes	no	no	no	yes
77191.65c	189.3200	endf66c	B-VI.4:X	1995	3000.1	64690	6116	20.0	yes	no	no	no	yes
77191.66c	189.3200	endf66c	B-VI.4:X	1995	293.6	90082	9290	20.0	yes	no	no	no	yes
** Ir-193 **													
77193.49c	191.3050	uresa	B-VI.4	1995	300.0	82966	8943	20.0	yes	no	no	no	yes
77193.65c	191.3050	endf66c	B-VI.4:X	1995	3000.1	69056	6751	20.0	yes	no	no	no	yes
77193.66c	191.3050	endf66c	B-VI.4:X	1995	293.6	88688	9205	20.0	yes	no	no	no	yes
Z = 78 ***** Platinum *****													
** Pt-nat**													
78000.35c	193.4141	rmccsa	LLNL	<1985	0.0	15371	1497	20.0	yes	no	no	no	no
78000.35d	193.4141	drmcsc	LLNL	<1985	0.0	6933	263	20.0	yes	no	no	no	no
78000.40c	193.4141	endl92	LLNL	<1992	300.0	43559	5400	30.0	yes	no	no	no	no
78000.42c	193.4141	endl92	LLNL:X	<1992	300.0	43559	5400	30.0	yes	no	no	no	no
Z = 79 ***** Gold *****													
** Au-197 **													
79197.50d	195.2740	dre5	B-V.0	1977	293.6	4882	263	20.0	no	no	no	no	no
79197.50c	195.2740	endf5p	B-V.0	1977	293.6	139425	22632	20.0	no	no	no	no	no
79197.55c	195.2740	rmccsa	LANL/T	1983[4]	293.6	134325	17909	20.0	yes	no	no	no	no
79197.55d	195.2740	drmcsc	LANL/T	1983[4]	293.6	7883	263	20.0	yes	no	no	no	no
79197.56d	195.2740	newxsd	LANL/T	1984	293.6	38801	263	20.0	yes	no	no	no	no
79197.56c	195.2740	newxs	LANL/T	1984	293.6	122482	11823	30.0	yes	no	no	no	no
79197.60c	195.2740	endf60	B-VI.1	1984	293.6	161039	17724	30.0	yes	no	no	no	no
79197.66c	195.2740	endf66c	B-VI.1	1984	293.6	377905	39417	30.0	yes	no	no	no	no
Z = 80 ***** Mercury *****													
** Hg-nat**													
80000.40c	198.8668	endl92	LLNL	<1992	300.0	29731	2507	30.0	yes	no	no	no	no
80000.42c	198.8668	endl92	LLNL:X	<1992	300.0	29731	2507	30.0	yes	no	no	no	no
** Hg-196 **													
80196.24c	194.2820	la150n	LANL	1998	293.6	153206	1690	150.0	yes	no	yes	no	no
** Hg-198 **													
80198.24c	196.2660	la150n	LANL	1998	293.6	172481	3205	150.0	yes	no	yes	no	no
** Hg-199 **													
80199.24c	197.2590	la150n	LANL	1998	293.6	173336	4126	150.0	yes	no	yes	no	no
** Hg-200 **													
80200.24c	198.2500	la150n	LANL	1998	293.6	192339	2560	150.0	yes	no	yes	no	no
** Hg-201 **													
80201.24c	199.2440	la150n	LANL	1998	293.6	166179	3492	150.0	yes	no	yes	no	no
** Hg-202 **													
80202.24c	200.2360	la150n	LANL	1998	293.6	154736	1887	150.0	yes	no	yes	no	no
** Hg-204 **													
80204.24c	202.2210	la150n	LANL	1998	293.6	140754	832	150.0	yes	no	yes	no	no
Z = 82 ***** Lead *****													
** Pb-nat**													
82000.42c	205.4200	endl92	LLNL	<1992	300.0	270244	18969	30.0	yes	no	no	no	no
82000.50d	205.4300	drmcsc	B-V.0	1976	293.6	20649	263	20.0	yes	no	no	no	no
82000.50c	205.4300	rmccsc	B-V.0	1976	293.6	37633	1346	20.0	yes	no	no	no	no

Table G.2 (Cont.)
Continuous-Energy and Discrete Neutron Data Libraries Maintained by X-5

<u>ZAID</u>	<u>AWR</u>	<u>Library</u> <u>Name</u>	<u>Source</u>	<u>Eval</u> <u>Date</u>	<u>Temp</u> <u>(°K)</u>	<u>Length</u> <u>words</u>	<u>NE</u>	<u>E_{max}</u> <u>(MeV)</u>	<u>GPD</u>	<u>\bar{U}</u>	<u>CP</u>	<u>DN</u>	<u>UR</u>
** Pb-206 **													
82206.24c	204.2000	la150n	B-VI.6	1996	293.6	424548	30415	150.0	yes	no	yes	no	no
82206.60c	204.2000	endf60	B-VI.0	1989	293.6	148815	12872	20.0	yes	no	no	no	no
82206.66c	204.2000	endf66c	B-VI.6	1997	293.6	420901	30414	150.0	yes	no	yes	no	no
** Pb-207 **													
82207.24c	205.2000	la150n	B-VI.6	1996	293.6	280309	10689	150.0	yes	no	yes	no	no
82207.60c	205.2000	endf60	B-VI.1	1991	293.6	111750	7524	20.0	yes	no	no	no	no
82207.66c	205.2000	endf66c	B-VI.6	1997	293.6	276136	10689	150.0	yes	no	yes	no	no
** Pb-208 **													
82208.25c	206.1900	la150n	LANL	1996	293.6	344772	6633	150.0	yes	no	yes	no	no
82208.60c	206.1900	endf60	B-VI.0	1989	293.6	70740	5105	20.0	yes	no	no	no	no
82208.66c	206.1900	endf66c	B-VI.6:X	1996	293.6	344865	6634	150.0	yes	no	yes	no	no
Z = 83 ***** Bismuth *****													
** Bi-209 **													
83209.24c	207.1850	la150n	LANL	1999	293.6	249386	11047	150.0	yes	no	yes	no	no
83209.42c	207.1851	endl92	LLNL	<1992	300.0	20921	1200	30.0	yes	no	no	no	no
83209.50c	207.1850	endf5u	B-V.0	1980	293.6	14939	1300	20.0	yes	no	no	no	no
83209.50d	207.1850	dre5	B-V.0	1980	293.6	7516	263	20.0	yes	no	no	no	no
83209.51d	207.1850	drmcscs	B-V.0	1980	293.6	7516	263	20.0	yes	no	no	no	no
83209.51c	207.1850	rmccs	B-V.0	1980	293.6	13721	1186	20.0	yes	no	no	no	no
83209.60c	207.1850	endf60	B-VI.0	1989	293.6	100138	8427	20.0	yes	no	no	no	no
83209.66c	207.1850	endf66c	B-VI.3	1989	293.6	161302	10906	20.0	yes	no	no	no	no
Z = 90 ***** Thorium *****													
** Th-230 **													
90230.60c	228.0600	endf60	B-VI.0	1977	293.6	35155	5533	20.0	no	tot	no	no	no
90230.66c	228.0600	endf66c	B-VI.0	1977	293.6	64761	8428	20.0	no	tot	no	no	no
** Th-231 **													
90231.42c	229.0516	endl92	LLNL	<1992	300.0	15712	187	30.0	yes	both	no	no	no
** Th-232 **													
90232.42c	230.0447	endl92	LLNL	<1992	300.0	109829	13719	30.0	yes	both	no	no	no
90232.48c	230.0400	uresa[16]	B-VI.0	1977	300.0	305942	41414	20.0	no	both	no	no	yes
90232.50d	230.0400	dre5	B-V.0	1977	293.6	11937	263	20.0	yes	both	no	no	no
90232.50c	230.0400	endf5u	B-V.0	1977	293.6	152782	17901	20.0	yes	both	no	no	no
90232.51d	230.0400	drmcscs	B-V.0	1977	293.6	11937	263	20.0	yes	both	no	no	no
90232.51c	230.0400	rmccs	B-V.0	1977	293.6	17925	1062	20.0	yes	both	no	no	no
90232.60c	230.0400	endf60	B-VI.0	1977	293.6	127606	16381	20.0	yes	both	no	no	no
90232.61c	230.0400	endf6dn	B-VI.0	1977	293.6	132594	16381	20.0	yes	both	no	yes	no
90232.65c	230.0400	endf66e	B-VI.0	1977	3000.1	238295	25915	20.0	yes	both	no	yes	yes
90232.66c	230.0400	endf66c	B-VI.0	1977	293.6	362871	41487	20.0	yes	both	no	yes	yes
** Th-233 **													
90233.42c	231.0396	endl92	LLNL	<1992	300.0	16015	206	30.0	yes	both	no	no	no
Z = 91 ***** Protactinium *****													
** Pa-231 **													
91231.60c	229.0500	endf60	B-VI.0	1977	293.6	19835	2610	20.0	no	both	no	no	no
91231.61c	229.0500	endf6dn	B-VI.0	1977	293.6	24733	2610	20.0	no	both	no	yes	no
91231.65c	229.0500	endf66e	B-VI.0	1977	3000.1	31463	2422	20.0	no	both	no	yes	yes
91231.66c	229.0500	endf66c	B-VI.0	1977	293.6	45111	4128	20.0	no	both	no	yes	yes
** Pa-233 **													
91233.42c	231.0383	endl92	LLNL	<1992	300.0	27720	1982	30.0	yes	both	no	no	no
91233.50d	231.0380	dre5	B-V.0	1974	293.6	3700	263	20.0	no	tot	no	no	no
91233.50c	231.0380	endf5u	B-V.0	1974	293.6	19519	2915	20.0	no	tot	no	no	no
91233.51d	231.0380	drmcscs	B-V.0	1974	293.6	3700	263	20.0	no	tot	no	no	no
91233.51c	231.0380	rmccs	B-V.0	1974	293.6	5641	637	20.0	no	tot	no	no	no
91233.65c	231.0380	endf66e	B-VI.0	1974	3000.1	34848	3993	20.0	no	tot	no	no	yes
91233.66c	231.0380	endf66c	B-VI.0	1974	293.6	50577	6240	20.0	no	tot	no	no	yes

Table G.2 (Cont.)
Continuous-Energy and Discrete Neutron Data Libraries Maintained by X-5

<u>Z</u> <u>A</u> <u>I</u> <u>D</u>	<u>A</u> <u>W</u> <u>R</u>	<u>L</u> <u>i</u> <u>b</u> <u>r</u> <u>a</u> <u>r</u> <u>y</u> <u>N</u> <u>a</u> <u>m</u> <u>e</u>	<u>S</u> <u>o</u> <u>u</u> <u>r</u> <u>c</u> <u>e</u>	<u>E</u> <u>v</u> <u>a</u> <u>l</u> <u>D</u> <u>a</u> <u>t</u> <u>e</u>	<u>T</u> <u>e</u> <u>m</u> <u>p</u> <u>(</u> <u>°</u> <u>K</u> <u>)</u>	<u>L</u> <u>e</u> <u>n</u> <u>g</u> <u>t</u> <u>h</u> <u>w</u> <u>o</u> <u>r</u> <u>d</u> <u>s</u>	<u>N</u> <u>E</u>	<u>E</u> _{max} <u>(</u> <u>M</u> <u>e</u> <u>V</u> <u>)</u>	<u>G</u> <u>P</u> <u>D</u>	<u>U</u>	<u>C</u> <u>P</u>	<u>D</u> <u>N</u>	<u>U</u> <u>R</u>
Z = 92 ***** Uranium *****													
** U-232 **													
92232.49c	230.0400	uresa	B-VI.0	1977	300.0	21813	2820	20.0	no	both	no	no	yes
92232.60c	230.0400	endf60	B-VI.0	1977	293.6	13839	1759	20.0	no	both	no	no	no
92232.61c	230.0400	endf6dn	B-VI.0	1977	293.6	18734	1759	20.0	no	both	no	yes	no
92232.65c	230.0400	endf66e	B-VI.0	1977	3000.1	29048	2318	20.0	no	both	no	yes	yes
92232.66c	230.0400	endf66c	B-VI.0	1977	293.6	32792	2786	20.0	no	both	no	yes	yes
92232.68c	230.0438	t16_2003	LANL/T16	2003	3000.0	183542	5757	30.0	yes	both	no	no	yes
92232.69c	230.0438	t16_2003	LANL/T16	2003	293.6	197150	7269	30.0	yes	both	no	no	yes
** U-233 **													
92233.42c	231.0377	endl92	LLNL	<1992	300.0	29521	2163	30.0	yes	both	no	no	no
92233.49c	231.0430	uresa	B-VI.0	1978	300.0	47100	4601	20.0	yes	both	no	no	yes
92233.50d	231.0430	drmcscs	B-V.0	1978	293.6	4172	263	20.0	no	both	no	no	no
92233.50c	231.0430	rmccs	B-V.0	1978	293.6	18815	2293	20.0	no	both	no	no	no
92233.60c	231.0430	endf60[15]	B-VI.0	1978	293.6	32226	3223	20.0	yes	both	no	no	no
92233.61c	231.0430	endf6dn	B-VI.0	1978	293.6	37218	3223	20.0	yes	both	no	yes	no
92233.65c	231.0430	endf66e	B-VI.0	1978	3000.1	49260	3354	20.0	yes	both	no	yes	yes
92233.66c	231.0430	endf66c	B-VI.0	1978	293.6	62463	4821	20.0	yes	both	no	yes	yes
92233.68c	231.0377	t16_2003	LANL/T16	2003	3000.0	323539	11206	30.0	yes	both	no	yes	yes
92233.69c	231.0377	t16_2003	LANL/T16	2003	293.6	441295	24290	30.0	yes	both	no	yes	yes
** U-234 **													
92234.42c	232.0304	endl92	LLNL	<1992	300.0	13677	149	30.0	yes	both	no	no	no
92234.49c	232.0300	uresa	B-VI.0	1978	300.0	161296	22539	20.0	no	both	no	no	yes
92234.50c	232.0300	endf5p	B-V.0	1978	293.6	89433	12430	20.0	no	tot	no	no	no
92234.50d	232.0300	dre5	B-V.0	1978	293.6	4833	263	20.0	no	tot	no	no	no
92234.51d	232.0300	drmcscs	B-V.0	1978	293.6	4833	263	20.0	no	tot	no	no	no
92234.51c	232.0300	rmccs	B-V.0	1978	293.6	6426	672	20.0	no	tot	no	no	no
92234.60c	232.0300	endf60	B-VI.0	1978	293.6	77059	10660	17.5	no	both	no	no	no
92234.61c	232.0300	endf6dn	B-VI.0	1978	293.6	82047	10660	17.5	no	both	no	yes	no
92234.65c	232.0300	endf66e	B-VI.0	1978	3000.1	144201	16318	20.0	no	both	no	yes	yes
92234.66c	232.0300	endf66c	B-VI.0	1978	293.6	196273	22827	20.0	no	both	no	yes	yes
92234.68c	232.0304	t16_2003	LANL/T16	2003	3000.0	286070	16719	30.0	yes	both	no	yes	yes
92234.69c	232.0304	t16_2003	LANL/T16	2003	293.6	344651	23228	30.0	yes	both	no	yes	yes
** U-235 **													
92235.11c	233.0250	endf62mt	B-VI.2	1993	77.0	696398	78912	20.0	yes	both	no	no	no
92235.12c	233.0250	endf62mt	B-VI.2	1993	400.0	411854	43344	20.0	yes	both	no	no	no
92235.13c	233.0250	endf62mt	B-VI.2	1993	500.0	379726	39328	20.0	yes	both	no	no	no
92235.14c	233.0250	endf62mt	B-VI.2	1993	600.0	353678	36072	20.0	yes	both	no	no	no
92235.15c	233.0250	endf62mt	B-VI.2	1993	800.0	316622	31440	20.0	yes	both	no	no	no
92235.16c	233.0250	endf62mt	B-VI.2	1993	900.0	300278	29397	20.0	yes	both	no	no	no
92235.17c	233.0250	endf62mt	B-VI.2	1993	1200.0	269062	25495	20.0	yes	both	no	no	no
92235.42c	233.0248	endl92	LLNL	<1992	300.0	72790	5734	30.0	yes	both	no	no	no
92235.49c	233.0250	uresa	B-VI.4	1996	300.0	647347	72649	20.0	yes	both	no	no	yes
92235.50c	233.0250	rmccs	B-V.0	1977	293.6	60489	5725	20.0	yes	both	no	no	no
92235.50d	233.0250	drmcscs	B-V.0	1977	293.6	11788	263	20.0	yes	both	no	no	no
92235.52c	233.0250	endf5mt[1]	B-V.0	1977	587.2	65286	6320	20.0	yes	both	no	no	no
92235.53c	233.0250	endf5mt[1]	B-V.0	1977	587.2	36120	2685	20.0	yes	both	no	no	no
92235.54c	233.0250	endf5mt[1]	B-V.0	1977	880.8	36008	2671	20.0	yes	both	no	no	no
92235.60c	233.0250	endf60	B-VI.2	1993	293.6	289975	28110	20.0	yes	both	no	no	no
92235.61c	233.0250	endf6dn	B-VI.2	1993	293.6	294963	28110	20.0	yes	both	no	yes	no
92235.64c	233.0250	endf66d	B-VI.5	1997	77.0	1115810	111154	20.0	yes	both	no	yes	yes
92235.65c	233.0250	endf66e	B-VI.5	1997	3000.1	332639	24135	20.0	yes	both	no	yes	yes
92235.66c	233.0250	endf66c	B-VI.5	1997	293.6	722105	67409	20.0	yes	both	no	yes	yes
92235.67c	233.0250	t16_2003	LANL/T16	2003	77.0	1119233	111037	20.0	yes	both	no	yes	yes
92235.68c	233.0250	t16_2003	LANL/T16	2003	3000.0	337079	24131	20.0	yes	both	no	yes	yes
92235.69c	233.0250	t16_2003	LANL/T16	2003	293.6	726320	67380	20.0	yes	both	no	yes	yes

Table G.2 (Cont.)
Continuous-Energy and Discrete Neutron Data Libraries Maintained by X-5

<u>ZAID</u>	<u>AWR</u>	<u>Library</u> <u>Name</u>	<u>Source</u>	<u>Eval</u> <u>Date</u>	<u>Temp</u> <u>(°K)</u>	<u>Length</u> <u>words</u>	<u>NE</u>	<u>E_{max}</u> <u>(MeV)</u>	<u>GPD</u>	<u>U</u>	<u>CP</u>	<u>DN</u>	<u>UR</u>
** U-236 **													
92236.42c	234.0178	endl92	LLNL	<1992	300.0	14595	311	30.0	yes	both	no	no	no
92236.49c	234.0180	uresa	B-VI.0	1989	300.0	159074	20865	20.0	no	both	no	no	yes
92236.50c	234.0180	endf5p	B-V.0	1978	293.6	138715	19473	20.0	no	tot	no	no	no
92236.50d	234.0180	dre5	B-V.0	1978	293.6	4838	263	20.0	no	tot	no	no	no
92236.51c	234.0180	rmccs	B-V.0	1978	293.6	7302	800	20.0	no	tot	no	no	no
92236.51d	234.0180	drmcsc	B-V.0	1978	293.6	4838	263	20.0	no	tot	no	no	no
92236.60c	234.0180	endf60	B-VI.0	1989	293.6	82819	10454	20.0	no	both	no	no	no
92236.61c	234.0180	endf6dn	B-VI.0	1989	293.6	87807	10454	20.0	no	both	no	yes	no
92236.65c	234.0180	endf66e	B-VI.0	1989	3000.1	153474	15331	20.0	no	both	no	yes	yes
92236.66c	234.0180	endf66c	B-VI.0	1989	293.6	199786	21120	20.0	no	both	no	yes	yes
92236.68c	234.0178	t16_2003	LANL/T16	2003	3000.0	276138	15549	30.0	yes	both	no	yes	yes
92236.69c	234.0178	t16_2003	LANL/T16	2003	293.6	328212	21335	30.0	yes	both	no	yes	yes
** U-237 **													
92237.42c	235.0123	endl92	LLNL	<1992	300.0	13465	210	30.0	yes	both	no	no	no
92237.50c	235.0120	endf5p	B-V.0	1976	293.6	32445	3293	20.0	yes	tot	no	no	no
92237.50d	235.0120	dre5	B-V.0	1976	293.6	8851	263	20.0	yes	tot	no	no	no
92237.51c	235.0120	rmccs	B-V.0	1976	293.6	10317	527	20.0	yes	tot	no	no	no
92237.51d	235.0120	drmcsc	B-V.0	1976	293.6	8851	263	20.0	yes	tot	no	no	no
92237.65c	235.0120	endf66e	B-VI.2	1976	3000.1	72824	6381	20.0	yes	both	no	yes	yes
92237.66c	235.0120	endf66c	B-VI.2	1976	293.6	87188	7977	20.0	yes	both	no	yes	yes
92237.68c	235.0124	t16_2003	LANL/T16	2000	3000.0	120768	6401	30.0	yes	both	no	yes	yes
92237.69c	235.0124	t16_2003	LANL/T16	2000	293.6	135303	8016	30.0	yes	both	no	yes	yes
** U-238 **													
92238.11c	236.0060	endf62mt	B-VI.2	1993	77.0	621385	74481	20.0	yes	both	no	no	no
92238.12c	236.0060	endf62mt	B-VI.2	1993	400.0	456593	53882	20.0	yes	both	no	no	no
92238.13c	236.0060	endf62mt	B-VI.2	1993	500.0	433681	51018	20.0	yes	both	no	no	no
92238.14c	236.0060	endf62mt	B-VI.2	1993	600.0	414185	48581	20.0	yes	both	no	no	no
92238.15c	236.0060	endf62mt	B-VI.2	1993	800.0	386305	45096	20.0	yes	both	no	no	no
92238.16c	236.0060	endf62mt	B-VI.2	1993	900.0	372625	43386	20.0	yes	both	no	no	no
92238.17c	236.0060	endf62mt	B-VI.2	1993	1200.0	348137	40325	20.0	yes	both	no	no	no
92238.21c	236.0060	100xs[3]	LANL/T:X	1993	300.0	279245	30911	100.0	yes	both	no	no	no
92238.42c	236.0058	endl92	LLNL	<1992	300.0	107739	7477	30.0	yes	both	no	no	no
92238.48c	236.0060	uresa[16]	B-VI.2	1993	300.0	705623	85021	20.0	no	both	no	no	yes
92238.50c	236.0060	rmccs	B-V.0	1979	293.6	88998	9285	20.0	yes	both	no	no	no
92238.50d	236.0060	drmcsc	B-V.0	1979	293.6	16815	263	20.0	yes	both	no	no	no
92238.52c	236.0060	endf5mt[1]	B-V.0	1979	587.2	123199	8454	20.0	yes	both	no	no	no
92238.53c	236.0060	endf5mt[1]	B-V.0	1979	587.2	160107	17876	20.0	yes	both	no	no	no
92238.54c	236.0060	endf5mt[1]	B-V.0	1979	880.8	160971	17984	20.0	yes	both	no	no	no
92238.60c	236.0060	endf60	B-VI.2	1993	293.6	206322	22600	20.0	yes	both	no	no	no
92238.61c	236.0060	endf6dn	B-VI.2	1993	293.6	211310	22600	20.0	yes	both	no	yes	no
92238.64c	236.0060	endf66d	B-VI.5	1993	77.0	976500	103602	20.0	yes	both	no	yes	yes
92238.65c	236.0060	endf66e	B-VI.5	1993	3000.1	425088	42334	20.0	yes	both	no	yes	yes
92238.66c	236.0060	endf66c	B-VI.5	1993	293.6	751905	78647	20.0	yes	both	no	yes	yes
92238.67c	236.0058	t16_2003	LANL/T16	2003	77.0	1099087	103664	30.0	yes	both	no	yes	yes
92238.68c	236.0058	t16_2003	LANL/T16	2003	3000.0	547675	42396	30.0	yes	both	no	yes	yes
92238.69c	236.0058	t16_2003	LANL/T16	2003	293.6	874492	78709	30.0	yes	both	no	yes	yes
** U-239 **													
92239.35d	237.0007	drmcsc	LLNL	<1985	yes	9286	263	20.0	yes	pr	no	no	no
92239.35c	237.0007	rmccsa	LLNL	<1985	yes	9809	394	20.0	yes	pr	no	no	no
92239.42c	237.0007	endl92	LLNL	<1992	300.0	14336	205	30.0	yes	both	no	no	no
92239.68c	237.0007	t16_2003	LANL/T16	2000	3000.0	111013	6340	30.0	yes	both	no	yes	yes
92239.69c	237.0007	t16_2003	LANL/T16	2000	293.6	125557	7956	30.0	yes	both	no	yes	yes
** U-240 **													
92240.42c	237.9944	endl92	LLNL	<1992	300.0	14000	128	30.0	yes	both	no	no	no
92240.68c	237.9944	t16_2003	LANL/T16	2003	3000.0	243398	11524	30.0	yes	both	no	yes	yes
92240.69c	237.9944	t16_2003	LANL/T16	2003	293.6	276968	15254	30.0	yes	both	no	yes	yes
** U-241 **													
92241.68c	238.9890	t16_2003	LANL/T16	2000	3000.0	117572	6309	30.0	yes	both	no	yes	yes
92241.69c	238.9890	t16_2003	LANL/T16	2000	293.6	132260	7941	30.0	yes	both	no	yes	yes

Table G.2 (Cont.)
Continuous-Energy and Discrete Neutron Data Libraries Maintained by X-5

<u>Z</u> <u>A</u> <u>I</u> <u>D</u>	<u>A</u> <u>W</u> <u>R</u>	<u>L</u> <u>i</u> <u>b</u> <u>r</u> <u>a</u> <u>r</u> <u>y</u> <u>N</u> <u>a</u> <u>m</u> <u>e</u>	<u>S</u> <u>o</u> <u>u</u> <u>r</u> <u>c</u> <u>e</u>	<u>E</u> <u>v</u> <u>a</u> <u>l</u> <u>D</u> <u>a</u> <u>t</u> <u>e</u>	<u>T</u> <u>e</u> <u>m</u> <u>p</u> <u>(</u> <u>°</u> <u>K</u> <u>)</u>	<u>L</u> <u>e</u> <u>n</u> <u>g</u> <u>t</u> <u>h</u> <u>w</u> <u>o</u> <u>r</u> <u>d</u> <u>s</u>	<u>N</u> <u>E</u>	<u>E</u> _{max} <u>(</u> <u>M</u> <u>e</u> <u>V</u> <u>)</u>	<u>G</u> <u>P</u> <u>D</u>	<u>U</u>	<u>C</u> <u>P</u>	<u>D</u> <u>N</u>	<u>U</u> <u>R</u>
Z = 93 ***** Neptunium *****													
** Np-235 **													
93235.42c	233.0249	endl92	LLNL	<1992	300.0	17717	660	30.0	yes	both	no	no	no
** Np-236 **													
93236.42c	234.0188	endl92	LLNL	<1992	300.0	13464	179	30.0	yes	both	no	no	no
** Np-237 **													
93237.42c	235.0118	endl92	LLNL	<1992	300.0	31966	2477	30.0	yes	both	no	no	no
93237.50c	235.0120	endf5p	B-V.0	1978	293.6	63223	8519	20.0	no	tot	no	no	no
93237.50d	235.0120	dre5	B-V.0	1978	293.6	5267	263	20.0	no	tot	no	no	no
93237.55d	235.0120	drmcscs	LANL/T	1984	293.6	20484	263	20.0	no	both	no	no	no
93237.55c	235.0120	rmccsa	LANL/T	1984	293.6	32558	1682	20.0	no	both	no	no	no
93237.60c	235.0118	endf60	B-VI.1	1990	293.6	105150	7218	20.0	yes	both	no	no	no
93237.61c	235.0118	endf6dn	B-VI.1	1990	293.6	110048	7218	20.0	yes	both	no	yes	no
93237.66c	235.0118	endf66c	B-VI.1	1990	293.6	255036	18967	20.0	yes	both	no	yes	no
93237.69c	235.0118	t16_2003	LANL/T16	2003	293.6	255036	18967	20.0	yes	both	no	yes	no
** Np-238 **													
93238.42c	236.0060	endl92	LLNL	<1992	300.0	13445	165	30.0	yes	both	no	no	no
** Np-239 **													
93239.60c	236.9990	endf60	B-VI.0	1988	293.6	7406	562	20.0	no	tot	no	no	no
93239.66c	236.9990	endf66c	B-VI.0	1988	293.6	17349	1087	20.0	no	tot	no	no	no
Z = 94 ***** Plutonium *****													
** Pu-236 **													
94236.60c	234.0180	endf60	B-VI.0	1978	293.6	33448	4610	20.0	no	tot	no	no	no
94236.66c	234.0180	endf66c	B-VI.4	1995	293.6	25187	1537	20.0	no	both	no	no	no
** Pu-237 **													
94237.42c	235.0120	endl92	LLNL	<1992	300.0	17284	279	30.0	yes	both	no	no	no
94237.60c	235.0120	endf60	B-VI.0	1978	293.6	3524	257	20.0	no	tot	no	no	no
94237.66c	235.0120	endf66c	B-VI.0	1978	293.6	10982	718	20.0	no	tot	no	no	no
** Pu-238 **													
94238.42c	236.0046	endl92	LLNL	<1992	300.0	30572	2177	30.0	yes	both	no	no	no
94238.49c	236.0045	uresa	B-VI.0	1978	300.0	41814	5337	20.0	no	both	no	no	yes
94238.50d	236.1670	dre5	B-V.0	1978	293.6	5404	263	20.0	no	tot	no	no	no
94238.50c	236.1670	endf5p	B-V.0	1978	293.6	18763	2301	20.0	no	tot	no	no	no
94238.51c	236.1670	rmccs	B-V.0	1978	293.6	6067	537	20.0	no	tot	no	no	no
94238.51d	236.1670	drmcscs	B-V.0	1978	293.6	5404	263	20.0	no	tot	no	no	no
94238.60c	236.0045	endf60	B-VI.0	1978	293.6	29054	3753	20.0	no	both	no	no	no
94238.61c	236.0045	endf6dn	B-VI.0	1978	293.6	33952	3753	20.0	no	both	no	yes	no
94238.65c	236.0045	endf66e	B-VI.0	1978	3000.1	50571	4565	20.0	no	both	no	yes	yes
94238.66c	236.0045	endf66c	B-VI.0	1978	293.6	58875	5603	20.0	no	both	no	yes	yes
** Pu-239 **													
94239.11c	236.9986	endf62mt	B-VI.2	1993	77.0	568756	62522	20.0	yes	both	no	no	no
94239.12c	236.9986	endf62mt	B-VI.2	1993	400.0	418556	43747	20.0	yes	both	no	no	no
94239.13c	236.9986	endf62mt	B-VI.2	1993	500.0	395964	40923	20.0	yes	both	no	no	no
94239.14c	236.9986	endf62mt	B-VI.2	1993	600.0	377116	38567	20.0	yes	both	no	no	no
94239.15c	236.9986	endf62mt	B-VI.2	1993	800.0	350292	35214	20.0	yes	both	no	no	no
94239.16c	236.9986	endf62mt	B-VI.2	1993	900.0	338236	33707	20.0	yes	both	no	no	no
94239.17c	236.9986	endf62mt	B-VI.2	1993	1200.0	312572	30499	20.0	yes	both	no	no	no
94239.42c	236.9986	endl92	LLNL	<1992	300.0	93878	6827	30.0	yes	both	no	no	no
94239.49c	236.9986	uresa	B-VI.2	1993	300.0	595005	64841	20.0	yes	both	no	no	yes
94239.50d	236.9990	dre5	B-V.0	1976	293.6	12631	263	20.0	yes	both	no	no	no
94239.50c	236.9990	endf5p	B-V.0	1976	293.6	74049	7809	20.0	yes	both	no	no	no

Table G.2 (Cont.)
Continuous-Energy and Discrete Neutron Data Libraries Maintained by X-5

<u>Z</u> <u>A</u> <u>I</u> <u>D</u>	<u>A</u> <u>W</u> <u>R</u>	<u>L</u> <u>i</u> <u>b</u> <u>r</u> <u>a</u> <u>r</u> <u>y</u> <u>N</u> <u>a</u> <u>m</u> <u>e</u>	<u>S</u> <u>o</u> <u>u</u> <u>r</u> <u>c</u> <u>e</u>	<u>E</u> <u>v</u> <u>a</u> <u>l</u> <u>D</u> <u>a</u> <u>t</u> <u>e</u>	<u>T</u> <u>e</u> <u>m</u> <u>p</u> <u>(</u> <u>°</u> <u>K</u> <u>)</u>	<u>L</u> <u>e</u> <u>n</u> <u>g</u> <u>t</u> <u>h</u> <u>w</u> <u>o</u> <u>r</u> <u>d</u> <u>s</u>	<u>N</u> <u>E</u>	<u>E</u> _{max} <u>(</u> <u>M</u> <u>e</u> <u>V</u> <u>)</u>	<u>G</u> <u>P</u> <u>D</u>	<u>̄</u> <u>U</u>	<u>C</u> <u>P</u>	<u>D</u> <u>N</u>	<u>U</u> <u>R</u>
94239.55d	236.9990	drmcscs	B-V.2	1983	293.6	20727	263	20.0	yes	both	no	no	no
94239.55c	236.9990	rmccs	B-V.2	1983	293.6	102099	10318	20.0	yes	both	no	no	no
94239.60c	236.9986	endf60	B-VI.2	1993	293.6	283354	26847	20.0	yes	both	no	no	no
94239.61c	236.9986	endf6dn	B-VI.2	1993	293.6	288252	26847	20.0	yes	both	no	yes	no
94239.64c	236.9986	endf66d	B-VI.5	1997	77.0	866231	83969	20.0	yes	both	no	yes	yes
94239.65c	236.9986	endf66e	B-VI.5	1997	3000.1	374390	29320	20.0	yes	both	no	yes	yes
94239.66c	236.9986	endf66c	B-VI.5	1997	293.6	685322	63868	20.0	yes	both	no	yes	yes
94239.67c	236.9986	t16_2003	LANL/T16	2003	77.0	887458	83969	20.0	yes	both	no	yes	yes
94239.68c	236.9986	t16_2003	LANL/T16	2003	3000.0	395617	29320	20.0	yes	both	no	yes	yes
94239.69c	236.9986	t16_2003	LANL/T16	2003	293.6	706549	63868	20.0	yes	both	no	yes	yes
** Pu-240 **													
94240.42c	237.9916	endl92	LLNL	<1992	300.0	198041	16626	30.0	yes	both	no	no	no
94240.49c	237.9920	uresa	B-VI.2	1986	300.0	341542	41596	20.0	yes	both	no	no	yes
94240.50d	237.9920	drmcscs	B-V.0	1977	293.6	9569	263	20.0	yes	both	no	no	no
94240.50c	237.9920	rmccs	B-V.0	1977	293.6	58917	6549	20.0	yes	both	no	no	no
94240.60c	237.9920	endf60	B-VI.2	1986	293.6	133071	15676	20.0	yes	both	no	no	no
94240.61c	237.9920	endf6dn	B-VI.2	1986	293.6	137969	15676	20.0	yes	both	no	yes	no
94240.65c	237.9920	endf66e	B-VI.2	1986	3000.1	283740	29451	20.0	yes	both	no	yes	yes
94240.66c	237.9920	endf66c	B-VI.2	1986	293.6	395889	41912	20.0	yes	both	no	yes	yes
** Pu-241 **													
94241.42c	238.9860	endl92	LLNL	<1992	300.0	14108	203	30.0	yes	both	no	no	no
94241.49c	238.9780	uresa	B-VI.3	1994	300.0	155886	17753	20.0	yes	both	no	no	yes
94241.50c	238.9780	endf5p	B-V.0	1977	293.6	38601	3744	20.0	yes	both	no	no	no
94241.50d	238.9780	dre5	B-V.0	1977	293.6	11575	263	20.0	yes	both	no	no	no
94241.51c	238.9780	rmccs	B-V.0	1977	293.6	13403	623	20.0	yes	both	no	no	no
94241.51d	238.9780	drmcscs	B-V.0	1977	293.6	11575	263	20.0	yes	both	no	no	no
94241.60c	238.9780	endf60	B-VI.1	1988	293.6	76453	8112	20.0	yes	both	no	no	no
94241.61c	238.9780	endf6dn	B-VI.1	1988	293.6	81351	8112	20.0	yes	both	no	yes	no
94241.65c	238.9780	endf66e	B-VI.3	1994	3000.1	104019	9145	20.0	yes	both	no	yes	yes
94241.66c	238.9780	endf66c	B-VI.3	1994	293.6	185478	18196	20.0	yes	both	no	yes	yes
** Pu-242 **													
94242.42c	239.9793	endl92	LLNL	<1992	300.0	48688	4287	30.0	yes	both	no	no	no
94242.49c	239.9790	uresa	B-VI.0	1978	300.0	130202	14922	20.0	yes	both	no	no	yes
94242.50c	239.9790	endf5p	B-V.0	1978	293.6	71429	7636	20.0	yes	both	no	no	no
94242.50d	239.9790	dre5	B-V.0	1978	293.6	12463	263	20.0	yes	both	no	no	no
94242.51c	239.9790	rmccs	B-V.0	1978	293.6	15702	728	20.0	yes	both	no	no	no
94242.51d	239.9790	drmcscs	B-V.0	1978	293.6	12463	263	20.0	yes	both	no	no	no
94242.60c	239.9790	endf60	B-VI.0	1978	293.6	73725	7896	20.0	yes	both	no	no	no
94242.61c	239.9790	endf6dn	B-VI.0	1978	293.6	78623	7896	20.0	yes	both	no	yes	no
94242.65c	239.9790	endf66e	B-VI.0	1978	3000.1	123314	11409	20.0	yes	both	no	yes	yes
94242.66c	239.9790	endf66c	B-VI.0	1978	293.6	157136	15167	20.0	yes	both	no	yes	yes
** Pu-243 **													
94243.42c	240.9740	endl92	LLNL	<1992	300.0	20253	745	30.0	yes	both	no	no	no
94243.60c	240.9740	endf60	B-VI.2	1976	293.6	45142	4452	20.0	yes	tot	no	no	no
94243.65c	240.9740	endf66e	B-VI.2	1976	3000.1	70649	6413	20.0	yes	tot	no	no	yes
94243.66c	240.9740	endf66c	B-VI.2	1976	293.6	97856	9436	20.0	yes	tot	no	no	yes
** Pu-244 **													
94244.60c	241.9680	endf60	B-VI.0	1978	293.6	23654	3695	20.0	no	tot	no	no	no
94244.65c	241.9680	endf66e	B-VI.0	1978	3000.1	51446	6450	20.0	no	tot	no	no	yes
94244.66c	241.9680	endf66c	B-VI.0	1978	293.6	61726	7931	20.0	no	tot	no	no	yes

Z = 95 ***** Americium *****

** Am-241 **

95241.42c	238.9860	endl92	LLNL	<1992	300.0	32579	2011	30.0	yes	both	no	no	no
95241.50c	238.9860	endf5u	B-V.0	1978	293.6	42084	4420	20.0	yes	tot	no	no	no
95241.50d	238.9860	dre5	B-V.0	1978	293.6	9971	263	20.0	yes	tot	no	no	no
95241.51c	238.9860	rmccs	B-V.0	1978	293.6	12374	713	20.0	yes	tot	no	no	no
95241.51d	238.9860	drmcscs	B-V.0	1978	293.6	9971	263	20.0	yes	tot	no	no	no
95241.60c	238.9860	endf60	LANL/T	1994	300.0	168924	13556	30.0	yes	both	no	no	no
95241.61c	238.9860	endf6dn	LANL/T	1994	300.0	173822	13556	30.0	yes	both	no	yes	no
95241.65c	238.9860	endf66e	B-VI.3:X	1994	3000.1	162566	8011	30.0	yes	both	no	yes	yes
95241.66c	238.9860	endf66c	B-VI.3:X	1994	293.6	267137	19630	30.0	yes	both	no	yes	yes
95241.68c	238.9860	t16_2003	LANL/T16	2003	3000.0	163034	8020	30.0	yes	both	no	yes	yes
95241.69c	238.9860	t16_2003	LANL/T16	2003	293.6	267605	19639	30.0	yes	both	no	yes	yes

Table G.2 (Cont.)
Continuous-Energy and Discrete Neutron Data Libraries Maintained by X-5

<u>Z</u> <u>A</u> <u>I</u> <u>D</u>	<u>A</u> <u>W</u> <u>R</u>	<u>Library</u> <u>Name</u>	<u>Source</u>	<u>Eval</u> <u>Date</u>	<u>Temp</u> <u>(°K)</u>	<u>Length</u> <u>words</u>	<u>NE</u>	<u>E_{max}</u> <u>(MeV)</u>	<u>GPD</u>	<u>U</u>	<u>CP</u>	<u>DN</u>	<u>UR</u>
** Am-242metastable **													
95242.42c	239.9801	endl92	LLNL	<1992	300.0	21828	1368	20.0	yes	both	no	no	no
95242.50c	239.9800	endf5u	B-V.0	1978	293.6	8593	323	20.0	yes	tot	no	no	no
95242.50d	239.9800	dre5	B-V.0	1978	293.6	9048	263	20.0	yes	tot	no	no	no
95242.51d	239.9800	drmcsc	B-V.0	1978	293.6	9048	263	20.0	yes	tot	no	no	no
95242.51c	239.9800	rmccs	B-V.0	1978	293.6	8502	317	20.0	yes	tot	no	no	no
95242.65c	239.9800	endf66c	B-VI.1	1978	3000.1	27793	945	20.0	yes	both	no	yes	yes
95242.66c	239.9800	endf66c	B-VI.1	1978	293.6	27625	933	20.0	yes	both	no	yes	yes
** Am-243 **													
95243.42c	240.9733	endl92	LLNL	<1992	300.0	52074	4867	30.0	yes	both	no	no	no
95243.50c	240.9730	endf5u	B-V.0	1978	293.6	92015	11921	20.0	yes	tot	no	no	no
95243.50d	240.9730	dre5	B-V.0	1978	293.6	11742	263	20.0	yes	tot	no	no	no
95243.51d	240.9730	drmcsc	B-V.0	1978	293.6	11742	263	20.0	yes	tot	no	no	no
95243.51c	240.9730	rmccs	B-V.0	1978	293.6	13684	757	20.0	yes	tot	no	no	no
95243.60c	240.9730	endf60	B-VI.0	1988	293.6	104257	11984	20.0	yes	both	no	no	no
95243.61c	240.9730	endf6dn	B-VI.0	1988	293.6	109155	11984	20.0	yes	both	no	yes	no
95243.65c	240.9734	endf66c	B-VI.5	1996	3000.1	160276	10268	30.0	yes	both	no	yes	yes
95243.66c	240.9734	endf66c	B-VI.5	1996	293.6	308812	26772	30.0	yes	both	no	yes	yes
95243.68c	240.9734	t16_2003	ENDF/B-VI.5	1996	3000.0	160276	10268	30.0	yes	both	no	yes	yes
95243.69c	240.9734	t16_2003	ENDF/B-VI.5	1996	293.6	308812	26772	30.0	yes	both	no	yes	yes
Z = 96 ***** Curium *****													
** Cm-241 **													
96241.60c	238.9870	endf60	B-VI.0	1978	293.6	3132	278	20.0	no	tot	no	no	no
96241.66c	238.9870	endf66c	B-VI.0	1978	293.6	9515	598	20.0	no	tot	no	no	no
** Cm-242 **													
96242.42c	239.9794	endl92	LLNL	<1992	300.0	37766	3141	30.0	yes	both	no	no	no
96242.50c	239.9790	endf5u	B-V.0	1978	293.6	30897	3113	20.0	yes	tot	no	no	no
96242.50d	239.9790	dre5	B-V.0	1978	293.6	8903	263	20.0	yes	tot	no	no	no
96242.51d	239.9790	drmcsc	B-V.0	1978	293.6	8903	263	20.0	yes	tot	no	no	no
96242.51c	239.9790	rmccs	B-V.0	1978	293.6	9767	472	20.0	yes	tot	no	no	no
96242.60c	239.9790	endf60	B-VI.0	1978	293.6	34374	3544	20.0	yes	both	no	no	no
96242.61c	239.9790	endf6dn	B-VI.0	1978	293.6	39269	3544	20.0	yes	both	no	yes	no
96242.65c	239.9790	endf66c	B-VI.0	1978	3000.1	54517	4410	20.0	yes	both	no	yes	yes
96242.66c	239.9790	endf66c	B-VI.0	1978	293.6	62059	5248	20.0	yes	both	no	yes	yes
** Cm-243 **													
96243.42c	240.9733	endl92	LLNL	<1992	300.0	21543	1099	30.0	yes	both	no	no	no
96243.60c	240.9730	endf60	B-VI.0	1978	293.6	18860	1445	20.0	yes	tot	no	no	no
96243.65c	240.9730	endf66c	B-VI.0	1978	3000.1	29796	1965	20.0	yes	tot	no	no	yes
96243.66c	240.9730	endf66c	B-VI.0	1978	293.6	32793	2298	20.0	yes	tot	no	no	yes
** Cm-244 **													
96244.42c	241.9661	endl92	LLNL	<1992	300.0	46590	4198	30.0	yes	both	no	no	no
96244.49c	241.9660	uresa	B-VI.0	1978	300.0	97975	11389	20.0	yes	pr	no	no	yes
96244.50d	241.9660	dre5	B-V.0	1978	293.6	9509	263	20.0	yes	tot	no	no	no
96244.50c	241.9660	endf5u	B-V.0	1978	293.6	45991	4919	20.0	yes	tot	no	no	no
96244.51d	241.9660	drmcsc	B-V.0	1978	293.6	9509	263	20.0	yes	tot	no	no	no
96244.51c	241.9660	rmccs	B-V.0	1978	293.6	10847	566	20.0	yes	tot	no	no	no
96244.60c	241.9660	endf60	B-VI.0	1978	293.6	73001	8294	20.0	yes	tot	no	no	no
96244.65c	241.9660	endf66c	B-VI.0	1978	3000.1	91371	8861	20.0	yes	tot	no	no	yes
96244.66c	241.9660	endf66c	B-VI.0	1978	293.6	116265	11627	20.0	yes	tot	no	no	yes
** Cm-245 **													
96245.42c	242.9602	endl92	LLNL	<1992	300.0	25678	1564	30.0	yes	both	no	no	no
96245.60c	242.9600	endf60	B-VI.2	1979	293.6	29535	2636	20.0	yes	both	no	no	no
96245.61c	242.9600	endf6dn	B-VI.2	1979	293.6	34433	2636	20.0	yes	both	no	yes	no
96245.65c	242.9600	endf66c	B-VI.2	1979	3000.1	44920	3214	20.0	yes	both	no	yes	yes
96245.66c	242.9600	endf66c	B-VI.2	1979	293.6	52336	4038	20.0	yes	both	no	yes	yes
** Cm-246 **													
96246.42c	243.9534	endl92	LLNL	<1992	300.0	24550	1376	30.0	yes	both	no	no	no
96246.60c	243.9530	endf60	B-VI.2	1976	293.6	37948	3311	20.0	yes	tot	no	no	no
96246.66c	243.9530	endf66c	B-VI.2	1976	293.6	56186	4704	20.0	yes	tot	no	no	no

Table G.2 (Cont.)
Continuous-Energy and Discrete Neutron Data Libraries Maintained by X-5

<u>ZAID</u>	<u>AWR</u>	<u>Library</u> <u>Name</u>	<u>Source</u>	<u>Eval</u> <u>Date</u>	<u>Temp</u> <u>(°K)</u>	<u>Length</u> <u>words</u>	<u>NE</u>	<u>E_{max}</u> <u>(MeV)</u>	<u>GPD</u>	<u>U</u>	<u>CP</u>	<u>DN</u>	<u>UR</u>
** Cm-247 **													
96247.42c	244.9479	endl92	LLNL	<1992	300.0	39971	3256	30.0	yes	both	no	no	no
96247.60c	244.9500	endf60	B-VI.2	1976	293.6	38800	3679	20.0	yes	tot	no	no	no
96247.65c	244.9500	endf66e	B-VI.2	1976	3000.1	49949	3849	20.0	yes	tot	no	no	yes
96247.66c	244.9500	endf66c	B-VI.2	1976	293.6	64799	5499	20.0	yes	tot	no	no	yes
** Cm-248 **													
96248.42c	245.9413	endl92	LLNL	<1992	300.0	40345	3355	30.0	yes	both	no	no	no
96248.60c	245.9410	endf60	B-VI.0	1978	293.6	83452	9706	20.0	yes	tot	no	no	no
96248.65c	245.9410	endf66e	B-VI.0	1978	3000.1	102038	10383	20.0	yes	tot	no	no	yes
96248.66c	245.9410	endf66c	B-VI.0	1978	293.6	130361	13530	20.0	yes	tot	no	no	yes
Z = 97 ***** Berkelium *****													
** Bk-249 **													
97249.42c	246.9353	endl92	LLNL	<1992	300.0	19573	809	30.0	yes	both	no	no	no
97249.60c	246.9400	endf60	B-VI.0:X	1986	293.6	50503	5268	20.0	no	both	no	no	no
97249.65c	246.9400	endf66e	B-VI.0	1986	3000.1	65384	5360	20.0	no	both	no	no	yes
97249.66c	246.9400	endf66c	B-VI.0	1986	293.6	85568	7883	20.0	no	both	no	no	yes
Z = 98 ***** Californium *****													
** Cf-249 **													
98249.42c	246.9352	endl92	LLNL	<1992	300.0	49615	4554	30.0	yes	both	no	no	no
98249.60c	246.9400	endf60	B-VI.0:X	1989	293.6	41271	4329	20.0	no	both	no	no	no
98249.61c	246.9400	endf66dn	B-VI.0:X	1989	293.6	46154	4329	20.0	no	both	no	yes	no
98249.65c	246.9400	endf66e	B-VI.0:X	1989	3000.1	62455	4376	20.0	no	both	no	yes	yes
98249.66c	246.9400	endf66c	B-VI.0:X	1989	293.6	78679	6404	20.0	no	both	no	yes	yes
** Cf-250 **													
98250.42c	247.9281	endl92	LLNL	<1992	300.0	17659	574	30.0	yes	both	no	no	no
98250.60c	247.9280	endf60	B-VI.2	1976	293.6	47758	5554	20.0	yes	tot	no	no	no
98250.65c	247.9280	endf66e	B-VI.2	1976	3000.1	66024	6701	20.0	yes	tot	no	no	yes
98250.66c	247.9280	endf66c	B-VI.2	1976	293.6	77434	8132	20.0	yes	tot	no	no	yes
** Cf-251 **													
98251.42c	248.9227	endl92	LLNL	<1992	300.0	17673	545	30.0	yes	both	no	no	no
98251.60c	248.9230	endf60	B-VI.2	1976	293.6	42817	4226	20.0	yes	both	no	no	no
98251.61c	248.9230	endf66dn	B-VI.2	1976	293.6	47715	4226	20.0	yes	both	no	yes	no
98251.65c	248.9230	endf66e	B-VI.2	1976	3000.1	64568	5257	20.0	yes	both	no	yes	yes
98251.66c	248.9230	endf66c	B-VI.2	1976	293.6	73253	6222	20.0	yes	both	no	yes	yes
** Cf-252 **													
98252.42c	249.9161	endl92	LLNL	<1992	300.0	21027	1210	30.0	yes	both	no	no	no
98252.60c	249.9160	endf60	B-VI.2	1976	293.6	49204	5250	20.0	yes	both	no	no	no
98252.65c	249.9160	endf66e	B-VI.2	1976	3000.1	66642	6250	20.0	yes	tot	no	no	yes
98252.66c	249.9160	endf66c	B-VI.2	1976	293.6	78378	7554	20.0	yes	tot	no	no	yes

Notes:

1. The data libraries previously known as EPRIXS and U600K are now a part of the data library ENDF5MT.
2. Data were translated to ENDF/B-VI format with some modifications by LANL.
3. The 100XS data library contains data for 9 nuclides up to 100 MeV. Heating numbers on this data library are known to be incorrect, overestimating the energy deposition.⁹
4. Photon production data were added to the existing ENDF evaluation for ¹¹B in 1984. A complete new evaluation was performed in 1986.
5. The natural carbon data 6000.50c are repeated here with the Z Aid of 6012.50c for the user's convenience. Both are based on the natural carbon ENDF/B-V.0 evaluation.
6. The delayed gamma ray at an energy of 1.7791 MeV from the reaction $n + {}^{27}\text{Al} \rightarrow {}^{28}\text{Al} \rightarrow {}^{28}\text{Si} + \beta^- + \gamma$ has been included in the thermal-capture photon-production data for these two ZAIDs.¹⁰
7. The data libraries previously known as ARKRC, GDT2GP, IRNAT, MISCXS, TM169, and T2DDC are now a part of the data library MISC5XS.
8. Photon production data were added to ENDF/B-V.0 neutron files for argon and krypton by T-16, with the intent to roughly estimate photon heating.¹¹
9. Data for Br, Rb, I, and Cs were taken from incomplete fission-product evaluations.¹²
10. This is ENDF/B-V.0 for ⁸⁹Y after modification by evaluator to get better agreement with ENDL85.^{13,14}
11. The following files for Zr have been replaced by the indicated ZAID, eliminating the rare problem of having a secondary neutron energy greater than the incident neutron energy caused by an ENDF/B-V.0 evaluation problem.¹⁵ Note that this correction has been made for the ENDF/B-VI evaluation.

40000.50c	rmccs	->	40000.56c	misc5xs
40000.50d	drmcscs	->	40000.56d	misc5xs
40000.51c	endf5p	->	40000.57c	misc5xs
40000.51d	dre5	->	40000.57d	misc5xs
40000.53c	eprixs	->	40000.58c	misc5xs

12. The ZAIDs for ENDL-based average fission product data files have been changed for the latest library, ENDL92, to 49120.42c and 49125.42c. Z is now set to 49 to ensure that the appropriate atomic fraction and photon transport library is used. You may need to update the atomic weight ratio table in your XSDIR file to include these entries.^{16,17} The ENDL92FP library is not publicly available.
13. The LANL/T-16 evaluation for I-127 was accepted for ENDF/B-VI.2 with modifications. These data are processed from the original LANL/T-16 evaluation.
14. Photon production data for Gd were added to the ENDF/B-V.0 neutron cross sections by T-16. These data are valid only to 1 MeV.¹⁸
15. Photon production data for ²³³U were added by LANL to the original evaluation in 1981.

16. There was a processing problem for the URES library that affected the photon production data for ¹⁸², ¹⁸³, ¹⁸⁴, ¹⁸⁶W, ²³²Th and ²³⁸U. The URESA library contains the same ACE files as the URES library except that photon-production data for the affected isotopes is zeroed. The IDs for the affected isotopes have been changed from “49c” to “48c”. Heating numbers in the unresolved region are known to be incorrect.

IV. MULTIGROUP DATA

Currently, only one coupled neutron-photon multigroup library is supported by the Data Team, MGXSNP.¹⁹ MGXSNP is comprised of 30-group neutron and 12-group photon data primarily based on ENDF/B-V for 95 nuclides. The MCNP-compatible multigroup data library was produced from the original Sn multigroup libraries MENDF5 and MENDF5G using the code CRSRD in April 1987.^{20,21} The original neutron data library MENDF5 was produced using the “TD-Division Weight Function,” also called “CLAW” by the processing code NJOY.^{22,23,24} This weight function is a combination of a Maxwellian thermal + 1/E + fission + fusion peak at 14.0 MeV. The data library contains no upscatter groups or self-shielding, and is most applicable for fast systems. All cross-sections are for room temperature, 300°K. P0 through P4 scattering matrices from the original library were processed by CRSRD into angular distributions for MCNP using the Carter-Forest equiprobable bin treatment. When available, both total and prompt nubar data are provided. The edit reactions available for each ZAID are fully described in Reference 19.

Table G .3 describes the MGXSNP data library. The ZAIDs used for this library correspond to the source evaluation in the same manner as the ZAID for the continuous-energy and discrete data; as an example, the same source evaluation for natural iron was used to produce 26000.55c, 26000.55d and 26000.55m. For coupled neutron-photon problems, specifying a particular isotope on a material card will invoke the neutron set for that isotope and the corresponding photon set for that element. For example, an entry of “1003” on a material card will cause MCNP to use ZAID=1003.50m for neutron data and 1000.01g for photon data.

Table G .3
MGXSNP: A Coupled Neutron-Photon Multigroup Data Library

<u>ZAID</u>	<u>Neutron AWR</u>	<u>Length</u>	<u>ZAID</u>	<u>Photon AWR</u>	<u>Length</u>
1001.50m	0.999172	3249	1000.01g	0.999317	583
1002.55m	1.996810	3542			
1003.50m	2.990154	1927			
2003.50m	2.990134	1843	2000.01g	3.968217	583
2004.50m	3.968238	1629			
3006.50m	5.963479	3566	3000.01g	6.881312	583
3007.55m	6.955768	3555			
4007.35m	6.949815	1598	4000.01g	8.934763	557
4009.50m	8.934807	3014			
5010.50m	9.926970	3557	5000.01g	10.717168	583
5011.56m	10.914679	2795			
6000.50m [1]	11.896972	2933	6000.01g	11.907955	583
6012.50m [1]	11.896972	2933			

Table G .3 (Cont.)
MGXSNP: A Coupled Neutron-Photon Multigroup Data Library

<u>ZAID</u>	<u>Neutron AWR</u>	<u>Length</u>	<u>ZAID</u>	<u>Photon AWR</u>	<u>Length</u>
7014.50m	13.882849	3501	7000.01g	13.886438	583
7015.55m	14.871314	2743			
8016.50m	15.857588	3346	8000.01g	15.861942	583
9019.50m	18.835289	3261	9000.01g	18.835197	583
11023.50m	22.792388	2982	11000.01g	22.792275	583
12000.50m	24.096375	3802	12000.01g	24.096261	583
13027.50m	26.749887	3853	13000.01g	26.749756	583
14000.50m	27.844378	3266	14000.01g	27.844241	583
15031.50m	30.707833	2123	15000.01g	30.707682	583
16032.50m	31.697571	2185	16000.01g	31.788823	583
17000.50m	35.148355	2737	17000.01g	35.148180	583
18000.35m	39.605021	2022	18000.01g	39.604489	557
19000.50m	38.762616	2833	19000.01g	38.762423	583
20000.50m	39.734053	3450	20000.01g	39.733857	583
22000.50m	47.455981	3015	22000.01g	47.455747	583
23000.50m	50.504104	2775	23000.01g	50.503856	583
24000.50m	51.549511	3924	24000.01g	51.549253	583
25055.50m	54.466367	2890	25000.01g	54.466099	583
26000.55m	55.366734	4304	26000.01g	55.366466	583
27059.50m	58.427218	2889	27000.01g	58.426930	583
28000.50m	58.182926	3373	28000.01g	58.182641	583
29000.50m	62.999465	2803	29000.01g	62.999157	583
31000.50m	69.124611	2084	31000.01g	69.124270	583
33075.35m	74.278340	2022	33000.01g	74.277979	557
36078.50m	77.251400	2108	36000.01g	83.080137	583
36080.50m	79.230241	2257			
36082.50m	81.210203	2312			
36083.50m	82.202262	2141			
36084.50m	83.191072	2460			
36086.50m	85.173016	2413			
40000.50m	90.440039	2466	40000.01g	90.439594	583
41093.50m	92.108717	2746	41000.01g	92.108263	583
42000.50m	95.107162	1991	42000.01g	95.106691	583
45103.50m	102.021993	2147	45000.01g	102.021490	583
45117.90m	115.544386	2709			
46119.90m	117.525231	2629	46000.01g	105.513949	557
47000.55m	106.941883	2693	47000.01g	106.941685	583
47107.50m	105.987245	2107			
47109.50m	107.969736	1924			
48000.50m	111.442911	1841	48000.01g	111.442363	583
50120.35m	115.995479	1929	50000.01g	117.667336	557
50998.99m	228.025301	1382			
50999.99m	228.025301	1413			
54000.35m	130.171713	1929	54000.01g	130.165202	557
56138.50m	136.721230	2115	56000.01g	136.146809	583
63000.35m	150.654333	1933	63000.01g	150.657141	557
63151.55m	149.623005	2976			
63153.55m	151.608005	2691			
64000.35m	155.898915	1929	64000.01g	155.900158	557

Table G .3 (Cont.)
MGXSNP: A Coupled Neutron-Photon Multigroup Data Library

<u>ZAID</u>	<u>Neutron AWR</u>	<u>Length</u>	<u>ZAID</u>	<u>Photon AWR</u>	<u>Length</u>
67165.55m	163.512997	2526	67000.01g	163.513493	583
73181.50m	179.394458	2787	73000.01g	179.393456	583
74000.55m	182.270446	4360	74000.01g	182.269548	583
74182.55m	180.386082	3687			
74183.55m	181.379499	3628			
74184.55m	182.371615	3664			
74186.55m	184.357838	3672			
75185.50m	183.365036	1968	75000.01g	184.607108	583
75187.50m	185.350629	2061			
78000.35m	193.415026	1929	78000.01g	193.404225	557
79197.56m	195.274027	3490	79000.01g	195.274513	583
82000.50m	205.437162	3384	82000.01g	205.436151	583
83209.50m	207.186158	2524	83000.01g	207.185136	583
90232.50m	230.045857	2896	90000.01g	230.044724	583
91233.50m	231.039442	1970	91000.01g	229.051160	479
92233.50m	231.038833	1988	92000.01g	235.984125	583
92234.50m	232.031554	2150			
92235.50m	233.025921	3164			
92236.50m	234.018959	2166			
92237.50m	235.013509	2174			
92238.50m	236.006966	3553			
92239.35m	236.997601	2147			
93237.55m	235.012957	2812	93000.01g	235.011799	479
94238.50m	236.005745	2442	94000.01g [2]	241.967559	583
94239.55m	236.999740	3038			
94240.50m	237.992791	3044			
94241.50m	238.987218	2856			
94242.50m	239.980508	2956			
95241.50m	238.987196	2535			
95242.50m	239.981303	2284			
95243.50m	240.974535	2480			
96242.50m	239.980599	1970			
96244.50m	241.967311	1950			

Notes:

1. The neutron transport data for ZAIDs 6012.50m and 6000.50m are the same.
2. Photon transport data are not provided for Z>94.

V. PHOTOATOMIC DATA

There are four photon transport libraries maintained by X-5 and distributed with MCNP: MCPLIB, MCPLIB02, MCPLIB03 and MCPLIB04. Their lineage is summarized below.

The official version of MCPLIB is unchanged since 1982.²⁵ Versions of MCPLIB existed prior to 1982. MCPLIB contains data from several sources. For Z equal 1 to 94 (excluding Z equal 84, 85, 87, 88, 89, 91, 93), the cross section data for incident energies from 1 keV to 100 MeV and all form factor data are from the ENDF/B-IV evaluation, which is available from RSICC as data package DLC-7e. The excluded elements are tabulated only on the energy range from 1 keV to 15 MeV and trace their cross-section data back to the Storm and Israel 1970 data compilation,²⁶ which is available from RSICC as data package DLC-15. The form factor data for the excluded elements is of forgotten origin. The fluorescence data were produced by Everett and Cashwell²⁷ from the Storm and Israel 1970 data, supplemented as necessary. MCPLIB does not contain momentum profile (CDBD) data.

MCPLIB02 was officially released in 1993²⁸ and was created as an extension to MCPLIB. The form factor and fluorescence data on MCPLIB and MCPLIB02 are identical. The cross section data below 10 MeV are also identical. From the maximum energy on the original MCPLIB table up to 100 GeV, the cross section data are derived from EPDL89.²⁹ Between 10 MeV and the highest energy of the MCPLIB data, the data are smoothly transitioned. MCPLIB02 does not contain momentum profile (CDBD) data.

MCPLIB03 was officially released in 2002³⁰ as another extension of the MCPLIB/MCPLIB02 data set. The cross section, form factor, and fluorescence data on MCPLIB02 and MCPLIB03 are identical. The only change is the addition of the momentum profile (CDBD) data, derived from the work of Biggs, Mendelsohn and Mann.³¹

MCPLIB04 was officially released in 2002.³² The cross section, form factor, and fluorescence data are all derived from the ENDF/B-VI.8 data library that are derived from EPDL97.³³ Cross section data are given for incident photon energies from 1 keV to 100 GeV. Fluorescence data are derived from the atomic relaxation data available in ENDF/B-VI.8 but use the storage and sampling scheme defined by Everett and Cashwell.²⁷ The momentum profile (CDBD) data are identical to the data found on MCPLIB03.³⁰

The entries in each of the columns of Table G .4 are described as follows:

ZAID	The nuclide identification number with the form ZZZAAA.nnX where ZZZ is the atomic number. AAA is always 000 for elemental photoatomic data. nn is the unique table identification number. X = P for continuous-energy neutron tables.
Library	Name of the library that contains the data file for that ZAID.

APPENDIX G - MCNP DATA LIBRARIES
PHOTOATOMIC DATA

Library Release Date	The date the library was officially released. This does not necessarily correspond to the source evaluation date; these tables contain data from many sources.
Length	The total length of a particular photoatomic table in words.
Number of Energies	The number of energy points (NE) on the grid used for the photoatomic cross sections for that data table. In general, a finer energy grid (or greater number of points) indicates a more accurate representation of the cross sections.
E_{max}	The maximum incident photon energy for that data table in GeV (multiply by 1000 to get the value in units of MeV). For all incident energies greater than E_{max} , MCNP assumes the last cross-section value given.
Cross Section Source	<p>This entry indicates the source from which the cross-section data are derived. There are four sources for the cross-section data:</p> <ol style="list-style-type: none">(1) S&I indicates data from the Storm and Israel 1970 compilation,(2) B-IV indicates data from ENDF/B-IV,(3) B-IV/89 indicates data from ENDF/B-IV merged with data from EPDL89, and(4) B/VI.8 indicates data from ENDF/B-VI release 8.
Form Factor Source	<p>This entry indicates the source from which the form factor data are derived. There are three sources for the form factor data:</p> <ol style="list-style-type: none">(1) Unknown indicates that data date back to unknown origins,(2) B/IV indicates data from ENDF/B-IV, and(3) B/VI.8 indicates data from ENDF/B-VI release 8.
Fluorescence Source	<p>This entry indicates the source from which the fluorescence data are derived. There are two sources for the fluorescence data:</p> <ol style="list-style-type: none">(1) E&C indicates data from Everett and Cashwell's original work, and(2) B/VI.8 indicates data in the Everett and Cashwell format derived from ENDF/B-VI release 8.
CDBD Source	This entry indicates the source from which the momentum profile (CDBD) data for Doppler broadening of the Compton scattered energy are derived. Currently the only source for the CDBD data is Biggs, Mendelsohn and Mann's 1975 compilation.

Table G.4
Continuous-Energy Photoatomic Data Libraries Maintained by X-5

<u>ZAID</u>	<u>Library Name</u>	<u>Release Date</u>	<u>Length Words</u>	<u>NE</u>	<u>E_{max} (GeV)</u>	<u>CS Source</u>	<u>FF Source</u>	<u>Fluor. Source</u>	<u>CDBD Source</u>
Z = 1 ***** Hydrogen *****									
1000.01p	mcplib	1982	389	43	0.1	B-IV	B-IV	E&C	n/a
1000.02p	mcplib02	1993	623	82	100	B-IV/89	B-IV	E&C	n/a
1000.03p	mcplib03	2002	722	82	100	B-IV/89	B-IV	E&C	BM&M
1000.04p	mcplib04	2002	1898	278	100	B-VI.8	B-VI.8	B-VI.8	BM&M
Z = 2 ***** Helium *****									
2000.01p	mcplib	1982	389	43	0.1	B-IV	B-IV	E&C	n/a
2000.02p	mcplib02	1993	623	82	100	B-IV/89	B-IV	E&C	n/a
2000.03p	mcplib03	2002	722	82	100	B-IV/89	B-IV	E&C	BM&M
2000.04p	mcplib04	2002	1970	290	100	B-VI.8	B-VI.8	B-VI.8	BM&M
Z = 3 ***** Lithium *****									
3000.01p	mcplib	1982	389	43	0.1	B-IV	B-IV	E&C	n/a
3000.02p	mcplib02	1993	623	82	100	B-IV/89	B-IV	E&C	n/a
3000.03p	mcplib03	2002	821	82	100	B-IV/89	B-IV	E&C	BM&M
3000.04p	mcplib04	2002	2339	335	100	B-VI.8	B-VI.8	B-VI.8	BM&M
Z = 4 ***** Beryllium *****									
4000.01p	mcplib	1982	389	43	0.1	B-IV	B-IV	E&C	n/a
4000.02p	mcplib02	1993	623	82	100	B-IV/89	B-IV	E&C	n/a
4000.03p	mcplib03	2002	821	82	100	B-IV/89	B-IV	E&C	BM&M
4000.04p	mcplib04	2002	2363	339	100	B-VI.8	B-VI.8	B-VI.8	BM&M
Z = 5 ***** Boron *****									
5000.01p	mcplib	1982	389	43	0.1	B-IV	B-IV	E&C	n/a
5000.02p	mcplib02	1993	623	82	100	B-IV/89	B-IV	E&C	n/a
5000.03p	mcplib03	2002	920	82	100	B-IV/89	B-IV	E&C	BM&M
5000.04p	mcplib04	2002	3116	448	100	B-VI.8	B-VI.8	B-VI.8	BM&M
Z = 6 ***** Carbon *****									
6000.01p	mcplib	1982	389	43	0.1	B-IV	B-IV	E&C	n/a
6000.02p	mcplib02	1993	623	82	100	B-IV/89	B-IV	E&C	n/a
6000.03p	mcplib03	2002	920	82	100	B-IV/89	B-IV	E&C	BM&M
6000.04p	mcplib04	2002	3152	454	100	B-VI.8	B-VI.8	B-VI.8	BM&M
Z = 7 ***** Nitrogen *****									
7000.01p	mcplib	1982	389	43	0.1	B-IV	B-IV	E&C	n/a
7000.02p	mcplib02	1993	623	82	100	B-IV/89	B-IV	E&C	n/a
7000.03p	mcplib03	2002	920	82	100	B-IV/89	B-IV	E&C	BM&M
7000.04p	mcplib04	2002	3194	461	100	B-VI.8	B-VI.8	B-VI.8	BM&M
Z = 8 ***** Oxygen *****									
8000.01p	mcplib	1982	389	43	0.1	B-IV	B-IV	E&C	n/a
8000.02p	mcplib02	1993	623	82	100	B-IV/89	B-IV	E&C	n/a
8000.03p	mcplib03	2002	920	82	100	B-IV/89	B-IV	E&C	BM&M
8000.04p	mcplib04	2002	3272	474	100	B-VI.8	B-VI.8	B-VI.8	BM&M

Table G.4 (Cont.)
Continuous-Energy Photoatomic Data Libraries Maintained by X-5

<u>ZAID</u>	<u>Library Name</u>	<u>Release Date</u>	<u>Length Words</u>	<u>NE</u>	<u>E_{max} (GeV)</u>	<u>CS Source</u>	<u>FF Source</u>	<u>Fluor. Source</u>	<u>CDBD Source</u>
Z = 9 ***** Fluorine *****									
9000.01p	mcplib	1982	389	43	0.1	B-IV	B-IV	E&C	n/a
9000.02p	mcplib02	1993	623	82	100	B-IV/89	B-IV	E&C	n/a
9000.03p	mcplib03	2002	920	82	100	B-IV/89	B-IV	E&C	BM&M
9000.04p	mcplib04	2002	3206	463	100	B-VI.8	B-VI.8	B-VI.8	BM&M
Z = 10 ***** Neon *****									
10000.01p	mcplib	1982	389	43	0.1	B-IV	B-IV	E&C	n/a
10000.02p	mcplib02	1993	623	82	100	B-IV/89	B-IV	E&C	n/a
10000.03p	mcplib03	2002	920	82	100	B-IV/89	B-IV	E&C	BM&M
10000.04p	mcplib04	2002	3278	475	100	B-VI.8	B-VI.8	B-VI.8	BM&M
Z = 11 ***** Sodium *****									
11000.01p	mcplib	1982	401	45	0.1	B-IV	B-IV	E&C	n/a
11000.02p	mcplib02	1993	635	84	100	B-IV/89	B-IV	E&C	n/a
11000.03p	mcplib03	2002	1031	84	100	B-IV/89	B-IV	E&C	BM&M
11000.04p	mcplib04	2002	3995	578	100	B-VI.8	B-VI.8	B-VI.8	BM&M
Z = 12 ***** Magnesium *****									
12000.01p	mcplib	1982	409	45	0.1	B-IV	B-IV	E&C	n/a
12000.02p	mcplib02	1993	643	84	100	B-IV/89	B-IV	E&C	n/a
12000.03p	mcplib03	2002	1039	84	100	B-IV/89	B-IV	E&C	BM&M
12000.04p	mcplib04	2002	3781	541	100	B-VI.8	B-VI.8	B-VI.8	BM&M
Z = 13 ***** Aluminum *****									
13000.01p	mcplib	1982	409	45	0.1	B-IV	B-IV	E&C	n/a
13000.02p	mcplib02	1993	643	84	100	B-IV/89	B-IV	E&C	n/a
13000.03p	mcplib03	2002	1138	84	100	B-IV/89	B-IV	E&C	BM&M
13000.04p	mcplib04	2002	4846	702	100	B-VI.8	B-VI.8	B-VI.8	BM&M
Z = 14 ***** Silicon *****									
14000.01p	mcplib	1982	409	45	0.1	B-IV	B-IV	E&C	n/a
14000.02p	mcplib02	1993	643	84	100	B-IV/89	B-IV	E&C	n/a
14000.03p	mcplib03	2002	1138	84	100	B-IV/89	B-IV	E&C	BM&M
14000.04p	mcplib04	2002	4792	693	100	B-VI.8	B-VI.8	B-VI.8	BM&M
Z = 15 ***** Phosphorus *****									
15000.01p	mcplib	1982	409	45	0.1	B-IV	B-IV	E&C	n/a
15000.02p	mcplib02	1993	643	84	100	B-IV/89	B-IV	E&C	n/a
15000.03p	mcplib03	2002	1138	84	100	B-IV/89	B-IV	E&C	BM&M
15000.04p	mcplib04	2002	4498	644	100	B-VI.8	B-VI.8	B-VI.8	BM&M
Z = 16 ***** Sulfur *****									
16000.01p	mcplib	1982	409	45	0.1	B-IV	B-IV	E&C	n/a
16000.02p	mcplib02	1993	643	84	100	B-IV/89	B-IV	E&C	n/a
16000.03p	mcplib03	2002	1138	84	100	B-IV/89	B-IV	E&C	BM&M
16000.04p	mcplib04	2002	4654	670	100	B-VI.8	B-VI.8	B-VI.8	BM&M

Table G.4 (Cont.)
Continuous-Energy Photoatomic Data Libraries Maintained by X-5

<u>ZAID</u>	<u>Library Name</u>	<u>Release Date</u>	<u>Length Words</u>	<u>NE</u>	<u>E_{max} (GeV)</u>	<u>CS Source</u>	<u>FF Source</u>	<u>Fluor. Source</u>	<u>CDBD Source</u>
Z = 17 ***** Chlorine *****									
17000.01p	mcplib	1982	409	45	0.1	B-IV	B-IV	E&C	n/a
17000.02p	mcplib02	1993	643	84	100	B-IV/89	B-IV	E&C	n/a
17000.03p	mcplib03	2002	1138	84	100	B-IV/89	B-IV	E&C	BM&M
17000.04p	mcplib04	2002	4738	684	100	B-VI.8	B-VI.8	B-VI.8	BM&M
Z = 18 ***** Argon *****									
18000.01p	mcplib	1982	409	45	0.1	B-IV	B-IV	E&C	n/a
18000.02p	mcplib02	1993	643	84	100	B-IV/89	B-IV	E&C	n/a
18000.03p	mcplib03	2002	1138	84	100	B-IV/89	B-IV	E&C	BM&M
18000.04p	mcplib04	2002	4696	677	100	B-VI.8	B-VI.8	B-VI.8	BM&M
Z = 19 ***** Potassium *****									
19000.01p	mcplib	1982	409	45	0.1	B-IV	B-IV	E&C	n/a
19000.02p	mcplib02	1993	643	84	100	B-IV/89	B-IV	E&C	n/a
19000.03p	mcplib03	2002	1237	84	100	B-IV/89	B-IV	E&C	BM&M
19000.04p	mcplib04	2002	5047	719	100	B-VI.8	B-VI.8	B-VI.8	BM&M
Z = 20 ***** Calcium *****									
20000.01p	mcplib	1982	417	45	0.1	B-IV	B-IV	E&C	n/a
20000.02p	mcplib02	1993	651	84	100	B-IV/89	B-IV	E&C	n/a
20000.03p	mcplib03	2002	1245	84	100	B-IV/89	B-IV	E&C	BM&M
20000.04p	mcplib04	2002	5013	712	100	B-VI.8	B-VI.8	B-VI.8	BM&M
Z = 21 ***** Scandium *****									
21000.01p	mcplib	1982	417	45	0.1	B-IV	B-IV	E&C	n/a
21000.02p	mcplib02	1993	651	84	100	B-IV/89	B-IV	E&C	n/a
21000.03p	mcplib03	2002	1344	84	100	B-IV/89	B-IV	E&C	BM&M
21000.04p	mcplib04	2002	5532	782	100	B-VI.8	B-VI.8	B-VI.8	BM&M
Z = 22 ***** Titanium *****									
22000.01p	mcplib	1982	417	45	0.1	B-IV	B-IV	E&C	n/a
22000.02p	mcplib02	1993	651	84	100	B-IV/89	B-IV	E&C	n/a
22000.03p	mcplib03	2002	1344	84	100	B-IV/89	B-IV	E&C	BM&M
22000.04p	mcplib04	2002	5742	817	100	B-VI.8	B-VI.8	B-VI.8	BM&M
Z = 23 ***** Vanadium *****									
23000.01p	mcplib	1982	417	45	0.1	B-IV	B-IV	E&C	n/a
23000.02p	mcplib02	1993	651	84	100	B-IV/89	B-IV	E&C	n/a
23000.03p	mcplib03	2002	1344	84	100	B-IV/89	B-IV	E&C	BM&M
23000.04p	mcplib04	2002	5814	829	100	B-VI.8	B-VI.8	B-VI.8	BM&M
Z = 24 ***** Chromium *****									
24000.01p	mcplib	1982	417	45	0.1	B-IV	B-IV	E&C	n/a
24000.02p	mcplib02	1993	651	84	100	B-IV/89	B-IV	E&C	n/a
24000.03p	mcplib03	2002	1344	84	100	B-IV/89	B-IV	E&C	BM&M
24000.04p	mcplib04	2002	5682	807	100	B-VI.8	B-VI.8	B-VI.8	BM&M

Table G.4 (Cont.)
Continuous-Energy Photoatomic Data Libraries Maintained by X-5

<u>ZAID</u>	<u>Library Name</u>	<u>Release Date</u>	<u>Length Words</u>	<u>NE</u>	<u>E_{max} (GeV)</u>	<u>CS Source</u>	<u>FF Source</u>	<u>Fluor. Source</u>	<u>CDBD Source</u>
Z = 25 ***** Manganese *****									
25000.01p	mcplib	1982	417	45	0.1	B-IV	B-IV	E&C	n/a
25000.02p	mcplib02	1993	651	84	100	B-IV/89	B-IV	E&C	n/a
25000.03p	mcplib03	2002	1344	84	100	B-IV/89	B-IV	E&C	BM&M
25000.04p	mcplib04	2002	5598	793	100	B-VI.8	B-VI.8	B-VI.8	BM&M
Z = 26 ***** Iron *****									
26000.01p	mcplib	1982	417	45	0.1	B-IV	B-IV	E&C	n/a
26000.02p	mcplib02	1993	651	84	100	B-IV/89	B-IV	E&C	n/a
26000.03p	mcplib03	2002	1344	84	100	B-IV/89	B-IV	E&C	BM&M
26000.04p	mcplib04	2002	5718	813	100	B-VI.8	B-VI.8	B-VI.8	BM&M
Z = 27 ***** Cobalt *****									
27000.01p	mcplib	1982	417	45	0.1	B-IV	B-IV	E&C	n/a
27000.02p	mcplib02	1993	651	84	100	B-IV/89	B-IV	E&C	n/a
27000.03p	mcplib03	2002	1344	84	100	B-IV/89	B-IV	E&C	BM&M
27000.04p	mcplib04	2002	5436	766	100	B-VI.8	B-VI.8	B-VI.8	BM&M
Z = 28 ***** Nickel *****									
28000.01p	mcplib	1982	429	47	0.1	B-IV	B-IV	E&C	n/a
28000.02p	mcplib02	1993	663	86	100	B-IV/89	B-IV	E&C	n/a
28000.03p	mcplib03	2002	1356	86	100	B-IV/89	B-IV	E&C	BM&M
28000.04p	mcplib04	2002	5826	831	100	B-VI.8	B-VI.8	B-VI.8	BM&M
Z = 29 ***** Copper *****									
29000.01p	mcplib	1982	429	47	0.1	B-IV	B-IV	E&C	n/a
29000.02p	mcplib02	1993	663	86	100	B-IV/89	B-IV	E&C	n/a
29000.03p	mcplib03	2002	1356	86	100	B-IV/89	B-IV	E&C	BM&M
29000.04p	mcplib04	2002	5754	819	100	B-VI.8	B-VI.8	B-VI.8	BM&M
Z = 30 ***** Zinc *****									
30000.01p	mcplib	1982	453	51	0.1	B-IV	B-IV	E&C	n/a
30000.02p	mcplib02	1993	687	90	100	B-IV/89	B-IV	E&C	n/a
30000.03p	mcplib03	2002	1380	90	100	B-IV/89	B-IV	E&C	BM&M
30000.04p	mcplib04	2002	6288	908	100	B-VI.8	B-VI.8	B-VI.8	BM&M
Z = 31 ***** Gallium *****									
31000.01p	mcplib	1982	457	51	0.1	B-IV	B-IV	E&C	n/a
31000.02p	mcplib02	1993	691	90	100	B-IV/89	B-IV	E&C	n/a
31000.03p	mcplib03	2002	1483	90	100	B-IV/89	B-IV	E&C	BM&M
31000.04p	mcplib04	2002	6787	974	100	B-VI.8	B-VI.8	B-VI.8	BM&M
Z = 32 ***** Germanium *****									
32000.01p	mcplib	1982	457	51	0.1	B-IV	B-IV	E&C	n/a
32000.02p	mcplib02	1993	691	90	100	B-IV/89	B-IV	E&C	n/a
32000.03p	mcplib03	2002	1483	90	100	B-IV/89	B-IV	E&C	BM&M
32000.04p	mcplib04	2002	7027	1014	100	B-VI.8	B-VI.8	B-VI.8	BM&M

Table G.4 (Cont.)
Continuous-Energy Photoatomic Data Libraries Maintained by X-5

<u>Z</u> <u>AID</u>	<u>Library</u> <u>Name</u>	<u>Release</u> <u>Date</u>	<u>Length</u> <u>Words</u>	<u>NE</u>	<u>E_{max}</u> <u>(GeV)</u>	<u>CS</u> <u>Source</u>	<u>FF</u> <u>Source</u>	<u>Fluor.</u> <u>Source</u>	<u>CDBD</u> <u>Source</u>
Z = 33	***** Arsenic *****								
33000.01p	mcplib	1982	457	51	0.1	B-IV	B-IV	E&C	n/a
33000.02p	mcplib02	1993	691	90	100	B-IV/89	B-IV	E&C	n/a
33000.03p	mcplib03	2002	1483	90	100	B-IV/89	B-IV	E&C	BM&M
33000.04p	mcplib04	2002	6595	942	100	B-VI.8	B-VI.8	B-VI.8	BM&M
Z = 34	***** Selenium *****								
34000.01p	mcplib	1982	457	51	0.1	B-IV	B-IV	E&C	n/a
34000.02p	mcplib02	1993	691	90	100	B-IV/89	B-IV	E&C	n/a
34000.03p	mcplib03	2002	1483	90	100	B-IV/89	B-IV	E&C	BM&M
34000.04p	mcplib04	2002	6655	952	100	B-VI.8	B-VI.8	B-VI.8	BM&M
Z = 35	***** Bromine *****								
35000.01p	mcplib	1982	457	51	0.1	B-IV	B-IV	E&C	n/a
35000.02p	mcplib02	1993	691	90	100	B-IV/89	B-IV	E&C	n/a
35000.03p	mcplib03	2002	1483	90	100	B-IV/89	B-IV	E&C	BM&M
35000.04p	mcplib04	2002	6853	985	100	B-VI.8	B-VI.8	B-VI.8	BM&M
Z = 36	***** Krypton *****								
36000.01p	mcplib	1982	457	51	0.1	B-IV	B-IV	E&C	n/a
36000.02p	mcplib02	1993	691	90	100	B-IV/89	B-IV	E&C	n/a
36000.03p	mcplib03	2002	1879	90	100	B-IV/89	B-IV	E&C	BM&M
36000.04p	mcplib04	2002	7177	973	100	B-VI.8	B-VI.8	B-VI.8	BM&M
Z = 37	***** Rubidium *****								
37000.01p	mcplib	1982	461	51	0.1	B-IV	B-IV	E&C	n/a
37000.02p	mcplib02	1993	695	90	100	B-IV/89	B-IV	E&C	n/a
37000.03p	mcplib03	2002	1982	90	100	B-IV/89	B-IV	E&C	BM&M
37000.04p	mcplib04	2002	7364	987	100	B-VI.8	B-VI.8	B-VI.8	BM&M
Z = 38	***** Strontium *****								
38000.01p	mcplib	1982	461	51	0.1	B-IV	B-IV	E&C	n/a
38000.02p	mcplib02	1993	695	90	100	B-IV/89	B-IV	E&C	n/a
38000.03p	mcplib03	2002	1982	90	100	B-IV/89	B-IV	E&C	BM&M
38000.04p	mcplib04	2002	7256	969	100	B-VI.8	B-VI.8	B-VI.8	BM&M
Z = 39	***** Yttrium *****								
39000.01p	mcplib	1982	461	51	0.1	B-IV	B-IV	E&C	n/a
39000.02p	mcplib02	1993	695	90	100	B-IV/89	B-IV	E&C	n/a
39000.03p	mcplib03	2002	2081	90	100	B-IV/89	B-IV	E&C	BM&M
39000.04p	mcplib04	2002	7583	1007	100	B-VI.8	B-VI.8	B-VI.8	BM&M
Z = 40	***** Zirconium *****								
40000.01p	mcplib	1982	461	51	0.1	B-IV	B-IV	E&C	n/a
40000.02p	mcplib02	1993	695	90	100	B-IV/89	B-IV	E&C	n/a
40000.03p	mcplib03	2002	2081	90	100	B-IV/89	B-IV	E&C	BM&M
40000.04p	mcplib04	2002	7703	1027	100	B-VI.8	B-VI.8	B-VI.8	BM&M

Table G.4 (Cont.)
Continuous-Energy Photoatomic Data Libraries Maintained by X-5

<u>ZAID</u>	<u>Library Name</u>	<u>Release Date</u>	<u>Length Words</u>	<u>NE</u>	<u>E_{max} (GeV)</u>	<u>CS Source</u>	<u>FF Source</u>	<u>Fluor. Source</u>	<u>CDBD Source</u>
Z = 41 ***** Niobium *****									
41000.01p	mcplib	1982	461	51	0.1	B-IV	B-IV	E&C	n/a
41000.02p	mcplib02	1993	695	90	100	B-IV/89	B-IV	E&C	n/a
41000.03p	mcplib03	2002	2081	90	100	B-IV/89	B-IV	E&C	BM&M
41000.04p	mcplib04	2002	7667	1021	100	B-VI.8	B-VI.8	B-VI.8	BM&M
Z = 42 ***** Molybdenum *****									
42000.01p	mcplib	1982	461	51	0.1	B-IV	B-IV	E&C	n/a
42000.02p	mcplib02	1993	695	90	100	B-IV/89	B-IV	E&C	n/a
42000.03p	mcplib03	2002	2180	90	100	B-IV/89	B-IV	E&C	BM&M
42000.04p	mcplib04	2002	7592	992	100	B-VI.8	B-VI.8	B-VI.8	BM&M
Z = 43 ***** Technetium *****									
43000.01p	mcplib	1982	461	51	0.1	B-IV	B-IV	E&C	n/a
43000.02p	mcplib02	1993	695	90	100	B-IV/89	B-IV	E&C	n/a
43000.03p	mcplib03	2002	2180	90	100	B-IV/89	B-IV	E&C	BM&M
43000.04p	mcplib04	2002	7946	1051	100	B-VI.8	B-VI.8	B-VI.8	BM&M
Z = 44 ***** Ruthenium *****									
44000.01p	mcplib	1982	461	51	0.1	B-IV	B-IV	E&C	n/a
44000.02p	mcplib02	1993	695	90	100	B-IV/89	B-IV	E&C	n/a
44000.03p	mcplib03	2002	2180	90	100	B-IV/89	B-IV	E&C	BM&M
44000.04p	mcplib04	2002	7988	1058	100	B-VI.8	B-VI.8	B-VI.8	BM&M
Z = 45 ***** Rhodium *****									
45000.01p	mcplib	1982	461	51	0.1	B-IV	B-IV	E&C	n/a
45000.02p	mcplib02	1993	695	90	100	B-IV/89	B-IV	E&C	n/a
45000.03p	mcplib03	2002	2180	90	100	B-IV/89	B-IV	E&C	BM&M
45000.04p	mcplib04	2002	7856	1036	100	B-VI.8	B-VI.8	B-VI.8	BM&M
Z = 46 ***** Palladium *****									
46000.01p	mcplib	1982	461	51	0.1	B-IV	B-IV	E&C	n/a
46000.02p	mcplib02	1993	695	90	100	B-IV/89	B-IV	E&C	n/a
46000.03p	mcplib03	2002	2081	90	100	B-IV/89	B-IV	E&C	BM&M
46000.04p	mcplib04	2002	7595	1009	100	B-VI.8	B-VI.8	B-VI.8	BM&M
Z = 47 ***** Silver *****									
47000.01p	mcplib	1982	461	51	0.1	B-IV	B-IV	E&C	n/a
47000.02p	mcplib02	1993	695	90	100	B-IV/89	B-IV	E&C	n/a
47000.03p	mcplib03	2002	2180	90	100	B-IV/89	B-IV	E&C	BM&M
47000.04p	mcplib04	2002	7772	1022	100	B-VI.8	B-VI.8	B-VI.8	BM&M
Z = 48 ***** Cadmium *****									
48000.01p	mcplib	1982	461	51	0.1	B-IV	B-IV	E&C	n/a
48000.02p	mcplib02	1993	695	90	100	B-IV/89	B-IV	E&C	n/a
48000.03p	mcplib03	2002	2180	90	100	B-IV/89	B-IV	E&C	BM&M
48000.04p	mcplib04	2002	7700	1010	100	B-VI.8	B-VI.8	B-VI.8	BM&M

Table G.4 (Cont.)
Continuous-Energy Photoatomic Data Libraries Maintained by X-5

<u>ZAID</u>	<u>Library Name</u>	<u>Release Date</u>	<u>Length Words</u>	<u>NE</u>	<u>E_{max} (GeV)</u>	<u>CS Source</u>	<u>FF Source</u>	<u>Fluor Source</u>	<u>CDBD Source</u>
Z = 49 ***** Indium *****									
49000.01p	mcplib	1982	461	51	0.1	B-IV	B-IV	E&C	n/a
49000.02p	mcplib02	1993	695	90	100	B-IV/89	B-IV	E&C	n/a
49000.03p	mcplib03	2002	2279	90	100	B-IV/89	B-IV	E&C	BM&M
49000.04p	mcplib04	2002	8291	1092	100	B-VI.8	B-VI.8	B-VI.8	BM&M
Z = 50 ***** Tin *****									
50000.01p	mcplib	1982	461	51	0.1	B-IV	B-IV	E&C	n/a
50000.02p	mcplib02	1993	695	90	100	B-IV/89	B-IV	E&C	n/a
50000.03p	mcplib03	2002	2279	90	100	B-IV/89	B-IV	E&C	BM&M
50000.04p	mcplib04	2002	8039	1050	100	B-VI.8	B-VI.8	B-VI.8	BM&M
Z = 51 ***** Antimony *****									
51000.01p	mcplib	1982	461	51	0.1	B-IV	B-IV	E&C	n/a
51000.02p	mcplib02	1993	695	90	100	B-IV/89	B-IV	E&C	n/a
51000.03p	mcplib03	2002	2378	90	100	B-IV/89	B-IV	E&C	BM&M
51000.04p	mcplib04	2002	8414	1096	100	B-VI.8	B-VI.8	B-VI.8	BM&M
Z = 52 ***** Tellurium *****									
52000.01p	mcplib	1982	473	53	0.1	B-IV	B-IV	E&C	n/a
52000.02p	mcplib02	1993	707	92	100	B-IV/89	B-IV	E&C	n/a
52000.03p	mcplib03	2002	2390	92	100	B-IV/89	B-IV	E&C	BM&M
52000.04p	mcplib04	2002	8162	1054	100	B-VI.8	B-VI.8	B-VI.8	BM&M
Z = 53 ***** Iodine *****									
53000.01p	mcplib	1982	473	53	0.1	B-IV	B-IV	E&C	n/a
53000.02p	mcplib02	1993	707	92	100	B-IV/89	B-IV	E&C	n/a
53000.03p	mcplib03	2002	2390	92	100	B-IV/89	B-IV	E&C	BM&M
53000.04p	mcplib04	2002	8492	1109	100	B-VI.8	B-VI.8	B-VI.8	BM&M
Z = 54 ***** Xenon *****									
54000.01p	mcplib	1982	473	53	0.1	B-IV	B-IV	E&C	n/a
54000.02p	mcplib02	1993	707	92	100	B-IV/89	B-IV	E&C	n/a
54000.03p	mcplib03	2002	2390	92	100	B-IV/89	B-IV	E&C	BM&M
54000.04p	mcplib04	2002	8324	1081	100	B-VI.8	B-VI.8	B-VI.8	BM&M
Z = 55 ***** Cesium *****									
55000.01p	mcplib	1982	497	57	0.1	B-IV	B-IV	E&C	n/a
55000.02p	mcplib02	1993	731	96	100	B-IV/89	B-IV	E&C	n/a
55000.03p	mcplib03	2002	2513	96	100	B-IV/89	B-IV	E&C	BM&M
55000.04p	mcplib04	2002	8417	1080	100	B-VI.8	B-VI.8	B-VI.8	BM&M
Z = 56 ***** Barium *****									
56000.01p	mcplib	1982	497	57	0.1	B-IV	B-IV	E&C	n/a
56000.02p	mcplib02	1993	731	96	100	B-IV/89	B-IV	E&C	n/a
56000.03p	mcplib03	2002	2513	96	100	B-IV/89	B-IV	E&C	BM&M
56000.04p	mcplib04	2002	8465	1088	100	B-VI.8	B-VI.8	B-VI.8	BM&M

Table G.4 (Cont.)
Continuous-Energy Photoatomic Data Libraries Maintained by X-5

<u>ZAID</u>	<u>Library Name</u>	<u>Release Date</u>	<u>Length Words</u>	<u>NE</u>	<u>E_{max} (GeV)</u>	<u>CS Source</u>	<u>FF Source</u>	<u>Fluor. Source</u>	<u>CDBD Source</u>
Z = 57 ***** Lanthanum *****									
57000.01p	mcplib	1982	497	57	0.1	B-IV	B-IV	E&C	n/a
57000.02p	mcplib02	1993	731	96	100	B-IV/89	B-IV	E&C	n/a
57000.03p	mcplib03	2002	2612	96	100	B-IV/89	B-IV	E&C	BM&M
57000.04p	mcplib04	2002	8744	1118	100	B-VI.8	B-VI.8	B-VI.8	BM&M
Z = 58 ***** Cerium *****									
58000.01p	mcplib	1982	497	57	0.1	B-IV	B-IV	E&C	n/a
58000.02p	mcplib02	1993	731	96	100	B-IV/89	B-IV	E&C	n/a
58000.03p	mcplib03	2002	2711	96	100	B-IV/89	B-IV	E&C	BM&M
58000.04p	mcplib04	2002	9173	1173	100	B-VI.8	B-VI.8	B-VI.8	BM&M
Z = 59 ***** Praseodymium *****									
59000.01p	mcplib	1982	497	57	0.1	B-IV	B-IV	E&C	n/a
59000.02p	mcplib02	1993	731	96	100	B-IV/89	B-IV	E&C	n/a
59000.03p	mcplib03	2002	2612	96	100	B-IV/89	B-IV	E&C	BM&M
59000.04p	mcplib04	2002	8750	1119	100	B-VI.8	B-VI.8	B-VI.8	BM&M
Z = 60 ***** Neodymium *****									
60000.01p	mcplib	1982	509	59	0.1	B-IV	B-IV	E&C	n/a
60000.02p	mcplib02	1993	743	98	100	B-IV/89	B-IV	E&C	n/a
60000.03p	mcplib03	2002	2624	98	100	B-IV/89	B-IV	E&C	BM&M
60000.04p	mcplib04	2002	9362	1221	100	B-VI.8	B-VI.8	B-VI.8	BM&M
Z = 61 ***** Promethium *****									
61000.01p	mcplib	1982	521	61	0.1	B-IV	B-IV	E&C	n/a
61000.02p	mcplib02	1993	755	100	100	B-IV/89	B-IV	E&C	n/a
61000.03p	mcplib03	2002	2636	100	100	B-IV/89	B-IV	E&C	BM&M
61000.04p	mcplib04	2002	9350	1219	100	B-VI.8	B-VI.8	B-VI.8	BM&M
Z = 62 ***** Samarium *****									
62000.01p	mcplib	1982	521	61	0.1	B-IV	B-IV	E&C	n/a
62000.02p	mcplib02	1993	755	100	100	B-IV/89	B-IV	E&C	n/a
62000.03p	mcplib03	2002	2636	100	100	B-IV/89	B-IV	E&C	BM&M
62000.04p	mcplib04	2002	9374	1223	100	B-VI.8	B-VI.8	B-VI.8	BM&M
Z = 63 ***** Europium *****									
63000.01p	mcplib	1982	521	61	0.1	B-IV	B-IV	E&C	n/a
63000.02p	mcplib02	1993	755	100	100	B-IV/89	B-IV	E&C	n/a
63000.03p	mcplib03	2002	2735	100	100	B-IV/89	B-IV	E&C	BM&M
63000.04p	mcplib04	2002	9323	1198	100	B-VI.8	B-VI.8	B-VI.8	BM&M
Z = 64 ***** Gadolinium *****									
64000.01p	mcplib	1982	521	61	0.1	B-IV	B-IV	E&C	n/a
64000.02p	mcplib02	1993	755	100	100	B-IV/89	B-IV	E&C	n/a
64000.03p	mcplib03	2002	2834	100	100	B-IV/89	B-IV	E&C	BM&M
64000.04p	mcplib04	2002	9560	1221	100	B-VI.8	B-VI.8	B-VI.8	BM&M

Table G.4 (Cont.)
Continuous-Energy Photoatomic Data Libraries Maintained by X-5

<u>ZAID</u>	<u>Library Name</u>	<u>Release Date</u>	<u>Length Words</u>	<u>NE</u>	<u>E_{max} (GeV)</u>	<u>CS Source</u>	<u>FF Source</u>	<u>Fluor. Source</u>	<u>CDBD Source</u>
Z = 65 ***** Terbium *****									
65000.01p	mcplib	1982	521	61	0.1	B-IV	B-IV	E&C	n/a
65000.02p	mcplib02	1993	755	100	100	B-IV/89	B-IV	E&C	n/a
65000.03p	mcplib03	2002	2735	100	100	B-IV/89	B-IV	E&C	BM&M
65000.04p	mcplib04	2002	9143	1168	100	B-VI.8	B-VI.8	B-VI.8	BM&M
Z = 66 ***** Dysprosium *****									
66000.01p	mcplib	1982	521	61	0.1	B-IV	B-IV	E&C	n/a
66000.02p	mcplib02	1993	755	100	100	B-IV/89	B-IV	E&C	n/a
66000.03p	mcplib03	2002	2735	100	100	B-IV/89	B-IV	E&C	BM&M
66000.04p	mcplib04	2002	9479	1224	100	B-VI.8	B-VI.8	B-VI.8	BM&M
Z = 67 ***** Holmium *****									
67000.01p	mcplib	1982	521	61	0.1	B-IV	B-IV	E&C	n/a
67000.02p	mcplib02	1993	755	100	100	B-IV/89	B-IV	E&C	n/a
67000.03p	mcplib03	2002	2735	100	100	B-IV/89	B-IV	E&C	BM&M
67000.04p	mcplib04	2002	9419	1214	100	B-VI.8	B-VI.8	B-VI.8	BM&M
Z = 68 ***** Erbium *****									
68000.01p	mcplib	1982	521	61	0.1	B-IV	B-IV	E&C	n/a
68000.02p	mcplib02	1993	755	100	100	B-IV/89	B-IV	E&C	n/a
68000.03p	mcplib03	2002	2735	100	100	B-IV/89	B-IV	E&C	BM&M
68000.04p	mcplib04	2002	9233	1183	100	B-VI.8	B-VI.8	B-VI.8	BM&M
Z = 69 ***** Thulium *****									
69000.01p	mcplib	1982	521	61	0.1	B-IV	B-IV	E&C	n/a
69000.02p	mcplib02	1993	755	100	100	B-IV/89	B-IV	E&C	n/a
69000.03p	mcplib03	2002	2735	100	100	B-IV/89	B-IV	E&C	BM&M
69000.04p	mcplib04	2002	9473	1223	100	B-VI.8	B-VI.8	B-VI.8	BM&M
Z = 70 ***** Ytterbium *****									
70000.01p	mcplib	1982	521	61	0.1	B-IV	B-IV	E&C	n/a
70000.02p	mcplib02	1993	755	100	100	B-IV/89	B-IV	E&C	n/a
70000.03p	mcplib03	2002	2735	100	100	B-IV/89	B-IV	E&C	BM&M
70000.04p	mcplib04	2002	9539	1234	100	B-VI.8	B-VI.8	B-VI.8	BM&M
Z = 71 ***** Lutetium *****									
71000.01p	mcplib	1982	521	61	0.1	B-IV	B-IV	E&C	n/a
71000.02p	mcplib02	1993	755	100	100	B-IV/89	B-IV	E&C	n/a
71000.03p	mcplib03	2002	2834	100	100	B-IV/89	B-IV	E&C	BM&M
71000.04p	mcplib04	2002	9914	1280	100	B-VI.8	B-VI.8	B-VI.8	BM&M
Z = 72 ***** Hafnium *****									
72000.01p	mcplib	1982	521	61	0.1	B-IV	B-IV	E&C	n/a
72000.02p	mcplib02	1993	755	100	100	B-IV/89	B-IV	E&C	n/a
72000.03p	mcplib03	2002	2834	100	100	B-IV/89	B-IV	E&C	BM&M
72000.04p	mcplib04	2002	9932	1283	100	B-VI.8	B-VI.8	B-VI.8	BM&M

Table G.4 (Cont.)
Continuous-Energy Photoatomic Data Libraries Maintained by X-5

<u>ZAID</u>	<u>Library Name</u>	<u>Release Date</u>	<u>Length Words</u>	<u>NE</u>	<u>E_{max} (GeV)</u>	<u>CS Source</u>	<u>FF Source</u>	<u>Fluor. Source</u>	<u>CDBD Source</u>
Z = 73 ***** Tantalum *****									
73000.01p	mcplib	1982	521	61	0.1	B-IV	B-IV	E&C	n/a
73000.02p	mcplib02	1993	755	100	100	B-IV/89	B-IV	E&C	n/a
73000.03p	mcplib03	2002	2834	100	100	B-IV/89	B-IV	E&C	BM&M
73000.04p	mcplib04	2002	9698	1244	100	B-VI.8	B-VI.8	B-VI.8	BM&M
Z = 74 ***** Tungsten *****									
74000.01p	mcplib	1982	521	61	0.1	B-IV	B-IV	E&C	n/a
74000.02p	mcplib02	1993	755	100	100	B-IV/89	B-IV	E&C	n/a
74000.03p	mcplib03	2002	2834	100	100	B-IV/89	B-IV	E&C	BM&M
74000.04p	mcplib04	2002	9716	1247	100	B-VI.8	B-VI.8	B-VI.8	BM&M
Z = 75 ***** Rhenium *****									
75000.01p	mcplib	1982	521	61	0.1	B-IV	B-IV	E&C	n/a
75000.02p	mcplib02	1993	755	100	100	B-IV/89	B-IV	E&C	n/a
75000.03p	mcplib03	2002	2933	100	100	B-IV/89	B-IV	E&C	BM&M
75000.04p	mcplib04	2002	9797	1244	100	B-VI.8	B-VI.8	B-VI.8	BM&M
Z = 76 ***** Osmium *****									
76000.01p	mcplib	1982	521	61	0.1	B-IV	B-IV	E&C	n/a
76000.02p	mcplib02	1993	755	100	100	B-IV/89	B-IV	E&C	n/a
76000.03p	mcplib03	2002	2933	100	100	B-IV/89	B-IV	E&C	BM&M
76000.04p	mcplib04	2002	9977	1274	100	B-VI.8	B-VI.8	B-VI.8	BM&M
Z = 77 ***** Iridium *****									
77000.01p	mcplib	1982	521	61	0.1	B-IV	B-IV	E&C	n/a
77000.02p	mcplib02	1993	755	100	100	B-IV/89	B-IV	E&C	n/a
77000.03p	mcplib03	2002	2933	100	100	B-IV/89	B-IV	E&C	BM&M
77000.04p	mcplib04	2002	9665	1222	100	B-VI.8	B-VI.8	B-VI.8	BM&M
Z = 78 ***** Platinum *****									
78000.01p	mcplib	1982	521	61	0.1	B-IV	B-IV	E&C	n/a
78000.02p	mcplib02	1993	755	100	100	B-IV/89	B-IV	E&C	n/a
78000.03p	mcplib03	2002	2933	100	100	B-IV/89	B-IV	E&C	BM&M
78000.04p	mcplib04	2002	9377	1174	100	B-VI.8	B-VI.8	B-VI.8	BM&M
Z = 79 ***** Gold *****									
79000.01p	mcplib	1982	521	61	0.1	B-IV	B-IV	E&C	n/a
79000.02p	mcplib02	1993	755	100	100	B-IV/89	B-IV	E&C	n/a
79000.03p	mcplib03	2002	2933	100	100	B-IV/89	B-IV	E&C	BM&M
79000.04p	mcplib04	2002	9881	1258	100	B-VI.8	B-VI.8	B-VI.8	BM&M
Z = 80 ***** Mercury *****									
80000.01p	mcplib	1982	521	61	0.1	B-IV	B-IV	E&C	n/a
80000.02p	mcplib02	1993	755	100	100	B-IV/89	B-IV	E&C	n/a
80000.03p	mcplib03	2002	2933	100	100	B-IV/89	B-IV	E&C	BM&M
80000.04p	mcplib04	2002	9281	1158	100	B-VI.8	B-VI.8	B-VI.8	BM&M

Table G.4 (Cont.)
Continuous-Energy Photoatomic Data Libraries Maintained by X-5

<u>ZAID</u>	<u>Library Name</u>	<u>Release Date</u>	<u>Length Words</u>	<u>NE</u>	<u>E_{max} (GeV)</u>	<u>CS Source</u>	<u>FF Source</u>	<u>Fluor. Source</u>	<u>CDBD Source</u>
Z = 81 ***** Thallium *****									
81000.01p	mcplib	1982	521	61	0.1	B-IV	B-IV	E&C	n/a
81000.02p	mcplib02	1993	755	100	100	B-IV/89	B-IV	E&C	n/a
81000.03p	mcplib03	2002	3032	100	100	B-IV/89	B-IV	E&C	BM&M
81000.04p	mcplib04	2002	10142	1285	100	B-VI.8	B-VI.8	B-VI.8	BM&M
Z = 82 ***** Lead *****									
82000.01p	mcplib	1982	521	61	0.1	B-IV	B-IV	E&C	n/a
82000.02p	mcplib02	1993	755	100	100	B-IV/89	B-IV	E&C	n/a
82000.03p	mcplib03	2002	3032	100	100	B-IV/89	B-IV	E&C	BM&M
82000.04p	mcplib04	2002	10010	1263	100	B-VI.8	B-VI.8	B-VI.8	BM&M
Z = 83 ***** Bismuth *****									
83000.01p	mcplib	1982	521	61	0.1	B-IV	B-IV	E&C	n/a
83000.02p	mcplib02	1993	755	100	100	B-IV/89	B-IV	E&C	n/a
83000.03p	mcplib03	2002	3131	100	100	B-IV/89	B-IV	E&C	BM&M
83000.04p	mcplib04	2002	10373	1307	100	B-VI.8	B-VI.8	B-VI.8	BM&M
Z = 84 ***** Polonium *****									
84000.01p	mcplib	1982	467	52	0.015	DLC-15	Unknown	E&C	n/a
84000.02p	mcplib02	1993	749	99	100	S&I/89	Unknown	E&C	n/a
84000.03p	mcplib03	2002	3125	99	100	S&I/89	Unknown	E&C	BM&M
84000.04p	mcplib04	2002	10247	1286	100	B-VI.8	B-VI.8	B-VI.8	BM&M
Z = 85 ***** Astatine *****									
85000.01p	mcplib	1982	479	54	0.015	DLC-15	Unknown	E&C	n/a
85000.02p	mcplib02	1993	761	101	100	S&I/89	Unknown	E&C	n/a
85000.03p	mcplib03	2002	3137	101	100	S&I/89	Unknown	E&C	BM&M
85000.04p	mcplib04	2002	10463	1322	100	B-VI.8	B-VI.8	B-VI.8	BM&M
Z = 86 ***** Radon *****									
86000.01p	mcplib	1982	533	63	0.1	B-IV	B-IV	E&C	n/a
86000.02p	mcplib02	1993	767	102	100	B-IV/89	B-IV	E&C	n/a
86000.03p	mcplib03	2002	3143	102	100	B-IV/89	B-IV	E&C	BM&M
86000.04p	mcplib04	2002	10325	1299	100	B-VI.8	B-VI.8	B-VI.8	BM&M
Z = 87 ***** Francium *****									
87000.01p	mcplib	1982	479	54	0.015	S&I	Unknown	E&C	n/a
87000.02p	mcplib02	1993	761	101	100	S&I/89	Unknown	E&C	n/a
87000.03p	mcplib03	2002	3236	101	100	S&I/89	Unknown	E&C	BM&M
87000.04p	mcplib04	2002	10532	1317	100	B-VI.8	B-VI.8	B-VI.8	BM&M
Z = 88 ***** Radium *****									
88000.01p	mcplib	1982	479	54	0.015	S&I	Unknown	E&C	n/a
88000.02p	mcplib02	1993	761	101	100	S&I/89	Unknown	E&C	n/a
88000.03p	mcplib03	2002	3236	101	100	S&I/89	Unknown	E&C	BM&M
88000.04p	mcplib04	2002	10346	1286	100	B-VI.8	B-VI.8	B-VI.8	BM&M

Table G.4 (Cont.)
Continuous-Energy Photoatomic Data Libraries Maintained by X-5

<u>ZAID</u>	<u>Library Name</u>	<u>Release Date</u>	<u>Length Words</u>	<u>NE</u>	<u>E_{max} (GeV)</u>	<u>CS Source</u>	<u>FF Source</u>	<u>Fluor. Source</u>	<u>CDBD Source</u>
Z = 89 ***** Actinium *****									
89000.01p	mcplib	1982	479	54	0.015	S&I	Unknown	E&C	n/a
89000.02p	mcplib02	1993	761	101	100	S&I/89	Unknown	E&C	n/a
89000.03p	mcplib03	2002	3335	101	100	S&I/89	Unknown	E&C	BM&M
89000.04p	mcplib04	2002	10133	1234	100	B-VI.8	B-VI.8	B-VI.8	BM&M
Z = 90 ***** Thorium *****									
90000.01p	mcplib	1982	533	63	0.1	B-IV	B-IV	E&C	n/a
90000.02p	mcplib02	1993	767	102	100	B-IV/89	B-IV	E&C	n/a
90000.03p	mcplib03	2002	3341	102	100	B-IV/89	B-IV	E&C	BM&M
90000.04p	mcplib04	2002	10565	1306	100	B-VI.8	B-VI.8	B-VI.8	BM&M
Z = 91 ***** Protactinium *****									
91000.01p	mcplib	1982	479	54	0.015	S&I	Unknown	E&C	n/a
91000.02p	mcplib02	1993	761	101	100	S&I/89	Unknown	E&C	n/a
91000.03p	mcplib03	2002	3434	101	100	S&I/89	Unknown	E&C	BM&M
91000.04p	mcplib04	2002	10670	1307	100	B-VI.8	B-VI.8	B-VI.8	BM&M
Z = 92 ***** Uranium *****									
92000.01p	mcplib	1982	533	63	0.1	B-IV	B-IV	E&C	n/a
92000.02p	mcplib02	1993	767	102	100	B-IV/89	B-IV	E&C	n/a
92000.03p	mcplib03	2002	3440	102	100	B-IV/89	B-IV	E&C	BM&M
92000.04p	mcplib04	2002	10808	1330	100	B-VI.8	B-VI.8	B-VI.8	BM&M
Z = 93 ***** Neptunium *****									
93000.01p	mcplib	1982	479	54	0.015	S&I	Unknown	E&C	n/a
93000.02p	mcplib02	1993	761	101	100	S&I/89	Unknown	E&C	n/a
93000.03p	mcplib03	2002	3434	101	100	S&I/89	Unknown	E&C	BM&M
93000.04p	mcplib04	2002	11120	1382	100	B-VI.8	B-VI.8	B-VI.8	BM&M
Z = 94 ***** Plutonium *****									
94000.01p	mcplib	1982	533	63	0.1	B-IV	B-IV	E&C	n/a
94000.02p	mcplib02	1993	767	102	100	B-IV/89	B-IV	E&C	n/a
94000.03p	mcplib03	2002	3341	102	100	B-IV/89	B-IV	E&C	BM&M
94000.04p	mcplib04	2002	10451	1287	100	B-VI.8	B-VI.8	B-VI.8	BM&M
Z = 95 ***** Americium *****									
95000.04p	mcplib04	2002	10640	1302	100	B-VI.8	B-VI.8	B-VI.8	BM&M
Z = 96 ***** Curium *****									
96000.04p	mcplib04	2002	10421	1249	100	B-VI.8	B-VI.8	B-VI.8	BM&M
Z = 97 ***** Berkelium *****									
97000.04p	mcplib04	2002	10478	1275	100	B-VI.8	B-VI.8	B-VI.8	BM&M
Z = 98 ***** Californium *****									
98000.04p	mcplib04	2002	10634	1301	100	B-VI.8	B-VI.8	B-VI.8	BM&M

Table G.4 (Cont.)
Continuous-Energy Photoatomic Data Libraries Maintained by X-5

<u>ZAID</u>	<u>Library Name</u>	<u>Release Date</u>	<u>Length Words</u>	<u>NE</u>	<u>E_{max} (GeV)</u>	<u>CS Source</u>	<u>FF Source</u>	<u>Fluor. Source</u>	<u>CDBD Source</u>
Z = 99	***** Einsteinium *****								
99000.04p	mcplib04	2002	11126	1383	100	B-VI.8	B-VI.8	B-VI.8	BM&M
Z = 100	***** Fermium *****								
100000.04p	mcplib04	2002	10916	1348	100	B-VI.8	B-VI.8	B-VI.8	BM&M

VI. PHOTONUCLEAR DATA

LA150U is the only photonuclear data library supported by X-5. It is derived from work done at Los Alamos National Laboratory in the Nuclear Physics Group (LANL/T-16).

The entries in each of the columns of Table G .5 are described as follows:

ZAID	The nuclide identification number with the form ZZZAAA.nnX where ZZZ is the atomic number AAA is the mass number (000 for elements). nn is the unique table identification number. X=U for continuous-energy photonuclear tables.
Atomic Weight Ratio	The atomic weight ratio (AWR) is the ratio of the atomic mass of the nuclide to a neutron, as contained in the original evaluation and used in the NJOY processing of the evaluation.
Library	Name of the library that contains the data file for that ZAID.
Evaluation Date	The date the evaluation was officially released.
Source	The source from which the evaluated data was obtained. The abbreviation LANL/T-16 indicates that the data were produced by the Nuclear Physics Group (T-16) at Los Alamos National Laboratory.
Length	The total length of a particular photonuclear table in words.
Number of Energies	The number of energy points (NE) on the grid used for the photonuclear cross sections for that data table. In general, a finer energy grid with a greater number of points provides a more accurate representation of the cross sections.
E_{max}	The maximum incident photon energy in MeV for that data table. For all incident energies greater than E_{max} , MCNP assumes the last cross section value given.
CP	“yes” indicates that secondary charged-particles data are present; “no” indicates that such data are not present.

Table G.5
Continuous-Energy Photonuclear Data Libraries Maintained by X-5

<u>ZAID</u>	<u>AWR</u>	<u>Library Name</u>	<u>Eval. Date</u>	<u>Source</u>	<u>Length (words)</u>	<u>NE</u>	<u>E_{max} (MeV)</u>	<u>CP</u>
Z = 1 ***** Hydrogen *****								
** H-2 **								
1002.24u	1.9963	la150u	2001	LANL/T-16	3686	35	30	No
Z = 6 ***** Carbon *****								
** C-12 **								
6012.24u	11.89691	la150u	1999	LANL/T-16	50395	98	150	Yes
Z = 8 ***** Oxygen *****								
** O-16 **								
8016.24u	15.85316	la150u	1999	LANL/T-16	72930	95	150	Yes
Z = 13 ***** Aluminum *****								
** Al-27 **								
13027.24u	26.74975	la150u	1999	LANL/T-16	68599	52	150	Yes
Z = 14 ***** Silicon *****								
** Si-28 **								
14028.24u	27.737	la150u	1999	LANL/T-16	70693	60	150	Yes
Z = 20 ***** Calcium *****								
** Ca-40 **								
20040.24u	39.736	la150u	1998	LANL/T-16	67051	54	150	Yes
Z = 26 ***** Iron *****								
** Fe-56 **								
26056.24u	55.454	la150u	1998	LANL/T-16	64043	50	150	Yes
Z = 29 ***** Copper *****								
** Cu-63 **								
29063.24u	62.389	la150u	1999	LANL/T-16	73548	57	150	Yes
Z = 73 ***** Tantalum *****								
** Ta-181 **								
73181.24u	179.4	la150u	1999	LANL/T-16	85094	50	150	Yes
Z = 74 ***** Tungsten *****								
** W-184 **								
74184.24u	182.3707	la150u	1998	LANL/T-16	78439	51	150	Yes
Z = 82 ***** Lead *****								
** Pb-206 **								
82206.24u	204.2	la150u	1998	LANL/T-16	78186	49	150	Yes
** Pb-207 **								
82207.24u	205.2	la150u	1998	LANL/T-16	78259	52	150	Yes
** Pb-208 **								
82208.24u	206.19	la150u	1998	LANL/T-16	77099	51	150	Yes

VII. DOSIMETRY DATA

The tally multiplier (FM) feature in MCNP allows users to calculate quantities of the form: $C \int \phi(E) R(E) dE$, where C is a constant, $\phi(E)$ is the fluence (n/cm^2), and $R(E)$ is a response function. If $R(E)$ is a cross section, and with the appropriate choice of units for C [atom/b-cm], the quantity calculated becomes the total number of some type of reaction per unit volume. If the tally is made over a finite time interval, it becomes a reaction rate per unit volume. In addition to using the standard reaction cross-section information available in our neutron transport libraries, dosimetry or activation reaction data can also be used as a response function. Often only dosimetry data is available for rare nuclides.

A full description of the use of dosimetry data can be found in Reference 34. This memorandum also gives a listing of all reaction data that is available for each Z Aid. There have been no major revisions of the LLNL/ACTL data since LLLDOS was produced. Users need to remember that dosimetry data libraries are appropriate only when used as a source of $R(E)$ for FM tally multipliers. Dosimetry data libraries cannot be used as a source of data for materials through which actual transport is required. Table G .6 lists the available dosimetry data libraries for use with MCNP, the evaluation source and date, and the length of the data in words.

Table G .6
Dosimetry Data Libraries for MCNP Tallies

<u>Z AID</u>	<u>AWR</u>	<u>Library</u>	<u>Source</u>	<u>Date</u>	<u>Length</u>
Z = 1 ***** Hydrogen *****					
1001.30y	1.00782	llldos	LLNL/ACTL	<1983	209
1002.30y	2.01410	llldos	LLNL/ACTL	<1983	149
1003.30y	3.01605	llldos	LLNL/ACTL	<1983	27
Z = 2 ***** Helium *****					
2003.30y	3.01603	llldos	LLNL/ACTL	<1983	267
Z = 3 ***** Lithium *****					
3006.24y	5.96340	531dos	ENDF/B-V	1978	735
3006.26y	5.96340	532dos	ENDF/B-V	1977	713
3006.30y	6.01512	llldos	LLNL/ACTL	<1983	931
3007.26y	6.95570	532dos	ENDF/B-V	1972	733
3007.30y	7.01601	llldos	LLNL/ACTL	<1983	201
Z = 4 ***** Beryllium *****					
4007.30y	7.01693	llldos	LLNL/ACTL	<1983	253
4009.30y	9.01218	llldos	LLNL/ACTL	<1983	335
Z = 5 ***** Boron *****					
5010.24y	9.92690	531dos	ENDF/B-V	1979	769
5010.26y	9.92690	532dos	ENDF/B-V	1976	589
5010.30y	10.01290	llldos	LLNL/ACTL	<1983	381
5011.30y	11.00930	llldos	LLNL/ACTL	<1983	119

Table G.6 (Cont.)
Dosimetry Data Libraries for MCNP Tallies

<u>ZAID</u>	<u>AWR</u>	<u>Library</u>	<u>Source</u>	<u>Date</u>	<u>Length</u>
Z = 6 ***** Carbon *****					
6012.30y	12.00000	llldos	LLNL/ACTL	<1983	97
6013.30y	13.00340	llldos	LLNL/ACTL	<1983	479
6014.30y	14.00320	llldos	LLNL/ACTL	<1983	63
Z = 7 ***** Nitrogen *****					
7014.26y	13.88300	532dos	ENDF/B-V	1973	1013
7014.30y	14.00310	llldos	LLNL/ACTL	<1983	915
Z = 8 ***** Oxygen *****					
8016.26y	15.85800	532dos	ENDF/B-V	1973	95
8016.30y	15.99490	llldos	LLNL/ACTL	<1983	215
8017.30y	16.99910	llldos	LLNL/ACTL	<1983	239
Z = 9 ***** Fluorine *****					
9019.26y	18.83500	532dos	ENDF/B-V	1979	31
9019.30y	18.99840	llldos	LLNL/ACTL	<1983	517
Z = 11 ***** Sodium *****					
11023.30y	22.98980	llldos	LLNL/ACTL	<1983	621
Z = 12 ***** Magnesium *****					
12023.30y	22.99410	llldos	LLNL/ACTL	<1983	333
12024.26y	23.98500	532dos	ENDF/B-V	1979	165
12024.30y	23.98500	llldos	LLNL/ACTL	<1983	309
12025.30y	24.98580	llldos	LLNL/ACTL	<1983	309
12026.30y	25.98260	llldos	LLNL/ACTL	<1983	321
12027.30y	26.98430	llldos	LLNL/ACTL	<1983	309
Z = 13 ***** Aluminum *****					
13026.30y	25.98690	llldos	LLNL/ACTL	<1983	447
13027.24y	26.75000	531dos	ENDF/B-V	1973	1165
13027.26y	26.75000	532dos	ENDF/B-V	1973	1753
13027.30y	26.98150	llldos	LLNL/ACTL	<1983	491
Z = 14 ***** Silicon *****					
14027.30y	26.98670	llldos	LLNL/ACTL	<1983	401
14028.30y	27.97690	llldos	LLNL/ACTL	<1983	377
14029.30y	28.97650	llldos	LLNL/ACTL	<1983	389
14030.30y	29.97380	llldos	LLNL/ACTL	<1983	395
14031.30y	30.97540	llldos	LLNL/ACTL	<1983	337

Table G.6 (Cont.)
Dosimetry Data Libraries for MCNP Tallies

<u>ZAID</u>	<u>AWR</u>	<u>Library</u>	<u>Source</u>	<u>Date</u>	<u>Length</u>
Z = 15 ***** Phosphorus *****					
15031.26y	30.70800	532dos	ENDF/B-V	1977	65
15031.30y	30.97380	llldos	LLNL/ACTL	<1983	263
Z = 16 ***** Sulfur *****					
16031.30y	30.97960	llldos	LLNL/ACTL	<1983	393
16032.24y	31.69740	531dos	ENDF/B-V	1979	145
16032.26y	31.69700	532dos	ENDF/B-V	1977	35
16032.30y	31.97210	llldos	LLNL/ACTL	<1983	417
16033.30y	32.97150	llldos	LLNL/ACTL	<1983	435
16034.30y	33.96790	llldos	LLNL/ACTL	<1983	437
16035.30y	34.96900	llldos	LLNL/ACTL	<1983	339
16036.30y	35.96710	llldos	LLNL/ACTL	<1983	293
16037.30y	36.97110	llldos	LLNL/ACTL	<1983	279
Z = 17 ***** Chlorine *****					
17034.30y	33.97380	llldos	LLNL/ACTL	<1983	401
17035.30y	34.96890	llldos	LLNL/ACTL	<1983	459
17036.30y	35.96830	llldos	LLNL/ACTL	<1983	563
17037.30y	36.96590	llldos	LLNL/ACTL	<1983	407
7038.30y	37.96800	llldos	LLNL/ACTL	<1983	33
Z = 18 ***** Argon *****					
18036.30y	35.96750	llldos	LLNL/ACTL	<1983	309
18037.30y	36.96680	llldos	LLNL/ACTL	<1983	311
18038.30y	37.96270	llldos	LLNL/ACTL	<1983	311
18039.30y	38.96430	llldos	LLNL/ACTL	<1983	337
18040.26y	39.61910	532dos	ENDF/B-V	1979	3861
18040.30y	39.96240	llldos	LLNL/ACTL	<1983	347
18041.30y	40.96450	llldos	LLNL/ACTL	<1983	317
18042.30y	41.96300	llldos	LLNL/ACTL	<1983	291
18043.30y	42.96570	llldos	LLNL/ACTL	<1983	295
Z = 19 ***** Potassium *****					
19038.30y	37.96910	llldos	LLNL/ACTL	<1983	603
19039.30y	38.96370	llldos	LLNL/ACTL	<1983	405
19040.30y	39.96400	llldos	LLNL/ACTL	<1983	675
19041.26y	40.60990	532dos	ENDF/B-V	1979	33
19041.30y	40.96180	llldos	LLNL/ACTL	<1983	369
19042.30y	41.96240	llldos	LLNL/ACTL	<1983	343
19043.30y	42.96070	llldos	LLNL/ACTL	<1983	277
19044.30y	43.96160	llldos	LLNL/ACTL	<1983	275
19045.30y	44.96070	llldos	LLNL/ACTL	<1983	283
19046.30y	45.96200	llldos	LLNL/ACTL	<1983	283

Table G.6 (Cont.)
Dosimetry Data Libraries for MCNP Tallies

<u>ZAID</u>	<u>AWR</u>	<u>Library</u>	<u>Source</u>	<u>Date</u>	<u>Length</u>
Z = 20 ***** Calcium *****					
20039.30y	38.97070	llldos	LLNL/ACTL	<1983	601
20040.30y	39.96260	llldos	LLNL/ACTL	<1983	309
20041.30y	40.96230	llldos	LLNL/ACTL	<1983	313
20042.30y	41.95860	llldos	LLNL/ACTL	<1983	285
20043.30y	42.95880	llldos	LLNL/ACTL	<1983	295
20044.30y	43.95550	llldos	LLNL/ACTL	<1983	269
20045.30y	44.95620	llldos	LLNL/ACTL	<1983	271
20046.30y	45.95370	llldos	LLNL/ACTL	<1983	255
20047.30y	46.95450	llldos	LLNL/ACTL	<1983	243
20048.30y	47.95250	llldos	LLNL/ACTL	<1983	239
20049.30y	48.95570	llldos	LLNL/ACTL	<1983	229
Z = 21 ***** Scandium *****					
21044.30y	43.95940	llldos	LLNL/ACTL	<1983	313
21044.31y	43.95940	llldos	LLNL/ACTL	<1983	311
21045.24y	44.56790	531dos	ENDF/B-V	1979	20179
21045.26y	44.56790	532dos	ENDF/B-V	1979	20211
21045.30y	44.95590	llldos	LLNL/ACTL	<1983	547
21046.30y	45.95520	llldos	LLNL/ACTL	<1983	323
21046.31y	45.95520	llldos	LLNL/ACTL	<1983	323
21047.30y	46.95240	llldos	LLNL/ACTL	<1983	331
21048.30y	47.95220	llldos	LLNL/ACTL	<1983	325
Z = 22 ***** Titanium *****					
22045.30y	44.95810	llldos	LLNL/ACTL	<1983	449
22046.24y	45.55780	531dos	ENDF/B-V	1977	53
22046.26y	45.55780	532dos	ENDF/B-V	1977	53
22046.30y	45.95260	llldos	LLNL/ACTL	<1983	391
22047.24y	46.54800	531dos	ENDF/B-V	1977	209
22047.26y	46.54800	532dos	ENDF/B-V	1977	209
22047.30y	46.95180	llldos	LLNL/ACTL	<1983	419
22048.24y	47.53600	531dos	ENDF/B-V	1977	145
22048.26y	47.53600	532dos	ENDF/B-V	1977	177
22048.30y	47.94790	llldos	LLNL/ACTL	<1983	415
22049.30y	48.94790	llldos	LLNL/ACTL	<1983	409
22050.26y	49.57000	532dos	ENDF/B-V	1979	33
22050.30y	49.94480	llldos	LLNL/ACTL	<1983	345
22051.30y	50.94660	llldos	LLNL/ACTL	<1983	389
Z = 23 ***** Vanadium *****					
23047.30y	46.95490	llldos	LLNL/ACTL	<1983	209
23048.30y	47.95230	llldos	LLNL/ACTL	<1983	399
23049.30y	48.94850	llldos	LLNL/ACTL	<1983	423
23050.30y	49.94720	llldos	LLNL/ACTL	<1983	407
23051.30y	50.94400	llldos	LLNL/ACTL	<1983	357
23052.30y	51.94480	llldos	LLNL/ACTL	<1983	401

Table G.6 (Cont.)
Dosimetry Data Libraries for MCNP Tallies

<u>ZAID</u>	<u>AWR</u>	<u>Library</u>	<u>Source</u>	<u>Date</u>	<u>Length</u>
Z = 24 ***** Chromium *****					
24049.30y	48.95130	llldos	LLNL/ACTL	<1983	377
24050.26y	49.51650	532dos	ENDF/B-V	1979	7405
24050.30y	49.94600	llldos	LLNL/ACTL	<1983	435
24051.30y	50.94480	llldos	LLNL/ACTL	<1983	377
24052.26y	51.49380	532dos	ENDF/B-V	1979	27
24052.30y	51.94050	llldos	LLNL/ACTL	<1983	417
24053.30y	52.94060	llldos	LLNL/ACTL	<1983	425
24054.30y	53.93890	llldos	LLNL/ACTL	<1983	461
24055.30y	54.94080	llldos	LLNL/ACTL	<1983	419
24056.30y	55.94070	llldos	LLNL/ACTL	<1983	297
Z = 25 ***** Manganese *****					
25051.30y	50.94820	llldos	LLNL/ACTL	<1983	417
25052.30y	51.94560	llldos	LLNL/ACTL	<1983	379
25053.30y	52.94130	llldos	LLNL/ACTL	<1983	425
25054.30y	53.94040	llldos	LLNL/ACTL	<1983	391
25055.24y	54.46610	531dos	ENDF/B-V	1977	119
25055.30y	54.93800	llldos	LLNL/ACTL	<1983	435
25056.30y	55.93890	llldos	LLNL/ACTL	<1983	423
25057.30y	56.93830	llldos	LLNL/ACTL	<1983	419
25058.30y	57.93970	llldos	LLNL/ACTL	<1983	285
Z = 26 ***** Iron *****					
26053.30y	52.94530	llldos	LLNL/ACTL	<1983	387
26054.24y	53.47620	531dos	ENDF/B-V	1979	517
26054.26y	53.47600	532dos	ENDF/B-V	1978	21563
26054.30y	53.93960	llldos	LLNL/ACTL	<1983	457
26055.30y	54.93830	llldos	LLNL/ACTL	<1983	373
26056.24y	55.45400	531dos	ENDF/B-V	1978	449
26056.26y	55.45400	532dos	ENDF/B-V	1978	581
26056.30y	55.93490	llldos	LLNL/ACTL	<1983	415
26057.30y	56.93540	llldos	LLNL/ACTL	<1983	447
26058.24y	57.43560	531dos	ENDF/B-V	1979	7077
26058.26y	57.43560	532dos	ENDF/B-V	1979	7097
26058.30y	57.93330	llldos	LLNL/ACTL	<1983	431
26059.30y	58.93490	llldos	LLNL/ACTL	<1983	397
26060.30y	59.93400	llldos	LLNL/ACTL	<1983	285
Z = 27 ***** Cobalt *****					
27057.30y	56.93630	llldos	LLNL/ACTL	<1983	629
27058.30y	57.93580	llldos	LLNL/ACTL	<1983	531
27058.31y	57.93580	llldos	LLNL/ACTL	<1983	569
27059.30y	58.93320	llldos	LLNL/ACTL	<1983	657
27060.30y	59.93380	llldos	LLNL/ACTL	<1983	435
27060.31y	59.93380	llldos	LLNL/ACTL	<1983	499
27061.30y	60.93250	llldos	LLNL/ACTL	<1983	613
27062.30y	61.93400	llldos	LLNL/ACTL	<1983	463
27062.31y	61.93400	llldos	LLNL/ACTL	<1983	519
27063.30y	62.93360	llldos	LLNL/ACTL	<1983	339

Table G.6 (Cont.)
Dosimetry Data Libraries for MCNP Tallies

<u>ZAID</u>	<u>AWR</u>	<u>Library</u>	<u>Source</u>	<u>Date</u>	<u>Length</u>
27064.30y	63.93580	llldos	LLNL/ACTL	<1983	323
Z = 28 ***** Nickel *****					
28057.30y	56.93980	llldos	LLNL/ACTL	<1983	441
28058.24y	57.43760	531dos	ENDF/B-V	1977	411
28058.26y	57.43760	532dos	ENDF/B-V	1978	4079
28058.30y	57.93530	llldos	LLNL/ACTL	<1983	509
28059.30y	58.93430	llldos	LLNL/ACTL	<1983	513
28060.24y	59.41590	531dos	ENDF/B-V	1977	435
28060.26y	59.41590	532dos	ENDF/B-V	1978	479
28060.30y	59.93080	llldos	LLNL/ACTL	<1983	503
28061.30y	60.93110	llldos	LLNL/ACTL	<1983	489
28062.26y	61.39630	532dos	ENDF/B-V	1978	3847
8062.30y	61.92830	llldos	LLNL/ACTL	<1983	459
28063.30y	62.92970	llldos	LLNL/ACTL	<1983	375
28064.30y	63.92800	llldos	LLNL/ACTL	<1983	397
28065.30y	64.93010	llldos	LLNL/ACTL	<1983	345
Z = 29 ***** Copper *****					
29062.30y	61.93260	llldos	LLNL/ACTL	<1983	507
29063.24y	62.93000	531dos	ENDF/B-V	1978	3375
29063.26y	62.93000	532dos	ENDF/B-V	1978	3615
29063.30y	62.92960	llldos	LLNL/ACTL	<1983	513
29064.30y	63.92980	llldos	LLNL/ACTL	<1983	437
29065.24y	64.92800	531dos	ENDF/B-V	1978	49
29065.26y	64.92800	532dos	ENDF/B-V	1978	49
29065.30y	64.92780	llldos	LLNL/ACTL	<1983	563
29066.30y	65.92890	llldos	LLNL/ACTL	<1983	397
Z = 30 ***** Zinc *****					
30064.30y	63.92910	llldos	LLNL/ACTL	<1983	555
30066.30y	65.92600	llldos	LLNL/ACTL	<1983	561
30067.30y	66.92710	llldos	LLNL/ACTL	<1983	411
30068.30y	67.92480	llldos	LLNL/ACTL	<1983	643
30070.30y	69.92530	llldos	LLNL/ACTL	<1983	619
Z = 31 ***** Gallium *****					
31069.30y	68.92560	llldos	LLNL/ACTL	<1983	197
31071.30y	70.92470	llldos	LLNL/ACTL	<1983	419
Z = 32 ***** Germanium *****					
32070.30y	69.92420	llldos	LLNL/ACTL	<1983	405
32072.30y	71.92210	llldos	LLNL/ACTL	<1983	423
32073.30y	72.92350	llldos	LLNL/ACTL	<1983	431
32074.30y	73.92120	llldos	LLNL/ACTL	<1983	629
32076.30y	75.92140	llldos	LLNL/ACTL	<1983	623

Table G.6 (Cont.)
Dosimetry Data Libraries for MCNP Tallies

<u>ZAID</u>	<u>AWR</u>	<u>Library</u>	<u>Source</u>	<u>Date</u>	<u>Length</u>
Z = 33 ***** Arsenic *****					
33075.30y	74.92160	lldos	LLNL/ACTL	<1983	987
Z = 34 ***** Selenium *****					
34074.30y	73.92250	lldos	LLNL/ACTL	<1983	159
34076.30y	75.91920	lldos	LLNL/ACTL	<1983	177
34080.30y	79.91650	lldos	LLNL/ACTL	<1983	205
34082.30y	81.91670	lldos	LLNL/ACTL	<1983	223
Z = 35 ***** Bromine *****					
35079.30y	78.91830	lldos	LLNL/ACTL	<1983	263
35081.30y	80.91630	lldos	LLNL/ACTL	<1983	695
Z = 37 ***** Rubidium *****					
37085.30y	84.91180	lldos	LLNL/ACTL	<1983	193
37087.30y	86.90920	lldos	LLNL/ACTL	<1983	199
Z = 38 ***** Strontium *****					
38084.30y	83.91340	lldos	LLNL/ACTL	<1983	163
38086.30y	85.90930	lldos	LLNL/ACTL	<1983	33
Z = 39 ***** Yttrium *****					
39089.30y	88.90590	lldos	LLNL/ACTL	<1983	419
Z = 40 ***** Zirconium *****					
40089.30y	88.90890	lldos	LLNL/ACTL	<1983	321
40090.26y	89.13200	532dos	ENDF/B-V	1976	37
40090.30y	89.90470	lldos	LLNL/ACTL	<1983	385
40091.30y	90.90560	lldos	LLNL/ACTL	<1983	407
40092.26y	91.11200	532dos	ENDF/B-V	1976	3821
40092.30y	91.90500	lldos	LLNL/ACTL	<1983	431
40093.30y	92.90650	lldos	LLNL/ACTL	<1983	371
40094.26y	93.09600	532dos	ENDF/B-V	1976	5255
40094.30y	93.90630	lldos	LLNL/ACTL	<1983	417
40095.30y	94.90800	lldos	LLNL/ACTL	<1983	375
40096.30y	95.90830	lldos	LLNL/ACTL	<1983	57
40097.30y	96.91090	lldos	LLNL/ACTL	<1983	339
Z = 41 ***** Niobium *****					
41091.30y	90.90700	lldos	LLNL/ACTL	<1983	491
41091.31y	90.90700	lldos	LLNL/ACTL	<1983	491
41092.30y	91.90720	lldos	LLNL/ACTL	<1983	285
41092.31y	91.90720	lldos	LLNL/ACTL	<1983	285
41093.30y	92.90640	lldos	LLNL/ACTL	<1983	493
41094.30y	93.90730	lldos	LLNL/ACTL	<1983	331
41095.30y	94.90680	lldos	LLNL/ACTL	<1983	333

Table G.6 (Cont.)
Dosimetry Data Libraries for MCNP Tallies

<u>ZAID</u>	<u>AWR</u>	<u>Library</u>	<u>Source</u>	<u>Date</u>	<u>Length</u>
41096.30y	95.90810	llldos	LLNL/ACTL	<1983	335
41097.30y	96.90810	llldos	LLNL/ACTL	<1983	339
41098.30y	97.91030	llldos	LLNL/ACTL	<1983	341
41100.30y	99.91420	llldos	LLNL/ACTL	<1983	349
Z = 42 ***** Molybdenum *****					
42090.30y	89.91390	llldos	LLNL/ACTL	<1983	261
42091.30y	90.91180	llldos	LLNL/ACTL	<1983	281
42092.26y	91.21000	532dos	ENDF/B-V	1980	7815
42092.30y	91.90680	llldos	LLNL/ACTL	<1983	537
42093.30y	92.90680	llldos	LLNL/ACTL	<1983	429
42093.31y	92.90680	llldos	LLNL/ACTL	<1983	461
42094.30y	93.90510	llldos	LLNL/ACTL	<1983	443
42095.30y	94.90580	llldos	LLNL/ACTL	<1983	523
42096.30y	95.90470	llldos	LLNL/ACTL	<1983	501
42097.30y	96.90600	llldos	LLNL/ACTL	<1983	427
42098.26y	97.06440	532dos	ENDF/B-V	1980	6489
42098.30y	97.90540	llldos	LLNL/ACTL	<1983	421
42099.30y	98.90770	llldos	LLNL/ACTL	<1983	445
42100.26y	99.04920	532dos	ENDF/B-V	1980	4971
42100.30y	99.90750	llldos	LLNL/ACTL	<1983	427
42101.30y	100.91000	llldos	LLNL/ACTL	<1983	447
Z = 43 ***** Technetium *****					
43099.30y	98.90620	llldos	LLNL/ACTL	<1983	469
43099.31y	98.90620	llldos	LLNL/ACTL	<1983	469
Z = 45 ***** Rhodium *****					
45103.30y	102.90600	llldos	LLNL/ACTL	<1983	275
Z = 46 ***** Palladium *****					
46110.30y	109.90500	llldos	LLNL/ACTL	<1983	417
Z = 47 ***** Silver *****					
47106.30y	105.90700	llldos	LLNL/ACTL	<1983	263
47106.31y	105.90700	llldos	LLNL/ACTL	<1983	265
47107.30y	106.90500	llldos	LLNL/ACTL	<1983	517
47108.30y	107.90600	llldos	LLNL/ACTL	<1983	275
47108.31y	107.90600	llldos	LLNL/ACTL	<1983	275
47109.30y	108.90500	llldos	LLNL/ACTL	<1983	583
47110.30y	109.90600	llldos	LLNL/ACTL	<1983	277
47110.31y	109.90600	llldos	LLNL/ACTL	<1983	281
Z = 48 ***** Cadmium *****					
48106.30y	105.90600	llldos	LLNL/ACTL	<1983	177
48111.30y	110.90400	llldos	LLNL/ACTL	<1983	317
48112.30y	111.90300	llldos	LLNL/ACTL	<1983	221
48116.30y	115.90500	llldos	LLNL/ACTL	<1983	231

Table G.6 (Cont.)
Dosimetry Data Libraries for MCNP Tallies

<u>ZAID</u>	<u>AWR</u>	<u>Library</u>	<u>Source</u>	<u>Date</u>	<u>Length</u>
Z = 49 ***** Indium *****					
49113.30y	112.90400	llldos	LLNL/ACTL	<1983	861
49115.24y	113.92000	531dos	ENDF/B-V	1978	26009
49115.26y	113.92000	532dos	ENDF/B-V	1978	26009
49115.30y	114.90400	llldos	LLNL/ACTL	<1983	1265
Z = 50 ***** Tin *****					
50112.30y	111.90500	llldos	LLNL/ACTL	<1983	789
50114.30y	113.90300	llldos	LLNL/ACTL	<1983	435
50115.30y	114.90300	llldos	LLNL/ACTL	<1983	389
50116.30y	115.90200	llldos	LLNL/ACTL	<1983	603
50117.30y	116.90300	llldos	LLNL/ACTL	<1983	313
50118.30y	117.90200	llldos	LLNL/ACTL	<1983	745
50119.30y	118.90300	llldos	LLNL/ACTL	<1983	311
50120.26y	118.87200	532dos	ENDF/B-V	1974	12881
50120.30y	119.90200	llldos	LLNL/ACTL	<1983	309
50122.26y	120.85600	532dos	ENDF/B-V	1974	1891
50122.30y	121.90300	llldos	LLNL/ACTL	<1983	275
50124.26y	122.84100	532dos	ENDF/B-V	1974	1693
50124.30y	123.90500	llldos	LLNL/ACTL	<1983	485
Z = 51 ***** Antimony *****					
51121.30y	120.90400	llldos	LLNL/ACTL	<1983	811
51123.30y	122.90400	llldos	LLNL/ACTL	<1983	1013
Z = 53 ***** Iodine *****					
53127.24y	125.81400	531dos	ENDF/B-V	1972	115
53127.26y	125.81400	532dos	ENDF/B-V	1980	14145
53127.30y	126.90400	llldos	LLNL/ACTL	<1983	221
Z = 55 ***** Cesium *****					
55133.30y	132.90500	llldos	LLNL/ACTL	<1983	215
Z = 57 ***** Lanthanum *****					
57139.26y	137.71300	532dos	ENDF/B-V	1980	15475
Z = 58 ***** Cerium *****					
58140.30y	139.90500	llldos	LLNL/ACTL	<1983	427
58142.30y	141.90900	llldos	LLNL/ACTL	<1983	265
Z = 59 ***** Praseodymium *****					
59141.30y	140.90800	llldos	LLNL/ACTL	<1983	215

Table G.6 (Cont.)
Dosimetry Data Libraries for MCNP Tallies

<u>ZAID</u>	<u>AWR</u>	<u>Library</u>	<u>Source</u>	<u>Date</u>	<u>Length</u>
Z = 60 ***** Neodymium *****					
60142.30y	141.90800	lldos	LLNL/ACTL	<1983	207
60148.30y	147.91700	lldos	LLNL/ACTL	<1983	255
60150.30y	149.92100	lldos	LLNL/ACTL	<1983	259
Z = 62 ***** Samarium *****					
62144.30y	143.91200	lldos	LLNL/ACTL	<1983	189
62148.30y	147.91500	lldos	LLNL/ACTL	<1983	245
62152.30y	151.92000	lldos	LLNL/ACTL	<1983	237
62154.30y	153.92200	lldos	LLNL/ACTL	<1983	247
Z = 63 ***** Europium *****					
63151.30y	150.92000	lldos	LLNL/ACTL	<1983	731
63153.30y	152.92100	lldos	LLNL/ACTL	<1983	565
Z = 64 ***** Gadolinium *****					
64150.30y	149.91900	lldos	LLNL/ACTL	<1983	237
64151.30y	150.92000	lldos	LLNL/ACTL	<1983	241
Z = 66 ***** Dysprosium *****					
66164.26y	162.52000	532dos	ENDF/B-V	1967	581
Z = 67 ***** Holmium *****					
67163.30y	162.92900	lldos	LLNL/ACTL	<1983	533
67164.30y	163.93000	lldos	LLNL/ACTL	<1983	327
67164.31y	163.93000	lldos	LLNL/ACTL	<1983	327
67165.30y	164.93000	lldos	LLNL/ACTL	<1983	589
67166.30y	165.93200	lldos	LLNL/ACTL	<1983	333
67166.31y	165.93200	lldos	LLNL/ACTL	<1983	333
Z = 69 ***** Thulium *****					
69169.30y	168.93400	lldos	LLNL/ACTL	<1983	453
Z = 71 ***** Lutetium *****					
71173.30y	172.93900	lldos	LLNL/ACTL	<1983	587
71174.30y	173.94000	lldos	LLNL/ACTL	<1983	417
71174.31y	173.94000	lldos	LLNL/ACTL	<1983	465
71175.30y	174.94100	lldos	LLNL/ACTL	<1983	559
71176.30y	175.94300	lldos	LLNL/ACTL	<1983	621
71176.31y	175.94300	lldos	LLNL/ACTL	<1983	637
71177.30y	176.94400	lldos	LLNL/ACTL	<1983	573
71177.31y	176.94400	lldos	LLNL/ACTL	<1983	573

Table G.6 (Cont.)
Dosimetry Data Libraries for MCNP Tallies

<u>ZAID</u>	<u>AWR</u>	<u>Library</u>	<u>Source</u>	<u>Date</u>	<u>Length</u>
Z = 72 ***** Hafnium *****					
72174.30y	173.94000	llldos	LLNL/ACTL	<1983	147
72175.30y	174.94100	llldos	LLNL/ACTL	<1983	121
72176.30y	175.94100	llldos	LLNL/ACTL	<1983	153
72177.30y	176.94300	llldos	LLNL/ACTL	<1983	157
72178.30y	177.94400	llldos	LLNL/ACTL	<1983	153
72179.30y	178.94600	llldos	LLNL/ACTL	<1983	433
72180.30y	179.94700	llldos	LLNL/ACTL	<1983	409
72181.30y	180.94900	llldos	LLNL/ACTL	<1983	365
72183.30y	182.95400	llldos	LLNL/ACTL	<1983	373
Z = 73 ***** Tantalum *****					
73179.30y	178.94600	llldos	LLNL/ACTL	<1983	629
73180.30y	179.94700	llldos	LLNL/ACTL	<1983	523
73180.31y	179.94700	llldos	LLNL/ACTL	<1983	435
73181.30y	180.94800	llldos	LLNL/ACTL	<1983	715
73182.30y	181.95000	llldos	LLNL/ACTL	<1983	435
73182.31y	181.95000	llldos	LLNL/ACTL	<1983	447
73183.30y	182.95100	llldos	LLNL/ACTL	<1983	425
73184.30y	183.95400	llldos	LLNL/ACTL	<1983	371
73186.30y	185.95900	llldos	LLNL/ACTL	<1983	377
Z = 74 ***** Tungsten *****					
74179.30y	178.94700	llldos	LLNL/ACTL	<1983	263
74180.30y	179.94700	llldos	LLNL/ACTL	<1983	397
74181.30y	180.94800	llldos	LLNL/ACTL	<1983	263
74182.30y	181.94800	llldos	LLNL/ACTL	<1983	415
74183.30y	182.95000	llldos	LLNL/ACTL	<1983	499
74184.30y	183.95100	llldos	LLNL/ACTL	<1983	443
74185.30y	184.95300	llldos	LLNL/ACTL	<1983	267
74186.30y	185.95400	llldos	LLNL/ACTL	<1983	413
74187.30y	186.95700	llldos	LLNL/ACTL	<1983	279
74188.30y	187.95800	llldos	LLNL/ACTL	<1983	271
Z = 75 ***** Rhenium *****					
75184.30y	183.95300	llldos	LLNL/ACTL	<1983	331
75184.31y	183.95300	llldos	LLNL/ACTL	<1983	335
75185.30y	184.95300	llldos	LLNL/ACTL	<1983	373
75186.30y	185.95500	llldos	LLNL/ACTL	<1983	381
75187.30y	186.95600	llldos	LLNL/ACTL	<1983	547
75188.30y	187.95800	llldos	LLNL/ACTL	<1983	339
75188.31y	187.95800	llldos	LLNL/ACTL	<1983	341
Z = 77 ***** Iridium *****					
77191.30y	190.96100	llldos	LLNL/ACTL	<1983	237
77193.30y	192.96300	llldos	LLNL/ACTL	<1983	243
77194.30y	193.96500	llldos	LLNL/ACTL	<1983	421

Table G.6 (Cont.)
Dosimetry Data Libraries for MCNP Tallies

<u>ZAID</u>	<u>AWR</u>	<u>Library</u>	<u>Source</u>	<u>Date</u>	<u>Length</u>
Z = 78 ***** Platinum *****					
78190.30y	189.96000	lldos	LLNL/ACTL	<1983	151
78192.30y	191.96100	lldos	LLNL/ACTL	<1983	153
78193.30y	192.96300	lldos	LLNL/ACTL	<1983	123
78193.31y	192.96300	lldos	LLNL/ACTL	<1983	123
78194.30y	193.96300	lldos	LLNL/ACTL	<1983	211
78195.30y	194.96500	lldos	LLNL/ACTL	<1983	157
78196.30y	195.96500	lldos	LLNL/ACTL	<1983	157
78197.30y	196.96700	lldos	LLNL/ACTL	<1983	427
78197.31y	196.96700	lldos	LLNL/ACTL	<1983	129
78198.30y	197.96800	lldos	LLNL/ACTL	<1983	183
78199.30y	198.97100	lldos	LLNL/ACTL	<1983	99
78199.31y	198.97100	lldos	LLNL/ACTL	<1983	99
Z = 79 ***** Gold *****					
79193.30y	192.96400	lldos	LLNL/ACTL	<1983	209
79194.30y	193.96500	lldos	LLNL/ACTL	<1983	261
79195.30y	194.96500	lldos	LLNL/ACTL	<1983	261
79196.30y	195.96700	lldos	LLNL/ACTL	<1983	265
79196.31y	195.96700	lldos	LLNL/ACTL	<1983	265
79197.30y	196.96700	lldos	LLNL/ACTL	<1983	307
79198.30y	197.96800	lldos	LLNL/ACTL	<1983	265
79199.30y	198.96900	lldos	LLNL/ACTL	<1983	269
79200.30y	199.97100	lldos	LLNL/ACTL	<1983	39
Z = 80 ***** Mercury *****					
80202.30y	201.97100	lldos	LLNL/ACTL	<1983	381
80203.30y	202.97300	lldos	LLNL/ACTL	<1983	379
80204.30y	203.97300	lldos	LLNL/ACTL	<1983	365
Z = 81 ***** Thallium *****					
81202.30y	201.97200	lldos	LLNL/ACTL	<1983	377
81203.30y	202.97200	lldos	LLNL/ACTL	<1983	375
81204.30y	203.97400	lldos	LLNL/ACTL	<1983	373
81205.30y	204.97400	lldos	LLNL/ACTL	<1983	369
Z = 82 ***** Lead *****					
82203.30y	202.97300	lldos	LLNL/ACTL	<1983	257
82204.30y	203.97300	lldos	LLNL/ACTL	<1983	405
82205.30y	204.97400	lldos	LLNL/ACTL	<1983	257
82206.30y	205.97400	lldos	LLNL/ACTL	<1983	347
82207.30y	206.97600	lldos	LLNL/ACTL	<1983	333
82208.30y	207.97700	lldos	LLNL/ACTL	<1983	263
82209.30y	208.98100	lldos	LLNL/ACTL	<1983	279
82210.30y	209.98400	lldos	LLNL/ACTL	<1983	351

Table G.6 (Cont.)
Dosimetry Data Libraries for MCNP Tallies

<u>ZAID</u>	<u>AWR</u>	<u>Library</u>	<u>Source</u>	<u>Date</u>	<u>Length</u>
Z = 83 ***** Bismuth *****					
83208.30y	207.98000	llldos	LLNL/ACTL	<1983	409
83209.30y	208.98000	llldos	LLNL/ACTL	<1983	551
83210.30y	209.98400	llldos	LLNL/ACTL	<1983	421
83210.31y	209.98400	llldos	LLNL/ACTL	<1983	421
Z = 84 ***** Polonium *****					
84210.30y	209.98300	llldos	LLNL/ACTL	<1983	441
Z = 90 ***** Thorium *****					
90230.30y	230.03300	llldos	LLNL/ACTL	<1983	209
90231.30y	231.03600	llldos	LLNL/ACTL	<1983	599
90232.30y	232.03800	llldos	LLNL/ACTL	<1983	347
90233.30y	233.04200	llldos	LLNL/ACTL	<1983	561
90234.30y	234.04400	llldos	LLNL/ACTL	<1983	37
Z = 91 ***** Protactinium *****					
91231.26y	229.05000	532dos	ENDF/B-V	1978	2861
91233.26y	231.03800	532dos	ENDF/B-V	1978	73
91233.30y	233.04000	llldos	LLNL/ACTL	<1983	361
Z = 92 ***** Uranium *****					
92233.26y	231.04300	532dos	ENDF/B-V	1978	75
92233.30y	233.04000	llldos	LLNL/ACTL	<1983	461
92234.30y	234.04100	llldos	LLNL/ACTL	<1983	393
92235.30y	235.04400	llldos	LLNL/ACTL	<1983	4629
92236.30y	236.04600	llldos	LLNL/ACTL	<1983	395
92237.30y	237.04900	llldos	LLNL/ACTL	<1983	609
92238.30y	238.05100	llldos	LLNL/ACTL	<1983	3103
92239.30y	239.05400	llldos	LLNL/ACTL	<1983	825
92240.30y	240.05700	llldos	LLNL/ACTL	<1983	389
Z = 93 ***** Neptunium *****					
93237.30y	237.04800	llldos	LLNL/ACTL	<1983	629
Z = 94 ***** Plutonium *****					
94237.30y	237.04800	llldos	LLNL/ACTL	<1983	487
94238.30y	238.05000	llldos	LLNL/ACTL	<1983	459
94239.30y	239.05200	llldos	LLNL/ACTL	<1983	497
94240.30y	240.05400	llldos	LLNL/ACTL	<1983	479
94241.30y	241.05700	llldos	LLNL/ACTL	<1983	559
94242.30y	242.05900	llldos	LLNL/ACTL	<1983	505
94243.30y	243.06200	llldos	LLNL/ACTL	<1983	511

Table G.6 (Cont.)
Dosimetry Data Libraries for MCNP Tallies

<u>ZAID</u>	<u>AWR</u>	<u>Library</u>	<u>Source</u>	<u>Date</u>	<u>Length</u>
Z = 95 ***** Americium *****					
95241.30y	241.05700	lldos	LLNL/ACTL	<1983	673
95242.30y	242.06000	lldos	LLNL/ACTL	<1983	473
95243.30y	243.06100	lldos	LLNL/ACTL	<1983	431
Z = 96 ***** Curium *****					
96242.30y	242.05900	lldos	LLNL/ACTL	<1983	467
96243.30y	243.06100	lldos	LLNL/ACTL	<1983	465
96244.30y	244.06300	lldos	LLNL/ACTL	<1983	483
96245.30y	245.06500	lldos	LLNL/ACTL	<1983	465
96246.30y	246.06700	lldos	LLNL/ACTL	<1983	491
96247.30y	247.07000	lldos	LLNL/ACTL	<1983	491
96248.30y	248.07200	lldos	LLNL/ACTL	<1983	495
Z = 97 ***** Berkelium *****					
97249.30y	249.07500	lldos	LLNL/ACTL	<1983	545
Z = 98 ***** Californium *****					
98249.30y	249.07500	lldos	LLNL/ACTL	<1983	491
98250.30y	250.07600	lldos	LLNL/ACTL	<1983	335
98251.30y	251.08000	lldos	LLNL/ACTL	<1983	485
98252.30y	252.08200	lldos	LLNL/ACTL	<1983	467

VIII. REFERENCES

1. V. McLane, C. L. Dunford, and P.F. Rose, ed., "ENDF-102: Data Formats and Procedures for the Evaluated Nuclear Data File ENDF-6," Brookhaven National Laboratory report, BNL-NCS-44945, revised (1995) (available URL: <http://www.nndc.bnl.gov/>).
2. S. C. Frankle and R. C. Little, "Cross-section and Reaction Nomenclature for MCNP Continuous-energy Libraries and DANTSYS Multigroup Libraries," Los Alamos National Laboratory internal memorandum, XTM:96-313 (July 15, 1996) (available URL: <http://www-xdiv.lanl.gov/PROJECTS/DATA/nuclear/pdf/scf-96-313.pdf>).
3. J. A. Halbleib, R. P. Kensek, G. D. Valdez, T. A. Mehlhorn, S. M. Seltzer and M. J. Berger, "ITS: The Integrated TIGER Series of Coupled Electron/Photon Monte Carlo Transport Codes Version 3.0," IEEE Transactions on Nuclear Science, Volume 39, pp. 1025–1030 (1992).
4. K. J. Adams, "Electron Upgrade for MCNP4B," Los Alamos National Laboratory internal memorandum, X-5-RN(U)-00-14 (May 25, 2000) (available URL: <http://www-xdiv.lanl.gov/PROJECTS/DATA/nuclear/pdf/X-5-RN-00-14.pdf>).
5. J. U. Koppel and D. H. Houston, "Reference Manual for ENDF Thermal Neutron Scattering Data," General Atomics report GA-8774 (also revised and reissued as ENDF-269 by the National Nuclear Data Center at the Brookhaven National Laboratory) (July 1978).
6. Robert E. MacFarlane, "Cold Moderator Scattering Kernals," *Advanced Neutron Sources 1988, Proceedings of the 10th Meeting of the International Collaboration on Advanced Neutron Sources (ICANS-X) held at Los Alamos, 3-7 October 1988*, Institute of Physics Conferences Series Number 97, p. 157 (Institute of Physics, Bristol and New York, 1988).
7. R. E. MacFarlane, "Cold Moderator Scattering Kernals," International Workshop on Cold Neutron Sources, March 5-8, 1990, Los Alamos, New Mexico, Los Alamos National Laboratory report LA-12146-C (August 1991).
8. R. E. MacFarlane, "New Thermal Neutron Scattering Files for ENDF/B-VI Release 2," Los Alamos National Laboratory report LA-12639-MS (also released as ENDF-356 by the National Nuclear Data Center at the Brookhaven National Laboratory) (August 1994).
9. R. C. Little, "Summary Documentation for the 100XS Neutron Cross Section Library (Release 1)," Los Alamos National Laboratory internal memorandum, XTM:RCL-95-259, and report LA-UR-96-24 (1995) (available URL: <http://www-xdiv.lanl.gov/PROJECTS/DATA/nuclear/doc/text100xs.html>).
10. S. C. Frankle, R. C. Reedy, and P. G. Young, "ACTI - A MCNP Continuous-Energy Neutron Data Library for Prompt Gamma-Ray Spectroscopy," Los Alamos National Laboratory report LA-UR-02-7783 (Dec. 2002) (available URL: <http://www-xdiv.lanl.gov/PROJECTS/DATA/nuclear/doc/acti.html>).
11. R. C. Little, "Argon and Krypton Cross-section Files," Los Alamos National Laboratory internal memorandum (June 30, 1982).

12. R. C. Little, "Cross Sections in ACE Format for Various IP Target Materials," Los Alamos National Laboratory internal memorandum (August 19, 1982).
13. R. C. Little, "Y-89 cross sections for MCNP," Los Alamos National Laboratory internal memorandum, X-6:RCL-85-419 (1985).
14. R. C. Little, "Modified ENDF/B-V.0 Y-89 cross sections for MCNP," Los Alamos National Laboratory internal memorandum, X-6:RCL-85-443 (1985).
15. R. E. Seamon, "Revised ENDF/B-V Zirconium Cross Sections," Los Alamos National Laboratory internal memorandum, X-6:RES-92-324 (1992) (available URL: http://www-xdiv.lanl.gov/PROJECTS/DATA/nuclear/doc/zr40_B5eval.html).
16. S. C. Frankle, "ENDL Fission Products, ENDL85 and ENDL92," Los Alamos National Laboratory internal memorandum, XTM:95-254 (1995).
17. S. C. Frankle, "Summary Documentation for the ENDL92 Continuous-Energy Neutron Data Library (Release 1)," Los Alamos National Laboratory internal memorandum, XTM:96-05, and report LA-UR-96-327 (1996) (available URL: <http://www-xdiv.lanl.gov/PROJECTS/DATA/nuclear/doc/textendl92.html>).
18. R. Little and R. Seamon, "ENDF/B-V.0 Gd Cross Sections with Photon Production," Los Alamos National Laboratory internal memorandum, X-6:RCL-87-132 (1986).
19. R. C. Little, "Neutron and Photon Multigroup Data Tables for MCNP3B," Los Alamos National Laboratory internal memorandum, X-6:RCL-87-225 (1987) (available URL: <http://www-xdiv.lanl.gov/PROJECTS/DATA/nuclear/doc/mgxsnp.html>).
20. R. C. Little and R. E. Seamon, "New MENDF5 and MENDF5G," Los Alamos National Laboratory internal memorandum, X-6:RCL-86-412 (1986).
21. J. C. Wagner et al., "MCNP: Multigroup/Adjoint Capabilities," Los Alamos National Laboratory report, LA-12704 (1994) (available URL: <http://www-xdiv.lanl.gov/PROJECTS/DATA/nuclear/pdf/la-ur-03-0164.pdf>).
22. R. E. Seamon, "Weight Functions for the Isotopes on Permfile THIRTY2," Los Alamos National Laboratory internal memorandum, TD-6 (July 23, 1976).
23. R. E. Seamon, "Plots of the TD Weight Function," Los Alamos National Laboratory internal memorandum, X-6:RES-91-80 (1980).
24. R. E. MacFarlane and D. W. Muir, "The NJOY Nuclear Data Processing System," Los Alamos National Laboratory report LA-12740 (1994) (available URL: <http://t2.lanl.gov/codes/codes.html>).
25. R. C. Little, "New Photon Library from ENDF Data," Los Alamos National Laboratory internal memorandum to Buck Thompson (February 26, 1982) (available URL: <http://www-xdiv.lanl.gov/PROJECTS/DATA/nuclear/pdf/la-ur-03-0164.pdf>).
26. E. Storm and H. I. Israel, "Photon Cross Sections from 1 keV to 100 MeV for Elements Z=1 to Z=100," Nuclear Data Tables, Volume A7, pp. 565-681 (1970).

APPENDIX G - MCNP DATA LIBRARIES
REFERENCES

27. C.J. Everett and E. D. Cashwell, "MCP Code Fluorescence Routine Discussion," Los Alamos National Laboratory report LA-5240-MS (1973).
28. H. G. Hughes, "Information on the Photon Library MCPLIB02 ," Los Alamos National Laboratory internal memorandum, X-6:HHG-93-77 (revised 1996) (available URL: <http://www-xdiv.lanl.gov/PROJECTS/DATA/nuclear/pdf/mcplib02.pdf>).
29. D. E. Cullen, M. H. Chen, J. H. Hubbell, S. T. Perkins, E. F. Plechaty, J. A. Rathkopf, and J. H. Scofield, "Tables and Graphs of Photon Interaction Cross Sections from 10 eV to 100 GeV Derived from the LLNL Evaluated Photon Data Library (EPDL)," Lawrence Livermore National Laboratory report UCRL-50400, Volume 6, Rev. 4, Part A: Z = 1 to 50 and Part B: Z = 51 to 100 (1989).
30. M. C. White, "Photoatomic Data Library MCPLIB03: An Update to MCPLIB02 Containing New Compton Doppler Broadening Data," Los Alamos National Laboratory internal memorandum X-5:MCW-02-110 (2002) (available URL: <http://www-xdiv.lanl.gov/PROJECTS/DATA/nuclear/pdf/mcw-02-110.pdf>).
31. F. Biggs, L. B. Mendelsohn, and J. B. Mann, "Hartree-Fock Compton Profiles for the Elements," Atomic Data and Nuclear Data Tables, Volume 16, pp. 201-309 (1975).
32. M. C. White, "Photoatomic Data Library MCPLIB04: A New Photoatomic Library Based on Data from ENDF/B-VI Release 8," Los Alamos National Laboratory internal memorandum X-5:MCW-02-111 (2002) (available URL: <http://www-xdiv.lanl.gov/PROJECTS/DATA/nuclear/pdf/mcw-02-111.pdf>).
33. D. E. Cullen, J. H. Hubbel, and L. D. Kissel, "EPDL97: The Evaluated Photon Data Library, '97 Version," Lawrence Livermore National Laboratory report, UCRL-50400, Volume 6, Rev. 5, (1997).
34. R. C. Little and R. E. Seamon, "Dosimetry/Activation Cross Sections for MCNP," Los Alamos National Laboratory internal memorandum, March 13, 1984 (available URL: <http://www-xdiv.lanl.gov/PROJECTS/DATA/nuclear/pdf/dosimetry.pdf>).

APPENDIX H - FISSION SPECTRA CONSTANTS AND FLUX-TO-DOSE FACTORS

Appendix H is divided into two sections: fission spectra constants to be used with the SP input card and ANSI standard flux-to-dose conversion factors to be used with the DE and DF input cards.

I. CONSTANTS FOR FISSION SPECTRA

The following is a list of recommended parameters for use with the MCNP source fission spectra and the SP input card described in Chapter 3. The constants for neutron-induced fission are taken directly from the ENDF/B-V library. For each fissionable isotope, constants are given for either the Maxwell spectrum or the Watt spectrum, but not both. The Watt fission spectrum is preferred to the Maxwell fission spectrum. The constants for spontaneously fissioning isotopes are supplied by Madland of Group T-16. If you desire constants for isotopes other than those listed below, contact X-5. Note that both the Watt and Maxwell fission spectra are approximations. A more accurate representation has been developed by Madland in T-16. If you are interested in this spectrum, contact X-5.

A. Constants for the Maxwell Fission Spectrum (Neutron-induced)

$$f(E) = CE^{1/2} \exp(-E/a)$$

	<u>Incident Neutron Energy (MeV)</u>	<u>a(MeV)</u>
n + ²³³ Pa	Thermal	1.3294
	1	1.3294
	14	1.3294
n + ²³⁴ U	Thermal	1.2955
	1	1.3086
	14	1.4792
n + ²³⁶ U	Thermal	1.2955
	1	1.3086
	14	1.4792
n + ²³⁷ U	Thermal	1.2996
	1	1.3162
	14	1.5063
n + ²³⁷ Np	Thermal	1.315
	1	1.315
	14	1.315

APPENDIX H - FISSION SPECTRA CONSTANTS AND FLUX-TO-DOSE FACTORS
CONSTANTS FOR FISSION SPECTRA

	Incident Neutron Energy (MeV)	a(MeV)
n + ²³⁸ Pu	Thermal	1.330
	1	1.330
	14	1.330
n + ²⁴⁰ Pu	Thermal	1.346
	1	1.3615
	14	1.547
n + ²⁴¹ Pu	Thermal	1.3597
	1	1.3752
	14	1.5323
n + ²⁴² Pu	Thermal	1.337
	1	1.354
	14	1.552
n + ²⁴¹ Am	Thermal	1.330
	1	1.330
	14	1.330
n + ^{242m} Pu	Thermal	1.330
	1	1.330
	14	1.330
n + ²⁴³ Am	Thermal	1.330
	1	1.330
	14	1.330
n + ²⁴² Cm	Thermal	1.330
	1	1.330
	14	1.330
n + ²⁴⁴ Cm	Thermal	1.330
	1	1.330
	14	1.330
n + ²⁴⁵ Cm	Thermal	1.4501
	1	1.4687
	14	1.6844
n + ²⁴⁶ Cm	Thermal	1.3624
	1	1.4075
	14	1.6412

B. Constants for the Watt Fission Spectrum

$$f(E) = C \exp(-E/a) \sinh(bE)^{1/2}$$

1. Neutron-Induced Fission

	Incident Neutron Energy (MeV)	a(MeV)	b(MeV⁻¹)
n + ²³² Th	Thermal	1.0888	1.6871
	1	1.1096	1.6316
	14	1.1700	1.4610
n + ²³³ U	Thermal	0.977	2.546
	1	0.977	2.546
	14	1.0036	2.6377
n + ²³⁵ U	Thermal	0.988	2.249
	1	0.988	2.249
	14	1.028	2.084
n + ²³⁸ U	Thermal	0.88111	3.4005
	1	0.89506	3.2953
	14	0.96534	2.8330
n + ²³⁹ Pu	Thermal	0.966	2.842
	1	0.966	2.842
	14	1.055	2.383

2. Spontaneous Fission

	a(MeV)	b(MeV⁻¹)
²⁴⁰ Pu	0.799	4.903
²⁴² Pu	0.833668	4.431658
²⁴² Cm	0.891	4.046
²⁴⁴ Cm	0.906	3.848
²⁵² Cf	1.025	2.926

II. FLUX-TO-DOSE CONVERSION FACTORS

This section presents several flux-to-dose rate conversion factor sets for use on the DE and DF tally cards to convert from calculated particle flux to human biological dose equivalent rate. These sets of conversion factors are not the only ones in existence, nor are they recommended by this

publication. Rather, they are presented for convenience should you decide that one is appropriate for your use. The original publication cited or other sources should be consulted to determine if they are appropriate for your application.

Although the various conversion factor sets differ from one another, it seems to be the consensus of the health physics community that they do not differ significantly from most health physics applications where accuracies of $\pm 20\%$ are generally acceptable. Some of the differences in the various sets are attributable to different assumptions about source directionality, phantom geometry, and depth of penetration. The neutron quality factors, derived primarily from animal experiments, are also somewhat different.

Be aware that conversion factor sets are subject to change based on the actions of various national and international organizations such as the National Council on Radiation Protection and Measurements (NCRP), the International Commission on Radiological Protection (ICRP), the International Commission on Radiation Units and Measurements (ICRU), the American National Standards Institute (ANSI), and the American Nuclear Society (ANS). Changes may be based on the reevaluation of existing data and calculations or on the availability of new information. Currently, a revision of the 1977 ANSI/ANS¹ conversion factors is underway and the ICRP and NCRP are considering an increase in the neutron quality factors by a factor of 2 to 2.5.

In addition to biological dose factors, a reference is given for silicon displacement kerma factors for potential use in radiation effects assessment of electronic semiconductor devices. The use of these factors is subject to the same caveats stated above for biological dose rates.

A. *Biological Dose Equivalent Rate Factors*

In the following discussions, dose rate will be used interchangeably with biological dose equivalent rate. In all cases the conversion factors will contain the quality factors used to convert the absorbed dose in rads to rem. The neutron quality factors implicit in the conversion factors are also tabulated for information. For consistency, all conversion factors are given in units of rem/h per unit flux (particles/cm²-s) rather than in the units given by the original publication. The interpolation mode chosen should correspond to that recommended by the reference. For example, the ANSI/ANS publication recommends log-log interpolation; significant differences at interpolated energies can result if a different interpolation scheme is used.

1. Neutrons

The NCRP-38² and ICRP-21³ neutron flux-to-dose rate conversion factors and quality factors are listed in Table H.1. Note that the 1977 ANSI/ANS factors referred to earlier were taken from NCRP-38 and therefore are not listed separately.

2. Photons

The 1977 ANSI/ANS¹ and the ICRP-21³ photon flux-to-dose rate conversion factors are given in Table H.2. No tabulated photon conversion factors have been provided by the NCRP as far as can be determined. Note that the 1977 ANSI/ANS and the ICRP-21 conversion factor sets differ

significantly (>20%) below approximately 0.7 MeV. Maximum disagreement occurs at ~0.06 MeV, where the ANSI/ANS value is about 2.3 times larger than the ICRP value.

B. Silicon Displacement Kerma Factors

Radiation damage to or effects on electronic components are often of interest. Of particular interest are the absorbed dose in rads and silicon displacement kerma factors. The absorbed dose may be calculated for a specific material by using the FM tally card discussed in Chapter 3 with an appropriate constant C to convert from the MCNP default units to rads. The silicon displacement kermas, however, are given as a function of energy, similar to the biological conversion factors. Therefore, they may be implemented on the DE and DF cards. One source of these kerma factors and a discussion of their significance and use can be found in Reference 4.

Table H.1
Neutron Flux-to-Dose Rate Conversion Factors and Quality Factors

NCRP-38, ANSI/ANS-6.1.1-1977*			ICRP-21	
Energy, E (MeV)	DF(E) (rem/hr)/(n/cm ² -s)	Quality Factor	DF(E) (rem/hr)/(n/cm ² -s)	Quality Factor
2.5E-08	3.67E-06	2.0	3.85E-06	2.3
1.0E-07	3.67E-06	2.0	4.17E-06	2.0
1.0E-06	4.46E-06	2.0	4.55E-06	2.0
1.0E-05	4.54E-06	2.0	4.35E-06	2.0
1.0E-04	4.18E-06	2.0	4.17E-06	2.0
1.0E-03	3.76E-06	2.0	3.70E-06	2.0
1.0E-02	3.56E-06	2.5	3.57E-06	2.0
1.0E-01	2.17E-05	7.5	2.08E-05	7.4
5.0E-01	9.26E-05	11.0	7.14E-05	11.0
1.0	1.32E-04	11.0	1.18E-04	10.6
2.0			1.43E-04	9.3
2.5	1.25E-04	9.0		
5.0	1.56E-04	8.0	1.47E-04	7.8
7.0	1.47E-04	7.0		
10.0	1.47E-04	6.5	1.47E-04	6.8
14.0	2.08E-04	7.5		
20.0	2.27E-04	8.0	1.54E-04	6.0

*Extracted from American National Standard ANSI/ANS-6.1.1-1977 with permission of the publisher, the American Nuclear Society.

Table H.2
Photon Flux-to-Dose Rate Conversion Factors

ANSI/ANS-6.1.1-1977		ICRP-21	
Energy, E (MeV)	DF(E) (rem/hr)/(p/cm ² -s)	Energy, E (MeV)	DF(E) (rem/hr)/(p/cm ² -s)
0.01	3.96E-06	0.01	2.78E-06
0.03	5.82E-07	0.015	1.11E-06
0.05	2.90E-07	0.02	5.88E-07
0.07	2.58E-07	0.03	2.56E-07
0.1	2.83E-07	0.04	1.56E-07
0.15	3.79E-07	0.05	1.20E-07
0.2	5.01E-07	0.06	1.11E-07
0.25	6.31E-07	0.08	1.20E-07
0.3	7.59E-07	0.1	1.47E-07
0.35	8.78E-07	0.15	2.38E-07
0.4	9.85E-07	0.2	3.45E-07
0.45	1.08E-06	0.3	5.56E-07
0.5	1.17E-06	0.4	7.69E-07
0.55	1.27E-06	0.5	9.09E-07
0.6	1.36E-06	0.6	1.14E-06
0.65	1.44E-06	0.8	1.47E-06
0.7	1.52E-06	1.	1.79E-06
0.8	1.68E-06	1.5	2.44E-06
1.0	1.98E-06	2.	3.03E-06
1.4	2.51E-06	3.	4.00E-06
1.8	2.99E-06	4.	4.76E-06
2.2	3.42E-06	5.	5.56E-06
2.6	3.82E-06	6.	6.25E-06
2.8	4.01E-06	8.	7.69E-06
3.25	4.41E-06	10.	9.09E-06
3.75	4.83E-06		
4.25	5.23E-06		
4.75	5.60E-06		
5.0	5.80E-06		
5.25	6.01E-06		
5.75	6.37E-06		
6.25	6.74E-06		

Table H.2
Photon Flux-to-Dose Rate Conversion Factors

ANSI/ANS-6.1.1-1977		ICRP-21	
Energy, E (MeV)	DF(E) (rem/hr)/(p/cm ² -s)	Energy, E (MeV)	DF(E) (rem/hr)/(p/cm ² -s)
6.75	7.11E-06		
7.5	7.66E-06		
9.0	8.77E-06		
11.0	1.03E-05		
13.0	1.18E-05		
15.0	1.33E-05		

III. REFERENCES

1. ANS-6.1.1 Working Group, M. E. Battat (Chairman), "American National Standard Neutron and Gamma-Ray Flux-to-Dose Rate Factors," ANSI/ANS-6.1.1-1977 (N666), American Nuclear Society, LaGrange Park, Illinois (1977).
2. NCRP Scientific Committee 4 on Heavy Particles, H. H. Rossi, chairman, "Protection Against Neutron Radiation," NCRP-38, National Council on Radiation Protection and Measurements (January 1971).
3. ICRP Committee 3 Task Group, P. Grande and M. C. O'Riordan, chairmen, "Data for Protection Against Ionizing Radiation from External Sources: Supplement to ICRP Publication 15," ICRP-21, International Commission on Radiological Protection, Pergamon Press (April 1971).
4. ASTM Committee E-10 on Nuclear Technology and Applications, "Characterizing Neutron Energy Fluence Spectra in Terms of an Equivalent Monoenergetic Neutron Fluence for Radiation-Hardness Testing of Electronics," American Society for Testing and Materials Standard E722-80, Annual Book of ASTM Standards (1980).

APPENDIX H - FISSION SPECTRA CONSTANTS AND FLUX-TO-DOSE FACTORS
REFERENCES

MCNP MANUAL INDEX

A

Absorption

Estimators, 2-171

Neutron, 2-34, 2-171

Accounting Arrays, E-35

Accuracy, 2-110

Accuracy, Factors Affecting, 2-111

ACE format, 2-17, 2-18, G-75

Adjoint option, 2-24, 3-125

Ambiguity

Cell, 2-10

Surfaces, 2-7, 2-9, **2-10**

Analog Capture, 2-34, 3-127

Angular Bins, 3-93

Angular Distribution

Functions for point detectors, 2-104

Sampling of, 2-36

Area calculation, 2-8, **2-187**

AREA card, 3-25

Arrays, 3-26

Asterisk, 3-11, 3-12, 3-31, 3-80, 3-86

Tally, 3-80

Atomic

Density, 3-9

Fraction, 3-118

Mass, 3-118

Number, 3-118

Weight (AWTAB) card, 3-123

Auger Electrons, 2-63, 2-78

Axisymmetric Surfaces

Defined by Points, 3-15

B

BBREM card, 3-52

Biasing

Cone, 2-153

Continuous, 2-153

Direction, 2-153

Energy, 3-52

Source, **2-152**, 3-61

Bin limit control, 2-105

Binning

By detector cell, 2-107

By multigroup particle type, 2-107

By particle charge, 2-107

By source distribution, 2-107

By the number of collisions, 2-107

Bins

Angular, 3-93

Cell, 3-81

Energy, 3-80

Multiplier, 3-80

Surface, 3-81

Tally, 3-80

Blank Line delimiter, 3-2

BOX, 3-18, 3-21

Bremsstrahlung, 2-77

Biasing (BBREM), 3-52

Model, 2-57

C

Capture

Analog, 2-34, 3-127

Implicit, 2-34

Neutron, 2-28, 2-34

Card Format, 3-4

Horizontal Input Format, 3-4

Vertical Input Format, 3-5

Cards

AREA, 3-25

Atomic Weight (AWTAB), 3-123

Bremsstrahlung Biasing (BBREM), 3-52

Cell, 3-2, 3-9 to 3-11

Cell Importance (IMP), 3-34

Cell Transformation (TRCL), 3-28

Cell Volume (VOL), 3-24

Cell-by-cell energy cutoff (ELPT), 3-136

Cell-flagging (CFn), 3-101

CFn, 3-101

CMn, 3-101

Cn, 3-93

Comment, 3-4

Computer time cutoff, 3-138

Coordinate Transformation (TRn), 3-30 to 3-32

Cosine (Cn), 3-93

Criticality Source (KCODE), 3-76

Cross-Section File (XS_n) Card, 3-123

CTME, 3-138
 CUT, 3-135
 DCBN, 3-142
 DDn, 3-108
 DE, 3-99
 DE / DF, H-3
 Debug Information (DBCN) card, 3-142
 Defaults, 3-7, 3-157
 Designators, 3-7
 Detector Contribution (PDn) card, 3-51
 Detector Diagnostics (DDn), 3-108
 Detector (F5), 3-82
 DF, 3-99
 Dose, 3-99
 DRXS, 3-121
 DSn, 3-65
 DXC (DXTRAN Contribution) card, 3-51
 DXTRAN (DXT), 3-110
 ELPT, 3-136
 En, 3-92
 Energy Multiplier (EMn), 3-100
 Energy Physics Cutoff (PHYS) card, 3-127 to 3-132
 Energy Splitting and Roulette (ESPLT) card, 3-35
 Energy-normed tally plots, B-27
 Exponential Transform (EXT) card, 3-40
 FCn, 3-91
 File creation (FILES) card, 3-144
 FILES, 3-144
 FILL, 3-29
 Fission Turnoff (NONU) card, 3-122
 Floating Point Array (RDUM) card, 3-139
 FMESH card, 3-114
 FMn, 3-95
 Fna, 3-80
 Forced collision card (FCL), 3-42
 Free-Gas Thermal Temperature (TMP) card, 3-132
 FSn, 3-102
 FTn, 3-112
 FUn, 3-105
 General Source (SDEF) card, 3-53
 History Cutoff (NPS) card, 3-137
 IDUM card, 3-138
 IMP, 3-34
 Integer Array (IDUM) card, 3-138
 KCODE card, 3-76
 KSRC, 3-77
 Lattice (LAT) card, 3-28
 Lost Particle (LOST) card, 3-141
 Material Specification Cards, 3-117
 Material Void (VOID) card, 3-124
 Material (Mm) card, 3-118
 Mesh Tally (FMESH), 3-114
 Message Block, 3-1
 MGOPT card, 3-125
 Mm, 3-118
 MODE card, 3-24
 MPLOT card, 3-147
 MPN Card, 3-120
 MTm card, 3-134
 Multigroup Adjoint Transport Option (MGOPT) card, 3-125
 NONU, 3-122
 NOTRN card, 3-137
 NPS, 3-137
 Output Print Tables (PRINT) card, 3-145, 3-147
 Particle Track Output (PTRAC) card, 3-148 to 3-152
 PDn card, 3-51
 Perturbation (PERTn) Card, 3-152 to 3-156
 Photon Weight (PWT) Card, 3-39
 Photon-Production Bias (PIKMT) card, 3-124
 PHYS card, 3-127 to 3-132
 PIKMT card, 3-124
 Plot tally while problem is running (MPLOT) card, 3-147
 PRDMP card, 3-139
 Print and Dump Cycle (PRDMP) card, 3-139
 PRINT card, 3-145, 3-147
 Problem Type (MODE) card, 3-24
 PTRAC card, 3-148 to 3-152
 PWT card, 3-39
 RDUM card, 3-139
 Repeated Structures cards, 3-25 to 3-32
 Ring detector, 3-82
 SBn card, 3-61
 SCn, 3-66
 SDEF, 3-53
 SDn card, 3-104

- Segment Divisor (SDn) card, 3-104
- SFn card, 3-102
- SIn card, 3-61
- Source Bias (SBn) card, 3-61
- Source Comment (SCn) card, 3-66
- Source Information (SIn) card, 3-61
- Source Points for KCODE Calculation (KSRC) card, 3-77
- Source Probability (SPn) Card, 3-61
- Special Treatments for Tallies (FTn), 3-112
- SPn card, 3-61
- SSR, 3-71
- SSW, 3-69
- Summary of MCNP Input Cards, 3-157
- Surface, **3-11 to 3-23**
- Surface Source Read (SSR) card, 3-71
- Surface Source Write (SSW) card, 3-69
- Surface-Flagging (SFn) card, 3-102
- $S(\alpha,\beta)$ Material (MTm) card, 3-134
- Tally Cards
 - Tally Comment (FCn) card, 3-91
 - Tally Energy card (En), 3-92
 - Tally Fluctuation (TFn) card, 3-107
 - Tally Multiplier (FMn) card, 3-95
 - Tally Segment (FSn card), 3-102
 - Tally Specification, 3-79
 - Tally Time (Tn) card, 3-92
 - Tally (Fna) cards, 3-80
- TALLYX (FUn) Input card, 3-105
- TALNP card, 3-147
- TFn, 3-107
- Thermal Times (THTME) card, 3-133
- THTME card, 3-133
- Time Multiplier (TMn) card, 3-100
- Title, 3-2
- TMn card, 3-100
- TMP card, 3-132
- Tn, 3-92
- Total Fission (TOTNU) card, 3-122
- TRCL, 3-28
- TRn, 3-30 to 3-32
- TSPLT card, 3-37
- Vector Input (VECT) card, 3-42
- VOID card, 3-124
- VOL, 3-24
- Weight Window Generator (WWG), 3-47
- WWG, 3-47
- X, 3-15
- XSn Card, 3-123
- Y, 3-15
- Z, 3-15
- Cell
 - Ambiguities, 2-10
 - Bins, 3-81
 - Complement, 2-8
 - Flux (F4) tally, 3-80
 - Tally, 3-80
- Cell Based Weight Window Bounds (WWN), 3-44
- Cell cards, 3-2, 3-9 to 3-11
 - Cell Importance (IMP) card, 3-34
 - Cell Transformation (TRCL) card, 3-28
 - Cell Volume (VOL) card, 3-24
 - Shorthand Cell Specification, 3-11
- Cell-by-cell Energy Cutoff (ELPT) Card, 3-136
- Cell-Flagging Card, 3-101
- Central Limit Theorem, **2-112**
- CFn Card, 3-101
- Change current tally reference vector, 2-106
- Characteristic X-rays, 2-78
- Charge Deposition Tally, 3-80
- CMn Card, 3-101
- Cn card, 3-93
- Code development, 3-132
- Coherent photon scattering
 - Detailed physics treatment, 2-61
- Coherent scattering
 - turning off, 2-62, 2-64
- Coincident detectors, 2-103
- Collision Nuclide Cross-section, 2-28
- Comment cards, 3-4
 - Source (SCn), 3-66
 - Tally, 3-91
- Complement Operator, 2-8
- Compton Scattering
 - Detailed physics treatment, 2-59
 - Simple physics treatment, 2-58
- Computer Time Cutoff, 3-138
- Cone, **2-9**
- Cone biasing, 2-153
- Confidence Intervals, **2-112**
- Continue-Run, 3-2 to 3-3, 3-143
- Continuous biasing, 2-153

Continuous-Energy data, 2-16
 Coordinate pairs, 3-15
 Coordinate Transformation (TRn) card, 3-30 to 3-32
 Correlated sampling, **2-163**
 Cosine
 bins, 2-18, 3-86, 3-93
 multiplier, 3-101
 (Cn) card, 3-93
 Criticality, **2-163**, 3-137, 3-140, 3-154
 Criticality Source (KCODE) card, 3-76
 Cross-Sections, 2-14
 Collision Nuclide, 2-28
 Default, 2-19
 Evaluations, 3-117
 File (XSn) Card, 3-123
 Library Identifier, 3-118
 Neutron, 3-118
 CTME card, 3-138
 Cumulative Tally, 5-61
 Current Tally, 2-84, 3-105
 CUT card, 3-135
 Cutoffs
 Cell-by-cell energy (ELPT), 3-136
 Computer time, 3-138
 Electron, 3-136
 Energy, 3-135
 Energy Physics (PHYS) card, 3-127 to 3-132
 History, 3-137
 Neutron, 3-135
 Photon, 3-136
 SWTM, 3-136
 Time, 2-69, 2-140, 3-135
 Weight, 3-135

D

Data arrays, 3-23, 3-26
 Data Cards (also see Cards), 3-23
 DBCN card, 3-142
 DDn Card, 3-108
 DE / DF cards, H-3, 3-99
 Debug Information Card, 3-142
 Debug Prints, 3-141
 Debugging, 3-109, 3-124, 3-132, 3-143
 Default Values, INP File, 3-7

Defaults, Card, 3-157
 Delayed Neutron (Data), G-11
 Density, Atomic, 3-9
 Dependent source distribution card, 3-65
 Detailed physics, 2-3, 2-7, 2-57, 3-129, D-8
 Treatment, 2-59
 Detectors
 Diagnostics card, 3-108
 Point, 3-82
 Reflecting/white/periodic surfaces, 2-101
 Ring, 3-82
 S(α,β) thermal treatment, 2-104
 Tallies, 2-5, D-6
 (F5) tallies, 2-80, 3-82
 Dimension Declarators, 3-30
 Direct vs. total contribution, 2-104
 Direction Biasing, 2-153
 Discrete Reaction Cross-Section Card, 3-121
 Discrete-Reaction data, 2-16
 Doppler Broadening
 Neutron, 2-29
 Photon, 2-61
 Dose Energy Card, 3-99
 Dose Function Card, 3-99
 DRXS Card, 3-121
 DSn Card, 3-65
 Dump cycle, 3-139
 DXC Card, 3-51
 DXTRAN, 2-12, 2-156 to 2-163
 Contribution Card (DXC), 3-51
 Sphere, 2-6, D-7, D-8
 Warnings, 3-74
 (DXT) card, 3-110

E

Elastic/Inelastic Scattering, 2-35
 Elastic cross-section adjusting, 2-29
 Energy from elastic scattering, 2-39
 Electron
 Cutoffs, 3-136
 Interaction data, 2-23
 Electron Transport, 2-67
 Angular Deflections, 2-76
 Bremsstrahlung, 2-77
 Condensed Random Walk, 2-69
 Energy Straggling, 2-72

Electrons, from photons, 2-57

Knock-On Electrons, 2-79

Multigroup, 2-79

Steps, 2-68

Stopping Power, 2-70

Electrons, from photons, 2-57

Elements, 3-118

ELPT Card, 3-136

EMAX, 3-130

EMn Card, 3-100

En card, 3-92

ENDF Emission Laws, 2-41

Energy

Biasing, 3-52

Bins, 3-80

Cutoffs, 3-135

Distribution sampling, 2-36

From elastic scattering, 2-39

Multiplier, 2-45

Multiplier (EMn) Card, 3-100

Physics Cutoff (PHYS) card, 3-127 to
3-132Roulette, **2-142**, 3-35

Spectra

Evaporation, 3-64

Gaussian fusion, 3-64

Maxwell fission, 3-64

Muir velocity Gaussian fusion, 3-64

Watt fission, 3-64

Splitting, **2-142**, 3-35

Tally, 3-92

Tally, F6 tally, 3-80

Entropy, 2-179, 3-77

Errors

Geometry, 3-8

Input, 3-7

ESPLT card, 3-35

Evaporation energy spectrum, 3-64

Event log, 3-8, 3-143

Printing, 3-142

Examples

Macrobody surfaces, 3-18

Surfaces by points, 3-16

Exponential transform, 3-10, 3-40

EXT card, 3-40

F

F1 (surface current) Tally, 3-80

F2 (surface flux) Tally, 3-80

F4 (cell flux) Tally, 3-80

F4, F6, F7 Tally Equivalence, 2-89

F5 (detector) flux tally, 3-80

F6 Neutrons, 2-88

F6 Photons, 2-88

F6 (cell energy) tally, 3-80

F7 Neutrons, 2-89

F7 (cell fission energy) Tally, 3-80

F8 (detector pulse energy) Tally, 3-80

Facets, 3-21

Fatal error message, 3-7

FATAL option, 3-7

FCL card, 3-42

FCn card, 3-91

Figure of Merit, 2-116, 3-35, 3-108, 3-140

File Creation (FILES) Card, 3-144

FILES (file creation) card, 3-144

FILL card, 3-29

Fission, 3-122

Neutron Multiplicity, 2-50

Spectra, 3-64

Turnoff (NONU) card, 3-122

Flagging, 2-105

Cell, 3-101

Surface, 3-102

Floating Point Array (RDUM) card, 3-139

Fluorescence, 2-57, 2-62

Flux at a Detector, 2-91

Flux Image Radiographs, 2-97

FIC, 3-82

FIP, 3-83

FIR, 3-82

Flux Tallies, 2-85

FMESH card, 3-114

FMn

card, 3-95

Reactions, G-1

FOM (also see Figure of Merit), 3-108

Forced collisions, 2-6, 2-136, 2-139, 2-151 to
2-152, 3-42, D-8

Fraction, Atomic, 3-118

Free Gas

Thermal temperature (TMP) card, 3-132

Thermal treatment, 2-28

FSn (tally segment) card, 3-102

FTn card, 3-112

FUn (TALLYX input) card, 3-105

Fusion Energy Spectrum (D-D), 3-64

G

Gas, Material Specification, 3-118

Gaussian Distribution

Position, 3-65

Time, 3-65

Gaussian energy broadening, 2-106

Gaussian fusion energy spectrum, 3-64

General Plane Defined by Three Points, 3-17

General Source (SDEF) card, 3-53

Geometry

Cone, 2-9

Surfaces, 2-9

Torus, 2-9

Geometry Cards, 3-24 to 3-32

AREA, 3-25

FILL, 3-29

LAT, 3-28

Repeated structures cards, 3-25 to 3-32

TRCL, 3-28

TRn, 3-30 to 3-32

Universe (U), 3-26

VOL, 3-24

Geometry Errors, 3-8

Geometry splitting, 2-6, 2-139, 2-140, D-8

Giant Dipole Resonance, 2-64

H

HEX, 3-19, 3-22

History

Cutoff (NPS) card, 3-137

Monte Carlo method, 2-1

History, Particle

Flow, 2-5, D-7

Horizontal Input Format, 3-4

HSRC, 3-77

HTGR Modeling, 3-32

I

IDUM array, 3-138

IDUM card, 3-138

IMP card, 3-34

Implicit Capture, 2-34

Importance, 3-7, 3-26, 3-34

Theory of, 2-146

Zero, 3-8, 3-12, 3-35, 3-44, 3-77, 3-85

Incoherent Photon Scattering

Detailed physics treatment, 2-59

Inelastic Scattering, 2-35, 2-39

Initiate-run, 3-1, 3-2, 3-3, 3-135

INP File, 3-1

Card Format, 3-4

Continue-Run, 3-2 to 3-3

Default Values, 3-7

Geometry Errors, 3-8

Initiate-Run, 3-2

Input Error Messages, 3-7

Message Block, 3-1

Particle Designators, 3-7

Installation, TC-1

Integer Array (IDUM) card, 3-138

Integers, 8 byte

DBCN, 3-142

DBUG, 3-142

MPLOT, 3-147

NPS, 3-137

PRDMP, 3-139

PTRAC, 3-148

RAND, 3-141

Interpolate (nI), 3-4

IPTAL Array, 3-106, E-31

J

Jerks/g, 3-80

Jump (nJ), 3-5

K

KCODE card, 3-76

Klein-Nishina, 2-58, 2-59, 2-60

KSRC card, 3-77

L

Lattice card, 3-28
 Lattice Tally, 3-81, 3-85
 Lattice Tally Enhancements, 3-116
 Lethargy-normed tally plots, B-27
 Lost Particle (LOST) card, 3-141
 Lost particles, 3-9, 3-141

M

Macrobodies, 3-18
 BOX, 3-18, 3-21
 Facets, 3-21
 HEX, 3-19, 3-22
 RCC, 3-19, 3-22
 RHP, 3-19, 3-22
 RPP, 3-18, 3-21
 SPH, 3-19, 3-22
 Mass
 Atomic, 3-118
 Density, 3-95, B-7
 Material Card
 Fraction, 3-118
 ZAID, 3-118
 Material number, 3-9, 3-10, 3-95, 3-96, 3-97,
 3-118, 3-124, 3-149, 3-152
 Material Specification Card, 3-117
 Material Void (VOID) card, 3-124
 Material (Mm) card, 3-118
 Maxwell fission energy spectrum, 3-64
 MCNP Input, 3-1
 MCNP Structure, 2-4, D-6
 Means, Variances, Standard Deviations, 2-109
 MESH Card, 3-48
 Mesh Tally, 2-83
 Mesh tally (FMESH), 3-114
 Mesh-Based Weight Window
 (MESH) card, 3-48
 Message Block, INP File, 3-1
 MGOPT card, 3-125
 Mm card (also see Material Card), 3-118
 MODE card, 3-24
 Monte Carlo Method History, 2-1
 MPLOT card, 3-147
 MPN Card, 3-120

MTm card, 3-134
 Muir velocity
 Gaussian fusion energy spectrum, 3-64
 Multigroup Adjoint Transport
 Option Card, 3-125
 Multigroup Tables, 2-24
 Multipliers and modification, 2-105
 Multiply (xM), 3-4

N

Neutron
 Absorption, 2-34, 2-171
 Capture, 2-28, 2-34
 Cross-sections, 3-118
 Cutoffs, 3-135
 Dosimetry cross sections, 2-23
 Interaction data, 2-16
 Interactions, 2-27
 Spectra, F-20
 Thermal $S(\alpha, \beta)$ tables, 2-24
 Neutron Emission
 Delayed, 2-52
 Prompt, 2-52
 nI (also see Interpolate), 3-4
 nJ (also see Jump), 3-5
 Normal, surface, 3-94
 NOTRN card, 3-137
 NPS card, 3-137
 nR (repeat), 3-4
 Nuclide identifier, 3-118

O

Output
 Print Tables (PRINT) Card, 3-145, 3-147

P

Pair Production
 Detailed physics treatment, 2-63
 Simple physics treatment, 2-58
 Parentheses, 3-9, 3-81, 3-95
 Particle
 Designators, 3-7

- History flow, 2-5, D-7
- Tracks, 2-27
- Weight, 2-25
- Particle Track Output
 - (PTRAC) card, 3-148 to 3-152
- Periodic boundaries, 2-7, **2-13**, 3-31
 - Limitations, 2-14
- Perturbation (PERTn) Card, 3-152 to 3-156
- Photoelectric Effect
 - Detailed physics treatment, 2-62
 - Simple physics treatment, 2-58
- Photon
 - Cross-sections, F-38
 - Cutoffs, 3-136
 - Generation, optional, 2-31
 - Interaction Data, 2-20
 - Interaction Treatment, 2-57
 - Production Bias (PIKMT) card, 3-124
 - Production Method
 - 30 x 20, 2-33
 - Expanded, 2-33
 - Scattering, 2-33
 - Spectra, F-20
 - Weight (PWT) Card, 3-39
- Photon Physics Treatment
 - Detailed, 2-59
 - Simple, 2-57
- Photonuclear Data
 - 4th entry on PHYS card, 2-66
 - Nuclide Selector, 3-120
- Photonuclear Physics, 2-64
- PHYS, 3-127
- PHYS Card, 2-57, 2-59, 3-127 to 3-132
 - Electrons, 3-130 to 3-132
 - Neutrons, 3-127 to 3-128
 - Photons, 3-128 to 3-129
- PIKMT card, 3-124
- Pinhole Camera Flux Tally, 3-83
- Pinhole Image Tally (FIP), 2-98
- Plot tally while problem is running
 - (MPLOT) Card, 3-147
- Plotting, 2-188 to 2-191, 3-8, 3-9, 3-10, 3-140, 3-148
- Plus, 3-11, 3-81, 3-86
- Point detectors, 2-91, 3-82
 - Cautions, 2-64
 - Contributions (NOTRN) Card, 3-137

- Power law source distribution, 3-65
- PRDMP card, 3-139
- Precision, 2-108, 2-110
 - Factors Affecting, 2-111
- Print and Dump Cycle (PRDMP) card, 3-139
- PRINT Card, 3-145
- Print cycle, 3-139
- Problem
 - Cutoff Cards, 3-135 to 3-138
 - Title card, 3-2
 - Type (MODE) card, 3-24
- Prompt v, 3-74, 3-122
- PTRAC card, 3-148 to 3-152
- Pulse Height Tallies, 2-89
- Pulse Height Tally
 - Variance Reduction, 3-87
 - Weight, 2-26
 - (F8), 3-85
- PWT card, 2-31, 2-32, 3-39

Q

- Quasi-deuteron photon absorption, 2-65

R

- Radiograph Image Tallies
 - FIC, 2-97
 - FIR, 2-97
- Radiography Tallies, 2-97, 3-82
- RAND Card, 3-141
- RCC, 3-19, 3-22
- RDUM array, 3-138
- RDUM card, 3-139
- Reflecting surface, 2-12, 3-11, 3-27, 3-79, 3-85, 3-111, 3-128
- Repeat (nR), 3-4
- Repeated Structures
 - Tally, 3-85
- Repeated structures, 3-10, 3-11, 3-88, 3-89, 3-90, 3-105, 3-143, 3-146
 - Cards, 3-25 to 3-32
 - Geometry, 2-9
 - Source, 3-59
 - Tally, 3-88
- Response function, 3-85, 3-96, 3-99, 3-100

RHP, 3-19, 3-22
 Ring detectors, 2-94, 3-82
 Cautions, 2-64
 Ring detector card, 3-82
 RPP, 3-18, 3-21
 Russian roulette, 2-6, 2-32, 2-140, 3-109, D-8
 Russian roulette (also see Energy roulette),
 2-142

S

Sampling Angular Distributions, 2-36
 SBn card, 3-61
 Scattering
 Elastic, 2-35, 2-39
 Inelastic, 2-35, 2-39
 Photon, 2-33
 $S(\alpha, \beta)$, 2-29
 $S(\alpha, \beta)$ Treatment, 2-28
 SCn card, 3-66
 SDEF card, 3-53
 SDn card, 3-104
 Segment Divisor (SDn) card, 3-104
 Segmenting card, 3-102
 Sense, 2-7, 3-12, 3-94, 5-114, E-44
 SFn (surface flagging) card, 3-102
 Simple physics treatment, 2-7, **2-57**, D-8
 SIn card, 3-61
 Source
 Bias (SBn) card, 3-61
 Comment (SCn) card, 3-66
 Dependent source distribution
 (DSn card), 3-65
 Direction Biasing, 2-153
 Energy biasing, 3-52
 Fission, 3-64
 Fusion, 3-64
 Information (SIn) card, 3-61
 Probability (SPn) Card, 3-61
 SDEF (General Source) card, 3-53
 SOURCE subroutine, 3-78
 Specification, 3-52
 Spectra, 3-64
 SRCDX subroutine, 3-78
 SSR card, 3-71
 SSW card, 3-69
 Surface, 3-26, 3-31, 3-50, 3-52, 3-57, 3-69,

3-71
 weight minimum cutoff, 3-136
 Source Biasing, 2-152
 Space-energy dependence, 2-142
 SPDTL, 3-116
 Special Treatments, 2-106
 Special Treatments for Tallies
 (FTn) card, 3-112
 SPH, 3-19, 3-22
 Splitting, 2-142
 Splitting (also see Energy Splitting), 3-33
 SPn card, 3-61
 SSR card, 3-71
 SSW card, 3-69
 Steradian, 3-101
 Stochastic Geometry, 3-32
 Storage Limitations, 3-160
 Subroutine Usage, **D-6**
 Subroutines
 SOURCE, 3-78
 SRCDX, 3-78
 Summary of MCNP Input Cards, 3-157
 Superimposed Importance Mesh for Mesh-
 Based Weight Window Generator
 (MESH) card, 3-48
 Superimposed Mesh Tally (FMESH), 3-114
 Surface
 Bins, 3-81
 Coordinate pairs, 3-15
 Current (F1) Tally, 3-80
 Flux (F2) Tally, 3-80
 Mnemonics, 3-11, **3-13**, 3-23
 Normal, 3-94
 Reflecting, 3-11
 Source, 3-26, 3-31, 3-50, 3-52, 3-57, 3-69,
 3-71
 White boundaries, 2-13, 3-11, 3-12
 Surface Area card, 3-25
 Surface Cards, 3-11 to 3-23
 Axisymmetric Surfaces
 Defined by Points, 3-15
 General Plane
 Defined by Three Points, 3-17
 Surfaces Defined by Equations, 3-11
 Surfaces Defined by Macrobodyes, 3-18
 Surface Flux (F2), 2-86
 Surface Source Read (SSR) card, 3-71

Surface Source Write (SSW) card, 3-69

Surface-Flagging (SF_n) Card, 3-102

Surfaces, **2-9**

Periodic boundaries, 2-13, 3-31

SWTM, 3-136

S(α , β) scattering, 2-28, 2-29

T

Tally

and DXTRAN, 3-110

Asterisk, 3-80

Bins, 3-80

Cell, 3-80

Cell flux (F₄), 3-80

Charge deposition (+F_{8E}) Tally, 3-80

Comment (FC_n) card, 3-91

Detector, 2-5, D-6

Detector diagnostics (DD_n) card, 3-108

Detector flux (F₅), 2-80, 3-80, 3-82

Dose, 3-99

F1(surface current), 3-80

F2 (surface flux), 3-80

F4 (cell flux), 3-80

F6 (cell avg. energy deposition), 3-80

F7 (cell fission energy deposition), 3-80

F8 (detector pulse energy
distribution), 3-80

Fluctuation (TF_n) card, 3-107

FMESH, 3-114

F_na cards, 3-80

FT_n (special treatments) card, 3-112

Lattice, 3-85

Mesh Tally, 2-83, 3-114

Multiplier (FM_n) card, 3-95

Pulse height, 3-85

Radiography, 3-82

Repeated Structures, 3-85, 3-88

Segment (FS_n) card, 3-102

Special treatments (FT_n) card, 3-112

Specification cards, **3-79** to 3-114

Surface current (F₁), 3-80

Surface Flux (F₂), 3-80

Time (T_n) card, 3-92

Types, 3-80

Union, 3-81

Units, 3-80

Weight, 3-80

Tally output format, 2-108

TALLYX

Subroutine, 3-105, **3-106**

(F_{Un}) Input card, 3-105

TALNP card, 3-147

Temperature, 3-10, 3-121, 3-127

TF_n card, 3-107

Thermal

Scattering treatment, 2-54

Temperature, 3-132

Times (THTME) card, 3-133

Treatment, 3-127

Thomson scattering, 2-58

Detailed physics treatment, 2-61

THTME card, 3-133

Time

Cutoff, 2-69, 2-140, 3-135

Multiplier (TM_n) card, 3-100

Time convolution, 2-106

Time Splitting (TSPLT) card, 3-37

Title card, 3-2

TM_n card, 3-100

TMP card, 2-30, 3-132

T_n card, 3-92

Torus, **2-9**, 3-13, 3-14

Total Fission (TOTNU) card, 3-122

TOTNU card, 2-50

TOTNU (Total ν card), 3-122

Track Length Cell Energy

Deposition Tallies, 2-87

Track Length Estimate of Cell Flux (F₄), 2-85

Transformation, 3-28

TRCL card, 3-28

TR_n card, 3-30 to 3-32

TSPLT card, 3-37

U

Universe, 3-25

Universe (U) card, 3-26

Unresolved neutron resonances, 2-55

Unresolved Resonance (Data), G-11

URAN, 3-32

User Data Arrays, 3-138 to 3-139

User modification, 2-108

VVariance Reduction, **2-134 to 2-163**

- and Accuracy, 2-134
- and Efficiency, 2-135
- DXTRAN, 2-156
- Energy Cutoff, 2-139, 3-135
- Energy roulette, **2-142**
- Energy splitting, **2-142**
- Exponential transform, 3-10, 3-40
- Forced collisions, **2-151 to 2-152**, 3-42
- Geometry splitting, 2-140
- Introduction, **2-134**
- Modified Sampling Methods, 2-139
- Partially-Deterministic Methods, 2-139
- Population Control Methods, 2-139
- Russian roulette, 2-140
- Schemes for detectors, 2-102
- Techniques, 2-139
- Time cutoff, **2-140**, 3-135
- Truncation Methods, 2-139
- Weight cutoff, 3-135

Variance Reduction Cards, 3-34 to 3-52

- BBREM, 3-52
- Detector Contribution (PDn) card, 3-51
- DXC, 3-51
- DXTRAN (DXT) card, 3-110
- ESPLT, 3-35
- EXT, 3-40
- FCL, 3-42
- IMP, 3-34
- MESH, 3-48
- PDn, 3-51
- PWT, 3-39
- Weight Window Cards, 3-43 to 3-47
- Weight Window Generation Cards, 3-46 to 3-51
- WWE, 3-44
- WWG, 3-47
- WWGE, 3-47
- WWN, 3-44
- WWP, 3-45

Vector Input (VECT) card, 3-42

Velocity sampling, 2-29

Vertical Input Format, 3-5

VOID card, 3-124

VOL card, 3-24

W

Warning Messages, 3-7

Watt fission energy spectrum, 3-64

Watt fission spectrum, 3-77

WC1, 3-128, 3-135, 3-136

WC2, 3-135

Weight cutoff, 3-135

Weight Window

- Cards, 3-43 to 3-47

- Energies or Times (WWE), 3-44

- Generation Cards, 3-46 to 3-51

- Generation Energies or Times (WWGE), 3-47

- Generator (WWG) card, 3-47

- Parameter Card (WWP), 3-45

White Boundaries, 2-13, 3-11, 3-12

WWE Card, 3-44

WWG Card, 3-47

WWGE Card, 3-47

WWN Card, 2-32, 3-44

WWP Card, 3-45

X

X Card, 3-15

xM (also see Multiply), 3-4

XS_n Card, 3-123**Y**

Y Card, 3-15

Z

Z Card, 3-15

ZA, **3-120**ZAID, 2-24, 3-118, **3-121**

- and $S(\alpha, \beta)$, 3-134

- and the AWTAB card, 3-123

ZA,ZB,ZC, E-44

Zero Importance, 3-8, 3-12, 3-35, 3-44, 3-77, 3-85

ZZZAAA (also see ZAID), 2-15

Symbols

#n (Complement Operator), 2-8

(), 3-9, 3-81, 3-95

*, 3-11, 3-12, 3-31, 3-80, 3-86

+, 3-11, 3-81, 3-86